

# Ninth International Conference On Molecular Beam Epitaxy



**August 5-9, 1996  
Pepperdine University  
Malibu, California**

**Sponsored by AVS  
Technical Cosponsorship by  
IEEE Electron Devices Society and MRS**

AIR FORCE OF SCIENTIFIC RESEARCH (AFSC)

THIS DOCUMENT IS UNCLASSIFIED AND HAS BEEN REVIEWED AND IS

APPROVED FOR RELEASE BY THE AIR FORCE OF SCIENTIFIC RESEARCH (AFSC) AFR 190-12

DISTRIBUTION STATEMENT UNCLASSIFIED

Joan Boga

STINFO Program Manager

## Abstract Book

19971002 044

Approved for public release;  
distribution unlimited

# MBE-IX

## Ninth International Conference on Molecular Beam Epitaxy

August 5-9, 1996  
Malibu, California, USA

### CONFERENCE CHAIR

Kang L. Wang, University of California, Los Angeles

### TECHNICAL PROGRAM COMMITTEE

Dwight C. Streit (Chair), TRW  
April Brown, Georgia Tech  
K.Y. Cheng, U. Illinois  
Karl Eberl, Max-Planck Institute  
C. Thomas Foxon, U. Nottingham  
Toshio Fujii, Fujitsu Labs  
Robert Gunshor, Purdue U.  
James S. Harris, Stanford U.  
Pin Ho, Lockheed-Martin  
Yoshiji Horikoshi, NTT Research Labs

Yung-Chung Kao (Editor), TI Corp. R&D  
Mei-Ying Kong, Chinese Academy Sciences  
Dan Mars, Hewlett-Packard Labs  
Jean Massies, CNRS  
Yasuhiro Shiraki, U. of Tokyo  
A.J. Springthorpe, Bell-Northern  
Ben Streetman, U. of Texas, Austin  
Won T. Tsang, Lucent Technologies  
Charles Tu, U. of California, San Diego  
Wen I Wang, Columbia U.  
Owen K. Wu, Hughes Research Labs

### ORGANIZING COMMITTEE

Owen K. Wu (Chair), Hughes Research Labs  
Jose Arias, Rockwell  
Ping Chen, U. of Southern California  
David Chow, Hughes Research Labs  
Ralph Dawson, Sandia National Labs  
Art Gossard, U. of California, Santa Barbara  
Frank Grunthaner, JPL

David Grider (Co-Chair), Hughes Research Labs  
John E. Jensen, Hughes Research Labs  
Leslie Kolodziejski, MIT  
Henry Lee, U. of California, Irvine  
Pat Gillis, University of California, Los Angeles  
Colin Wood, U. of Maryland  
Yong Zhang, Hughes Research Labs

### INTERNATIONAL ADVISORY COMMITTEE

Ben Streetman (Chair), U. of Texas, Austin  
Pallab Bhattacharya, U. of Michigan  
Leroy L. Chang, Hong Kong U.  
Alfred Y. Cho, Lucent Technologies  
Leo Esaki, Tsukuba U.  
Jean Pierre Faurie, CNRS  
Shun-ichi Gonda, Osaka U.  
Kia-Feng Huang, National Chiao Tung U.  
Derek Houghton, NRC Canada  
Erich Kasper, U. Stuttgart  
Bruce Joyce, U. of London  
Herbert Kroemer, UC Santa Barbara

Ai-Zhen Li, Shanghai Inst. Metal.  
Thomas G. McGill, Cal Tech  
Jeffery Miller, Hewlett-Packard  
Linh T. Nuyen, PicoGiga  
Evan H.C. Parker, U. Warwick  
Markus Pessa, Tempera U.  
Klaus H. Ploog, Paul-Drude-Institute  
Hiroyuki Sakaki, U. of Tokyo  
Jan F. Schetzina, North Carolina State U.  
Kang L. Wang, UCLA  
G. Weimann, Walter-Schottky Institute



## MBE-IX

Sponsored by the  
American Vacuum Society

Technical co-sponsorship provided by  
IEEE Electron Devices Society  
Materials Research Society

MBE-IX gratefully acknowledges the following vendors who have provided financial support by exhibiting their products and services during the conference:

ADDON Creative Epitaxy Equipment  
American Xtal Technology (AXT)  
Bede Scientific, Inc.  
CI Systems, Inc.  
D&T International Company  
EPI MBE Products Group  
Granville-Phillips Company  
MCP Wafer Technology  
O. S. Technology  
Pacific Lightwave  
Shin-etsu Chemical  
Sumitomo Electric (SEMIA, Inc.)  
SVT / EPI MBE Group  
Thermionics Laboratory, Inc.  
Univeral Systems of Tokyo  
VSI Vacuum Science  
Woolam Company

Advanced Ceramics Corporation  
ASTeX/Applied Science Tech.  
Charles Evans & Associates  
CVD Products, Inc.  
DCA Instruments  
Fisons Instruments/VG Semicon  
Johnson Matthey  
NIMTEC Inc. / Japan Energy  
Oxford Applied Research  
Riber Division / Instruments SA, Inc.  
Staib Instruments, Inc.  
Surface / Interface, Inc.  
SVT Associates, Inc.  
United Mineral & Chemical Corp.  
Varian Vacuum Products  
VTS J. Schwarz GmbH

MBE-IX gratefully acknowledges the following agencies for providing financial support for students and invited speakers:

AFOSR	Air Force Office of Scientific Research
ARO	Army Research Office
ONR	Office of Naval Research
NSF	National Science Foundation
DARPA	Defense Advanced Research Projects Agency

# REPORT DOCUMENTATION PAGE

Form Approved  
OMB No. 0704-0188

Public reporting burden for this collection of information is estimated to average 1 hour per response, including the time for reviewing instructions, searching existing data sources, gathering and maintaining the data needed, and completing and reviewing the collection of information. Send comments regarding this burden estimate or any other aspect of this collection of information, including suggestions for reducing this burden, to Washington Headquarters Services, Directorate for Information Operations and Reports, 1215 Jefferson Davis Highway, Suite 1204, Arlington, VA 22202-4302, and to the Office of Management and Budget, Paperwork Reduction Project (0704-0188), Washington, DC 20503.

1. AGENCY USE ONLY (Leave blank)		2. REPORT DATE		3. REPORT TYPE AND DATES COVERED FINAL REPORT 01 Jul 96 - 30 Jun 97	
4. TITLE AND SUBTITLE PROPOSAL FOR PARTIAL SUPPORT OF THE 9TH INTERNATIONAL MOLECULAR BEAM EPITAXY (MBE) CONFERENCE				5. FUNDING NUMBERS 61102F 2305/CS	
6. AUTHOR(S) Professor Kang L. Wang					
7. PERFORMING ORGANIZATION NAME(S) AND ADDRESS(ES) Electrical Engineering Department University of California, Los Angeles P O Box 951594 Los Angeles, CA 90095-1594				AFOSR-TR-97 0323	
9. SPONSORING/MONITORING AGENCY NAME(S) AND ADDRESS(ES) AFOSR/NE 110 Duncan Avenue Suite B115 Bolling AFB DC 20332-8050				10. SPONSORING/MONITORING AGENCY REPORT NUMBER F49620-96-1-0303	
11. SUPPLEMENTARY NOTES					
12a. DISTRIBUTION/AVAILABILITY STATEMENT APPROVED FOR PUBLIC RELEASE: DISTRIBUTION UNLIMITED				12b. DISTRIBUTION CODE	
13. ABSTRACT (Maximum 200 words)  The Ninth International Conference on Molecular Beam Epitaxy (MBE-IX) was held on the campus of the Pepperdine University, Malibu, California, from August 5 to 9, 1996. Prof. Kang L. Wang (UCLA) served as the Conference Chairman for this conference along with Dr. Dwight C. Streit (TRW) as the Program Chairman, and Drs. Owen K. Wu and David E. Grider (Hughes) as the Organizing Committee Chairmen, and Prof. Benjamin G. Streetman (Univ. Texas, Austin) as the International Advisory Committee Chairman. There were over 500 participants who attended from 27 countries including US. There were 110 presentations in 15 oral sessions and 145 posters in 4 poster sessions.					
14. SUBJECT TERMS  DTIC QUALITY INSPECTED 4				15. NUMBER OF PAGES	
				16. PRICE CODE	
17. SECURITY CLASSIFICATION OF REPORT UNCLASSIFIED	18. SECURITY CLASSIFICATION OF THIS PAGE UNCLASSIFIED	19. SECURITY CLASSIFICATION OF ABSTRACT UNCLASSIFIED	20. LIMITATION OF ABSTRACT		

**Final Report**  
**on the**  
**Ninth International Conference on Molecular Beam Epitaxy (MBE-IX)**  
**by Prof. Kang L. Wang, Chairman, MBE-IX**

The Ninth International Conference on Molecular Beam Epitaxy (MBE-IX) was held on the campus of the Pepperdine University, Malibu, California, from August 5 to 9, 1996. Prof. Kang L. Wang (UCLA) served as the Conference Chairman for this conference along with Dr. Dwight C. Streit (TRW) as the Program Chairman, and Drs. Owen K. Wu and David E. Grider (Hughes) as the Organizing Committee Chairmen, and Prof. Benjamin G. Streetman (Univ. Texas, Austin) as the International Advisory Committee Chairman. There were over 500 participants who attended from 27 countries including US. There were 110 presentations in 15 oral sessions and 145 posters in 4 poster sessions.

This conference is one in a biennial series, which rotates between the United States, Japan and Europe, and thus, takes place in this country every six years. Previous meetings were held in Sapporo, Japan (1988), York, United Kingdom (1986), San Francisco (1984), Tokyo (1982), Paris (1978), UC San Diego, California (1990), Stuttgart, Germany (1992), and Osaka, Japan (1994) and Los Angeles, (1996). The next MBE conference will be chaired by Dr. Jean-Pierre Faurie of CNRS, and to be held in France (1998).

In this conference, the major theme highlighted the success of MBE technology to the state that it is now a commercial tool for manufacturing integrated circuits. The topics critical to the development and advance of MBE were covered and they ranged from material aspects of growth, processing and characterization to relevant physics and device properties of the resulting films and structures. Specific topics included growth and growth mechanisms of MBE, characterization of MBE films and interfaces, advances in MBE and related techniques, such as MEE, GSMBE, and MOMBE Physics and MBE grown devices and structures.

The magnitude of the success of this International MBE Conference has certainly exceeded the original expectation. This was hinged on the ability to attract active researchers of various disciplines to address different aspects of topics and problems while interacting under the common theme of molecular beam epitaxy. The ability of the conferences to grow with the field in keeping the vitality of new emerging science and technology on one hand and on the other to maintain a manageable size to provide a collegiate environment contributed in part to their success. This conference served as an effective medium to introduce the new comers in the field

to this forefront area of materials science and electronics. This series of the Conferences, we believe, have also helped shape the field of molecular beam epitaxy as it is known today. Major developments in the field of MBE have always involved international efforts. Indeed, this MBE conference owes much of its success to the close collaboration of the MBE community worldwide.

For the past half century, MBE has been of fundamental importance in the creation of advanced new materials and device structures for electronics and optoelectronics, and photonics. The papers presented reflected tremendous progress in molecular beam epitaxy since the first international conference held 16 years ago. To date, MBE has progressed to the point that it is now an important tool for both research and production applications as reflected in the plenary session and other invited and contributed presentations in this conference.

## CONFERENCE COMMITTEE'S FOREWORD

Dear MBE Colleagues,

This year the United States once again hosts the International Conference on Molecular Beam Epitaxy. MBE-VI was held in La Jolla, California six years ago, and now MBE-IX has returned to Southern California. In the interim MBE-VII was held in Germany in 1992, and MBE-VIII was held in Japan in 1994. MBE-IX is being held at the spectacular Pepperdine University campus in Malibu California the week of August 5-9. Its beautiful scenery and sunny weather provide a perfect setting for both scientific discussions as well as social and professional interactions.

There has been tremendous growth in molecular beam epitaxy since the first international conference was held 16 years ago. MBE is now of fundamental importance in the creation of advanced new materials and device structures for electronics, optoelectronics, and photonics applications. MBE has progressed to the point that it is now an important tool for both research and production applications. The plenary session reflects this ongoing evolution, with overview talks on MBE-based system insertions as well as new MBE materials and technologies.

Over 390 abstracts from 27 countries were submitted for MBE-IX, resulting in an exciting and interesting program. The most recent advances in MBE-based material growth, characterization, and devices will be presented through 110 presentations in 15 oral sessions and 145 posters in 4 poster sessions. The conference proceedings will be published as a special issue of the Journal of Crystal Growth in 1997.

The social agenda includes user's meetings throughout the week for each of the major equipment makers, parallel rump sessions on Tuesday evening, a lunchtime barbecue in a park-like setting overlooking the Pacific Ocean followed by tours of research facilities and museums on Wednesday afternoon, and a conference banquet at the Hyatt Westlake Village Hotel on Thursday evening.

We welcome you to Malibu for an exciting week of scientific and social activities in a spectacular coastal setting.

*Kang L. Wang*      *Dwight C. Streit*      *Owen K. Wu*      *David E. Grider*  
Conference Chair      Program Chair      Organizing Committee Chair, Co-Chair

### NINTH INTERNATIONAL CONFERENCE ON MOLECULAR BEAM EPITAXY

MBE-IX	Morning	Afternoon		Evening
Sunday 4 Aug.		Registration and Check-In 14:00 - 22:00		VG Users Meeting
Monday 5 Aug.	1. Plenary	2. Nitrides 3. Quantum Dots		EPI Users Meeting
Tuesday 6 Aug.	4. III-V Growth 5. II-VI Growth	6. III-V Growth 7. IV-IV Growth	Poster 1. III-V Poster 2. IV, II-VI	Rump 1. Production Rump 2. New Materials
Wed. 7 Aug.	8. Regrowth 9. Sb and Other Materials	Barbecue	Free Afternoon & Tours	Riber Users Meeting
Thursday 8 Aug.	10. In-Situ Characterization & Control 11. Lasers and Growth Issues	12. In-Situ 13. VCSELs	Poster 3. Sb, N, P Poster 4. Devices	Banquet
Friday 9 Aug.	14. Devices and Quantum Wires 15. Lasers and Detectors			



**Applications and Future Directions of MBE Material**

Session Chair: Dwight Streit, TRW, Redondo Beach, California

09:00 1.0 **Welcoming Remarks**

Kang Wang, Conference Chair

Owen Wu, Organizing Co-Chair

Dave Grider, Organizing Co-Chair

Arthur N. Chester, Chairman &amp; President, Hughes Research Laboratories, Inc.

09:15 1.1 **Applications of MBE-grown PHEMTs, (Invited)**

James V. DiLorenzo

Raytheon Advanced Device Center, Andover, Massachusetts, USA.

09:40 1.2 **Millimeter wave and digital applications of InP-based MBE-grown HEMTs and HBTs, (Invited)**

Paul Greiling

Hughes Research Laboratories, Malibu, USA

10:05 1.3 **Commercial business development and growth of MBE-based GaAs HBT products and services, (Invited)**

Bob Van Buskirk

TRW Electronics and Technology Division, Redondo Beach, California, USA.

Break

10:50 1.4 **Mass production of InAs Hall elements by MBE, (Invited)**

Ichiro Shibasaki

Asahi Chemical Industry Co. Ltd., Shizuoka, Japan.

11:20 1.5 **Quantum cascade lasers operating with high power above room temperature, (Invited)**

Jerome Faist

Bell Laboratories, Lucent Technologies, Murray Hill, New Jersey, USA.

11:50 1.6 **Progress and prospects of Group III nitride semiconductors, (Invited)**

Isamu Akasaki and H. Amano

Meijo University, Tempaku, Nagoya, Japan.

# **Applications of MBE Grown PHEMTs**

**James V. DiLorenzo  
Raytheon Advanced Device Center  
Andover, MA 01810 USA**

In the last decade Pseudomorphic High Electron Mobility Transistors (PHEMTs) have gone from a laboratory curiosity with unique low noise performance to a high volume commercial product for a variety of power and low noise applications. At Raytheon Microelectronics we currently use several thousand 4 inch PHEMT wafers per year and expect this quantity to grow to tens of thousands of wafers per year in 5 years. These wafers are all grown by MBE and obtained from a combination of commercial vendors and Raytheon internal MBE systems. At ADC we have 2 Riber automated production MBE systems capable of growing over forty 4 inch PHEMT wafers per day in round-the-clock operation plus an additional 3 single wafer experimental systems.

Technological advances in PHEMT fabrication - delta doping from both sides of the channel for high carrier densities, short gate length T gates for high transconductance, with double recesses for high breakdown voltage - have made PHEMTs suitable for power applications. The resulting high power along with high efficiency and linearity have allowed PHEMTs to be employed in a wide variety of applications in our foundry from cellular based products below 1 Ghz to ICC radar/transceivers at 77 Ghz. In 1995 the number of PHEMT wafers produced at ADC exceeded that of ion-implanted MESFETs and that trend is accelerating today.

We describe here the variety of programs at Raytheon using PHEMT circuits. Military programs make use of PHEMTs for high efficiency power amplifiers and low noise receivers at X-band (Advanced Ground Based Radar), C-band (Navy Cooperative Engagement Capability), and Q-band (Milstar Satellite terminals such as Smart T). Space applications include a variety of commercial consumer satellite communications system components for such systems as Globalstar<sup>TM</sup>, IRIDIUM, Inmarsat, and Odyssey operating at L and S band. There are also commercial applications consisting of high frequency converters, transceivers, and power amplifiers at L and S bands for personal communications products and cellular telephones.

The growing need for very large quantities of PHEMT wafers having a precisely defined material structure presents significant challenges to be MBE grower. We will discuss these challenges and our approach to meeting them.

## **Millimeter Wave and Digital Applications of InP-Based MBE Grown HEMTs and HBTs**

Paul Greiling  
Hughes Research Laboratories  
3011 Malibu Cyn. Rd., Malibu, CA 90265

The growth of semiconductor device layers by MBE has allowed designers to develop a range of bandgap engineered devices including: 1) low noise HEMTs; 2) high power and power added efficiency HEMTs and HBTs; and 3) high speed digital/analog HBT ICs with an order of magnitude performance improvement over standard Si CMOS, Si bipolar transistors or GaAs MESFETs. The superior performance of MBE-grown, heterojunction devices has motivated the analysis, development, and optimization of Si, GaAs and InP-based HBT and HEMT technologies for military systems such as radar, communications, EW, as well as smart munitions. The transition of these technologies into commercial applications, however, is dependent on a rather different set of criteria than those for military applications.

MBE-grown heterojunction devices offer significant advantages in speed and frequency range of operation. Si bipolar ICs offer a 25 GHz device technology, for example, with practical operation at frequencies up to 5 GHz. Half-micron gate length GaAs MESFETs represent a 40 GHz technology, with effective operation at up to 20 GHz. In sharp contrast, MBE-grown, heterojunction devices currently being developed (e.g., SiGe-, GaAs-, and InP-based HBTs, and GaAs- and InP-based HEMTs) offer over 100 GHz device technologies, with operation extending well into the millimeter wave frequency range.

The enhanced performance of these MBE-grown heterojunction device technologies will help meet the requirements of future military systems. In particular, the next generation of phased-array radar systems will require reduced weight and volume as well as enhanced power/efficiency performance parameters to fulfill military needs. System operating frequencies will extend from the ultra-high frequency (UHF) range up through the microwave and millimeter wave frequency regimes. The GaAs MESFET technology, which has evolved rapidly over the past several years, is approaching its perceived ultimate performance limits and is therefore unlikely to meet these advanced radar performance requirements. As a result, heterojunction device technologies are being developed in order to produce T/R modules with octave bandwidths, noise figures (NF) under 2 dB, output power of 20 W and power added efficiencies (PAE) greater than 30%. These improved radar system will offer improved power-aperture products, broader bandwidths, reduced prime power consumption, and enhanced reliability.

There is also a growing need for MBE-grown heterojunction devices to meet the performance requirements of current and future satellite communication systems, which are also moving to higher frequencies for increased bandwidth. For satellite communications, device performance, (i.e., noise figure, power added efficiency and reliability), is all-important, and cost is not as critical an issue. Systems are being developed requiring devices operating from X through V band. These systems require low noise devices

with less than 0.3 dB NF at X band, rising with frequency to less than 1 dB NF at V-band. Solid State Power Amplifiers (SSPAs) with 20 W and 40 % PAE at Ku band and 1 W and 30 % PAE at V-band are also needed. With the exploding market for data/voice/video communication, future satellites will also require on-board, high performance signal processing with 40 GBPS or greater capacity. Devices for satellite applications must also have a MTTF of greater than  $10^7$  hr. at operating temperature. These performance requirements are helping expand the envelope of performance for MBE grown heterojunction device technologies.

For both radar and satellite systems as well as EW applications, designers want to digitize the signal as close to the front end as possible. This is driving the development of a 100 GHz or greater IC technology for A/D converters, synthesizers, MUX/DEMUXs, DDSs, and PRNs. Requirements for A/D converters with 16 bits @ 100-200 MHz and up to 10-12 bits @ 10 GHz. are appearing for advanced radar and EW systems. Synthesizers and DDSs operating in the 5 GHz to 20 GHz frequency range are being designed for the next generation of satellite systems. These needs are encouraging the development of an MBE-grown heterojunction IC technology with  $f_T$  and  $f_{MAX}$  well above 100 GHz and a speed-power product in the range of 10 to 30 femtojoules.

For military systems, the emphasis has almost always been on the enhanced performance of MBE-grown heterojunction devices and ICs. Cost of production has always played a secondary role, if it has been considered at all. Today, performance at an affordable cost, utilizing a dual-use industrial base, governs both R&D investment and procurement. In the future, the cost-driven, commercial markets of automotive collision warning radar, personnel communication systems, and digital radios will determine the direction of device and IC R&D investment. Therefore, researchers developing MBE technology must be cognizant of the accelerating changes that are taking place in the marketplace. No longer is it possible to develop heterojunction devices and ICs based solely on improved performance (e.g., higher operating frequencies, lower noise figure, higher power output, higher power added efficiencies, wider bandwidths, and higher dynamic range). Now, cost-related issues (e.g., growth on larger area substrates, across-wafer uniformity, wafer-to-wafer reproducibility, and reduced cost per wafer growth) must be included in the development of MBE-grown heterojunction device and IC technologies for future system applications.

## **Commercial Business Development and Growth of MBE-based GaAs HBT Products and Services**

Robert M. Van Buskirk

TRW Electronics & Technology Division  
One Space Park D1/1302, Redondo Beach, CA 90278  
310.814.1978 fax 310.812.7011 bob.van.buskirk@trw.com

TRW has been actively developing a commercial GaAs business operation since 1991 featuring our MBE-based HBT and HEMT production processes. This business has grown from approximately \$50,000 in 1991 sales to over \$20,000,000 in projected sales for 1996. A vital part of this successful growth is attributed to our proprietary MBE technology and production capabilities.

Our MBE-based HBT and HEMT components meet critical market needs in the highly competitive wireless and wired telecommunications markets. These needs include:

- low cost: an imperative linked closely to uniformity/yield
- reliability: commercial markets/products require highly reliable, predictable device/component performance.
- uniformity/yield: key for both low cost and product development cycle times
- performance: competitive discriminator necessary to win and hold product design-ins

Specific commercial applications of our HBT and HEMT components and services are described including examples of end-use products and customers. In the wireless telecommunication arena TRW has recently announced a strategic alliance and series of investments in RF Micro Devices of North Carolina, a leading provider of RF ICs for the wireless market. Plans for the expansion of TRW's GaAs HBT manufacturing capacity at our Redondo Beach wafer fab and the transfer of our process to a RF Micro Devices wafer fab now under development are described. This strategic alliance features a unique capability to meet our customers needs for MBE-based GaAs HBTs that we call Cross-Linked Manufacturing®. TRW is also selling products and services in the wired telecommunication market and these specific applications are also described.

Our perspective on exploding, global commercial opportunities for HBT and HEMT components and services and the successful growth of our MBE-based business at TRW are outlined. Key market forces and the prospects for both wireless and wired markets are highlighted. A historical perspective of commercial GaAs at TRW as well as current status and future projections are provided. Concluding statements summarize and conceptualize future MBE-based commercial opportunities at TRW.



## Mass production of InAs Hall elements by MBE

Ichiro Shibasaki

Corporate Research & Development Administration (Fuji)

Asahi Chemical Industry Co., Ltd.

2-1 Samejima, Fuji-city, Shizuoka, 416, JAPAN

Recently there have been strong demands for Hall elements in the field of electronic equipments such as video cassette recorders(VCR), personal computers with floppy disk drives(FDD), and compact disk read-only memory(CD-ROM) drives and other electronic systems. Hall elements are mainly used for brushless motors in those equipments as magnetic sensors.

For these applications, we developed InSb thin film Hall elements having high sensitivity by vacuum deposition.<sup>1)</sup> Over 800 millions of this InSb Hall elements were produced and served commercially in 1995 which covers 70% of world market.

The only problem of the InSb Hall elements is operation temperature range restricted near room temperature. GaAs Hall elements having wide operation temperature range have been also produced. However, there are still strong demands for Hall element with high sensitivity and wide operation range from low to high temperature for recent application such as current sensors, car sensors, industrial sensors, and so on.

InAs has larger band gap energy than InSb and higher electron mobility than GaAs. Thus, InAs is one of the promising material for Hall element with both high sensitivity and wide operation temperature range as practical magnetic sensors.

A Si-doped InAs with 0.5  $\mu\text{m}$  thickness on GaAs substrate by MBE has high electron mobility of  $\sim 10,000\text{cm}^2/\text{V} \cdot \text{sec}$ . By using this InAs thin film, we developed InAs Hall elements having about 50% higher sensitivity than GaAs Hall element and wider operation temperature range than InSb Hall element.<sup>1,2)</sup>

For mass production of this InAs Hall elements, we designed a production MBE system with multi-wafers substrate holder having large growth area (eg. a substrate holder with twelve 2 inches wafers). After a rather long installation efforts, we found a standard production growth condition for Si-doped InAs thin films. High device yield was obtained for production of InAs Hall elements. The fabrication process of the InAs Hall element is shown in Fig.1. The electron mobility of Si-doped InAs by this production system are shown in Fig.2. The electron mobility of Si-doped InAs thin film and the InSb thin film is shown in Table 1. Their typical Hall output voltage at room temperature and temperature dependence are compared in Table 2 and Fig.3, respectively. The Si-doped InAs Hall elements has excellent properties compared to InSb Hall element such as wide range of operation temperature as seen from Fig.3,<sup>2,3)</sup> moreover, stability for pulse voltage noise, low offset drift, and low noise properties, all of which are effective for low magnetic field sensing in practical applications. In 1995, 2 millions of this InAs Hall elements have been applied to DC current sensors, brushless motors, and etc., as practical magnetic sensors.

However, simply grown InAs thin film on GaAs has not so high electron mobility observed in bulk InAs single crystal. To obtain more high electron mobility, InAs deep quantum well structure(InAs DQW) has been investigated using AlGaAsSb insulating layer lattice matched to InAs by MBE i.e., AlGaAsSb(35nm)/InAs(15nm)/AlGaAsSb(600nm)/GaAs.<sup>4,5)</sup> This InAs DQW has high electron mobility of 20,000-32,000  $\text{cm}^2/\text{V} \cdot \text{sec}$ . Hall output voltage of InAs DQW Hall element and its temperature dependence is shown in Table 2 and Figure 3, respectively. InAs DQW Hall element has both high sensitivity and excellent stability for wide range of temperature. This InAs DQW Hall element is hopeful as a future magnetic sensor.

Thin film technologies such as vacuum deposition and MBE are useful for production of InSb thin films, InAs thin films and InAs DQW and thus for mass production of Hall elements as practical magnetic sensors.

### References

- 1) I. Shibasaki, in: Technical Digest 8 Sensors Symp. 1989, p.211
- 2) I. Shibasaki, et.al., IEEE, in: Digest Tech. Papers on Transducers, 1991, p.1069.
- 3) T. Iwabuchi, et.al., J. Cryst. Growth, Vol. 150, 1995, p.1302.
- 4) K. Nagase, et.al. in: Digest Technical Papers; Late News, Transducers 1993, p.
- 5) N. Kuze, et.al., J. Cryst. Growth, Vol. 150, 1995, p.1307.

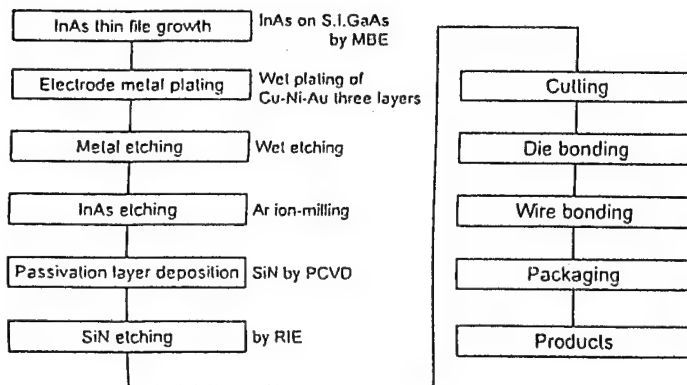


Fig.1, Fabrication process of the InAs Hall element

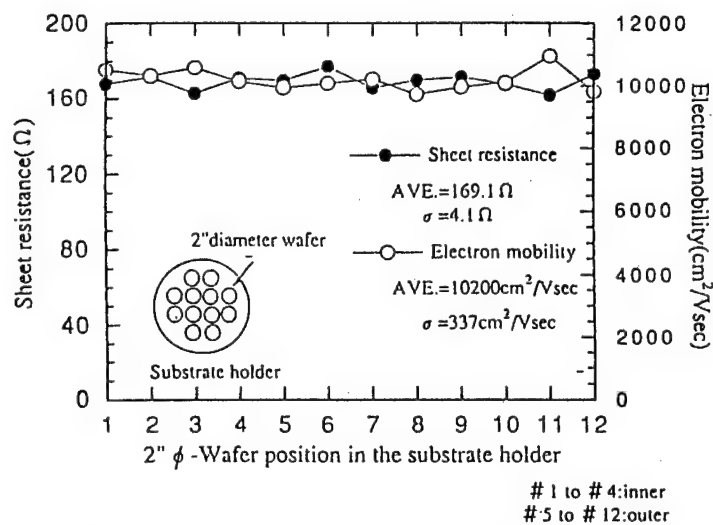


Fig.2, Uniformity of InAs thin film by production MBE

Table.1 Properties of InSb, InAs thin films and InAs DQW

	Dope	Electron mobility $\mu_H$ (cm²/Vsec)	Electron density $n$ ( $\times 10^{16}$ cm³)	Thickness $d$ (μm)
InSb	non	20000 ~ 30000	2	0.8
InAs	Si	11000	8	0.5
DQW	non	20000 ~ 32000	50	0.015

Table.2 Characteristics of InSb, InAs and InAs DQW Hall elements

	Driving voltage $V_{in}$ (V)	Hall output voltage $V_H$ (mV) ( $B=0.05T$ )	Offset voltage $V_o$ (mV) ( $B=0T$ )	Resistance $R_{in}$ (Ω)
InSb	1	150 ~ 320	$< \pm 7$	240 ~ 550
InAs	6	100	$< \pm 16$	400
DQW	6	250 ~ 300	$< \pm 16$	700

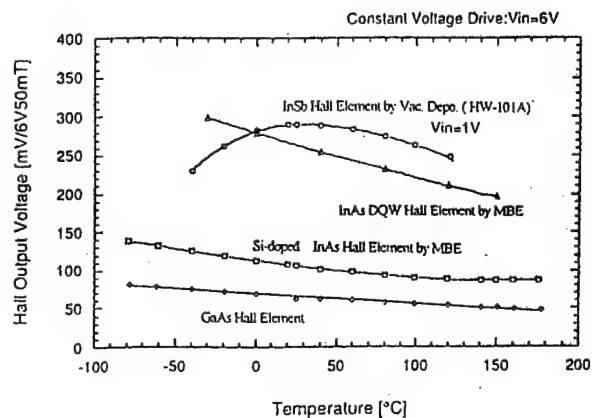


Fig.3, Temperature dependence of Hall output voltage

## Quantum Cascade Lasers Operating with High Powers at Room Temperature

*J. Faist*

Bell Laboratories, Lucent technologies  
700 Mountain ave, Murray Hill, NJ 07974  
Tel (908) 582 2336  
Fax (908) 582 7660

We have recently demonstrated room temperature operation of a quantum cascade (QC) laser based on a vertical transition with a modified design enhancing the injection efficiency and reducing the thermal backfilling at high temperatures<sup>2</sup>.

We show that, at the original operating wavelength ( $\lambda=5.2\mu\text{m}$ ), substitution of the AlInAs cladding by a molecular beam epitaxy grown InP cladding which exhibits a much lower thermal resistance significantly improve the performances. We also show that room temperature operation can also be obtained in devices operating at  $\lambda = 8.5\mu\text{m}$ .

Fig. 1 shows the optical power versus drive current from a single using f/0.8 optics and a calibrated, room temperature HgCdTe detector. Very good performances are obtained, with maximum peak output powers of about 200mW at 300K and 100mW at 320K.

The devices were also tested at room temperature in pulsed mode with a relatively large (3.3%) duty cycle. The pulse length was 50ns and the repetition rate 670kHz. The light was collected by a non-imaging energy concentrator and its average intensity measured by a broadband laser power meter. As shown on Fig. 2 the high peak powers observed translate into average powers in the 2-10mW range at and above room temperature. These devices also operated in continuous wave with a maximum operating temperature of  $T = 140\text{K}$ .

In Fig. 3, optical power versus drive current is reported for a device with an AlInAs cladding and a vertical transition design<sup>2</sup> operating at  $\lambda = 8.5\mu\text{m}$  (see inset). Peak optical power of 10 mW are obtained.

This is the first demonstration of high power, room-temperature operation of any semiconductor source in the mid-infrared (3.5-12 $\mu\text{m}$  wavelength).

1. J. Faist, F. Capasso, C. Sirtori, D. L. Sivco, A. L. Hutchinson, and A. Y. Cho, *Electron. Lett.* **32**, 560 (1996)
2. C. Sirtori, J. Faist, F. Capasso, D. L. Sivco, A.L. Hutchinson, and A. Y. Cho, *Appl. Phys. Lett.* **68**, 1745 (1996)

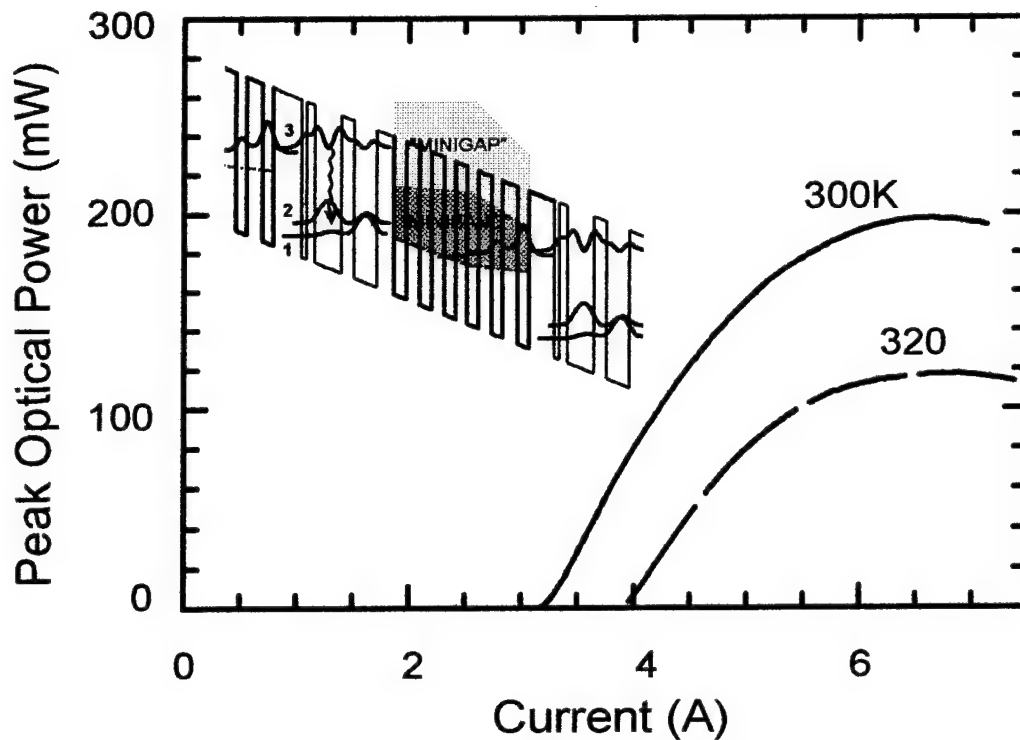


Fig. 1 Pulsed optical output power from a single facet versus injection current for heat sink temperatures of  $T = 300$  K and  $T = 320$  K. The device is 2.9 mm long and  $14 \mu\text{m}$  wide. Inset: Schematic conduction band diagram of a portion of the active region.

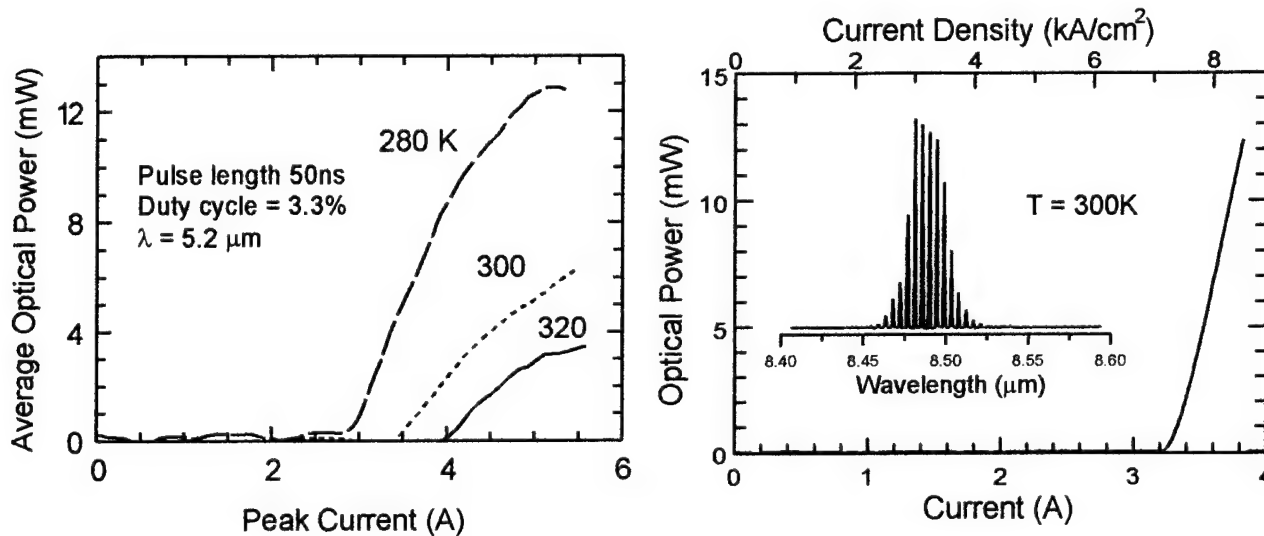


Fig. 2 Average power as a function of current for various temperatures. The pulse length is 50ns and the repetition rate is 670kHz.

Fig. 3 Pulsed optical output power from a single facet versus injection current at  $T = 300$  K for the device designed for long wavelengths operation. The device is 3.2 mm long and  $14 \mu\text{m}$  wide. Inset: optical spectrum showing the operation at  $8.5 \mu\text{m}$ .

## Progress and Prospects of Group III Nitride Semiconductors

Isamu Akasaki and H.Amano

Department of Electrical and Electronic Engineering, Meijo University,  
1-501 Shiogamuaguchi, Tempaku-ku, Nagoya 468, Japan

Group III nitrides with the exception of BN, that is wurtzite polytypes of AlN, GaN, InN and their alloy AlGaInN are one of the most promising materials for applications to short wavelength light emitters, such as light emitting diodes(LEDs) and laser diodes(LDs) in the green to ultraviolet(UV) regions.

To realize such devices, it is essential to grow high-quality epitaxial films and control their electrical conductivity. On the contrary to other III-V compounds such as GaAs and InP, however, it had been quite difficult to grow high-quality epitaxial nitride films with a flat surface free from cracks. This is mainly due to the lack of substrate materials with lattice constant and thermal expansion coefficient close to those of GaN and nitride alloys. Moreover, it has been well-known that undoped nitrides were of strong n-type conductivity, and p-type nitrides had never been realized. These problems had prevented from making the actual application of nitride devices for a long time.

Recent development of the technology and the understanding of growth mechanism in the heteroepitaxial growth of nitrides on highly-mismatched substrates(e.g. sapphire) have enabled us to grow high-quality GaN, AlGaIn, GaInN and their heterostructures. Conductivity control of both n-type and p-type nitrides has also been achieved. These achievements have led to the fabrication of high-brightness UV/blue, blue and bluish green LEDs with efficiencies in excess of 1%. UV stimulated emission from nitrides operating at RT by optical pumping has also been achieved. Recently, nitride-based LD operating at RT has been also realized.

To date, hexagonal nitrides, grown by MOVPE on sapphire substrate, have been mostly used in these devices.

In addition to hexagonal nitrides, cubic nitrides and so-called III-V nitrides which include GaNAs, GaNP, AlNSiC and other materials containing nitrogen as one of the major constituents have also attracted the



attention by many researchers.

On the other hand, various kinds of substrates, that is less-mismatched and/or electrically conductive substrates are being used for a variety of reasons.

Nowadays, nitride people are employing MOVPE as well as several kinds of growth methods such as MBE, HVPE etc. Selective area growth and several kinds of etching of nitrides are being studied for the fabrication of desirable device structures, such as the optical cavity and waveguide structures.

This paper reviews the recent progress of crystal growth, conductivity control and nitride-based short wavelength light emitters. Future prospects of group III nitride semiconductors will also be presented.

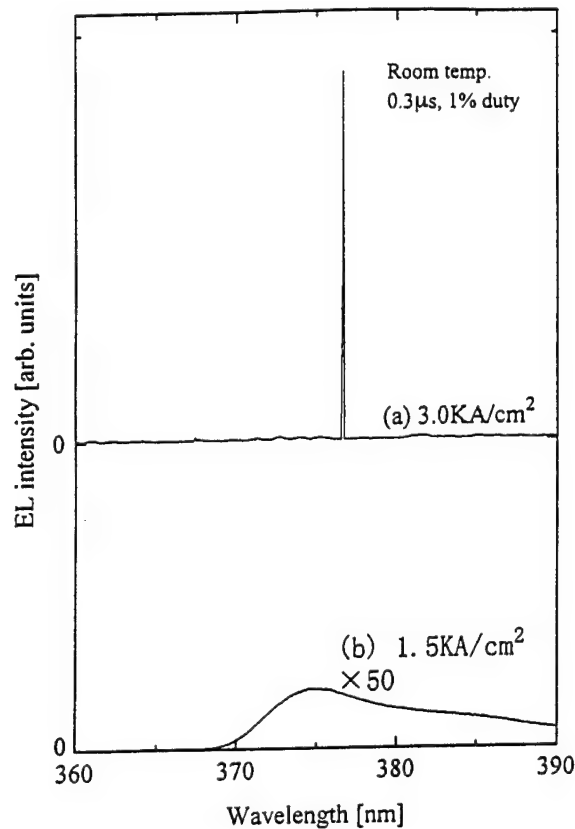


Fig.1 EL spectra from a diode with AlGaInN SCH structure at a forward current of 3KA/cm<sup>2</sup>(a) and 1.5KA/cm<sup>2</sup>(b) , respectively.

## 2. NITRIDES

MONDAY AFTERNOON (SMOTHERS)

Session Chair: Wen Wang, Columbia University

Co-Chair: April Brown, Georgia Institute of Technology

- 13:40 2.1 **Growth of GaN, InGaN, AlGaN films and quantum well structures by molecular beam epitaxy**  
M.A.L. Johnson, W.C. Hughes, W.H. Roland, J.W., Cook Jr., and J.F. Schetzina  
North Carolina State University, USA.
- 14:00 2.2 **Optimization of AlGaN films grown by rf atomic nitrogen plasma using in-situ cathodoluminescence**  
J.M. Van Hove, P.P. Chow, A.M. Wowchak, M.F. Rosamond, and D.R. Croswell,  
SVT Associates, USA.
- 14:20 2.3 **Erbium doping of Group III-nitrides during growth by metalorganic molecular beam epitaxy**  
J.D. MacKenzie, C.R. Abernathy, S.J. Pearton, R.N. Schwartz, R.G. Wilson, and J.M. Zavada, University of Florida, Gainesville, USA.
- 14:40 2.4 **Growth kinetics in GSMBE of GaN**  
K.R. Evans, C.R. Jones, and R. Kaspi  
Wright Laboratory, USA.
- 15:00 2.5 **Growth of high quality GaN on GaAs(111)B by molecular beam epitaxy**  
C.T. Foxon, T.S. Cheng, R.G. Boa, N.J. Jeffs, J.W. Orton, and D.E. Lacklison,  
University of Nottingham, England.
- Break
- 15:40 2.6 **N incorporation in  $\text{GaN}_x\text{P}_{1-x}$  and  $\text{InN}_x\text{P}_{1-x}$  grown by gas-source molecular beam epitaxy**  
W.G. Bi and C.W. Tu  
University of California, San Diego, USA.
- 16:00 2.7 **Gas source MBE growth of GaN rich side of  $\text{GaN}_{1-x}\text{P}_x$  using ion-removed ECR radical cell**  
K. Iwata, H. Asahi, K. Asami, and S. Gonda  
Osaka University, Japan.
- 16:20 2.8 **Stability of surface reconstructions for MBE grown GaN**  
H. Okumura, G. Feuillet, P. Hacke, and S. Yoshida  
Electrotechnical Laboratory, Ibaraki, Japan.
- 16:40 2.9 **Growth and doping of GaN/AlGaN heterostructure on c-plane sapphire and 6-H SiC by nitrogen plasma-assisted molecular beam epitaxy,**  
Myung C. Yoo, M.Y. Park, S.K. Kang and J.W. Lee  
Samsung Advanced Institute of Technology, Suwon, Korea

## **Growth of GaN, InGaN, and AlGaN Films and Quantum Well Structures by Molecular Beam Epitaxy**

M.A.L. Johnson, W.C. Hughes, W.H. Rowland, Jr., J.W. Cook, Jr., and J.F. Schetzina  
Department of Physics, North Carolina State University, Raleigh, NC 27695-8202

J. Zavada

US Army Research Office, Triangle Research Park, North Carolina 27709-2211

III-V nitrides are attracting significant attention because of the recent demonstrations of high-brightness blue/green LEDs and violet laser diodes. Two significant issues relating to the MBE growth of these materials has been (1) the determination of an optimum substrate for epitaxy and (2) the evaluation of the MBE process parameters for high quality nitride film growth. At North Carolina State University (NCSU), we have evaluated MBE growth of these materials by a two-fold approach: the homoepitaxial growth of nitride films and quantum well structures on MOVPE-grown GaN/SiC substrates and the heteroepitaxial nucleation and growth of nitride layers on alternative substrates such as sapphire and LiGaO<sub>2</sub>. In these MBE experiments, we have used an rf nitrogen plasma source for the generation of active nitrogen. Recently, by employing two nitrogen plasma sources, we have achieved GaN film growth rates of up to 0.8  $\mu\text{m/hr}$ . For quantum well structures emitting visible light, InGaN is essential as the active recombination layer material in double-heterostructure devices. The growth of high quality InGaN is complicated by thermodynamic limitations: InN is unstable and tends to dissociate at typical MBE growth temperatures of 600-800°C. Furthermore, the surface energies of InGaN are such that the indium tends to coalesce into metal droplets rather than migrate freely to lattice incorporation sites. The formation of indium droplets results in a low incorporation rate of indium in the growing film and a weak photoluminescence (PL) signal dominated by deep level emission. To overcome these difficulties, we have developed a modulated beam technique which employs alternating layers of (In,Ga)N and (Ga)N, analogous to the techniques used for the growth of InGaN by MOVPE. The intermittent deposition of a brief GaN layer stabilizes the indium containing layer before droplets can nucleate and results in high quality epitaxy. Factors which influence the InGaN composition include the metal flux ratios, substrate temperature, and the relative lengths of the beam modulation periods. RHEED analysis indicates a two dimensional growth surface during modulated beam deposition. InGaN quantum well structures (~26% In) based on this growth technique display a strong band-edge emission PL spectrum peaking at 408 nm. Recent results, including the growth at higher indium moles and optimized nucleation, will also be presented. AlGaN and GaN QW structures have been grown on LiGaO<sub>2</sub> substrates. LiGaO<sub>2</sub> has an ordered variant of the wurtzite structure with oxygen occupying the anion sites, and lithium and gallium alternating on cation sites. The (001) plane of the orthorhombic LiGaO<sub>2</sub> is a close lattice-match to the (0001) plane of GaN. In order to grow GaN by MBE, a thin buffer of AlN was first nucleated on the LiGaO<sub>2</sub> at low temperatures. The substrate temperature was then increased to ~800 °C for optimum MBE growth of GaN. GaN films up to 3.25  $\mu\text{m}$  thick were grown which exhibit x-ray diffraction rocking curves as narrow as 103 arcsec FWHM. Multiple quantum well structures of AlGaN/GaN exhibit strong 300K PL emission at 3.46 eV.

Work supported by grants from ARO and DARPA.

## **Optimization of AlGa<sub>N</sub> films grown by RF Atomic Nitrogen Plasma using In-situ Cathodoluminescence**

J.M. Van Hove\*, P.P. Chow, A.M. Wowchak, M.F. Rosamond and D. R. Croswell

SVT Associates, 7620 Executive Drive, Eden Prairie MN 55344

\*(612) 934-2100 ext. 225, Fax number (612) 934-2737, jvanhove@svta.com

The III-nitride material system has experienced a rapid growth in the past five years with the recent demonstration of a blue nitride based laser. MOCVD has been the chosen method of deposition of this material with Molecular Beam Epitaxy only recently producing comparable material quality. One inherent advantage of MBE is the ability to monitor the growth and composition in-situ using techniques such as reflection high energy electron diffraction and Auger spectroscopy. In this paper, we present information on the use of in-situ cathodoluminescence on GaN and AlGa<sub>N</sub> films deposited by MBE onto buffered sapphire substrates. Both the composition and optical quality of the films can be quickly determined using this method.

A cathodoluminescence system was added to the preparation chamber of the MBE system. Excitation of the films was done with a electron gun operating between 1 to 10 KeV and the emission monitored using a 3 nm resolution monochromator. Reactive nitrogen was produced using a RF plasma source optimized to produce atomic nitrogen based on plasma emission spectra. Growth rates of AlGa<sub>N</sub> and GaN films were between 0.5 to 1  $\mu\text{m/hr}$ . Growth was done on basal plane sapphire substrates with the substrate temperature varying between 750 and 900°C. A low temperature AlN buffer was used producing GaN films with FWHM x-ray diffraction (0002) peaks as low as 33 arc sec. Cathodoluminescence was done by removing the sample from the growth chamber and measuring the emission spectra of the film. The sample was then re-inserted, and growth conditions and composition varied.

Optimization of the growth process will be discussed using in-situ cathodoluminescence. Figure 1 shows the reduction of the "yellow" defect level present in GaN before and after changes to the growth temperature and III/N ratios. Figure 2 shows the emission of various AlGa<sub>N</sub> films whose composition and quality can be determined quickly from the peak position and width. These measurements are extremely useful in the nitride system where RHEED oscillations are not routinely observed. Data on the quality of GaN and AlGa<sub>N</sub> films deposited under various growth rates, III/N ratios, substrate temperatures and doping levels will be presented.

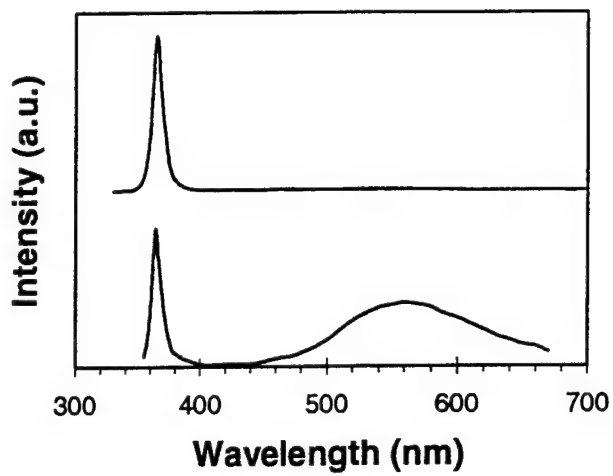


Figure 1. In-situ Cathodoluminescence spectrum from GaN taken after growth at two different growth conditions. The reduction of the yellow defect emission demonstrates in-situ Cathodoluminescence usefulness for nitride growth.

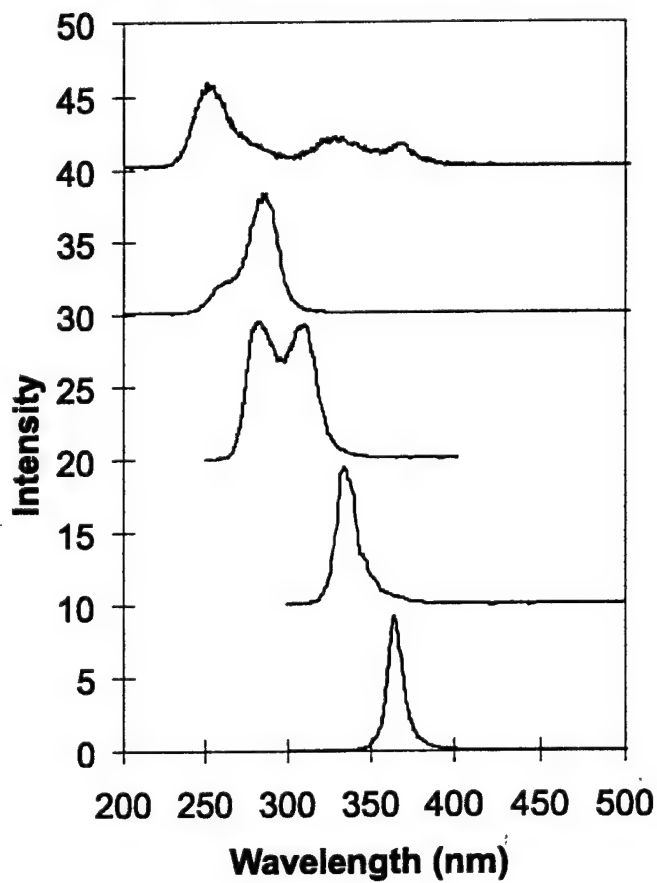


Figure 2. In-situ Cathodoluminescence spectrum from several different Al content AlGaN films.



## **Erbium Doping of Group III-Nitrides During Growth by Metalorganic Molecular Beam Epitaxy**

J. D. MacKenzie,\* C. R. Abernathy, and S. J. Pearton  
Department of Materials Science and Engineering  
University of Florida, Gainesville, FL 32611

R. N. Schwartz and R. G. Wilson  
Hughes Research Laboratories  
Malibu, CA 90265

J. M. Zavada  
US Army Research Laboratory  
RTP, NC 27709

Optical communications systems based on the 1.54  $\mu\text{m}$  emission of  $\text{Er}^{3+}$  exploit the intrinsic attenuation loss minima of silica fibers to achieve efficient, temperature-stable long-distance signal transmission. Optoelectronic components based on Er doping of Si and III-V materials have been sought to replace the extensive pumping systems required in conventional Er doped fiber amplifier systems. Recent developments in Group III-nitride growth have focused on developing blue/UV emitters and high temperature electronics. However, the wide band gap, environmental insensitivity and the ionic character of the III-nitrides also make them an attractive medium for Er-based devices with superior temperature stability, high thermal quenching temperature and high emission efficiency. To evaluate this potential, the growth and properties of Er-doped III-N films grown by ECR plasma-assisted metalorganic molecular beam epitaxy (ECR-MOMBE) with a solid Er source have been studied.

For the first time, strong 1.54  $\mu\text{m}$  room temperature photoluminescence (PL) from  $\text{AlN}:\text{Er}$  doped during growth has been demonstrated (Figure 4). Secondary ion mass spectrometry (SIMS), PL, and high resolution x-ray diffraction (HRXRD) results will be presented as a function of growth parameters and comparisons will be made with implanted material. Figures 1 and 2 show representative SIMS profiles of  $\text{AlN}:\text{Er}$  and  $\text{InAlN}$  implanted with Er. The effects of Er incorporation on surface morphology, as determined by scanning electron microscopy (SEM), will be shown. Solubility, segregation during growth and diffusion upon post-growth annealing will be addressed. Also, incorporation and activation of Er in other III-nitrides, ternaries, and device structures (Fig. 3 shows a micrograph of an  $\text{AlN}$ -based microdisk structure) will be discussed.

\*Rhines Hall  
University of Florida  
Gainesville, FL 32611

phone: (904) 846-1091  
fax: (904) 846-1182  
email: jdmacken@silica.mse.ufl.edu

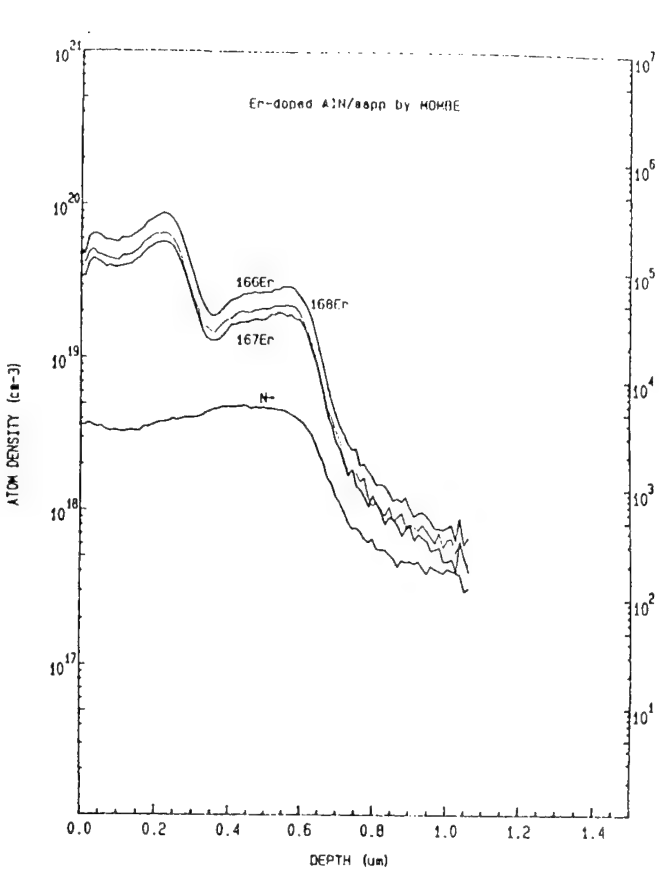


FIG. 1

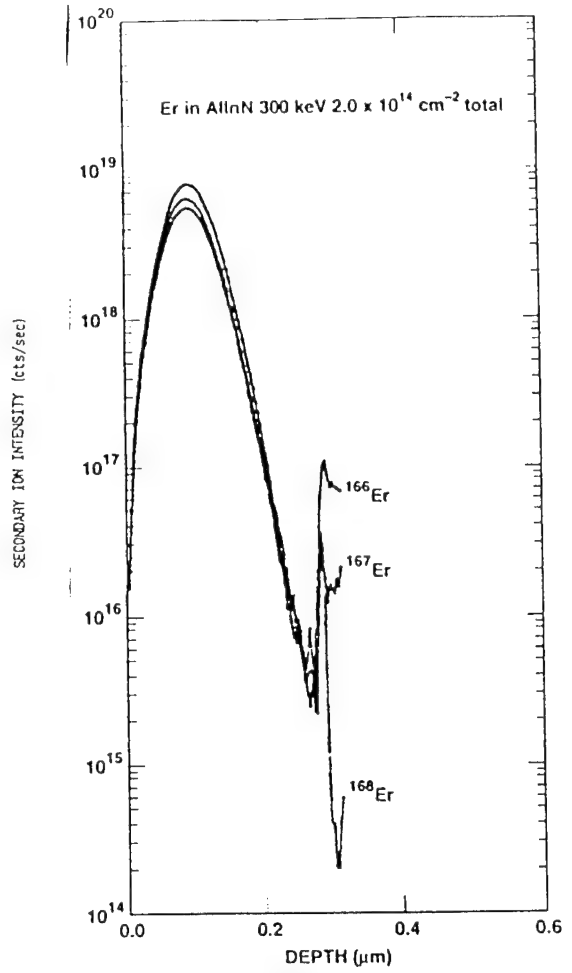


FIG. 2

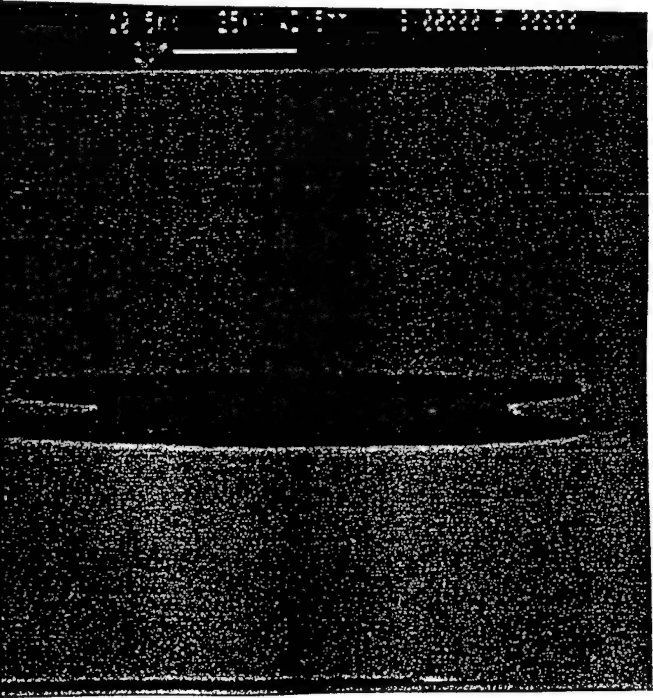


FIG. 3

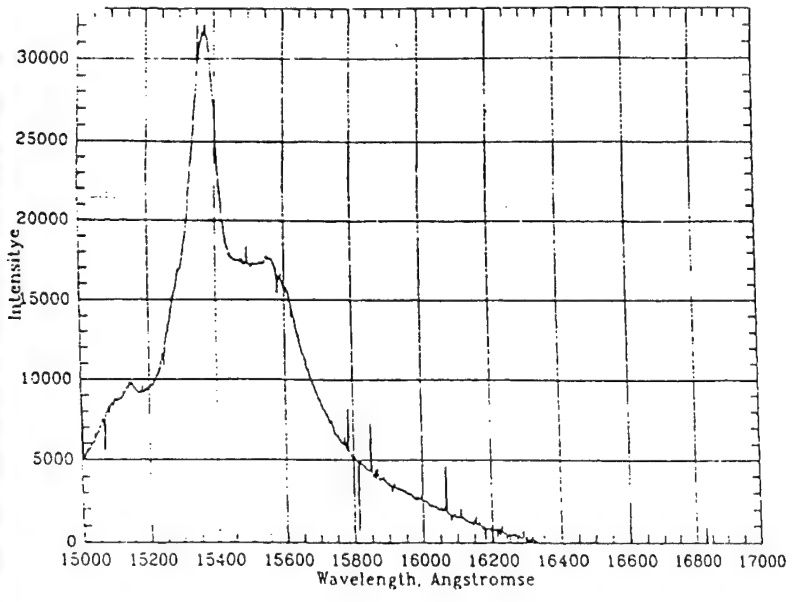


FIG. 4.

# Growth Kinetics in GSMBE of GaN

K. R. Evans<sup>1</sup>, C. R. Jones<sup>2</sup>, and R. Kaspi<sup>2</sup>

<sup>1</sup>Wright Laboratory (WL/ELDM), Wright-Patterson Air Force Base, Ohio 45433-7323

<sup>2</sup>University Research Center, Wright State University, Dayton, Ohio 45435

Recent advances in semiconductor device technology based on III-arsenides is due in part to important early fundamental studies of III-arsenide epitaxial growth. In contrast, development of III-nitride device technology has been hampered in part due to the lack of such fundamental studies. Present issues of concern in III-nitride growth include those associated with 1) low growth rates, 2) high intrinsic point defect generation rates, 3) the role of hydrogen (if present) during growth, and 4) the lack of available substrates. Progress in each of these issues would benefit from fundamental studies of the epitaxial growth process.

We report our most recent results on, and our current understanding of, the kinetics of gallium and nitrogen incorporation during gas source molecular beam epitaxy (GSMBE) of GaN using a Ga effusion cell and a  $\text{NH}_3$  cracker<sup>1</sup> for sources. Results are reported for varying Ga flux,  $\text{NH}_3$  flux,  $\text{NH}_3$  cracker current, and substrate temperature. Desorption mass spectrometry (DMS) is used to measure Ga desorption during growth; temperature-programmed desorption (TPD) analysis performed immediately after growth interruption is employed to quantify the population of surface accumulated Ga; and GaN formation rates are determined by subtracting surface accumulation rates and desorption rates from the incident Ga flux.

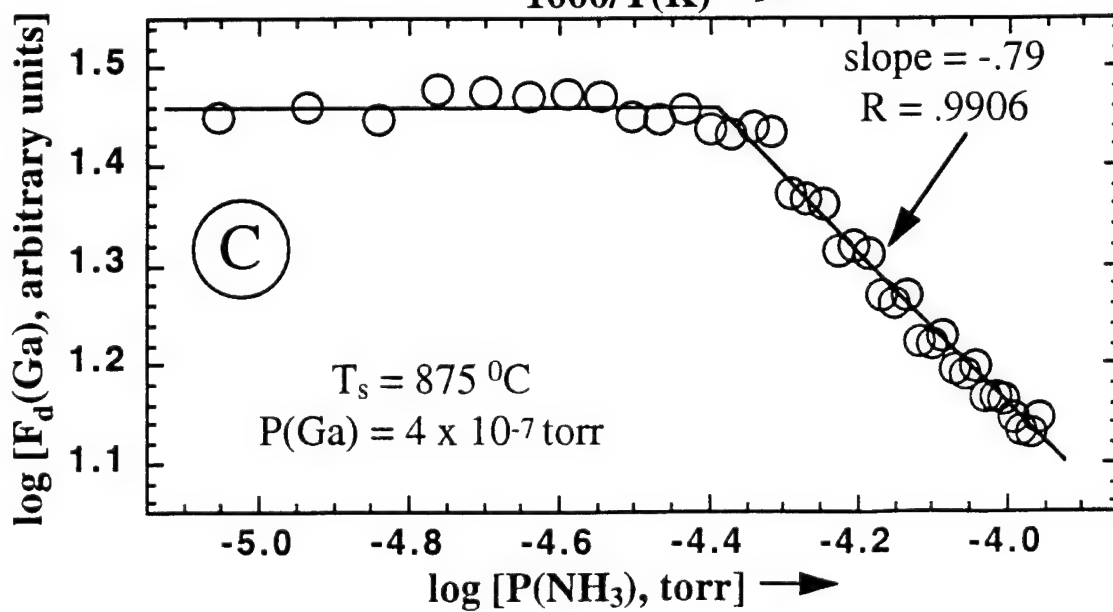
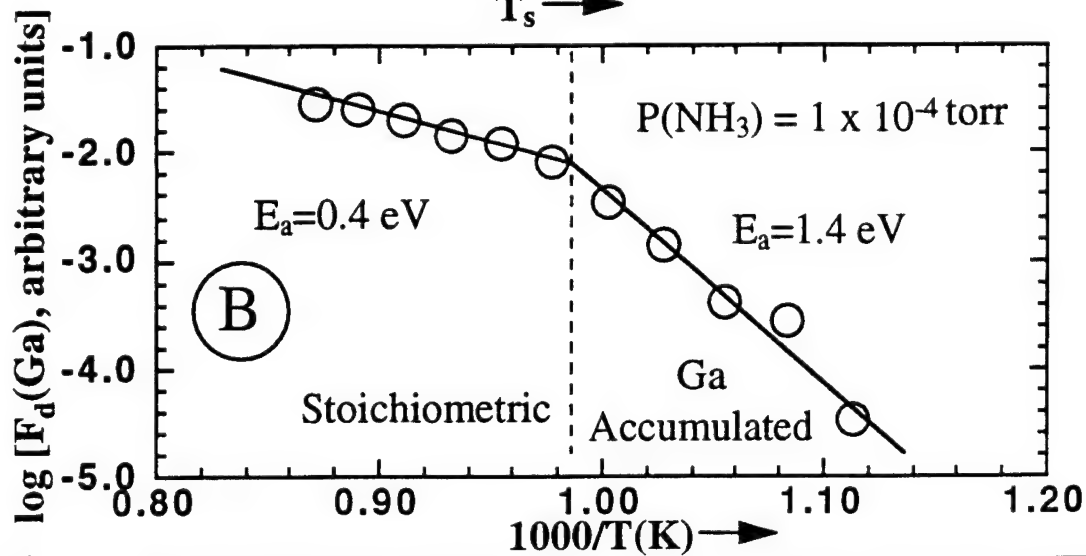
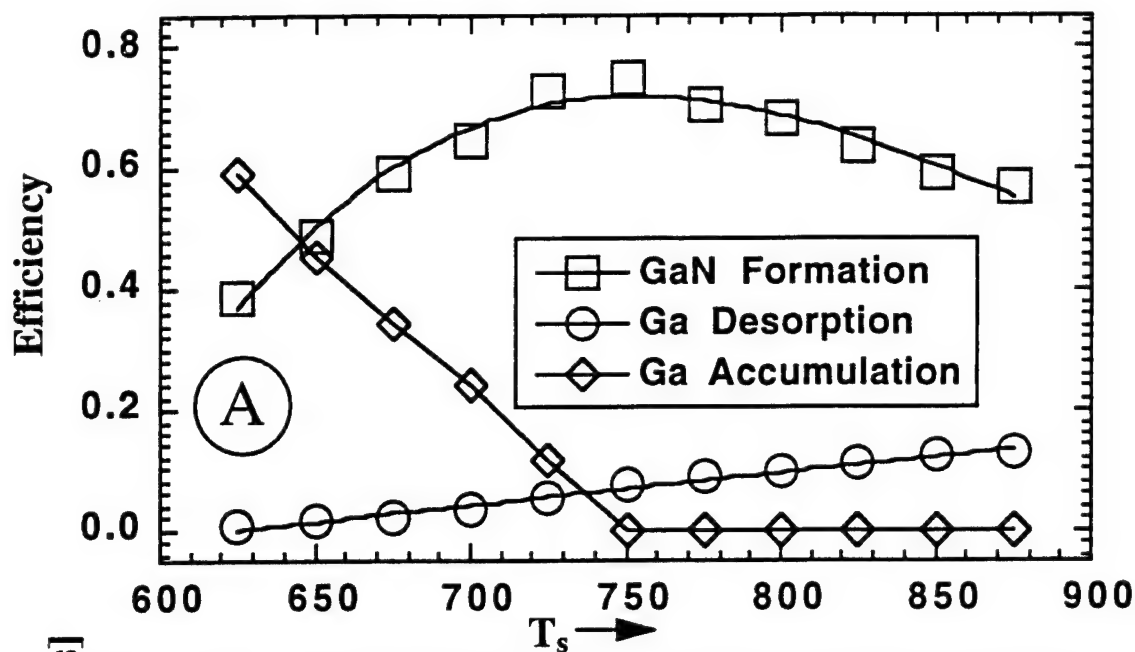
For uncracked  $\text{NH}_3$ , high substrate temperatures are found to give rise to significant Ga desorption, the rate of which decreases with increasing  $\text{NH}_3$  flux. Low substrate temperatures give rise to significant Ga surface accumulation, the rate of which decreases with increasing  $\text{NH}_3$  flux. The GaN formation rate increases with  $\text{NH}_3$  flux and peaks at an intermediate temperature, as shown in Figure A. The temperature dependence of the Ga desorption rate obeys Arrhenius behavior, with two different associated activation energies  $E_a$ , depending on whether or not Ga surface accumulation occurs. When Ga surface accumulation is significant,  $E_a=1.4$  eV, while  $E_a=0.4$  eV when the Ga surface accumulation rate is negligible. Both values of  $E_a$  are relatively small and are highly suggestive of the presence of a hydrogen-terminated surface which serves as the Ga desorption precursor site. The relatively high growth rates observed, coupled with the likelihood that hydrogen has an important role at the surface, are consistent with a recent study<sup>2</sup> of GaN growth using an  $\text{N}_2$  RF plasma as the nitrogen source, which found that the presence of an atomic H beam resulted in approximately a doubling of the GaN growth rate.

The effect of cracker current ( $I_c$ ), which controls the cracking region temperature, on the Ga incorporation rate was studied. At a substrate temperature of 800 °C, the highest  $I_c$  levels investigated gave rise to a dramatic decrease in the GaN formation rate, due to a corresponding increase in the Ga desorption rate. Results of chamber pressure measurements as a function of cracker current suggest that nearly complete conversion of  $\text{NH}_3$  into  $\text{N}_2$  and  $\text{H}_2$  occurs at the highest  $I_c$  levels investigated, and partial cracking of  $\text{NH}_3$  occurs at intermediate  $I_c$  levels. It was hoped that partially cracking of  $\text{NH}_3$  would produce highly reactive  $\text{NH}$  and  $\text{NH}_2$ , which would enhance the Ga incorporation rate (and possibly reduce the nitrogen vacancy generation rate). However, no enhancement in the Ga incorporation rate was observed for any cracker current, relative to the completely uncracked case, under the conditions investigated.

**Acknowledgments:** The authors thank C. Huang, L. Kyle, and C. Litton for technical support. Authors RK and CRJ were supported by US Air Force Contract # F33615-95-C-1765. This work was partially supported by the US Air Force Office of Scientific Research (AFOSR).

<sup>1</sup>Supplied by EPI MBE Products Group, Saint Paul, MN, USA.

<sup>2</sup>T. Myers, et al., to be published.



# Growth of High Quality GaN on GaAs(111)B by Molecular Beam Epitaxy

C.T. Foxon, T.S. Cheng, R.G. Boa, N.J. Jeffs, J.W. Orton, D.E. Lacklison

*Department of Physics, University of Nottingham, Nottingham NG7 2RD, England*

*Tel: +44-115-9515138 Fax: +44-115-9515184*

*e-mail: ppzctf@ppn1.nott.ac.uk*

Growth of the III-nitride materials system has been increasingly studied due to its use in devices operating in the visible/uv part of the electromagnetic spectrum. Since GaN grows naturally in a wurtzite form and GaAs(111) has a hexagonal symmetry, this provides a good template onto which we can deposit the wurtzite GaN. In addition, we have previously shown that the growth of GaN on (111)B is superior to that grown on (111)A and/or (100)GaAs<sup>1</sup>.

We have studied the growth of GaN grown on GaAs(111)B as a function of different growth temperatures, V/III ratios and the effect of substrate nitridation. The active nitrogen used in the growth is supplied by an RF activated plasma source which generates predominantly atomic species. We show that high quality, stoichiometric materials can be obtained by using the appropriate growth conditions. In-situ RHEED and ex-situ low temperature PL and X-ray diffraction techniques are used to characterize the epitaxial films.

Since controllable n- and p-type doping in GaN are required for producing useful device structures, we will also report on the respective doping in GaN using Si and Mg/C.

<sup>1</sup> To be presented at The first European GaN Workshop (EGW-1), Rigi, Switzerland, 2-4 June, 1996

# N Incorporation in $\text{GaN}_x\text{P}_{1-x}$ and $\text{InN}_x\text{P}_{1-x}$ Grown by Gas-Source Molecular Beam Epitaxy

W. G. Bi and C. W. Tu

Department of Electrical and Computer Engineering

University of California, San Diego, La Jolla, CA 92093-0407

E-mail: wbi@sdcc3.ucsd.edu, Fax: (619)534-2486, Phone: (619)534-3014

Recently much attention has been paid to N incorporation in GaP and GaAs because of potential applications in optoelectronic devices on Si. Due to the large miscibility gap, however, the N composition is limited. N incorporation in InP, an important member of the III-V family, and its properties have not been investigated.

In this talk we will present a study of the N incorporation behavior into GaP and InP as a function of growth conditions, and show that N composition well above the predicted value can be incorporated. The N composition was determined from X-ray (511) asymmetric reflections to account for strain-induced lattice constant change of the  $\text{InN}_x\text{P}_{1-x}$  and  $\text{GaN}_x\text{P}_{1-x}$  films. As in other mixed group-V compounds (e.g.,  $\text{GaAs}_x\text{P}_{1-x}$  and  $\text{InAs}_x\text{P}_{1-x}$ <sup>1</sup>), the N composition in  $\text{GaN}_x\text{P}_{1-x}$  and  $\text{InN}_x\text{P}_{1-x}$  is smaller than in the gas phase, but the overall behavior is somewhat different. With increasing the  $\text{N}_2$  flow-rate fraction ( $\text{N}_2$  flow rate over total group-V gas flow rate), the N composition increases up to a point and then levels off, while for  $\text{GaAs}_x\text{P}_{1-x}$ <sup>1</sup>, no saturation was observed. This might be due to the small solubility of N in these materials or the leveling off of the active N species at higher  $\text{N}_2$  flow rate. At a fixed  $\text{N}_2$  flow-rate fraction, the higher the growth temperature  $T_s$ , the less the N can be incorporated; e.g., with a  $\text{N}_2$  flow-rate fraction being fixed at  $\sim 0.37$ , the N concentration in  $\text{InN}_x\text{P}_{1-x}$  is decreased from 0.93% to 0.44% as  $T_s$  is increased from 310 °C to 420 °C, and that in  $\text{GaN}_x\text{P}_{1-x}$  is decreased from 16% to 4.5% as  $T_s$  is increased from 500 to 600 °C. This decreasing N incorporation with increasing growth temperature might be due to the lowering of the sticking coefficient of nitrogen at higher  $T_s$ . Similar behavior was also observed in  $\text{GaN}_x\text{As}_{1-x}$ <sup>2</sup>. Although the general trend of the growth condition dependence is the same for N incorporation in InP and GaP, the amount of N can be incorporated is quite different. With GaP, as high as 16% N can be obtained, while with InP, only less than 1% can be incorporated. This is due to the very high vapor pressure of  $\text{N}_2$  over InN.

Optical properties of  $\text{InN}_x\text{P}_{1-x}$  and  $\text{GaN}_x\text{P}_{1-x}$  films were studied by optical absorption measurement. For  $\text{InN}_x\text{P}_{1-x}$ , the absorption coefficient obeys a square law, indicating the optical absorption is from a direct-bandgap material, while for  $\text{GaN}_x\text{P}_{1-x}$ , a square-root law holds, indicating indirect bandgap nature of the material. As the N composition is increased, the band-edges of both materials shift to longer wavelength, revealing a large bowing of the bandgap energy.

<sup>1</sup>H. Q. Hou and C. W. Tu, J. Electron. Mat. 21, 137 (1992).

<sup>2</sup>M. Weyers and M. Sato, Appl. Phys. Lett

## Gas source MBE growth of GaN rich side of $\text{GaN}_{1-x}\text{P}_x$ using ion-removed ECR radical cell

K. Iwata, H. Asahi, K. Asami and S. Gonda

The Institute of Scientific and Industrial Research, Osaka University,  
8-1, Mihogaoka, Ibaraki, Osaka 567, Japan.

Tel:+81-6-879-8406;Fax:+91-6-879-8509;e-mail:iwata21@sanken.osaka-u.ac.jp

Recently, it was proved that wide-band gap III-V nitrides are suitable to fabricate blue-green light emitting diodes, and the pulsed operation of violet laser diodes was demonstrated [1]. This material system can also cover wide wavelengths from ultra-violet to longer than  $2\mu\text{m}$  by adding As or P. Several authors reported the growth of GaAs or GaP-rich side of GaAsN or GaPN. In this paper, we report the gas source MBE growth of GaN rich side of GaNP and their band gap variation with P composition, for the first time.

GaN-rich side of GaNP layers were grown on sapphire substrates after the high temperature growth of GaN buffer layers (thickness :  $0.3\mu\text{m}$ ) by using ion removed ECR (electron cyclotron resonance) radical cell for nitrogen source. Advantage of the use of ion-removed cell was demonstrated by the observation of x2 RHEED patterns during growth of GaN [2,3]. The ion removal efficiency by ion removal magnets in this ECR radical cell was over 99%. Elemental Ga, radical  $\text{N}_2$  and thermally cracked  $\text{PH}_3$  were used as group III and group V sources. The flow rate of  $\text{N}_2$  was 1.5 SCCM. The  $\text{PH}_3$  flow rate was varied from 0.1 to 1.0 SCCM. The substrate temperature was  $750^\circ\text{C}$ .

We have succeeded to grow GaN rich side of GaNP. However, in the growth with high  $\text{PH}_3$  flow rate of 1.0 SCCM, the phase separation into GaN rich GaNP and GaP (or GaP rich GaPN) was observed, as shown in Fig.1 (X-ray diffraction (XRD) rocking curve). The growth of GaNP was confirmed by the XRD curve around GaN (0002) angle (Fig.2). Two peaks are observed: one comes from high temperature grown GaN buffer layer and the other from GaNP alloy layer (P composition=1.5%). The full width at half maximum (FWHM) of GaNP (0002) peak was only 237.6 arc sec, which was comparable to that of GaN (0002). This phase separation was also observed in the RHEED pattern during GaNP growth (Fig.3). In addition to the streak patterns from GaNP, the spotty patterns from phase separated GaP (or GaP rich GaPN) was observed.

77K photoluminescence (PL) emissions were observed from  $\text{GaN}_{1-x}\text{P}_x$  layers, where  $x=0, 0.0026, 0.0077$  (Fig.4). The red shift of near band edge emission was observed. The relation between the band gap energy and P composition  $x$  of  $\text{GaN}_{1-x}\text{P}_x$  agrees with the theoretical calculation by Miyoshi et al [4] rather than those by Baillargeon et al [5] and Sakai et al [6] suggesting the existence of bowing bandgap, but no existence of semimetallic region.

In the conference, we also report the growth temperature dependence of GaNP growth characteristics.

- [1] S.Nakamura, M.Senoh, S.Nagahama, N.Iwasa, T.Yamada, T.Matsushita, H.Kiyoku and Y.Sugimoto : Jpn.J.Appl.Phys. 35 (1996) pp.L74-L76.
- [2] K.Iwata, H.Asahi, S.J.Yu, K.Asami, H.Fujita, M.Fushida and S.Gonda : Jpn.J.Appl.Phys. 35 (1996) pp.L289-L292.
- [3] K.Iwata, H.Asahi, S.J.Yu, M.Fushida, K.Asami and S.Gonda : TWN'95 (1995) H-1.
- [4] S.Miyoshi and K.Onabe : TWN'95 (1995) P-1.
- [5] J.N.Baillargeon, K.Y.Cheng, G.E.Hofler, P.J. Pearah, and K.C. Hsieh : Appl.Phys.Lett. 60 (1992) 2540.
- [6] S.Sakai, Y.Ueta and Y.Terauchi : Jpn.J.Appl.Phys. 32 (1993) 4413.



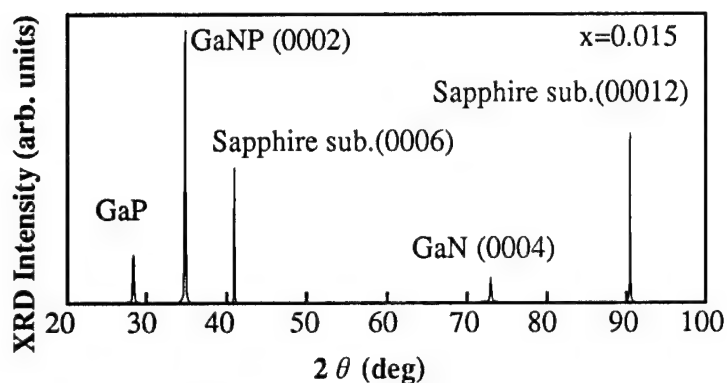


Fig.1 XRD rocking curve from GaN-rich side of  $\text{GaN}_{1-x}\text{P}_x$  on sapphire substrate.

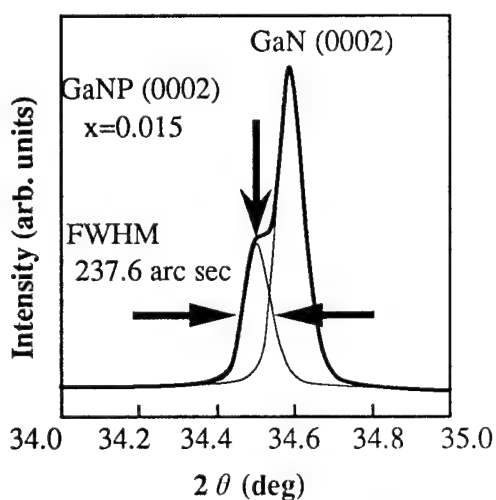


Fig.2 XRD rocking curve around angle of GaN-rich side of  $\text{GaN}_{1-x}\text{P}_x$ .

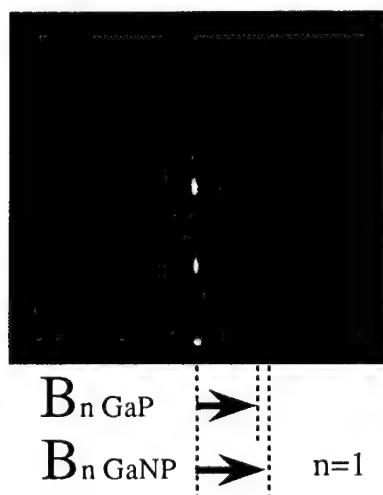


Fig.3 RHEED pattern during GaNP growth.

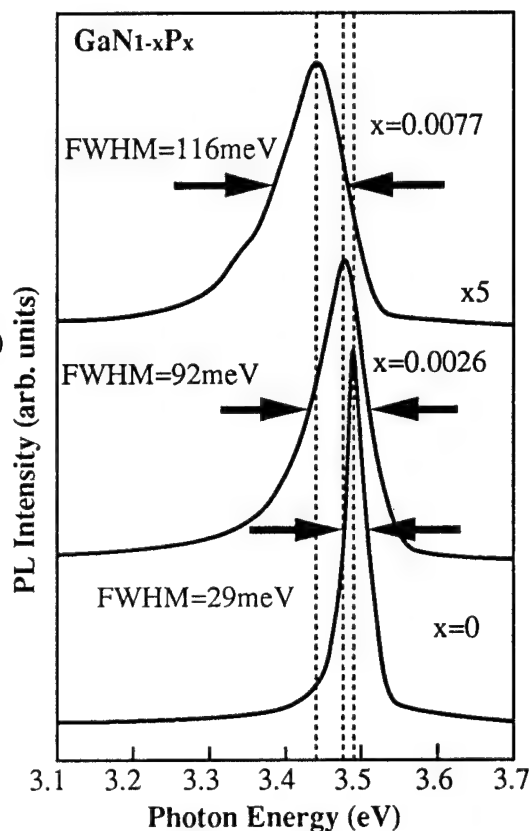


Fig.4 77K photoluminescence spectra for  $\text{GaN}_{1-x}\text{P}_x$

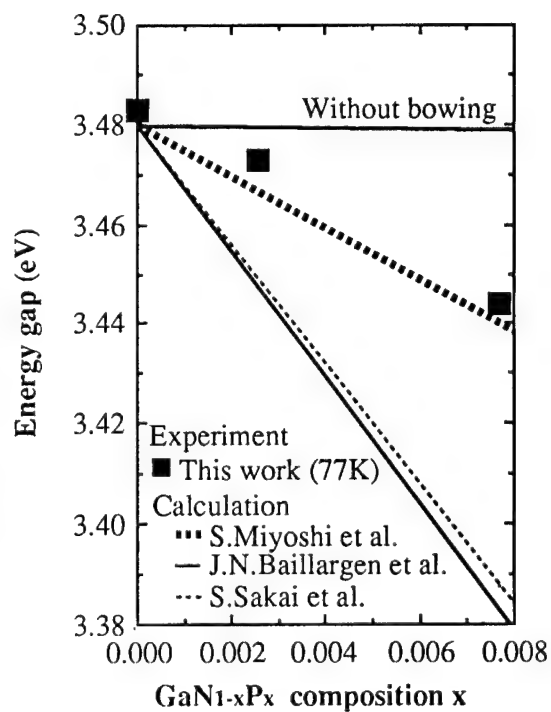


Fig.5  $\text{GaN}_{1-x}\text{P}_x$  :  $E_g$  vs composition

## Stability of surface reconstructions for MBE grown GaN

H.Okumura, G.Feuillet, P.Hacke, S.Yoshida  
Electrotechnical Laboratory  
1-1-4 Umezono, Tsukuba, Ibaraki 305, Japan

It is the purpose of this paper to investigate the stability of surface reconstructions for GaN as a function of the different growth parameters ; conversely, it will be shown how these reconstructions can be used as a very efficient tool to scale the growth parameters and to gain a better insight into the physics of growth itself.

When grown under optimised conditions, MBE grown cubic and hexagonal GaN layers evidence surface reconstructions as seen by RHEED. In the case reported here where hexagonal GaN is grown by MBE on homoepitaxial GaN layers deposited by MOCVD on (0001) sapphire, these reconstructions are of the  $\times 2$  type on all crystallographic azimuths in the c plane (Fig. 1).

Once stabilized, the  $\times 2$  reconstructions disappear if the Ga flux is too high or the substrate temperature too low. The transition is totally reversible and path independant if the parameters are varied slowly enough to achieve quasi equilibrium conditions. The appearance - disappearance of the  $\times 2$  RHEED pattern can be followed as a function of the different growth parameters. Represented in Fig.2 are these transition points in a Ga flux vs substrate temperature graph, for a set of different nitrogen flow rates. The experimental curves appear to be exponential in nature with a y axis offset we found to depend linearly on the  $N_2$  flow rate.

The exponential shape strongly suggests a thermally activated process which can be attributed to Ga reevaporation from the growing surface. These observations are accounted for in a model whereby the conditions for appearance/disappearance of these  $\times 2$  reconstructions are related to a given Ga to active nitrogen flux stoichiometry :  $\Phi(Ga) = \alpha \Phi(N)$ . Because of Ga reevaporation from the surface, this can be written:

$$\Phi(Ga)_{\text{incident}} - A \exp(-E_a/kT) = \alpha \Phi(N),$$

where the first term is the incident Ga flux, the second term describing Ga reevaporation from the surface with  $E_a$  its activation energy. Very good fits are obtained this way (Fig.2). Interestingly no N desorption has to be taken into account to explain the experimental results.

Based on this approach, one can first deduce the Ga sticking coefficient as a function of substrate temperature, hence the growth rate itself. The activation energy for Ga reevaporation  $E_a$  is found to be  $3.3\text{eV} \pm 0.4\text{eV}$ ; the sample thicknesses as measured when the samples are grown in the  $\times 2$  regime agree well with this evaluation. This indicates further that, when  $\times 2$  reconstructions are observed, the growth rate is Ga limited, growth being carried out in N-rich conditions. The other implication of these observations and model is that the y-axis offset of these transition curves is directly proportional to the active nitrogen species which can be followed as a function of ECR power, nitrogen flow rate and system pressure.

In conclusion, the surface reconstructions that we have observed are not only the signature of equilibrium growth fronts for MBE grown GaN; the study of their stability domain can also be used to scale growth parameters and as an efficient feedback to control and optimise growth conditions.

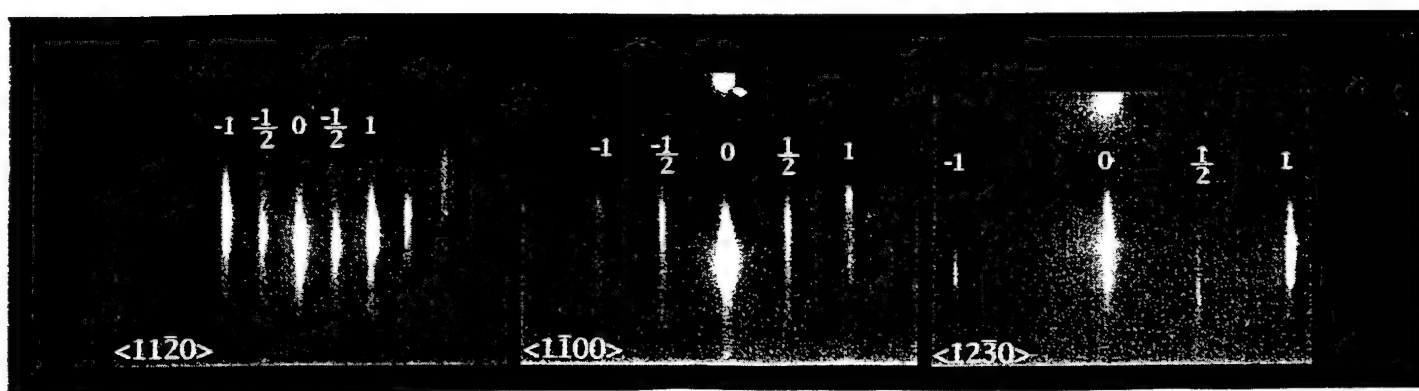


Fig. 1. RHEED patterns of the (0001) GaN surface growing in a  $\times 2$  reconstruction-stabilized mode. Reconstructions are clearly observable on the  $\langle 11\bar{2}0 \rangle$ ,  $\langle 1\bar{1}00 \rangle$ , and  $\langle 12\bar{3}0 \rangle$  zone axes.

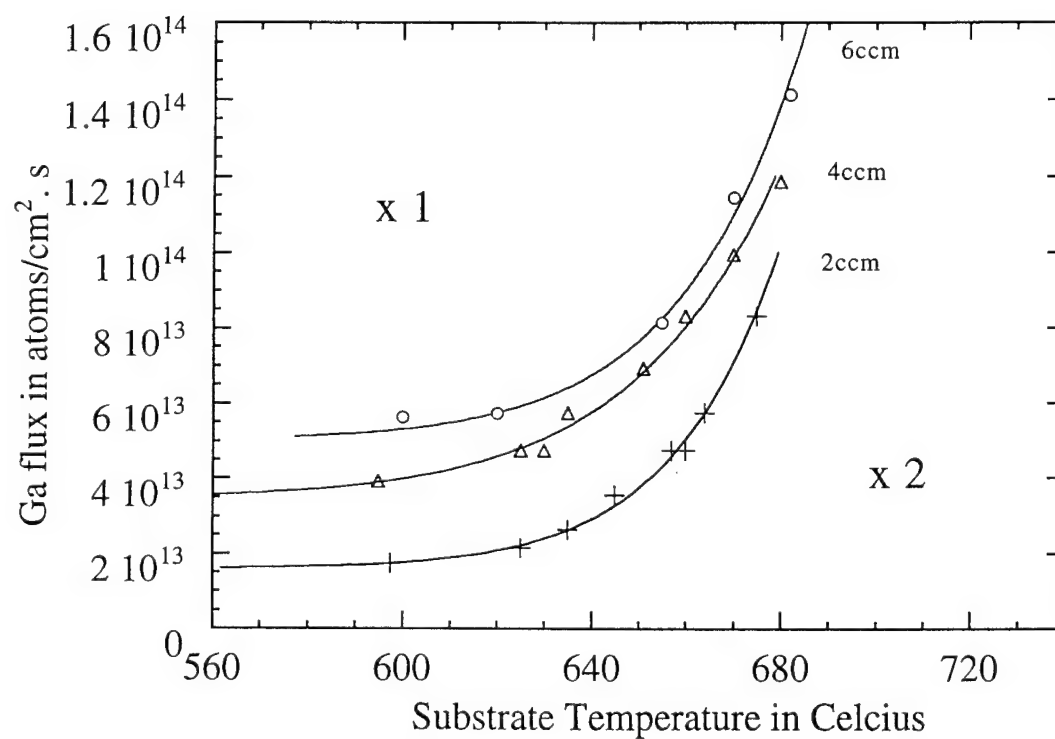


Fig.2. Stability domain for the  $\times 2$  reconstruction for different  $N_2$  flow rates.

# **Growth and Doping of GaN/AlGa<sub>N</sub> Hetrostructure on c-Plane Sapphire and 6-H SiC by Nitrogen Plasma-Assisted Molecular Beam Epitaxy**

Myung C. Yoo\*, M.Y. Park, S.K. Kang, and J.W. Lee  
Photonics Semiconductor Laboratory  
Samsung Advanced Institute of Technology, Suwon, Korea

## **ABSTRACT**

High quality GaN/AlGa<sub>N</sub> heterostructure has been grown on c-plane sapphire and 6-H SiC substrates by using nitrogen plasma-assisted MBE. The growth system is consisted of inductively coupled rf nitrogen plasma source, III-family solid sources and Mg and Si dopant sources. Without deteriorating epi-quality, 0.5  $\mu\text{m}/\text{hour}$  growth rate was achieved by using high capacity turbomolecular pump and high efficiency  $\text{N}_2$  plasma source. Prior to GaN/AlGa<sub>N</sub> growth, 50nm-thick AlN buffer layer was grown on sapphire and SiC substrates at 600 °C. The RHEED pattern of buffer layer shows very streaky (2x2) pattern, while GaN and AlGa<sub>N</sub> films exhibit (4x4) patterns indicating the grown epilayers are crystallographically very smooth and flat throughout the epitaxial growth. The FWHM of x-ray locking curve is as low as 39 arcsec for 1  $\mu\text{m}$ -thick GaN and 80 arcsec for 0.2  $\mu\text{m}$ -thick AlGa<sub>N</sub> films. In-growth doping was sucessfully performed using Mg and Si as a p-type and a n-type dopant in the stream of nitrogen plasma, respectively. Results from the vander Pauw Hall measurement indicate that p-type doping concentration is  $1.2 \times 10^{19}/\text{cm}^3$  and that of n-type is  $2.0 \times 10^{20}/\text{cm}^3$ . Room temperature photoluminescence spectra of GaN epilayer is peaked at 3.42eV and no discernible yellow luminescence resulted from ion damages is observed.

\* person to be contacted

Dr. Myung Cheol Yoo  
Photonics Semiconductor Labolatory  
Samsung Advanced Institute of Technology  
P.O. Box 111  
Suwon 440-600, Korea

Tel) +82-331-280-8830  
Fax) +82-331-280-9357  
e-mail: mcyoo@saitgw.sait.samsung.co.kr

### 3. QUANTUM DOTS

MONDAY AFTERNOON (ELKINS)

Session Chair: Art Gossard, University of California, Santa Barbara

Co-Chair: Ben Streetman, University of Texas, Austin

- 13:40 3.1 **Low-threshold ( $100\text{A}/\text{cm}^2$ ) injection lasers based on vertically coupled InGaAs/GaAs quantum dots** (Invited)  
V.M. Ustinov, A. Yu Egorov, A.E. Zhukov, N.N. Ledentsov, M.V. Maksimov, A.F. Tsatsul'nikov, S.V. Zaitsev, N.Yu. Gordeev, A.O. Kosogov, P.S. Kop'ev, D. Bimberg, Zh.I. Alferov, Russian Academy of Sciences, St. Petersburg, Russia.
- 14:10 3.2 **Alternating MBE formation of multiple layers of InGaAs quantum dots and application to quantum dot lasers**  
Richard Mirin, John Bowers, and Arthur Gossard  
University of California, Santa Barbara, USA.
- 14:30 3.3 **Self-assembling InP quantum dots for red laser diodes**  
K. Eberl, A. Kurtencach, M. Zundel, J.Y. Phillipp, A. Moritz, and A. Hangleiter  
Max-Planck-Institut FKF, Stuttgart, Germany.
- 14:50 3.4 **Vertical coupling and lateral transport in growth induced InAs quantum dot columns**  
G.S. Solomon, Y. Yamamoto, and J.S. Harris, Jr.  
Stanford University, USA.
- 15:10 3.5 **Self assembled structures of closely stacked InAs islands grown on GaAs by molecular beam epitaxy**  
Yoshiaki Nakata, Yoshihiro Sugiyama, Toshiro Futatsugi, and Naoki Yokoyama  
Fujitsu Laboratories Ltd., Japan.
- Break
- 15:50 3.6 **Room temperature luminescence from self-organized  $\text{In}_x\text{Ga}_{1-x}\text{As}/\text{GaAs}$  ( $0.35 \leq x \leq 0.45$ ) quantum boxes with high size uniformity**  
K. Kamath, P. Bhattacharya and J. Phillips  
University of Michigan, Ann Arbor, USA.
- 16:10 3.7 **Growth and characterization of self-organized InSb quantum dots and quantum-dashes in InP**  
T. Utzmeier, G. Armelles, P.A. Postigo, J. Tamayo, M. Dotor, R. García, and F. Briones, Inst. de Microelectrónica de Madrid, Spain.
- 16:30 3.8 **MBE growth of novel GaAs/n-AlGaAs field effect transistor structures with embedded InAs quantum traps and their transport characteristics**  
G. Yusa and H. Sakaki  
University of Tokyo, Japan.
- 16:50 3.9 **Selective MBE growth of n-type GaAs wire and dot structures using atomic hydrogens and their electronic properties**  
T. Noda, Y. Nagamune, Y. Ohno, S. Koshihara, and H. Sakaki  
University of Tokyo, Japan.

## LOW-THRESHOLD ( $100 \text{ A/cm}^2$ ) INJECTION LASERS BASED ON VERTICALLY COUPLED InGaAs/GaAs QUANTUM DOTS.

V.M.Ustinov, A.Yu.Egorov, A.E.Zhukov, N.N.Ledentsov, M.V.Maksimov, A.F.Tsatsul'nikov, S.V.Zaitsev, N.Yu.Gordeev, A.O.Kosogov, P.S.Kop'ev, D.Bimberg\*, and Zh.I.Alferov

A.F.Ioffe Physico-Technical Institute, Russian Academy of Sciences, Politekhnikeskaya 26, St. Petersburg, Russia; tel: (812)-247-9132; fax: (812)-247-8640;  
e-mail: VMUST@BEAM.IOFFE.RSSI.RU

\*Institut für Festkörperphysik, Technische Universität Berlin, Hardenbergstr. 36, D-10623 Berlin, Germany

Quantum dot lasers have been predicted to exhibit improved characteristics as compared to quantum well lasers owing to modification of the density of states [1]. Previously [2] we reported high  $T_0$  (350K) at low temperatures and extremely narrow lasing linewidth for injection laser based on (In,Ga)As quantum dots in GaAs matrix. Using the concept of vertically coupled quantum dots allowed us to reduce room temperature threshold current density and to extend the range of current thermal stability up to 160-180K [3].

In the present work we study the effects of emitter growth temperature and active layer design on lasing characteristics of quantum dot lasers grown by MBE.

We have found, that annealing the dots at  $700^\circ\text{C}$  results in a marked shift of PL emission toward higher energies. TEM studies show, that the reason for this is the decrease in In content in a quantum dot, while the dot size is affected only slightly. When the emitters of a GRINSCH laser are grown at  $700^\circ\text{C}$  (i.e., the quantum dot region is subjected to  $700^\circ\text{C}$  for  $\sim 1.5$  hours), room temperature threshold current density is decreased owing to the improvement of the structural quality of low-temperature GaAs covering quantum dots, lasing wavelength shifts due to the In composition reduction in a quantum dot, and the range of current thermal stability is decreased owing to reduction of the carrier localization energy.

Increasing the number of quantum dot sheets leads to a dramatic decrease in threshold current density due to improvement of optical confinement factor. The lasing wavelength of lasers based on vertically coupled quantum dots is considerably higher as compared to that of single-sheet dot lasers due to electronic coupling between neighboring dots. Laser based on 10 sheet vertically coupled quantum dots showed room temperature threshold current density as low as  $97 \text{ A/cm}^2$  ( $\lambda = 1.05 \mu\text{m}$ ).

### REFERENCES

1. Y.Arakawa and H.Sakaki, Appl. Phys. Lett. 40, 939 (1982).
2. N.Kirstaedter, N.N.Ledentsov, M.Grundmann, D.Bimberg, V.M.Ustinov, S.S.Ruvimov, M.V.Maksimov, P.S.Kop'ev, Zh.I.Alferov, U.Richter, P.Werner, U.Gosele, and J.Heydenreich, Electron. Lett. 30, 1416 (1994).
3. V.M.Ustinov, A.Yu.Egorov, A.E.Zhukov, N.N.Ledentsov, M.V.Maksimov, A.F.Tsatsul'nikov, N.A.Bert, A.O.Kosogov, P.S.Kop'ev, D.Bimberg, and Zh.I.Alferov, to be published in Proc. MRS 1995 Fall Meeting (Nov.27-Dec.01, 1995, Boston, USA).

## **Alternating MBE Formation of Multiple Layers of InGaAs Quantum Dots and Application to Quantum Dot Lasers**

Richard Mirin, John Bowers, and Arthur Gossard  
University of California, Santa Barbara  
Santa Barbara, CA 93106

Quantum dots formed by highly strained epilayers undergoing a Stranski-Krastanow transition (2D-3D) have recently been demonstrated in several III-V semiconductor systems such as InGaAs/GaAs, GaSb/GaAs, and InP/GaInP. We have previously reported optical and structural characteristics of  $\text{In}_{0.3}\text{Ga}_{0.7}\text{As}$  quantum dots grown using alternating molecular beam epitaxy (MBE), in which submonolayer amounts of In and Ga are deposited without any As flux. This deposition method allowed indium segregation to the growth front. The reflection high energy electron diffraction (RHEED) pattern showed that the 2D-3D transition occurred between 7.1 and 8.0 monolayers of deposition. We continued to deposit  $\text{In}_{0.3}\text{Ga}_{0.7}\text{As}$  until 22.1 monolayers had been deposited. The quantum dots demonstrated room temperature photoluminescence (RTPL) at  $1.32\text{ }\mu\text{m}$  with a full width at half maximum of only 28 meV. The dot density was  $2\text{--}3 \times 10^{10}\text{ cm}^{-2}$ , the dot height was around 24 nm, and the areal coverage was about 40%.

The overgrowth of GaAs on top of the three dimensional InGaAs islands is an area that is important to understand for realization of practical devices. In the present work, we vary the thickness of GaAs that is deposited at the InGaAs growth temperature of  $515^\circ\text{C}$ , and then pause the growth while raising the substrate temperature to about  $570^\circ\text{C}$ . Additional layers of GaAs and AlGaAs are then grown at  $570^\circ\text{C}$ . Substantial differences in the optical properties of the quantum dots are observed. Nine nm of GaAs grown at  $515^\circ\text{C}$  is the optimum thickness for obtaining the best RTPL. If we deposit less than 9 nm of GaAs at  $515^\circ\text{C}$ , the PL peak wavelength is progressively blue-shifted. If more than 9 nm of GaAs are grown at  $515^\circ\text{C}$ , the PL intensity is decreased and the linewidth is increased. The blue-shift is attributed to partial island evaporation during the growth pause. The PL intensity decrease with thicker GaAs is due to non-radiative defects in the overlying GaAs caused by the low temperature growth.

The overgrowth conditions also have important consequences for the growth of multiple layers of InGaAs quantum dots. We have studied the RTPL properties of single and multiple layers of InGaAs quantum dots of varying sizes. The multiple layer structures have 25 nm of GaAs as a barrier. We find that when growing multiple layers of smaller dots (13.3 monolayers of  $\text{In}_{0.3}\text{Ga}_{0.7}\text{As}$ ), it is possible to increase the RTPL intensity and the pump power required to saturate the ground state luminescence while still maintaining the same peak position and linewidth as for a single layer. However, larger dot sizes (more than about 17.7 monolayers of  $\text{In}_{0.3}\text{Ga}_{0.7}\text{As}$ ) do not allow the growth of good optical quality multiple layers. We find that there is often a **reduction** in PL peak intensity, which indicates that the second (and subsequent) layers of islands have non-radiative defects.

Finally, we will present results on how the overgrowth properties affect the device performance of quantum dot lasers. At 295 K, these quantum dot lasers show a saturation of the ground state emission at  $120\text{ A/cm}^2$  and lasing occurs from excited states of the quantum dots at  $1200\text{ A/cm}^2$ . At 85 K, the ground state emission saturates at  $32\text{ A/cm}^2$  and lasing occurs at a current density of  $510\text{ A/cm}^2$ .

This research is supported by the NSF Center for Quantized Electronic Structures (QUEST), Grant No. DMR91-20007.

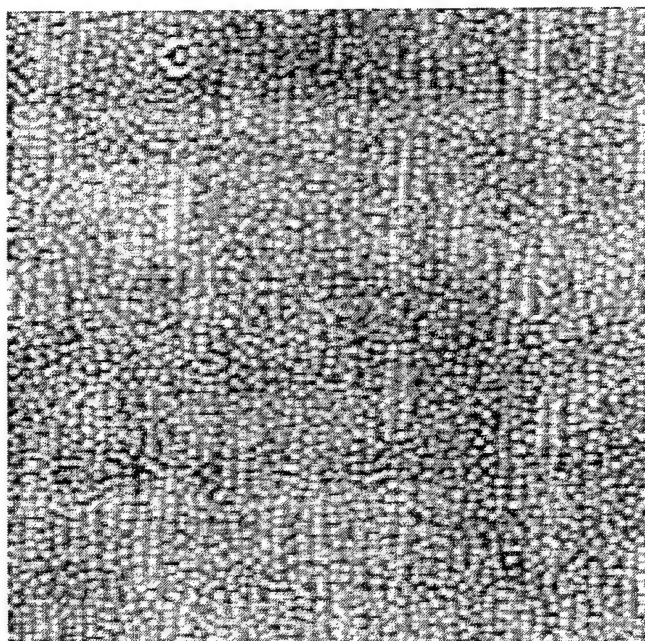


Figure 1: 5  $\mu\text{m}$  x 5  $\mu\text{m}$  AFM image of quantum dots formed by depositing 17.7 monolayers of  $\text{In}_{0.3}\text{Ga}_{0.7}\text{As}$  with alternating MBE.

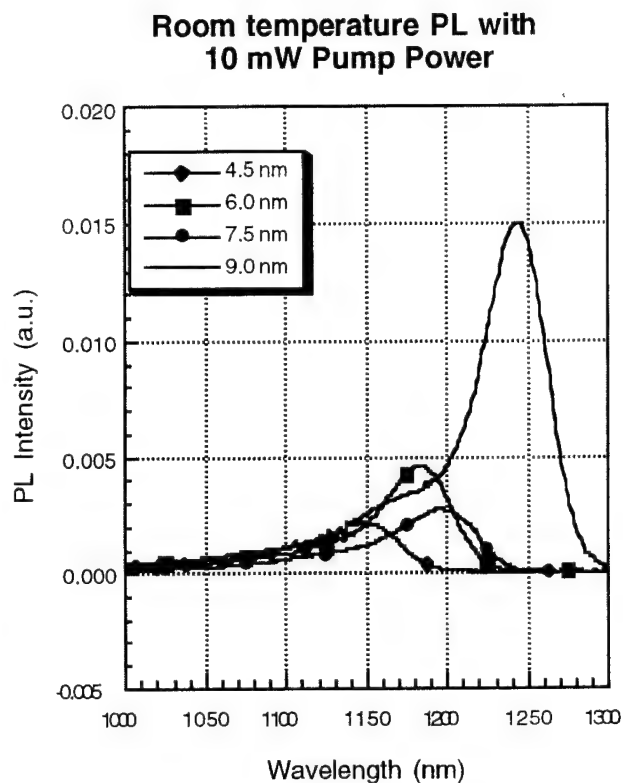


Figure 2: 9 nm of GaAs grown at 515°C gives the best room temperature PL results. Thicker layers of GaAs lead to reduced PL intensity. Quantum dots are 17.7 monolayers of  $\text{In}_{0.3}\text{Ga}_{0.7}\text{As}$

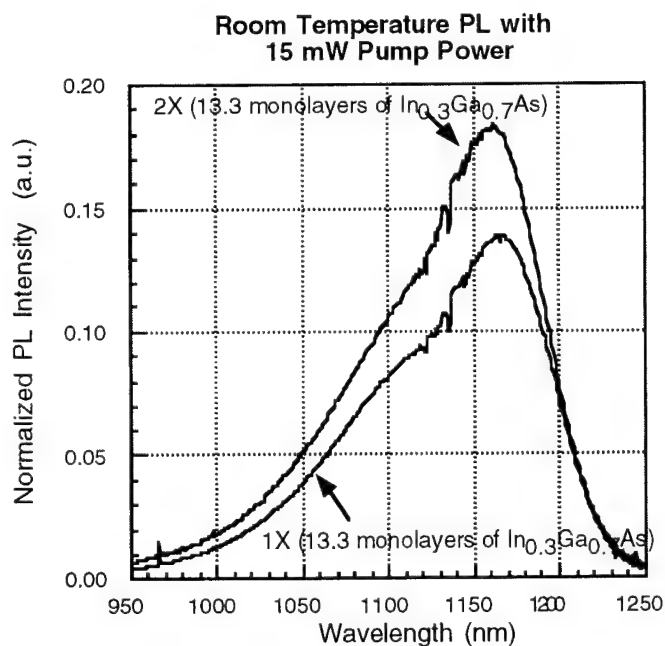


Figure 3: Two layers of quantum dots have an increased RTPL intensity compared to a single layer. These dots are formed by depositing 13.3 monolayers of  $\text{In}_{0.3}\text{Ga}_{0.7}\text{As}$ . The single dot layer sample also shows stronger band-filling as indicated by the more pronounced high energy shoulder.

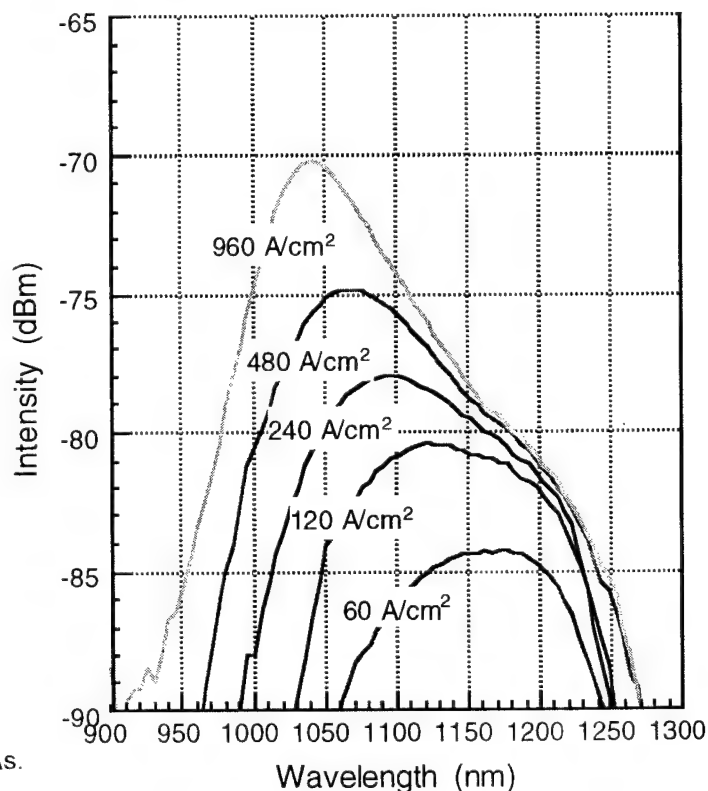


Figure 4: Subthreshold electroluminescence from quantum dot laser at 295 K.



## SELF-ASSEMBLING INP QUANTUM DOTS FOR RED LASER DIODES

**K. Eberl<sup>1</sup>, A. Kurtenbach<sup>1</sup>, M. Zundel<sup>1</sup>, J.Y. Phillipp<sup>1</sup>, A. Moritz<sup>2</sup>, and A. Hangleiter<sup>2</sup>**

<sup>1</sup> Max-Planck-Institut FKF, 70569 Stuttgart, Germany

<sup>2</sup> Physikalisches Inst. University Stuttgart 70569 Stuttgart, Germany

Self-assembling InP quantum dots are prepared by solid source molecular beam epitaxy [1]. The dots have a diameter of 15 to 50 nm and a height of 5 to 15 nm depending on the nominally deposited InP layer thickness between 1.5 and 7 monolayers [2]. Transmission electron microscopy and atomic force microscopy studies are presented to provide information about the structural properties. The InP quantum dots are embedded in InGaP lattice matched to the GaAs (100) substrate and show a strong and narrow photoluminescence (PL) at room temperature in the energy range from 1.6 to 1.85 eV as shown in figure 2. PL measurements on samples with several closely packed layers of dots indicate a degradation of the PL intensity and line width for distances below 30 nm between the layers.

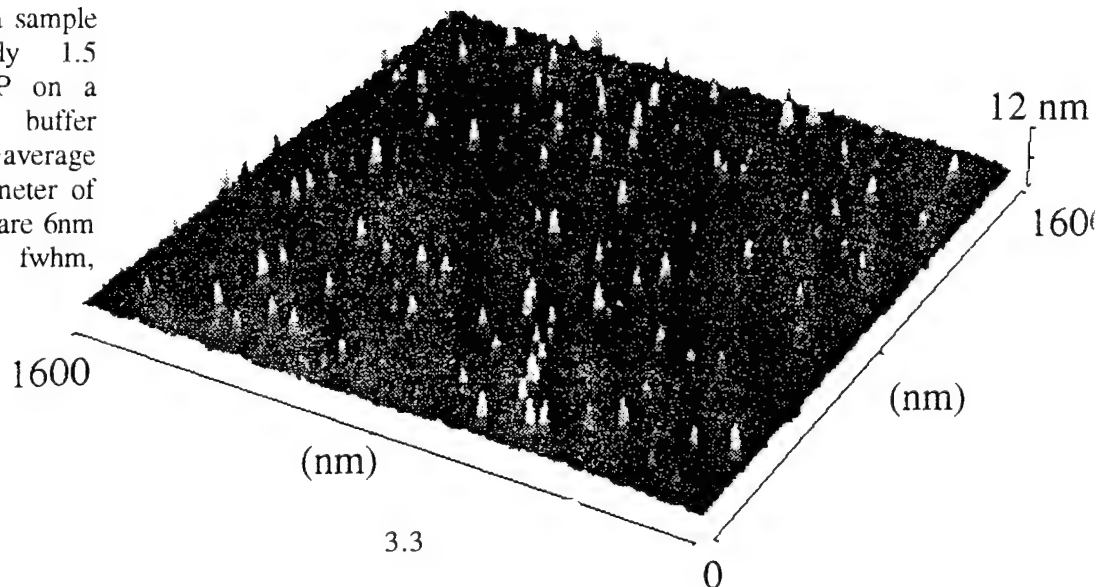
Laser structures are prepared with one and several layers of InP quantum dots within the 160 nm thick InGaP wave guide region. There are 0.7  $\mu\text{m}$  thick AlInP layers below and above the InGaP wave guide. In optical gain measurements we observe two gain peaks, which can be attributed to the wetting layer and the quantum dots. We have optically pumped cleaved samples with a length of 500  $\mu\text{m}$ . As expected from the results of the gain measurements we observe lasing at room temperature of either the quantum dots or the wetting layer depending on the experimental conditions. An example is shown in figure 4. Latest results on electrically pumped laser diodes with one and two layers of dots are presented.

Ref.:

1. A. Kurtenbach et al. Appl. Phys. Lett. 66, 361 (1995).
2. K. Eberl et. al. Mat. Res. Soc. Symp. Proc. Vol 378, 185, (1995).
3. A. Moritz et. al. Mat. Res. Soc. Symp. Fall Meeting Boston (1995).

Figures 1:

AFM scan of a sample with nominally 1.5 monolayers InP on a thick InGaP buffer layer. The average height and diameter of the InP islands are 6 nm and 15 nm fwhm, respectively.



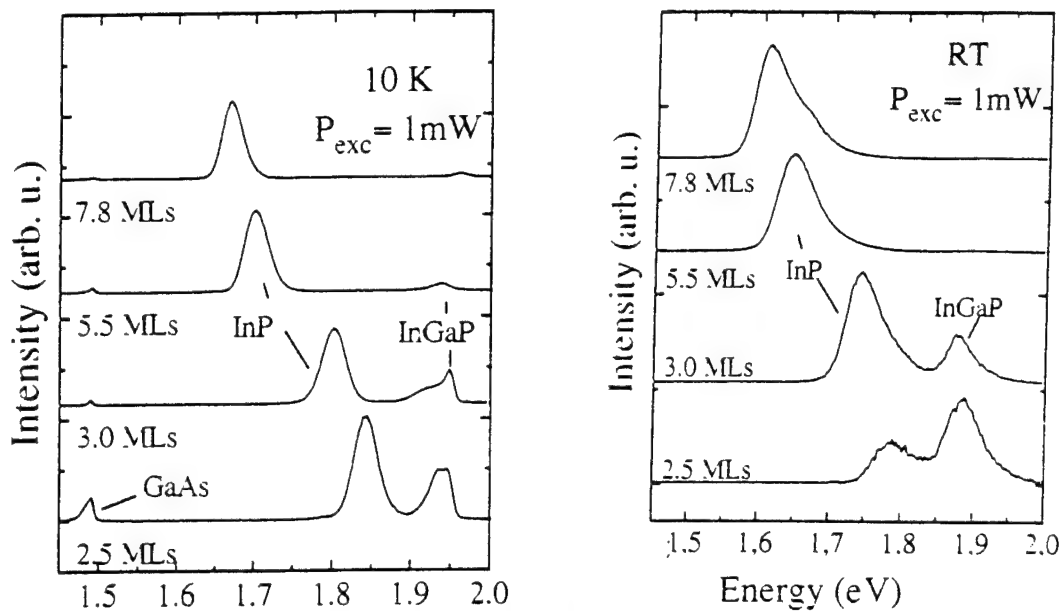


Figure 2: PL spectra measured at a) 10 K and b) room temperature (RT) for samples with InP islands embedded in InGaP. The nominal InP thickness is 2.5, 3, 5.5 and 7.8 monolayers. The typical PL linewidth is 30 meV at 10 K and 60 meV at RT.

Figure 3: Intensity of the optical output as a function of the pumping intensity for InP dots/InGaP/AlInP laser structures with 500  $\mu\text{m}$  length.

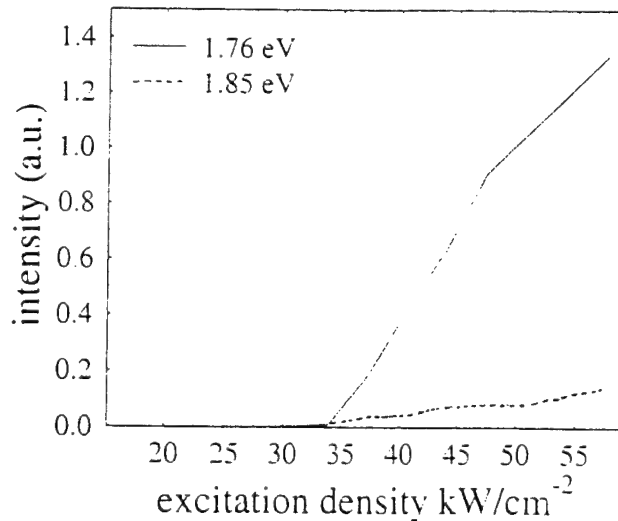
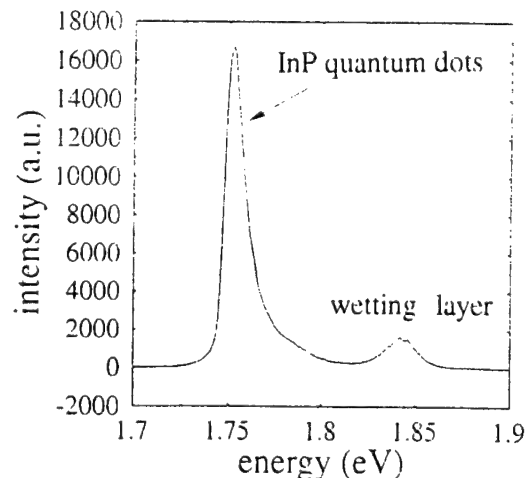


Figure 4: Emission spectrum of the laser structures shown in figure 3 showing the laser lines originating from the wetting layer and the InP quantum dots



Contact and presenting author:

Karl Eberl, Max-Planck-Institut FKF, Heisenbergstr. 1, 70569 Stuttgart (Germany)  
Tel.: 49 (0)711 689 1312 / Fax: 49 (0)711 689 1010 / email: eberl@servix.mpi-stuttgart.mpg.de

## Vertical Coupling and Lateral Transport in Growth Induced InAs Quantum Dot Columns

G. S. Solomon<sup>1</sup>, Y. Yamamoto<sup>1</sup> and J. S. Harris, Jr.<sup>2</sup>

<sup>1</sup> *Ginzton Laboratory, Stanford University, Stanford CA, 94305-4085*

<sup>2</sup> *Solid State Laboratory, Stanford University, Stanford, CA, 94305-4055*

*tele: 415-725-6910, fax: 415-723-5320, email: solomon@loki.stanford.edu*

It is naturally desirable to extend the device performance successes gained using quantum wells in electronic and optoelectronic devices, to structures with more reduced density of states (DOS), such as quantum wires and quantum dots (QDs). Using a growth induced islanding technique, we have constructed vertical columns of InAs QDs in a GaAs matrix, without post growth lithography. The InAs quantum dots are approximately 150 Å in base width and 40 Å high. The quantum dots form spontaneously in a random array in response to the 7% lattice mismatch between InAs and GaAs. Their size and density is well controlled by adjusting the growth temperature, growth rate and V/III beam flux ratio if the amount of InAs deposited is below a critical limit.

After the InAs quantum dots have formed, further GaAs growth quickly smoothes the growth front. This smoothing growth process is also a response to the lattice mismatch. If the GaAs thickness is small, when additional InAs is deposited the quantum dots nucleate directly above the previous quantum dot layer, and if this growth sequence is continued, vertical columns of InAs QDs are formed from dots of different layers. Transmission-electron microscopy indicates that the dots remain in the column formation up to the 10 layers of QDs investigated, and no large scale plastic relaxation is observed. Atomic-force microscopy, conducted by halting the growth at various stages, indicates the QD size and density is unchanged between the first layer of QDs and the fifth layer, while the dot density is reduced by the tenth dot layer.

8K photoluminescence measurements show a red shift in the spectral peak position, and a reduction in the spectral linewidth as the number of dots in a column is increased. We attribute these spectral feature changes to electronic coupling within the vertical dot columns.<sup>1</sup> This coupling is adjusted by adjusting the GaAs spacer region between the dots in a column. Room temperature electroluminescence on single dot layers and dot columns show a spectral peak shift with increased bias that we have attributed to transport between dots perpendicular to the columns, in the in-plane direction. I-V measurements conducted at 100K show Coulomb blockade steps that support the electroluminescence measurements. Thus, our experiments support strong coupling vertically within the dot columns, and weaker transport perpendicular to the columns.

---

<sup>1</sup> G. S. Solomon, J. A. Trezza, A. F. Marshall and J. S. Harris, Jr. *Phys. Rev. Lett.* **76** (952) 1996.

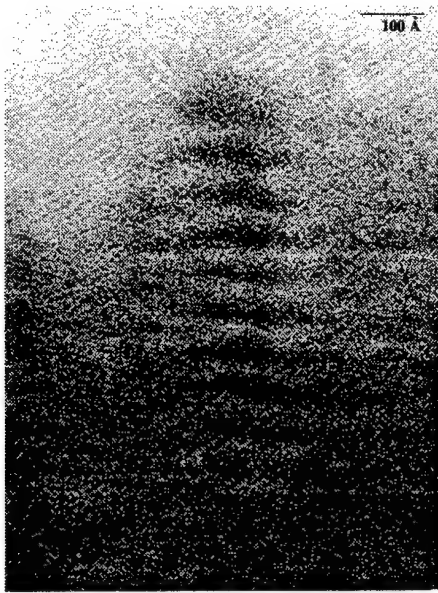
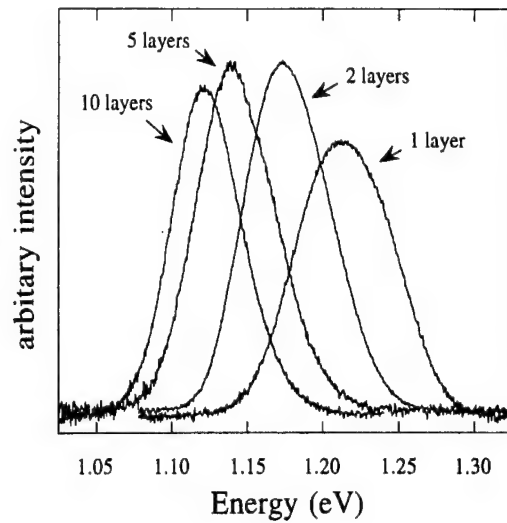


Fig.1 TEM of a column of 10 vertically aligned InAs quantum dots. The dots are approximately 40 Å tall.



8K PL showing red shift in peak position and linewidth reductions with increased number of dots in a column.

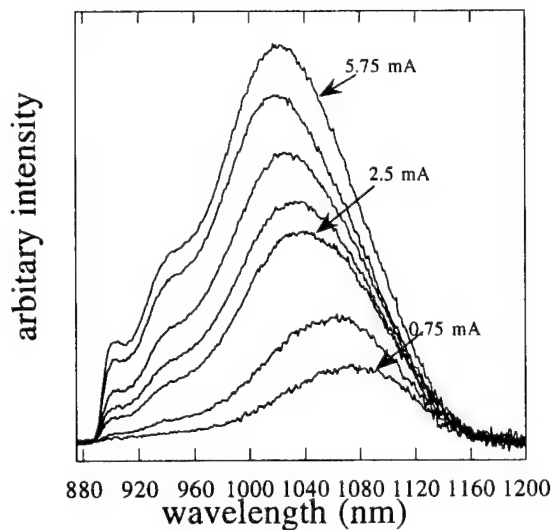


Fig. 3. Peak shift in electroluminescence as the bias is increased indicating transport in the in-plane direction.

# **Self assembled structures of closely stacked InAs islands grown on GaAs by molecular beam epitaxy**

Yoshiaki Nakata, Yoshihiro Sugiyama, Toshiro Futatsugi and Naoki Yokoyama

Fujitsu Laboratories Ltd.

10 - 1 Morinosato-Wakamiya, Atsugi, Kanagawa 243 - 01 Japan

Tel. +81-462-50-8247 (dial in), Fax. +81-462-50-8844, E-mail KXA0444@fjcug.fujitsu.co.jp.

Islands formed at the initial stage in highly mismatched heteroepitaxy have attractive much interests in device applications. Recently, we have reported the vertically aligned InAs islands on GaAs stacked with the 10 and 15 nm interval layers [1]. If the upper islands could be stacked closely just on the lower islands with the thin interval layers, the effective island height can be controlled by the stacked layer numbers, keeping the island lateral size and density as those of the first island layer. In this paper, we describe closely stacked InAs island structures grown with 2 and 3 nm interval layers.

We stacked InAs islands with the 3 and 2 nm GaAs interval layers by molecular beam epitaxy. The growth temperature for the InAs islands was fixed at 510°C and InAs nominal thickness for the island formation was about 1.8 monolayer (ML). Stacked island structures were evaluated by atomic force microscopy (AFM), transmission electron microscopy (TEM) and photoluminescence (PL) measurements. We found that the islands were formed even when stacking with 3 nm intervals (Fig. 1). The upper islands expanded gradually with stacked layer numbers (Fig. 2). The TEM images of the 5 stacked structures grown with 2 nm intervals indicated that upper islands were grown closely just on the lower islands (Fig. 3). The closely stacked structures were almost columnar with about 28 nm diameter and 16 nm height. The broad PL spectrum of the single island layer transformed to be sharp and high-intensity spectra with increasing island layers (Fig. 4). The peak energies shifted to the lower energy side. The line width of the 5 stacked structure was 27 meV and the peak intensity was about three times higher than that of the single layer structure. These renovated characteristics were useful for the laser applications.

## Reference

- [1] Y. Sugiyama, Y. Nakata, S. Muto, and N. Yokoyama, Extended Abstracts of the Int. Conf. on Solid State Devices and Materials, Osaka, 1995, pp. 773-775.

# Self assembled structures of closely stacked InAs islands grown on GaAs by molecular beam epitaxy

Fujitsu Laboratories Ltd., 10 - 1 Morinosato-Wakamiya, Atsugi 243- 01 Japan

Y. Nakata, Y. Sugiyama, T. Futatsugi and N. Yokoyama

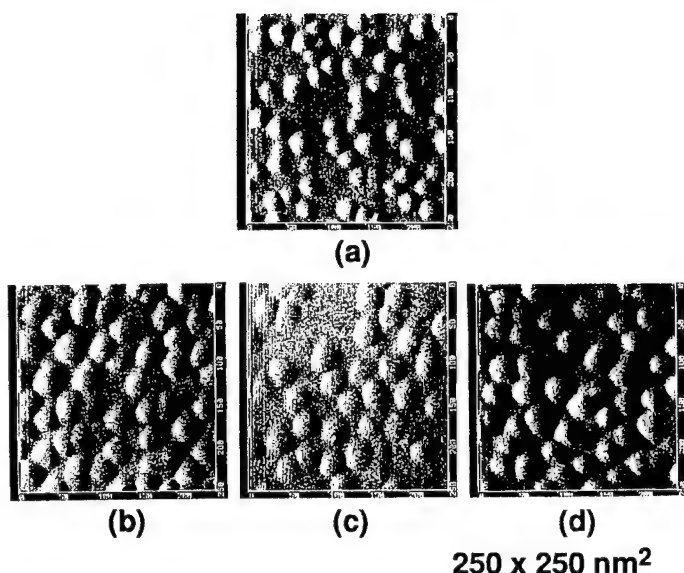


Fig. 1. AFM images of stacked InAs islands grown with 3 nm intervals. (a) 1st layer, (b) 3rd layer, (c) 5th layer and (d) 10th layer.

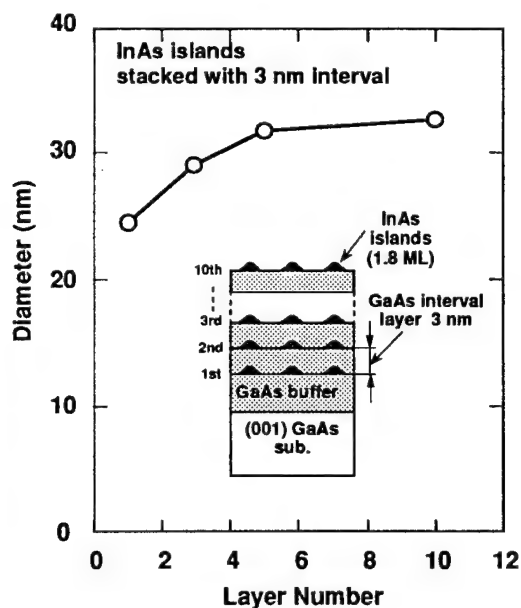


Fig. 2. InAs island size dependence on the stacked layer numbers evaluated by AFM.



Fig.3. TEM image of the cross-section obtained from the 5 stacked InAs island layers grown with 2 nm intervals.

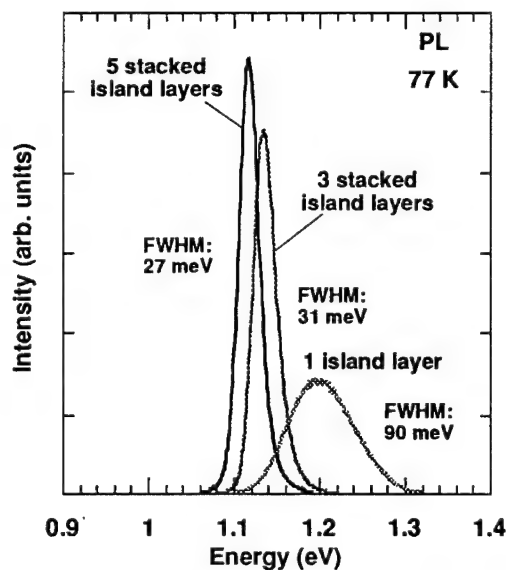


Fig. 4. PL spectra of stacked InAs island layers grown with 3 nm intervals.

## Room temperature luminescence from self-organized $\text{In}_x\text{Ga}_{1-x}\text{As}/\text{GaAs}$ ( $0.35 \leq x \leq 0.45$ ) quantum boxes with high size uniformity

K.Kamath, P.Bhattacharya and J.Phillips  
Department of Electrical Engineering and Computer Science  
University of Michigan, Ann Arbor, MI 48109 USA

e-mail : pkb@eecs.umich.edu, Phone : (313)-763-6678, FAX : (313)-763-9324

### Abstract

A powerful technique for the realization of quantum boxes is by self organization during the epitaxial growth of highly mismatched layers. Such quantum boxes can be disorder-free and when grown on patterned substrates they can be arranged in regular linear or two dimensional arrays. Most of the work reported in this area has been done with  $\text{In}_x\text{Ga}_{1-x}\text{As}/\text{GaAs}$  systems with  $x > 0.5$ . Such 3-dimensional growth with  $\text{In}_x\text{Ga}_{1-x}\text{As}/\text{GaAs}$  for  $x < 0.5$  would extend the energy bandgap range of the quasi-zero dimensional system. Additionally a lower mismatch allows a thicker 2D layer growth before the onset of the island growth mode (transition from Vollmer-Weber to Stranski-Krastanow growth mode). This would provide efficient carrier injection into the boxes in devices such as LEDs and lasers. To our knowledge, there has been no report of strong room temperature luminescence from self-organized quantum dots. In this paper we report on the growth and optical property of self organized  $\text{In}_x\text{Ga}_{1-x}\text{As}/\text{GaAs}$  ( $0.35 \leq x \leq 0.45$ ) quantum dots. Sharp excitonic resonances with narrow line widths are seen in low temperature photoluminescence (PL). The PL emission was observed upto room temperature.

MBE growth of the mismatched heterostructures were monitored by in-situ RHEED measurements. The structures grown on (001) GaAs consist of an  $\text{In}_x\text{Ga}_{1-x}\text{As}$  layer sandwiched between GaAs layers. The growth temperatures were  $640^\circ\text{C}$  and  $540^\circ\text{C}$  for GaAs and  $\text{In}_x\text{Ga}_{1-x}\text{As}$ , respectively, and the growth rate was 1 monolayer (ML) per second. We have used the change in RHEED spectrum from streaked (layer by layer growth) to a spotty (3D growth) pattern for estimating the nominal  $\text{InGaAs}$  wetting layer (initial 2D growth mode) thickness. It has been reported earlier that a wetting layer of only 1.75 ML's is required before the onset of island growth of InAs on GaAs, whereas, 4 ML's are needed for  $x=0.5$  on GaAs. We have observed that island growth commences after about 6 ML's for  $x=0.4$  and 10 ML's for  $x=0.35$ . No change in RHEED pattern was observed for  $x=0.3$  even after 20 ML's. The typical quantum boxes grown and characterized in this study are around 15nm in lateral extent as observed by scanning electron microscopy.

High resolution photoluminescence measurements were made with varying excitation levels in the temperature range of 16-300K. Very strong excitonic luminescence is observed in  $\text{In}_{0.35}\text{Ga}_{0.65}\text{As}(15\text{ML's})/\text{GaAs}$  upto 300K. A second peak emerges at higher excitation levels which, we believe, originates from a higher order state. For the material with  $x=0.3$ , on the other hand there is only a broadening of the excitonic peak with increased excitation, as is expected for a quantum well. This is in conformity with the RHEED measurements which indicate the formation of quantum boxes only for  $x \geq 0.35$ . The linewidth of the PL emission peak is about 33meV which is much lower than the 40-50 meV linewidths usually reported.

An important observation made in spatially resolved PL excitonic spectra is the presence of additional fine structures superimposed on the emission peaks. We believe that these features, observed for the first time, represent groups of boxes of identical dimensions and are a measure of the high degree of size uniformity. Time resolved PL measurement of carrier dynamics in these boxes is in progress and the results will be presented and discussed.

---

This work is supported by the Army Research Office.

# Growth and Characterization of Self-Organized InSb Quantum-Dots and Quantum-Dashes in InP

T. Utzmeier, G. Armelles, P.A.Postigo, J.Tamayo, M.Dotor, R.García, and F.Briones  
*Inst. de Microelectrónica de Madrid, CNM, CSIC, Serrano 144, 28006 Madrid, Spain*  
**Tel.:** (34-1) 562 53 11 - 216 **Fax:** (34-1) 411 76 51 **e-mail:** thomas@imm.cnm.csic.es

Self-organized InSb Quantum-Dots (QD) on semi-insulating InP (001) substrates have been grown by atomic layer molecular beam epitaxy (fig.1). This system is especially interesting because of the high lattice mismatch of 10.4%. Atomic force microscopy has been used to determine the size-dependency of the uncapped quantum dots on the nominal thickness of the deposited InSb layer. The dot-size shows a pronounced minimum for about 2.2 monolayers (ML) of nominal InSb thickness with an dot-diameter of  $24 \pm 4$  nm and a height of  $6 \pm 3$  nm. Above 3.2 ML we observe a drastic change of the dot shape from a point-like to a strikingly elongated one, aligned in the (1-10) direction (fig. 2). The resulting features we call quantum-dashes. Quantum-dots, in general, repel each other due to the overlap of their mismatch-induced strain field in the substrate. This repelling force depends quadratically of the dot diameter. In the case of quantum-dashes, their elongated shape causes an highly anisotropic strain-field, that gives rise to higher repulsion in the (1-10) than in the (110) direction, as observed experimentally measuring the inter-dash distribution in the two directions, respectively. Photoluminescence (PL) at 12K of the QD samples with and without cap-layer was measured. Both type of samples show PL emission at 1.1 eV and 1.2 eV (fig.3), respectively, but the emission energy does not change significantly with the dot-size. This, together with the fact that the PL emission is relatively broad ( $\approx 100$ meV) and that the QDs do not show any signal in photo-absorption measurements indicates a type II band-alignment between the strained InSb and InP. This agrees with theoretical estimations from biaxially strained quantum-wells. Therefore, in the system studied the hole are confined in the InSb, while the electrons are located the InP.



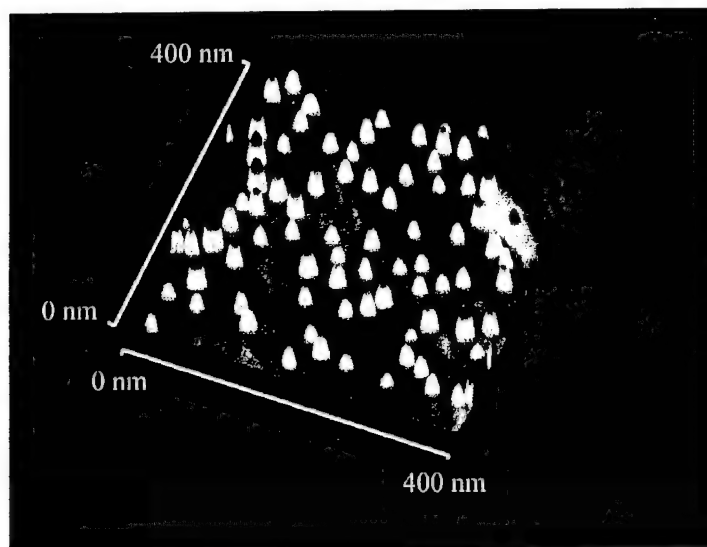


Figure 1

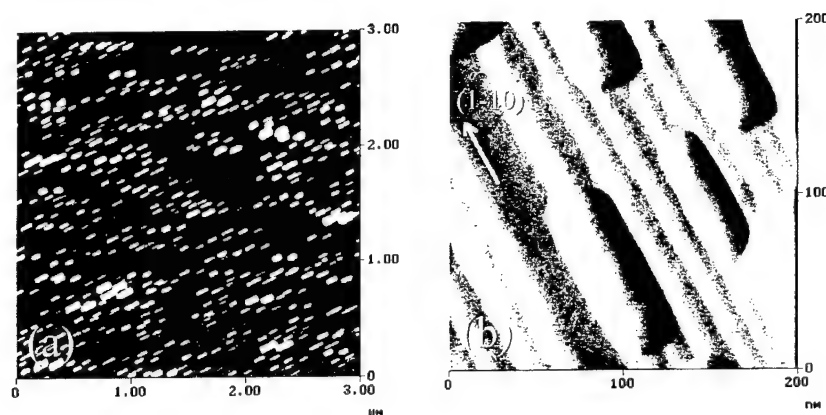


Figure 2

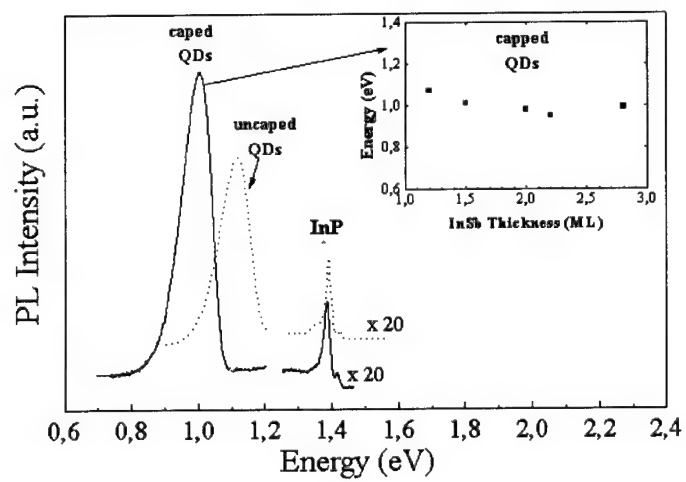


Figure 3

# MBE growth of novel GaAs/n-AlGaAs field-effect transistor structures with embedded InAs quantum traps and their transport characteristics

G. Yusa and H. Sakaki

We have grown by molecular beam epitaxy (MBE) selectively doped GaAs/n-AlGaAs FET structures, in which InAs quantum dots are embedded near the channel. It is found that the electron concentration  $N_s$  of this FET increases linearly with the gate voltage ( $V_g$ ) but its threshold voltage can be programmed by the gate controlled trapping of electrons in these dots. Analysis has shown that one electron is trapped by each dot.

Selectively doped inverted HEMT structures (A, B and C) have been grown by MBE on a semi-insulating GaAs (100) substrate. Figure 1 shows the structure of sample A, in which InAs dots (1.75 ML) are embedded inside of 600 nm thick GaAs layer at a position of 200 nm from the hetero interface. Note that the dots are empty, as their states are pulled up by the surface Fermi level. In sample B, 1 ML InAs was embedded in place of dots, whereas sample C was prepared without InAs layer.

These wafers were processed into FETs in order to modulate  $N_s$  as a function of gate voltage  $V_g$ . Figure 2 shows that  $N_s$  measured by the Hall effect at 4.2 K increases linearly with  $V_g$  up to  $V_g = 0.8$  V for all samples. In sample B and C, we could not raise  $V_g$  beyond 0.8 V, as the gate-to-source current increases. In sample A, however, the leakage current remained low even for  $V_g > 0.8$  V and  $N_s$  was found to saturate as shown in Fig. 2. When  $V_g$  is reduced from 1.9 V,  $N_s$  of sample A is found to reduce with the same slope but  $N_s$ - $V_g$  characteristics are shifted by  $4.50 \times 10^{10} \text{ cm}^{-2}$ . This unique behavior can be ascribed to the trapping of electrons by InAs dots, which is schematically shown in Fig. 3. By analyzing the shift of threshold voltage, the density  $N_{dot}$  of trapped electrons is estimated to be  $6.56 \times 10^{10} \text{ cm}^{-2}$ . As the density  $D_{dot}$  of InAs dots estimated by AFM is  $(5 \sim 10) \times 10^{10} \text{ cm}^{-2}$ , we find that one dot traps one electron each. The temperature dependence and other features of this interesting trapping effect will be reported.

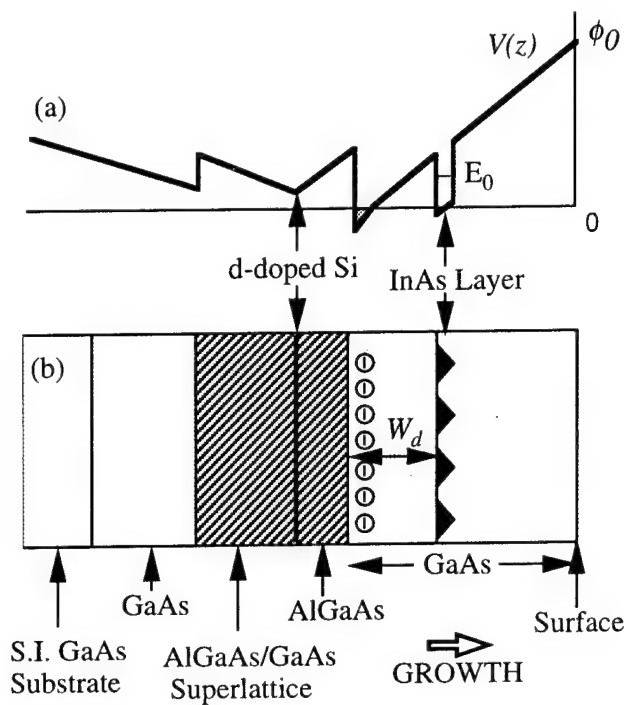


**Figure 1**  
Schematic illustration of the conduction band diagrams of the dot-embedded GaAs/n-AlGaAs modulation doped field-effect transistors.

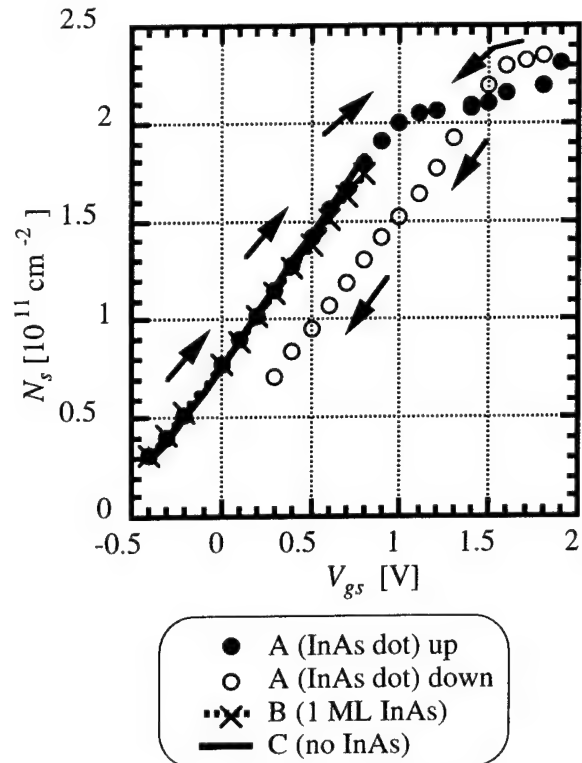


**Figure 2**  
The concentrations  $N_s$  of electrons in the channel of three FETs measured as functions of the gate-source voltage at 4.2 K.

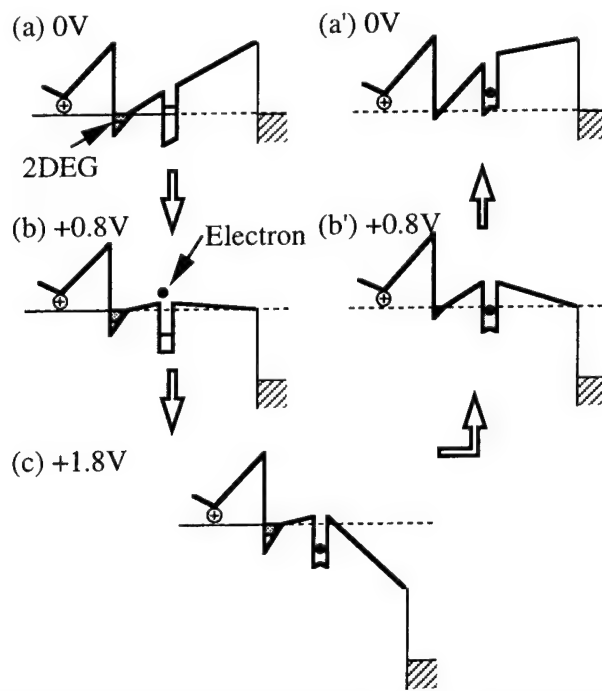


**Figure 3**  
Illustration of the potential profile of a dot-inserted MODFET at various values of  $V_g$ . (a), (b), and (c) show how an empty dot traps one electron when  $V_g$  increases, while (a') and (b') show the band diagram after the dot is charged up with the electron.

# Selective MBE growth of n-type GaAs wire and dot structures using atomic hydrogens and their electronic properties

T.Noda 1), Y.Nagamune 2), Y.Ohno 3), S. Koshiha 4), and H.Sakaki 3,4)

1) IIS, University of Tokyo, 7-22-1 Roppongi, Minato-ku, Tokyo 106, Japan  
TEL:81-3-3402-6231 ext. 2344, FAX:81-3-3796-1249; E-mail:noda@kyokusho.rcast.u-tokyo.ac.jp

2) Electrotechnical Laboratory, 1-1-4 Umezono, Tsukuba-shi, Ibaraki 305, Japan

3) RCAST, University of Tokyo, 4-6-1 Komaba, Meguro-ku, Tokyo 153, Japan

4) QTP, JRDC, Park Bldg, 4F 4-7-6 Komaba, meguro-ku, Tokyo 153, Japan

Fabrication of quantum wires (QWIs) and quantum dots (QDs) is important not only for device applications but also for physics of low dimensional systems. Among various methods, selective growth of GaAs with SiNx or SiO<sub>2</sub> mask pattern is attractive. Indeed, selective metalorganic chemical vapour deposition and molecular beam epitaxy (MBE) with atomic hydrogens [1] have been used to produce nearly damage-free nanostructures.

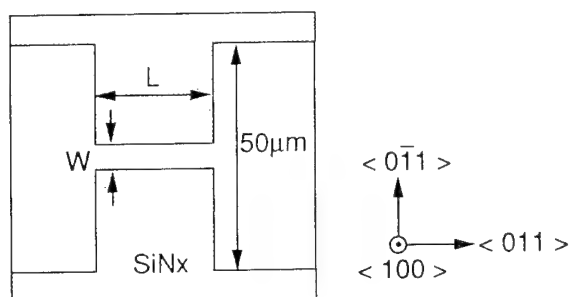
In this work we investigated structural features and electronic properties of QWI and QD prepared by the selective MBE growth with atomic hydrogens [2]. We grew 610 ~ 620 °C a GaAs layer (.9 μm), then GaAs/AlGaAs superlattices and selectively-doped 6 nm single quantum wells (QWs) on (100) GaAs substrates, covered with SiNx mask patterns. Hydrogen of 0.90 ccm was supplied and the temperature of the craking cell was ~ 1600 °C. The growth rate was 0.23 μm/hr for GaAs and 0.1 μm/hr for AlAs. The flux ratio As<sub>4</sub>/Ga was ~6.

To fabricate QWIs, (100) GaAs substrate with a SiNx mask pattern of Fig.1(a) was prepared. The window consists of a narrow constrictions ( $L = 3 \sim 6 \mu\text{m}$  length and  $W = 0.8 \sim 4.0 \mu\text{m}$  width) running along  $\langle 011 \rangle$  to connect two 50 μm wide regions. By the selective growth of GaAs and QW structure, a QWI is formed. Figure 1 (b) shows an SEM of the final structure seen from the top, whereas Fig.1(c) is a cross-sectional illustration of the structure, cut along the line A of Fig.1(a). When we grew a long wire, the diffusion of Ga from the side (111)B plane to the top (100) plane is dominant, resulting in a very sharp ridge structure. In a short wire, however, Ga migrates along the wire and the narrowing of the top (100) plane is strongly hindered. Indeed, spatially resolved photoluminescence (PL) study shows that the thickness of the QW in the middle region of the wire is close to 6 nm, suggesting that the material diffusion from the (111)B to the (100) is small. These morphological features indicate the important roles of additional facets formed due to the finite length of the wire. Hence, we have found that the width of the top (100) plane can be squeezed most effectively by employing a long constriction. Using the constriction pattern of 0.8 μm in width, an n-type conductive wire with the geometrical width of 0.3 μm have been formed and the electrons transport has been studied.

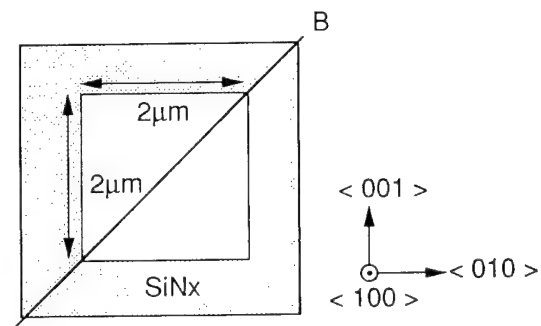
By using 2μm x 2μm square window along  $\langle 001 \rangle$  and  $\langle 010 \rangle$  (Fig.2(a)), a quantum dot was formed, whose cross-section is shown in Figs.2(b) and (c). MBE growth of GaAs and 6 nm GaAs QW was performed at  $T_s = 620 \text{ C}$ . Note that the lateral size of QD is ~100 nm and the facet is close to (320) plane, though the (110) plane usually appears for the long wire. PL of the QD studied at 15 K shows a broad spectrum with a shoulder at 15 meV higher than the main peak. Although the origin of this shoulder is not clear, it is probably due to the electron accumulation in higher levels of the dot.

In conclusion, we have fabricated n-type nanostructures in MBE with assist of atomic hydrogens and found that the facets interaction is strongly modified by the presence of additional facets at least in this pattern studied here.

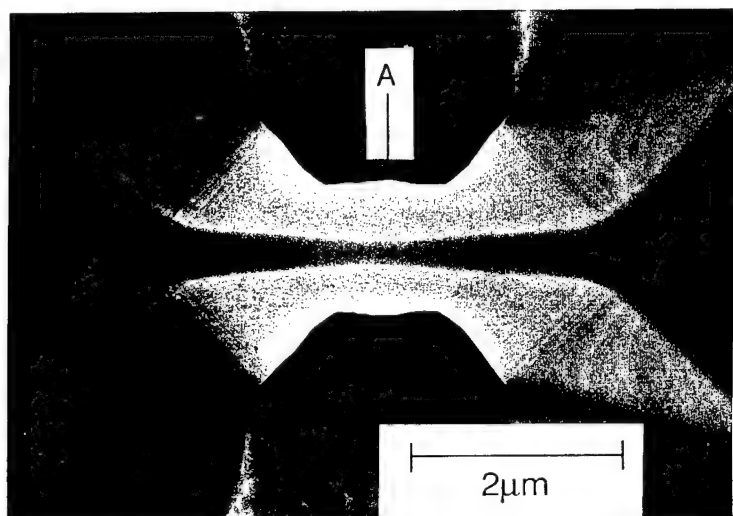
**References** [1] T.Sugaya, M.Kaneko, Y.Okada, and M.kawabe, Jpn. J. Appl. Phys. **32**, L1834 (1993), [2] T. Sugaya and M. Kawabe, Jpn. J. Appl. Phys. **30**, L402 (1991)



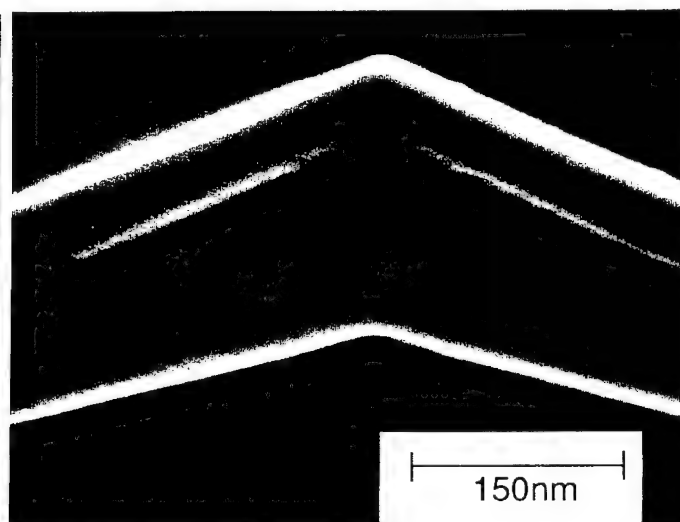
(a) An illustration of the wire pattern



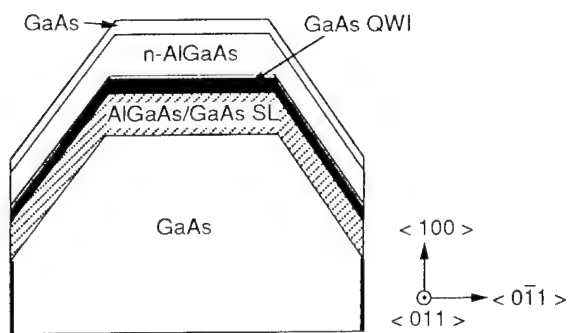
(a) An illustration of the dot pattern



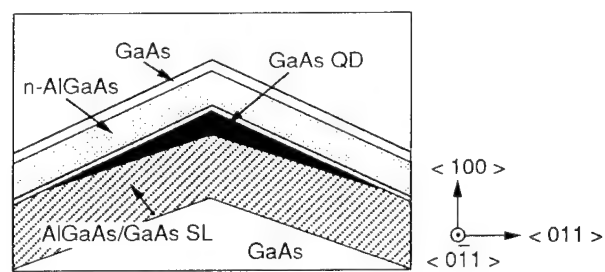
(b) A SEM picture of the wire grown on the pattern with  $W = 0.8 \mu\text{m}$  and  $L = 3 \mu\text{m}$ .



(b) A cross-sectional SEM picture cleaved along the line B in Fig.2(a).



(c) A cross-sectional illustration of the wire structure.



(c) A schematic illustration of the QD in Fig.2(b).

Fig.1

Fig.2

#### 4. III-V GROWTH

TUESDAY MORNING (SMOTHERS)

Session Chair: Yung-Chung Kao, Texas Instruments Corporate R&D, Dallas, Texas

Co-chair: Henry Lee, University of California, Irvine, California

09:00 4.1 **Surface chemistry during metalorganic molecular beam epitaxy studied by pulsed molecular beam scattering**, (Invited)  
Masahiro Sasaki and Seikoh Yoshida  
Optoelectronics Research Laboratory, Ibaraki, Japan.

09:30 4.2 **Laterally nonuniform Ga segregation at GaAs/AlGaAs interfaces during MBE growth**  
W. Braun, A. Trampert, L. Däweritz, and K.H. Ploog  
Paul-Drude-Institute für Festkörperelektronik, Berlin, Germany

09:50 4.3 **Suppression of AlGaAs/GaAs superlattice intermixing by p-type doping**  
K. Muraki and Y. Horikoshi  
NTT Basic Research Laboratories, Kanagawa, Japan

10:10 4.4 **Iodine assisted molecular beam epitaxy**  
M. Micovic, D. Lubychev, W.Z. Cai, F. Flack, and D.L. Miller  
The Pennsylvania State University, USA

Break

10:50 4.5 **Incorporation of  $As_2$  in  $InAs_xP_{1-x}$  grown using valved cracker sources; application to  $InAs_xP_{1-x}/InP$  and  $InAs/InAs_xP_{1-x}$  quantum well structures**  
M. Hopkinson and J.P.R. David  
University of Sheffield, United Kingdom

11:10 4.6 **Contamination in molecular beam epitaxy: the role of arsenic drag effect**  
Z.R. Wasilewski, S.J. Rolfe, and R.A. Wilson  
National Research Council of Canada, Ottawa, Canada

11:30 4.7 **A cell for producing carbon atoms deposition producing no carbon clusters**,  
N.R. Gall, E.V. Rut'kov, A. Ya. Tontegode, P.B. Kuznetsov, and R.N. Gall, A.F. Ioffe  
Physico-Teschnical Institute RAS, St. Petersburg, Russia

11:50 4.8 **Sensor controlled linear motion oven (S-LIMO) for precision group III flux operation**  
P.P. Chow, K. Evans, and A.J. SpringThorpe  
SVT Associates, Eden Prairie, MN, USA

# **Surface chemistry during metalorganic molecular beam epitaxy studied by pulsed molecular beam scattering**

Masahiro Sasaki<sup>1</sup> and Seikoh Yoshida<sup>2</sup>

Optoelectronics Technology Research Laboratory (OTL)  
5-5 Tohkodai, Tsukuba, Ibaraki 300-26, Japan

The high controllability of metalorganic molecular beam epitaxy (MOMBE) is attributed to the surface chemical reaction which is very sensitive to the substrate surface condition. In this paper, we report on the surface chemistry during MOMBE on variously controlled GaAs surfaces, studied by the scattering of pulsed trimethylgallium (TMG) beams.

The experiments were carried out in a UHV system comprising an MOMBE facility and a pulsed molecular beam scattering chamber equipped with a quadrupole mass spectrometer having a liquid-nitrogen cooled shroud and aperture. We measured the time-of-flight (time-of-arrival) distributions of TMG molecules scattered from stoichiometry- and structure-controlled GaAs (100), GaAs(110) and GaAs(111)B surfaces to obtain the information on the dynamical behavior of the surface reaction.

In this study we conclude that the TMG surface chemical reaction is described within the framework of the precursor-mediated chemisorption, where the stability and the charge distribution of the relaxed or reconstructed surface are important.

In the case of the scattering from less stabilized GaAs surfaces, TMG molecules are mainly chemisorbed dissociatively. On the other hand, in the case of the scattering from highly stabilized surfaces, such as GaAs(100)-(2×4), GaAs(110) and GaAs(111)B-( $\sqrt{19}\times\sqrt{19}$ ) surfaces, most of TMG molecules are desorbed without decomposition although they are temporarily trapped in a deep precursor state.

The depth of the precursor state are estimated from the temperature dependence of the surface residence time during scattering. The surface structure dependence of the precursor state is explained by taking into account the charge distribution in the relaxed or reconstructed surface.

On the basis of this result, the mechanisms of the growth controls by MOMBE, such as the selective area growth and the lateral growth, are discussed.

---

<sup>1</sup> Corresponding author. Present address: Institute of Applied Physics, University of Tsukuba, 1-1-1 Tennoudai, Tsukuba, Ibaraki 305, Japan FAX:+81-298-53-5205

<sup>2</sup> Present address: The Furukawa Electric Co.,Ltd. Yokohama R&D Laboratories, 2-4-3 Okano, Nishi-ku, Yokohama 220, Japan

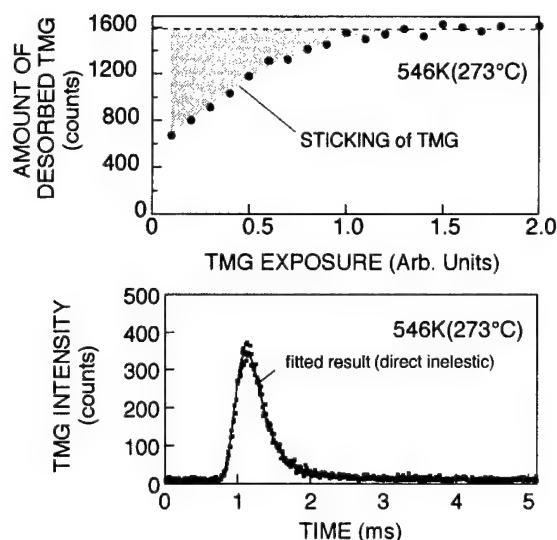


**Fig.1** (a) The amount and (b) the time-of-flight spectrum of TMG scattered from less stabilized GaAs(100)-(1x6) surface. The shaded area in (a) corresponds to the sticking of TMG. The time-of-flight spectrum in (b) is well reproduced by the single component for the scattering without surface residence. This result suggests that TMG molecules are mainly adsorbed with dissociation, although TMG molecules may be trapped in the precursor state.

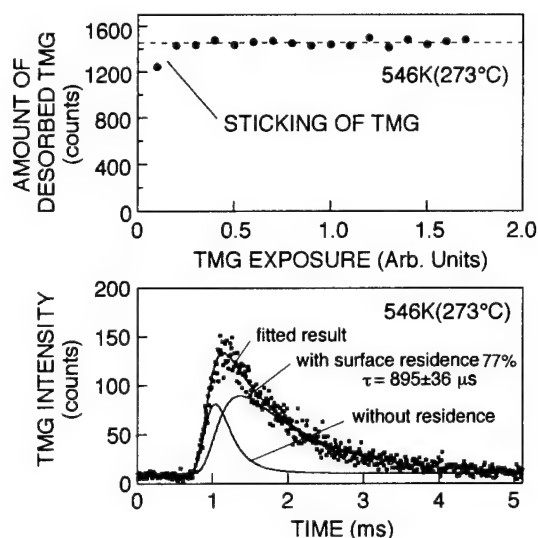


**Fig.2** (a) The amount and (b) the time-of-flight spectrum of TMG scattered from highly stabilized GaAs(100)-(2x4) surface. The shaded area in (a) corresponds to the sticking of TMG. The time-of-flight spectrum in (b) is well reproduced by the sum of two components for scattering with and without surface residence. This result suggests that most of TMG molecules are desorbed without dissociation after a long surface residence in the precursor state.

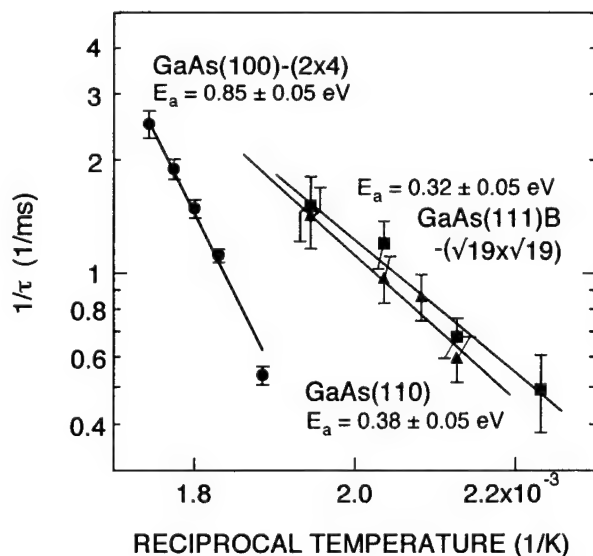


**Fig.3** Arrhenius plots of the reciprocal of the surface residence time during scattering (escape rate from the precursor state) for the highly stabilized GaAs surfaces. The depths of the precursor state are estimated from the slopes. In addition to the results for these surfaces, we observe no surface residence in the precursor state for the GaAs(111)B-(2x2) surface. The obtained surface structure dependence of the precursor state is interpreted by taking into account the charge distribution in the reconstructed or relaxed surface structure.



## Laterally nonuniform Ga segregation at GaAs/AlAs interfaces during MBE growth

W. Braun\*, A. Trampert, L. Däweritz and K.H. Ploog

Paul-Drude-Institut für Festkörperelektronik, Hausvogteiplatz 5-7, D-10117 Berlin, Germany

When RHEED intensity oscillations from homoepitaxial growth are compared to oscillations during heterointerface formation, a relative phase shift is detected that is *independent of diffraction conditions*. Instead, this phase shift depends only on the pair of surface reconstructions before and after the completion of the heterointerface. The phase difference can be explained by the difference of group III element content of both surface reconstructions involved. With group V overpressure, the constant group III flux defines the time axis of the oscillations in III-V-MBE. A loss or gain of group III material at the heterointerface shifts the oscillations with respect to this time axis, resulting in a phase shift.

The phase shift depends monotonously on the alloy composition of  $\text{Al}_x\text{Ga}_{1-x}\text{As}$  (fig. 1), allowing an assessment of segregation in-situ and during growth. Whereas no Al segregation is found for GaAs growth on AlAs, Ga is found to segregate up to 20 ML for growth of AlAs on GaAs. At this interface, the phase shift signal shows a distinctly different time evolution on the specular spot compared to the first-order diffraction streak (fig. 2) when recording the RHEED signal with the incident beam along the  $[\bar{1}10]$  direction. We interpret this difference by a real-space sensitivity of RHEED with respect to surface morphology. Whereas for diffraction into the higher-order streaks good lateral periodicity is required, this constraint does not apply to the specular spot. We therefore obtain the oscillating signal from the disordered surface regions close to the specular position on the screen. The results are interpreted in terms of preferential segregation at the step edges parallel to  $[\bar{1}10]$ . This leads to laterally confined segregation and we obtain elongated intermixed regions at the normal heterointerface with a strongly anisotropic shape. The results are confirmed by TEM images (fig. 3) along both  $[\bar{1}10]$  and  $[110]$  that *clearly show the anisotropic intermixed regions*. The implications on current growth and segregation models as well as RHEED theory are discussed.

\* corr. author, phone: +49-30-20377-356, fax: +49-30-20377-201, email: braun@pdi.wias-berlin.de

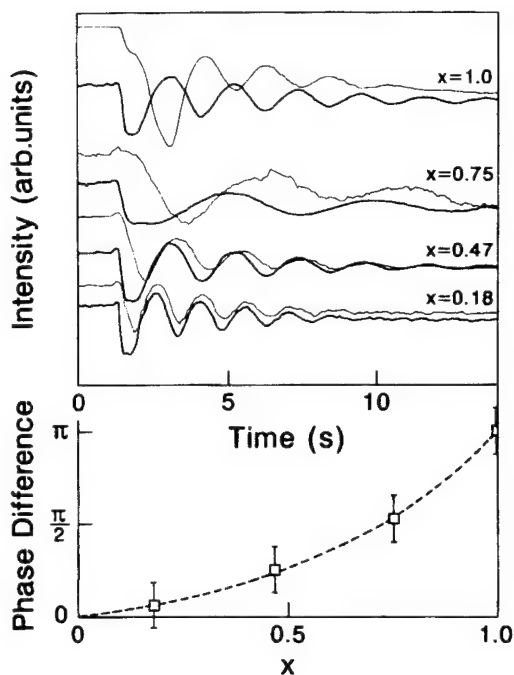


Figure 1: Phase shift as a function of Al fraction  $x$  of the  $\text{Al}_x\text{Ga}_{1-x}\text{As}$ . GaAs on GaAs growth in green, GaAs on  $\text{Al}_x\text{Ga}_{1-x}\text{As}$  in black.

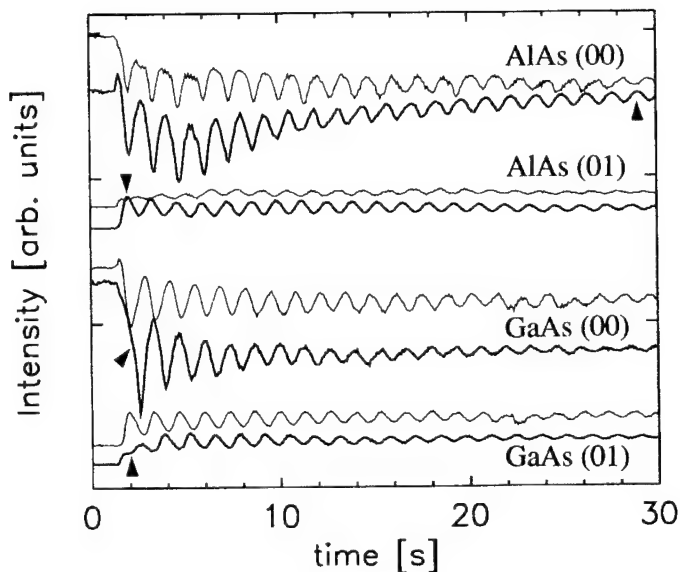


Figure 2: Evolution of the phase shift for the two interfaces on both the (00) and (01) streaks. Homoepitaxial references in green. The saturation distance is very large on the specular spot along  $[\bar{1}10]$ .

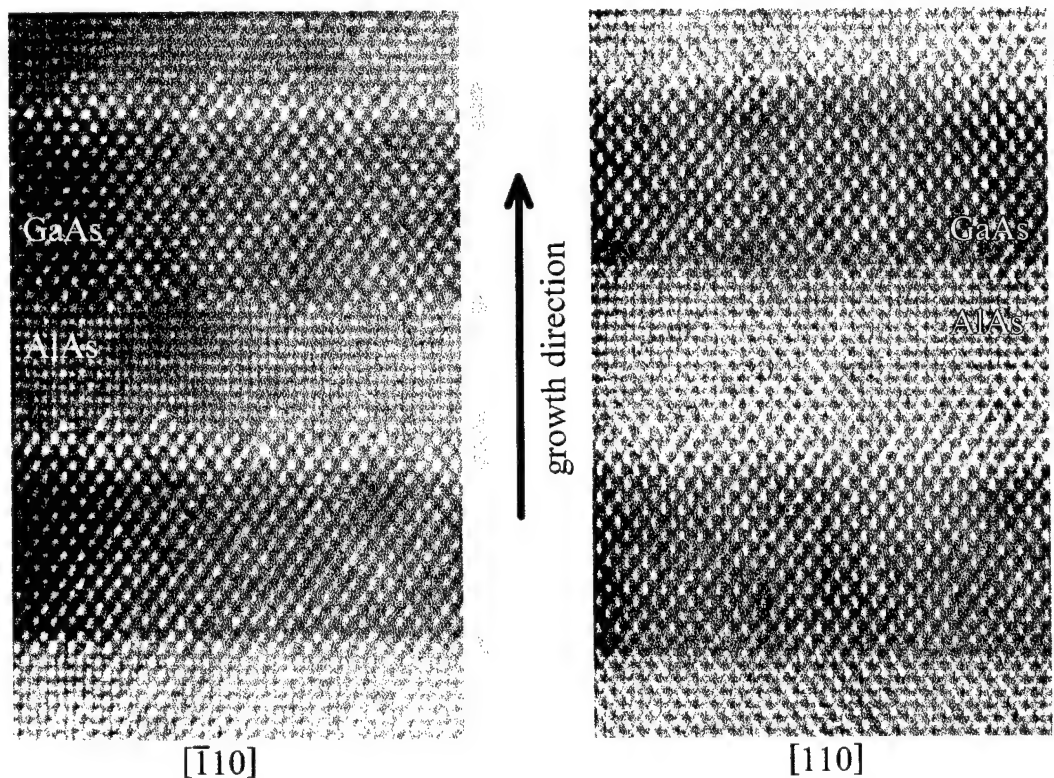


Figure 3: TEM pictures taken along the main directions of the surface anisotropy. The specimen thickness is in the range of 50 to 100 crystal planes. The intermixed regions at the normal interface show as triangular areas of enhanced contrast along  $[\bar{1}10]$ , whereas no lateral structure is resolved along  $[110]$ . The inverted interfaces are abrupt.

# Suppression of AlGaAs/GaAs Superlattice Intermixing by *p*-type Doping

K. Muraki\* and Y. Horikoshi

*NTT Basic Research Laboratories,*

*3-1 Morinosato-Wakamiya, Atsugi, Kanagawa 243-01, Japan*

We have studied the effects of *p*-type doping on the intermixing of Al<sub>0.3</sub>Ga<sub>0.7</sub>As/GaAs superlattices (SLs) where the dopants are introduced during the molecular-beam epitaxy (MBE) growth of the SLs. In contrast to the case of post-growth in-diffusion or implantation of *p*-type dopants, for which striking enhancement of the SL intermixing is reported to occur, we find that *p*-type doping during the growth results in a significant reduction of the SL intermixing during the post-growth annealing, as compared with the undoped case. The results are compared with the case of *n*-type doping, and shown to be explained in terms of the Fermi-level effect.

The samples studied are Al<sub>0.3</sub>Ga<sub>0.7</sub>As/GaAs (10 nm/10 nm) SLs grown by MBE on undoped GaAs (001) substrates at 580 °C. Both *n*- and *p*-doped ([Si], [Be] = 3 × 10<sup>17</sup> and 7 × 10<sup>17</sup> cm<sup>-3</sup>) samples as well as nominally undoped samples are investigated. These SLs were annealed at 800-950 °C for 1 hour in sealed quartz ampoules with or without excess As. The Al-Ga interdiffusion coefficients have been determined from the photoluminescence (PL) peak energy shift of the thermally treated SLs (Fig. 1).

In the As-rich condition (*p*<sub>As4</sub> = 1 atm) neither Si or Be affected the intermixing significantly. On the other hand, striking effects have been found for the Ga-rich conditions (no excess As); the interdiffusion is enhanced by Si, while it is suppressed by Be (Fig. 1, 2). As a result, the effective activation energy for the interdiffusion varies from 2.6 eV for *n* = 3 × 10<sup>17</sup> cm<sup>-3</sup> to 4.0 eV for *p* = 3 × 10<sup>17</sup> cm<sup>-3</sup> (Fig. 2).

The effects of *n*- and *p*-doping on the interdiffusion are found to be symmetric with respect to the intrinsic case (Fig. 3). The dependence of the diffusion coefficient on log(*n*/*n*<sub>i</sub>) (= log(*n*/*p*)), where *n*<sub>i</sub> is the intrinsic carrier concentration, is almost linear in both *n*- and *p*-regions. Hence, the effects of *n*- and *p*-doping are interpreted consistently in terms of the Fermi-level effect. That is, the thermal equilibrium concentration of native defects is thought to be modulated through the Fermi level. Although previous in-diffusion studies suggest doubly-positively-charged Ga interstitials, I<sub>Ga</sub><sup>2+</sup>, as the diffusion vehicle, our results suggest that the column-III diffusion is mediated by acceptor-like defects with single negative charge in the Ga-rich conditions.

---

\* the author to be contacted  
Tel: +81-462-3478 Fax: +81-462-4727 E-mail: muraki@will.brl.ntt.jp

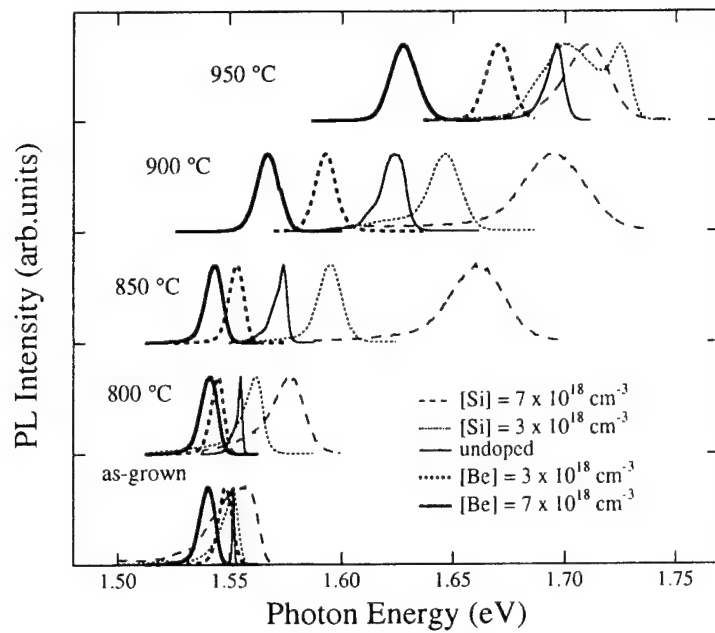


Fig. 1 9-K PL spectra of as-grown and thermally treated SLs with various doping conditions. The intensities are normalized for clarity.

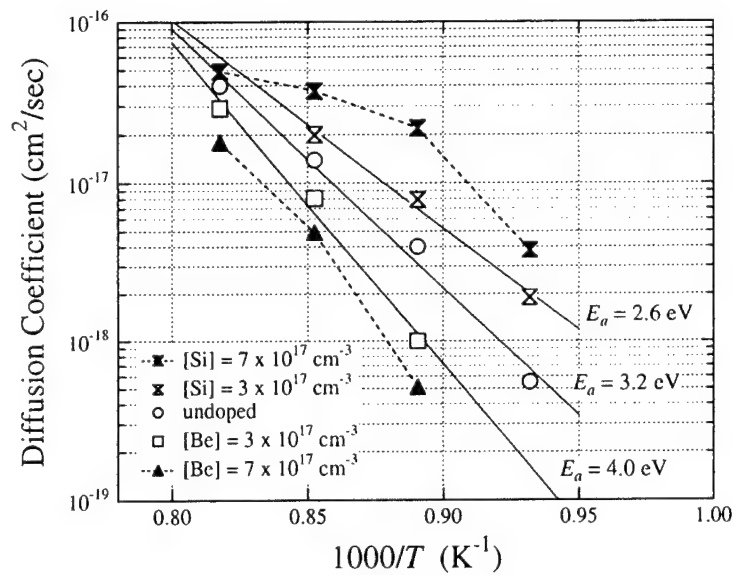


Fig. 2 Al-Ga interdiffusion coefficients for various doping conditions shown as a function of inverse temperature.

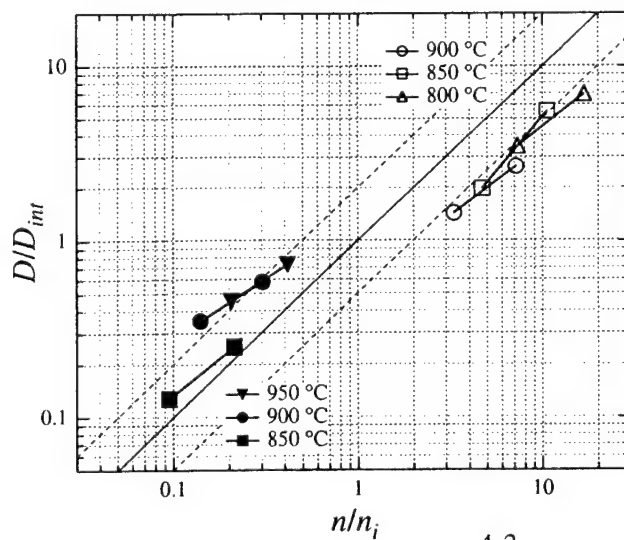


Fig. 3 Diffusion coefficients normalized by the intrinsic values plotted as a function of the normalized electron concentration  $n/n_i$ . The solid and dashed lines are guides to the eye.

## **Iodine assisted Molecular Beam Epitaxy**

M. Micovic<sup>+</sup>, D. Lubychev, W. Z. Cai, F. Flack\*, and D. L. Miller

*Electronic Material and Processing Research Laboratory, Department of Electrical Engineering, The Pennsylvania State University, University Park, Pa 16802 USA*

*\* Department of Physics, The Pennsylvania State University, University Park, Pa 16802, USA*

### **Abstract**

Iodine was introduced into our Solid Source Molecular Beam Epitaxy (MBE) chamber during the growth of bulk GaAs and AlGaAs layers, and strained layer InGaAs quantum wells (QW). Liquid Helium Photoluminescence (PL) spectra of these samples were compared to PL spectra of a series of test samples which were grown in the absence of iodine flux.

The 4.2 K PL spectra suggest that the iodine presence promotes incorporation of carbon into GaAs films, increases the intensity of PL lines obtained from the AlGaAs films by more than a factor of 10, and also increases the ratio between the exciton and shallow impurity PL peaks in AlGaAs by more than an order of magnitude. We have also observed that the PL intensity of the strained layer InGaAs AlGaAs QW structures was reduced when the structures were grown under iodine flux. We have obtained strong room temperature PL from all samples under the 25 W/cm<sup>2</sup> excitation by HeNe laser light including Al<sub>0.2</sub>Ga<sub>0.8</sub>As layers which were grown at the substrate temperature of only 600 C. Room temperature PL intensities of the GaAs and AlGaAs layers grown with iodine flux were higher than intensities of layers grown in the absence of iodine flux. Our results clearly indicate that AlGaAs material quality improves when material is grown in the presence of iodine. These results suggest that Iodine assisted MBE can be used to improve the quality of AlGaAs containing device structures.

<sup>+</sup> *Person to be contacted regarding the abstract: Miroslav Micovic, The Pennsylvania State University, 121 EE East, University Park, Pa 16802, USA, Tel: 814 865 7400, Fax: 814 865 7065, E-mail: miro@ecl.psu.edu*

# **Incorporation of As<sub>2</sub> in InAs<sub>x</sub>P<sub>1-x</sub> grown using valved cracker sources; application to InAs<sub>x</sub>P<sub>1-x</sub>/InP and InAs/InAs<sub>x</sub>P<sub>1-x</sub> quantum well structures**

M.Hopkinson and J.P.R.David

*Department of Electronic and Electrical Engineering, University of Sheffield,  
Mappin Street, Sheffield S1 3JD, UK.*

*Phone: +44 114 2825211 Fax: +44 114 2726391*

*e-mail: m.hopkinson@sheffield.ac.uk*

We report studies on the incorporation of arsenic in InAs<sub>x</sub>P<sub>1-x</sub> layers grown on InP and InAs substrates using solid-source MBE with groupV valved cracker sources. The results are applied to a wide range of strained, strain-balanced and strain-relaxed quantum well (QW) structures which demonstrate excellent optical properties covering the wavelength range 0.9-2.2μm.

The preferential adsorption of arsenic, co-evaporated during the growth of InP under high P<sub>2</sub> overpressure, allows the growth of precise InAs<sub>x</sub>P<sub>1-x</sub> fractions by control over the As<sub>2</sub> flux alone. The effect is fortuitous for solid-source MBE since the control and stability of As<sub>2</sub> from valved cracker sources is often considerably better than that from equivalent P<sub>2</sub> sources. Using a calibrated EPI-500V arsenic valved cracker we have applied this technique to the growth of InAs<sub>x</sub>P<sub>1-x</sub> layers on InP and InAs substrates. Fig.1. shows the relationship between the incident (As/In) ratio and the incorporated arsenic fraction (x) in a series of InAs<sub>x</sub>P<sub>1-x</sub> /InP multi-quantum well (MQW) structures, with (x) determined by post-growth x-ray diffraction. Two regions are observed; for x≤0.4, As<sub>2</sub> is incorporated with near-unity efficiency, whilst for higher x the dependency is increasingly non-linear. We have also investigated the incorporation of As<sub>2</sub> & P<sub>2</sub> in InAs<sub>x</sub>P<sub>1-x</sub> grown on InAs substrates. On InAs we find P<sub>2</sub> is incorporated up to fractions ~0.25, this despite incident (As/In) ratios of close to unity.

A range of InAs<sub>x</sub>P<sub>1-x</sub>/InP strained MQW structures with 0≤x≤0.6 have been grown. Excellent optical and electrical properties are obtained for λ≈1.06 (x~0.28) and 1.3μm (x~0.41) structures. For longer wavelengths strain-balanced MQW's, using In<sub>y</sub>Ga<sub>1-y</sub>P barriers, show significantly better optical and electrical properties. X-ray diffraction and 300K PL data from a range of 10-30 period MQW samples is shown in Figs. 2& 3 respectively. Fig.2. also includes the InAs-based structure, which has thin InAs<sub>x</sub>P<sub>1-x</sub> tensile barriers. The structure is of little interest optically, but its growth provides a useful means to measure (As/P) incorporation on InAs substrates. The data in Fig.3. illustrates the narrow PL linewidths which are achievable in this material system, with typical 300K values <20meV and 10K values ≤5meV.

Graded InAs<sub>x</sub>P<sub>1-x</sub> compositions can be easily grown using valved cracker sources. We have performed preliminary measurements on InAs MQW structures grown on linearly-graded, buffer layers. Our interest is to extend the band gap of InP (or InAs) based structures to λ~2μm. InAs<sub>x</sub>P<sub>1-x</sub> layers are graded to compositions (x) of 0.5-0.75 over thicknesses ~2-3μm. The strain-relaxed InAs<sub>x</sub>P<sub>1-x</sub> then forms the barrier for InAs QW's, allowing thicknesses of up to 80Å to be grown without significant further relaxation. Fig.4. shows 10K PL data from 10 period InAs/InAs<sub>x</sub>P<sub>1-x</sub> (-InP substrate) and InAs/InAs<sub>x</sub>P<sub>1-x</sub> (-InAs substrate).MQW structures. The samples exhibit PL intensities typically 50-100x higher than previously reported InAs/InP structures. PL linewidths are 6-8meV for the InP-based structures and 11meV for the InAs-based structure. The 80Å InAs/InAs<sub>x</sub>P<sub>1-x</sub> (x~0.63) structure exhibits 10K(300K) PL at λ≈2.2(2.4)μm, and represents the longest wavelength we have yet achieved for InP-based materials.

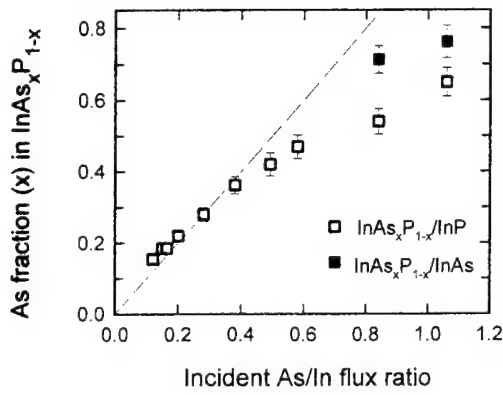


Fig.1: Incorporated As fraction (x) in  $\text{InAs}_x\text{P}_{1-x}$  as a function of incident flux ratio

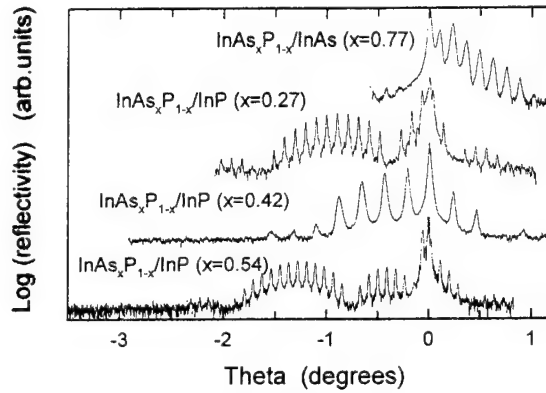


Fig.2: x-ray diffraction data from  $\text{InAs}_x\text{P}_{1-x}/\text{InP}$  and  $\text{InAs}_x\text{P}_{1-x}/\text{InAs}$  multi-quantum well structures

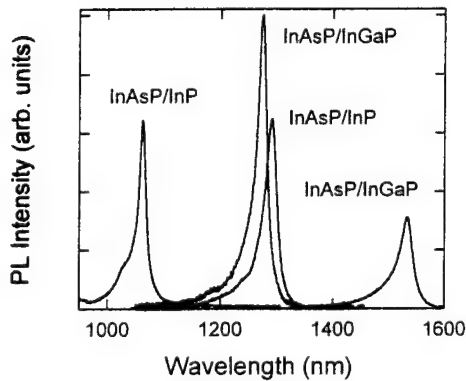


Fig.3: Room temperature photoluminescence data for  $\text{InAsP}/\text{In}(\text{Ga})\text{P}$  MQW structures with  $\lambda \sim 1.06, 1.3$  &  $1.55 \mu\text{m}$ . The PL linewidths are in the range 15-20 meV.

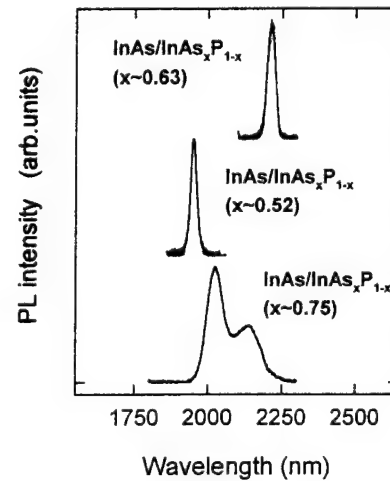


Fig.4: 10K PL of  $\text{InAs}/\text{InAs}_x\text{P}_{1-x}$  multi-quantum well structures grown using linearly-graded  $\text{InAs}_x\text{P}_{1-x}$  buffer layers on InP and InAs substrates.

# Contamination in Molecular Beam Epitaxy: the Role of Arsenic Drag Effect

Z. R. Wasilewski and S. J. Rolfe

*Institute for Microstructural Sciences, National Research Council of Canada,  
Montreal Road, Ottawa, ON K1A 0R6, Canada  
tel. (613) 990 4557, fax.(613) 941 4667, e-mail:Zbig.Wasilewski@nrc.ca*

R. A. Wilson

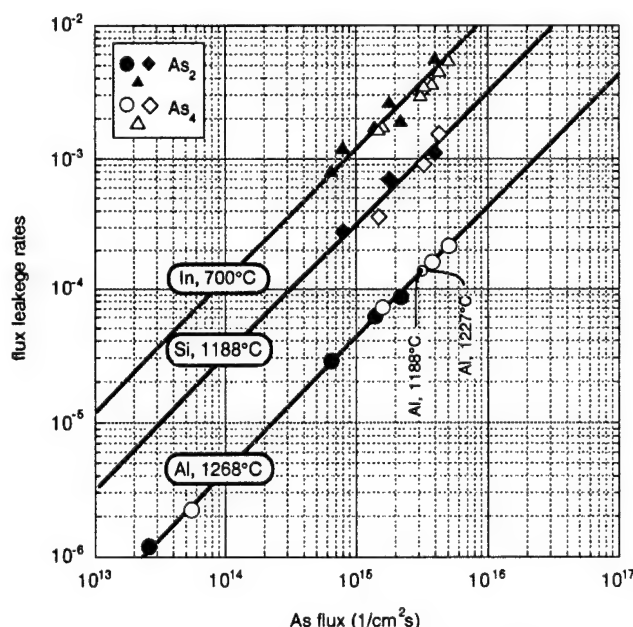
*Laboratory for Physical Sciences, University of Maryland,  
College Park MD 20740, USA*

Much progress has been made in the field of purification of elements used for Molecular Beam Epitaxy with the result that in many areas quality of sources available on the market is no longer the limiting factor. In spite of that, large gaps still exist between the quality of the best and "typical" layers grown in any given class. In order to bridge this gap, a better understanding of the remaining factors is needed in areas such as MBE system design, its preparation and growth procedures.

In the present work we examine a contamination source which for the past four years has been controversial, namely unintentional doping with elements from idling effusion cells. Proposed mechanisms ranged from suboxide transport<sup>1</sup> to direct re-evaporation from coated shutters and inadequately cooled cell ports.<sup>2</sup> Although plausible under some circumstances, none of the proposed mechanisms explains the growing evidence that such contamination is quite common, even in the absence of either of the conditions considered. We demonstrate that this contamination is linked to the direct interaction between molecular beams traversing the chamber, a process which has been regarded so far as negligible in the typical MBE environment.

We measured levels of Al, In and Si in nominally pure GaAs layers grown in our modified V80H MBE system, as a function of  $\text{As}_2$  or  $\text{As}_4$  flux for a number of temperatures of Al, In and Si cells. We find that the number of atoms arriving at the wafers surface in spite of closed shutters is proportional to the arsenic flux used (see figure) and to the equilibrium vapor pressure over the considered element. We present arguments for the existence of the "arsenic drag" effect that deflects a fraction of atoms that bypassed their effusion cell shutter towards the wafer. This mechanism explains not only the undesired doping or alloying of the layer, but also the often observed and so far elusive cross-contamination of sources and memory effects. These problems are best taken care of by proper MBE system

design. However, with existing systems most of the negative consequences can be avoided by altering certain growth procedures and simple modification of the flux



Flux leakage rate is defined here as the ratio of the flux incident on the wafer with the cell shutter closed to the nominal flux with the cell shutter open. It has intuitive meaning of the "effective transparency of the shutter."

blocking structures adjacent to the cell ports. Indeed, realizing the mechanism of this contamination helped us considerably to sustain an excellent quality of layers grown in our system as demonstrated by peak mobilities for 2D electron gases of  $6,400,000 \text{ cm}^2/\text{Vs}$ ,<sup>3</sup> and record low threshold currents of  $44 \text{ A/cm}^2$  for our 980nm strained GaAs/InGaAs quantum well lasers.<sup>4</sup>

<sup>1</sup> C. E. C. Wood and R. A. Wilson, *J. Vac. Sci. Technol. B* **11**, pp.1036-1040 (1993).

<sup>2</sup> A. J. SpringThorpe, W. T. Moore, A. Majeed, and R. W. Streater, *J. Vac. Sci. Technol. B* **11**, pp.1275-1280 (1993).

<sup>3</sup> P. T. Coleridge, Z. R. Wasilewski, and P. Zawadzki, *15th North American Conference on Molecular Beam Epitaxy*, University of Maryland, USA, 1995 (American Vacuum Society).

<sup>4</sup> M. Dion, Z. R. Wasilewski, F. Chatenoud, and R. L. Williams, *7th Canadian Semiconductor Technology Conference*, Ottawa, Canada, 1995 (Canadian Journal of Physics).



## **A CELL FOR CARBON ATOMS DEPOSITION PRODUCING NO CARBON CLUSTERS.**

N.R.Gall, E.V.Rut'kov, A.Ya.Tontegode, P.B.Kuznetsov(\*), R.N.Gall(\*)

A.F.Ioffe Physico-Teshnical Institute RAS,

26, Polytechnicheskaya str., St.Petersburg , 194223, Russia

(\*) CADIX(R),Ltd., St.Petersburg, 195053, P.O.BOX 576, Russia

Tel: (007)812.2134406 Fax: (007)812.2135835 E-mail: pavel@cadix.spb.su

The UHV ( $p=10^{-10}$  Torr) source of the carbon atoms beam containing no carbon clusters (SBCA) has been developed, constructed, produced and tested. The SBCA is a tool designed to be built in scientific and technological UHV units. It consists of a getter of carbon atoms, from which they release under annealing, and a regenerator unit used periodically to replenish a stock of initial carbon in the getter. A density of carbon beam on the 20mm distance from the source is  $10^{11} - 10^{13}$  at/cm<sup>2</sup>\*sec, its nonhomogeneity on the area of 5\*25mm<sup>2</sup> is 10%. Purity of the beam was tested by means of mass-spectrometry. The tests showed less than 0.1% of foreign atoms and less than 0.01% of carbon clusters in the beam. Such purity characteristics make possible to use the SBCA in the MBE technology.

The presented device (method) has obvious advantages over the existing methods of the carbon deposition. For example, thermal evaporation of graphite performs up to 70% of carbon clusters in the total volume of produced carbon. Usage of plasma methods is accompanied by huge percentage of foreign atomic particles. Both cause serious difficulties when being applied to the processes of SiC and diamond films growing.

The SBCA was tested in growing of ultrathin SiC films on metal substrates. It appears that in atomic form carbon is much more reactive than in cluster (C<sub>2</sub>, C<sub>3</sub>,...) one and its utilisation permits to grow SiC films on (10-10) Re at T=400-600°K. It seems to be very promising in diamond, diamondlike and silicon carbide films growing using MBE technology.

## Sensor Controlled Linear Motion Oven (S-LIMO) for Precision Group III Flux Operation

P. P. Chow<sup>1\*</sup>, K. Evans<sup>2</sup>, and A. J. SpringThorpe<sup>3</sup>

1.SVT Associates, 7620 Executive Drive, Eden Prairie, MN 55344

2.WL/ELR, Wright Laboratory, WPAFB, Ohio 45433-7323

3.Bell-Northern Research, 5C14, Ontario K1Y 4H7, Canada

In solid source MBE the source is usually maintained at a very stable temperature to supply a constant beam flux for the growth process. When composition change is desired the growth process must be interrupted for the cell temperature to reach a new set point. The response of the source however is often slow, and the flux change can not be made smoothly and reproducibly. There are many bandgap-engineered devices that require composition or dopant changes, therefore precise control of layer profiles is important to key MBE applications. For example, continuously graded index confinement layers have been suggested to reduce conductance in a Vertical Cavity Surface Emitting Laser (VCSEL). A suitable means to achieve smooth group III flux variation is to employ the Linear Motion Oven (LIMO) concept(Ref.1). The source is coupled to a linear motion feedthrough to vary the source to substrate distance. As a result the flux and thus the composition can be varied by moving the source. In addition the flux transient can be eliminated by moving the source to avoid thermal perturbation due to the shutter action.

In the latest operation of the LIMO source we have incorporated a novel Atomic Absorption (AA) beam sensing technique, so that flux can be accurately measured and adjusted in real time; long term drift may also be corrected. Layer composition can then be controlled by taking into account the ratio of the beam fluxes. The growth was also monitored with surface sensitive optical interferometric (PI) (Ref.2) measurement that correlates well with post-growth characterization.

A PI measurement of a sample structure consisting of 5 parabolic  $\text{Al}_{0.5}\text{Ga}_{0.5}\text{As}$  quantum wells, each 15 nm thick, sandwiched between 50 nm thick  $\text{Al}_{0.3}\text{Ga}_{0.7}\text{As}$  barriers is illustrated in Fig. 1. The sample was grown with an Al LIMO and a regular Ga source. The five vertical markers highlighted the well regions. The upper trace indicated the substrate temperature variation due to heating from the Al source as its position was changed. The lower trace is the reflected signal from a normal incidence 980 nm LED whose slope changed at each individual layer as a result of the difference in layer composition. Figure 2 displays the SIMS profiling result of the sample revealing the very reproducible Al content variation in the sample.

\*Ph:(612)941-1898, Fax:(612)934-2737, chowx005@tc.umn.edu

Ref.(1). C.R. Jones, D.L. Beasley, E.N. Taylor, K.R. Evans, and J.S. Solomon, JVST B13(1995)739.

Ref.(2).F.G. Böbel, H. Möller, A. Wowchak, B. Hertl, J. Van Hove, L.A. Chow and P.P. Chow, JVST B12(1994)1207.

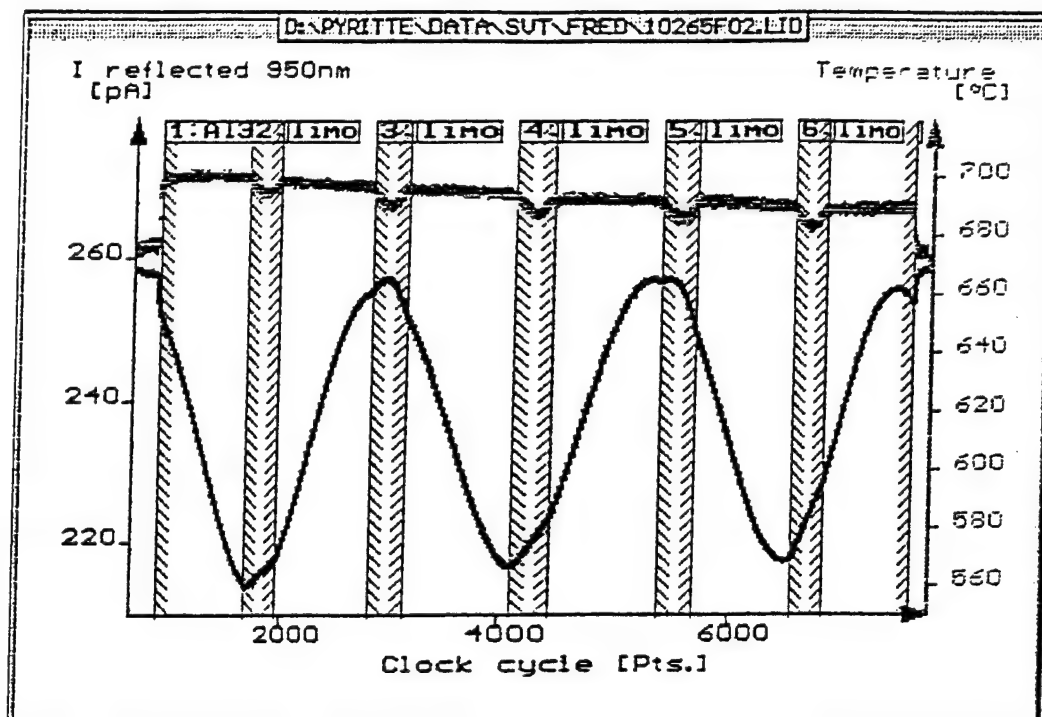


Figure 1. Pyrometric Interferometry real time monitoring of the temperature and the layer thickness of the 5 parabolic AlGaAs well sample.

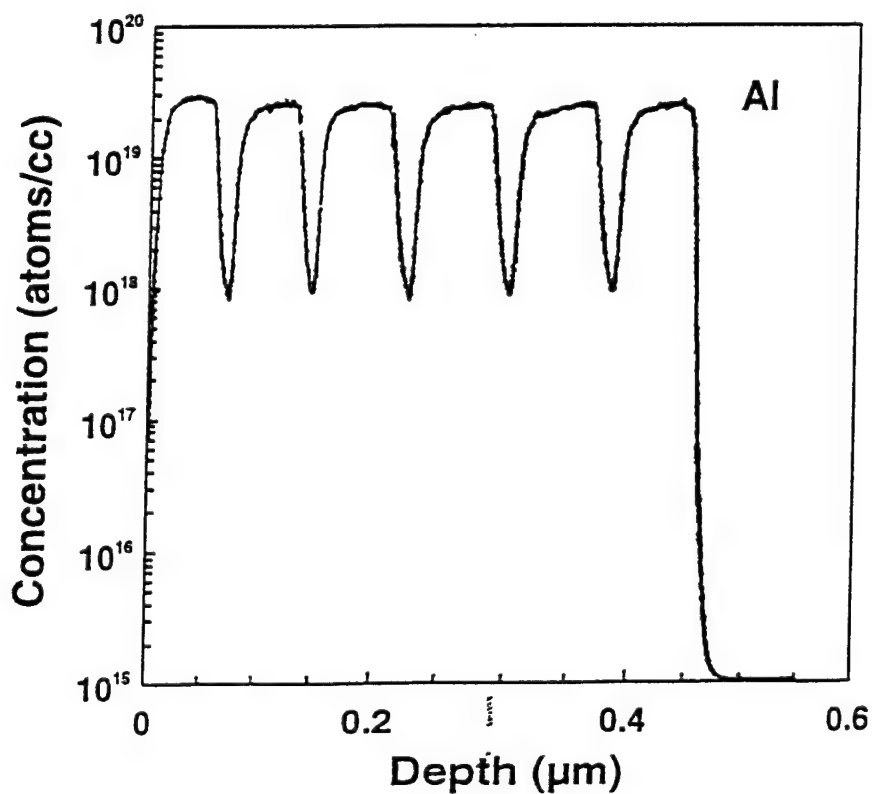


Figure 2. SIMS depth profiling of the parabolic AlGaAs well structure.

## 5. II-VI MATERIALS

TUESDAY MORNING (ELKINS)

Session chair: Owen Wu, Hughes Research Laboratories, Malibu, California

Co-Chair: Leslie Kolodziejski, Massachusetts Institute of Technology

- 09:00 5.1 **The fabrication of II-VI light emitting devices based on Be compounds**  
(Invited) F. Fischer, H.J. Lugauer, Th. Litz, J. Laubender, A. Weigärtner, Th. Gergard,  
U. Zehnder, W. Ossau, U. Lunz, A. Waag, G. Landwehr  
Physikalisches Institut, Würzburg, Germany.
- 09:30 5.2 **MBE growth of high quality lattice-matched ZnCdMgSe quaternaries on InP substrates**, L. Leng, A. Cavus, B.X. Yang, N. Dai, F. Naz, M.C. Tamargo, Y. Guo, G. Ayzin, Y.C. Chen, N. Bambha, A. Gray, and F. Semendy  
City College of New York, USA.
- 09:50 5.3 **Surface preparation of ZnSe substrates for MBE growth of II-VI light emitters**, W.C. Hughes, C. Boney, M.A.L. Johnson, J.W. Cook, Jr., J.F. Schetzina, and F.A. Ponce, North Carolina State University, USA.
- 10:10 5.4 **Reduction of extended defects in II-VI blue green laser diodes**  
T.B. Ng, C.-C. Chu, G.C. Hua, J. Han, R.L. Gunshor, E. Ho, E.L. Warlick, L.A. Kolodziejski, and A.V. Nurmikko  
Purdue University, USA.
- Break
- 10:50 5.5 **Highly improved quality of lattice-matched ZnCdSe on InP substrates: use of III-V buffer layers and doping**  
A. Cavus, B.X. Yang, L. Zeng, M. Wright, B. Schewareged, M.C. Tamargo, City College of New York, USA, E. Snoeks and L. Zhao, Philips Laboratories, New York, USA.
- 11:10 5.6 **Reducing the defect density in MBE-ZnSe/III-V heterostructures**  
E.L. Warlick, J.L. House, E. Ho, G.S. Petrich, and L.A. Kolodziejski  
Massachusetts Institute of Technology, USA.
- 11:30 5.7 **Arsenic incorporation in MBE-HgCdTe layers using planar doping approach**, F. Aqariden, P.S. Wijewarnasiriya, C. Grein, J.P. Faurie, and S. Sivananthan, University of Illinois at Chicago, USA.
- 11:50 5.8 **High performance two-color infrared photodetectors grown by molecular beam epitaxy**, R.D. Rajavel, D.M. Jamba, O.K. Wu, J.E. Jensen, J.A. Wilson, E.A. Patten, K. Kosai, P. Goetz, B. Baumgratz, G.R. Chapman, and W.A. Radford  
Hughes Research Laboratories, Malibu, CA, USA

# **The Fabrication of II-VI Light Emitting Devices Based on Be-Compounds**

F.Fischer, H.J.Lugauer, Th.Litz, J.Laubender, A.Weingärtner, Th.Gerhard, U.Zehnder, W.Ossau,  
U.Lunz, A.Waag, G.Landwehr  
Physikalisches Institut, Am Hubland, 97074 Wuerzburg, Germany

Light emitters and detectors for green, blue and near ultraviolet light are of great interest, e.g. for applications in the field of information technology, display technology or medicine. Several semiconductor materials are under investigation, which are candidates for the realization of such laser diodes and LEDs. Laser diodes based on ZnSe and GaN have been demonstrated. The electrical and optical properties of the best II-VI lasers seem to be sufficient for commercial application, but not their long term stability. The device lifetimes, e.g. of blue-green laser diodes are still restricted to 100 hours under cw excitation at room temperature. The degradation is usually attributed to the motion of extended defects along with the formation of dark line defects and their impact on the device characteristics.

Recently, investigations on Be-chalcogenides as a novel class of II-VI semiconductors indicated new possibilities for the design of optoelectronic devices. The incorporation of Be modifies mechanical properties of the mixed crystals, e.g. the critical layer thickness or the microhardness, leading to an improvement of the crystalline quality. Additionally, the use of ZnSe and BeTe provides the possibility to form strained layer superlattices in order to retard the motion of threading dislocations. Moreover, the covalent character of the Be-X bonding (X: S, Se or Te) might influence the dopability of this class of semiconductors, leading to a reduction of compensation effects. Finally, the Be-chalcogenides (BeMgZn)(TeSe) can be considered for band gap engineering of alternative heterostructures fully lattice matched to GaAs substrates.

In our contribution the properties of Be-compounds are discussed with regard to their use in light emitting devices like LEDs and laser diodes. We present results from optical and electrical measurements on BeMgZnSe diodes grown by MBE. Blue and green LEDs were fabricated with peak wavelengths of the electroluminescence between 450 nm and 540 nm at room temperature. The long term stability of these structures turned out to be surprisingly high, e.g. several thousands of hours, even at high current densities. We will discuss electrical transport behaviour of the devices, focussing on the role of BeTe and BeTe/ZnSe superlattices at the II-VI/III-V interface. The properties of BeTe/ZnSe superlattice contacts schemes to p-type ZnSe will also be addressed.

Corresponding author:

Frank Fischer  
Physikalisches Institut, Uni Wuerzburg, Germany  
Am Hubland  
97074 Wuerzburg

Tel.: ++ 49 (0)931 - 888 5757  
FAX: ++ 49 (0)931 - 888 5142

e-mail: [fischer@physik.uni-wuerzburg.de](mailto:fischer@physik.uni-wuerzburg.de)

# MBE GROWTH OF HIGH QUALITY LATTICE-MATCHED ZnCdMgSe QUATERNARIES ON InP SUBSTRATES

L. ZENG, A. CAVUS, B.X. YANG, N. DAI, F. NAZ, M. C. TAMARGO  
*CUNY Center for Advanced Technology (CAT) on Photonic Materials and Applications*  
*Center for Analysis of Structures and Interfaces (CASI) and Department of Chemistry,*  
City College-CUNY, New York, NY 10031

Y. GUO, G. AYZIN and Y.C.CHEN  
*CUNY Center for Advanced Technology (CAT) on Photonic Materials and Applications*  
*and Department of Physics, Hunter College-CUNY, New York, NY 10021*

N. BAMBHA, A. GRAY and F. SEMENDY  
*IR Optical Technology OFS, Army Research Laboratory, Fort Belvoir, VA 22060*

We have recently reported<sup>1</sup> the growth and properties of a new materials system, ZnCdMgSe, that can be used in the design and fabrication of blue (visible) semiconductor lasers. By growing these on InP substrates, entirely lattice-matched heterostructures can be obtained. These lattice-matched quaternaries encompass a wide range of bandgaps, from 2.18 eV to above 3.5 eV, enabling the growth of device structures that emit in a large segment of the visible range, useful for the design of high performance semiconductor lasers.

In this paper, we report the MBE growth conditions and properties for high quality lattice-matched ZnCdMgSe quaternaries of a wide range of compositions. The main results are:

1). For a given Cd/Zn flux ratio (keeping Zn flux constant) we can control the bandgap and lattice mismatch by varying the Mg flux. From our study we can predict the best conditions for the growth of different bandgap quaternaries that are lattice-matched ( $|\Delta a/a| < .2\%$ ) to InP substrate. We find that: For Cd/Zn = 2 (the condition for ZnCdSe lattice-matched to InP) changing the Mg flux does not affect the mismatch very much, but the mismatch is always greater than 0 and the layers tend to have spotty RHEED patterns. To obtain lattice-matched quaternaries we must reduce the Cd/Zn ratio: as the bandgap of the lattice-matched quaternary increases, one must lower the Cd/Zn ratio further.

2). Combining the X-ray and PL data, we can calculate the Mg composition of our quaternaries. We find that the PL full width at half maximum (FWHM) increases with increasing Mg composition. When the Mg composition is 0.4, the FWHM at 10 K is about 50 meV which represents a very significant improvement relative to the best reported data<sup>2</sup> of 100 meV for quaternaries of the same Mg composition.

3). With the optimal growth conditions and with the incorporation of a III-V buffer layer, we have grown the best quality ZnCdMgSe having double crystal x-ray rocking curve FWHM about 120 arcsec for a bandgap of 2.8 eV. Low temperature PL data show that the quaternaries have very strong bandedge photoluminescence peaks without any significant deep-level emission.

Using ZnCdSe as the quantum well and ZnCdMgSe as cladding and barrier layers, we have grown several separate confinement heterostructures, lattice-matched to the InP substrates which exhibit optically pumped stimulated emission at room temperature.

1. M. C. TAMARGO, et. al. *J Elect. Mat.* 25, 259(1996)

2. T. MORITA, et. al. *J Elect. Mat.* 25, 425(1996)

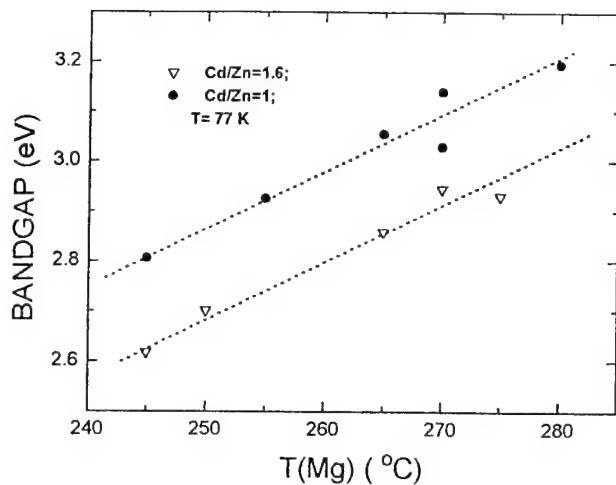


Fig.1. Bandgap of ZnCdMgSe quaternaries versus Mg Flux for two different Cd/Zn ratios ( Keeping Zn flux as  $2.0 \times 10^{-7}$  Torr).

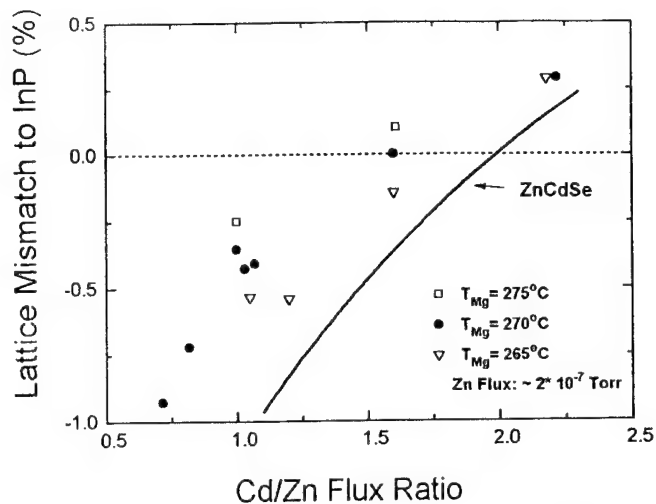


Fig.2. Lattice Constant Dependence on Cd/Zn Flux Ratio

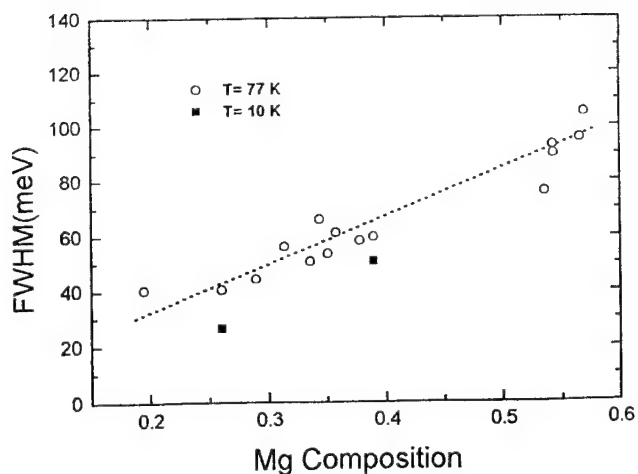


Fig.3. The PL full width at half maximum (FWHM) versus the calculated Mg compositions.

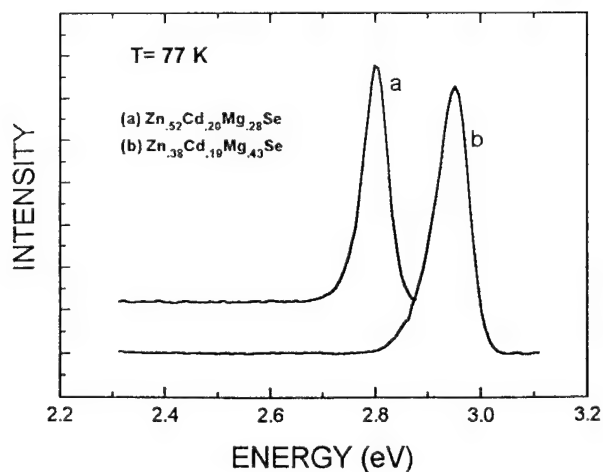


Fig.4. Low temperature PL spectra for two ZnCdMgSe quaternaries.

## Surface Preparation of ZnSe Substrates for MBE Growth of II-VI Light Emitters

W.C. Hughes, C. Boney, M.A.L. Johnson, J.W. Cook, Jr., and J.F. Schetzina  
Department of Physics, North Carolina State University, Raleigh, NC 27695-8202

F.A. Ponce  
Xerox Palo Alto Research Center, Palo Alto, California 94304

The quality of ZnSe-based heterostructures grown on GaAs substrates is presently limited by the density of defects, particularly twins, that originate at the substrate-epilayer interface. To avoid these unwanted defects, we have focused on developing II-VI light-emitting diode and laser diode structures using high-quality, bulk ZnSe substrates supplied by Eagle-Picher Industries. While the use of ZnSe substrates eliminates many of the problems associated with lattice mismatch, defects still form during nucleation of an epitaxial layer because of surface roughness, surface contamination, and surface defects. At NCSU, we have employed a variety of wet chemical etches, vacuum anneals, plasma treatments, and other procedures in an attempt to improve the ZnSe substrate surface prior to MBE film growth. Processed ZnSe surfaces were evaluated by RHEED, Auger electron spectroscopy, SEM/TEM studies, and etch-pit density counts. These studies revealed that nearly all of the wet etches employed left large amounts of carbon and in some cases oxygen and chlorine, on the ZnSe surface. In addition, some of the etchants such as bromine/methanol left the surface roughened and unusable, even when hydroplane-polishing techniques developed originally for preparing very high quality CdTe and CdZnTe substrate surfaces, were employed. Vacuum annealing of ZnSe produced a noticeable improvement in the RHEED patterns observed, but films grown on substrates treated only with this anneal showed evidence of poor film nucleation and large densities of defects, principally twins, in the epilayer. We have also systematically subjected the surface of selected ZnSe substrates to plasma etches. Auger spectra of hydrogen-plasma-etched ZnSe show that carbon and chlorine contamination can be eliminated and oxygen minimized by proper use of this etchant, and RHEED patterns from these surfaces are streaky, denoting 2-dimensional surfaces. However, ZnSe films and devices grown on hydrogen-cleaned ZnSe surfaces showed larger twin densities and poorer device performance than those grown on ZnSe substrates which were only subject to thermal annealing. We speculate that hydrogen-terminated ZnSe is very reactive to a flux of Se, Te, or S such that hydrogen compounds may be formed. In contrast, Cl-based plasma etchants produce smooth ZnSe surfaces with minimum surface defects. Under proper conditions, we have used plasma etchants to prepare ZnSe substrate surfaces with minimum defect densities (less than  $10^4$  per  $\text{cm}^2$ ). High-brightness blue LEDs (1.7 mW at 10 mA), green LEDs (6.9 mW at 10 mA), and blue/green laser diodes operating at room temperature have been successfully synthesized and tested using properly-prepared ZnSe substrates. Issues related to MBE growth of quaternary II-VI materials will also be discussed.

Work supported by grants from ARO, ONR, DARPA, and by Eagle-Picher Industries.



## **Reduction of Extended Defects in II-VI Blue Green Laser Diodes**

T-B. Ng, C-C. Chu, G.C. Hua, J. Han, and R. L. Gunshor

School of Electrical and Computer Engineering, Purdue University, West Lafayette, IN 47907

E. Ho, E.L. Warlick, and L.A. Kolodziejski

Department of Electrical Engineering and Computer Science, MIT, Boston, MA 02139

A.V. Nurmikko

Division of Engineering and Department of Physics, Brown University, Providence, RI 02912

Early blue/green laser diodes based on ZnSe exhibited room temperature lifetimes of the order of a minute. Similar to the history of (Al,Ga)As lasers, the source of the degradation was the presence of extended crystalline defects. Complexes of defects consisting of stacking faults, which are nucleated at or near the II-VI/GaAs interface, and associated threading dislocations, are the most commonly observed extended defects present throughout the separate confinement heterostructure (SCH) laser structures. Plan-view TEM imaging of the degraded lasers identified the degradation as originating from patches of dislocation networks developed at the quantum-well region during lasing. The dislocation networks appeared to be nucleated at threading dislocations originated from stacking faults. The early room temperature cw lasers exhibited defect densities of the order of  $10^6 \text{ cm}^{-2}$ . Currently, laser diodes with CW lifetimes between 1 to 3 hours are reported to generally have a defect density of between  $5 \times 10^4$  to  $1 \times 10^5 \text{ cm}^{-2}$ . Since TEM studies have shown the extended defects to be nucleated at or near the ZnSe/GaAs interface, a systematic study of test structures consisting of a ZnSe nucleation followed by a 1 or 2  $\mu\text{m}$  of ZnSSe test epilayers were used to explore means to minimize extended defects. The same nucleation techniques were then employed for the growth of laser structures. For the test structures, the density of extended defects soon moved below the ability to accurately apply plan view TEM imaging, and etch pit counts became the primary evaluation procedure. (In the case of laser structures, cathodoluminescence served as an independent confirmation.)

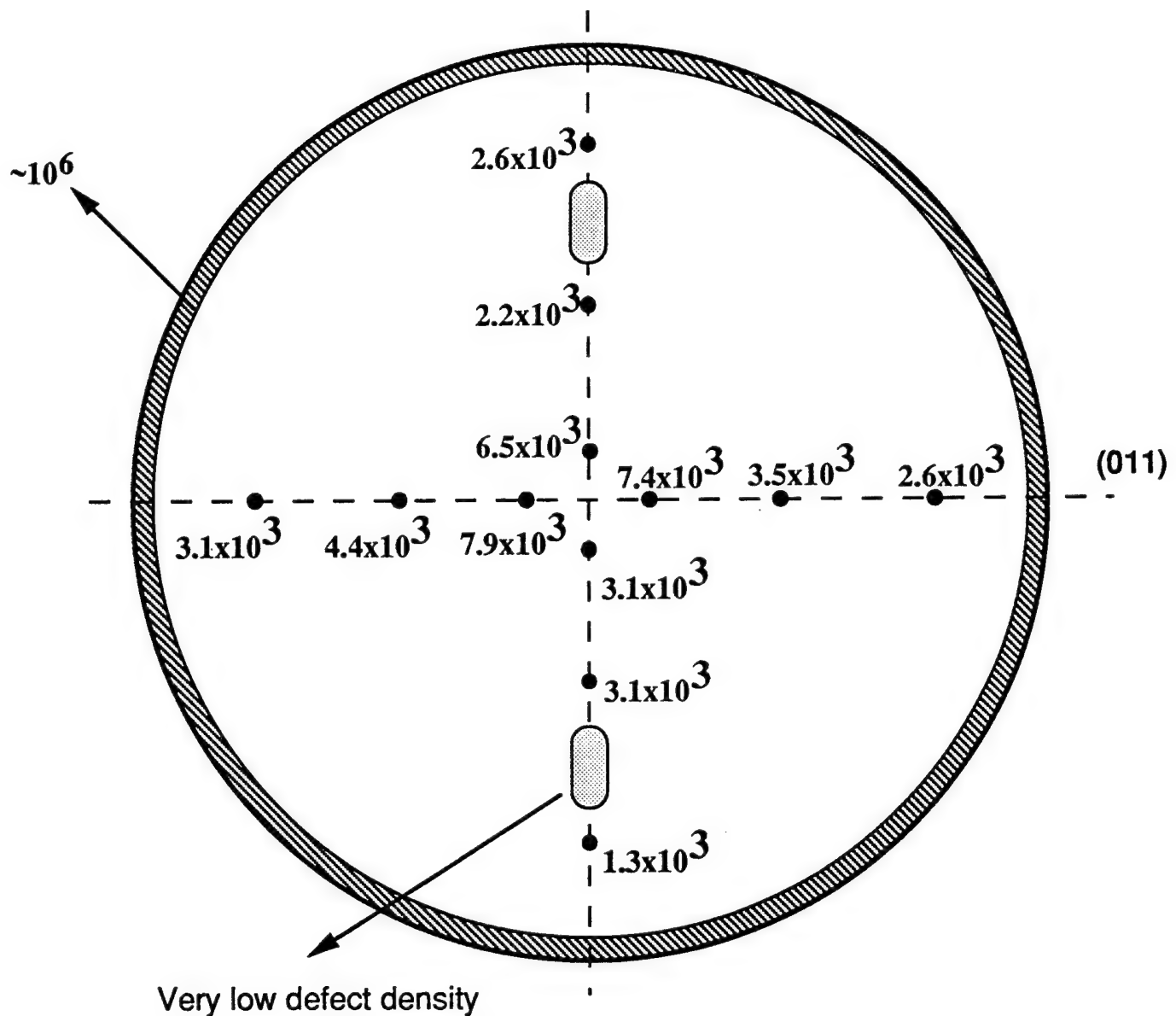
Here we report an investigation of ZnSe/GaAs heterovalent nucleation and show that the 2-D growth mode of ZnSe on GaAs could be facilitated by the use of the MEE technique (Gaines et al., 1993), and this technique was used as one step to achieve the defect reduction described in this paper. Influence from extrinsic factors such as GaAs wafer handling as well as the stoichiometry and morphology of homoepitaxial GaAs buffer layers will be discussed. The means for a consistent reduction in the density of the extended defects into the mid to low  $10^3 \text{ cm}^{-2}$  range over a significant portion of a 3-inch wafer (see attached figure) will be presented.

\*Research was supported by DARPA/ONR URI, AFOSR, and NSF/MRG.

**Corresponding Author:** R. L. Gunshor, PH: 317-494-3509, FAX: 317-494-2706,  
gunshor@ecn.purdue.edu

# EPD ( $1/\text{cm}^2$ ) over a whole 3-inch wafer

Zn-irradiation + MEE on c(4x4) GaAs surface



Counting window :  $550 \mu\text{m} \times 400 \mu\text{m}$

91ZSS260-5

## Highly Improved Quality of Lattice-Matched ZnCdSe on InP Substrates: Use of III-V Buffer Layers and Doping

A. Cavus, B.X. Yang, L. Zeng, M. Wright, B. Shewareged and M.C. Tamargo  
*CUNY Center for Advanced Technology on Photonic Materials and Applications  
Center for Analysis of Structures and Interfaces (CASI) and Department of Chemistry,  
City College-CUNY, NY 10031*

and

E. Snoeks and L. Zhao  
*Philips Laboratories, Briarcliff Manor, NY 10510*

Recently, we proposed a new family of II-VI alloys, ZnCd(Mg)Se that are completely lattice-matched to InP with their band gaps ranging from yellow to blue, being very promising in visible laser applications. We have successfully grown these materials by MBE directly on the InP substrate. The ZnCd(Mg)Se quality was shown to be very sensitive to the initial InP substrate surface, which largely depended on the thermal deoxidation. To obtain two dimensional nucleation, an initial low temperature growth was used. However, the control of the interface remains an essential issue to obtain reliable and reproducible materials. In this paper, we report the details of the initiation of the II-VI layer growth and remarkable improvement of ZnCdSe ternary quality obtained by using InGaAs or InP as buffer layers. We also report on the n-type doping with chlorine of these lattice-matched layers.

ZnCdSe was grown on InP substrates and on InGaAs or InP buffer layers. Growth was initiated either at 170 C or at the typical growth temperature of 270 C. The VI/II flux ratio was  $\sim 4$  and growth rates were  $\sim 1$  micron/hour. The buffer layers were grown in a III-V MBE chamber that is connected by UHV modules with the II-VI chamber. The sources for both III-V and II-VI growth were elemental sources except for polycrystalline InP used as phosphorus source. Both InGaAs and InP buffer layers were grown under standard III-V growth conditions. The thicknesses were about 500-700 Å. The RHEED patterns were streaky ( $2 \times 4$ ) before the start of ZnCdSe growth.

Very sharp and intense bandedge photoluminescence (PL) peaks were obtained in micron thick ZnCdSe layers with either InGaAs or InP buffer layers. The PL full width at half maximum (FWHM) was 4 meV at 10 K, compared to our best result of 8 meV without the buffer layer. The PL intensities of samples with buffer layers were reproducible and generally stronger than those without a buffer layer, grown under the same conditions. TEM results show that the density of stacking faults is reduced by about 2 orders of magnitude by using buffer layers. X-ray diffraction measurements showed that the FWHM of double crystal rocking curves was reduced to about 60 arcsec (the lowest value reported so far for ZnCdSe), compared with  $\sim 300$  arcsec without buffer layers. Similar improvements were obtained for ZnCdMgSe quaternaries grown with III-V buffer layers. Contrary to our results of growth directly on InP substrates, we find that, when we grow on InGaAs or InP buffer layers 2-dimensional nucleation is achieved immediately even when growth is started at high temperature (270 °C), as evident from RHEED. This suggests that the chemical differences between phosphides and arsenides are less pronounced when a smooth, high quality epitaxial surface is provided for the growth.

Carrier concentrations as high as  $2 \times 10^{18}$  carriers/cm<sup>2</sup>, with mobilities of 205 cm<sup>2</sup>/Vsec at 300K were achieved in doped ZnCdSe layers using a ZnCl<sub>2</sub> source. Photoluminescence spectra (at 77K) of the doped layers show a gradual increase of the bandedge emission linewidth with increased doping. No deep level emission was observed.

Contact: Maria C. Tamargo, Phone: (212)650-6147, Fax: (212)650-6848. E-mail: tamar@scisun.sci.ccny.cuny.edu

## **Reducing the Defect Density in MBE-ZnSe/III-V Heterostructures**

E. L. Warlick, J. L. House, E. Ho, G. S. Petrich and L. A. Kolodziejski

Research Laboratory of Electronics  
Department of Electrical Engineering and Computer Science  
Massachusetts Institute of Technology, Cambridge, MA 02139

The state-of-the-art ZnSe-based injection laser diodes that have been demonstrated to date are primarily pseudomorphic structures grown on GaAs substrates with GaAs epitaxial buffer layers. Recent electrical degradation studies have led to a growing consensus that defects arising from the ZnSe/GaAs interface presently play the limiting role in the lifetime performance of these devices. Various reports have also suggested that different nucleation procedures can lead to significant changes in the structural properties of the ZnSe overlayer. In this study, we have examined the effects of the GaAs surface reconstruction and the use of Zn or Se pre-exposure prior to growth on the resultant defect densities observed in 1  $\mu\text{m}$  ZnSe films grown by molecular beam epitaxy. Cathodoluminescence imaging of the II-VI/III-V interface has been used to provide a rapid and non-destructive method to characterize the defect densities and was found to be in agreement with both etch pit density and transmission electron microscopy characterizations. Films grown without special nucleation precautions on c(4x4) GaAs were typically found to result in defect densities  $>10^6 \text{ cm}^{-2}$ . Using Zn pre-exposure on (2x4) reconstructed GaAs, the defect densities were found to be decreased by over an order of magnitude. Note that these 1  $\mu\text{m}$  layers of ZnSe are relaxed and lattice-mismatched (0.27%) from the GaAs.

In order to examine the role of lattice-mismatch on the ZnSe defect density, we have also studied ZnSe grown on lattice-matched novel buffer layers of (In,Ga,Al)P on GaAs substrates. These relaxed buffer layers, each with 4  $\mu\text{m}$  thickness, were characterized by x-ray diffraction, photoluminescence, cathodoluminescence, and transmission electron microscopy. By varying the In content of (In,Ga,Al)P, it is possible to grade the lattice constant of the buffer layer from that of GaAs to that of ZnSe. Study of these buffer layers is further motivated by their use as a p-type ohmic contact to a p-type ZnSe overlayer. We are currently studying defect generation in ZnSe epilayers grown on relaxed buffer layers of (In,Ga)P (lattice-matched to ZnSe) with the phosphide surface capped with 8 monolayers of GaAs exhibiting various reconstructions. In this manner, surface chemistry is removed as a variable while simultaneously achieving a lattice-matched buffer layer to ZnSe. In this paper, the microstructural, optical, and electrical properties of these novel heterostructures will be described and contrasted to the more conventional ZnSe/GaAs heterostructure.

The research described herein was sponsored by an ARPA/ONR University Research Initiative (Cont. No. 284-25041) and ARO/JSEP (Cont. No. DAAL 03-92-C-0001).

Contact: Leslie A. Kolodziejski, 77 Massachusetts Avenue, Cambridge, MA 02139  
Tel: (617) 253-6868, FAX: (617) 258-6640, e-mail: lak@mtl.mit.edu

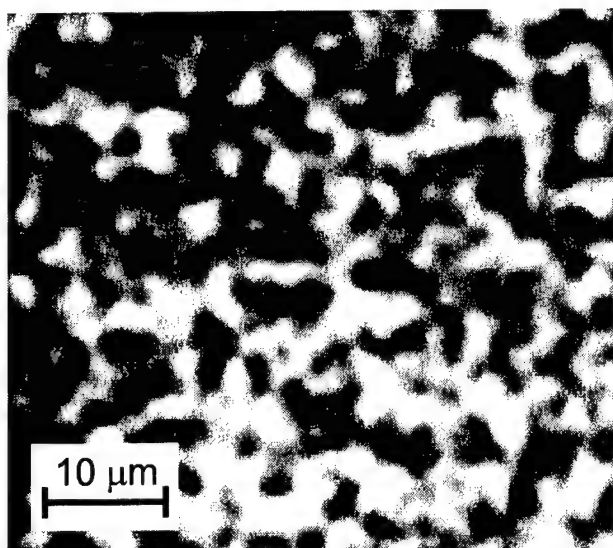


Figure 1) The room-temperature cathodoluminescence of a 1  $\mu\text{m}$  ZnSe film grown by MBE on a c(4x4) GaAs buffer layer at a magnification of 1700. The defect density is  $>10^6 \text{ cm}^{-2}$ . The electron probe parameters were: 30nA, 20kV.

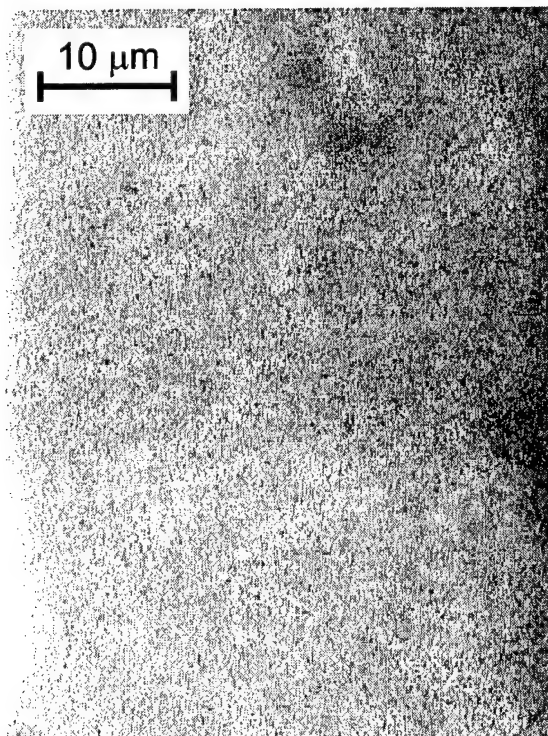


Figure 2) The room-temperature cathodoluminescence of a 1  $\mu\text{m}$  ZnSe film grown by MBE on a Zn-exposed (2x4) GaAs buffer layer at a magnification of 1700. Based on the observation that no defects were detected in the area shown, the defect density is less than  $2 \times 10^5 \text{ cm}^{-2}$ . The electron probe parameters were: 30nA, 20kV.

# ARSENIC INCORPORATION IN MBE-HgCdTe LAYERS USING PLANAR DOPING APPROACH

F. Aqariden, P.S Wijewarnasiriya, C. Grein, J.P. Faurie, and S. Sivananthan.

Microphysics Laboratory, Dept. Of Physics (M/C 173). The University of Illinois at Chicago. 845 W Taylor Street, Room# 2236, Chicago, IL, 60680.

MBE-HgCdTe is extensively investigated for its capability and flexibility in developing new compounds and device structures. Advanced electro-optical devices require homojunction or heterojunction structures. MBE offers precise control over the thickness of the epilayers, allows abrupt junctions, and it guarantees the reproducibility of the epilayers by making use of in-situ analysis capabilities and doping techniques. Doping MBE-HgCdTe has led to the development of a variety of advanced devices, including p-i-n photodetectors; n-p-n dual color photodiodes; and light emitting devices. Recently MBE-HgCdTe doped and undoped epilayers were grown with low defect densities. N-type doped epilayers with a  $10^{15} \text{ cm}^{-3}$  doping level are obtained easily with indium as dopant. At the present time, arsenic, which is the dopant of choice for p-type MBE-HgCdTe epilayers, has the tendency to go in the cation sublattice and act as donor. Doping MBE-HgCdTe p-type in-situ (as grown) is still a problem. To overcome it, layers have to be grown at a lower temperature in order to improve the sticking of As, and a high mercury flux is needed. Under these conditions, the HgCdTe structural quality will be lowered, and therefore the electrical performance will suffer. The planar doping (delta-doping) method is a new way to incorporate arsenic as an acceptor in-situ, and can lead to obtaining as-grown MBE-HgCdTe p-type epilayers.

In this paper, we will report on the MBE growth and characterization of p-type MBE-HgCdTe epilayers. We used the planar doping technique in which Te and CdTe effusion cell shutters were periodically closed and the arsenic shutter was open during the growth. The periodicity interval ranges from 30 to 200 Å, and the duration of the arsenic shutter opening is a few seconds. The arsenic flux is around  $10^{15} \text{ atm s}^{-1}$ , while the Hg is still impinging on the surface, which is expected to enhance the Hg-As bond formation. We have successfully incorporated As as dopant in MBE-HgCdTe epilayers. Fig.1 shows the transport measurement of as-grown planar doped HgCdTe epilayers revealing p-type behavior. Furthermore, these results show that arsenic is activated at the MBE growth temperature. We will present some comparisons between MBE-HgCdTe p-type epilayers grown using planar doping and conventional doping in which Te, Cd, and As shutters are all opened at once. These layers have been characterized by a variety of techniques. We will present some of our data obtained from IR transmission, Hall measurements, scanning electron microscopy (SEM), second ion mass spectroscopy (SIMS), and transport measurement after carrying out different annealing experiments. A detailed analysis of these results will be presented.

Contact author: F. Aqariden

Address: The University of Illinois at Chicago

Department of Physics (M/C 273)

845 W Taylor, Rm# 2236 SES

Chicago, Ill 60607 . Tel: 312-996-5876, Fax: 312-996-9016, e-mail Aqariden@uicws.phy.uic.edu

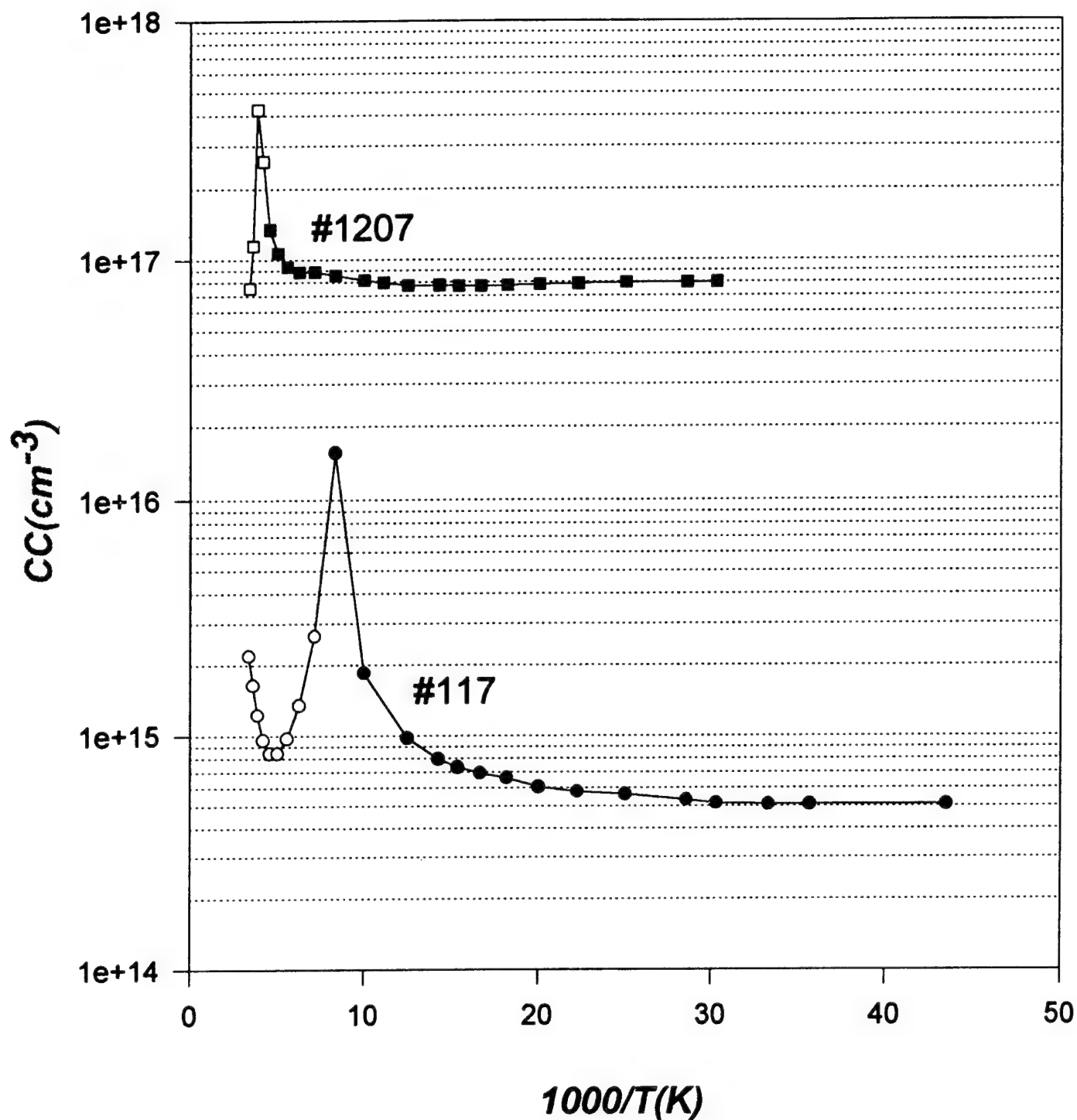


Fig. (1) Carrier concentration vs reciprocal temperature of as-grown arsenic planar doped HgCdTe layers with Cd composition ~33%.



## HIGH PERFORMANCE TWO-COLOR INFRARED PHOTODETECTORS GROWN BY MOLECULAR BEAM EPITAXY

R.D. Rajavel, D.M. Jamba, O.K. Wu, and J.E. Jensen  
Hughes Research Laboratories, Malibu, CA 90265

J.A. Wilson, E.A. Patten, K. Kosai, P. Goetz, B. Baumgratz, G.R. Chapman, and  
W.A. Radford  
Santa Barbara Research Center, Goleta, CA 93117

Integrated multi-spectral detectors that can detect radiation in two different bands of the infrared spectrum offer performance advantages such as improved contrast and signature recognition, automatic pixel registry and savings in weight and power over two independent detectors used for the same application. We report on high performance HgCdTe n-p-n two-color detector structures grown by MBE that operate in the mid-wave infrared (MWIR) and long-wave infrared (LWIR) bands of the infrared spectrum.

A schematic of the n-p-n two-color detector structure is shown in Fig. 1. The n-type layers were doped with indium at  $1\text{-}2 \times 10^{15} \text{ cm}^{-2}$ , and the p-type layer was in situ doped with As at  $\approx 1 \times 10^{18} \text{ cm}^{-2}$ . Infrared radiation is incident on the transparent substrate and the MWIR component is absorbed by the 6  $\mu\text{m}$  thick HgCdTe layer that is adjacent to the substrate, while the LWIR radiation is absorbed in the narrow band-gap HgCdTe layer at the top of the structure. The layers were fabricated as mesa diodes and electrical contacts were made to the top LWIR layer and the common MWIR layer. The diodes were operated in the sequential mode which does not require an electrical contact to the p-type layer for this back-to-back diode geometry. The LWIR diode is active when the LWIR layer is biased positive with respect to the n-type MWIR layer and the MWIR diode is made active when the n-type MWIR common layer is biased positive with respect to the LWIR layer.<sup>1,2</sup> The spectral response of a MWIR/LWIR two-color detector that was grown by MBE is shown in Fig. 2. The data are shown as response per Watt, and measured at  $f/2$  field of view. At 80K, the cutoff wavelengths for MWIR and LWIR photodiodes were 5.5 and 10.5  $\mu\text{m}$ , respectively. Based on I-V measurements, the  $R_0A$  product of the LWIR diode of the two color detector is estimated to be  $> 100 \Omega\text{cm}^2$ , and compares very favorably with state-of-the-art LWIR diodes. Details of MBE growth and properties of MWIR/LWIR detectors, as well as two-color detectors that operate in other bands of the IR spectrum will be presented.

1. J.A. Wilson, E.A. Patten, G.R. Chapman, K. Kosai, B. Baumgratz, P. Goetz, S. Tighe R. Risser, R. Herald, W.A. Radford, T. Tung and W.A. Terre, SPIE 2274, 117 (1994).
2. E.R. Blazejewski, J.M. Arias, G.M. Williams, W. McLevige, M. Zandian and J. Pasko, J. Vac. Sci. Technol. B10, 1626 (1992).



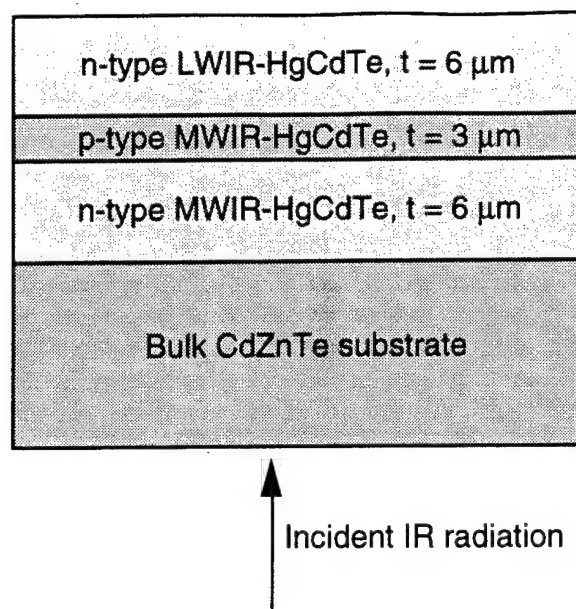


Fig. 1. Schematic of the MWIR/LWIR n-p-n two-color detector structure.

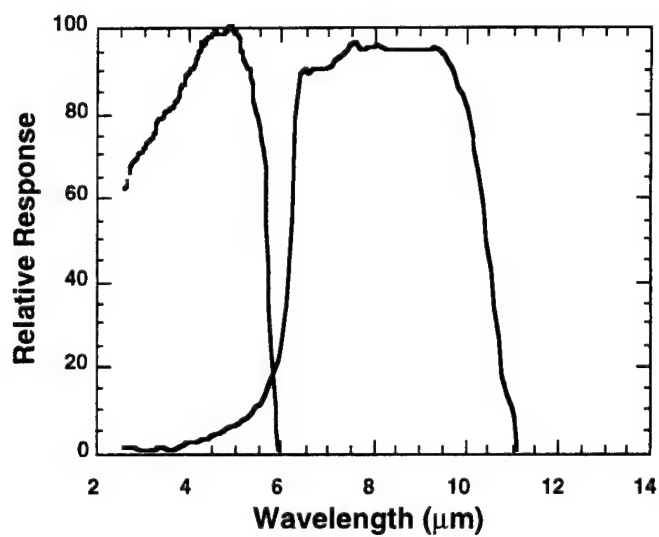


Fig. 2. MWIR and LWIR spectral response at 77K of the two-color detector.

## 6. III-V MATERIALS

TUESDAY AFTERNOON (SMOTHERS)

Session Chair: K.Y. Cheng, University of Illinois, USA.

- 13:40 6.1 **Molecular beam epitaxy with solid phosphorus and arsenic valved cracking cells** (Invited)  
J.N. Baillargeon and A.Y. Cho, Bell Laboratories  
Lucent Technologies, USA.
- 14:10 6.2 **Growth parameter dependence of step patterns in AlGaAs molecular beam epitaxy on vicinal GaAs(110) inclined toward (111)A**  
Shigehiko Hasegawa, Kazuki Sato, Satoshi Torii, and Hisao Nalashima  
Osaka University, Japan
- 14:30 6.3 **Effects of tensile strain and substrate off-orientation on the CBE growth of GaInAs/InP multiple quantum well structures**  
T. Marschner, R.T.H. Rongen, M.R. Leys, H. Vonk, J.H. Wolter, and F.D. Tichelaar  
Eindhoven University of Technology, The Netherlands
- 14:50 6.4 **Improved MBE-grown GaAs using a novel, high capacity Ga effusion cell,**  
R.N. Sacks, P. Colombo, George A. Patterson, and Kathleen A. Stair  
Ohio State University, USA
- 15:10 6.5 **Strain-compensated AlGaInAs/InP heterostructures with up to 50 QWs by MBE,** H. Hillmer, R. Lösch, and W. Schlapp  
Deutsche Telekom, Darmstadt, Germany
- 15:30 6.6 **InAs/GaAs in-plane strained superlattices grown on slightly misoriented (110) InP substrates by molecular beam epitaxy**  
Yoshiaki Nakata, Osamu Ueda, Yuji Nishikawa, Shunichi Muto, and Naoki Yokoyama  
Fujitsu Laboratories, Atsugi, Japan

Break

- 16:00-18:00 **Poster Session 1. III-V Materials and Growth Issues**  
Please see end of abstract book for poster session abstracts.

Dinner

- 19:30-21:30 **Rump Session 1.**  
**Production MBE Technology**  
Chair: April Brown, Georgia Institute of Technology, USA.

Tuesday Evening (Smothers)

## Molecular Beam Epitaxy with Solid Phosphorus and Arsenic Valved Cracking Cells

J. N. Baillargeon, and A. Y. Cho

Bell Laboratories, Lucent Technologies, 600 Mountain Avenue, Murray Hill, NJ 07974

Molecular beam epitaxy (MBE) of III-V phosphorus compounds (without hydrides or metalorganic sources) is now possible as a direct result of the ability to convert *in-situ*, amorphous red to  $\alpha$ -white phosphorus. This recent technological advance enables red phosphorus to be used as a starting source for producing a highly stable and reproducible beam flux. It is now possible to manufacture fiber lightwave communication components requiring  $\text{Ga}_x\text{In}_{1-x}\text{As}_y\text{P}_{1-y}$ , previously thought unachievable with all solid sources. All solid source MBE is distinctive in that it is environmentally safe and the least costly precision growth technique available.

In this talk, we will address two prime issues that have historically limited the viability of MBE as a manufacturing platform for 1.3  $\mu\text{m}$  and 1.55  $\mu\text{m}$  optical fiber communication lasers. The first is the reproducible control of the quaternary composition lattice matched to InP. Reproducible growth of the quaternary can only be achieved through the accurate, stable control of the incident P, As, In and Ga beam fluxes, and substrate temperature. Extensive data will be presented showing the complex nature of the interdependent relationships amongst the growth parameters, as viewed across the entire composition range. A run-to-run emission wavelength variation of less than 1% will be demonstrated using this information. The second issue is the formation of a mechanically smooth, defect-free over-grown surface using lattice matched  $\text{Ga}_x\text{In}_{1-x}\text{As}_y\text{P}_{1-y}$  on an etched, periodic InP grating. The periodic grating is an essential element of which the fiber lightwave distributed feedback (DFB) laser is comprised. Preliminary results will be presented, clearly showing that morphologically flat or planarized surfaces are attainable on the DFB laser grating. Devices grown with *in-situ* produced  $\alpha$ -white phosphorus will also be discussed.

# **Growth parameter dependence of step patterns in AlGaAs molecular beam epitaxy on vicinal GaAs(110) inclined toward (111)A**

Shigehiko HASEGAWA, Kazuki SATO, Satoshi TORII, and Hisao NAKASHIMA

*The Institute of Scientific and Industrial Research, Osaka University*

*8-1 Mihogaoka, Ibaraki, Osaka 567, JAPAN*

TEL : +81-6-879-8412, FAX : +81-6-879-8414, E-mail: hasegawa@sanken.osaka-u.ac.jp

We have demonstrated that molecular beam epitaxial (MBE) growth on vicinal GaAs(110) induces macrosteps being several tens nm high [1], and that such macrostep system is one of fairly good candidates as substrates for fabricating nanostructures such as quantum wires, since macrosteps formed by MBE using AsH<sub>3</sub> gas source are coherently aligned along  $[\bar{1}10]$  direction perpendicular to the misorientation direction of the vicinal (110) substrates [2]. However, MBE growth using solid As source (As<sub>4</sub>) produces rather fluctuated macrostep patterns. In order to fabricate excellent nanostructures, it is necessary to control macrostep patterns, that is, to know what growth parameters make straight and uniform macrosteps stable.

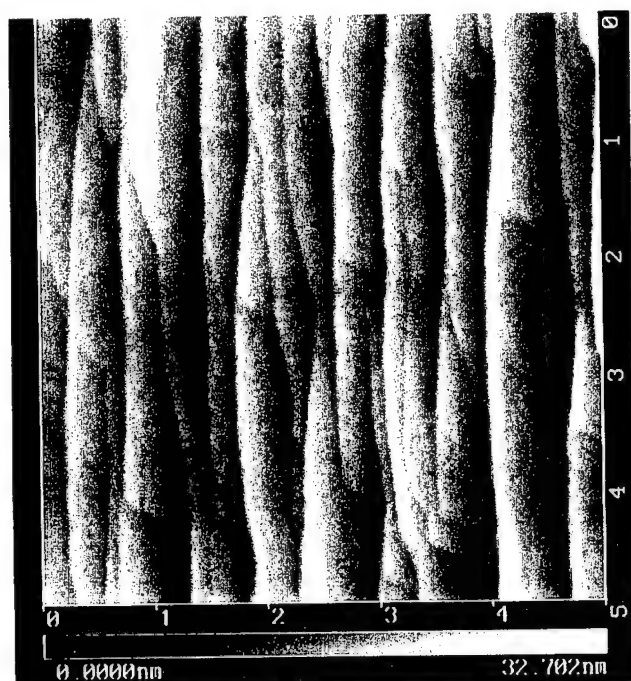
In this paper, we present growth parameter dependence of macrostep patterns in AlGaAs MBE growth using As<sub>2</sub> molecular beams with the use of atomic force microscopy (AFM). In particular, our interest is concentrated both on how the macrostep patterns are changed by varying growth temperature and V/III ratio and on what the difference in the resulting step patterns is, when compared with the results using As<sub>4</sub> molecular beams.

AlGaAs layers of 400 nm in thickness were grown by MBE at temperatures ranging from 430 to 580 °C on vicinal GaAs(110) substrates inclined at 3° toward (111)A. As<sub>2</sub> molecular beams were obtained by dissociating GaAs polycrystalline into As<sub>2</sub> using Knudsen cell. Before AlGaAs growth, 200 nm thick GaAs buffer layers were grown at 580 °C. AFM measurements were carried out in air in contact mode. In situ reflection high-energy electron diffraction (RHEED) observation were done to examine how the atomic steps were changed into macrosteps during MBE growth.

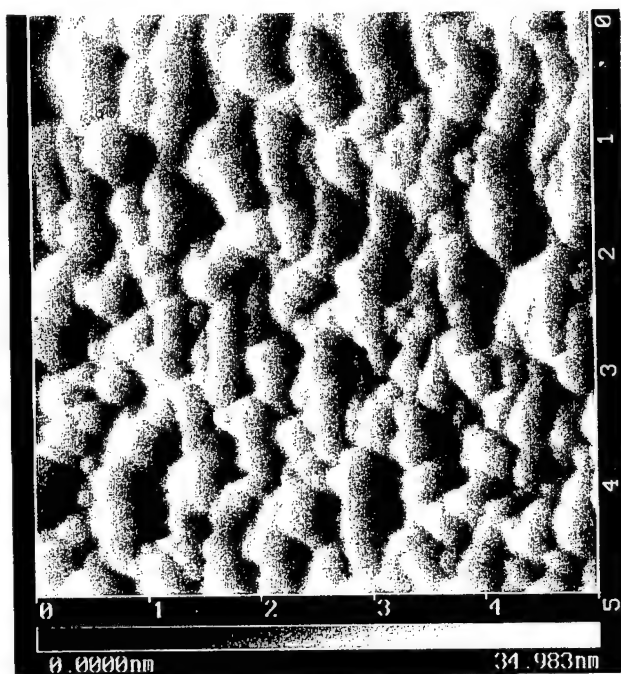
AFM investigation of AlGaAs layers grown by using As<sub>2</sub> molecular beams reveals that coherently aligned macrosteps are formed, and that increasing growth temperatures leads to the formation of straighter macrostep patterns. Simultaneously, terrace width becomes wider. In contrast, MBE growth using solid As source (As<sub>4</sub>) leads to highly connected zigzag networks of macrosteps rather than fairly straight and uniformly spaced macrosteps. We will discuss the difference in macrostep patterns between MBE growth using As<sub>2</sub> and As<sub>4</sub> in terms of diffusion length of As species.

[1] S. Hasegawa *et al.*, *Surf. Sci.* **267**, 5 (1992).

[2] M. Takeuchi *et al.*, *Jpn. J. Appl. Phys.* **34**, 4411 (1995), and references therein.



(a)



(b)

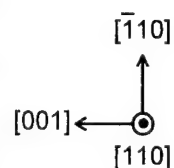


Fig.1 AFM images ( $5\mu\text{m} \times 5\mu\text{m}$ ) of AlGaAs layers grown by MBE at  $580^\circ\text{C}$  on vicinal GaAs(110) substrates when using (a)  $\text{As}_2$  molecular beams and (b)  $\text{As}_4$  molecular beams. It is apparent that MBE growth using  $\text{As}_2$  molecular beams produces fairly straight and uniformly spaced macrosteps.

## Effects of Tensile Strain and Substrate Off-Orientation on the CBE Growth of GaInAs/InP Multiple Quantum Well Structures

T. Marschner<sup>1,a</sup>, R. T. H. Rongen<sup>1</sup>, M. R. Leys<sup>1</sup>, H. Vonk<sup>1</sup>, J. H. Wolter<sup>1</sup>, F. D. Tichelaar<sup>2</sup>

<sup>1</sup>COBRA Inter-University Research Institute, Eindhoven University of Technology,  
P.O. Box 513, NL-5600 MB Eindhoven, The Netherlands

<sup>2</sup>Laboratory of Metallurgy, Delft University of Technology,  
Rotterdamseweg 137, NL-2628 AL Delft, The Netherlands

<sup>a</sup>Corresponding author, phone: +31 40 2474228, Fax: +31 40 2453587,  
e-mail: t.marschner@phys.tue.nl

Ga<sub>x</sub>In<sub>1-x</sub>As/InP multiple quantum well (MQW) structures with high Ga content are becoming increasingly important for device-applications because of the possibility to reduce the optical birefringence in waveguide components by tensile strain.

In our work we investigate in detail the influence of the growth parameters on the optical and structural properties of GaInAs/InP MQW structures grown by chemical beam epitaxy (CBE). In particular we discuss the influence of the tensile strain in the GaInAs-layers and the substrate off-orientation.

A series of 10 periods 5nm Ga<sub>x</sub>In<sub>1-x</sub>As / 9nm InP MQW structures with  $x_{Ga}$  up to 0.77 was grown by CBE in a growth temperature range between 485°C and 545°C. The used substrates were (100) InP 2° off-oriented towards [110] and exactly oriented, respectively. In each growth run both substrate orientations were used.

The structures were investigated by double crystal X-ray diffraction (XRD), low-temperature photoluminescence (PL) and cross-sectional transmission electron microscopy (TEM).

XRD investigations reveal that the InP as well as the GaInAs growth rate is larger for off-oriented substrates than for exactly oriented substrates. This behaviour is independent of the strain in the GaInAs layers and of the growth temperature within the chosen range, although the individual values of the GaInAs- and InP-growth-rate are dependent of the growth temperature (Fig.1). This can be explained by the fact that on off-oriented substrates the growth takes place by a step-flow mechanism, while on exactly oriented substrates 2-D nucleation is required. This leads to a higher evaporation probability.

The XRD-linewidths of the MQW-reflections are near the theoretical values for layers of the respective thickness indicating that no relaxation by misfit dislocation formation has occurred up to  $x_{Ga} = 0.77$  in the individual GaInAs layers. This corresponds to a lattice mismatch  $(\Delta d/d)^\perp = -4 \times 10^{-2}$  in the individual GaInAs layers and an average mismatch of the whole MQW structure  $(\Delta d/d)^\perp = -1.1 \times 10^{-2}$ . The dependence of the position of the zeroth order satellite reflection on the azimuthal angle shows that the layers grown on off-oriented substrates are tilted with respect to the InP-substrate. The tilt increases with increasing strain in the MQW layers. The samples grown on exactly oriented substrates do not reveal this feature.

MQW structures grown on off-oriented substrates have a larger PL linewidth of the MQW-peak than structures grown on exactly oriented substrates (Fig.2). Additionally, for the off-oriented substrates the linewidth increases linearly with increasing lattice mismatch in the GaInAs layers. In contrast, the linewidth remains constant for exactly oriented substrates up to the maximum Ga-content  $x_{Ga} = 0.77$ .

Cross sectional TEM reveals that MQW structures with high tensile strain have a wavy surface structure (Fig.3). This applies to both exactly and off-oriented substrates. Surface undulations are known to decrease strain by elastic deformation. Although such quantum well thickness variations might lead to a broadening of the PL peaks, this cannot be the cause for the trend observed in fig.2. Therefore, the increase in the PL linewidth for highly strained MQWs grown on off-oriented substrates must be due to the lattice tilting occurring on stepped substrates.

Our results indicate that devices containing strained quantum wells have to be grown preferably on substrates with the lowest possible off-orientation to decrease the lattice tilt.

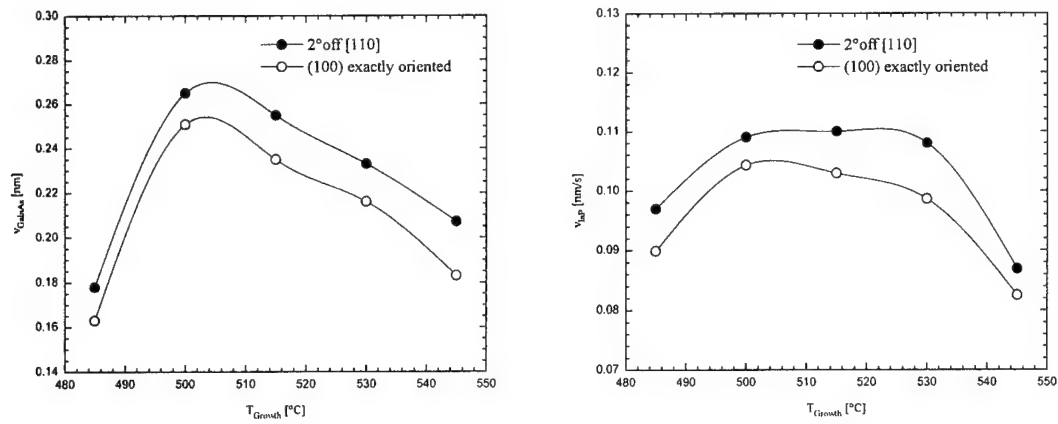


Fig.1 GaInAs growth rate  $v_{\text{GaInAs}}$  (left) and InP growth rate  $v_{\text{InP}}$  (right) for off-oriented and exactly oriented (100) InP substrates as a function of the growth temperature.

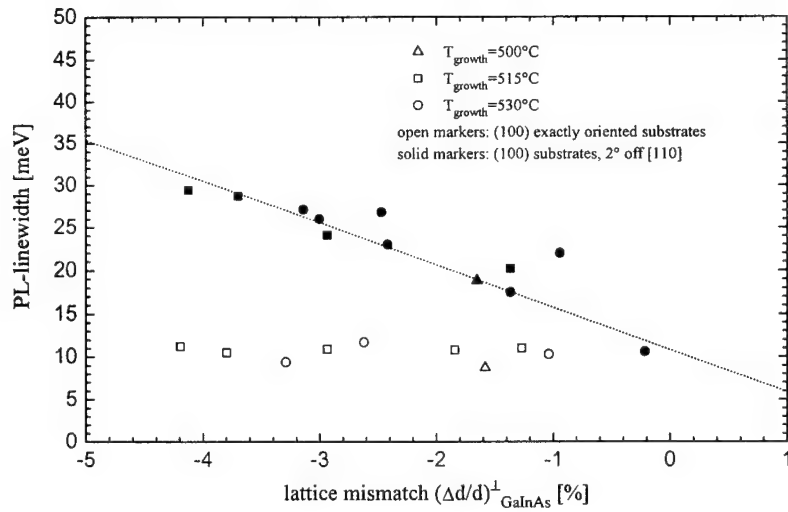


Fig.2 Photoluminescence linewidth of the GaInAs quantum well peak as a function of the lattice mismatch  $(\Delta d/d)_{\perp}^{\text{GaInAs}}$  of the GaInAs layers for off-oriented and exactly oriented (100) InP substrates.

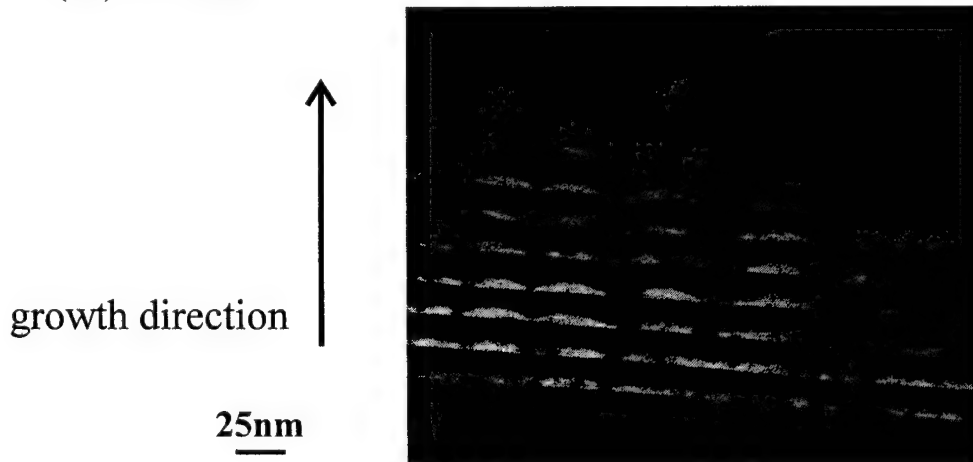


Fig.3 Cross-sectional TEM micrograph of a 10 periods GaInAs/InP MQW with  $x_{\text{Ga}} = 0.70$  grown on a (100) InP substrate  $2^{\circ}$  off towards [110].

## Improved MBE-Grown GaAs Using a Novel, High Capacity Ga Effusion Cell

R. N. Sacks<sup>1</sup>, P. Colombo<sup>2</sup>, George A. Patterson<sup>3</sup>, and Kathleen A. Stair<sup>4</sup>

1)Dept. of Electrical Engineering, Ohio State University, Columbus, Ohio 43210\*

2) EPI MBE Products, St. Paul, Minnesota 55110

3) Hewlett-Packard - Microwave Technology Division, Santa Rosa, California 95403

4) Materials Research Center, Northwestern University, Evanston, Illinois 60208

The use of a novel PBN crucible has allowed the design of a new high capacity group III source incorporating a unique heat shielding cap. The crucible is cylindrical in overall shape, but necks down to a small orifice with a short cone. The extra heat shielding at the front of the effusion cell, in conjunction with dual heater filaments allows hot lip operation with considerably lower power than for previous designs. Thus the tip of the source can be held hot enough to completely eliminate Ga droplets without incurring a deleterious penalty in the form of impurities generated by an inordinately high heat load on the cell materials or the surrounding cryoshrouding. This source has been mounted on an EPI (Varian-style) GEN II MBE growth chamber using a water cooled nipple to reduce heat loading even further. Use of this source has resulted in dramatically reduced visible defect densities in GaAs and (Al,Ga)As layers. It is important to note that this has been achieved with no sacrifice in other operating characteristics of the source. To be more specific, this effusion cell exhibits low flux transient and low flux drift, and has generated GaAs with good uniformities, low background doping, high mobility, and low trap concentrations.

The new cell was compared with another high capacity, low flux transient cell: an EPI 125DF mounted in the same position on the same growth chamber. Operating these cells at a  $1\mu\text{m/hr}$  GaAs growth rate with 100% power to the tip required 210W for the new cell, but 380W for the 125DF. To test defect densities, wafers were grown on 2" diameter substrates taken from the same boule. The structure grown was a MODFET with a  $1\mu\text{m}$  GaAs buffer, and a total thickness of  $1.1\mu\text{m}$ . The growth rate for all runs was  $1\mu\text{m/hr}$ . Defect densities were measured with a Tencor Surfscan 6200 set to count all defects larger than  $1.28\mu\text{m}$ . Defect densities of 22-27 defects/ $\text{cm}^2$  have been obtained for the new source, representing the lowest defect densities ever reported from a GEN II using large capacity sources. This compares with 88-92 defects/ $\text{cm}^2$  from the 125DF. In addition, an  $18.7\mu\text{m}$  thick GaAs layer grown with the new cell had only 277 defects/ $\text{cm}^2$ . Electrical results with the new source were: A  $17.8\mu\text{m}$  thick GaAs layer with no intentional doping was fully depleted at zero bias, implying a background doping of  $< 2 \times 10^{13}/\text{cm}^3$ . Deep level transient spectroscopy indicated that a GaAs layer doped  $n = 1 \times 10^{15}/\text{cm}^3$  had a total trap density of  $1.5\text{--}2.0 \times 10^{12}/\text{cm}^3$ . MODFET's have yielded 77°K mobilities of  $132,000\text{cm}^2/\text{V-sec}$  for  $n_s = 4 \times 10^{11}/\text{cm}^2$ .

Flux transients for both sources were below the detection limit for our measurement technique ( $< 2\%$ ). From the beginning to the end of the growth of an  $18.7\mu\text{m}$  thick GaAs layer, the flux dropped by  $\sim 2\%$ , at the edge of our flux gauge reproducibility. Uniformity was tested by growing a 20 period AlAs( $160\text{\AA}$ )/GaAs( $59\text{\AA}$ ) MQW on two 3" diameter wafers, one each with the old and new design. Layer thicknesses were measured with photoluminescence and double-crystal x-ray diffraction. Both cells give a center-to-edge decrease in GaAs thickness of  $\sim 2\%$ , and only a  $\sim 1\%$  drop from the center out to a 2" diameter. The uniformity of the new cell was also measured using reflectometry on an  $18.7\mu\text{m}$  thick GaAs layer grown on top of a  $200\text{\AA}$  AlAs "reflection" layer, yielding the same results as above.

\*phone: (614) 292-3462, fax: (614) 292-7596, e-mail: sacks@ee.eng.ohio-state.edu



## Strain-compensated AlGaInAs/InP heterostructures with up to 50 QWs by MBE

H. Hillmer, R. Lösch and W. Schlapp

Deutsche Telekom, Technologiezentrum, P. O. Box 100003, 64276 Darmstadt, Germany

Tel: +49 6151 83 3062, Fax: +49 6151 83 4912, e-mail: hillmer@fz.telekom.de

### Abstract :

For applications in 1.55 $\mu$ m photonic communication systems, AlGaInAs quantum well (QW) structures were rarely grown in recent years compared to the GaInAsP material system, although AlGaInAs has several advantages for the optoelectronic device performance.

Strain-compensated QW samples with compressively strained Al<sub>0.09</sub>Ga<sub>0.20</sub>In<sub>0.71</sub>As wells ( $\sim 8.2$ nm,  $\Delta a/a \sim +1.2\%$ ), tensile strained Al<sub>0.21</sub>Ga<sub>0.46</sub>In<sub>0.33</sub>As barriers ( $\Delta a/a \sim -1.4\%$ ) and unstrained Al<sub>0.23</sub>Ga<sub>0.24</sub>In<sub>0.53</sub>As cladding layers have been grown by solid source MBE on InP at 515°C using two In-furnaces and one furnace, respectively, for the Al, Ga and As source materials. We have grown samples with different numbers of QWs between 1 and 50 and observed excellent crystalline quality without any indications of strain relaxation. Fig. 1 shows very narrow photoluminescence (PL) linewidths for a structure with 50 QWs. Disregarding statistical fluctuations, the PL linewidths at 10K are independent of the number of QWs as shown in Fig. 2. This demonstrates excellent homogeneity from well to well. The absolute values can be explained by alloy disorder fluctuations and well width fluctuations. X-ray diffraction (XRD) and PL were used in combination with model calculations to determine the layer widths and compositions. Fig. 3a depicts a measured and a simulated XRD rocking curve of a structure containing 50 QWs. Fig. 3b (3c) displays a blow up indicating the 48 (28) side-maxima corresponding to 50 (30) wells. Note that the total strained stack has a very large width of 0.65 $\mu$ m. Due to alloy disorder fluctuation the PL linewidths in our QWs are higher than in binary QWs, therefore, monolayer splittings are difficult to observe. Fig. 4 displays PL spectra of a sample grown without any interruption at the heterointerfaces indicating indeed monolayer splittings. At low carrier densities (low laser excitation power  $P_L$ ) the islands of wider well width (lower quantization energy) are preferentially populated. Island areas of reduced well widths increase in population with growing excitation energy and show a rising contribution to the PL emission. To the best of our knowledge, this is the first report both on a very high number of strain-compensated AlGaInAs QWs and on monolayer splittings in AlGaInAs QWs.

The use of quaternary QWs in photonic devices allows strain and well width to be varied independently of each other while maintaining e.g. 1.55 $\mu$ m emission wavelength. The use of strain compensation overcomes the total critical layer thickness restrictions and enables a free choice of the number of QWs in photonic device design. Recently, we reported a record modulation bandwidth of 26 GHz for 1.55 $\mu$ m AlGaInAs lasers<sup>1</sup>.

1. H. Hillmer A. Greiner F. Steinhagen R. Lösch W. Schlapp T. Kuhn H. Burkhard, 9. HCIS (95).

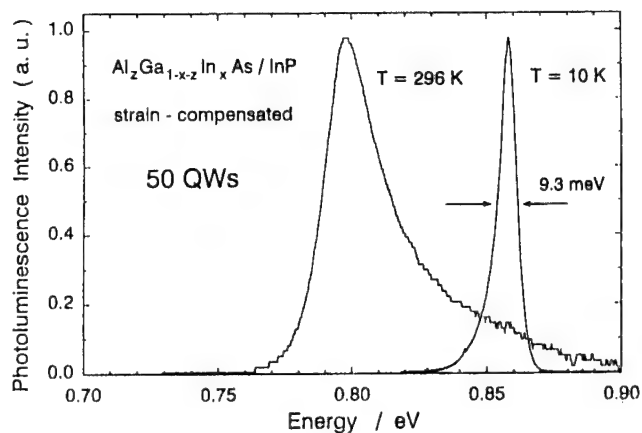


Fig. 1

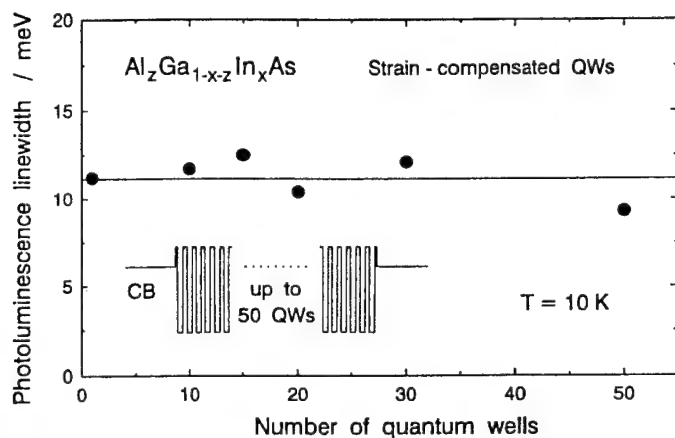


Fig. 2

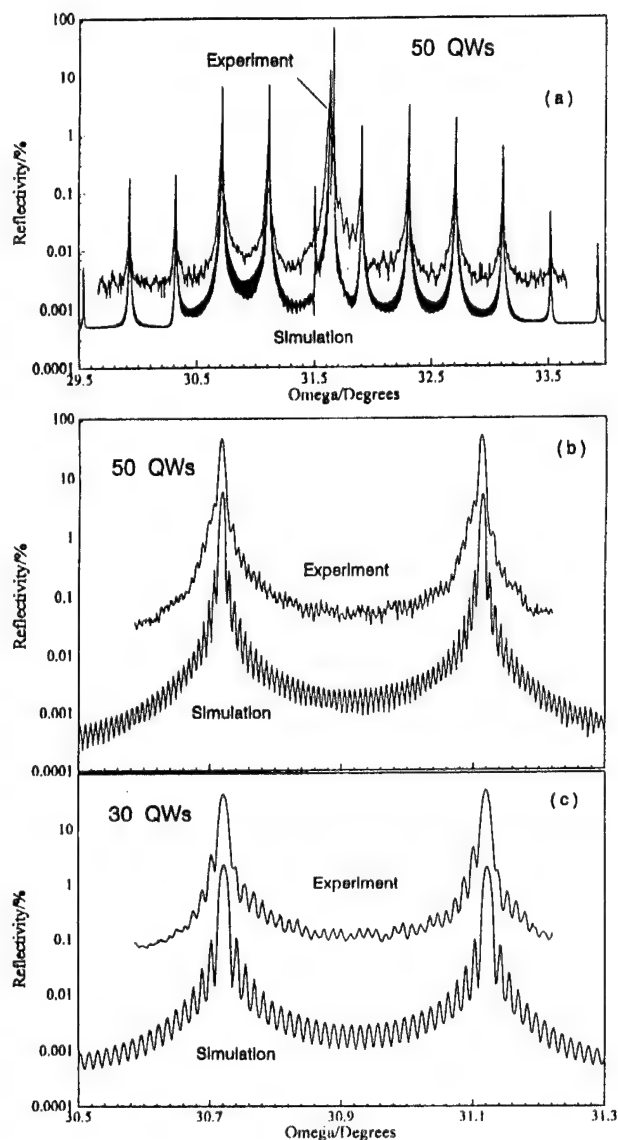


Fig. 3

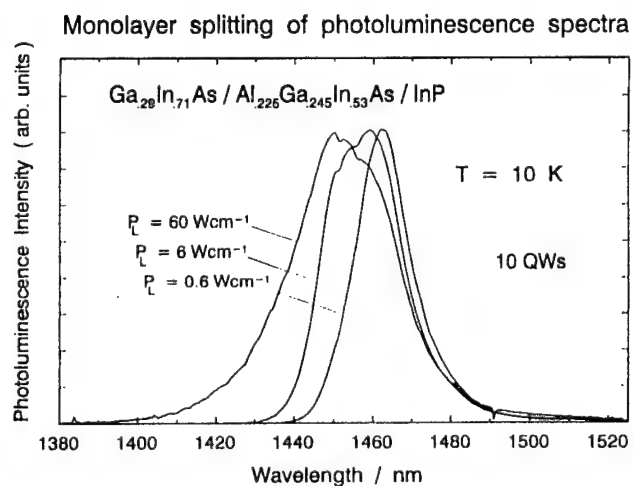


Fig. 4

# **InAs/GaAs in-plane strained superlattices grown on slightly misoriented (110) InP substrates by molecular beam epitaxy**

Yoshiaki Nakata, Osamu Ueda, Yuji Nishikawa, Shunichi Muto\*), Naoki Yokoyama

Fujitsu Laboratories Ltd.

10 - 1 Morinosato-Wakamiya, Atsugi, Kanagawa 243 - 01 Japan

Tel. +81-462-50-8247 (dial in), Fax. +81-462-50-8844, E-mail KXA0444@fjcug.fujitsu.co.jp.

Growth of laterally periodic structures using step flow growth on misoriented substrates is a very important for directly forming quantum wire and box array structures. Successful works had been extensively done, but most studies focused on the lattice matched materials. Highly strained materials have not yet been reported. In this paper, we describe the growth of the InAs/GaAs strained in-plane superlattices (IPSSLs) on InP substrates by molecular beam epitaxy (MBE).

The substrates used were misoriented (110) InP tilted toward the  $[00\bar{1}]$  direction. On these substrates the straight steps could be ordered [1]. We grew half monolayers of InAs and GaAs alternately without growth interruption (Fig. 1). Structural features were evaluated by transmission electron microscopy (TEM) and photoluminescence (PL) measurements. In the electron diffraction (TED) pattern of the  $(1\bar{1}0)$  cross-section obtained from the sample grown on a substrate tilted at  $1.5^\circ$ , extra spots were observed at about  $\{h, k, l \pm 1/13.5\}$  in which  $h, k, l$  are all even or all odd, corresponding to fundamental spots as 002, 220, 111, etc. (Fig. 2). These findings are satisfactorily explained by the formation of the laterally periodic structures. A dark field TEM image of the  $(1\bar{1}0)$  cross-section revealed a periodic structure formed almost in the  $[001]$  direction (Fig. 3). The mean contrast period (about 10 nm) is comparable to the terrace width (10 nm) expected from the substrate tilt angle ( $1.2^\circ$ ). The PL spectrum of the IPSSL has a peak at the energy of 0.77 eV which are about 40 meV lower than that of the  $\text{In}_{0.53}\text{Ga}_{0.47}\text{As}$  alloy (Fig. 4). From the energy band calculations of the  $\text{In}_{1-x}\text{Ga}_x\text{As}/\text{In}_x\text{Ga}_{1-x}\text{As}$  superlattices based on nearest-neighbor  $\text{sp}^3\text{s}$  tight-binding approximation, we deduced  $x$  was 0.26. Thus the compositional difference between the barriers and wells is about 0.48 which is highest value ever reported. These results suggest the potential for growing as-grown quantum wire array structures whose wavelengths of practical 1.3 or 1.55  $\mu\text{m}$ .

## References:

- [1] Y. Nakata, O. Ueda, and S. Muto, Proc. 7th Intern.Conf. InP and Related Materials, p.165..

\*) Present address: Faculty of Engineering, Hokkaido Univ., Sapporo

# InAs/GaAs in-plane strained superlattices grown on slightly misoriented (110) InP substrates by molecular beam epitaxy

Y. Nakata, O. Ueda, Y. Nishikawa, S. Muto, and N. Yokoyama

Fujitsu Laboratories Ltd., 10 - 1 Morinosato-Wakamiya, Atsugi 243-01 Japan

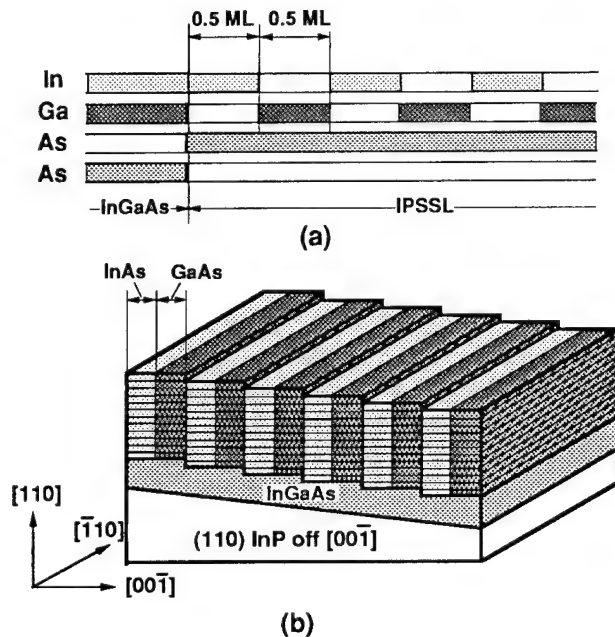


Fig. 1. (a) Growth sequence and (b) schematic diagram of the InAs/GaAs IPSSL structure.

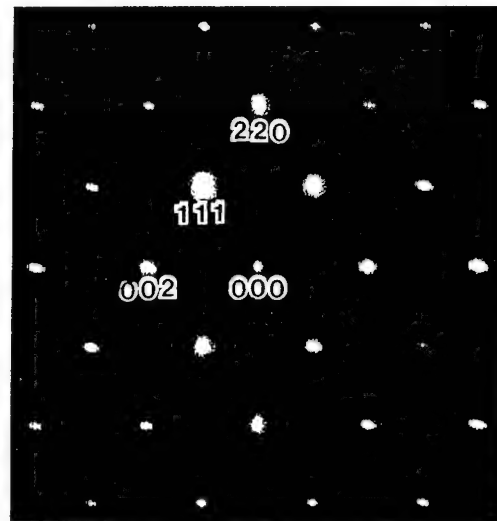


Fig. 2. TED pattern from the (110) cross-section of the IPSSL grown on a substrate tilted at 1.5°.

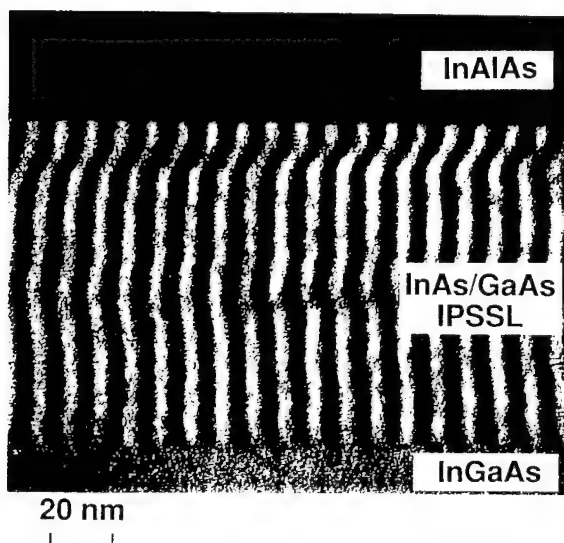


Fig. 3. TEM dark field image of the (110) cross-section of the IPSSL grown on a substrate tilted at 1.2°.

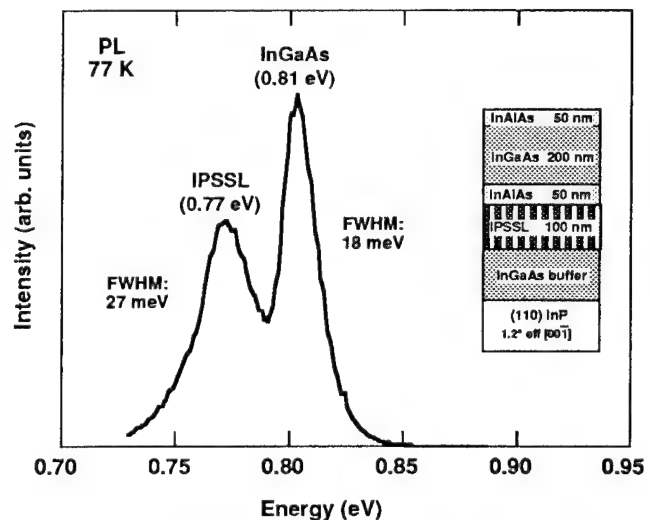


Fig. 4. PL spectrum of the IPSSL sample grown with the In<sub>0.53</sub>Ga<sub>0.47</sub>As alloy on a substrate tilted at 1.2°.

## 7. GROUP IV MATERIALS

TUESDAY AFTERNOON (ELKINS)

Session Chair: Karl Eberl, Max-Planck-Institut FKF, Stuttgart, Germany.

- 13:40 7.1 **Fabrication and band alignment of pseudomorphic  $\text{Si}_{1-y}\text{C}_y$ ,  $\text{Si}_{1-x-y}\text{Ge}_x\text{C}_y$  and coupled  $\text{Si}_{1-y}\text{C}_y/\text{Si}_{1-x-y}\text{Ge}_x\text{C}_y$  quantum well structures on Si substrates, (Invited)**  
K. Brunner, W. Winter, and K. Eberl  
Max-Planck-Institut für FKF, Stuttgart, Germany.
- 14:10 7.2 **Dynamical STM studies of the growth of Si and Ge on silicon by MBE**  
Bert Voigtländer  
Institut für Grenzflächenforschung und Vakuumphysik, Jülich, Germany.
- 14:30 7.3 **MBE-growth and structural characterization of  $\text{Si}_{1-y}\text{C}_y/\text{Si}_{1-x}\text{Ge}_x$  superlattices**  
S. Zerlauth, J. Stangel, A.A. Darhuber, F. Schäffler, and G. Bauer  
Institut für Halbleiterphysik, Linz, Austria
- 14:50 7.4 **Why is a quantum confined Stark shift absent in type-I strained  $\text{Si}_{1-x}\text{Ge}_x/\text{Si}$  typeI symmetric quantum wells?**  
Y. Miyake, S. Fukatsu, J.Y. Kim, and Y. Shiraki  
The University of Tokyo, Japan
- 15:10 7.5 **Photoluminescence and X-ray characterization of relaxed  $\text{Si}_{1-x}\text{Ge}_x$  alloys grown on silicon on insulator (SOI) and implanted SOI substrates**  
Michael A. Chu, Martin O. Tanner, Fengyi Huang, Kang L. Wang, Gordon G. Chu, and Mark S. Goorsky, University of California, Los Angeles, USA.
- 15:30 7.6 **Growth of abrupt GaAs/Ge interfaces by atomic hydrogen-assisted MBE**  
Y. Okada, J.S. Harris, Jr., A. Sutoh, and M. Kawabe  
Stanford University, USA.

Break

- 16:00-18:00 **Poster Session 2. Group IV Material and Growth Issues**  
Please see end of abstract book for poster session abstracts.

Dinner

- 19:30-21:30 **Rump Session 2. New Materials and Structures** Tuesday Evening (Elkins)  
Chair: Pallab K. Bhattacharya, University of Michigan, USA.

# Fabrication and band alignment of pseudomorphic $\text{Si}_{1-y}\text{C}_y$ , $\text{Si}_{1-x-y}\text{Ge}_x\text{C}_y$ and coupled $\text{Si}_{1-y}\text{C}_y/\text{Si}_{1-x-y}\text{Ge}_x\text{C}_y$ quantum well structures on Si substrates

K. Brunner, W. Winter, and K. Eberl

Max-Planck-Institut für FKF, Heisenbergstraße 1, D-70569 Stuttgart, Germany.  
Tel: (711) 6891347, Fax: (711) 6891010, e-mail: brunner@servix.mpi-stuttgart.mpg.de

We will describe the structural and photoluminescence (PL) properties of several types of pseudomorphic  $\text{Si}_{1-y}\text{C}_y/\text{Si}_{1-x-y}\text{Ge}_x\text{C}_y$  quantum well (QW) structures which are grown by solid-source molecular beam epitaxy on (001) Si substrates. The systematic studies of band-edge PL from high quality multi-layer samples with varied sequence, composition and width of the layers provide a consistent picture of the band alignments attainable by these new heterostructures on Si.

Optimum  $\text{Si}_{1-y}\text{C}_y$  growth takes place at a substrate temperature of 550°C and a growth rate  $\leq 1 \text{ Å/s}$ . Well-defined alloy layers with no defects or SiC precipitates are observed by TEM. Substitutional C introduces lateral tensile strain  $\varepsilon = 0.35y$  in pseudomorphic  $\text{Si}_{1-y}\text{C}_y$  layers on Si. The C content and layer widths in  $\text{Si}_{1-y}\text{C}_y/\text{Si}$  multi-quantum well (MQW) structures are determined by X-ray diffraction. Excitonic band-edge PL is observed from  $\text{Si}_{1-y}\text{C}_y$  MQW's and even single QW's. Distinct no-phonon, Si-like TO and TA phonon transitions of bound excitons are resolved. The  $\text{Si}_{1-y}\text{C}_y$  band gap is drastically reduced by about  $\Delta E = -y(6.5 \text{ eV})$  for C contents up to about 2% (Fig. 1, [1]). Even thin 11 Å  $\text{Si}_{0.936}\text{C}_{0.064}$  QW's reveal band-edge PL. Reducing the width of  $\text{Si}_{0.99}\text{C}_{0.01}$  layers from 110 Å to 11 Å results in a PL blueshift up to 45 meV caused by quantum confinement (Fig. 2). There is good agreement of the PL energies and effective mass calculations based on a strong and weak confinement of  $\Delta(2)$ -valley electrons and light holes, respectively. The band alignment in  $\text{Si}_{1-y}\text{C}_y/\text{Si}$  QW's is well explained by the strain-induced shift of levels due to C incorporation. In  $\text{Si}_{1-x-y}\text{Ge}_x\text{C}_y$  QW's, compressive strain caused by Ge is partially compensated by C. The strain-induced level splitting is decreased and the band gap increases with y.

A qualitatively different band alignment is realized in closely spaced  $\text{Si}_{1-y}\text{C}_y/\text{Si}_{1-x}\text{Ge}_x$  double quantum wells (DQW) embedded in Si. The PL observed is lower in energy than that of isolated  $\text{Si}_{1-y}\text{C}_y$  and  $\text{Si}_{1-x}\text{Ge}_x$  reference QW's.  $\Delta(2)$  electrons confined in the  $\text{Si}_{1-y}\text{C}_y$  layers and heavy holes localized in the  $\text{Si}_{1-x}\text{Ge}_x$  layers cause spatially indirect PL transitions with no-phonon contributions dominating. The PL from thin DQW's is strongly enhanced compared to  $\text{Si}_{1-x}\text{Ge}_x$  and  $\text{Si}_{1-y}\text{C}_y$  reference QW's but it is quenched at layer widths  $\geq 40 \text{ Å}$  (Fig. 3). This can be assigned to the decreasing overlap of electron and hole wavefunctions in neighbouring QW's of increasing width. It confirms the spatially indirect origin of the PL. In principle, the Si conduction and valence band shifts with C or Ge alloying can be studied independently applying PL spectroscopy from  $\text{Si}_{1-y}\text{C}_y/\text{Si}_{1-x-y}\text{Ge}_x\text{C}_y$  DQW's. This is demonstrated by varying one layer composition and keeping the other constant.

The fundamental physical properties of C-based alloys on Si, which are a reduced lattice constant and a large modulation of the conduction band-edge induced by strain, provide a significant broadening of the possibilities in band structure engineering of Group IV semiconductors. Potential improvement of the structural, optical, and electronic properties of Si and  $\text{Si}_{1-x}\text{Ge}_x$  by C alloying and future devices will be discussed.

[1] K. Brunner, K. Eberl, and W. Winter, Phys. Rev. Lett. 76, 303 (1996).

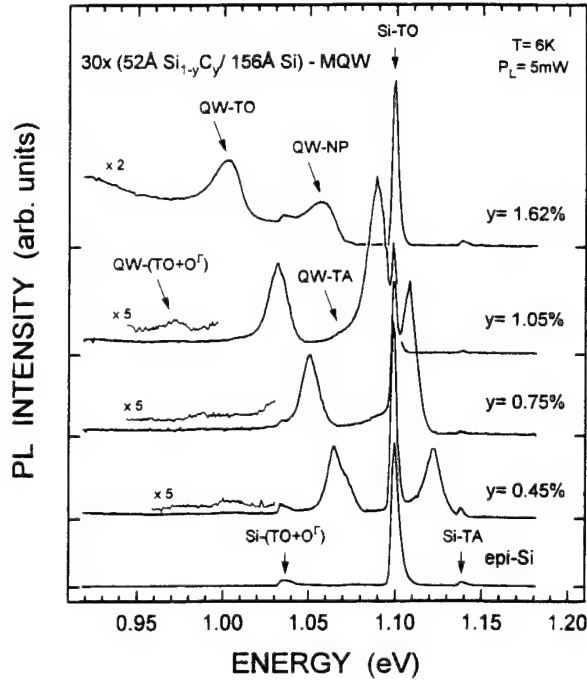


Fig.1

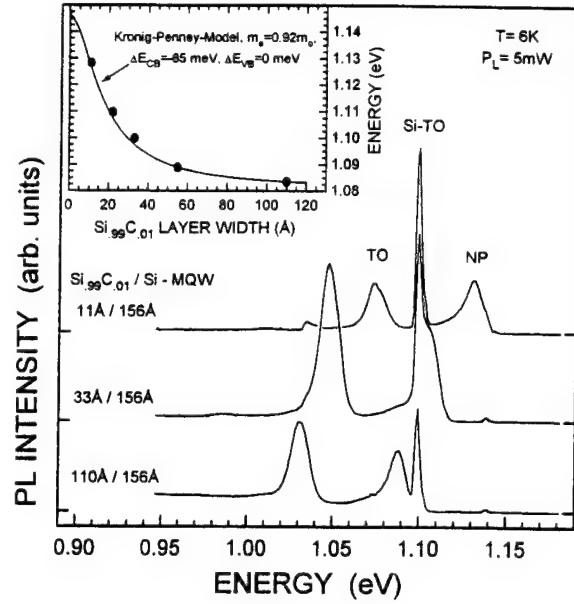


Fig.2

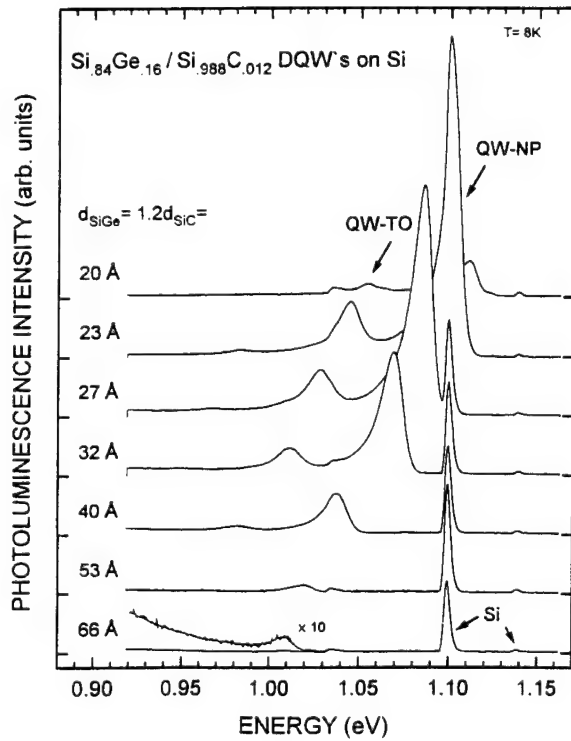


Fig.3

**Fig. 1:** PL spectra from 52Å  $\text{Si}_{1-y}\text{C}_y$  / 156Å Si QW structures on Si. No-phonon and TO phonon PL lines at decreasing energy  $\Delta E = -y \cdot 5.2 \text{ eV}$  originate from the  $\text{Si}_{1-y}\text{C}_y$  QW layers. The PL red-shift is mainly attributed to the strain-induced splitting and lowering of  $\Delta(2)$  electron states.

**Fig. 2:** The PL shifts to higher energy for decreasing the  $\text{Si}_{99}\text{C}_{01}$  QW width. This agrees well with simple effective mass model calculations assuming a strong electron confinement with mass  $m_{\Delta(2)} = 0.92m_0$  in growth direction.

**Fig. 3:** PL spectra from  $\text{Si}_{84}\text{Ge}_{16}$  /  $\text{Si}_{988}\text{C}_{012}$  double quantum well structures of varied width embedded in Si. The PL is dominated by no-phonon transitions (QW-NP) and is attributed to spatially indirect recombination of  $\Delta(2)$  electrons and heavy holes within the SiC and SiGe layers, resp.. For decreasing  $d_{\text{SiGe}} = 1.2d_{\text{SiC}}$ , the PL is blueshifted due to carrier confinement and it is strongly enhanced in intensity.

## **Dynamical STM Studies of the Growth of Si and Ge on Silicon by MBE**

Bert Voigtländer

Institut für Grenzflächenforschung und Vakuumphysik

Forschungszentrum Jülich, 52425 Jülich, Germany

A high temperature scanning tunneling microscope (STM) capable of imaging during MBE-growth is described. We studied the epitaxial growth of Germanium on Silicon at 600 - 900 K sample temperature "in vivo". This technique gives access to the dynamics of the growth process on an atomic scale. The potential of the method is demonstrated by the following results:

- The layer-by-layer growth of the two-dimensional Stranski-Krastanov layer of Ge on Si(111) and the formation of three-dimensional islands during further growth of Ge was observed. An inversion of the aspect ratio of the islands with increasing coverage indicates a transition from coherent to dislocated islands.
- The transition from initial multilayer to pure layer-by-layer growth was imaged in Si(111) homoepitaxy.
- In Si(111) homoepitaxy growth was observed along stripes of the width of a (7x7) unit cell. Upon coalescence of islands new growth facets with different growth speeds are observed.
- Nucleation of next layer growth on Si(111) occurs at domain boundaries of the (7x7) reconstruction.
- In Si/Si(100) homoepitaxy the fractional coverage of the non-equivalent terraces was studied as function of coverage and a theoretically predicted transient growth mode was observed.

Some of the results will be presented on videotape. This method (MBSTM) opens the possibility to follow MBE growth processes dynamically on a nanometer scale and gives access to the evolution of specific features during growth.



## Si(100) homoepitaxy

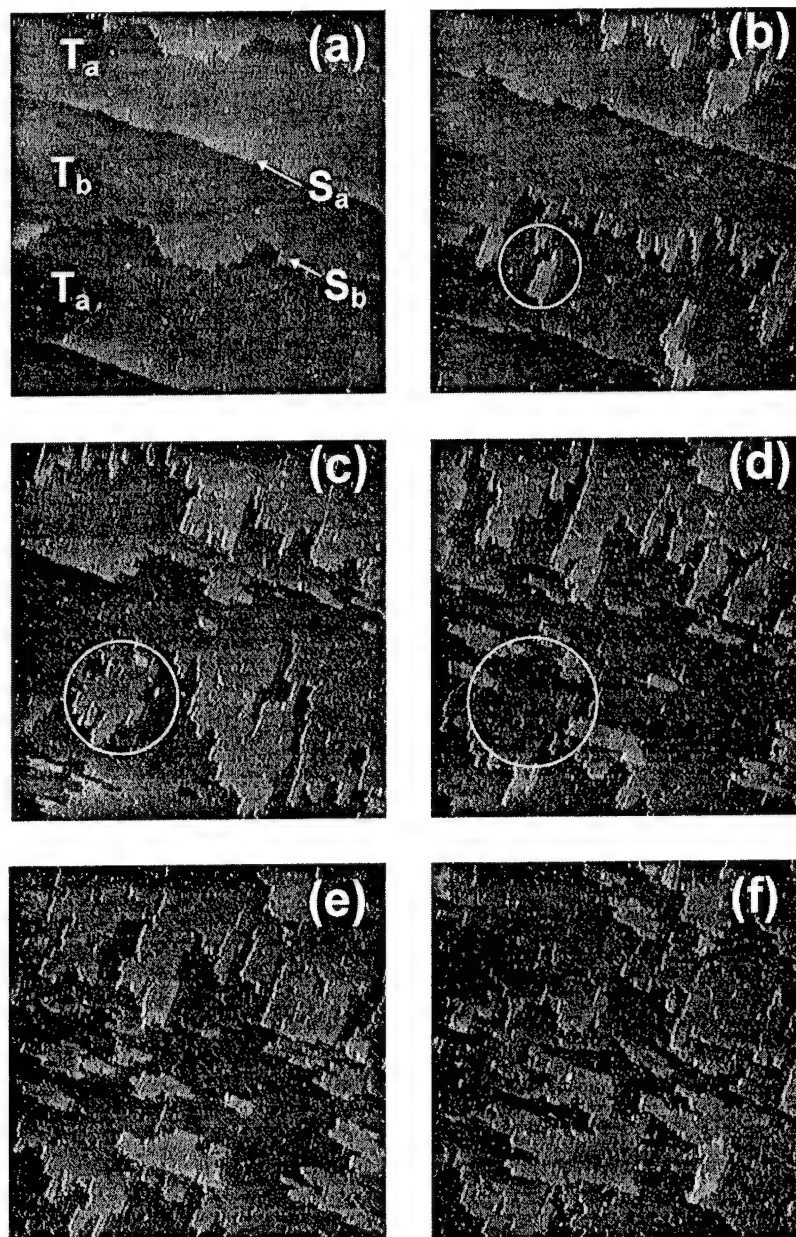


Fig.: STM images ( $2900 \times 2900 \text{ \AA}$ ) of the growth of Si on Si(100) at 725K. Images a-f were recorded at 0.22, 0.53, 0.94 and 1.14 layers Si coverage respectively. In (b-d) an island is indicated where the (2x1) reconstruction is out of phase with the upper terrace. This induces nucleation of islands upon coalescence of this island with the upper terrace.

## MBE growth and structural characterization of $\text{Si}_{1-y}\text{C}_y/\text{Si}_{1-x}\text{Ge}_x$ superlattices

S.Zerlauth<sup>1</sup>, J.Stangl, A.A.Darhuber, F.Schäffler and G.Bauer

Institut für Halbleiterphysik, Johannes Kepler Universität Linz, A-4040 Linz, Austria

We have investigated the MBE growth of strain compensated SiGe/SiC superlattices deposited on (001) Si substrates. The lattice constant of  $\text{Si}_{1-y}\text{C}_y$  alloys is smaller than that of Si and decreases strongly with carbon concentration, in contrast to  $\text{Si}_{1-x}\text{Ge}_x$  alloys where the lattice constant increases. As a consequence the biaxial compressive strain of  $\text{Si}_{1-x}\text{Ge}_x$  layers on Si can be compensated by introducing tensilely strained  $\text{Si}_{1-y}\text{C}_y$  layers, the compensation ratio Ge:C is about 8.5:1. Thus by a proper choice of both the carbon and germanium contents of the alloy layers and their thicknesses, a completely strain symmetrized superlattice structure can be engineered. MBE growth was performed in a chamber equipped with three electron beam evaporators for Si, Ge, and C. The beam fluxes were monitored and controlled with a quadrupole mass spectrometer. Samples were grown at temperatures between 400 and 500°C with periods between 6 and 40 nm, with Ge contents up to 27 % and C contents up to 3%. The structural properties of these superlattices were investigated by high resolution x-ray diffraction and their interface roughness by x-ray reflectivity. From high resolution x-ray reciprocal space mapping around the (004) and (224) reflections quantitative information on their strain states was obtained. It was established that the superlattices were completely pseudomorphic. Using dynamical simulations of the rocking curves ( $\omega$ -2 $\theta$  scans) the superlattice periods, the  $\text{Si}_{1-y}\text{C}_y$  and  $\text{Si}_{1-x}\text{Ge}_x$  layer thicknesses and the Ge and C contents were obtained. The morphology of the  $\text{Si}_{1-y}\text{C}_y/\text{Si}_{1-x}\text{Ge}_x$  interfaces, in particular their roughness and its correlations were determined by specular x-ray reflectivity measurements using synchrotron radiation (Optics beamline of the ESRF, Grenoble). From these measurements, the thickness of the layers, their chemical composition as well as the root mean square roughness of the interfaces have been obtained. Apart from the  $\omega$ -2 $\theta$  scans, in the non-specular mode also  $\omega$  scans were performed at different 2 $\theta$  settings, corresponding to several satellite maxima around (000) of the specular reflectivity. Thus information on the correlation properties of the interfaces were obtained as well. For the simulations, we assumed according to Ref.3 a correlation function of the roughness replication, and the calculations of the diffuse scattering were performed by means of the distorted wave Born approximation. As a result we find from the fits to the experimental data of the sample with  $y=0.01$  and  $x=0.09$  it turned out that the RMS roughness is  $(4 \pm 1)\text{\AA}$ , a value which is comparable to that of pseudomorphic Si/SiGe superlattices. The values for the in-plane as well as interplane (vertical) correlations of the roughness profiles are of the order of 200 and 120 nm.

- [1] K.Eberl, S.S.Iyer, and F.K.LeGoues, Appl.Phys.Lett. **64**, 793 (1994)
- [2] W.Faschinger, S.Zerlauth, J.Stangl, G.Bauer, Appl. Phys.Lett. **67**, 2630 (1995)
- [3] Z.H.Ming, A.Krol, Y.L.Soo, Y.H.Kao, J.S.Park, K.L.Wang, Phys.Rev. **B47**,16373 (1993)
- [4] R.L.Headrick, J.M.Baribeau, Y.E.Strausser, Appl.Phys.Lett. **66**, 96 (1995)

<sup>1</sup> S.Zerlauth: Phone: +43-732-2468-9607; Fax:+43-732-2468-650; E-Mail: S.Zerlauth@hlphys.uni-linz.ac.at

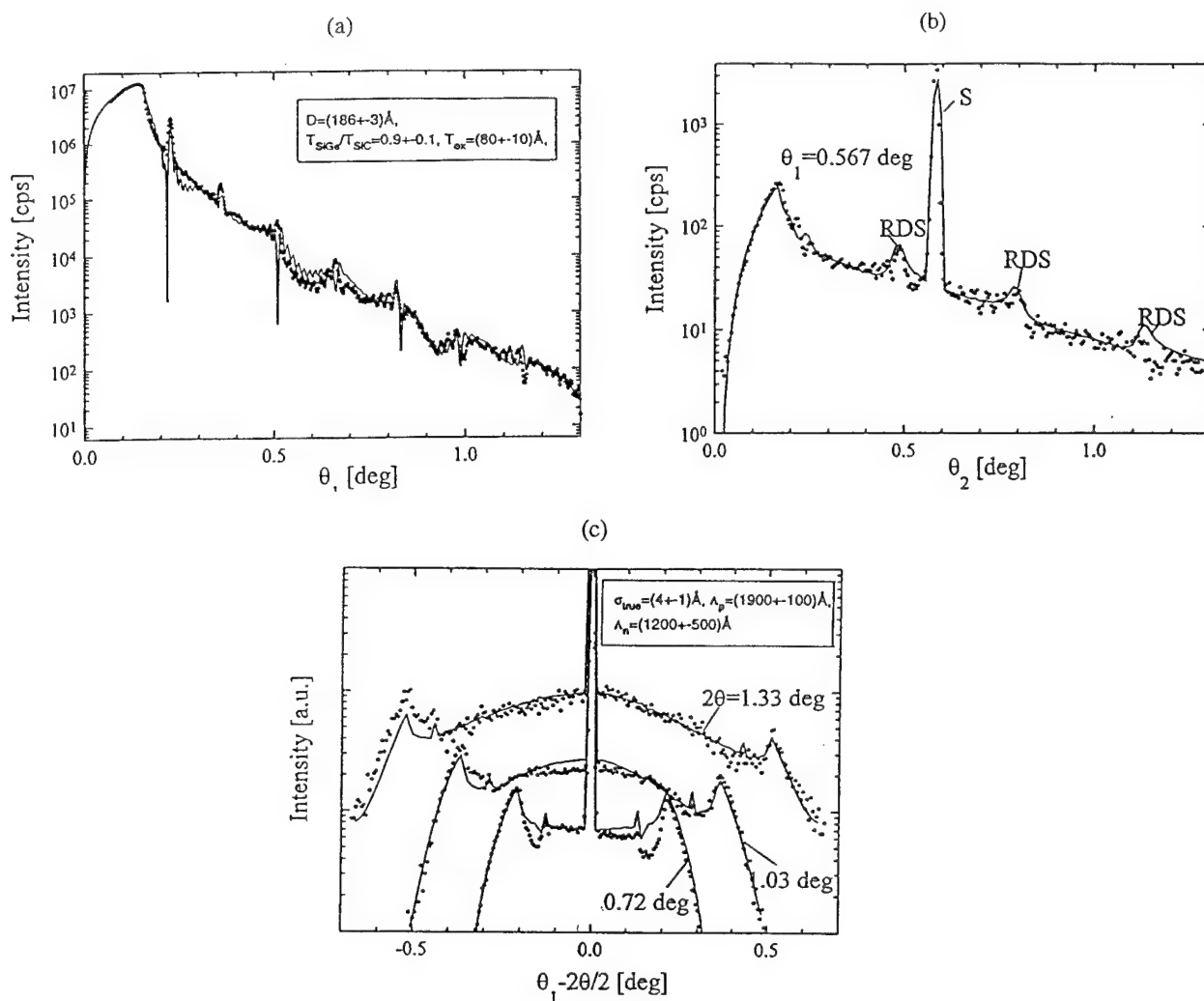


**Figure 1:** (a) Measured and simulated specular reflectivity ( $\omega$ - $2\theta$ -scan)  
 (b)  $2\theta$ -scan  
 (c)  $\omega$ -scans at different  $2\theta$ -settings around (000) of the specular reflectivity

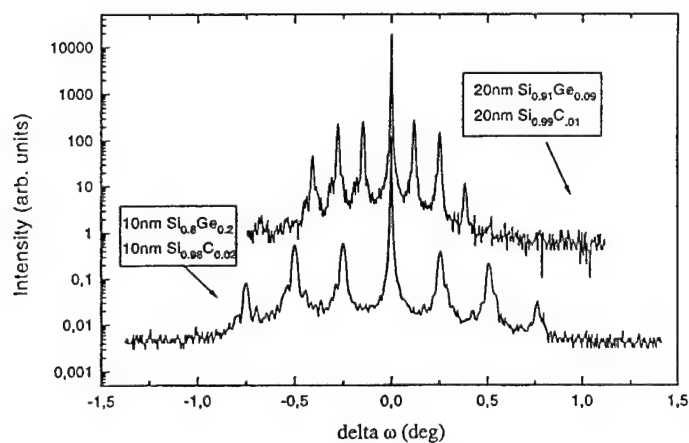


**Figure 2:** Measured rocking curves of 2 different strain compensated superlattices

## Why is a quantum confined Stark shift absent in type-I strained $\text{Si}_{1-x}\text{Ge}_x/\text{Si}$ type-I symmetric quantum wells ?

Y.Miyake, and S. Fukatsu

Department of Pure and Applied Sciences,  
The University of Tokyo, 3-8-1 Komaba, Meguro-ku, Tokyo 153, Japan

J.Y.Kim, and Y.Shiraki

RCAST, The University of Tokyo, 4-6-1 Komaba, Meguro-ku, Tokyo 153, Japan

Electrical control is a key feature in tuning semiconductor devices and there has been a surge of demand for development of optoelectronic devices utilizing electrically controlled optical phenomena based on quantum effects. Application of a dc field across a quantum confined exciton leads to distinct electro-optic effects such as quantum-confined Stark (QCS) shift. For GaAs/AlGaAs, purely excitonic optic modulation based on dc field control has been demonstrated. An intriguing point is that the free exciton (FE) binding energy,  $E_B$ , in GaAs is  $\approx 4\text{--}8\text{meV}$  and relatively small. This is contrasted with  $E_B=15\text{--}30\text{meV}$  for SiGe strained quantum wells (QWs). However, for these "type-I QWs", early attempts were not successful in identifying the QCS effects as opposed to fairly large shifts observed in type-II QWs.

In this paper, we present a study of electric field effects on FE recombination in type-I strained  $\text{Si}_{1-x}\text{Ge}_x/\text{Si}$  symmetric QWs. The extreme vulnerability of free excitons to electric field is demonstrated, accounting for the apparent loss of QCS effects.

The field effect was studied over a series of single QWs ( $x=0.18$ ,  $L_z=10\text{--}216\text{\AA}$ ) grown by gas source MBE at  $740^\circ\text{C}$ . The electric bias was applied on Al contact pads on both sides of the wafer using a dc voltage source. Thus the field is applied along the quantization axis.

With increasing electric field,  $F<2\text{kV/cm}$ , free-excitonic photoluminescence exhibited a steady blue-shift, up to  $3\text{meV}$ , of the peak energies. This was consistently observed for all well width, thereby the anticipated downward shift due to the QCS effect being suppressed. The blue shifts are attributed to a reduction of  $E_B$  with increasing field strength even in the weak field regime. To confirm this,  $E_B$  was calculated as functions of electric field and well width by the variational method taking account of appropriate QCS red-shifts. We found that the blue-shifts due to  $E_B$  reduction are always greater than the QCS shifts at lower fields, clearly confirming the observation. As expected, the calculated results well reproduce the field dependence of the blue-shifts observed. Interestingly, the blue shifts followed a quadratic increase with field both theoretically and experimentally reflecting the symmetric QW potential.

There still remains a question as to why SiGe FE is vulnerable to field compared to FE in GaAs despite its large binding energy.  $E_B$  was calculated for different conduction band offsets and the answer was that the realistic conduction band offset,  $\approx 7\text{meV}$ , is too small to withstand  $F$ . In addition, this also accounts for the mixed dimensionality as confirmed for FE.

The results seem to encompass the future direction of electro-optic device fabrication.

---

Contact author:

S. Fukatsu

Department of Pure and Applied Sciences,

The University of Tokyo, 3-8-1 Komaba, Meguro-ku, Tokyo 153, Japan,

Tel: +81-3-5454-6754; Fax: +81-3-5454-4311, E-mail: fkatz@srv.bme.rcast.u-tokyo.ac.jp

Why is a quantum confined Stark shift absent in type-I strained  $\text{Si}_{1-x}\text{Ge}_x/\text{Si}$  type-I symmetric quantum wells ?

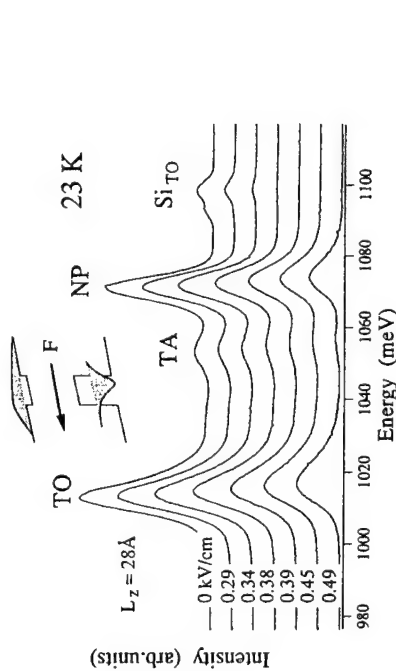


FIG.1. 23K photoluminescence spectra of a single strained  $\text{Si}/\text{SiGe}$  type-I symmetric QW under electric fields.

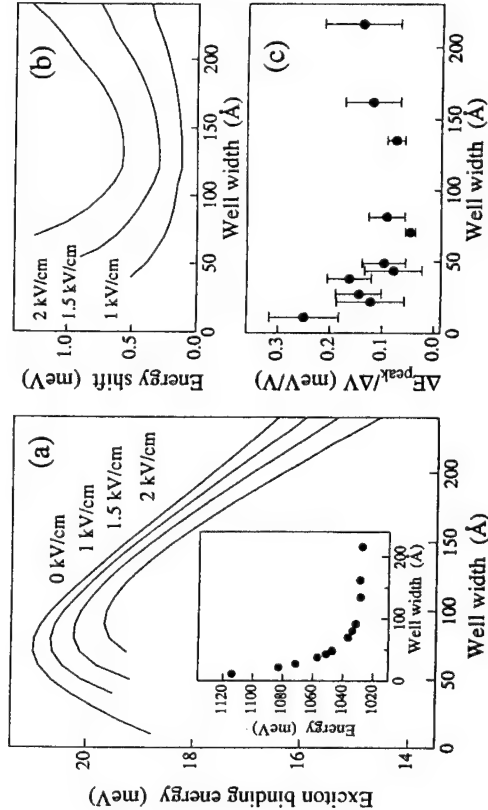


FIG.3. (a) Exciton binding energy vs well width as functions of electric field. Inset shows the peak energies vs well width. Theoretical (b) and experimental (c) peak shift vs well width.

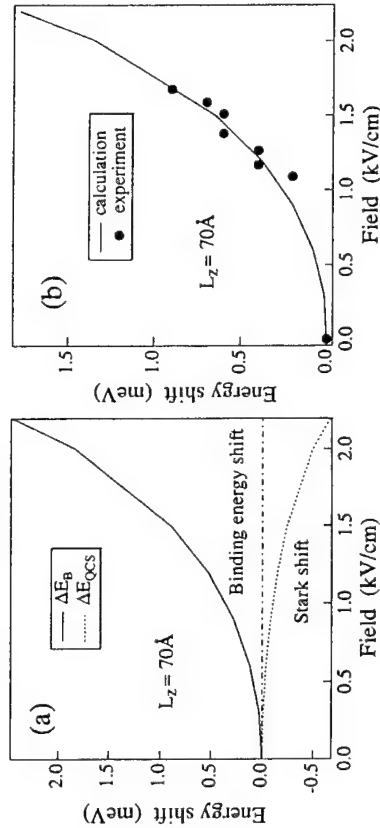


FIG.2. Field dependence of FE binding energy and QCS shifts. Left: calculation. Right: Experiment (line is the fit).

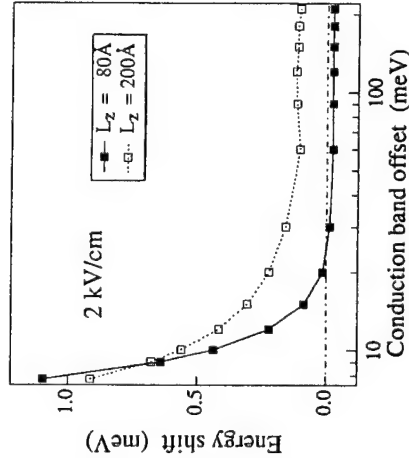


FIG.4. Field driven peak shift as a function of conduction band offset. The realistic one is 7.7meV and at the left extreme. Note the QCS red shift is expected to show up only at larger conduction band offsets.

# Photoluminescence and X-ray Characterization of relaxed $\text{Si}_{1-x}\text{Ge}_x$ alloys grown on Silicon on Insulator (SOI) and implanted SOI substrates

MICHAEL A. CHU\*, Martin O. Tanner, Fengyi Huang, and Kang L. Wang

Device Research Laboratory  
Department of Electrical Engineering  
UCLA, Los Angeles, CA 90095-1594

Gordon G. Chu and Mark S. Goorsky  
Department of Materials Science and Engineering  
UCLA, Los Angeles, CA 90095

Recently, there has been an interest in relaxed low-dislocation films of  $\text{Si}_{1-x}\text{Ge}_x$  for the growth of commensurately strained SiGe heterostructures. These relaxed films allow for increased flexibility in designing heterostructures and offer benefits that are just beginning to surface such as enhanced electron mobilities for strained silicon on relaxed  $\text{Si}_{1-x}\text{Ge}_x$ <sup>1,2</sup>.

We have previously studied the growth and relaxation of  $\text{Si}_{0.86}\text{Ge}_{0.14}$  on very thin Bond-Etchback Silicon on Insulator (BESOI)<sup>3</sup>. In this work, we examined  $\text{Si}_{0.86}\text{Ge}_{0.14}$  layers grown on BESOI and the effect of ion-implantation of the viscous flow of the  $\text{SiO}_2$  layer which allows relaxation of the SiGe layer. The objective of this work is to reduce the reflow temperature of the  $\text{SiO}_2$  layer to allow in-situ growth and anneal and improve the relaxation of SiGe layers. In this experiment, a BESOI substrate was implanted with boron and subsequently with oxygen in an attempt to create a borosilicate glass in the  $\text{SiO}_2$  region. Then,  $\text{Si}_{0.7}\text{Ge}_{0.3}$  layers were grown using solid source MBE on both implanted and unimplanted BESOI substrates. Samples were then annealed at temperatures from 700 °C to 1000 °C for as little as 30 minutes.

Photoluminescence (PL) and triple-axis x-ray diffraction were used to characterize film quality, Ge concentration and percent relaxation. We see a dramatic decrease in the annealing temperature required (roughly a difference of 200-300 °C) to relax the  $\text{Si}_{0.7}\text{Ge}_{0.3}$  layer fully. The PL spectra shows a broad band around 800 meV that we believe is related to the relaxation of the SiGe layer. It can be seen to increase in intensity and then decrease dramatically when the layer begins to relax. For the sample grown on implanted BESOI, it is shown to disappear completely at an annealing temperature of 900 °C. Above 900 °C, we also begin to see the evolution of near bandgap luminescence for the  $\text{Si}_{0.7}\text{Ge}_{0.3}$  layer grown on boron and oxygen implanted BESOI. The energy peak which shifts to higher energies with greater relaxation, from 970 meV to 1025 meV, is only observed for the sample grown on the implanted substrate. It is believed that this is primarily due to the reduced reflow temperature and low dislocation concentration of the  $\text{Si}_{0.7}\text{Ge}_{0.3}$  film. High resolution triple-axis x-ray diffraction was used to confirm the Ge concentration and percent relaxation.

<sup>1</sup>K. Ismail, M. Arafa, et al., *Appl. Phys. Lett.* **66** 1995.

<sup>2</sup>Y. H. Xie, E. A. Fitzgerald, et al., *J. Appl. Phys.* **73** (12) 1993.

<sup>3</sup>M. O. Tanner, M. O., M. A. Chu, et al., *J. Crystal Growth*, **157** 1995.

\* Contact Person. Address: Device Research Laboratory, Department of Electrical Engineering, University of California, Los Angeles, Los Angeles, California 90095-1594. Telephone: (310) 206-1693. Fax: (310) 206-8495. E-mail: mchu@ee.ucla.edu

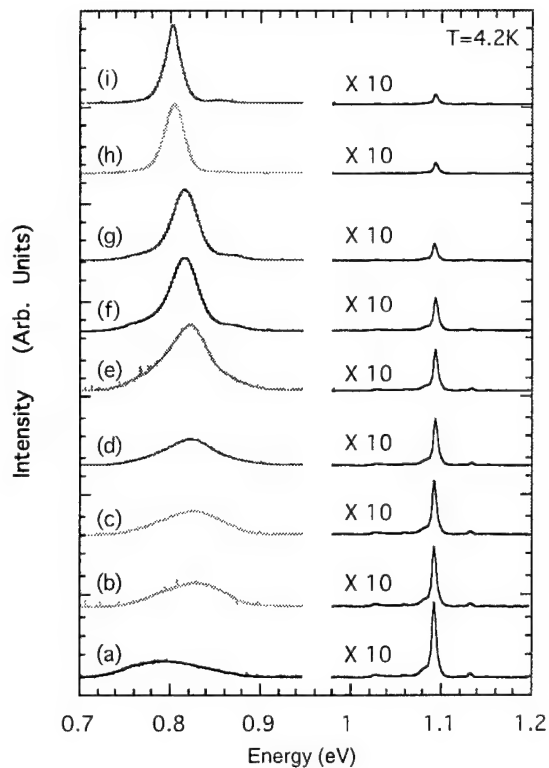


Figure 1 - PL spectra of Sample A as a function of annealing temperature and time -  $\text{Si}_7\text{Ge}_3$  alloy layer on a p-Si substrate; (a) As grown (b)  $800^\circ\text{C}$  - 30 min. (c)  $800^\circ\text{C}$  - 60 min. (d)  $900^\circ\text{C}$  - 30 min. (e)  $900^\circ\text{C}$  - 60 min. (f)  $1000^\circ\text{C}$  - 30 min. (g)  $1000^\circ\text{C}$  - 60 min. (h)  $1100^\circ\text{C}$  - 30 min. (i)  $1100^\circ\text{C}$  - 60 min.

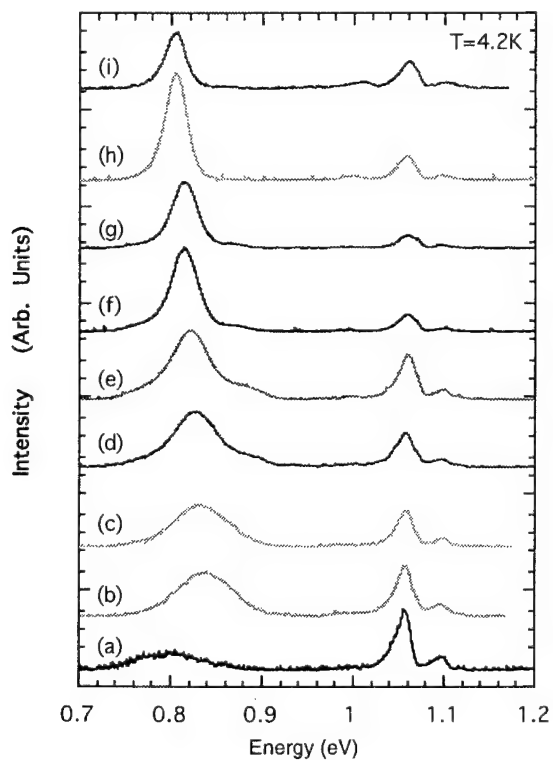


Figure 2 - PL spectra of Sample B as a function of annealing temperature and time -  $\text{Si}_7\text{Ge}_3$  alloy layer on unimplanted BESOI substrate; (a) As grown (b)  $800^\circ\text{C}$  - 30 min. (c)  $800^\circ\text{C}$  - 60 min. (d)  $900^\circ\text{C}$  - 30 min. (e)  $900^\circ\text{C}$  - 60 min. (f)  $1000^\circ\text{C}$  - 30 min. (g)  $1000^\circ\text{C}$  - 60 min. (h)  $1100^\circ\text{C}$  - 30 min. (i)  $1100^\circ\text{C}$  - 60 min.

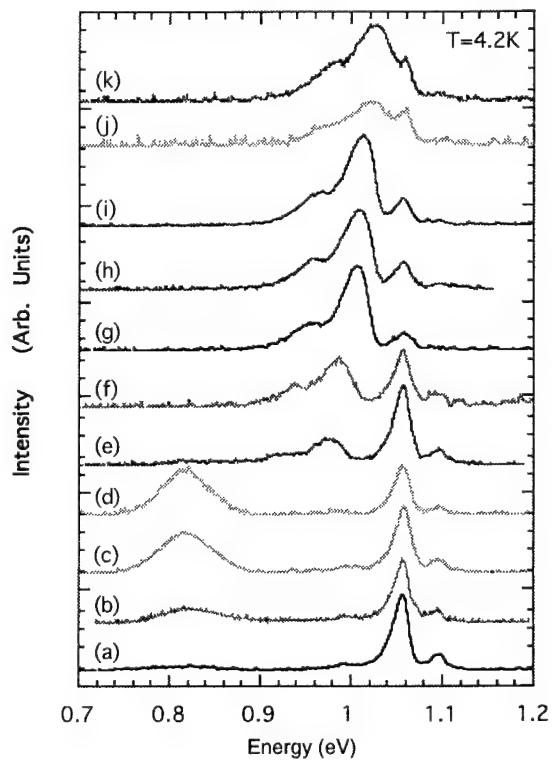


Figure 3 - PL spectra of Sample C as a function of annealing temperature and time -  $\text{Si}_7\text{Ge}_3$  alloy layer on a boron and oxygen implanted BESOI substrate; (a) As grown (b)  $700^\circ\text{C}$  - 30 min. (c)  $800^\circ\text{C}$  - 30 min. (d)  $800^\circ\text{C}$  - 60 min. (e)  $900^\circ\text{C}$  - 30 min. (f)  $900^\circ\text{C}$  - 60 min. (g)  $1000^\circ\text{C}$  - 30 min. (h)  $1000^\circ\text{C}$  - 60 min. (i)  $800^\circ\text{C}$  - 60 min. and  $1000^\circ\text{C}$  - 30 min. (j)  $1100^\circ\text{C}$  - 30 min. (k)  $1100^\circ\text{C}$  - 60 min.



Correspondence; Professor Yoshitaka OKADA

324 CIS-X, Solid State Electronics Laboratory, Stanford University, Stanford, CA 94305

Tel. (415)723-7537 Fax. (415)723-4659

E-mail. okada@luciano.stanford.edu

---

### **Growth of Abrupt GaAs/Ge Interfaces by Atomic Hydrogen-Assisted MBE**

Y. Okada, J. S. Harris, Jr.

Solid State Electronics Laboratory, Stanford University, Stanford, CA 94305

A. Sutoh and M. Kawabe

Institute of Materials Science, University of Tsukuba, 1-1-1 Tennodai, Tsukuba, Ibaraki, Japan

The GaAs/Ge system is attracting increasing interest for low-cost, high-efficiency solar cells and patterned growth for non-linear optics. Its heteroepitaxy is somewhat facilitated by the fact that GaAs and Ge(100) not only have a small lattice-mismatch ( $\Delta a / a \sim 0.1\%$ ), but the difference in their thermal expansion coefficients  $\Delta\alpha$  and thus thermal stress is also favorably small in comparison to a more popular GaAs/Si system ( $\Delta a / a \sim 4.0\%$  and  $\Delta\alpha \sim 60\%$ ). There is, however, a problem of significant Ge segregation into the GaAs when GaAs is grown on Ge(100) at high growth temperatures ( $> 450^\circ\text{C}$ ). As a consequence, the nucleation and initial growth stage proceeds by an islanded three-dimensional (3D) growth which degrades the surface smoothness as well as interface abruptness.

We have developed high-quality heteroepitaxy of GaAs-on-Ge using a low growth temperature of  $\sim 400^\circ\text{C}$  combined with atomic hydrogen-assisted MBE (H-MBE). Continuous generation and irradiation of atomic H inside a conventional MBE growth chamber is done with a cracker that fits into one of the effusion cell ports. The hydrogen cracker consists of a spirally-wound tungsten filament, which when heated  $> \sim 1500^\circ\text{C}$ , dissociates the molecular hydrogen into atomic H. The important concept in the H-MBE growth technique is that atomic H is employed as a *surfactant*, which acts to modify the kinetics and energetics of the growth that are in general very difficult to control at the atomic-scale unless a third element, like a surfactant, is introduced into both heteroepitaxy and homoepitaxy.

Using RHEED, AFM and SIMS as main characterization tools, we demonstrate that H-MBE growth results in significant reduction of Ge segregation during GaAs-on-Ge heteroepitaxy and consequently, atomically smooth surfaces (as shown in Fig. 1) and abrupt GaAs/Ge heterointerfaces are formed. For example, SIMS profiles measured for samples grown at  $400^\circ\text{C}$  (as plotted in Fig. 2 and 3) show that after an initial decrease of Ge concentration at the GaAs/Ge interface with a slope of  $\sim 7.6\text{nm/dec}$ , the slope levels off to  $\sim 17\text{ nm/dec}$  at a concentration of  $\sim 1.4 \times 10^{20}\text{ cm}^{-3}$  in the MBE-grown sample, while the slope is almost unchanged for the H-MBE case and the Ge concentration drops abruptly down to a measurement limit of  $< 2.2 \times 10^{18}\text{ cm}^{-3}$ . Both the Ge concentration at the bending point and level-off slope in the SIMS profiles were found to be smaller for the H-MBE than MBE for the temperature range of  $330$  and  $560^\circ\text{C}$ . It was further found that irradiation of atomic H during the MBE growth favorably brings up additional effects, such as removal of surface contaminants such as oxygen (as from Fig. 4).

Segregation is closely related to the strength of bonding energy, the surface and interface energies of the system, the dislocations and defects, and the charge neutrality requirements especially in polar-on-nonpolar heteroepitaxy. We will discuss the mechanisms responsible for these observed Ge segregation reduction in H-MBE technique in terms of surfactant nature of atomic H.



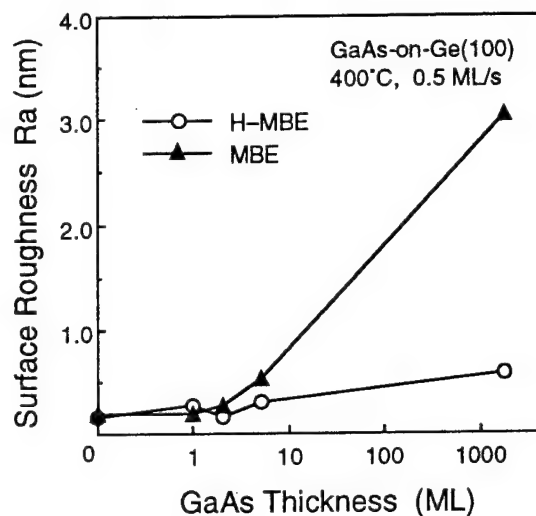


Fig. 1 Average surface roughness measured by AFM. H-MBE gives atomically flat surface of GaAs/Ge.

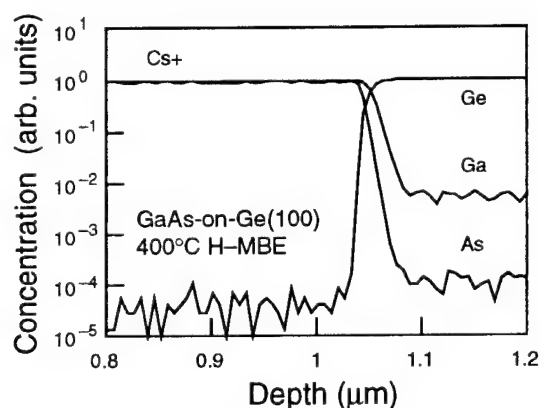


Fig. 2 SIMS depth profiles for samples grown by H-MBE. Ge segregation is significantly reduced.

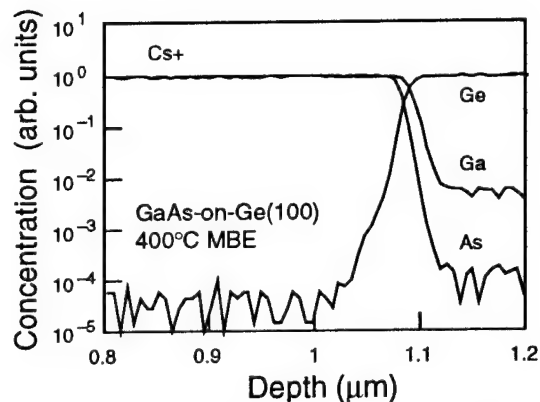


Fig. 3 SIMS depth profiles for samples grown by conventional MBE.

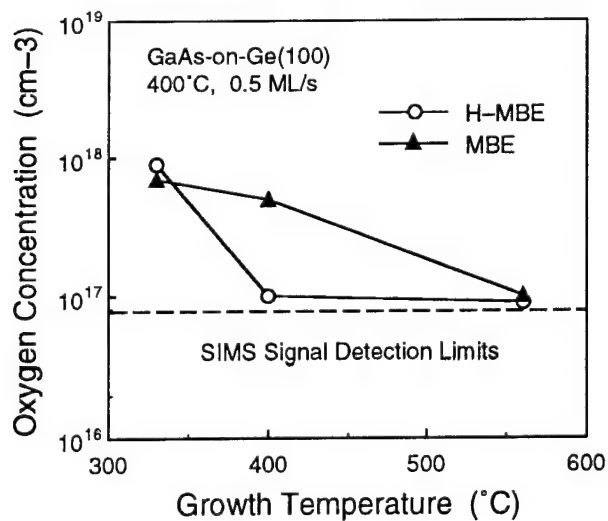


Fig. 4 Oxygen concentrations in GaAs epilayers on Ge. Oxygen incorporation is lower for H-MBE.

## 8. REGROWTH

WEDNESDAY MORNING (SMOTHERS)

Session Chair: Charles Tu, University of California, San Diego

Co-Chair: Larry Sadwick, University of Utah, Salt Lake City, Utah

- 09:00 8.1 **Improving the etched/regrown GaAs interface by in-situ etching and chemical beam epitaxy using tris-dimethylaminoarsenic**  
N.Y. Li, Y.M. Hsin, W.G. Bi, P.M. Asbeck, and C.W. Tu  
University of California, San Diego, USA
- 09:20 8.2 **Micro-reversibility during MBE growth and in situ etching of GaAs/AlGaAs heterostructures**, T. Kaneko, T. Säger, M. Ritz, and K. Eberl  
Max-Planck-Institut für Festkörperforschung, Stuttgart, Germany.
- 09:40 8.3 **Analysis of in-situ etched and regrown  $\text{Al}_{0.48}\text{In}_{0.52}\text{As}$ - $\text{Ga}_{0.47}\text{In}_{0.53}\text{As}$  interfaces**  
P. Chavarkar, D.S.L. Mui, T. Strand, L.A. Coldren, U.K. Mishra  
University of California, Santa Barbara, USA.
- 10:00 8.4 **Lateral coupling of InP/GaInAsP/InP structures by selective area MOMBE**  
M. Wachter, U. Schöffel, M. Schier, and H. Heinecke  
University of Ulm, Germany
- Break
- 10:40 8.5 **Selective area epitaxy of GaAs using combined very low energy Ga+ focused ion beam deposition and molecular beam epitaxial growth**  
H.E. Beere, J.H. Thompson, G.A.C. Jones, and D.A. Ritchie  
Univeristy of Cambridge, United Kingdom.
- 11:00 8.6 **Selective area chemical beam epitaxial regrowth of Si-doped GaAs and InP by using silicon tetraiodide for HFET application**, Shigekazu Izumi, Norio Hayafuji, Testsuro Kunii, Shinichi Miyakuni, Kazuhiko Ito, Kazuhiko Sato, and Mutsuyuki Otsubo, Mitsubishi Electric Corporation, Hyogo, Japan.
- 11:20 8.7 **MBE regrowth on AlGaInAs DFB gratings using in-situ hydrogen radical cleaning**, H. Künael, J. Böttcher, A. Hase, H.-J. Hensel, K. Janiak, A. Paraskevopoulos, and G. Urmann  
Heinrich-Hertz-Institut für Nachrichtentechnik, Berlin, Germany.
- 11:40 8.8 **Hydrogen radical surface cleaning of GaAs for MBE regrowth**  
T.M. Burke, E.H. Linfield, M.A. Quierin, D.A. Ritchie, M. Pepper, and J.H. Burroughes, University of Cambridge, United Kingdom.

## Improving the etched/regrown GaAs interface by in-situ etching and chemical beam epitaxy using tris-dimethylaminoarsenic

N. Y. Li, Y. M. Hsin, W. G. Bi, P. M. Asbeck, and C. W. Tu

*Department of Electrical and Computer Engineering*

*University of California at San Diego, La Jolla, CA 92093-0407, USA*

E-mail address: nli@sdcc3.ucsd.edu, Fax: (619) 534-2486, Tel: (619) 534-3014

Multiple processes of ex-situ etching and passivation of semiconductor heterostructures before regrowth are commonly used to improve the performance of advanced electronic and optoelectronic devices, but one can not expect to obtain a clean etched/regrown interface by these ex-situ processes due to possible contamination in the atmosphere. Mui et al.<sup>1</sup> reported a high quality etched/regrown GaAs interfaces using an in-situ  $\text{Cl}_2$  etching process, but a complicated interlocking system of separate growth and etching chambers was used. Tsang et al.<sup>2</sup> reported in-situ etching of GaAs and InP using  $\text{AsCl}_3$  and  $\text{PCl}_3$  prior to regrowth in the same chemical beam epitaxy (CBE) chamber; therefore, possible contamination in the etched/regrown interface can be minimized. However,  $\text{Cl}_2$  decomposed from  $\text{AsCl}_3$  or  $\text{PCl}_3$  may etch filaments in the growth chamber, and the long term use of  $\text{AsCl}_3$  or  $\text{PCl}_3$  could be a concern. Recently, Villaflor et al. found that tris-dimethylaminoarsenic (TDMAs) has an etching effect on GaAs<sup>3</sup>, but the TDMAs etched/regrown interface of GaAs has not been reported. In this talk, we report our studies on etching of  $\text{Al}_x\text{Ga}_{1-x}\text{As}$  ( $0 \leq x \leq 0.25$ ) by TDMAs at different substrate temperatures and the etched/regrown GaAs interface.

The in-situ etching experiments were conducted in a modified Perkin-Elmer 425 CBE chamber. Reflection high-energy electron diffraction (RHEED) study shows that TDMAs can remove efficiently the oxide layer of GaAs at a substrate temperature of  $470^\circ\text{C}$ . This low-temperature cleaning process of GaAs prior to regrowth is very important for high-quality regrown devices. A 2500Å-thick  $\text{SiO}_2$  film was deposited on  $\text{Al}_x\text{Ga}_{1-x}\text{As}$  epilayers as the mask for determining the TDMAs etch rate at different substrate temperatures. The etch rate of  $\text{Al}_x\text{Ga}_{1-x}\text{As}$  increases with increasing substrate temperature, but decreases with increasing Al composition.

To study quantitatively the interface trap density in the etched/regrown interfaces, n-GaAs epilayers ( $4 \times 10^{17} \text{ cm}^{-3}$ ) were exposed at  $600^\circ\text{C}$  to  $\text{As}_4$  for 10 minutes (sample A) or to TDMAs for ~ 30 seconds (sample B) to desorb the oxide layers. Prior to regrowth Sample B was etched by TDMAs for another 10 minutes (removing ~ 65Å). Capacitance-voltage carrier profiles show that the interface trap density of the TDMAs etched/regrown interface was reduced by about a factor of 3. Further experimental results with different in-situ etching/regrowth conditions will be reported.

In summary, TDMAs is shown to be an effective precursor for etching GaAs at a lower substrate temperature as well as for regrowing GaAs, thus providing a cleaner etched/regrown interface for novel device applications.

This work is supported by the U. S. Air Force Wright Laboratory.

<sup>1</sup> D. S. L. Mui, T. A. Strand, B. J. Thibeault, L. A. Coldren, P. M. Petroff, and E. L. Hu, Inst. Phys. Conf. Ser. 141 (1995) 69.

<sup>2</sup> W. T. Tsang, R. Kapre, and P. F. Sciortino, Jr., J. Crystal Growth 136 (1994) 42.

<sup>3</sup> A. B. Villaflor, H. Asahi, D. Marx, K. Miki, K. Yamamoto, S. Gonda, J. Crystal Growth 150 (1994) 638.

## Micro-reversibility during MBE growth and *in situ* etching of GaAs/AlGaAs heterostructures

T. Kaneko, T. Säger, M.Ritz and K. Eberl

Max-Planck-Institut für Festkörperforschung, Stuttgart, Germany

Fax: +44-711-689-1010, Tel+44-711-689-1313, e-mail: kaneko@servix.mpi-stuttgart.mpg.de

Recently, RHEED intensity oscillations have been observed during the etching of GaAs using  $\text{AsCl}_3$  [1],  $\text{AsBr}_3$  [2,3] and tris-dimethylaminoarsenic (TDMAs) [4]. This *in situ* etching occurs via a layer-by-layer mechanism analogous to the reverse process of growth and enables control on the atomic scale. A combination of *in situ* etching and growth within the same UHV chamber offers considerable potential for fabricating novel low dimensional structures.

In this work, we demonstrate the first *in situ* etching of GaAs/AlGaAs/AlAs heterostructures using  $\text{AsBr}_3$ . The observation of RHEED intensity oscillations allows to distinguish the etchings between AlAs, AlGaAs and GaAs because of large selectivity in etching rates between GaAs and AlAs. The availability of two reverse functions: removal and deposition, for controlling thickness and selectivity of heterostructures with atomic layer precision represents micro-reversibility between etching and growth. The experiments were carried out in a modified conventional solid source MBE system equipped with a gas manifold for  $\text{AsBr}_3$  (6N) to be introduced without any carrier gas.

Fig. 1 shows the substrate temperature dependence of the etching rate for  $\text{Al}_x\text{Ga}_{1-x}\text{As}$  ( $0 \leq x \leq 1$ ) at a fixed  $\text{AsBr}_3$  flow rate of 0.080 sccm, where the etching rate was obtained from the period of the RHEED oscillations. The removal of AlAs indicates a reaction rate limited mode for the whole temperature range, in contrast with the case of GaAs where the reaction rate limited region ( $< 500^\circ\text{C}$ ) can be distinguished from a supply rate limited region ( $> 500^\circ\text{C}$ ). The removal of AlGaAs seems rather complicated reflecting the more feature of the AlAs etching. The scaling of etching rate as a function of Al content can be used to determine the Al content for any AlGaAs samples. Fig. 2 shows the RHEED specular beam intensities during the etching of the heterostructure: GaAs(9ML)/AlGaAs(9ML)/AlAs(6ML)/GaAs substrate at a fixed  $\text{AsBr}_3$  flow rate. As a comparison, the beam intensities during the growth are also shown in the same figure. Three different etching rates are observed as the etching proceeds, where lower etching rate corresponds to the etching of AlGaAs with higher Al-content, as shown in Fig. 1. At the interface between GaAs and AlGaAs during etching, one can see the larger number of oscillations corresponding to the GaAs etching rate than the actual number of GaAs (9ML). This is considered to be associated with surface segregation of Ga on the AlGaAs layer. *In situ* etching through different materials could provide a new technique to investigate surface/ interface roughness on the atomic scale.

We will also discuss about optimum etching conditions to minimise the degradation of surface morphology and reduce interface roughness, and selective etching through  $\text{SiO}_2$  mask.

1. W.T.Tsang, T.H.Chui and R.M.Kapre, Appl.Phys.Lett. **63** (1993) 3500
2. T.Kaneko, P.Smilauer, B.A.Joyce, T.Kawamura and D.D.Vvedensky, Phys.Rev.Lett. **74** (1995) 3289
3. T.Kaneko, T. Säger and K. Eberl, Mater.Res;Soc.Proc. 1995 (to be published)
4. H.Asahi, X.F.Liu, K.Inoue, D.Marx, K.Asami, M.Miki and S.Gonda, J.Crystal Growth **145** (1994) 668

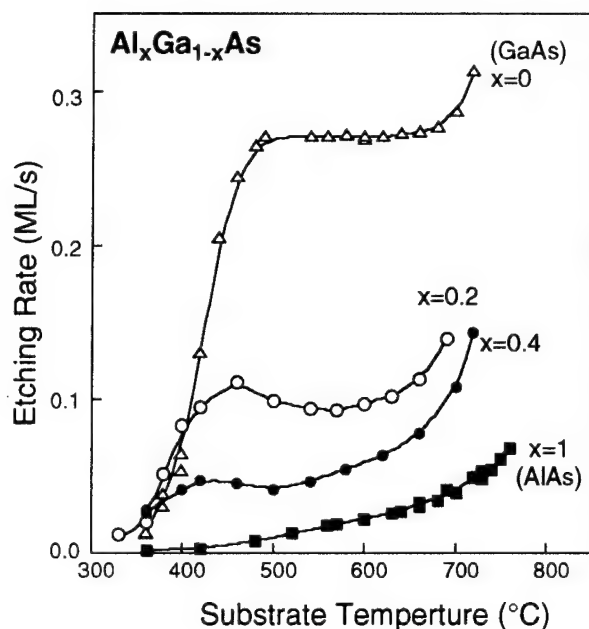


**Fig. 1** The variation with temperatures in the etching rates of  $\text{Al}_x\text{Ga}_{1-x}\text{As}(100)$  at an  $\text{AsBr}_3$  flow rate of 0.080 sccm and a concomitant  $\text{As}_4$  flux of 1.5 ML/s. The etching rate is determined from the period of the RHED oscillations.

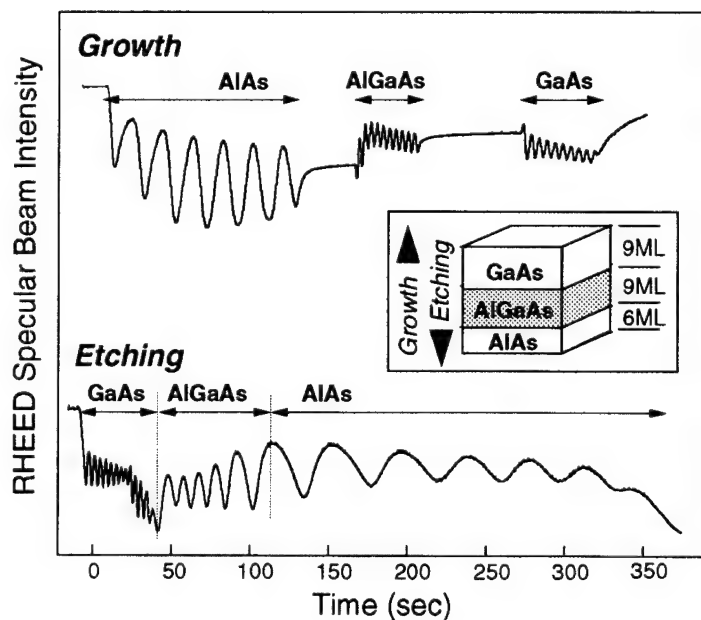


**Fig. 2** The RHEED specular-beam intensity evolution during the growth (upper) and etching (lower) of  $\text{GaAs}(9\text{ML})/\text{Al}_{0.2}\text{Ga}_{0.8}\text{As}(9\text{ML})/\text{AlAs}(6\text{ML})$  on  $\text{GaAs}(100)$  substrate at substrate temperature of  $600^\circ\text{C}$ , an  $\text{AsBr}_3$  flow rate of 0.080 sccm and a concomitant  $\text{As}_4$  flux of 1.5 ML/s

## Analysis of *in-situ* etched and regrown $\text{Al}_{0.48}\text{In}_{0.52}\text{As}$ - $\text{Ga}_{0.47}\text{In}_{0.53}\text{As}$ interfaces

P. Chavarkar, D.S.L.Mui, T. Strand, L.A.Coldren, U.K.Mishra

Department of Electrical and Computer Engineering

University of California, Santa Barbara CA 93106

Tel : 805 - 893- 3812, Fax : 805 - 893 - 3262

Email :prashant@nemesis.ece.ucsb.edu

*This work funded by ARPA ( Thunder and Lightning) and QUEST*

### Abstract

*In-situ* processing has recently been investigated for the fabrication of quantum structures. This technique also holds promise for fabrication of high performance optoelectronic and electronic devices and the integration of different type of devices on the same substrate. This necessitates the development of a damage free, *in-situ* etch and regrowth technique.

We present the analysis of *in-situ* etched and regrown  $\text{AlInAs}/\text{GaInAs}$  interfaces and the dependence of interface quality on the etching temperature. Chlorine gas etching has been investigated as a part of *in-situ* processing for GaAs based materials. However in the case of In containing semiconductors like  $\text{GaInAs}$  and  $\text{AlInAs}$ , higher etching temperatures are required due to the low volatility of Indium chloride which is a etch by-product. More important is the selection of proper etching temperature where the etch rates of both the Group III etch by-products are equal. Thus the roughness of the etched surface and the characteristics of the subsequently regrown interface depend critically on the etching temperature.

n- $\text{GaInAs}$  layers are grown on a  $n^+$   $\text{GaInAs}$  contact layer lattice matched to InP. The substrates are then transferred to the etching chamber which is connected to the MBE growth chamber through a UHV transfer tunnel. The  $\text{GaInAs}$  epilayers are etched using chlorine gas at temperatures ranging from 250 - 325 °C. The  $\text{Cl}_2$  gas flow is 2.5 sccm and the pressure is  $5 \times 10^{-5}$  Torr. The substrates are then transferred back to the MBE growth chamber and  $\text{AlInAs}$  is regrown. Fig. 1 shows the schematic of the regrown N-n heterojunction. C-V analysis of the *in-situ* etched and regrown interface is used to calculate the interface charge and the interface state density by the technique described by D. Biswas et.al.<sup>1</sup>. The surface roughness of as-etched  $\text{GaInAs}$  surface is measured using a atomic force microscope.

A minimum surface roughness of 10 Å is obtained at 275 °C, this also corresponds to low interface charge and mid-gap interface state density of  $2 \times 10^{11} / \text{cm}^2 \text{ eV}$  in  $\text{GaInAs}$  as shown in Figs. 2 and 3. As reported by Furuhashi et.al.<sup>2</sup> the etch rates of GaAs and InP are equal at this temperature. Thus it is clear that surface roughness and interface state density are minimum when the desorption rates of both Ga and In chloride etch by-products are the same. Also the interface state density directly correlates with the surface roughness. A comparison of the regrown interface with as-grown  $\text{AlInAs}/\text{GaInAs}$  interface shows only a minor degradation, indicating the suitability of this technique for *in-situ* processing in the  $\text{AlInAs}/\text{GaInAs}/\text{InP}$  material system.

<sup>1</sup>D.Biswas, P.R.Berger, U.Das, J.E.Oh, P.K.Bhattacharya, J. Electronic Materials, Vol.18, No.2, pp 137, 1989.

<sup>2</sup>N.Furuhashi, H.Miyamoto, A.Okamoto, K. Ohata, J. Applied Physics, Vol. 65, pp168, 1989.

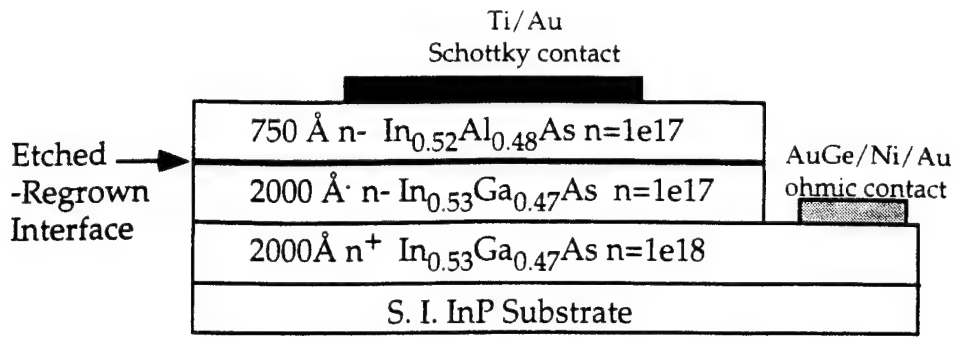


Fig. 1: Schematic of Regrown N-n Heterojunction Capacitor

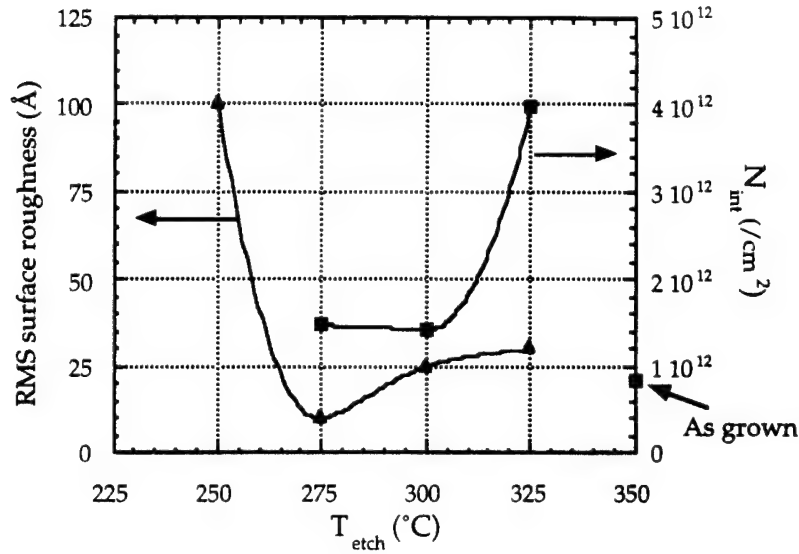


Fig. 2: Variation of surface roughness of as-etched GaInAs and interface charge at the etched - regrown AlInAs / GaInAs interface with GaInAs etching temperature

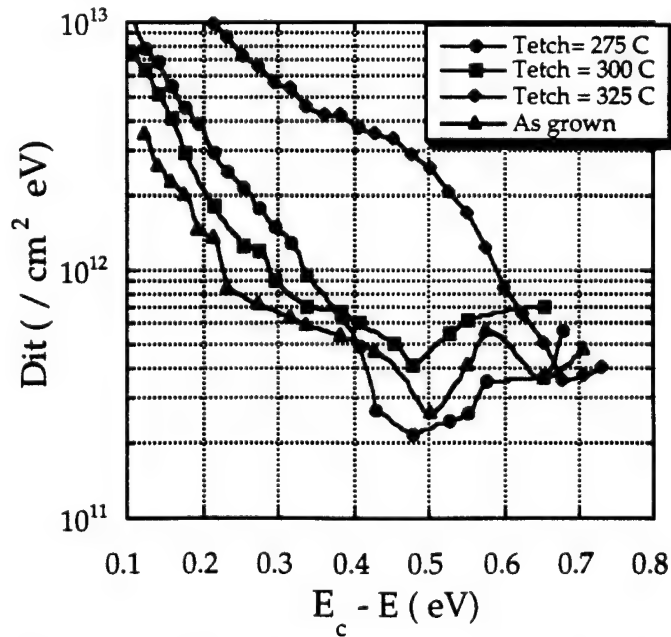


Fig. 3: Variation of interface state density at the AlInAs / GaInAs interface with etching temperature

## Lateral coupling of InP/GaInAsP/InP structures by selective area MOMBE

M. Wachter, U. Schöffel, M. Schier\*, and H. Heinecke

University of Ulm, Dept. of Semiconductor Physics, D-89069 Ulm, Germany

\*Siemens AG, Corporate Research and Development, D-81730 Munich, Germany

Phone: + 49 731 502-6101 Fax: - 6108 e-mail: heinecke@sunrise.e-technik.uni-ulm.de

In this study we have investigated systematically the *embedded selective area epitaxy (SAE)* of InP/GaInAsP/InP heterostructures which is an attractive pathway for the integration of photonic devices by butt coupling like lasers and waveguides. In addition for the production of such devices there is a significant driving force for replacing the hydrides by less toxic precursors. Hence we have investigated the SAE of InP/GaInAsP/InP structures using the hydrides AsH<sub>3</sub> and PH<sub>3</sub> as well as using *tertiarybutylphosphine (TBP)* and *tertiarybutylarsine (TBA)* as group V precursors in a prototype of a multi wafer metalorganic molecular beam epitaxy (MOMBE) system.

The InP/GaInAsP/InP starting layers from a full 2" wafer process were patterned with 120 nm thick SiO<sub>2</sub> mask stripes by conventional photolithography and trenches (up to 2 µm in depth) were reactive ion etched. The width of the structures varies from 1.5 to 250 µm. The trenches were filled in a second growth run by SAE of various InP/GaInAsP/InP structures. Thus a lateral coupling of InP/GaInAsP/InP double heterostructures of different material compositions is achieved.

The characterization of these lateral heterojunctions was performed by Nomarski interference microscopy, scanning electron microscopy (SEM), and spatially resolved photoluminescence (µ-PL) measurements at 300 K (excitation spot 5 µm in diameter).

Nomarski interference micrographs show that also in the TBA, TBP process no growth takes place on the mask (SAE). The SEM investigations reveal lateral heterojunctions with planar infill-layers and smooth contacts of the quaternary layer. Fig. 1 gives a cross-sectional view of two lateral coupled InP/GaInAsP/InP heterostructures with a gap-wavelength of  $\lambda_g = 1.55 \mu\text{m}$  for both quaternary layers. The shown planarity of the SAE layers is independent of the aspect ratio of the masked to the unmasked surface. The thin vertical InP separation layer between the two quaternary coupled layers is adjustable in the thickness by changing the growth parameters and the molecular beam geometry.

Fig. 2 shows linescans of the PL intensity in dependence on the lateral position of the laser spot for the transitions between quaternary materials with gap-wavelengths of  $\lambda_g = 1.047 \mu\text{m}$  (infill) and  $\lambda_g = 1.540 \mu\text{m}$  (structure see insert). The oxide capped ridge structure was grown by using the hydrides AsH<sub>3</sub> and PH<sub>3</sub> and for the embedded SAE heterostructure TBA and TBP was used. The SAE quaternary layer exhibits a bright luminescence and a sharp decay at the boundary of the locally grown structure indicating a high crystal quality *up to the lateral junction*. This decay of the PL intensity at  $\lambda_g = 1.047 \mu\text{m}$  coincidences spatially with the increase at  $\lambda_g = 1.540 \mu\text{m}$  and vice versa. The measured decay / increase length of 4 - 5 µm is limited by the spot size of the exciting laser beam. Consequently a sharp transition area (butt coupling) is realized. This is supported by the fact, that the *measured* wavelength shift at the lateral heterojunction in the coupling zone is less than  $\pm 4$  nm in [011] or  $[0\bar{1}\bar{1}]$  directions. The nature of this fine wavelength variation as well as comparative data on a number of different lateral material transitions in various crystal directions will be presented. These results demonstrate that the state of the art lateral couplings of GaInAsP heterostructures can be achieved by SAE MOMBE using either the hydrides or the replacement precursors TBA and TBP.



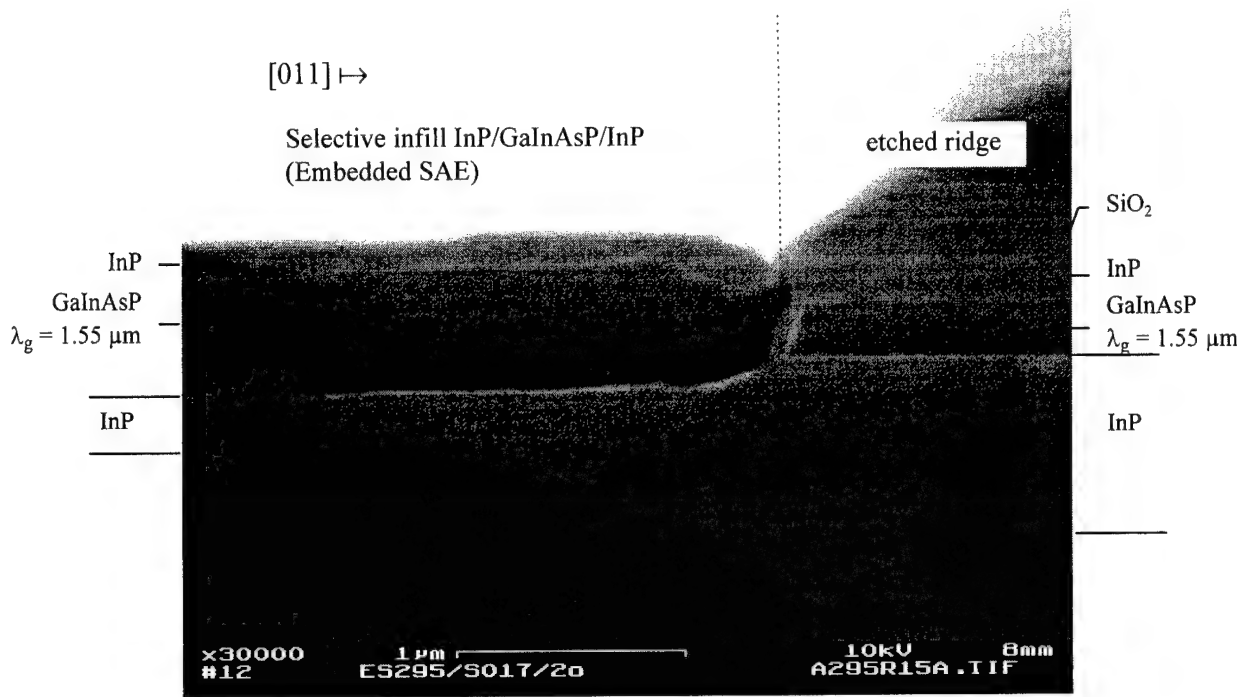


Fig. 1: SEM micrograph of the cross-section of a lateral coupling of two InP/InGaAsP ( $\lambda_g = 1.55 \mu\text{m}$ )/InP heterostructures in the [011] direction, (looking on  $(0\bar{1}1)$  plane).

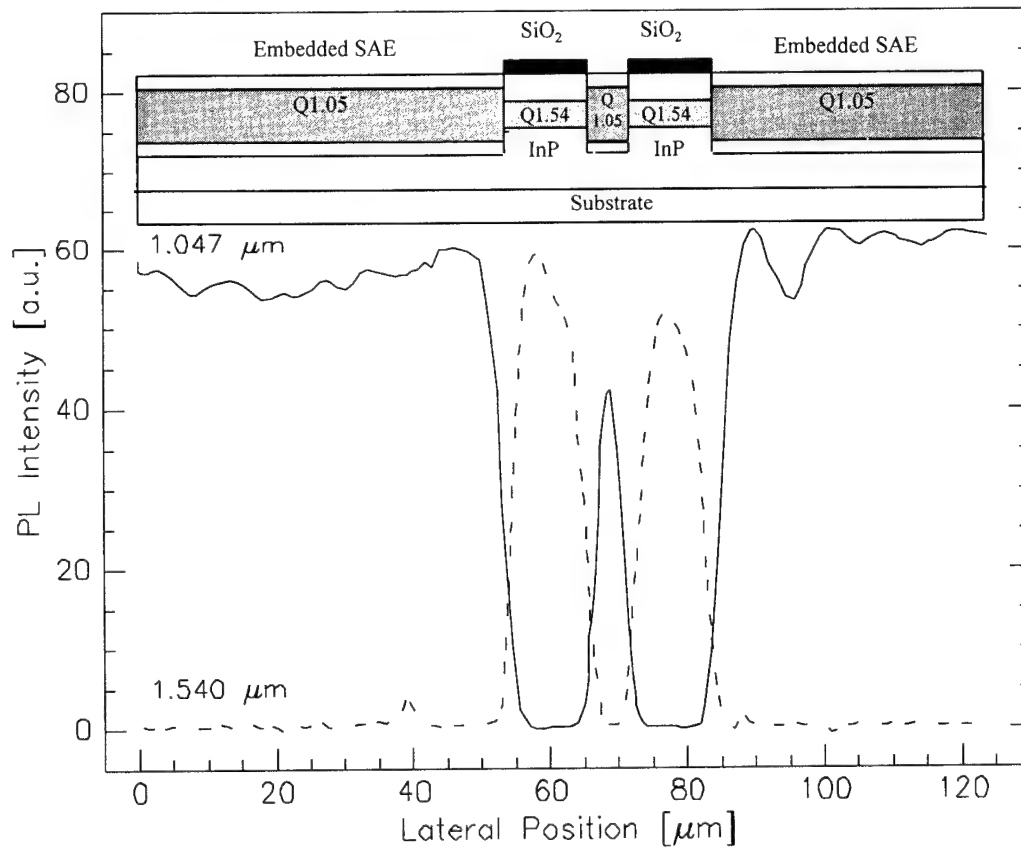


Fig. 2: PL spatial linescans across a structure as in Fig. 1, but SAE infill using GaInAsP with  $\lambda_g = 1.047 \mu\text{m}$  (see insert; lateral heterojunction achieved by embedded SAE; the quaternary layers are indicated by Q1.05 ( $\lambda_g = 1.047 \mu\text{m}$ ) and Q1.54; all other layers are InP).

# SELECTIVE AREA EPITAXY OF GaAs USING COMBINED VERY LOW ENERGY Ga<sup>+</sup> FOCUSED ION BEAM DEPOSITION AND MOLECULAR BEAM EPITAXIAL GROWTH

H. E. Beere, J. H. Thompson, G. A. C. Jones, and D. A. Ritchie.

University of Cambridge, Cavendish Laboratory, Madingley Road, Cambridge CB3 0HE, UK.

The selective area epitaxy of III-V compound semiconductors could become an important technique in the preparation of sophisticated integrated semiconductor structures. A novel system has been developed at the Cavendish in which a conventional thermal molecular beam epitaxy (MBE) source is replaced with a focused ion beam (FIB) column located directly opposite the sample on a standard MBE deposition chamber (Fig. 1). Initial studies used a Sn FIB to dope n-type GaAs/AlGaAs structures with three-dimensionally patterned doping profiles<sup>[1]</sup>. This technique has been further developed to facilitate the lateral selective area epitaxy of GaAs by supplying the group III matrix element via a FIB. In order to minimise crystalline damage during growth, very low ion energies (less than 100eV) are necessary. Thus the ions are deposited rather than implanted. To overcome the problem of focusing an ion beam in this low energy regime, retarding field optics were employed<sup>[2]</sup>.

For the first time, a FIB has been used to grow conducting n-type GaAs in lithographically defined areas. A low energy (25 to 100eV) mass separated <sup>69</sup>Ga<sup>+</sup> FIB was rastered over a 210μm x 210μm area on a GaAs(100) substrate, once per second, with thermal Si and As<sub>4</sub> molecular beams impinging upon the sample under conventional MBE growth conditions. The FIB grown samples were grown ~1μm thick at a typical growth rate of 0.6μm/hr (Fig. 2). Electrical characterisation of the 25eV FIB grown layer gave a 77°K mobility of 1550cm<sup>2</sup>V<sup>-1</sup>s<sup>-1</sup> at a carrier concentration of 2.5 x 10<sup>17</sup> cm<sup>-3</sup> (Fig. 3). Hall mobility versus temperature measurements showed the mobility for the FIB grown sample is lower than an equivalent MBE grown sample, suggesting the FIB sample's mobility is dominated by scattering centres within the crystal. These results imply that there is ion-induced lattice damage within the grown film, however it is expected that this damage would be reduced by decreasing the incident ion energy from 25 to 10eV.

The use of a low energy ion source with MBE may also provide technologically important improvements in semiconductor crystal growth. The extra energy supplied to the wafer surface by low energy ion irradiation has allowed the growth of semiconductor layers with lower defect densities and reduced surface roughness at lower temperatures than conventional MBE growth alone<sup>[3]</sup>. The capability of growing high quality MBE crystal structures with improved heterointerfaces and at low growth temperatures would lead to an enhancement in both optical and electrical device performance.

1. J.H.Thompson, G.A.C.Jones, D.A.Ritchie, E.H.Linfield, M.Houlton, G.W.Smith, and C.R.Whitehouse. *J. Cryst. Growth* **127**, pp 732 (1993)
2. H. Kasahara, H. Sawaragi, R. Aihara, K. Gamo, S. Namba, and M. Hassal Shearer. *J. Vac. Sci. Technol. B* **6**, pp 974 (1988)
3. S. Shimuzu, O. Tsukakoshi, and S. Komiya. *J. Vac. Sci. Technol. B* **3**, pp 554 (1985)

Harvey Beere  
e-mail:heb1000@cus.cam.ac.uk

Tel: +44 (0) 1223 337471  
Fax: +44 (0) 1223 337271

# SELECTIVE AREA EPITAXY OF GaAs USING COMBINED VERY LOW ENERGY $\text{Ga}^+$ FOCUSED ION BEAM DEPOSITION AND MOLECULAR BEAM EPITAXIAL GROWTH

H. E. Beere, J. H. Thompson, G. A. C. Jones, and D. A. Ritchie.

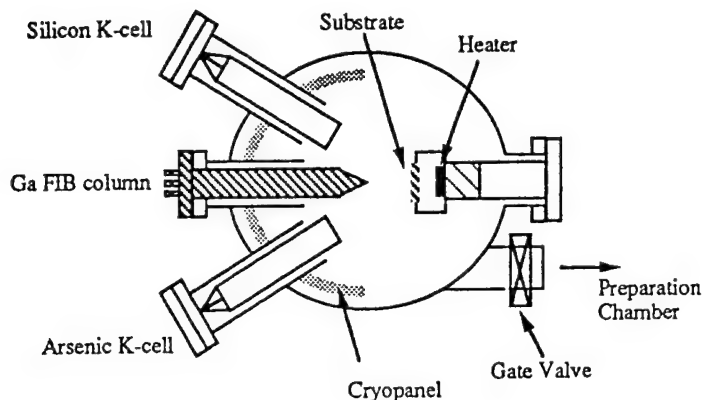


Figure 1. A schematic diagram of the experimental apparatus showing the focused-ion-beam matrix element source attached to the growth chamber of a MBE machine.

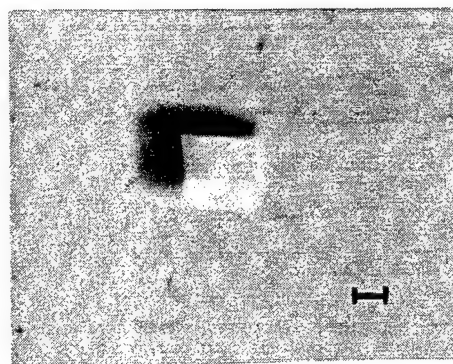


Figure 2. Nomarski micrograph of a selectively grown n-GaAs sample using a 25eV  $\text{Ga}^+$  FIB with Si and  $\text{As}_4$  molecular beams. The marker represents 100  $\mu\text{m}$ .

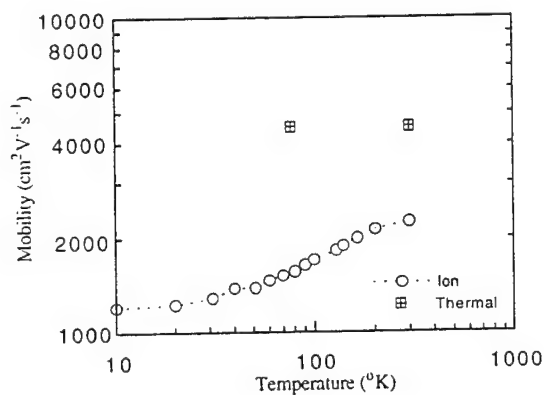


Figure 3. Hall mobility versus temperature for the 25eV  $\text{Ga}^+$  FIB grown sample thermally doped with Si at a level of  $1.3 \times 10^{18} \text{ cm}^{-3}$  (note the logarithmic axes). For comparison a conventionally grown MBE n-GaAs sample is also shown. Both samples have a free carrier concentration of  $2.5 \times 10^{17} \text{ cm}^{-3}$ .

## Selective Area Chemical Beam Epitaxial Regrowth of Si-Doped GaAs and InP by Using Silicon Tetraiodide for HFET Application

Shigekazu Izumi, Norio Hayafuji, Tetsuro Kunii, Shinichi Miyakuni,  
Kazuhiko Ito, Kazuhiko Sato, and Mutsuyuki Otsubo  
Optoelectronic & Microwave Devices Laboratory, Mitsubishi Electric Corporation,  
4-1 Mizuhara, Itami, Hyogo 664, Japan  
Phone number : 81-727-84-7436, Fax number : 81-727-80-2694  
E-mail : izumi@oml.melco.co.jp

In this presentation, we propose a novel silicon (Si) dopant source of silicon tetraiodide ( $\text{SiI}_4$ ) for CBE growth of GaAs and InP. High electrical quality has been ascertained for both of GaAs and InP with linear Si doping controllability in the wide range. Abrupt interfaces and precise on-off controllability without any memory effect have been confirmed as well.

Si is one of the most commonly used n-type dopant for III-V compound semiconductors due to low thermal diffusivity and little surface segregation.  $\text{Si}_2\text{H}_6$  has been mainly used in every sort of growth method such as metalorganic vapor phase epitaxy (MOVPE) and gas source molecular beam epitaxy (GS-MBE). Carrier concentration up to  $1.4 \times 10^{18} \text{cm}^{-3}$  was obtained by using  $\text{Si}_2\text{H}_6$  in chemical beam epitaxial (CBE) grown InP<sup>(1)</sup>. Controllability especially at low doping level, however, is still insufficient for device application such as the collector layer of heterojunction bipolar transistor (HBT). Recently, it has been reported that somewhat high Si doping efficiency and controllability are obtained for InP and InGaAs growth by using  $\text{SiBr}_4$  having relatively weak (87.9 kcal/mol) Si-Br bond strength<sup>(2)</sup>, which suggests that the facile decomposition of Si is an inevitable item for Si dopant source.

Si-doped GaAs and InP were grown by CBE on undoped GaAs and Fe-doped InP (100) substrates with three inch diameters, respectively. GaAs layer was grown at  $510^\circ\text{C}$  with a growth rate of  $0.65 \mu\text{m/h}$  by using triethylgallium (TEGa) and arsine ( $\text{AsH}_3$ ). InP layer was grown at  $460^\circ\text{C}$  with a growth rate of  $0.5 \mu\text{m/h}$  by using trimethylindium (TMIn) and phosphine ( $\text{PH}_3$ ). Si dopant was the specially provided 5N grade purity  $\text{SiI}_4$ , which was supplied with helium (He) carrier gas through a mass flow controller without any precracking. 10%  $\text{Si}_2\text{H}_6$  diluted with hydrogen ( $\text{H}_2$ ) was used as a reference in some experiments.

High electrical quality has been ascertained for both of GaAs and InP with linear Si doping controllability in the range from  $2 \times 10^{16} \text{cm}^{-3}$  to  $6 \times 10^{18} \text{cm}^{-3}$  with the uniformity less than 2% within 3 inch diameter area. Electron mobility in GaAs with carrier concentration of  $1 \times 10^{17} \text{cm}^{-3}$  is  $4400 \text{ cm}^2/\text{Vs}$  and that in InP with carrier concentration of  $4 \times 10^{17} \text{cm}^{-3}$  is  $2400 \text{ cm}^2/\text{Vs}$ , respectively. Abrupt interfaces and precise on-off controllability without any memory effect have been confirmed by secondary ion mass spectroscopy (SIMS) measurements. Electrical activation ratio of Si in  $\text{SiI}_4$  for both of GaAs and InP is found to be almost 100% in the range studied here, while that in  $\text{Si}_2\text{H}_6$  is 80% or less. These versatile features are thought to be due to the very weak Si-I bond strength in  $\text{SiI}_4$  (70 kcal/mol).

This technique has been applied to the heterostructure field effect transistor (HFET) fabrication. Selective area regrowth of  $0.3 \mu\text{m}$  thick Si-doped GaAs with a concentration of  $3 \times 10^{18} \text{cm}^{-3}$  has been successfully achieved on patterned trench structure fabricated by ECR plasma etching without any polycrystalline deposition on the dielectric mask film as well. Sufficient low contact resistance as low as  $3 \times 10^{-7} \Omega \text{cm}^2$  has achieved with alloyed Ni/AuGe/Au contact metals on Si-doped GaAs source and drain surfaces.

These satisfactory results indicate that  $\text{SiI}_4$  is a promising candidate as a Si dopant source and that the combination of the CBE growth and the use of  $\text{SiI}_4$  has a potential ability of constructing any planar type devices.

- 1) H.Ando, N.Okamoto, A.sandhu, T.Fujii, Jpn. J. Appl. Phys.**30**, (1991)L1696.
- 2) S.L.Jackson, M.T.Fresina, J.E.Baker, G.E.Stillman, Appl.Phys.Lett. **64**, (1994)2867.

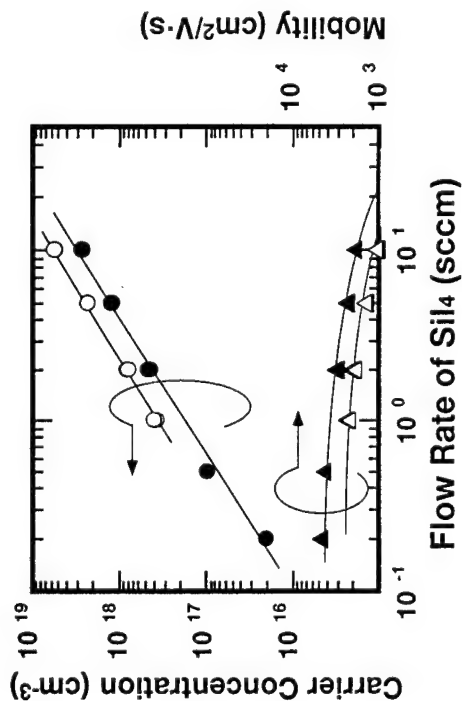


Fig. 1 Dependence of net carrier concentration and electron mobility in GaAs (●) and InP (○, △) on flow rate of SiH<sub>4</sub> diluted with He carrier gas. High electrical quality has been obtained for both of GaAs and InP with linear Si doping controllability.

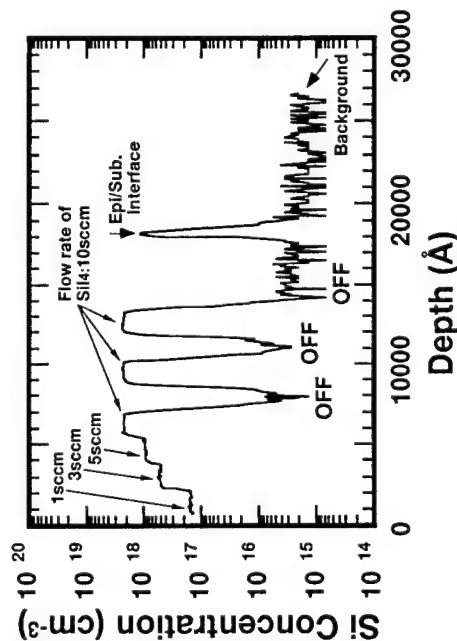


Fig. 2 SIMS profile of Si modulation doped GaAs layer by using SiH<sub>4</sub>. Abrupt interfaces and precise on-off controllability have been obtained without any memory effect.

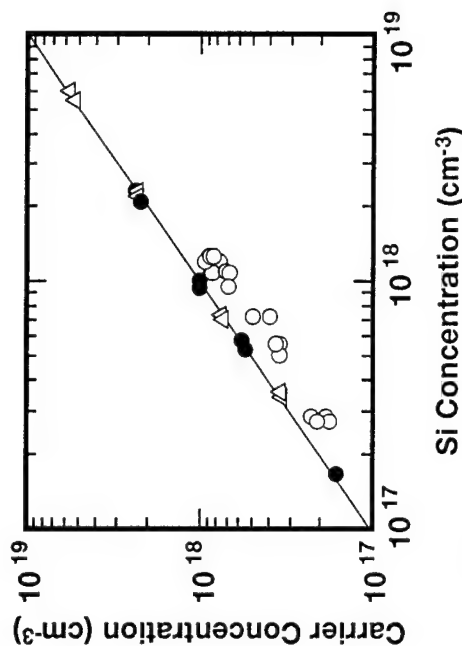


Fig. 3 Relation between carrier concentration and Si concentration in Si doped GaAs by using SiH<sub>4</sub> (●), by using Si<sub>2</sub>H<sub>6</sub> (○), and Si doped InP by using SiH<sub>4</sub> (△). Electrical activation ratio of Si in SiH<sub>4</sub> for both of GaAs and InP is almost 100% in the range studied, while that in Si<sub>2</sub>H<sub>6</sub> is 80% or less.

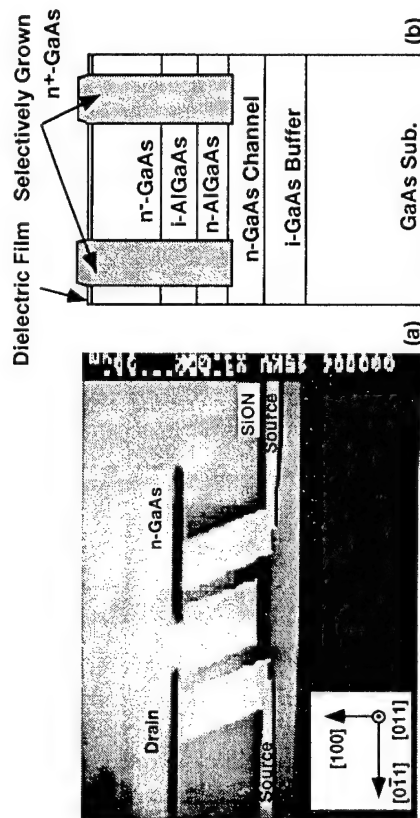


Fig. 4 SEM photograph (a) and cross sectional drawing (b) of selectively CBE regrown Si doped GaAs (source and drain) layer on patterned HFET structure in which trench has been fabricated by ECR plasma etching. Thickness of buried layer is 0.3 μm.

# MBE Regrowth on AlGaInAs DFB Gratings Using In-Situ Hydrogen Radical Cleaning

H. Künzel, J. Böttcher, A. Hase, H.-J. Hensel, K. Janiak, A. Paraskevopoulos and G. Urmann

Heinrich-Hertz-Institut für Nachrichtentechnik Berlin GmbH,  
Einsteinufer 37, D-10587 Berlin, Germany

Phone: ++49.30.31002.546, FAX: ++49.30.31002.558, e-mail: kuenzel@mails.hhi.de

## Abstract

Recently, MBE regrowth on Al-containing surfaces was made feasible by the implementation of in-situ, UHV-compatible cleaning/etching techniques to remove the thermally stable native oxide layer /1,2/. Particularly when thin layers are involved, hydrogen radical ( $H^*$ ) cleaning is the method of choice since no material removal is observed /3/. The suitability of the  $H^*$  cleaning technique was demonstrated by MBE growth of high quality InGaAs quantum wells on  $Al_{0.24}Ga_{0.24}In_{0.52}As$  surfaces.

In this contribution, the  $H^*$  radical treatment was applied for the first time prior to InP regrowth on  $Al_{0.16}Ga_{0.32}In_{0.52}As$  DFB-gratings, a crucial step towards the realization of GaInAs / AlGaInAs DFB-lasers with solid source MBE. The following three topics involved in the elaboration of the regrowth process will be separately addressed: 1)  $H^*$  process conditions for  $Al_{0.16}Ga_{0.32}In_{0.52}As$  surfaces, 2) a suitable stabilization procedure of DFB gratings prior to MBE regrowth and 3) adequate MBE conditions for a final planar regrown surface.

The basic results can be summarized as follows:

- 1) As compared to  $Al_{0.24}Ga_{0.24}In_{0.52}As$  /3/, for the sufficient removal of the native oxide film from  $Al_{0.16}Ga_{0.32}In_{0.52}As$  surfaces only short  $H^*$  processing times are required, as determined from Auger measurements. An increase of the processing time results in a decrease of the crystalline quality of the regrown material (cf. Fig. 1 in the example of InGaAs) and simultaneously of the optical quality as judged from 300K PL. Time resolved PL measurements on regrown AlGaInAs/GaInAs heterostructures indicate similar lifetimes as those found in continuously grown material.
- 2)  $As_4$ -stabilization of grating structures indicated no influence of  $As$  pressure, stabilization time and  $H^*$ -processing on the grating profiles. The influence of  $P_2$ -stabilization is presently under investigation.
- 3) Regrowth of 1.5  $\mu m$  thick InP layers results in smooth and planar surfaces (c.f. Fig. 2). The optical quality, in terms of PL intensity of the regrown material on grating areas, is in good agreement with that of InP on non-structured AlGaInAs as well as on an InP reference substrate. Regrowth was performed both on dry (RIE) as well as wet chemically etched grating structures. A comparative study of regrowth with different materials (i.e. AlInAs, GaInAs and InP) is currently under investigation to study of the influence of the mobility of the growth constituents on regrowth behaviour.

/1/ A. Hase et al., Appl. Phys. Lett. **65**, 1406 (1994).

/2/ K.D. Choquette et al., Appl. Phys. Lett. **62**, 735 (1993).

/3/ H.Künzel et al., J. Crystal Growth **150**, 18 (1995).

# Part of the work was conducted under contract with Bosch-Telecom GmbH, Backnang.

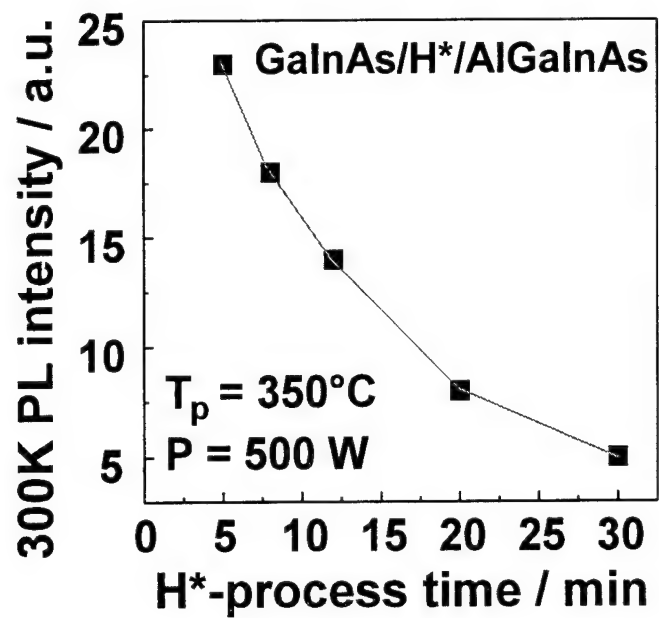


Fig. 1: 300K PL intensity of GaInAs regrown on H\*-treated  $\text{Al}_{0.16}\text{Ga}_{0.32}\text{In}_{0.52}\text{As}$  as a function of H\*-exposure time.

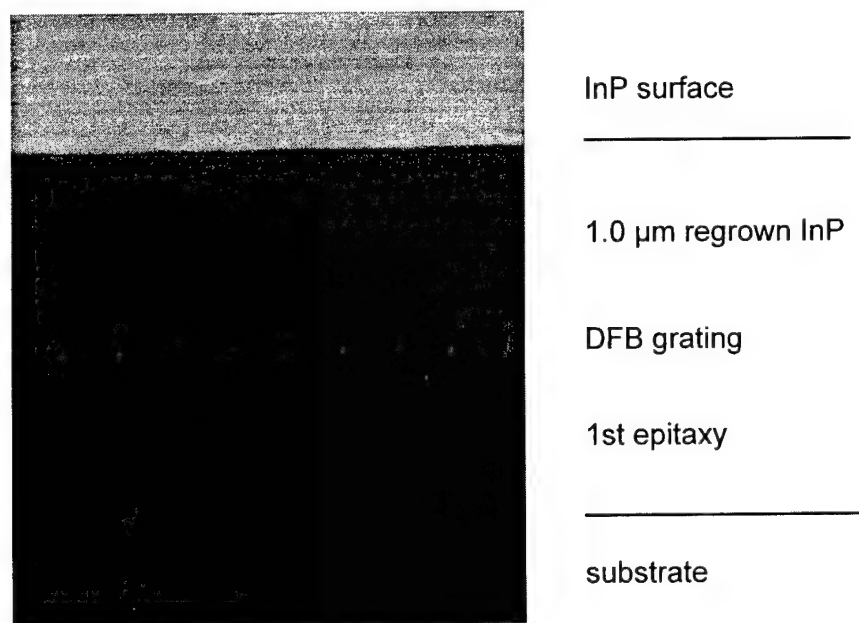


Fig. 2: REM of a tilted stained cross-section of a 1.5  $\mu\text{m}$  thick InP layer regrown on a 195 nm deep DFB grating defined by RIE.

## Hydrogen Radical Surface Cleaning of GaAs for MBE Regrowth

T.M.Burke, E.H.Linfield, M.A.Quierin, D.A.Ritchie, M.Pepper\*

Cavendish Laboratory, University of Cambridge, Madingley Road, Cambridge CB3 0HE, UK.

J.H.Burroughes

Toshiba Cambridge Research Centre Ltd, 260 Cambridge Science Park, Milton Road, Cambridge CB4 4WE, UK.

\* Also at Toshiba Cambridge Research Centre

MBE regrowth on *ex-situ* patterned GaAs substrates provides a promising technique for the wafer-scale production of novel three dimensional device structures [1]. Optimal substrate preparation prior to regrowth to remove contaminants such as oxygen and carbon which are incurred at the surface during *ex-situ* processing is essential. Hydrogen radical ( $H^*$ ) surface cleaning can provide an effective method for the removal of such contamination resulting in both smoother and cleaner surfaces than those that can be achieved by standard thermal cleaning [2,3].

A dedicated decontamination chamber has been commissioned incorporating an r.f. plasma hydrogen radical source for surface cleaning and an integrated SIMS system. This cleaning chamber is connected to a V80H MBE growth system via a UHV transfer chamber. SIMS characterisation before and after the  $H^*$  cleaning of patterned wafers has been used to measure reductions of up to three orders of magnitude in the surface oxide levels and a significant removal of hydrocarbon contamination at cleaning temperatures as low as 450°C. To assess the effectiveness of this cleaning technique for device production the impact on a two dimensional electron gas (2DEG) of the close proximity of a hydrogen cleaned regrowth interface has been assessed and compared with that for a corresponding thermally cleaned interface. For regrowth interface/2DEG separations below 2000Å the thermally cleaned interface was found to rapidly degrade the 2DEG carrier concentration and low temperature mobility. Following  $H^*$  cleaning this degradation is found to be much reduced leading to the growth of a 2DEG lying only 500Å from a  $H^*$  cleaned regrowth interface with a mobility after illumination of  $5.26 \times 10^5 \text{ cm}^2 \text{ V}^{-1} \text{ s}^{-1}$  at a carrier concentration of  $4.20 \times 10^{11} \text{ cm}^{-2}$ .

To further investigate the effectiveness of thermal/ $H^*$  cleaning, resonant tunnelling devices have been fabricated where the regrowth interface lies between the collector and the double barrier structure. The current-voltage characteristics of these devices again indicate a significant improvement in the quality of a hydrogen cleaned interface in comparison to that achieved by standard thermal decontamination.

These results show the applicability of the MBE regrowth technique combined with hydrogen radical cleaning to the fabrication of complex device structures in which active layers are required to be regrown in close proximity to the regrowth interface.

- [1] R.J.Evans, T.M.Burke, M.P.Grimshaw, D.A.Ritchie, M.Pepper and J.H.Burroughes, Mat. Sci. and Eng. B, **35**(1-3), 1995, 203.
- [2] C.M.Rouleau and R.M.Park, J. Appl. Phys. **73**(9), 1993, 4610.
- [3] A. Takamori, S. Sugata, K. Asakawa, E. Miyauchi and H. Hashimoto, Jap. J. Appl. Phys., **26**(2), 1987, L142.

**Theresa Burke**  
Address as above  
Tel: 44 1223 337323  
Fax: 44 1223 337271  
email: tmb1001@cus.cam.ac.uk



## 9. Sb AND OTHER MATERIALS.

WEDNESDAY MORNING (ELKINS)

Session Chair: Pin Ho, Lockheed-Martin Electronics Labs, USA

Co-Chair: Takyiu Liu, Hughes Research Labs, Malibu, California

- 09:00 9.1 **MBE growth of high-power InAsSb/InAlAsSb quantum-well diode lasers emitting at 3.5  $\mu\text{m}$**  (Invited)  
G.W. Turner, M.J. Manfra, and H.K. Choi  
Lincoln Laboratory, Massachusetts Institute of Technology, USA.
- 09:30 9.2 **Microstructure properties of  $\text{InAs}/\text{InAs}_x\text{Sb}_{1-x}$  superlattices and  $\text{InAs}_x\text{Sb}_{1-x}$  ordered alloys grown by modulated molecular beam epitaxy**  
Y.-H. Zhang, A. Lew, E. Yu, and Y. Chen, Hughes Research Laboratories, Malibu, CA
- 09:50 9.3 **Sb-surface segregation and the control of compositional abruptness at the GaAs/GaAsSb interface**  
Ron Kaspi, and Keith R. Evans, Wright State University, Dayton, OH, USA.
- 10:10 9.4 **MBE growth of Si-doped InAsSb layers lattice-matched with InAs**  
Makoto Kudo and Tomoyoshi Mishima  
Central Research Laboratory, Hitachi, Ltd., Tokyo, Japan.

Break

- 10:50 9.5 **Molecular beam epitaxial GaInSbBi for infrared detector applications**  
Q. Du, J. Alpern, and W.I. Wang  
Columbia University, New York, USA.
- 11:10 9.6 **New semiconductors  $\text{TiInGaP}$  and their gas source MBE growth**  
H. Asahi, K. Yamamoto, K. Iwata, S. Gonda, and K. Oe  
Osaka University, Japan.
- 11:30 9.7 **Thin heterogeneous (MnAs/III-V) magnetic layers buried in high quality III-V heterostructures**  
J. De Boeck, A. Van Esch, and G. Borghs, IMEC, Leuven, Belgium.
- 11:50 9.8 **GaMnAs: GaAs-based III-V diluted magnetic semiconductors grown by molecular beam epitaxy**  
T. Hayashi, M. Tanaka, and H. Shimada  
The University of Tokyo, Japan.

# MBE Growth of High-Power InAsSb/InAlAsSb Quantum-Well Diode Lasers Emitting at $3.5\ \mu\text{m}$ \*

G.W. Turner, M.J. Manfra, and H.K. Choi  
Lincoln Laboratory, Massachusetts Institute of Technology  
Lexington, Massachusetts 02173-9108

High-performance diode lasers emitting in the wavelength region of  $2\text{--}5\ \mu\text{m}$  have numerous potential applications in gas detection, spectroscopy, pollution monitoring, and military systems. Recently, diode lasers fabricated from the antimonide-based III-V compounds have been receiving increased attention for such applications since excellent results have already been demonstrated for room-temperature quantum-well devices emitting near  $2\ \mu\text{m}$ . For longer wavelengths, however, performance of such antimonide-based lasers has been more limited.

In this paper, we will report the MBE growth and fabrication of high-performance multiple quantum-well diode lasers incorporating compressively strained  $\text{InAs}_{0.935}\text{Sb}_{0.065}$  wells and tensile-strained  $\text{In}_{0.85}\text{Al}_{0.15}\text{As}_{0.9}\text{Sb}_{0.1}$  barriers in the active region and lattice-matched  $\text{AlAs}_{0.16}\text{Sb}_{0.84}$  as the cladding layers. These lasers, which were grown on InAs substrates, have emission wavelengths between  $3.2$  and  $3.55\ \mu\text{m}$ . Broad-stripe lasers have exhibited  $215\ \text{mW/facet}$  cw at  $80\ \text{K}$ , with pulsed threshold current densities as low as  $30\ \text{A/cm}^2$  at  $80\ \text{K}$ . The maximum pulsed operating temperature is  $225\ \text{K}$ . Ridge-waveguide lasers have exhibited cw threshold currents of  $12\ \text{mA}$  at  $100\ \text{K}$ , with the maximum cw operating temperature of  $175\ \text{K}$ .

We will describe the MBE materials growth issues that determine the characteristics of the present high-performance lasers. We will also present some new approaches that could minimize unsolved problems in the present lasers. Such approaches may lead to even higher performance diode lasers in this wavelength region.

---

\*This work was sponsored by the Air Force Phillips Laboratory.

## Microstructure Properties of InAs/InAs<sub>x</sub>Sb<sub>1-x</sub> Superlattices and InAs<sub>x</sub>Sb<sub>1-x</sub> Ordered Alloys Grown by Modulated Molecular Beam Epitaxy

Y.-H. Zhang<sup>1</sup>, A. Lew<sup>2</sup>, E. Yu<sup>2</sup>, and Y. Chen<sup>3</sup>

<sup>1</sup>Hughes Research Laboratories, 3011 Malibu Canyon Road, Malibu, CA 90265.

Tel: (310)317-5696, FAX: (310)317-5450, E-mail: zhang@madmax.hrl.hac.com.

<sup>2</sup>Department of Electrical Engineering and Computer Science, University of California at San Diego, La Jolla, CA 92093

<sup>3</sup>Lawrence Berkeley Lab, University of California, Berkeley, CA 94720

Control of the composition of group-V alloys has been problematic for molecular beam epitaxy (MBE). The problem is even more acute for the epitaxial growth of InAs<sub>x</sub>Sb<sub>1-x</sub> random alloys due to the spontaneous CuPt-orderings, which are not desirable for device applications [1-3]. Previously, we reported a straightforward and accurate means of controlling the incorporation of As and Sb by rapidly alternating As<sub>2</sub> and Sb fluxes, i.e. Modulated MBE (MMBE), for As/Sb alloys [4]. In this paper we will present detailed cross-sectional Scanning Tunneling Microscopy (STM), Transmission Electron Diffraction (TED), and optical spectroscopy study of the MMBE grown InAs/InAs<sub>x</sub>Sb<sub>1-x</sub> superlattices (SL) and InAs<sub>x</sub>Sb<sub>1-x</sub> ordered alloys. The new results show that MMBE provides not only a better control of the composition but also a way to overcome the problem of spontaneous CuPt orderings in InAs<sub>x</sub>Sb<sub>1-x</sub> random alloys.

For the STM study, we focus on a 172Å-InAs/52Å-InAs<sub>0.76</sub>Sb<sub>0.24</sub> SL grown on a GaSb substrate. Each of the 52 Å InAs<sub>0.76</sub>Sb<sub>0.24</sub> layers consists of 4 periods of nominal 7.8Å-InAs/5.2Å-InSb sub-superlattice structures. Figure 1 (a) shows a high-resolution constant-current cross-sectional STM image of a single InAs<sub>0.76</sub>Sb<sub>0.24</sub> ordered-alloy layer surrounded by InAs. Contrast between the InAs layers and the InAs<sub>0.76</sub>Sb<sub>0.24</sub> ordered-alloy layer can be seen clearly in the image. The growth direction is indicated in the figure. Figure 1 (b) shows an averaged topographic line scan of the InAs<sub>0.76</sub>Sb<sub>0.24</sub> layer and the surrounding InAs layers. Also visible in the image is contrast caused by the ordered structure within the InAs<sub>0.76</sub>Sb<sub>0.24</sub> layer produced by the MMBE growth technique. These features are observed consistently with different cleaved samples and tips. Differences in topographic height, caused by differences in electronic structure, between the sub-superlattices and the darker InAs layers become larger as more InAs<sub>0.76</sub>Sb<sub>0.24</sub> is grown. The maximum contrast in height (corresponding to maximum content) is consistently observed at the next-to-last (i.e. the third) grown InSb-like layer in the InAs<sub>0.76</sub>Sb<sub>0.24</sub> ordered alloy region. This non-uniformity in the electronic structure in the InAs<sub>0.76</sub>Sb<sub>0.24</sub> layers suggests the presence of atomic cross-incorporation within the InAs<sub>0.76</sub>Sb<sub>0.24</sub> layers during the MMBE growth.

TED study of InAs/InAs<sub>0.924</sub>Sb<sub>0.076</sub> SL in a laser structure grown on an InAs substrate reveals additional detailed information about the microstructure properties of the SL. The sample is examined in a <110> direction perpendicular to the [001] growth direction. TED pattern of the InAs/InAs<sub>0.924</sub>Sb<sub>0.076</sub> SL active region is shown in Fig. 2. Only zinc-blende reflections have been seen on the photographs. Special attention is paid to the reflections caused by CuPt ordering. But no reflection spots at half the distance between (000) and {111} reflection spots are visible, indicating that the lack of CuPt orderings in the InAs<sub>0.924</sub>Sb<sub>0.076</sub> ordered alloys. This finding is confirmed by photoluminescence study of MMBE grown thick InAs<sub>0.9</sub>Sb<sub>0.1</sub> ordered alloy layers lattice matched to GaSb substrates. The bandgaps of these samples show no reduction. In contrast, CuPt-orderings in InAs<sub>x</sub>Sb<sub>1-x</sub> random alloys grown by MOCVD and MBE are evidenced by detailed TED and optical spectroscopy studies [1-3]. Due to the spontaneous nature, this kind of orderings is difficult to control and not desirable for device applications. In view of the present results, the ordered alloys grown by MMBE technique provide an alternative way to bypass the CuPt ordering issue. Laser structures grown by using MMBE have demonstrated very high performance.

1. H. R. Jen, K. Y. Ma, and G. B. Stringfellow, Appl. Phys. Lett. **54**, 1154 (1989).
2. S. R. Kurtz, L. R. Dawson, R. M. Bielfeld, D. M. Follstaedt, and B. L. Doyle, Phys. Rev. B **46**, 1909 (1992).
3. D. M. Follstaedt, R. M. Bielfeld, S. R. Kurtz, L. R. Dawson, and K. C. Baucom, Narrow Gap Semiconductors 1995, Proceedings of the International Conference on Narrow Gap Semiconductors, Edited by J. L. Reno, Institute of Physics Publishing, London, 1995, p. 225.
4. Y.-H. Zhang, J. of Crystal Growth **150**, 838 (1995).

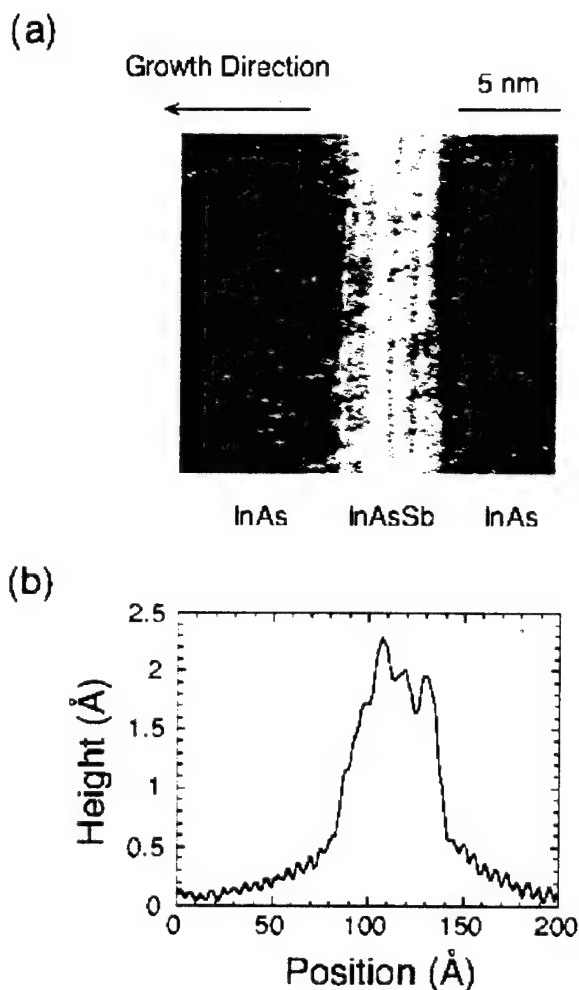


Fig. 1 (a) A high-resolution constant-current cross-sectional STM image of a single  $\text{InAs}_{0.76}\text{Sb}_{0.24}$  ordered-alloy layer surrounded by InAs. (b) An averaged topographic line scan of the layer and the surrounding InAs layers.

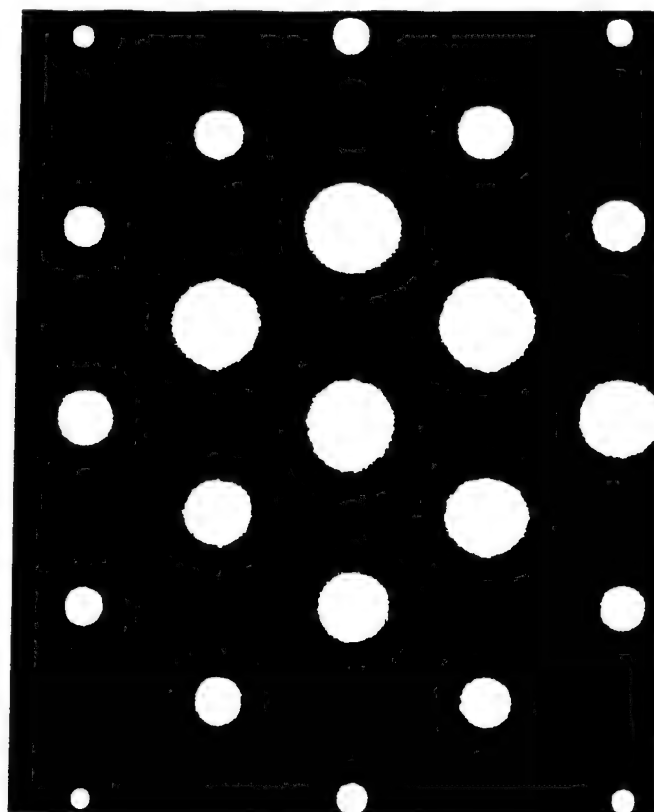


Fig. 2 TED pattern of the  $\text{InAs}/\text{InAs}_{0.76}\text{Sb}_{0.24}$  SL active region in a midwave infrared laser structure.

## **Sb-Surface Segregation and the Control of Compositional Abruptness at the GaAs/GaAsSb Interface**

Ron Kaspi, *University Research Center, Wright State University, Dayton, OH 45435,*  
Keith R. Evans, *Wright Laboratory (WL/AADP) Wright-Patterson AFB, OH 45433-7323*

The compositional abruptness at interfaces between ternary and binary III-V layers is inherently limited by surface segregation effects. We observe that Sb exhibits strong surface segregation during pseudomorphic GaAs<sub>1-x</sub>Sb<sub>x</sub> layer deposition by molecular beam epitaxy (MBE). This is observed to result in compositionally graded, generally Sb-deficient regions near the GaAs<sub>1-x</sub>Sb<sub>x</sub> on GaAs normal interface, and Sb-enriched regions near the GaAs on GaAsSb inverted interface. Our results suggest that compositionally abrupt normal and inverted interfaces in this system can be formed by the intelligent control of incident fluxes during interface formation.

Line-of-sight mass spectrometry was used to quantify the amount of surface accumulated Sb,  $x_{ss}$ , by interrupting growth and measuring the amount of Sb which leaves the film surface when the surface is held under a sole As flux and becomes As-capped. Surface accumulation of Sb was measured in this manner with an accuracy of  $\pm 0.05$  monolayers (ML). It was observed, for example, that  $\sim 0.95$  monolayers of Sb surface accumulation persist at steady-state during growth of GaAs<sub>0.8</sub>Sb<sub>0.2</sub> at  $T=500^\circ\text{C}$  despite a Sb sticking coefficient near unity. This amount was observed to diminish to  $\sim 0.2$  monolayers (negligible surface segregation) at  $T=350^\circ\text{C}$ . The segregation coefficient  $R$ , defined as  $R=1-(x/x_{ss})$ , was observed to exhibit an Arrhenius relationship with  $T$  for which the extracted activation energy was  $\sim 0.27$  eV.

Surface segregation measurements were performed at various distances from the intended normal interface to delineate the compositional grading. It was observed, for example, that during growth at  $T=450^\circ\text{C}$ , the intended GaAs<sub>0.8</sub>Sb<sub>0.2</sub> composition was not reached until nearly  $30\text{\AA}$  away from the intended GaAsSb on GaAs interface. Moreover, the compositional profile near this interface was observed to depend strongly on the shutter sequence during GaAsSb growth initiation. For example, if the Sb beam is introduced concurrently with Ga, then surface segregation occurs at the expense of Sb incorporation and a Sb-deficient interfacial layer analogous to that near the InGaAs on GaAs interface is formed. Alternatively, if both group-V beams are incident on the surface before growth begins, then the region near the interface may become enriched in Sb if the amount of Sb at the surface on the static surface is in excess of the steady-state value reached during growth.

A compositionally abrupt normal interface can be formed by populating the surface with the same amount of Sb that will surface segregate at steady state during growth in order to eliminate the transient behavior. This can be accomplished either by a measured amount of Sb deposition or a propitious choice of growth parameters for which the amount of Sb at the surface at steady state will be equivalent for both the static and the growth surface. For example, the latter was observed to occur when incident fluxes of  $J(\text{As}_2)=2\times 10^{-6}$  Torr,  $J(\text{Ga})=0.75$  ML/s, and  $J(\text{Sb}_2)=0.15$ , and  $T=485^\circ\text{C}$  were used to deposit GaAs<sub>0.8</sub>Sb<sub>0.2</sub> on GaAs where  $x_{ss}\sim 0.65$  ML.

A compositionally abrupt inverted interface can be formed by selective use of the As/Sb surface exchange reaction to deplete the excess surface Sb during a growth interrupt. Line-of-sight mass spectrometry is the ideal tool with which to accomplish this task.

Author RK is supported under U.S. Air Force contract F33615-95-C-1619. This work was partially supported by the Air Force Office of Scientific Research. Please contact regarding the abstract, author RK by mail at the above address, by phone at (513)255-1736, by FAX at (513)255-3374, or by e-mail at [kaspi@el.wpafb.af.mil](mailto:kaspi@el.wpafb.af.mil).

Figure 1.  
Measured amount of Sb surface segregation on  $\text{GaAs}_{0.8}\text{Sb}_{0.2}$  as a function of growth temperature.

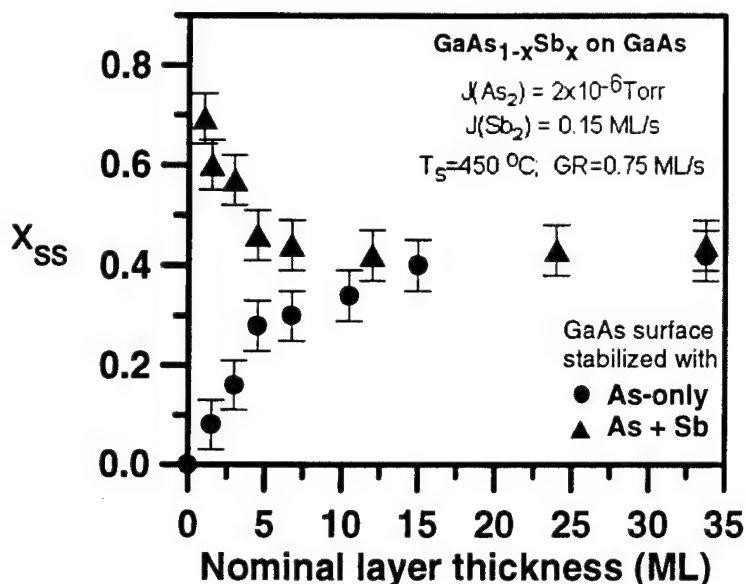
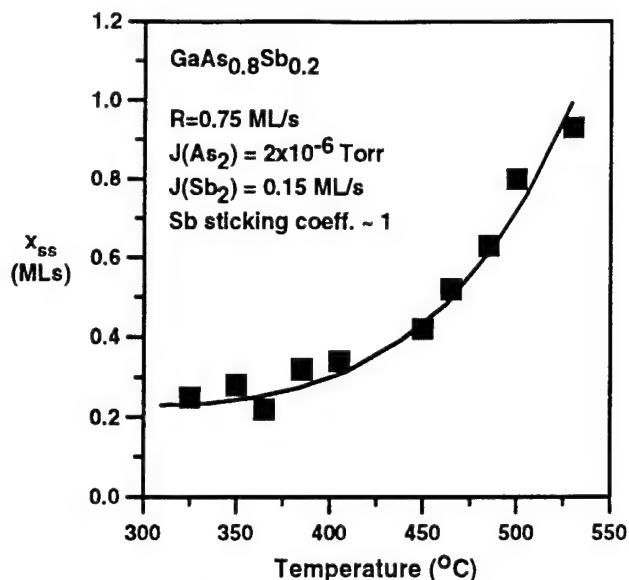
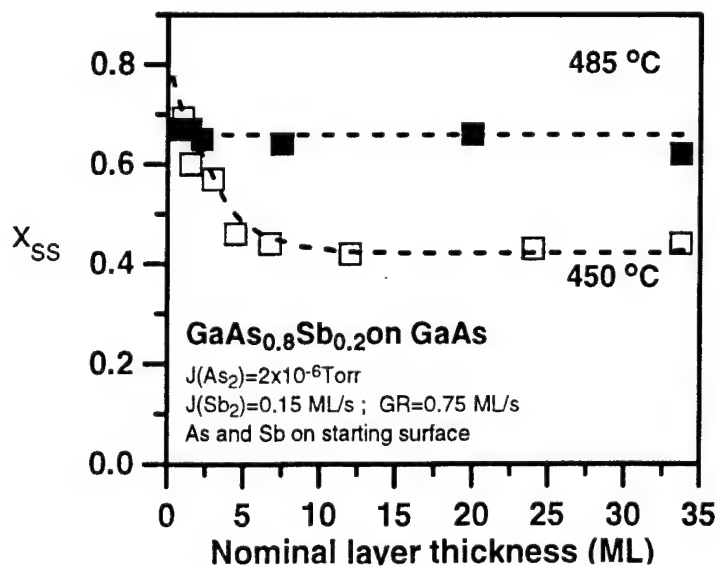


Figure 2.  
Evolution of Sb surface accumulation ( $x_{ss}$ ) near the normal interface. Prior to  $\text{GaAs}_{0.8}\text{Sb}_{0.2}$  deposition, the GaAs surface is stabilized with  $\text{As}_2$  only (circle), or with both  $\text{As}_2$  and  $\text{Sb}_2$  (diamond).

Figure 3.  
Evolution of Sb surface accumulation on  $\text{GaAs}_{0.8}\text{Sb}_{0.2}$  deposited on GaAs at two different temperatures. The graded composition interfacial layer at  $T=450^\circ\text{C}$  is eliminated at  $T=485^\circ\text{C}$  because the amount of Sb present at the surface before the ternary layer growth is equivalent to that during the growth.



# MBE growth of Si-doped InAlAsSb layers lattice-matched with InAs

Makoto Kudo and Tomoyoshi Mishima

Central Research Laboratory, Hitachi, Ltd., Kokubunji, Tokyo, Japan

Phone: +81-423-23-1111 (ext. 3139), Fax: +81-423-27-7679

e-mail: mkudo@crl.hitachi.co.jp

## **Abstract**

We describe a method to control the 2DEG concentration in the InAs/AlSb material system heterostructures. This was done by using an  $\text{In}_{0.5}\text{Al}_{0.5}\text{As}_{0.56}\text{Sb}_{0.44}$  quaternary alloy, in which n-type doping using Si as a donor was achieved for the first time.

InAs/AlSb (or AlGaSb, AlGaAsSb) heterostructures have been widely studied for future high-frequency FET applications because of their very high 2DEG mobility which exceeds  $20,000 \text{ cm}^2/\text{Vs}$  at room temperature. Accurate control of the 2DEG concentration in InAs channels, however, has not previously been achieved. N-type doping of AlSb, which is normally used as the barrier material in InAs channel FETs, is difficult when MBE is used. The Si, which behaves only as a donor for GaAs, turns into partially compensated acceptors in GaSb and AlSb [1]. Although column VI materials, such as S, Se, and Te, become donors for GaSb and AlSb, the vapor pressure of these materials is too high for accurate control of the doping concentration in MBE. Therefore, we have concentrated on studying an  $\text{In}_{0.5}\text{Al}_{0.5}\text{As}_{0.56}\text{Sb}_{0.44}$  alloy whose electron concentration can be controlled through Si doping.

The lattice constant and Sb content of  $\text{In}_{0.5}\text{Al}_{0.5}\text{As}_{1-x}\text{Sb}_x$  as a function of the  $\text{Sb}_4$  beam pressure is shown in Fig. 1. The growth rate was about  $1.2 \mu\text{m/h}$ , the  $\text{As}_4$  pressure was  $1 \times 10^{-5}$  torr, and the substrate temperature was  $350^\circ\text{C}$ . The lattice-matching with InAs is given at an Sb beam pressure of  $9 \times 10^{-7}$  torr. The mobility and free electron concentration of Si-doped  $\text{In}_{0.5}\text{Al}_{0.5}\text{As}_{1-x}\text{Sb}_x$  as a function of the Sb content is also shown in Fig. 2. Under growth conditions suitable for lattice-matching with InAs, an electron concentration of more than  $4 \times 10^{18} \text{ cm}^{-3}$  was obtained. This indicates that  $\text{In}_{0.5}\text{Al}_{0.5}\text{As}_{0.56}\text{Sb}_{0.44}$  is a suitable material for use as the electron-supply layer for an InAs channel.

We then grew an undoped- $\text{In}_{0.5}\text{Al}_{0.5}\text{As}_{0.56}\text{Sb}_{0.44}$ /undoped-InAs structure and a Si-doped  $\text{In}_{0.5}\text{Al}_{0.5}\text{As}_{0.56}\text{Sb}_{0.44}$ /undoped-InAs structure. The 2DEG concentrations of the undoped and Si-doped heterostructures were  $7 \times 10^{11} \text{ cm}^{-2}$  and  $1.3 \times 10^{11} \text{ cm}^{-2}$ , respectively. This is the first time that the 2DEG concentration in InAs channel modulation-doped structures has been controlled by Si-doping.

More detailed results, including TEM and PL measurements, will be given at the coming conference.

[1] G. Pindoria et al., Surf. Sci. **234**, 17 (1990).

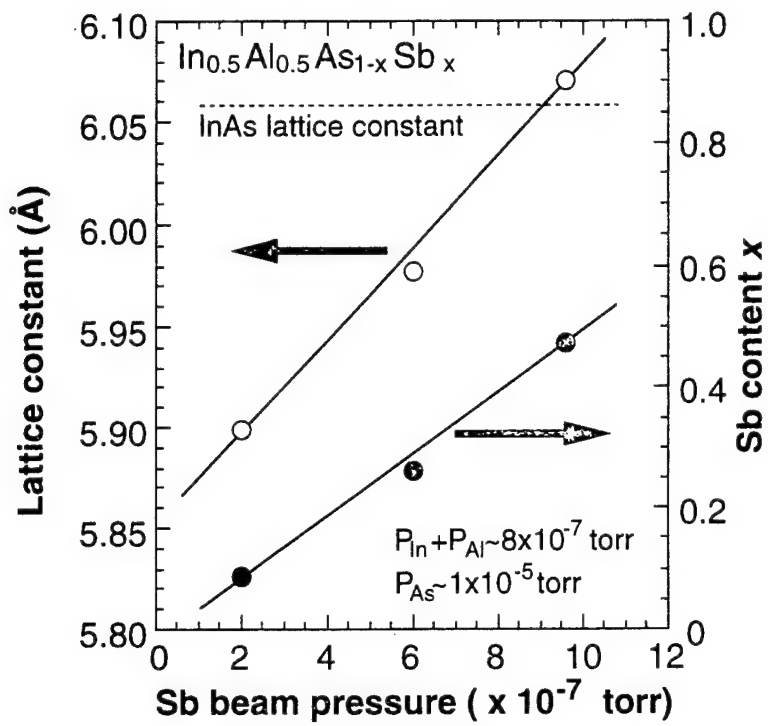


Fig. 1

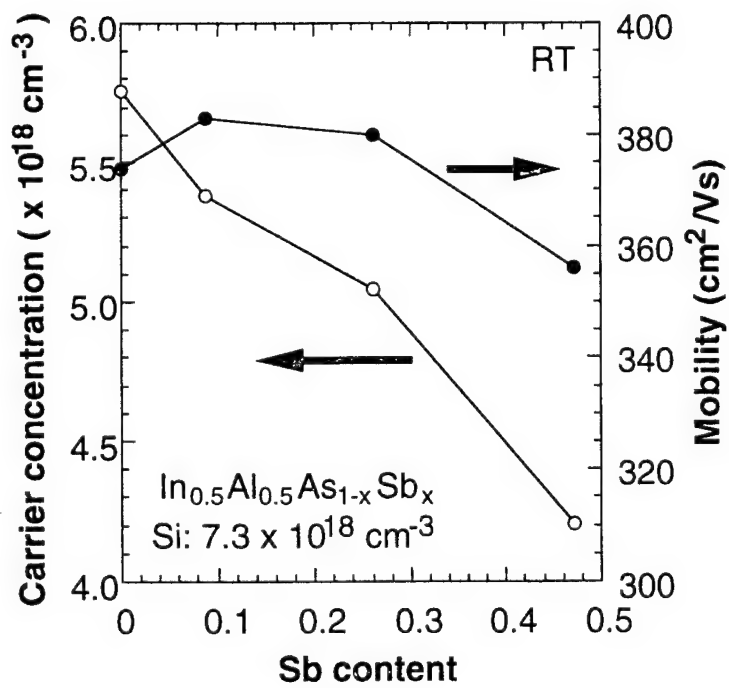


Fig. 2

kudo, et al.



## Molecular beam epitaxial GaInSbBi for infrared detector applications

Q. Du, J. Alperin, and W.I. Wang  
Department of Electrical Engineering  
Columbia University, New York, NY 10027

There have been efforts in recent years to incorporate Bi into narrow gap III-V's such as InAsSb to further reduce the band gap for 8-12  $\mu\text{m}$  infrared (IR) detector applications. To date, all published results indicated that although some Bi was incorporated into the films as evidenced by secondary ion mass spectroscopy (SIMS), the IR absorption spectra failed to show increase in the band edge response. Although one problem has been associated with molten InBi compounds which prevented the incorporation of Bi, we believe that the real difficulty is due to the fact that increasing the Bi content increases the lattice constant and thus increases lattice-mismatch between the Bi-containing alloys and the substrates (such as InSb). In other words, the Bi will be "squeezed" out of the epilayer.

In order to increase the Bi content, our approach is to add Ga to the InSbBi alloy. Since the covalent radius of Ga is relatively small compared to that of In, Sb, and Bi, the addition of Ga into InSbBi can significantly decrease the lattice constant and make the Bi-containing alloy lattice-matched to the available III-V substrates. Conventional wisdom works against adding Ga to InSbBi since this is expected to increase the band gap which is exactly opposite to what needs to be achieved (i.e., "narrow gap"). However, we realized that for the ternary compound GaInSb, adding a small mole fraction of Ga to InSb does not really enlarge the band gap compared to that of InSb due to band gap bowing. Furthermore, GaInSb is a group III alloy which makes composition control easy to achieve. To date, all published results indicate that Ga was never added in narrow gap III-V compounds such as InAsSbBi and TlInSb.

We have grown a new quaternary alloy GaInSbBi for the first time. With the addition of 3% Bi, the 77K absorption spectra showed a sharp band edge at 10.66  $\mu\text{m}$ , a wavelength range that was previously inaccessible through narrow gap III-V compounds such as InAsSb. This is the first time that adding Bi into narrow gap III-V's clearly extended the band edge absorption to a longer wavelength. The novel approach of taking advantage of "band gap bowing" to achieve lattice-matching as demonstrated here is applicable to other narrow gap materials. The details of molecular beam epitaxial growth and the effect of off-axis substrates will be presented.

## New semiconductors $\text{TlInGaP}$ and their gas source MBE growth

H. Asahi, K. Yamamoto, K. Iwata, S. Gonda and K. Oe\*

The Institute of Scientific and Industrial Research, Osaka University  
8-1, Mihogaoka, Ibaraki, Osaka 567, Japan  
Tel.+81-6-879-8407, Fax.+81-6-879-8509, E-mail: asahi@sanken.osaka-u.ac.jp

\*NTT Opto-electronics Laboratories  
Morinosato Wakamiya, Atsugi, Kanagawa 243-01

We here propose new III-V compound semiconductors  $\text{Tl}_x\text{In}_{1-x-y}\text{Ga}_y\text{P}$  (Thallium Indium Gallium Phosphide) lattice-matched to InP. This material system can cover the wavelength range from 0.92  $\mu\text{m}$  (InP) to over 10  $\mu\text{m}$  (TiGaP) and is suitable for the optical devices, especially for 1  $\mu\text{m}$  range laser diodes (LDs) for optical fiber communication and mid-infrared (longer than 2  $\mu\text{m}$ ) LDs. Furthermore, these LDs have a possibility to operate without change of wavelength with ambient temperature variation.

The estimated band gap energy variation with alloy composition is shown in Fig.1. This semiconductor materials are the alloys consisting of semiconductor InGaP and semimetal TIP. This alloy system has only one group V anion atoms and the type-I band lineup having a wider conduction band discontinuity than that of valence band is expected. This characteristics is very suitable for the optical devices. Furthermore, the semiconductors whose band gap does not change with ambient temperature are expected because of the alloy of semiconductor and semimetal like  $\text{Hg}_{0.4}\text{Cd}_{0.6}\text{Te}$ . This characteristics is very promising to fabricate semiconductor lasers whose wavelength does not change with ambient temperature variation, which is very important for the advance in WDM (wavelength division multiplexing) optical fiber communication, because one problem in using InGaAsP/InP LDs in WDM system is that the lasing wavelength fluctuates with ambient temperature variation due to the temperature dependence of band gap energy and LDs in WDM system must be equipped with Peltier elements that works to stabilize LD temperature.

We have successfully grown TlInP and TlInGaP alloys on InP (100) substrates by gas source molecular beam epitaxy (MBE) for the first time. The growth was conducted in the gas source MBE. Elemental Tl (Thallium), In (Indium), Ga (Gallium) and thermally cracked  $\text{PH}_3$  were used as group III and group V sources. The substrates used were InP (100). The substrate temperature was varied from 350°C to 450°C.  $\text{PH}_3$  flow rate was 0.3-0.5 SCCM. The vapor pressure of Tl is similar to that of Sb (Antimony) at low cell temperatures and higher at high cell temperatures, and Tl vaporizes from melt. Therefore, the Tl flux controllability is much better than that of Sb.

RHEED (reflection high energy electron diffraction) patterns revealed (2x4) reconstruction at substrate temperatures of 400-450 °C showing phosphorus-stabilized surfaces. However, at lower temperatures RHEED pattern showed phosphorus-excess (2x2) reconstruction. The surface exhibited mirror-smooth. The alloy composition of TlInP was found to vary with Tl flux. Fig.3 shows double crystal X-ray rocking curves, where the diffraction peak from InP and that from TIP and TlInP are clearly observed. In the conference, the growth of quaternary TlInGaP alloys as well as their electrical and optical properties are also presented.

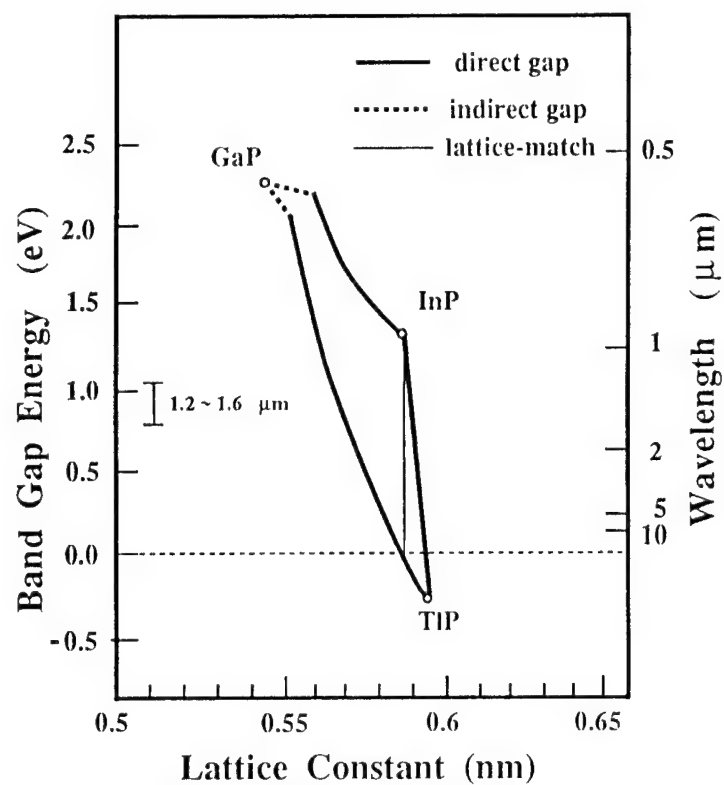


Fig.1 Band gap energy versus lattice constant for TIInGaP.

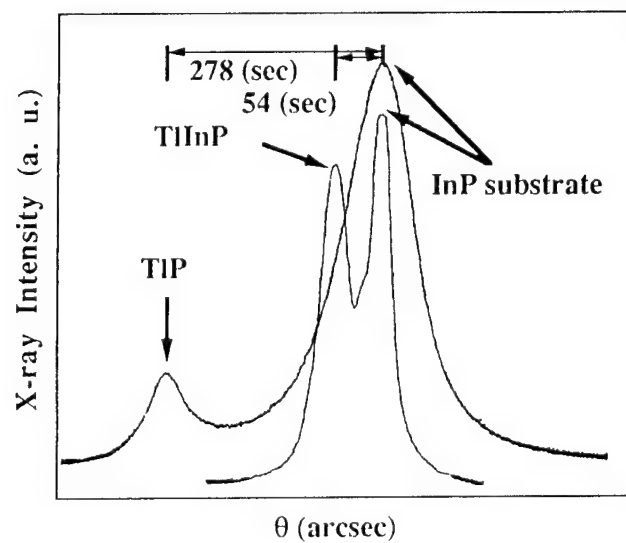


Fig.2 Double crystal X-ray diffraction rocking curves for TIInP on (100) InP.

## **Thin heterogeneous (MnAs / III-V) magnetic layers buried in high quality III-V heterostructures**

J. De Boeck, A. Van Esch <sup>(a)</sup>, and G. Borghs  
IMEC, Kapeldreef 75, B-3001 Leuven, Belgium

Recently we have demonstrated the formation of magnetic MnAs particles in GaAs using the technique of low-temperature GaMnAs growth followed by annealing as a unique way of fabricating magnetic thin films embedded in high quality semiconductor structures [1]. This type of buried magnetic heterostructures is difficult to achieve by overgrowth on a metal thin film or by implantation of transition metals [2]. The as-grown  $\text{Ga}_{1-x}\text{Mn}_x\text{As}$  layers are found to have high structural quality for uniform layers of 6 % Mn and for peak Mn concentrations up to 15%. The magnetic particles of 1 to 25 nm in size, depending on the annealing treatment, are very well confined to the regions which were Mn doped during growth. Hence, embedded magnetic layers can be incorporated in high quality semiconductor heterostructures, such as quantum wells and superlattices.

In this report the structural and magnetic properties of Mn doped III-V heterogeneous materials are briefly reviewed and we will concentrate on the fabrication of nearly two dimensional buried magnetic layers with a high density of MnAs clusters.

The structural quality of the semiconductor overgrowth will be discussed. We consider two approaches for III-V overgrowth: (i) the low-temperature growth under shuttered  $\text{As}_4$ -supply followed by post-growth annealing and (ii) regrowth at normal temperatures (600 °C) during which the MnAs phase separation takes place *in situ*.

Electronic transport properties through the 2D III-V/MnAs cluster chain are modified using Al(Ga)As barriers, Si (modulated) doping and In(Ga)As in the Mn doped region.

These new heterogeneous magnetic/semiconductor structures offer potential for designing novel magneto-electronic devices.

### References:

- [1] J. De Boeck, R. Oesterholt, A. Van Esch, H. Bender, C. Bruynseraede, C. Van Hoof, and G. Borghs, to be published in Appl. Phys. Lett. (may 1996).
- [2] J. Shi, J. Kikkawa, R. Proksch, T. Schäffer, D. Awschalom, G. Medeiros-Ribeiro, P. Petroff, Nature 377,707 (1995)

Work supported by the European Community under contract ESPRIT 20.027.  
(a) KU Leuven Physics Dept. Celestijnenlaan 200D, B-3001 Leuven, Belgium

### Contact author:

J. De Boeck  
IMEC  
Kapeldreef 75 B-3001 Leuven  
Belgium  
Tel +32 16 281 518  
Fax +32 16 281 501  
e-mail: deboeck@imec.be

## Supporting figures on magnetic and structural properties of the MnAs / (III-V) material system.

showing:

Fig 1: Magnetic behavior

Fig 2: size of clusters and incorporation in GaAs lattice

Fig 3 and 4: Feasibility of building well controlled layers (thicknesses larger than the ones studied in the present work)

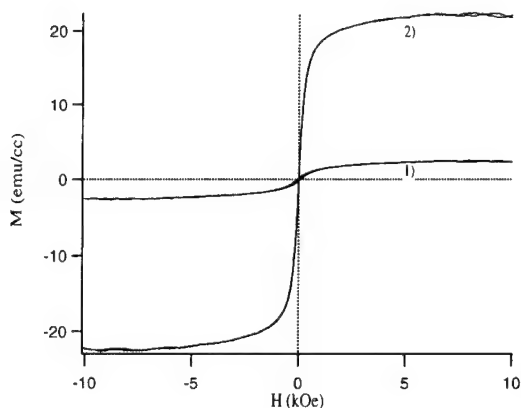


Fig. 1. Magnetisation data from a  $\text{Ga}_{0.94}\text{Mn}_{0.06}\text{As}$  layer, (1) as-grown and (2) after annealing, demonstrating the strong magnetic behaviour of the annealed film.

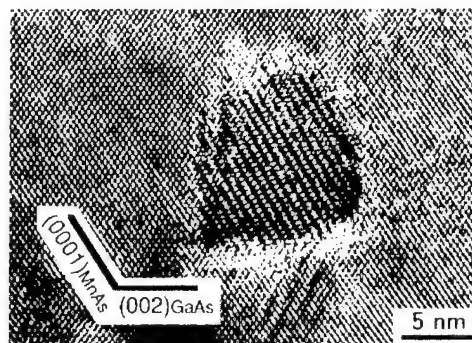


Fig. 2. High resolution TEM image of a MnAs cluster in a GaAs matrix.

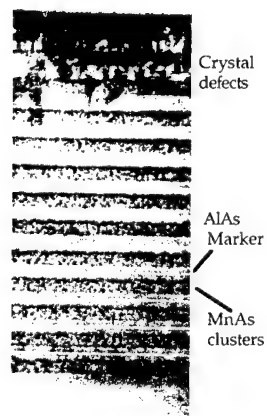


Fig 3 Multilayer GaAs/ (MnAs-III-V) structure comprising regions with high MnAs concentration (after anneal 600 °C).

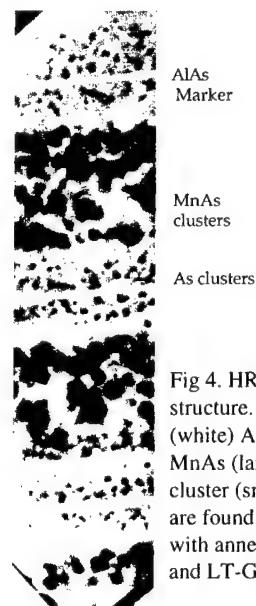


Fig 4. HREM of multilayer structure. In between two (white) AlAs markers, MnAs (larger) and As cluster (smaller) regions are found. Corresponding with annealed LT-GaMnAs and LT-GaAs regions.

## GaMnAs: GaAs-based III-V Diluted Magnetic Semiconductors Grown by Molecular Beam Epitaxy

T. Hayashi<sup>1)</sup>, M. Tanaka<sup>1,2)</sup>, and H. Shimada<sup>3)</sup>

<sup>1)</sup> *Department of Electronic Engineering, The University of Tokyo*

<sup>2)</sup> *PRESTO(Sakigake-21), Research and Development Corporation of Japan*

<sup>3)</sup> *Cryogenic Center, The University of Tokyo*

The person to be contacted: Masaaki Tanaka, phone +81-3-3812-2111 ext 6729,

Fax: +81-3-3816-4996, Email: masaaki@ee.t.u-tokyo.ac.jp

Recent progress of epitaxial growth techniques, such as molecular beam epitaxy (MBE) enabled us to prepare a variety of new artificial materials. One of the most interesting but unexplored directions for materials science will be the hybridization of semiconductors and magnetic materials. Recently, we have done a series of work on epitaxial heterostructures consisting of ferromagnetic metals (e.g. MnAs) and semiconductors (e.g. GaAs) [1]. In this paper, a different approach is presented, in which we prepare new GaAs-based III-V diluted magnetic semiconductors, GaMnAs, and explore their structural and magneto-transport properties. Although InMnAs was studied in the past [2], the present work will give new opportunities for research to explore an interdisciplinary field, because GaMnAs can be easily coupled with the existing GaAs-based III-V electronics/photonics.

We have successfully grown  $(\text{Ga}_{1-x}\text{Mn}_x)\text{As}$  with a Mn content  $x$  of 0.01 - 0.05 by MBE at 200°C - 300°C on GaAs(001) semi-insulating substrates. Reflection high energy electron diffraction (RHEED) and X-ray measurements indicate that the crystal structure of the epitaxial GaMnAs is of zinc-blende type, with a lattice constant slightly larger than that of GaAs. Figure 1 shows a X-ray rocking curve of a GaMnAs ( $x=0.02$ ) film with a thickness of 500 nm. The lattice mismatch to the GaAs substrate was estimated to be 0.0615 %, which linearly increases with  $x$ . The narrow linewidth of the GaMnAs peak indicates high structural quality. No indication of MnAs formation was seen either in X-ray measurements ( $\theta$ - $2\theta$  and rocking curves) or in high sensitivity magnetization measurements. These results indicate that the GaMnAs with low  $x$  (up to 0.05) is homogeneous alloy. During the MBE growth, clear RHEED oscillations were observed at the initial stage of the epitaxial growth, indicating that the growth mode is two-dimensional. Throughout the growth of GaMnAs, very streaky RHEED patterns with (1x2) reconstruction were seen.

In contrast, when we grew  $(\text{Ga}_{1-x}\text{Mn}_x)\text{As}$  with a Mn content  $x$  of 0.08 or more at 300°C, the formation of hexagonal MnAs was seen as well as GaMnAs of zinc-blende type. RHEED and X-ray analyses revealed that the MnAs clusters were formed with the epitaxial orientation of  $(-1101)\text{MnAs} // (001)\text{GaAs}$ ,  $[1120]\text{MnAs} // [110]\text{GaAs}$ , similar to the "type-B" MnAs/GaAs heterostructures [3]. The formation of these inhomogeneous films at higher Mn content shows the limitation of the Mn solubility in GaAs grown by low temperature MBE.

Magneto-transport properties were also studied for the homogeneous GaMnAs samples. In Hall measurements at room temperature and at 77 K, all samples showed  $p$ -type conduction with the hole concentration of  $5 \times 10^{17} \text{ cm}^{-3}$  -  $2 \times 10^{18} \text{ cm}^{-3}$  with no ferromagnetic behavior. At low temperature (4.2K or below), however, ferromagnetic properties have appeared. Figure 2 shows a magneto-resistance (MR) curve of a 1.0  $\mu\text{m}$ -thick  $(\text{Ga}_{1-x}\text{Mn}_x)\text{As}$  ( $x=0.05$ ) film measured at 1.6K. The magnetic field was applied in-plane, along the  $[110]$  axis of GaAs (and GaMnAs). The clear hysteretic behavior indicates ferromagnetic ordering in the GaMnAs, and the abrupt drop of the resistance at low magnetic field ( $\sim 0.1\text{T}$ ) indicates that the coercive field of the present sample is about 0.1T. Similar MR measurements were done with the applied magnetic field normal to the film plane, and we have found that our GaMnAs films have in-plane magnetic anisotropy.

[1] see for example, M. Tanaka, *Materials Sci. & Eng.* B31, 117 (1995).

[2] H. Munekata et al. *Phys. Rev. Lett.* 63, 1849 (1989).

[3] M. Tanaka et al. *Appl. Phys. Lett.* 65, 1964 (1994).

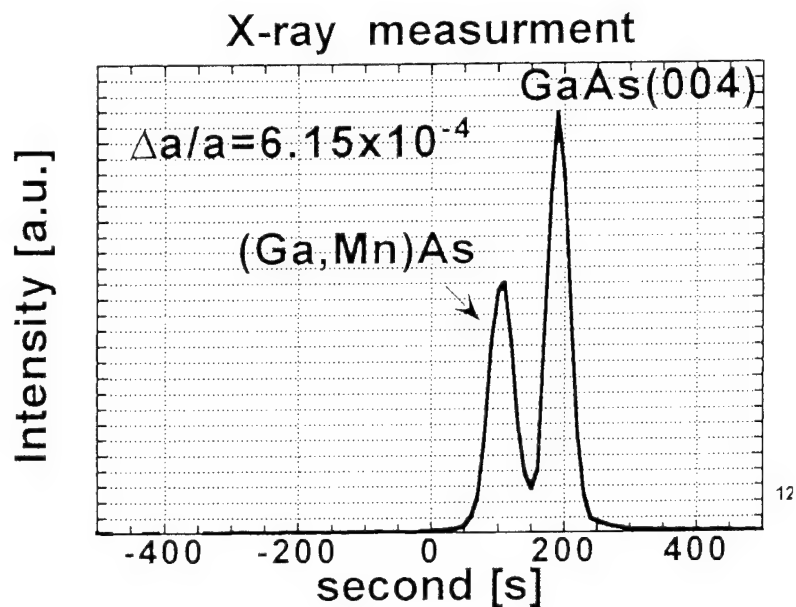


Figure 1: X-ray rocking curve of a  $(\text{Ga}_{1-x}\text{Mn}_x)\text{As}$  ( $x=0.02$ ) film with a thickness of 500 nm grown on a GaAs (001) substrate. The lattice mismatch to the GaAs substrate was 0.0615 %, which linearly increases with  $x$ .

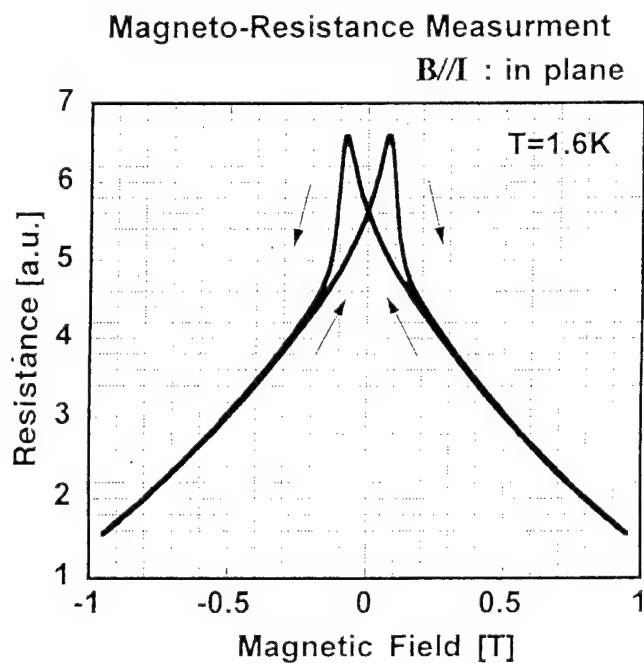


Figure 2: Magneto-resistance curve of a 1000 nm-thick  $(\text{Ga}_{1-x}\text{Mn}_x)\text{As}$  ( $x=0.05$ ) film measured at 1.6K. The magnetic field was applied in-plane, along the [110] axis of GaAs (and GaMnAs). The current was also along the [110]. The clear hysteresis behavior indicates ferromagnetic ordering.

## 10. IN-SITU CHARACTERIZATION AND CONTROL

THURSDAY MORNING (SMOTHERS)

Session Chair: A.J. SpringThorpe, Bell-Northern, Canada

Co-Chair: Parvez Uppal, Lockheed-Martin

- 09:00 10.1 **Integrated multi-sensor control of III-V MBE** (Invited)  
J.A. Roth, Hughes Research Laboratories, Malibu, CA, USA.
- 09:30 10.2 **Two-dimensional - one-dimensional mode change in GaAs molecular beam epitaxy revealed by in-situ scanning electron microscopy**  
N. Inoue, Y. Homma, J. Osaka, and T. Araki, Osaka Prefecture University, Japan.
- 09:50 10.3 **Monitoring growth and desorption of InGaAs epitaxial layers using atomic absorption**, Andrew Jackson, Paul Pinsukanjana, Larry Coldren, and Art Gossard  
University of California, Santa Barbara, California, USA.
- 10:10 10.4 **Real time in-situ thickness control of Fabry Perot cavities in MBE by 88 wavelength ellipsometry**  
C.H. Kuo, M.D. Boonzaayer, D.K. Schreder, G.N. Maracas, and B. Johs  
Arizona State University, USA.
- Break
- 10:50 10.5 **Application of pyrometric interferometry to the *in situ* monitoring of  $\text{In}_{0.525}(\text{Al}_x\text{Ga}_{1-x})_{0.475}\text{As}$  growth on InP substrates**  
R.M. Sieg, R.N. Sacks, and S.A. Ringel, Ohio State University, USA.
- 11:10 10.6 **Use of optical fiber thermometry in molecular beam epitaxy**  
K.G. Eyink, J.K. Patterson, S. Adams, T.W. Haas, and W.V. Lampert  
Wright Laboratory, USA.
- 11:30 10.7 **Measurement of MBE substrate temperature by photoluminescence**  
Y. Takahira and H. Okamoto, Chiba University, Japan.
- 11:50 10.8 **Simultaneous in situ measurement of substrate temperature and layer thickness using diffused reflectance spectroscopy (DRS) during molecular beam epitaxy growth**, Y. Li, J.J. Zhou, P. Thompson, D.L. Sato, and H.P. Lee  
University of California, Irvine, USA.



# Integrated Multi-Sensor Control of III-V MBE

J. A. Roth  
Hughes Research Laboratories  
Malibu, CA 90265

The control of MBE through the use of *in situ* sensors is a rapidly evolving technology that promises to revolutionize the growth of complex multilayer device structures by eliminating run-to-run variability, reducing the reliance on pre-growth calibration runs, and increasing the probability of first-pass success. Practical sensors are now available for substrate temperature, epitaxial layer composition and thickness, and effusion cell fluxes, and feedback control of each of these parameters has been demonstrated on an individual basis. However, the full benefits of sensor-based control can only be realized in a multiple-sensor environment, where the complementary information available from a host of sensors can be used to compensate for limitations in the domain of validity of each individual sensor. This permits a more accurate and complete picture of the state of the growing epitaxial layer to be achieved. With appropriate control algorithms that make use of the full complement of sensor data available in such a system, robust real-time control of the properties of MBE-grown epitaxial films can be achieved.

In the present talk we describe the design and operation of an integrated multi-sensor MBE system that includes sensors for all key growth parameters, and which incorporates flexible control software that utilizes the sensor information to achieve precise real-time regulation of the composition, thickness and temperature of growing films. In this system, substrate temperature is sensed by the shift in the substrate absorption edge (bandgap) determined from transmission spectra taken using a chopped white light source incident on the front side and a quartz light-pipe placed behind the substrate to collect the transmitted light. Fluxes of the In, Ga and Al effusion cells are determined from measurements of resonant atomic (optical) absorption of light directed through the source beams transversely. Composition and thickness of the growing epitaxial layer is determined by spectroscopic ellipsometry measurements over the photon energy range from 1.6 to 4.5 eV. For extremely thin (monolayer) films, the thickness is determined by analyzing oscillations in the UV photoelectric yield. The performance of these various sensors under MBE growth conditions will be reviewed, and data acquired during the growth of various device structures, including HBTs and RTDs, will be presented. The control algorithms and software used in this system will be discussed and contrasted with conventional approaches to MBE control, and the benefits of sensor-based control will be illustrated through results on the performance characteristics and yield of devices grown with and without sensor feedback. Finally, plans for future enhancements to the system will be described.

---

\* Work partially supported by DARPA through Agreement No. MDA972-95-3-0046

Contact:  
John A. Roth  
Hughes Research Labs  
3011 Malibu Canyon Road  
Malibu, CA 90265  
(310) 317-5339 (VOICE)  
(310) 317-5450 (FAX)  
email: jroth1@msmail4.hac.com

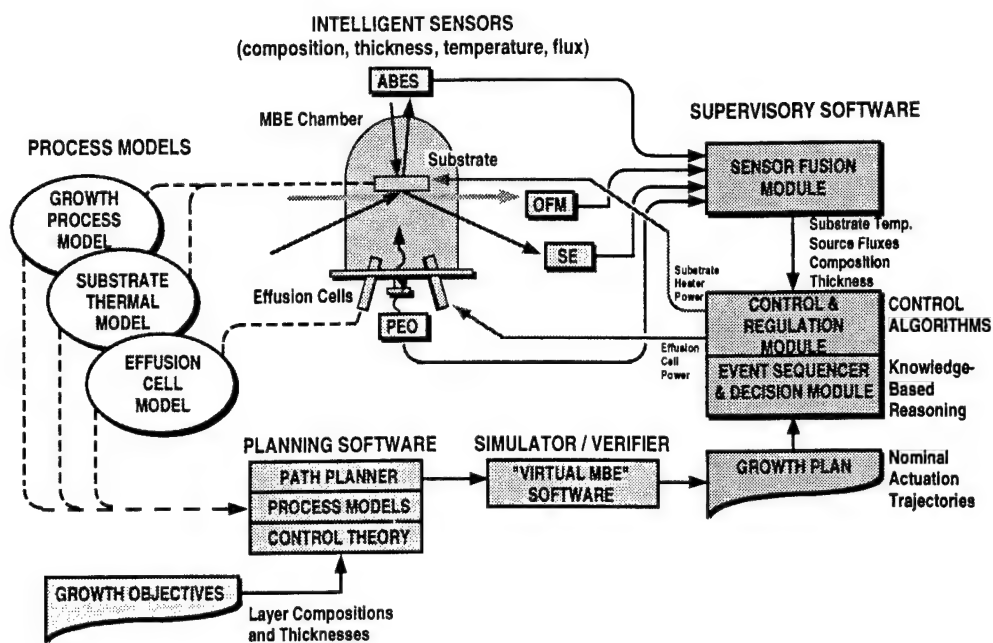


Figure 1. Integrated multi-sensor control system comprising intelligent sensors, process models, supervisory control algorithms, growth planning software, and system simulation. Sensors include: absorption-edge spectroscopy (ABES) for substrate temperature, spectroscopic ellipsometry (SE) for film composition and thickness, optical absorption flux monitoring (OFM), and a photoemission oscillation (PEO) sensor for monolayer thicknesses.

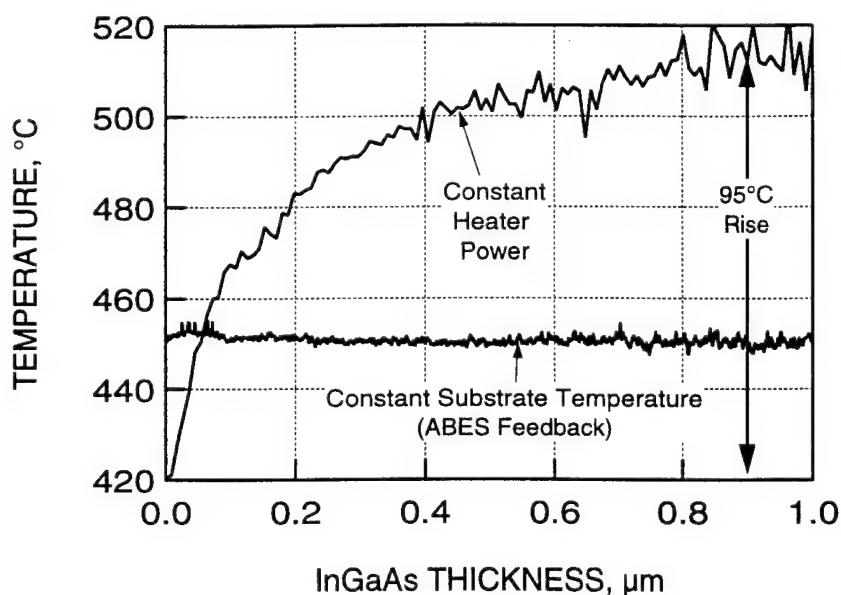


Figure 2. ABES data show that the true substrate temperature rises by 95-100°C during the growth of  $\text{In}_{0.53}\text{Ga}_{0.47}\text{As}$  on  $\text{InP}$ , at constant heater power (or constant thermocouple temperature). By using ABES sensor feedback, the spurious temperature increase due to  $\text{InGaAs}$  growth can be completely eliminated. Constant substrate temperature is advantageous in the growth of HBTs and other devices based on lattice-matched  $\text{InGaAs}$  on  $\text{InP}$ .

# Two-dimensional-one dimensional mode change in GaAs molecular beam epitaxy revealed by in-situ scanning electron microscopy

N. Inoue<sup>a</sup>, Y. Homma<sup>b</sup>, J. Osaka<sup>c</sup> and T. Araki<sup>a</sup>

<sup>a</sup>Osaka Prefecture University, Gakuencho, Sakai, Osaka 593 Japan

<sup>b</sup>NTT Interdisciplinary Research Labs, Musashino, Tokyo 180 Japan

<sup>c</sup>NTT LSI Laboratories, Morinosato, Atsugi, Kanagawa 243-01 Japan  
(T:+81-722-52-1161,F: 52-1163,mail:inouen@riast.osakafu-u.ac.jp)

We have developed in-situ scanning electron microscopy of GaAs MBE and shown that the actual MBE growth process is inhomogeneous and unsteady.<sup>1,2)</sup> In the present study we study the two dimensional (2D) nucleation mode in detail and show that the local growth mode changes from 2D to one dimensional (1D) step propagation mode under a critical growth condition.

The experiment was done using an MBE-UHV SEM hybrid system. The substrate was (001) GaAs misoriented 0.2° to the [110] direction which had nominal interstep spacing of about 80 nm. A smooth surface was prepared by a buffer layer growth. The growth was performed at a substrate temperature of about 540 °C and a growth rate of 1 ML per 100 sec. SEM observation was performed with a resolution of about 5nm and an observation rate of 1 frame per 80 sec.

Figure 1 shows an example of the morphology change with such a transition. Surface feature at the beginning of growth is shown in Fig. 1(a). The curved lines are the monolayer steps. White small features appeared on the very wide terraces as marked by the big arrows. These are the monolayer island clusters. Isolated island also appeared in medium wide terraces as marked by the small arrows. There were no islands on the narrow terraces. This shows that step propagation growth occurs there. Therefore the two growth modes coexist under a critical growth condition. This is due to an inhomogeneity of terrace width introduced by unavoidable surface undulation and step bunching during annealing before growth.

It is to be noted that as the growth proceeded, island nucleation became scarce. Finally only a few islands nucleated between the steps and the 1D growth became dominant.

As for the step configuration, two important changes took place. (1) The step shape was curved and smooth initially, but aligned with small zigzag later. (2) The step interval was inhomogeneous initially but ordered later. The latter caused local growth mode change to 1D step propagation. Step propagation growth also made the step ordering. In addition, as the islands were coalesced to the steps, step interval was homogeneized. Thus, this 2D+1D mixed mode makes the surface smooth.

There have been no reports on the phase boundary between 3D and 2D growth modes. Various intermediate growth modes between pure 3D and 1D growths were observed as shown in Fig. 2, including the multi-level 2D growth (transition from 2-level).

1)J.Osaka, MBE8,J.Cryst.Growth 150(1995)73, 2)N.Inoue, ibid, 107.

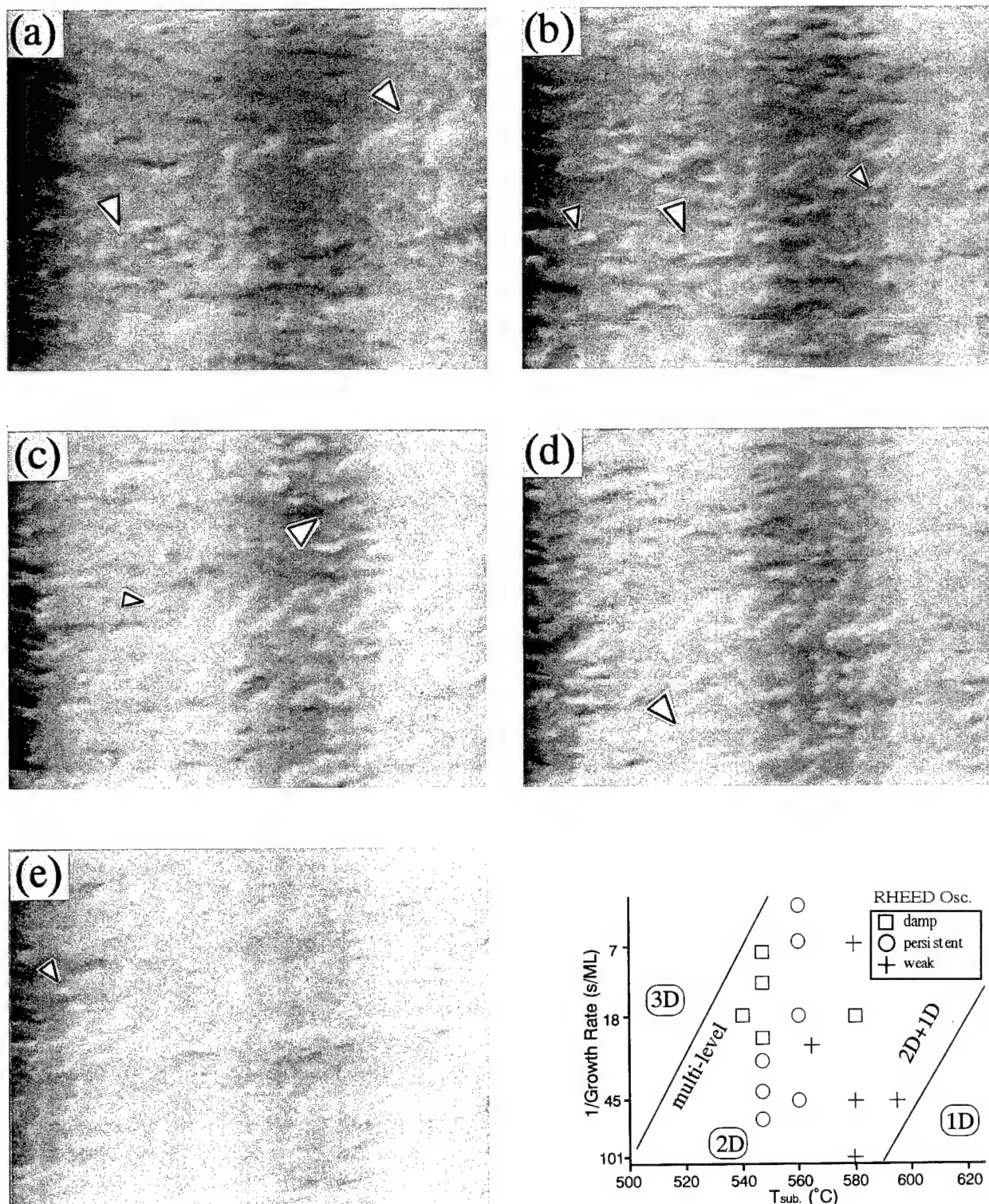


Fig. 1 SEM observation of morphology change. (a)beginning of growth, (b)1 min, (c)2 min, (d)3 min, (e)5 min.

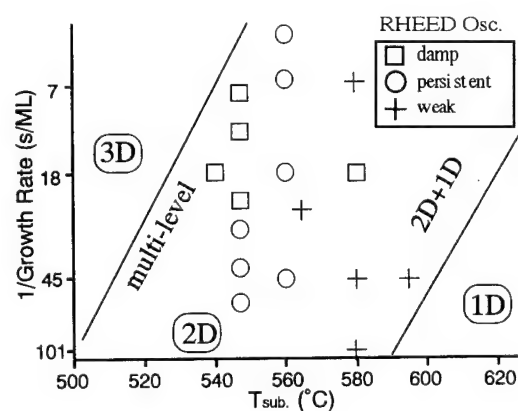


Fig. 2 Phase diagram of growth modes with various 2D growths correspondig to RHEED behaviors.

# Monitoring growth and desorption of InGaAs epitaxial layers using atomic absorption

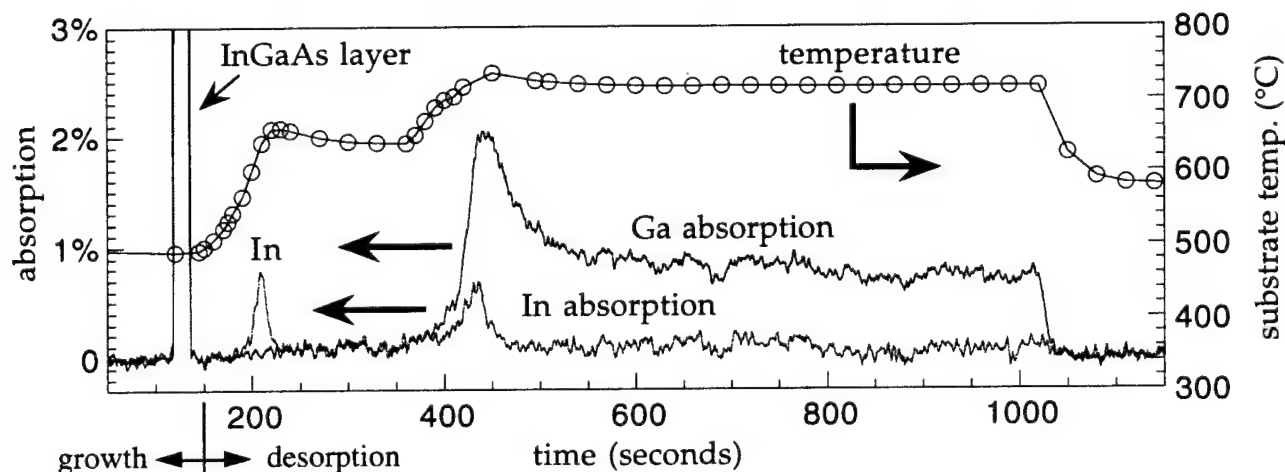
Andrew Jackson<sup>1</sup>, Paul Pinsukanjana<sup>2</sup>, Larry Coldren<sup>2</sup>, and Arthur Gossard<sup>1</sup>

1) Materials Department, 2) ECE Department  
University of California, Santa Barbara, CA 93106

The growth dynamics of InGaAs quantum wells were recently investigated by measuring thermal desorption of In using a quadrupole mass spectrometer (QMS) mounted on the pyrometer port of an MBE system<sup>1</sup>. The technique was used to measure the surface and bulk indium concentrations of an InGaAs epitaxial layer. In this work, we use an optical-based flux monitor (OFM)<sup>2</sup> to study both the MBE growth and the thermal desorption process of a ternary InGaAs layer on a GaAs substrate. The desorption is accomplished by raising the substrate temperature following the layer deposition. With the OFM, we measure the atomic absorption of Ga and In molecular beam fluxes simultaneously. Additionally, in our system we retain the use of the optical pyrometer for substrate temperature measurement.

The OFM uses atomic emission lines from Al, Ga, and In hollow cathode lamps. The light from each of the three lamps is mechanically chopped at a different frequency and combined into a single beam using a trifurcating fiber bundle. This beam is then split into a reference beam and a probe beam, each coupled into an optical fiber. The probe beam passes through the growth chamber in front of the substrate and is then reflected back by a pair of flat mirrors. The returning probe beam is collected by another optical fiber which carries the beam to the signal detector. This dual pass configuration increases the measured absorption signal for a given flux. The signal is measured using a PMT and lock-in amplifiers. Another PMT measures the reference beam, which does not pass through the chamber, to account for lamp intensity drifts.

The figure below shows the Ga and In optical absorption signal for the growth of a 110Å In<sub>0.2</sub>Ga<sub>0.8</sub>As layer and its subsequent desorption as the temperature, as measured by optical pyrometry, is raised. During the growth of the InGaAs layer ( $T_{\text{substrate}} \approx 490^\circ\text{C}$ ) the absorption signals for In and Ga are 5.4% and 12.1%, respectively. The first peak appears upon heating above 600°C and corresponds to desorption of excess indium that segregates at the surface during growth of InGaAs. The second peak, as the substrate is raised above 700°C, is from desorption of the InGaAs layer itself, followed by continued desorption of the underlying GaAs.



<sup>1</sup> K.R. Evans, R. Kaspi, J.E. Ehret, M. Skowronski, C.R. Jones, *Journal of Vacuum Science and Technology B*, **13** 1820 (1995)

<sup>2</sup> P. Pinsukanjana, A. Jackson, K. Maranowski, J. Tofte, S. Campbell, J. English, S. Chalmers, L. Coldren, A. Gossard, *Journal of Vacuum Science and Technology B*, **14** May/Jun (1996) (in press)



## **Real time in-situ thickness control of Fabry Perot cavities in MBE by 88 wavelength ellipsometry**

**C. H. Kuo, M. D. Boonzaayer, D.K. Schreder, G. N. Maracas\*, and B. Johs<sup>+</sup>**

**Department of Electrical Engineering,  
Center for Solid State Electronic Research  
Arizona State University , Tempe, AZ 85287-6206**

**\* Motorola Phoenix Corporate Research Labs  
2100 E. Elliot Road  
Tempe, AZ 85284**

**+J.A. Woollam Co., Inc.  
650 J st. suite 39  
Lincoln, NE 68508**

We have demonstrated the use of closed-loop feedback control of MBE by in-situ spectroscopic ellipsometry (SE) to grow reproducible AlAs/GaAs Fabry Perot vertical cavity which is used for surface emitting laser cavities. Tracking of layer thickness in real-time was accomplished by using a virtual substrate model to reduce the time required to perform data reduction on multilayer epitaxial structure data. A 44 wavelength ellipsometer (Woollam Co.), ( $4150 \text{ \AA} < \lambda < 7554 \text{ \AA}$ ), capable of obtaining three spectra per second, was used to measure material optical properties in real time. A new ultra-stable substrate manipulator design (DCA instruments) was implemented in which piezoelectric crystals were used to vary the tilt and thus improve the stability of reflected light from substrate surface under rotation. The variation of incident angle under rotation was typically 0.02 degree (0.005 degree was the best obtained), reduced from ~0.1 degree in conventional MBE manipulators. This stability reduced the noise in the ellipsometry data and also improved the accuracy of thickness information during growth by eliminating the need to fit for angle of incidence.

To test the reproducibility of SE control among successive growth runs, a 1 lambda cavity structure (with mode centered at 970nm) was tested by normal incident reflectance measurement. Sample-to-sample reproducibility of the mode positions in wavelength among the structures was observed to be better than a  $\pm 0.2\%$  variation in thickness control for Fabry Perot cavity.

A new 88 wavelength ellipsometer ( $2500 \text{ \AA} < \lambda < 7554 \text{ \AA}$ ) has been constructed by J.A. Woollam Co.. The improvement over the UV range will cover the critical point transition of the III-V compound material. This will enable us to obtain a better information of thickness during the growth. It is especially important for the thickness control for the  $\text{Al}_x\text{Ga}_{1-x}\text{As}$ . In this paper, we will demonstrated the growth control of AlAs/GaAs Fabry Perot vertical cavity and the comparison of the thickness control between 44 and 88 wavelength ellipsometer. We will also demonstrated the thickness control of the AlGaAs/GaAs Fabry Perot vertical cavity (with mode centered at 850nm) from the new 88 wavelength ellipsometer.

From this study, we will demonstrated of non-destructive ellipsometry technique is a better way for real time in-situ thickness control in MBE or MOCVD. This will allowed us to have a thickness control of better than  $\pm 0.2\%$  which is important in the optoelectronic device.

**Chau-Hong Kuo  
ERC 163  
Center for Solid State Electronic Research  
Arizona State University , Tempe, AZ 85287-6206  
Tel: (602) 965-3196  
FAX: (602) 965-0775  
e-mail: [chkuo@enuxsa.eas.asu.edu](mailto:chkuo@enuxsa.eas.asu.edu)**

**Application of pyrometric interferometry to the *in situ* monitoring  
of  $\text{In}_{0.525}(\text{Al}_x\text{Ga}_{1-x})_{0.475}\text{As}$  growth on InP substrates**

R.M. Sieg, R.N. Sacks, and S.A. Ringel

Department of Electrical Engineering, 205 Drees Lab, 2015 Neil Avenue

The Ohio State University, Columbus, OH 43210-1272

Telephone: (614) 292-1721 E-mail: rsieg@magnus.acs.ohio-state.edu

The alloy system  $\text{In}_{0.525}(\text{Al}_x\text{Ga}_{1-x})_{0.475}\text{As}$ , which is lattice matched to InP, covers the technologically important wavelength range 0.8-1.6  $\mu\text{m}$ , including the fiber optic communications wavelengths 1.3  $\mu\text{m}$  and 1.55  $\mu\text{m}$ . However, growth of these alloys on InP substrates by MBE would be improved by convenient *in situ* methods of monitoring the epitaxial growth. In this study we extend quantitative pyrometric interferometry (PI), which was developed by Springthorpe et al<sup>1</sup> and applied to the  $\text{Al}_x\text{Ga}_{1-x}\text{As}$  system, to  $\text{In}_{0.525}(\text{Al}_x\text{Ga}_{1-x})_{0.475}\text{As}$  for the first time. Because PI requires the epitaxial layer to be partially transparent at the pyrometer wavelength (0.94  $\mu\text{m}$ ) we find that obtaining usable oscillations is easier for higher Al-content layers due to their larger bandgaps. For this reason, we concentrate on obtaining quantitative results for the endpoint  $\text{In}_{0.52}\text{Al}_{0.48}\text{As}$ . However, PI oscillations are observable even for the  $\text{In}_{0.53}\text{Ga}_{0.47}\text{As}$  endpoint. We also find that stray radiation can be a problem due to the low growth temperature, especially when using indium-free holders with gaps around the wafer edge. The holders used in this study had such gaps, and we observed up to 10°C pyrometer variations during substrate rotation due to stray heater radiation passing through the sapphire back plate. For comparison, typical PI oscillations were 2°C peak-to-valley. This problem is solvable by deposition of a relatively thin (~0.5  $\mu\text{m}$  or less) initial layer of  $\text{In}_{0.53}\text{Ga}_{0.47}\text{As}$ . The low bandgap  $\text{In}_{0.53}\text{Ga}_{0.47}\text{As}$  layer largely eliminates stray heater radiation noise by coating the sapphire in the gaps between the InP substrate and the holder. Another source of error we observed are changes in the apparent surface temperature during initial layer growth. As was observed previously for  $\text{Al}_x\text{Ga}_{1-x}\text{As}$ ,<sup>2</sup> these transients are in the direction of increasing apparent surface temperature for growth of smaller bandgap material on top of larger bandgap material, and vice versa.

PI yields the growth rate  $R=\lambda/(2Tn)$  where  $\lambda=0.94$   $\mu\text{m}$  is the pyrometer wavelength,  $T$  is the measured oscillation period, and  $n$  is the effective refractive index. Conversely, to obtain  $n$  the composition and growth rate must be known. In this study, double crystal x-ray diffractometry (DCXRD) was used to measure both the composition ratio  $[\text{In}]/[(\text{Al},\text{Ga})]$  and the growth rate. In addition, photoluminescence was used to obtain the  $[\text{Al}]/[\text{Ga}]$  composition in the case of quaternary layers, using published calibration curves.<sup>3</sup> The growth rate was obtained from DCXRD using both  $\text{In}_{0.53}\text{Ga}_{0.47}\text{As}/\text{In}_{0.52}\text{Al}_{0.48}\text{As}$  superlattices and  $\text{In}_{0.52}\text{Al}_{0.48}\text{As}/\text{GaAs}$  superlattices where the GaAs layer was sufficiently thin to be coherently strained. The lattice matched  $\text{In}_{0.52}\text{Al}_{0.48}\text{As}/\text{In}_{0.53}\text{Ga}_{0.47}\text{As}$  superlattices were found to produce relatively weak satellite peaks. In contrast, we found that only a six period strained 50 nm  $\text{In}_{0.52}\text{Al}_{0.48}\text{As}/0.8$  nm GaAs superlattice was sufficient to produce numerous strong satellite peaks in the rocking curves. We corrected for the strain-reduction of the GaAs thickness; however, due to the overall thickness ratio, this amounts to less than a 0.25% correction in the  $\text{In}_{0.52}\text{Al}_{0.48}\text{As}$  growth rate. The much stronger satellite peaks obtained for the strained  $\text{In}_{0.52}\text{Al}_{0.48}\text{As}/\text{GaAs}$  superlattice, combined with a smaller overall superlattice thickness and elimination of the  $\text{In}_{0.53}\text{Ga}_{0.47}\text{As}$  sub-layers as a source of error, lead us to consider the strained  $\text{In}_{0.52}\text{Al}_{0.48}\text{As}/\text{GaAs}$  superlattice structure superior for determination of growth rate. In the case of a quaternary alloy, the strained structure has an additional advantage in that only one Ga and Al cell each is required. Growth conditions were setup using a combination of RHEED on GaAs substrates and flux measurements. RHEED was used to establish the  $\text{Al}_x\text{Ga}_{1-x}\text{As}$  composition and growth rate. By correcting for the difference in total group III flux and unit cell volume between  $\text{Al}_x\text{Ga}_{1-x}\text{As}$  and  $\text{In}_{0.525}(\text{Al}_x\text{Ga}_{1-x})_{0.475}\text{As}$  the growth rate on InP could be calculated from the  $\text{Al}_x\text{Ga}_{1-x}\text{As}$  RHEED with an accuracy of 3% or better versus the DCXRD standard. Flux gauge measurement of the indium was found to be sufficient to reproducibly obtain the  $[\text{In}]/[\text{Al},\text{Ga}]$  composition to within .005 as long as the In-to-Ga flux sensitivity factor was known to three decimal places. Using these techniques and *ex situ* DCXRD the effective refractive index was obtained for  $\text{In}_{0.52}\text{Al}_{0.48}\text{As}$  to be  $n=3.515 \pm 1\%$ .

1. A.J. Springthorpe, T.P. Humphreys, A. Majeed, and W.T. Moore, Appl. Phys. Lett. **55**, 2138 (1989).
2. R.N. Sacks, R.M. Sieg, and S.A. Ringel, J. Vac. Sci. Technol. **B**, in print.
3. R.F. Kopf, J.M. Kuo, and M. Ohring, J. Vac. Sci. Technol. **B9**, 1920 (1991).

Application of pyrometric interferometry to the *in situ* monitoring  
of  $\text{In}_{0.525}(\text{Al}_x\text{Ga}_{1-x})_{0.475}\text{As}$  growth on InP substrates

R.M. Sieg, R.N. Sacks, and S.A. Ringel

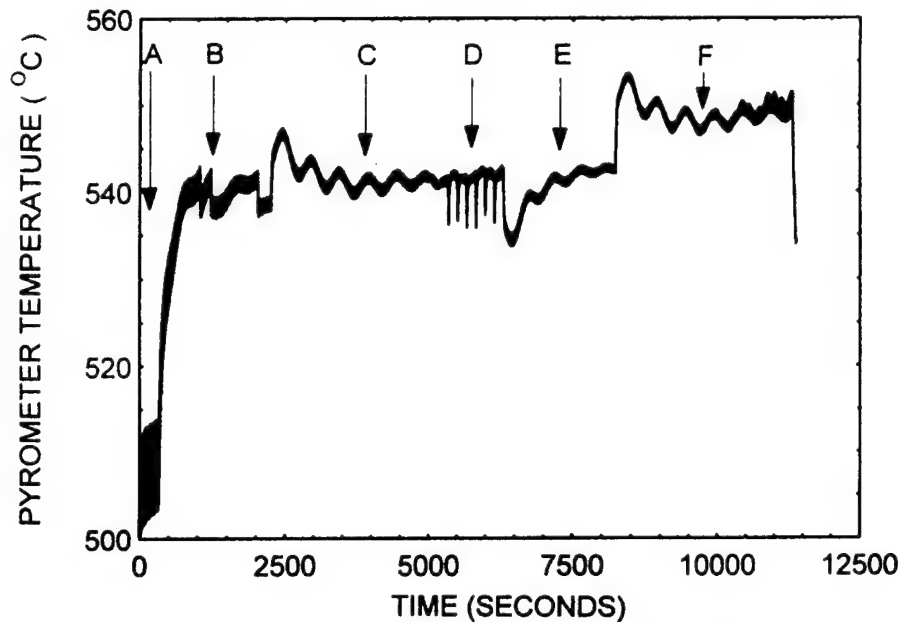


Figure 1. Pyrometer trace for a typical  $\text{In}_{0.52}\text{Al}_{0.48}\text{As}$  calibration run. Region A is before the start of the run: note the large noise ( $\sim 10^\circ\text{C}$  width) during substrate rotation due to stray heater radiation. Region B is the  $\text{In}_{0.53}\text{Ga}_{0.47}\text{As}$  coating layer. The three nearly instantaneous temperature jumps in this region are manual heater adjustments to correct for an increasing surface temperature due to deposition of the low bandgap  $\text{In}_{0.53}\text{Ga}_{0.47}\text{As}$ . Region C is the first  $\text{In}_{0.52}\text{Al}_{0.48}\text{As}$  layer. Region D is the 6 period  $\text{In}_{0.52}\text{Al}_{0.48}\text{As}/\text{GaAs}$  superlattice used for DCXRD analysis. Region E is a second  $\text{In}_{0.53}\text{Ga}_{0.47}\text{As}$  layer, used to provide a large refractive index step for the second  $\text{In}_{0.52}\text{Al}_{0.47}\text{As}$  layer, which is region F. Note that both low bandgap  $\text{In}_{0.53}\text{Ga}_{0.47}\text{As}$  layers exhibit an increase in apparent surface temperature during initial growth, while both high bandgap  $\text{In}_{0.52}\text{Al}_{0.48}\text{As}$  layers exhibit an initial decrease in apparent surface temperature. Also notice that pyrometric interference oscillations are observable for the second  $\text{In}_{0.53}\text{Ga}_{0.47}\text{As}$  layer (region E), as well as in both  $\text{In}_{0.52}\text{Al}_{0.48}\text{As}$  layers (regions C and F).

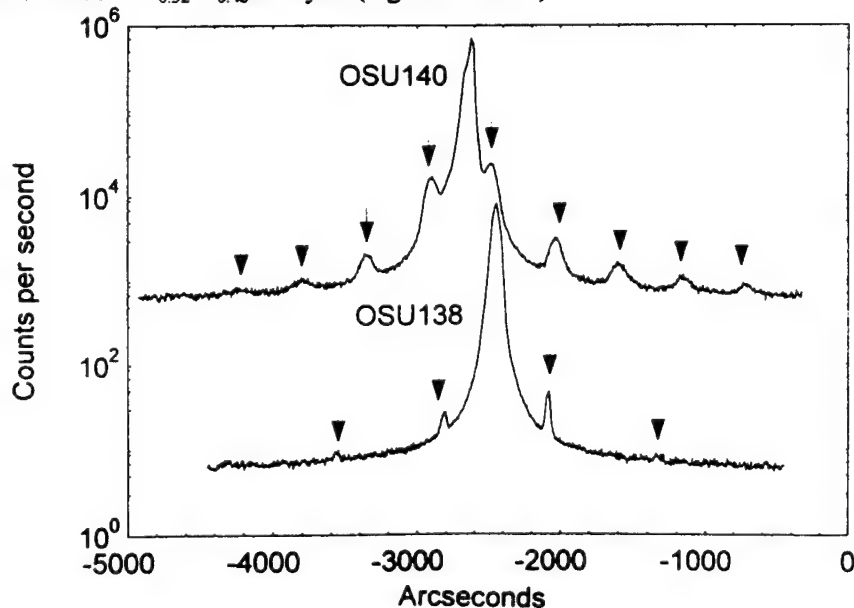


Figure 2. DCXRD rocking curves. OSU138 has a 30 period 25 nm/25 nm  $\text{In}_{0.53}\text{Ga}_{0.47}\text{As} / \text{In}_{0.52}\text{Al}_{0.48}\text{As}$  superlattice, while OSU140 has a 6 period 41 nm/0.9 nm  $\text{In}_{0.52}\text{Al}_{0.48}\text{As} / \text{GaAs}$  superlattice. Arrows denote observed superlattice satellite peaks. OSU140 has been raised by 2 orders of magnitude to separate the rocking curves in the figure. Note that for OSU138 the even diffraction orders are symmetry forbidden according to rocking curve simulations.



**“Use of Optical Fiber Thermometry in Molecular Beam Epitaxy”, K. G. Eyink, J. K. Patterson, S. Adams, T. W. Haas, and W. V. Lampert  
Wright Laboratory-Materials Directorate WPAFB, OH 45433-7750**

**ABSTRACT**

The measurement of temperature in the practice of solid source MBE is a very important process. Substrate and cell temperatures are dominant in determining growth modes, alloy compositions, defects, etc of the epitaxial films. A variety of means are currently used to make these measurements with contact and non-contact thermocouple and optical pyrometry being the commonest and simplest. The need for precise temperature control can be appreciated when it is realized that as little as  $\pm 0.5^{\circ}\text{C}$  in the operating temperature of a group III cell can affect films composition by over  $\pm 0.1\%$  —a value which can be of importance when attempting to grow lattice matched films. In this work we will present results using optical fiber thermometry (OFT) for the measurement and control of temperature in MBE. Examples of substrate temperature measurements using 2 color OFT will be given and compared to standard optical pyrometry, thermocouple readout, and spectroscopic ellipsometry (SE)). SE depends upon having an adequate data base of spectra as a function of temperature and depends to some extent on sample roughness. The growth of a narrow bandgap material on a wide bandgap substrate will be presented with GaSb on GaAs as an example. Modeling of changes in IR absorbance to be expected for this case have been carried out using ellipsometric modeling and show significant effects in agreement with experimental results. In another example, OFT has been integrated into a standard MBE effusion cell. The OFT measurement is considerably more sensitive than the usual thermocouple used in these applications and can give reproducible temperature resolution of  $\pm 0.01^{\circ}\text{C}$  at  $800^{\circ}\text{C}$ . This cell design has exhibited long term stability of  $\pm 0.02^{\circ}\text{C}$  when cell temperatures are controlled by OFT. This is about an order of magnitude better than what is typically available using thermocouples. In addition, because the OFT is measuring light from the crucible it does not depend on thermal contact to an insulator as a thermocouple does. We will present data showing the improved time response possible using the OFT control, in particular short term flux transient response. In addition we will point out the robustness of the OFT sensor to cell failure modes such as crucible cracking, contamination, and the like.

## Measurement of MBE Substrate Temperature by Photoluminescence

Y. Takahira, and H. OKAMOTO

Chiba University, Faculty of Engineering  
1-33 Yayoi-Cho, Inage-ku, Chiba 263, JAPAN

Tel: +81-43-290-3441, Fax: +81-43-290-3442, E-mail: okamoto@tcom.tech.chiba-u.ac.jp.

In conventional MBE, the substrate temperature is measured by a thermocouple and by a pyrometer, both of which are inaccurate because the thermocouple is not in touch to the substrate nor to the Mo block, and because the pyrometer suffers from the ambient light such as room light and a light from an ionization gauge, thereby making it very difficult to measure accurately a low substrate temperature necessary for the low temperature MBE growth (200~300°C). Lee et. al., [1] reported another method using an infra-red spectroscopic technique to measure the temperature dependence of the bandgap energy or the refractive index of the substrate. Both transmission and reflection modes of the measurement were proposed, which are free from any adjustable parameters such as emissivity and unaffected by window absorption or coating. The transmission mode is suitable for a non-In-bonded, radiatively heated substrate, thereby the substrate heater is used as the light source. But any change in current flowing through the heater gives a change in the blackbody radiation spectrum of the heater. Ambient lights such as filaments of the RHEED gun and the ionization gauge will also give an error in the measured absorption or refractive index spectrum. The reflection mode of the refractive index measurement is suitable to the substrate mounted on a Mo block with or without In solder. But two viewing ports facing to the substrate are needed, and furthermore the refractive index is not well known at high temperature. An example of the measurement shows that wavelength change corresponding to a temperature change by 100°C is comparable with the spectrum broadening of a transmission peak [1].

In this paper, a new method is presented, which utilizes PL from the substrate. PL measurement system very familiar to every MBE engineers is used, except an optical fiber through which an excited light (Ar laser) is introduced into the vacuum chamber and incident perpendicularly on the substrate. Photoluminescence light is also gathered into this fiber and supplied to the measuring system outside vacuum. An uv silica fiber with core diameter as large as 400  $\mu\text{m}$  is used to gather much amount of PL (fig.1). A specially designed UHV flange with optical fiber feedthrough is used here (fig.2), which exhibits negligible amount of vacuum leakage measured at  $1 \times 10^{-9}$  torr by QMS. Optical insertion loss of this feedthrough is also negligible. This fiber flange is bakable up to 150°C, which is limited by the plastic coat of the fiber. In the experiment a GaAs/AlGaAs MQW wafer is used for the substrate, because the FWHM of the PL spectrum is as narrow as 10nm at 20°C, which is only to 1/3 the wavelength change corresponding to the temperature change of 100°C (fig.3).

[1] W.S.Lee, G.W.Yoffe, D.G.Schlom and J.S.Harris, Jr.: J. Cryst. Growth 111 (1991) 131.

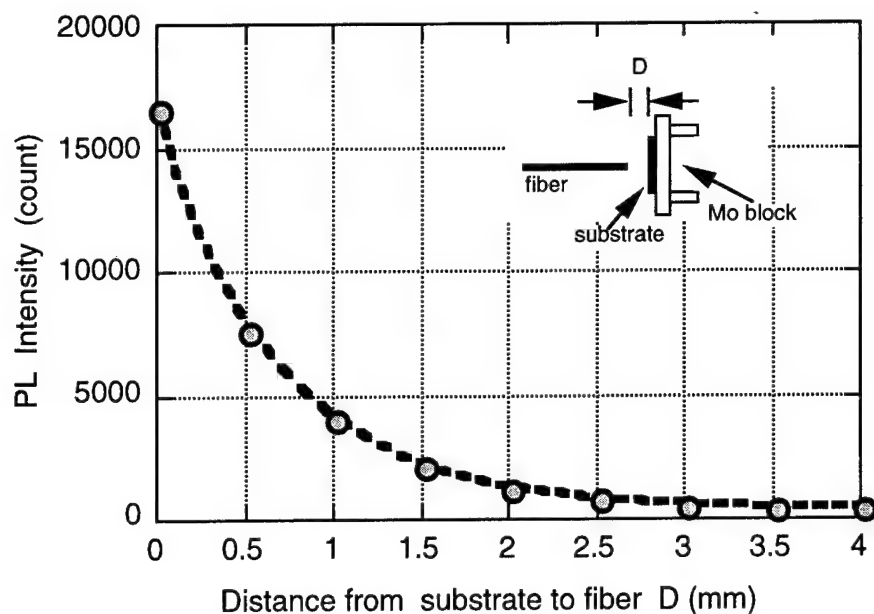


Fig.1 : Measured PL intensity as a function of separation between substrate surface and edge of fiber.

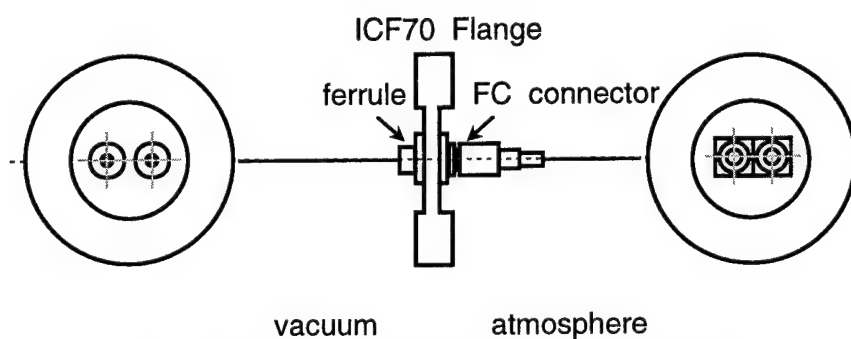


Fig.2 : UHV flange with optical fiber feedthrough.

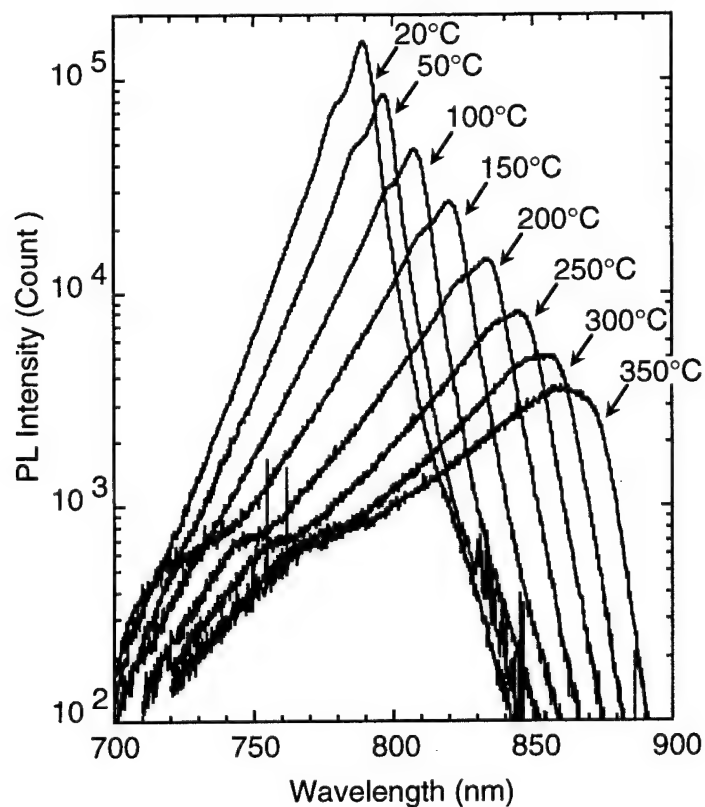


Fig.3 : PL spectrum of GaAs/AlGaAs MQW as a function of temperature.

# **Simultaneous *In situ* Measurement of Substrate Temperature and Layer Thickness Using Diffused Reflectance Spectroscopy (DRS) During Molecular Beam Epitaxy Growth**

Y. Li\*, J. J. Zhou, P. Thompson, D. L. Sato and H.P. Lee

Department of Electrical and Computer Engineering

University of California, Irvine CA 92717

Tel: (714)824-8309 Fax: (714)824-3732

\*email: yli@ece.uci.edu

*In situ* temperature and layer thickness measurements have always been integral parts of MBE technology development. The use of Diffused Reflectance Spectroscopy (DRS) for *in situ* temperature monitoring and feedback control have been established recently [1]. However, nearly all previous measurements were carried out during the growth of homoepitaxial GaAs on GaAs substrates. In this work, we explore the use DRS for simultaneous measurements of substrate temperature and layer thickness during MBE growth of AlAs/GaAs layered structure. The experimental results are analyzed with the aids of numerical simulation.

The technique relies on non-specular scattering of the probing light from a non-polished backside of the wafer for detection. The working principle is very similar to optical transmission measurement with two notable differences: (i) both the incident and the detection ports are located in front of the sample (at non-specular angles) and therefore alleviate the technical difficulties of installing a light source at the backside of the substrate, and (ii) the spectroscopic probing light passes through the sample twice with slight difference in path length before detection. The measured DRS signal over the entire spectrum yields useful information on the sample temperature, incremental change in layer thickness and surface morphology. From the cutoff wavelength of the band edge absorption, the band gap (Urbach edge) can be determined, from which the substrate temperature can be inferred [2]. As a temperature sensor, DRS has two major advantages over pyrometry: (i) it is capable of measuring much lower substrate temperature, and (ii) the measured data is unaffected by the background radiation of the heated Knudsen cells from the chamber.

We have utilized DRS [3] for measuring temperature transient arising from shutter opening of Ga and Si Knudsen cells at various substrate temperature, which is nearly impossible to obtain from any other measurement techniques. We found that the effect of Knudsen cells induced substrate heating becomes steadily more prominent at lowered temperature. An abrupt change in the X-ray diffraction peak for as-grown LTG GaAs is identified at a temperature range between 260-270°C for the first time. Such data are especially valuable for achieving reproducible growth of low-temperature grown GaAs and AlGaAs layers respectively. We have also used the DRS to measure the drift of substrate temperature (not detectable from the substrate thermocouple) of thick AlAs/GaAs layered structures arising from the change of effective sample emissivity due to optical interference effect. The results not only confirmed earlier measurement using pyrometric interferometry but provide vital data for building a temperature simulator during MBE growth. For the growth of AlAs/GaAs heterostructure, a clear oscillation of the DRS signal is observed at the transparent wavelength, due to incremental change of optical phase which can be used for thickness monitoring. We have carried out numerical modeling of the DRS spectrum for layered structures to explain such interference oscillation as well as to access the impact of optical interference effect on the band-edge absorption where the sample temperature is inferred.

[1] S.R. Johnson, C. Laviue, T. Tiedje, and J.A. Mackenzie, J. Vac. Sci. Technol. **B11**, 1007(1993).

[2] S.R. Johnson and T. Tiedje, J. Appl. Phys. **78**, 5609, (1995).

[3] Manufactured by Thermionics Laboratory model DRS-1000.

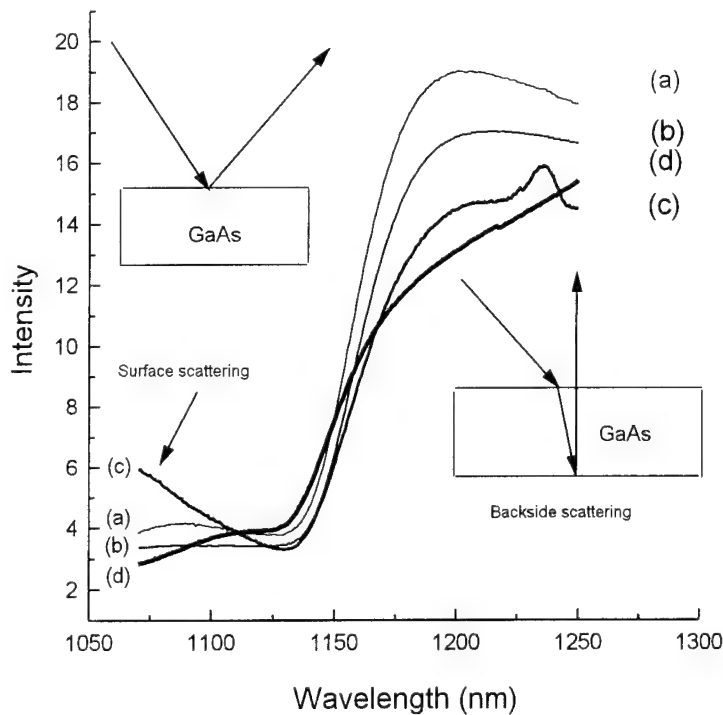


Figure 1. (a) and (b) show typical DRS spectrum of GaAs sample measured at different view ports at 560°C; (c) GaAs sample with a hazy surface due to low As vapor pressure; and (d) an increase of surface scattering of an  $\text{In}_{0.2}\text{Ga}_{0.8}\text{As}$  on GaAs sample grown beyond critical thickness.

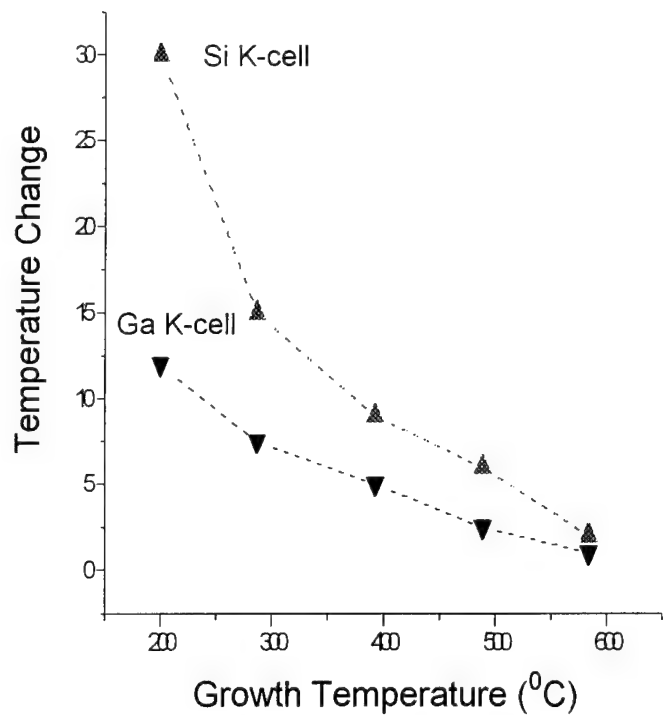


Figure 2. The Ga and Si Knudsen cells induced temperature change at various growth temperatures. The Ga and Si K-cells are at 1020 and 1180°C respectively. Corresponding to a growth rate of 1  $\mu\text{m/hr}$  and doping density of  $5 \times 10^{18}/\text{cm}^3$  respectively.

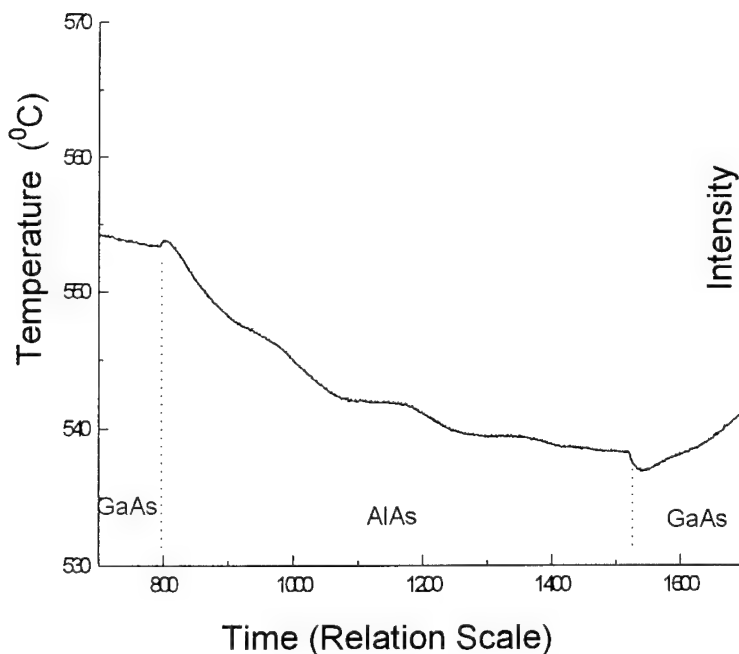


Figure 3. The temperature drift of thick AlAs layer grown on GaAs substrate under constant heater power supply. The quasi-periodic undulation of the temperature drift is attributed to the interference of the pyrometric emission from the sample due to the AlAs layer.

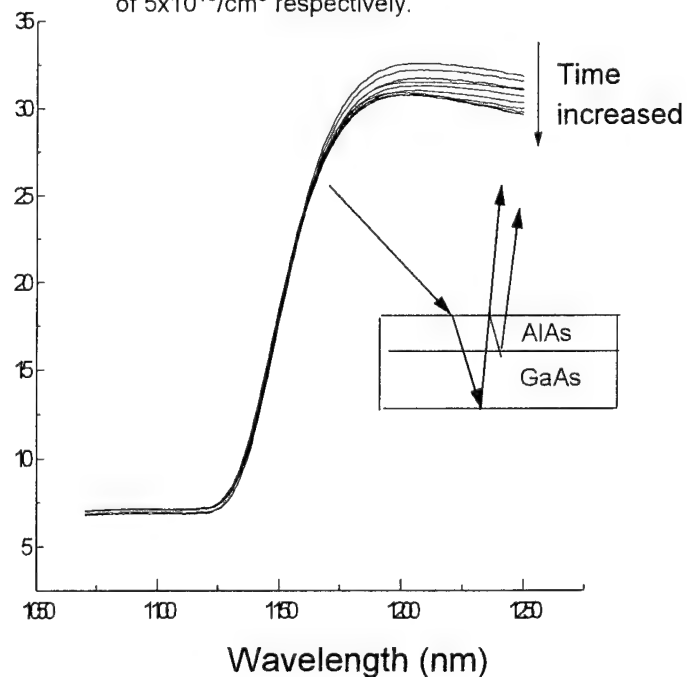


Figure 4. Interference of the DRS signal at transparent wavelength of an AlAs/GaAs layered structure. Such interference effect can potentially be utilized for layer thickness monitoring.

## 11. LASER GROWTH

THURSDAY MORNING (ELKINS)

Session Chair: Dan Mars, Hewlett-Packard Laboratories, USA

Co-Chair: Kathleen Stair, Northwestern University, USA

09:00 11.1 **Multispectral InGaAs/GaAs/AlGaAs laser arrays by MBE growth on patterned substrates**, K. Kamath, P. Bhattacharya, and J. Singh  
University of Michigan, Ann Arbor, Michigan, USA

09:20 11.2 **Molecular beam epitaxy of vertical compact  $\text{Al}_x\text{Ga}_{1-x}\text{As}/\text{GaAs}$  laser-HEMT structures for monolithic integration**  
A. Gaymann, J. Schaub, W. Bronner, N. Grün, J. Hornung, and K. Köhler,  
Fraunhofer-Institut für Angewandte Festkörperphysik, Freiburg, Germany

09:40 11.3 **Solid-source MBE for growth of laser diode materials**  
M. Toivonen, P. Savolainen, H. Asonen, and M. Pessa  
Tampere University of Technology, Finland.

10:00 11.4 **Low threshold 1.3  $\mu\text{m}$  InAsP/GaInAsP lasers by solid source molecular beam epitaxy**, C.C. Wamsley, M.W. Koch, and G.W. Wicks  
University of Rochester, USA.

Break

10:40 11.5 **Growth of  $\text{Ga}_x\text{In}_{1-x}\text{As}_y\text{P}_{1-y}$  on InP distributed feedback laser gratings by solid source molecular beam epitaxy**, W.Y. Hwang, J.N. Baillargeon, A.Y. Cho, S.N.G. Chu, and P.F. Sciortino, Lucent Technologies, USA.

11:00 11.6 **Solid source MBE growth and regrowth of 1.55  $\mu\text{m}$  wavelength GaInAsP/InP ridge lasers**, F.G. Johnson, O. King, F. Seiferth, K.S. Mobarhan, D.R. Stone, R.D. Whaley, M. Dagenais, and Y.J. Chen, University of Maryland, USA

11:20 11.7 **MBE growth of high-quality InP for AlGaInAs/InP laser structures using incongruent evaporation of GaP**  
H. Künzel, J. Böttcher, P. Harde, and R. Maessen  
Heinrich-Hertz-Institut für Nachrichtentechnik, Berlin, Germany.

11:40 11.8 **Late news papers.**

# Multispectral InGaAs/GaAs/AlGaAs laser arrays by MBE growth on patterned substrates

K.Kamath, P.Bhattacharya and J.Singh  
Department of Electrical Engineering and Computer Science  
University of Michigan, Ann Arbor, MI 48109, USA

e-mail : pkb@eecs.umich.edu, Phone : (313)-763-6678, FAX : (313)-763-9324

## Abstract

Semiconductor laser arrays with spectrally separated emission wavelengths in close spatial proximity are of interest in applications such as wavelength division multiplexing and multi-wavelength optical recording. Two different techniques have been tried with molecular beam epitaxy in order to get dual and multiple wavelength lasers. In the first approach, active layers with multiple quantum wells with different composition and well widths are first grown and the wavelength selectivity is obtained by selective etching of the quantum wells under neighboring stripes. The upper cladding and the contact layers are then regrown to complete the structure. In the second approach, impurity induced intermixing from a doped layer adjacent to the quantum well by post-growth annealing is utilized to realize the change in bandgap of the quantum well. These techniques have the disadvantages that they involve either regrowths or high temperature annealing which seriously degrade the laser performance. There is also a limitation on the number of wavelengths and the minimum wavelength spacing that can be achieved. In this paper we present a new technique wherein multiple wavelength laser arrays with close spectral proximity are obtained in a single growth step on patterned substrates.

In this technique of patterned growth, an alloy such as InGaAs is grown on a patterned substrate having ridges and trenches with *vertical* side walls obtained by dry etching. When the ridge and trench widths are of the order of the In adatom migration length ( $\sim 25\mu\text{m}$ ), the corners of the vertical side walls act as additional kink sites for growth. As a result InGaAs with increasing blue shift in the bandgap can be obtained by reducing the ridge or trench width. Thus a series of lasers, spectrally shifted in their emission energy, can be obtained by growing on a patterned substrate with gradually changing ridge width. An important point to note is that since the devices are grown on the top of the ridge they are essentially placed on the substrate surface and problems associated with regrowth do not exist. Photoluminescence spectra of quantum wells grown on the patterned substrate therefore exhibit linewidths as narrow as those on unpatterned substrates.

Laser structures consisting of  $\text{In}_{0.2}\text{Ga}_{0.8}\text{As}$ /GaAs quantum wells, GaAs confinement layers and  $\text{Al}_{0.3}\text{Ga}_{0.7}\text{As}$  cladding layers were grown by MBE on (001) GaAs substrates patterned with ridges. The widths of the ridges varied from 10-80 $\mu\text{m}$ . Single mode lasers were fabricated on top of the ridges and on the unpatterned regions. Light-current measurements showed similar threshold characteristics for lasers from patterned and unpatterned regions. Threshold currents were around 12mA for a cavity length of 400 $\mu\text{m}$ .

Spectral measurements made at a current level of  $1.5I_{\text{th}}$  showed a shift in the emission wavelength towards higher photon energies for the lasers in patterned regions compared to those in unpatterned region. The amount of shift increases with decreasing ridge width, and a maximum shift of 110Å is observed for the minimum ridge width of 10 $\mu\text{m}$  used in this study. An important feature of these results is that a good control over the emission wavelength spacing has been achieved by varying the dimensions of the pre-growth patterns. Thus we conclude that, this technique is highly useful in applications where a large number of lasers with relatively small wavelength shift is needed with precise control over the wavelength spacing.

This work is supported by ARPA (COST program).

# MOLECULAR BEAM EPITAXY OF VERTICAL COMPACT $\text{Al}_x\text{Ga}_{1-x}\text{As}/\text{GaAs}$ LASER-HEMT STRUCTURES FOR MONOLITHIC INTEGRATION

A. Gaymann, J. Schaub, W. Bronner, N. Grün, J. Hornung, and K. Köhler

Fraunhofer-Institut für Angewandte Festkörperphysik, Tullastr. 72, D-79108 Freiburg, Germany,  
Phone: +49-761-5159-339, Fax: -200, email: gaymann@iaf.fhg.de

The monolithic integration of laser and electronic circuits represents a promising device technology to meet the growing demand for future information data transfer systems. An ideal semiconductor for short-haul communication is the  $\text{GaAs}/\text{Al}_x\text{Ga}_{1-x}\text{As}$  system since even sophisticated vertical structures can be routinely grown by molecular beam epitaxy (MBE). In our laboratory, we grow the laser structure on top of the HEMT structure during a single epitaxial run. The Al-content of the ternary compound is 30%, other Al mole fractions are realized by short-period superlattices (SPSL). In order to obtain an easy to manufacture HEMT process, a vertical design of the laser structure is necessary. This can be achieved by a moderate thickness of the cladding layers with high aluminum content realized by short-period  $\text{AlGaAs}/\text{AlAs}$ -SPSLs. The aim of this work is to study the influence of the layer sequence of the SPSLs on the series resistance  $R_s$  of the laser diode which is a crucial parameter for the performance of the transmitter chip. Additionally, we present dc data of lasers grown on top of a double-delta doped MODFET structure suitable for high bit-rate transmission. Finally, we report on successful reduction of p-cladding layer thickness.

Samples with different SPSL-cladding layer sequences were grown by MBE.  $\text{AlAs}$ - and  $\text{AlGaAs}$ -layer thicknesses varied from 2 to 6 nm and 0.8 to 2.4 nm, respectively. Total thicknesses of the cladding layers and doping profile were kept constant. Mesas with cavity length of  $200\text{ }\mu\text{m}$  and widths from 3 to  $32\text{ }\mu\text{m}$  were processed. We found an exponential dependence of series resistance  $R_s$  with  $\text{AlAs}$  and  $\text{AlGaAs}$  SPSL-layer thickness, respectively. For example,  $R_s$  of a  $3\times 200\text{ }\mu\text{m}^2$  laser with low-doped claddings drops from 88 to  $5\text{ }\Omega$  with decreasing the  $\text{AlAs}$  layer from 4 to 2 nm.

Laser-HEMT structures with  $\text{AlAs}$ - and  $\text{AlGaAs}$  layers of 3 and 1.2 nm in the SPSL-claddings, respectively, were grown by MBE and processed including dry-etched mirrors. Be doping concentration of the p-cladding was raised from  $1\times 10^{18}\text{ cm}^{-3}$  to  $2\times 10^{18}\text{ cm}^{-3}$  after 300 nm while the substrate temperature was simultaneously lowered from  $700^\circ\text{C}$  to  $670^\circ\text{C}$  (thermocouple read-out). This leads to an effective lowering of Be diffusion into the active region since the Be concentration is thus held below the maximum attainable Be concentration. (The maximum Be concentrations as a function of Al mole fraction were found in heavily Be doped samples by depth profiling with Secondary Ion Mass Spectroscopy.) Lasers were characterized by on-wafer dc measurements. We found threshold currents  $I_{th}$  below 20 mA and serial resistances below  $12\text{ }\Omega$  for  $3\times 200\text{ }\mu\text{m}^2$  3 QW-lasers.  $I_{th}$  and  $R_s$  were determined for mesas with fixed cavity length of  $200\text{ }\mu\text{m}$  and widths between 3 and  $32\text{ }\mu\text{m}$ . Linear regression yields a threshold current density  $j_{th}$  of  $480\text{ A/cm}^2$ .

Finally, laser structures with different p-cladding thicknesses but identical doping profiles were grown and processed. p-grading and cap layer were doped throughout with  $2\times 10^{18}\text{ cm}^{-3}$ . Threshold current densities below  $480\text{ A/cm}^2$  were found for lasers with p-cladding thicknesses of 700 and 550 nm, respectively. Thus, no increase in  $j_{th}$  was observed upon reducing the cladding layer thickness by 150 nm. This clearly demonstrates that laser structures for monolithic integration can be designed even more compact if p-dopants are kept from diffusing into the active region.



**Supporting Material: A.Gaymann et. al**  
**Molecular beam epitaxy of vertical compact**  
 **$\text{Al}_x\text{Ga}_{1-x}\text{As}/\text{GaAs}$  Laser-HEMT structures**  
**for monolithic integration**

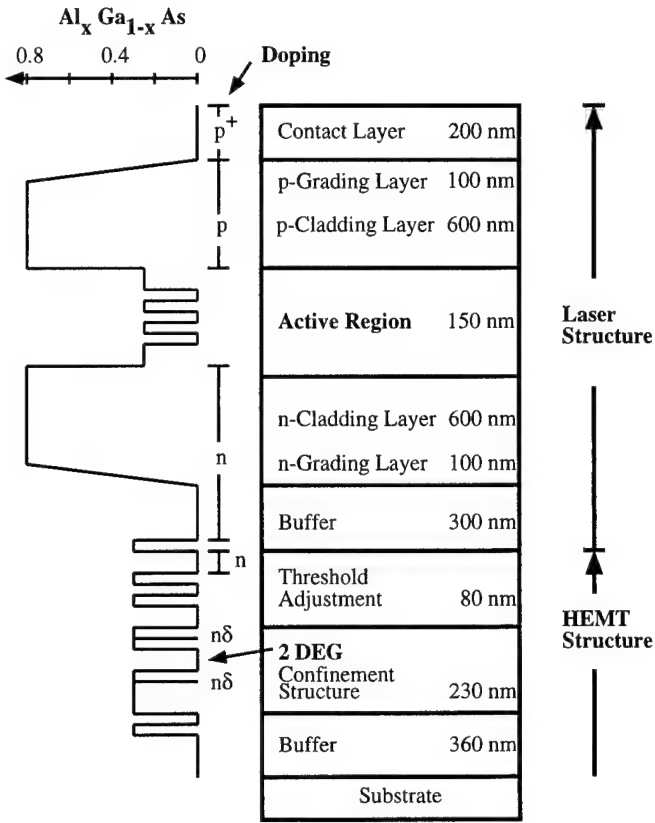


**Fig. 1**  
 Layer sequence of Laser-HEMT structure for monolithic integration

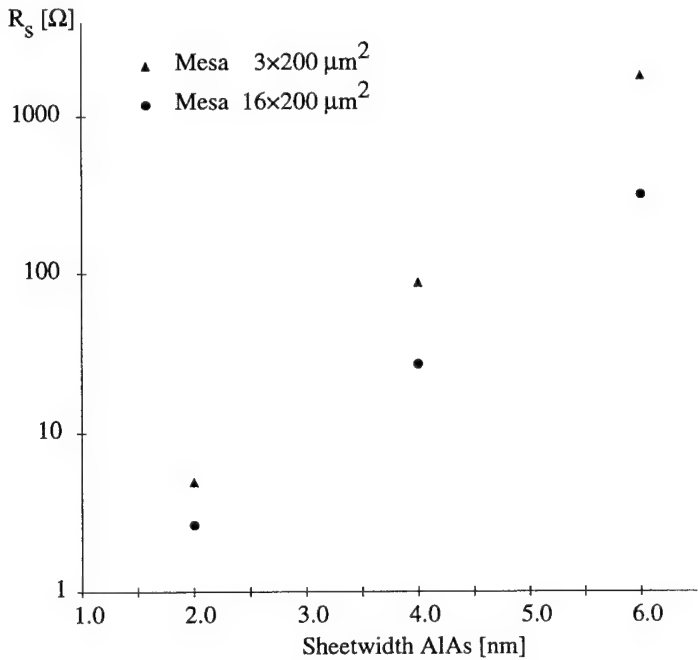


**Fig. 2**  
 Serial resistances of laser mesas as a function of AlAs-sheetwidth of short-period superlattice claddings

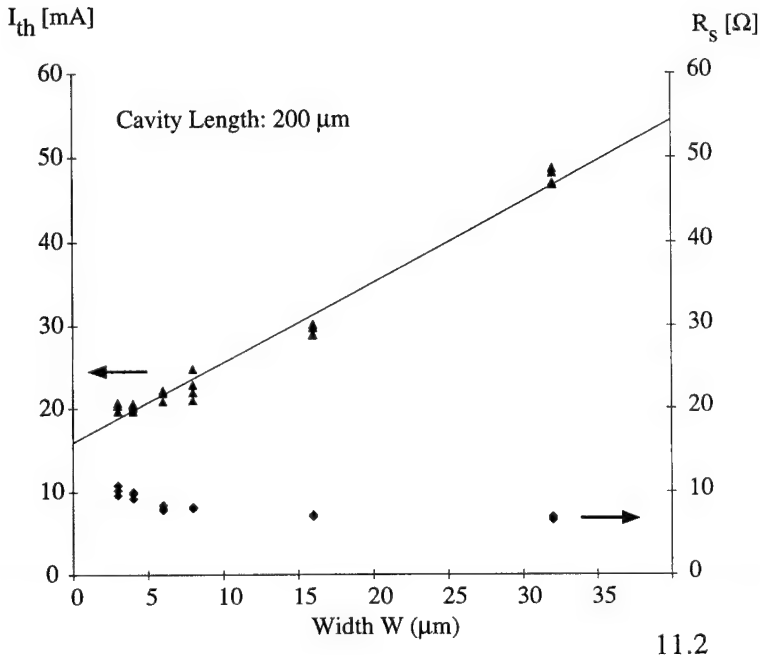


**Fig. 3**  
 Threshold current and serial resistance of 3x200  $\mu\text{m}^2$  3 QW-Lasers grown on top of a HEMT structure

# Solid-source MBE growth of InGaAsP lasers emitting at 1.5 $\mu\text{m}$

Mika Toivonen, Pekka Savolainen, Harry Asonen\*, Richard Murison\*, and Markus Pessa

*Department of Physics, Tampere University of Technology, P. O. Box 692,  
FIN-33101 Tampere, FINLAND*

*Tel: +358 31 3652609, Fax: +358 31 3652600, E-mail: toivonen@ee.tut.fi*

*\*TUTCORE Ltd., P. O. Box 48, FIN-33721 Tampere, FINLAND*

*\*EG&G Optoelectronics Canada, 22001 Dumberry, Vaudreuil (Quebec), Canada J7V 8P7*

We report on the first 1.5  $\mu\text{m}$  InGaAsP/InP laser grown by solid-source MBE method. This novel, environmentally friendly method is a viable alternative to more conventional techniques which use toxic  $\text{PH}_3$  and  $\text{AsH}_3$  as sources of group-V elements. Solid-source MBE has already proved to be a cost-effective way of preparing phosphorus-containing semiconductors with reduced safety precautions. Valved cracker cells produce stable  $\text{As}_2$  and  $\text{P}_2$  molecular beams without switching problems often encountered with conventional effusion cells.

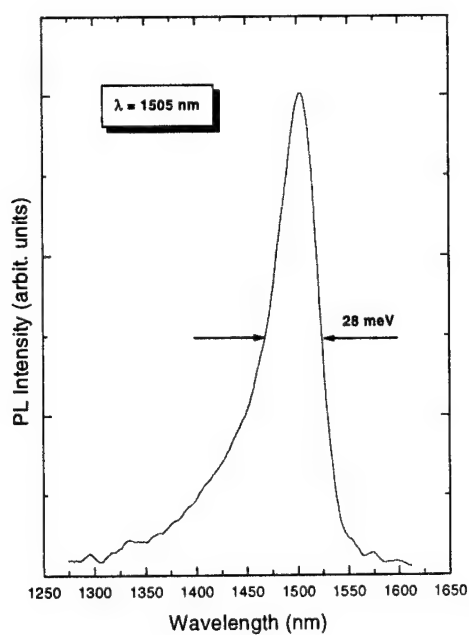
The growth chamber of our MBE system is evacuated using an ion pump. It is equipped with two valved cracker cells, one for arsenic, the other for phosphorus, and with six effusion cells for group-III elements and the dopants (Be and Si). We grew a separate confinement heterostructure (SCH) multi-quantum well (MQW) laser which was designed for emitting at the wavelength  $\lambda \approx 1.5 \mu\text{m}$ . The laser consisted of 1  $\mu\text{m}$  thick  $n$ -type and  $p$ -type InP cladding layers, an active region, and a 0.2  $\mu\text{m}$   $p^+$ -InGaAs contact layer. The active region was undoped, and it contained five 6 nm thick compressively strained ( $\Delta a/a = 0.75\%$ ) InGaAsP quantum wells, separated by 20 nm thick lattice-matched  $\lambda_g = 1.25 \mu\text{m}$  InGaAsP barriers, and 70 nm  $\lambda_g = 1.25 \mu\text{m}$  InGaAsP SCH-layers on both sides of the QW region.

Fig. 1 shows the room temperature photoluminescence spectrum for the laser structure. A peak wavelength of 1.505  $\mu\text{m}$  and the full width at half maximum of 28 meV were measured. Strong luminescence and narrow linewidth indicate that this material is of high optical quality.

The layer structure was processed into broad-area lasers for the assessment of device performance. Fig. 2 shows the threshold current density ( $J_{\text{th}}$ ) of a laser with uncoated mirror facets *versus* inverse cavity length ( $1/L$ ). The extrapolated current density for infinite cavity length is 310  $\text{A}/\text{cm}^2$ . A threshold current density of 387  $\text{A}/\text{cm}^2$  was measured for a 1400  $\mu\text{m}$  long device. These results are comparable with those of 1.55  $\mu\text{m}$  lasers grown by other methods. For example, Ougazzaden *et al.* have reported  $J_{\text{th}}$  of 328  $\text{A}/\text{cm}^2$  for MOCVD grown 5-QW InGaAsP lasers<sup>1</sup> and Starck *et al.* have obtained  $J_{\text{th}}$  of 760  $\text{A}/\text{cm}^2$  ( $L = 400 \mu\text{m}$ ) for gas-source MBE grown 5-QW lasers.<sup>2</sup> In the last diagram, Fig. 3, we show a light-current curve and a lasing spectrum for our 520  $\mu\text{m}$  long device.

<sup>1</sup> A. Ougazzaden, A. Mircea, R. Mellet, G. Primot, and C. Kazmierski, *Electron. Letters* 28 (1992) 1078

<sup>2</sup> C. Starck, J.-Y. Emery, R. J. Simes, M. Matabon, L. Goldstein, and J. Barrau, *J. Crystal Growth* 120 (1992) 180



**Fig. 1** Room-temperature photoluminescence from the laser structure.

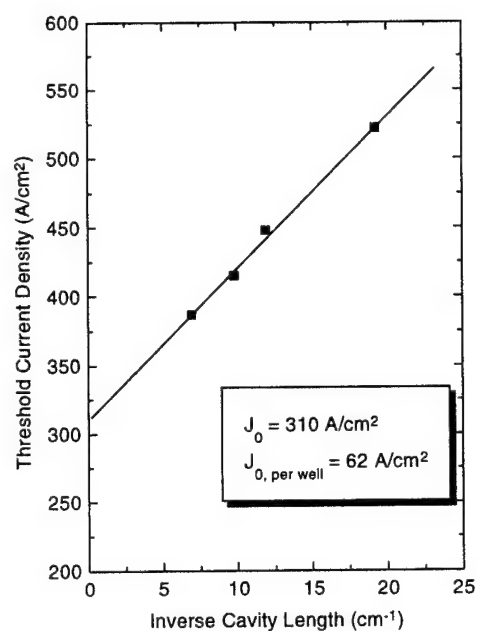


**Fig. 2** Threshold current density plotted against inverse cavity length.

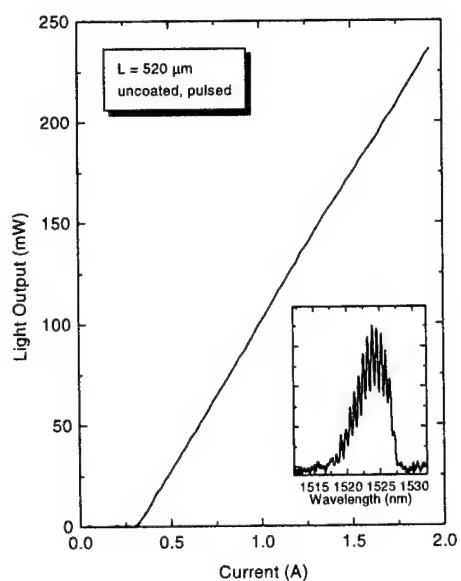


**Fig. 3** Light-current curve for an as-cleaved broad-area laser. The inset shows the lasing spectrum at 150 mW.

# Low Threshold 1.3 $\mu\text{m}$ InAsP/GaInAsP Lasers by Solid Source Molecular Beam Epitaxy

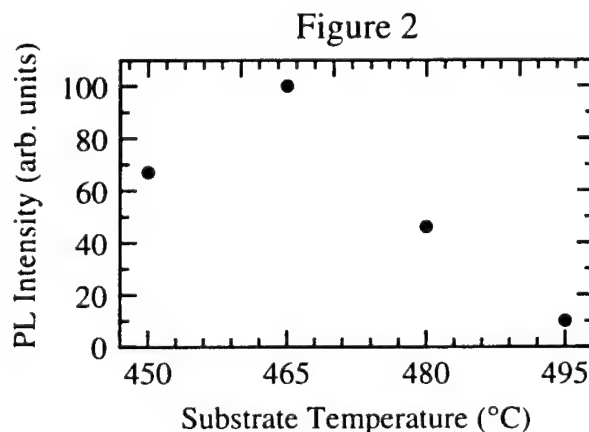
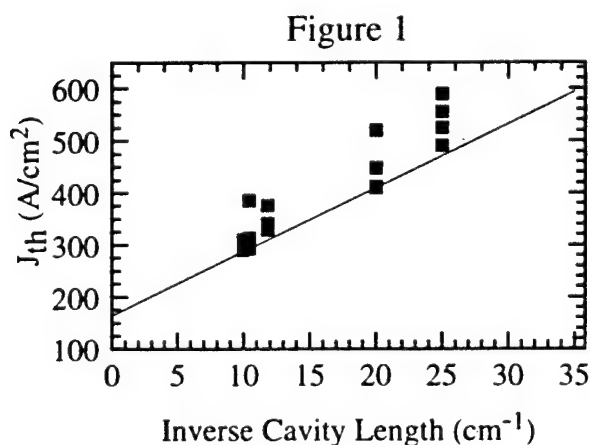
C. C. Wamsley, M. W. Koch, and G. W. Wicks

*The Institute of Optics, University of Rochester, Rochester, NY 14627*

This paper reports on the growth and fabrication of strained InAsP/GaInAsP MQW lasers grown by solid source molecular beam epitaxy (SSMBE). The lasers emit near 1.3  $\mu\text{m}$  at room temperature. Broad area devices with 1 mm long cavities exhibit a threshold current density,  $J_{\text{th}}$ , as low as 290  $\text{A}/\text{cm}^2$ . To our knowledge this is the lowest reported threshold current density for  $\lambda \sim 1.3 \mu\text{m}$  lasers by any type of MBE growth technique. The MBE machine was configured with two EPI valved group V solid sources. The phosphorus species used was  $\text{P}_2$ ; the arsenic was  $\text{As}_4$ .

The SCH-MQW laser structure consisted of 1  $\mu\text{m}$  thick n and p doped InP clads, the active region, and a 0.1  $\mu\text{m}$  p+ GaInAsP cap with bandgap emission at  $\lambda_{\text{bg}} \sim 1.1 \mu\text{m}$ . The active region consisted of three 41  $\text{\AA}$  InAsP strained quantum wells separated by 200  $\text{\AA}$  lattice matched GaInAsP ( $\lambda_{\text{bg}} \sim 1.1 \mu\text{m}$ ) barriers sandwiched between 1500  $\text{\AA}$  GaInAsP ( $\lambda_{\text{bg}} \sim 1.1 \mu\text{m}$ ) confining regions. The barrier and well compositions were designed so that no growth stops or cell temperature changes were necessary for the growth of these lasers. At the start of the quantum well regions, the gallium was shuttered closed and the arsenic valve opened to get the desired InAsP emission. This allowed the gallium and indium cell temperatures to remain fixed throughout the growth at the fluxes needed to grow the GaInAsP ( $\lambda_{\text{bg}} \sim 1.1 \mu\text{m}$ ) quaternary.

The lasers were grown at a substrate temperature of 465  $^\circ\text{C}$ . This optimum growth temperature had been previously determined in a PL study using the active region described above as the test structure. Figure 2 shows the influence of substrate temperature on the PL intensity. The maximum PL intensity was observed for a substrate temperature of 465  $^\circ\text{C}$ . The typical room temperature PL FWHM energy value was 25 meV, indicative of the high quality material and abrupt interfaces produced by SSMBE. During this study we also compared samples grown on (100) exact InP substrates with (100) misoriented 4  $^\circ$  (111)A InP substrates. The misoriented substrates consistently had lower PL intensities and longer PL emission wavelengths. The surface quality as well as the laser threshold was also found to be worse for the misoriented substrate.



## **Growth of $\text{Ga}_x\text{In}_{1-x}\text{As}_y\text{P}_{1-y}$ on InP Distributed Feedback Laser Gratings by Solid Source Molecular Beam Epitaxy**

W.-Y. HWANG, J. N. Baillargeon, A. Y. Cho, S. N. G. Chu, and P. F. Sciortino  
Bell Laboratories, Lucent Technologies, 600 Mountain Ave., Murray Hill, NJ 07974

Distributed feedback (DFB) lasers at 1.3 and 1.55  $\mu\text{m}$  wavelength employing GaInAsP/InP materials are essential components for optical fiber communications. Fabrication of a high quality DFB laser structure requires growth on a corrugated crystal surface with precise control of material composition and layer thickness. When growing a DFB laser structure directly on a grating substrate, the growth surface must be mechanically smooth after only a few hundred angstroms of the quaternary is deposited. Presently, all commercially available DFB lasers are prepared exclusively by metalorganic chemical vapor deposition. Due to the lack of a stable phosphorous source, solid source MBE growth of GaInAsP on nonplanar substrates has never been investigated. Here, the study of MBE growth of GaInAsP directly on DFB grating surfaces and the mass transport of InP gratings are first reported.

Elemental In and Ga, and  $\text{P}_2$  and  $\text{As}_2$  supplied via solid phosphorous and arsenic valved sources were used for MBE growth of quaternary GaInAsP layers on etched (100) InP grating surfaces. Gratings with a periodicity of 0.2  $\mu\text{m}$  were optically patterned parallel to the  $[0\bar{1}1]$  direction using holographic photolithography, and then wet chemically etched to form (111)A side-walls. The etched depth of the V-groves was about 600 Å. The mass transport properties for InP under a  $\text{P}_2$  beam flux in relation to the grating profile and depth were first studied. Surface temperature was found to be the most critical parameter for reshaping the grating surface. The corrugation depth of the grating was reduced to 300 Å after heating at 480 °C and was nearly eliminated when heated at 510 °C. When using a combination of  $\text{P}_2$  and  $\text{As}_2$  fluxes, a grating depth of up to 500 Å can be preserved. GaInAsP layers were grown on the InP grating surfaces at temperatures ranging from 500 °C to 530 °C immediately following heat treatment. As expected, higher growth temperature required thinner GaInAsP growth to produce a smooth surface. Transmission electron microscopy revealed that only 340 Å of GaInAsP growth was required to achieve a mechanically flat surface on a heat-treated 300 Å-deep gratings. Photoluminescence measurements indicate that there is a compositional shift of the GaInAsP grown before the surface was totally planarized. This composition shift is most likely due to the differences in the arsenic and phosphorous incorporation ratio on the different crystallographic surfaces.

## Solid source MBE growth and regrowth of 1.55 $\mu\text{m}$ wavelength GaInAsP/InP ridge lasers.

F.G. Johnson, O. King, F. Seiferth, K.S. Mobarhan, and D.R. Stone  
Laboratory for Physical Sciences, University of Maryland, College Park, MD 20740  
phone: (301)-935-6436 fax: (301)-935-6723 e-mail: fred@lps.umd.edu

R.D. Whaley and M. Dagenais  
Department of Electrical Engineering, University of Maryland, College Park, MD 20742

Y.J. Chen  
Department of Electrical Engineering, University of Maryland, Baltimore, MD 21228

InP-based separate confinement heterostructure lasers were grown by molecular beam epitaxy using all solid sources. The Ga, In, Si, and Be fluxes were obtained from conventional elemental effusion cells. Two independent, valved, cracking effusion cells containing elemental arsenic and white phosphorus (converted from red phosphorus) were used to generate  $\text{As}_4$  and  $\text{P}_2$  fluxes, respectively. The laser structures consisted of InP cladding layers, a lattice matched  $\text{Ga}_{0.27}\text{In}_{0.73}\text{As}_{0.57}\text{P}_{0.43}$  core ( $E_\lambda = 1.27 \mu\text{m}$ ), and four quantum wells. The material composition of the four quantum wells was varied to achieve compressive strains of  $\epsilon=0\%$  ( $\text{Ga}_{0.47}\text{In}_{0.53}\text{As}$ ),  $\epsilon=0.7\%$  ( $\text{Ga}_{0.27}\text{In}_{0.73}\text{As}_{0.8}\text{P}_{0.2}$ ), and  $\epsilon=1.9\%$  ( $\text{InAs}_{0.6}\text{P}_{0.4}$ ) while maintaining an emission wavelength near 1.55  $\mu\text{m}$ . Secondary ion mass spectrometry (SIMS) results show that there is little diffusion of the dopants from the cladding layers into the core.

After initial calibrations, quaternary compositions were reproducible from run to run by simply adjusting the valves to obtain a particular beam equivalent pressure ratio of  $\text{As}_4$  to  $\text{P}_2$ . Five laser growths with quaternary quantum wells ( $\epsilon=0.7\%$ ) were grown over a period of several weeks, and the photoluminescence peak position varied within the range 1.550 to 1.575  $\mu\text{m}$ . Narrow photoluminescence peak linewidths of 22 meV (300K) and 6 meV (15K) as well as the observation of superlattice satellite peaks in the symmetric (004) x-ray diffraction spectrum (resulting from the four period quantum well in the core of the laser) both indicate that the interfaces between the quaternary quantum wells and barriers are abrupt.

Threshold current densities for broad area lasers made from the laser material with  $\epsilon=0.7\%$  compressive strain were as low as 275  $\text{A}/\text{cm}^2$  for 2.5mm long devices. Ridge lasers, with dimensions 5  $\mu\text{m}$  x 1mm, were processed using reactive ion etching (RIE) and  $\text{Si}_3\text{N}_4$  isolation, and threshold currents of 39 mA were achieved. The performance of these devices will be compared to the performance of ridge lasers that use MBE regrown InP layers for electrical and optical confinement. Tungsten stripes are first deposited, and RIE is used to etch through the active region and define the ridges. This tungsten forms an ohmic contact when annealed above 500° C in the MBE chamber during oxide removal. A p-n-p InP current blocking layer is then regrown over the ridges. This layer is later selectively removed to expose the tungsten contacts and apply metallization to the individual lasers.

# MBE Growth of High-Quality InP for AlGaInAs/InP Laser Structures Using Incongruent Evaporation of GaP

H. Künzel, J. Böttcher, P. Harde and R. Maessen

Heinrich-Hertz-Institut für Nachrichtentechnik Berlin GmbH,

Einsteinufer 37, D-10587 Berlin, Germany

Phone: +49.30.31002.546, FAX: +49.30.31002.558, e-mail kuenzel@mails.hhi.de

## Abstract

Growth of phosphorus containing materials in an MBE environment was recently made possible by application of specific effusion cell design. While the evaporation of elemental red phosphorus from valved cracker cells offers a high degree of control and flexibility /1/, the incongruent evaporation of GaP from a conventional effusion cell equipped with a scavenger at the orifice is a simple and cost-effective way to generate a pure  $P_2$  molecular beam, suitable for the growth of materials containing phosphorus as the only group-V element /2/. In this contribution, a systematic study on growth of high-quality InP from a GaP source is presented for the first time, to our knowledge, and its potential for InP/(Al)GaInAs device structures is demonstrated.

InP growth was investigated in a temperature ( $T_g$ ), range from 400 to 500°C. Smooth and featureless surfaces were obtained even for  $BEP(P_2/In)$ -ratios as low as 10 (at  $T_g = 500^\circ\text{C}$ ), demonstrating the effectiveness of phosphorus incorporation. Best electrical characteristics were obtained at low  $BEP(P_2/In)$ -ratios or correspondingly high  $T_g$ -values. Residual carrier concentrations below  $10^{15}\text{ cm}^{-3}$  (cf. Fig. 1) in combination with 77K mobilities of the order of  $50.000\text{ cm}^2/\text{V}\cdot\text{s}$  were achieved. A high optical quality is observed even at a low  $T_g$ . The 10K PL spectra are exciton dominated and the intensity is comparable with typical characteristics of state-of-the-art MOMBE or MOVPE grown InP layers, as demonstrated in Fig. 2 for  $T_g = 420^\circ\text{C}$ . Parasitic incorporation of Ga and As was analyzed by SIMS measurements. Using an adequate scavenger design, the Ga-level could be kept negligibly low ( $< 0.1\%$ ). The As-content was found to be strongly influenced by  $T_g$ . Values below 0.3% were achieved resulting in a lattice-mismatch of  $10^{-4}$ , however, a reduction of  $T_g$  favours incorporation of residual As and enhances lattice strain.

Si and Be doping of the MBE InP layers up to  $10^{19}\text{ cm}^{-3}$  level were achieved which indicates high incorporation rates in InP, in particular for Be doping. Mobilities were found to agree with recent literature values, obtained with a valved cracker cell /3/.

InP/(Al)GaInAs heterostructures were grown with moderate growth interruptions to ramp  $T_{GaP}$ , while the surface was stabilized with As from a valved cracker cell. The successful achievement of abrupt changes in As and P incorporation was demonstrated by SIMS profiling (Fig. 3). Implementation of InP as cladding layers for AlGaInAs/GaInAs QW-lasers is currently under investigation.

/1/ G.W. Wicks et al., Appl. Phys. Lett. **59**, 342 (1991)

/2/ T. Shitara et al., Appl. Phys. Lett. **65**, 356 (1994) and references therein

/3/ J.N. Baillargeon et al., IEEE Catalog #95CH35720 Library of Congress #94-79424, 148 (1995)

# Part of the work was conducted under contract with Bosch-Telecom GmbH, Backnang.

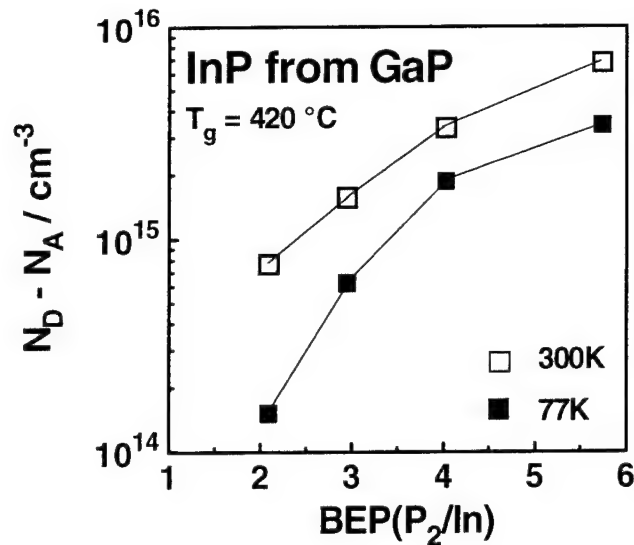


Fig. 1: Dependence of the residual carrier concentration on the V/III-ratio in InP grown from a GaP source at  $T_g=420^\circ\text{C}$ .

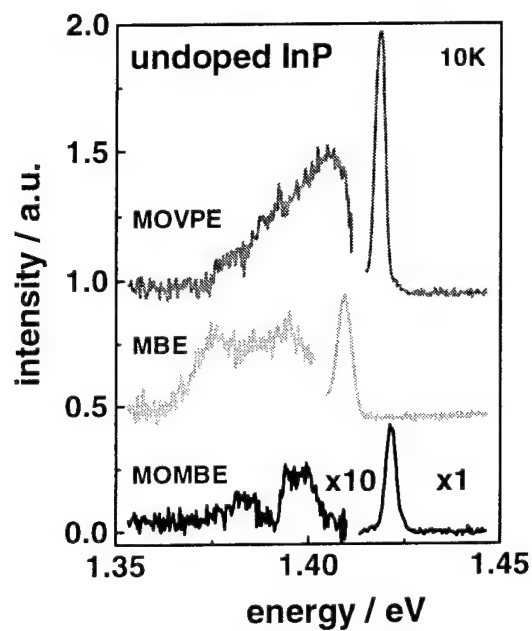


Fig. 2: Comparison of typical 10K PL spectra of MOMBE, MOVPE and MBE InP layers. The energetic shift of the dominant excitonic emission of the MBE InP grown at  $420^\circ\text{C}$  from a GaP source is indicative of As-incorporation while the slightly enhanced FWHM is related to a  $10^{15} \text{ cm}^{-3}$  residual carrier background.

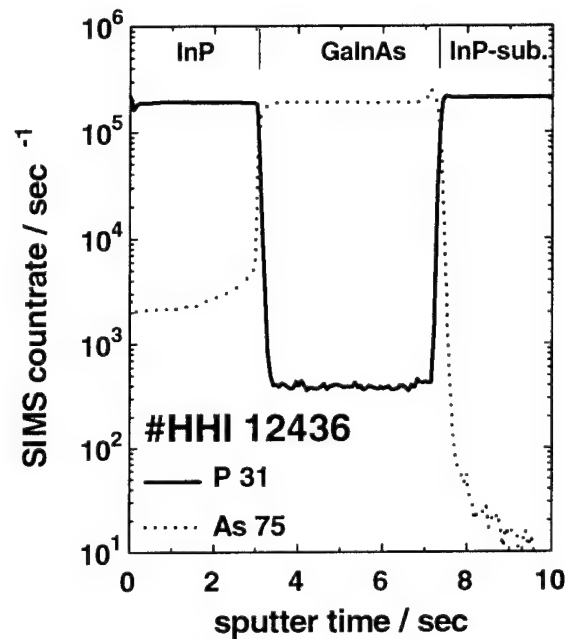


Fig. 3: SIMS As- and P-profile across a InP/GaInAs/InP heterostructure grown by MBE using a GaP source and an As valved cracker.



## 12. IN-SITU CHARACTERIZATION

THURSDAY AFTERNOON (SMOTHERS)

Session Chair: Won Tsang, Bell Labs, Lucent Technologies, USA

- 13:40 12.1 **In Situ observation of MEE GaAs growth using scanning electron microscopy**, (Invited) Y. Homma, H. Yamaguchi, and Y. Horikoshi  
NTT Interdisciplinary Research Laboratories, Tokyo, Japan.
- 14:10 12.2 **A new in-situ III-V surface characterization technique: chemical modulation spectroscopy**, P.A. Postigo, T. Utzmeier, G. Armelles, and F. Briones  
Instituto de Microelectrónica de Madrid, Spain.
- 14:30 12.3 **Surface morphology evolution and reconstruction in highly strained InAs epilayer growth on the GaAs(001) surface**  
Quikun Xue, T. Ogino, H. Kiyama, Y. Hasegawa, and T. Sakurai  
Tohoku University, Sendai, Japan
- 14:50 12.4 **Real space imaging of GaAs/AlAs(001) heterointerfaces**  
J. Behrend, M. Wassermeier, W. Braun, P. Krispin, and K.H. Ploog  
Paul-Drude-Institute für Festkörperelektronik, Berlin, Germany.
- 15:10 12.5 **Electronic properties of monolayer steps on GaAs (001) surfaces studied by scanning tunneling microscopy**  
Kiyoshi Kanisawa, Hiroshi Yamaguchi, and Yoshiji Horikoshi  
NTT Basic Research Laboratories, Atsugi, Japan.

Break

- 15:30-17:30 **Poster Session 3. Sb, N, P, and Patterned Growth**  
Please see end of abstract book for poster abstracts.

## ***In Situ* Observation of MEE GaAs Growth Using Scanning Electron Microscopy**

Y. Homma<sup>1\*</sup>, H. Yamaguchi<sup>2</sup> and Y. Horikoshi<sup>2</sup>

<sup>1</sup>NTT Interdisciplinary Research Laboratories, Musashino-shi, Tokyo 180, Japan

<sup>2</sup>NTT Basic Research Laboratories, Atsugi-shi, Kanagawa 243-01, Japan

\*Phone: +81 422 59 2558, Fax: +81 422 59 3695, E-mail: yhonma@ilab.ntt.jp

Scanning electron microscopy (SEM) is useful to obtain real-time images of GaAs MBE processes. It can provide 2D nucleation island images as well as step images during growth [1, 2]. We used *in situ* SEM to investigate the surface morphology during migration enhanced epitaxy (MEE) [3] of GaAs, thereby showing enhanced migration in real-space [4].

*In situ* observations were performed using an ultrahigh vacuum SEM/MBE system [1]. The comparative experiment between MBE and MEE was performed at a substrate temperature of 500°C. The growth rate of GaAs was determined to be about 12 s per monolayer (ML) from surface morphology oscillation observed at 580°C.

Figures 1 and 2 show secondary electron (SE) images of GaAs surfaces before and after 10 ML growth in the MEE mode, respectively. Although small islands remain on the MEE surface, monolayer steps similar to the initial surface can be seen. Thus the surface remains smooth; surface roughness during MEE growth is about one monolayer. The MEE surface recovered its smoothness during 100 s-annealing at 500°C after growth termination. On the other hand, an MBE grown surface became much rougher at 500°C due to small island formation as shown in Fig. 3. Monolayer steps are hard to recognize with the growth of islands. The MBE surface never recovered its initial smoothness at 500°C.

Two types of morphology were observed just after MEE growth; monolayer islands or monolayer holes. This depended on the Ga supply per cycle relative to the Ga atom density in 1 ML. When the Ga supply was over 1 ML, islands were formed as seen in Fig. 2. Holes were observed with a short Ga supply to 1 ML. However, even when the Ga supply was not equal to 1 ML, the resulting islands or holes did not develop more than 1 ML high or deep. This is because Ga atoms supplied in each cycle moved to island edges or between islands, and never stayed on top of the islands. This mechanism suppressed surface roughening during growth. The monolayer islands or holes disappear immediately after growth termination. These results directly confirm enhancement of surface atom migration in MEE.

[1] Y. Homma, J. Osaka, and N. Inoue, Jpn. J. Appl. Phys. 33, L563 (1994); Jpn. J. Appl. Phys. 34, L1187 (1995).

[2] N. Inoue, J. Osaka, and Y. Homma, J. Cryst. Growth 150, 107 (1995).

[3] Y. Horikoshi, M. Kawashima, and H. Yamaguchi, Jpn. J. Appl. Phys. 25, L868 (1986).

[4] Y. Homma, H. Yamaguchi, and Y. Horikoshi, Appl. Phys. Lett. 68, 63 (1996).

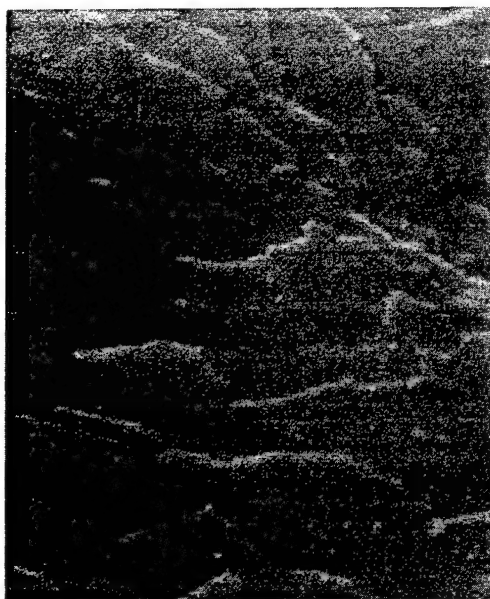


Fig. 1. SE image of initial GaAs (001) surface.

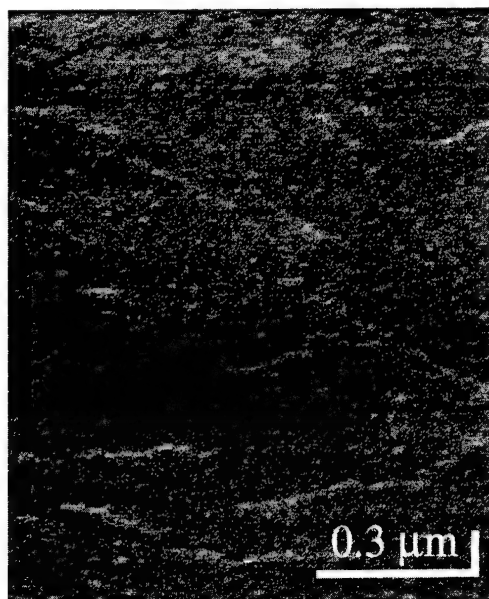


Fig. 2. GaAs (001) surface just after MEE growth (10 ML).

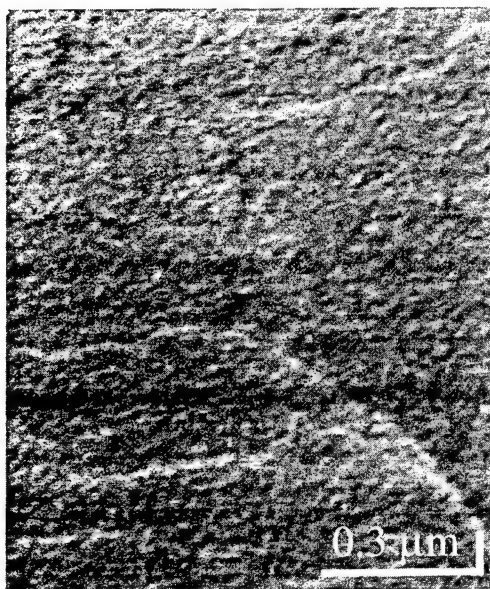


Fig. 3. GaAs (001) surface just after MBE growth (10 ML).

# **A new in-situ III-V surface characterization technique: Chemical Modulation Spectroscopy.**

P.A. Postigo, T. Utzmeier, G. Armelles and F. Briones  
Instituto de Microelectrónica de Madrid (CNM-CSIC), Serrano 144, 28006 Madrid,  
Spain.

Tel: +34 1 562 53 11  
Fax: +34 1 411 76 51  
e-mail: aitor@pinar1.csic.es

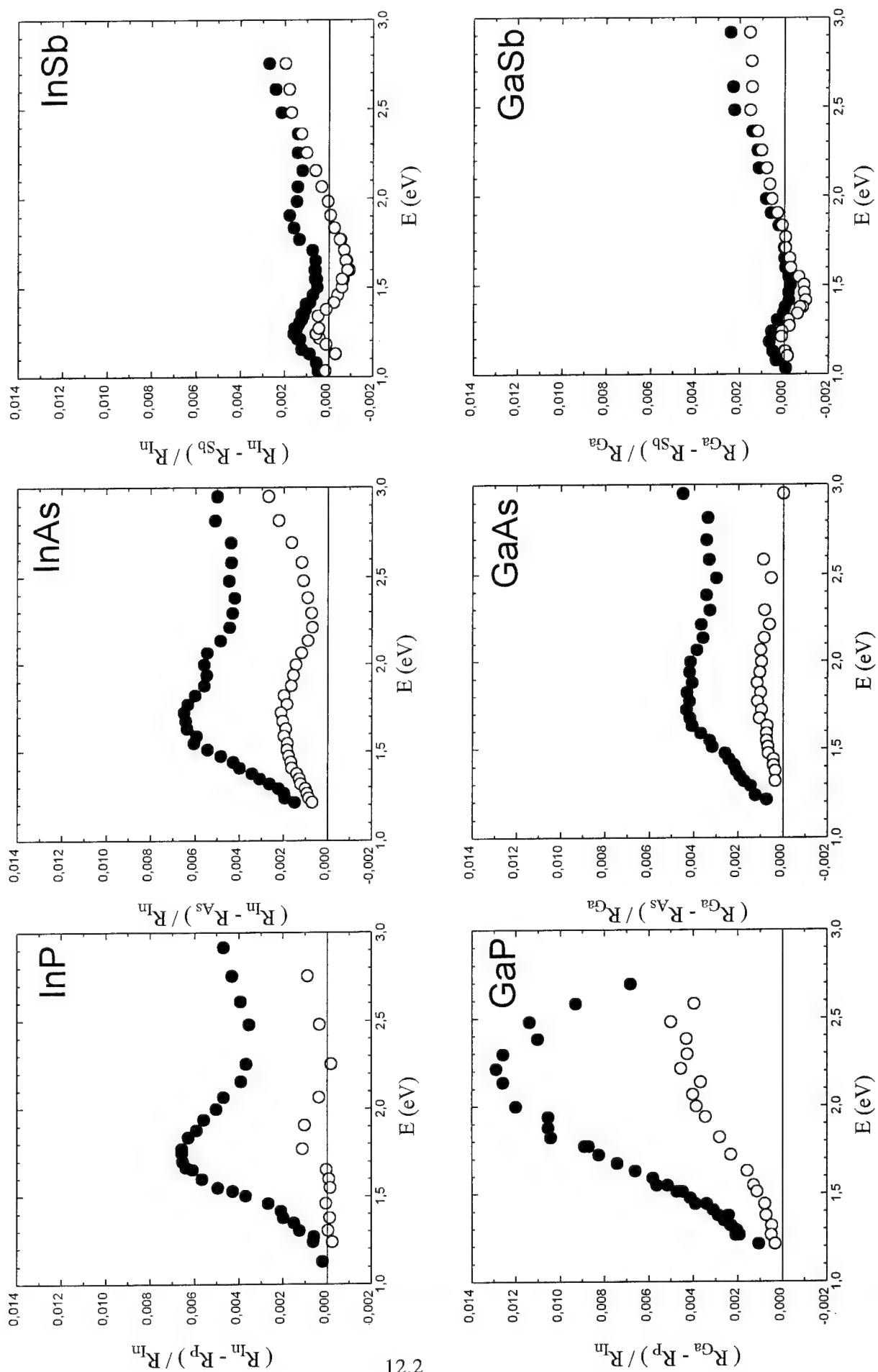
A new *in-situ* technique for the study of the MBE growth process of III-V compounds based on the chemical modulation of the surface has been developed. In this technique, the anisotropic optical reflectivity is modulated by a periodic variation of the surface stoichiometry induced by using group-V pulsed molecular beams. Pulses are produced by valved pulsed cells for V-group elements (As, P, Sb) that we use for atomic layer molecular beam epitaxy (ALMBE) growth. The substrate is maintained at sufficiently high temperature in order to obtain rapid desorption of group-V molecules from surface during flux interruptions. Corresponding changes in the surface reconstruction due to this modulation are monitored by reflection high energy electron diffraction (RHEED). Linearly polarized light, reflected at near normal incidence by the sample, is collected in a similar way as for Reflectance Difference technique<sup>1</sup> along one of the two principal axes of the crystal, [110] and [1-10]. Change in surface coverage induce changes in the intensity of the polarized reflected light, and the normalized variation,  $\Delta R/R$ , is recorded as a function of wavelength.

This chemical modulation reflectance spectroscopy technique has been applied to the surfaces of epitaxial (100) layers of GaP, GaAs, GaSb, InP, InAs, InSb and their alloys, such as GaInP, grown by MBE. In the 1 - 3 eV range, all the spectra show well-defined absorption peaks for light polarized along [110] direction, parallel to III-group dimers, at energies specific for each compound. In the case of GaAs, the position of the absorption agrees with that observed by RDS measurements<sup>2</sup> and has been related with Ga dimers absorption ( $d-I^*$ ). This is the first time that this kind of modulation spectroscopy have been used for a large set of III-V compounds, providing a new method for *in-situ* monitoring of surface composition during MBE or ALMBE growth.

---

<sup>1,2</sup> D.E. Aspnes, Y. C. Chang, A. A. Studna, L. T. Florez, H. H. Farrell, and J. P. Harbison, Phys. Rev. Lett. 64, 192 (1990).

Fig.1 Spectra obtained for a set of the binary III-V compounds.



ORIGINAL

Abstract submitted to MBE-IX'96 at Malibu, CA, USA

## Surface Morphology Evolution and Reconstruction in Highly Strained InAs Epilayer Growth on the GaAs(001) Surface

Qikun Xue, T. Ogino, H. Kiyama, Y. Hasegawa, and T. Sakurai

Institute for Materials Research (IMR), Tohoku University, Sendai 980-77, JAPAN

### Abstract

Highly strained heterostructure of InAs/GaAs(001) grown by molecular beam epitaxy (MBE) up to 10ML has been studied by an *in situ* -scanning tunneling microscope (STM) and reflection high energy electron diffraction (RHEED), with emphasis on the realization of the sharp interface. By carefully controlling growth kinetics, such as III/V flux ratio, virtual surfactant, growth interruption, the well-known 3-dimensional (3D) island formation after the critical thickness ( $\sim 2$  monolayers) for this system can be significantly suppressed, and the layer-by-layer growth has been achieved for the InAs deposition of up to 10 monolayers. We attribute differences between the present 2D planar growth and the commonly-reported Stranski-Krastanov (SK) mode to the surface tension difference of the overlayer. Moreover, the strain from the large lattice mismatch between the InAs adlayer and GaAs substrate is coherently accumulated in the 2D adlayer at this stage of growth. No evidence of strain relaxation was observed by the STM. A striking new feature of our observations is the formation of one dimensional domain walls, which separate the coherent  $4 \times 2$  or a new  $6 \times 2$  reconstructing domain with a periodicity of  $L=4Na_0$  ( $a_0=4\text{\AA}$ , the surface lattice constant of GaAs(001)). These domain walls with a characteristic width of  $\lambda=na_0$  ( $n=2, 4, 6, 8$ ) are extremely long and straight, extending from one terrace to another along the  $[110]$  direction. The interaction of the neighboring domain is found to be of long-range repulsive force and decays as  $L^{-2}$ , indicating a new strain relaxation mechanism, never being observed. The atomic structures of the In-stabilized  $4 \times 2/c(8 \times 2)$  phase and a newly observed  $6 \times 2/c(12 \times 2)$  phase will also be discussed, based on the voltage-dependent high resolution images. We will present the tentative models for these two reconstructions.

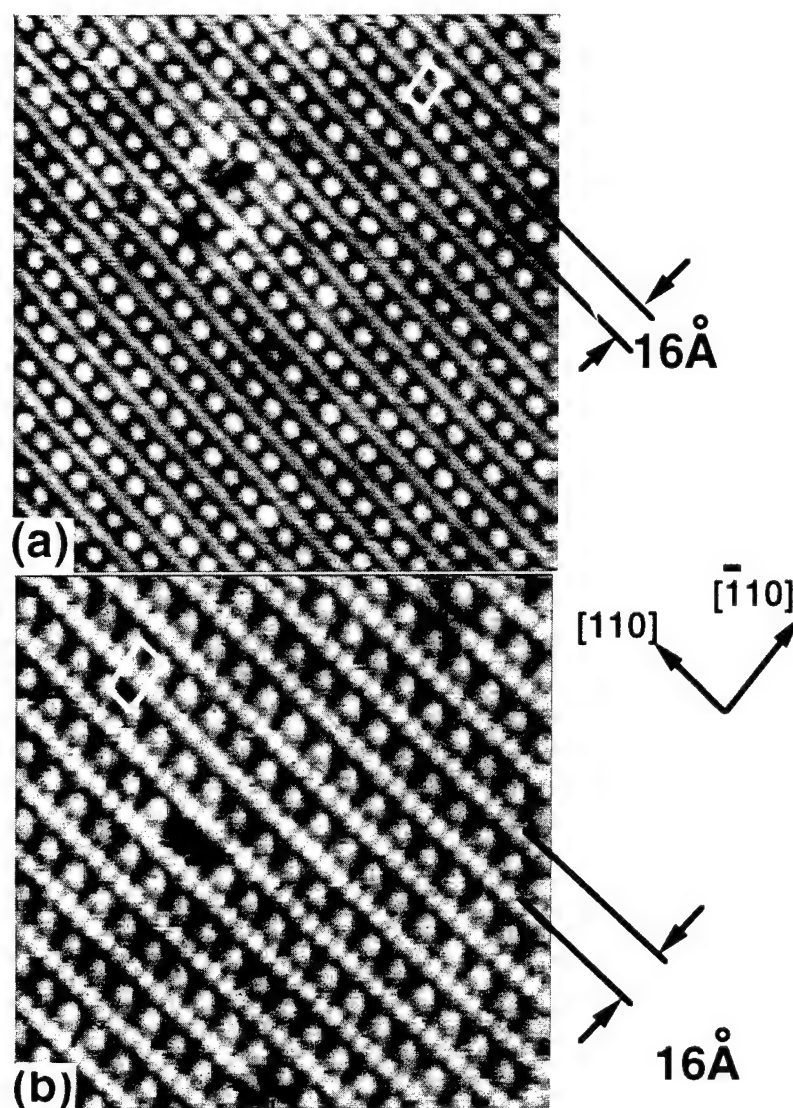
Corresponding author: **Prof. Toshio Sakurai**

Address: Institute for Materials Research, Tohoku University, Sendai 980-77, JAPAN

Tel: +81-22-215-2021

FAX: +81-22-215-2020

E-mail: sakurai@apfim.imr.tohoku.ac.jp



Filled states images of the In-rich 4x2 reconstruction grown on the GaAs(001) surface, showing the bias-dependent character of the surface. Figures (a) and (b) were recorded with bias voltages of 2.2V and 1.6V, respectively. In both images, larger individual humps are uniformly separated by 8Å along the [110] direction, clearly revealing the 2x periodicity of the surface in this direction. Note that the humps were imaged brighter than the lines in (a), while the humps and lines have almost the same contrast in (b). Also note that in (b) the smaller humps, which were not able to be resolved in (a), display a distinct 1x periodicity of the line along the [110] direction.

## Real space imaging of GaAs/AlAs(001) heterointerfaces

*J. Behrend, M. Wassermeier, W. Braun, P. Krispin, and K.H. Ploog*

*Paul-Drude-Institut für Festkörperelektronik, Hausvogteiplatz 5 - 7, D - 10117 Berlin,*

*Germany, Tel.: (+49-30) 20 377 364, e-mail: behrend@pdi.wias-berlin.de*

We have studied the formation of GaAs/AlAs(001) interfaces and the AlAs(001) surface grown by molecular beam epitaxy (MBE) using scanning tunneling microscopy in ultrahigh vacuum (UHV-STM) and reflection high-energy electron diffraction (RHEED).

At the *normal interface* (AlAs on GaAs) we observe a continuous change from the (2x4) reconstruction of the GaAs surface to a diffuse (2x3) symmetry of the AlAs surface extending about 10 ML into the AlAs layer. STM images show a large amount of kinks that are created in the As dimer rows disturbing the order of the (2x4) reconstruction gradually. We relate this finding to a strong Ga segregation that leads to a graded compositional profile at the normal interface.

In contrast to the behaviour at the normal interface, the formation of the *inverted interface* takes place very rapidly. The phase transition of the reconstruction is already complete after the deposition of the first GaAs monolayer on the AlAs surface when the (2x4) structure appears again. Also in this case the STM images reveal a high degree of disorder introduced by kink formation accompanied by a decreased As coverage (see Fig.1.).

As a new mechanism we find the creation of compensating surface defects (kinks) in response to deep-level defects of the bulk material close to the surface. We relate the observed kink formation at both interfaces to intrinsic point defects inherent to the AlAs growth that are identified as As vacancies in recent deep level transient spectroscopy (DLTS) measurements on such GaAs/AlAs heterostructures.

The incorporation of the defect layer consisting mainly of As vacancies at the growing AlAs surface during the abrupt formation of the inverted interface contributes to the known asymmetry of the electronic properties between both interface types. This finding is supported by the surprisingly smooth morphology of the as-grown AlAs(001) surface that is evident for the first time from our large scale STM images. They indicate that the morphological differences between the normal and inverted interfaces are less important as expected (see Fig.2.).



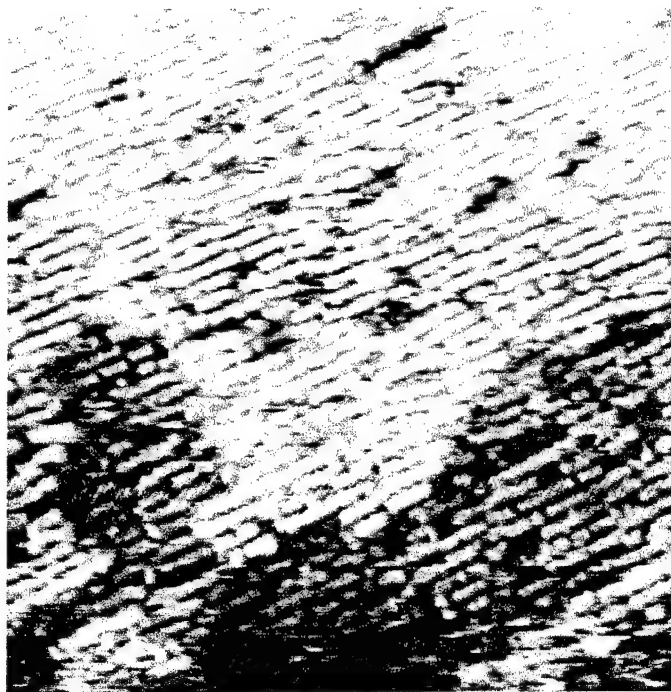


Fig.1: STM image of the inverted AlAs/GaAs interface after the deposition of 1 ML GaAs onto the AlAs(001) surface ( $500 \times 500 \text{ \AA}^2$ )

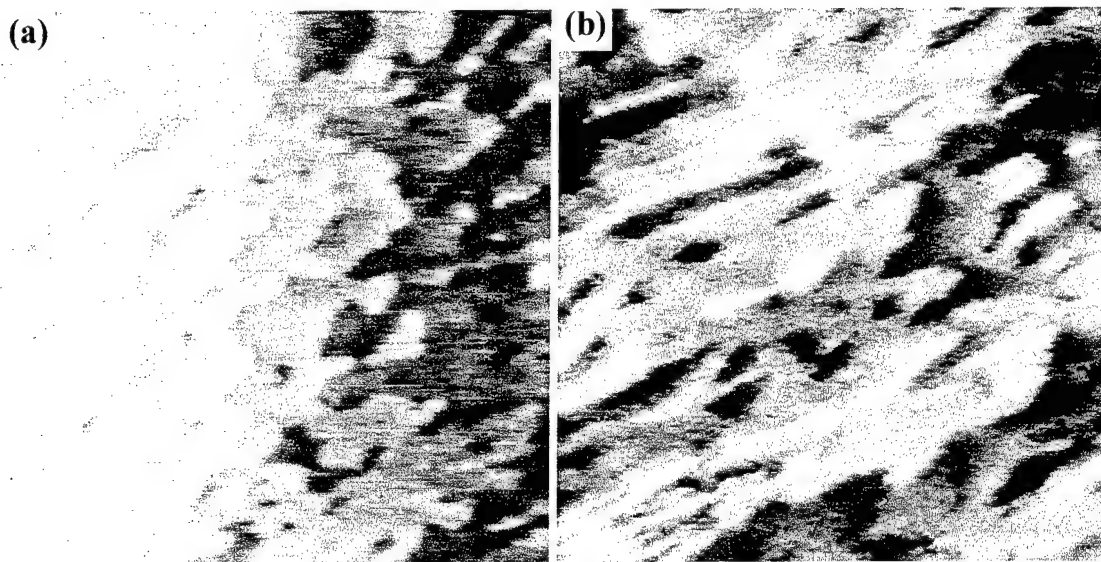


Fig.2: **(a)** large scale STM image of the pure AlAs(001) surface and **(b)** of the initial stage of the inverted interface formation after the deposition of 1 ML GaAs onto the AlAs(001) surface ( $4000 \times 4000 \text{ \AA}^2$ )

# Electronic Properties of Monolayer Steps on GaAs (001) Surfaces Studied by Scanning Tunneling Microscopy

Kiyoshi Kanisawa, Hiroshi Yamaguchi, and Yoshiji Horikoshi  
NTT Basic Research Laboratories,  
3-1 Wakamiya, Morinosato, Atsugi, Kanagawa, 243-01, Japan

contact : Kiyoshi Kanisawa  
TEL : +81 462 40 3567  
FAX : +81 462 40 4727  
e-mail : kani@will.brl.ntt.jp

Studying the microscopic relationship between atomistic configurations and their electronic properties on a surface is important in surface physics and semiconductor technology. In this paper, we clarify the relation between atomistic structures of monolayer steps and their electronic properties on  $(2 \times 4)/c(2 \times 8)$  reconstructed GaAs (001) surfaces. It is found that the monolayer steps make equivalent acceptor-type surface states similar to electron traps caused by kinks in the As dimer rows.

Experiments were carried out in an ultra-high-vacuum scanning tunneling microscopy (UHV-STM) system, which was combined with a molecular beam epitaxy (MBE) system. The  $n^+$ -GaAs layers with Si concentration of  $4 \times 10^{18}$  ( $\text{cm}^{-3}$ ) and  $2 \times 10^{19}$  ( $\text{cm}^{-3}$ ) were grown on GaAs (001) substrates misoriented in the [111]A and the [111]B directions. Figure 1(a) and 1(b) shows the STM images of the vicinal surfaces. There are As dimer row kinks which act as single acceptor-type traps.[1] We found that a higher step density with a larger misorientation angle induced lower kink densities, and this depended on the misorientation direction. Figure 2(a) and 2(b) shows the kink densities on the various misoriented surfaces. The horizontal lines L and H indicate the surface electron densities corresponding to the space-charge densities in the depletion region for different Si doping levels ( $4 \times 10^{18}$  and  $2 \times 10^{19} \text{ cm}^{-3}$ ). We explained the reduced surface kink density with the increasing misorientation angle by assuming that the monolayer steps behave as acceptor-type surface traps similar to the kinks in the As dimer rows. The solid and the broken lines in Fig. 2 indicate estimated surface kink densities based on the above assumption. Indeed, the sum of the observed kink density and the density of traps caused by monolayer steps agrees very well with the space charge density in the depletion region. Here, the density of acceptor-type traps due to steps was established by applying electron counting consideration to atomistic structures of steps obtained by STM. Experimental results show that acceptor-type traps at steps have equivalent properties to those at kinks. This strongly suggests that the surface acceptor state is formed at the surface defect by steps and kinks which disturb the coherency of the semiconducting  $(2 \times 4)$  unit cell arrangement on  $(2 \times 4)/c(2 \times 8)$  reconstructed surfaces.

[1] M. D. Pashley and K. W. Haberern, Phys. Rev. Lett. 67 (1991) 2697.

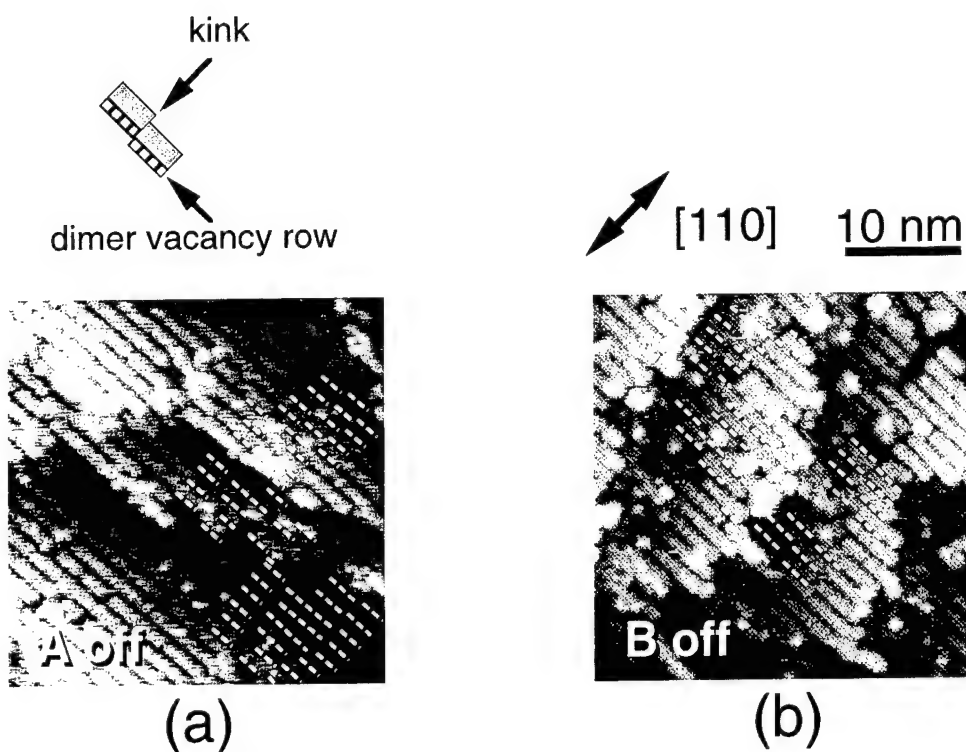


Fig. 1 STM images of vicinal GaAs (001) surfaces. Misorientation is  $1^\circ$  in (a) the [111]A direction and (b) the [111]B direction. Dotted lines are As dimer vacancy rows near the kinks in As dimer rows.

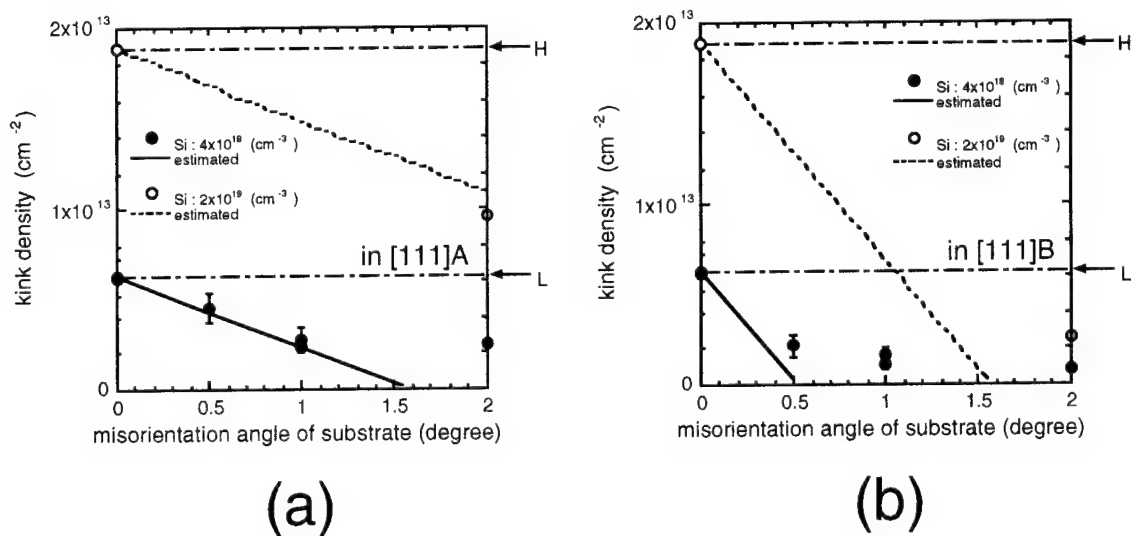


Fig. 2 Kink densities as a function of misorientation angles of substrates. Misorientation direction is (a) [111]A and (b) [111]B. Circles are experimental results by STM, and the solid and the broken lines are estimated results assuming the monolayer steps are acceptor-type surface traps.

### 13. VCSEL GROWTH

THURSDAY AFTERNOON (ELKINS)

Session Chair: Gary Wicks, University of Rochester

- 13:40 13.1 **MBE growth of highly reproducible VCSELs**, (Invited)  
Y.M. Houngh and M.R.T. Tan  
Hewlett-Packard Laboratories, Palo Alto, CA, USA
- 14:10 13.2 **High performance MBE-grown top surface emitting vertical-cavity laser diodes**, G. Reiner, B. Weigl, M. Grabherr, and K.J. Ebeling  
University of Ulm, Germany
- 14:30 13.3 **Fabrication of InGaAs vertical-cavity surface-emitting lasers by molecular beam epitaxy on (411) GaAs substrates and its room temperature operation**  
Yoshihiko Hanamaki, Tetsuya Takeuti, Nagaatsu Ogawawara, and Yasuhiro Shiraki  
The University of Tokyo, Japan
- 14:50 13.4 **Growth of vertical cavity surface emitting laser material on (311)B GaAs by MBE**, D.E. Mars, Y. Kaneko, S. Nakagawa, T. Takeuchi, and N. Yamada  
Hewlett-Packard Laboratories, Palo Alto, CA, USA and Kanagawa, Japan
- 15:10 13.5 **Molecular beam epitaxy of AlGaAsSb system for 1.55 $\mu$ m Bragg mirrors**,  
J.C. Harmand and A. Kohl  
France Telecom/CNET laboratoire de Bagneux, France

Break

- 15:30-17:30 **Poster Session 4. Devices and Characterization.**  
Please see end of abstract booklet for poster abstract listings.

## MBE Growth of Highly Reproducible VCSEL's

Y.M. Houn, and M.R.T. Tan  
Hewlett-Packard Laboratories  
3500 Deer Creek Road  
Palo Alto, CA94304  
USA

### ABSTRACT

Advances in the design of heterojunction devices have placed stringent demands on the epitaxial materials technologies required to fabricate these structures. The increased demand for more stringent tolerance and complex device structures have resulted in a situation where acceptable growth yields will be realized only if epitaxial growth is directly monitored and controlled in real time. We report the growth of 980-, 850-, and 780-nm vertical cavity surface emitting lasers (VCSEL's) by gas-source molecular beam epitaxy (GSMBE), in which the pyrometric interferometry technique is used for in-situ monitoring and feedback control of layer thickness to obtain a highly reproducible Distributed Bragg reflectors (DBR) for VCSEL structures. This technique uses an optical pyrometer to measure emissivity oscillations of the growing epi-layer surface. The growing layer thickness can then be related to the emissivity oscillation signals. When the layer reaches the desired thickness, the growth of the subsequent layer is then initiated. By making layer thickness measurements and control in real-time throughout the entire growth cycle of the structure, the Fabry-Perot resonance at the desired wavelength is reproducibly obtained. The center wavelength and FWHM of the reflectivity stop-band with a run-to-run variation of  $<\pm 0.2\%$  and  $<\pm 0.4\%$  for the AlAs/GaAs and AlAs/AlGaAs mirror stacks, respectively, were achieved. The run-to-run variation of the Fabry-Perot wavelength of VCSEL structures is  $<\pm 0.4\%$ . Using this technique, the group III fluxes can also be calibrated and corrected for flux drifts, thus we are able to control the gain peak of the active region with a run-to-run variation of less than 0.3%. Surface emitting laser diodes were fabricated and operated CW at room temperature. CW threshold currents of 3, 3, and 6 mA are measured at room temperature for 10  $\mu\text{m}$  diameter 980-, 850-, and 780-nm lasers, respectively. Output powers higher than 25 mW for 980-nm, 15 mW for 850-nm, and 1.2 mW for 780-nm devices are obtained.

# HIGH PERFORMANCE MBE-GROWN TOP SURFACE-EMITTING VERTICAL-CAVITY LASER DIODES

G. Reiner, B. Weigl, M. Grabherr, and K.J. Ebeling  
University of Ulm, Dept. of Optoelectronics, D-89069 Ulm, Germany  
Phone: ++49(0)7315026048, Fax: ++49(0)7315026049  
E-mail: gerner@e-technik.uni-ulm.de

## Abstract

Short wavelength vertical-cavity surface-emitting lasers (VCSELs) are interesting light sources for short distance, high data rate optical interconnects. VCSELs with active InGaAs quantum wells emitting around 980 nm [1] as well as VCSELs with active GaAs quantum wells emitting around 850 nm [2] are discussed as light sources for transmitter-receiver modules. Here we report on the optimization of MBE-grown devices with active InGaAs as well as GaAs quantum wells. A comparison of optimized growth parameters for both kind of quantum wells will be given. The influence of structure parameters like Bragg mirror composition and mirror doping on the operation characteristics will be shown. The devices were grown in a solid source MBE system using As<sub>2</sub> from a valved cracker as the Arsenic species. Beryllium is used for p-type doping and Silicon for the n-type doping. Fig. 1 shows the structure of a VCSEL with 3 active In<sub>0.2</sub>Ga<sub>0.8</sub>As/GaAs quantum wells. The upper p-type mirror consists of 24 Al<sub>0.7</sub>Ga<sub>0.3</sub>As-GaAs quarter wavelength stacks. A 30 nm thick AlAs layer in the first low index layer just above the active zone is used for lateral current confinement by selective oxidation. The lower n-type mirror consists of 32.5 AlAs-GaAs pairs. In between the low and high index layers of both Bragg reflectors are 5nm thick AlGaAs layers for reduction of series resistance. The modulation doping profile applied in the p-mirror is described in [3]. Fig. 2 shows the cw output characteristics of a not heat sunked device with 20  $\mu$ m active diameter. A maximum wall plug efficiency of 47% is achieved for a driving current of 10 mA. At higher driving currents, wall plug efficiency decreases due to increased series resistance, however output power further increases to a maximum of 40 mW. Fig. 3 shows the cw output characteristics of a not heat sunked 4  $\mu$ m device with GaAs quantum wells. The upper mirror consists of 24 Al<sub>0.9</sub>Ga<sub>0.1</sub>As-Al<sub>0.2</sub>Ga<sub>0.8</sub>As Bragg pairs while the lower n-type mirror consists of 30.5 AlAs-Al<sub>0.2</sub>Ga<sub>0.8</sub>As pairs. Between the low and high index layers are 5 nm thick Al<sub>0.5</sub>Ga<sub>0.5</sub>As layers for reduction of series resistance. The active region consists of 3 GaAs quantum wells with Al<sub>0.2</sub>Ga<sub>0.8</sub>As barriers and Al<sub>0.5</sub>Ga<sub>0.5</sub>As spacer layers. Lateral current confinement is again achieved by selective oxidation of a 30 nm AlAs layer just above the active zone. The devices fabricated from such a wafer showed threshold currents of 730  $\mu$ A at a threshold voltage of 1.7 V. Wall plug efficiency reaches a maximum of 40% and maximum output power is around 8 mW.

## References:

- [1] Kenneth H. Hahn, "POLO-Parallel Optical Links for Gigabyte Data Communications", Proceedings of ECTC'95, pp. 368-375, 1995.
- [2] Daniel B. Schwartz et al., "A Low Cost, High Performance Optical Interconnect", Proceedings of ECTC'95, pp. 376-379, 1995.
- [3] G. Reiner et al., "Optimization of Planar Be-Doped InGaAs VCSELs with Two-Sided Output", Photon. Technol. Lett., Vol. 7, pp. 730-732, 1995.

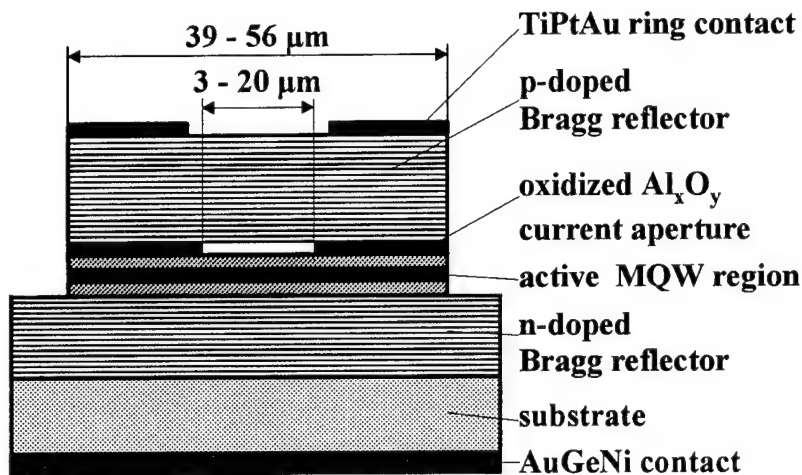


Fig. 1: Schematic of top emitting VCSEL

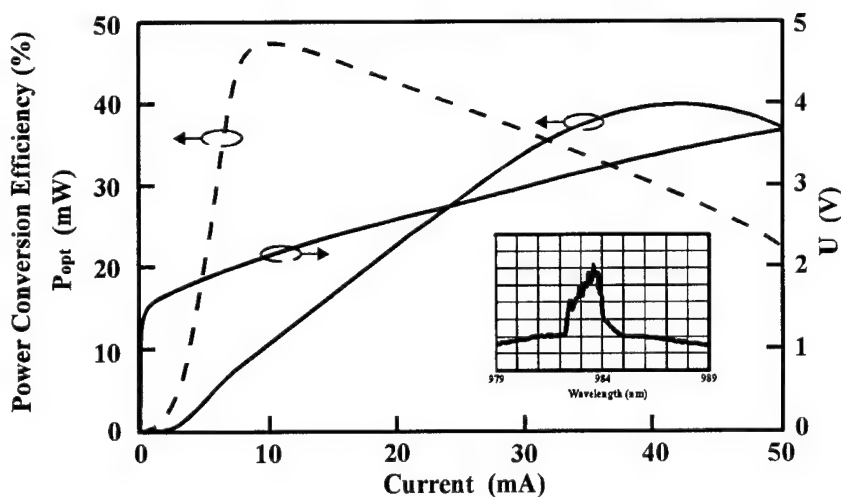


Fig. 2: Output characteristics of InGaAs VCSEL

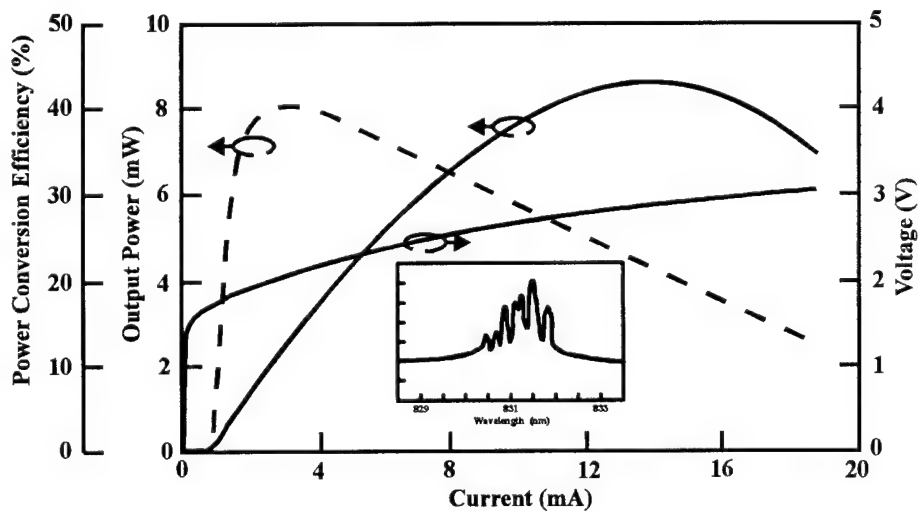


Fig. 3: Output characteristics of GaAs VCSEL

# **Fabrication of InGaAs Vertical-Cavity Surface-Emitting Lasers by Molecular Beam Epitaxy on (411)A GaAs Substrates and Its Room Temperature Operation**

Yoshihiko Hanamaki, Tetsuya Takeuti\*, Nagaatsu Ogasawara\*\* and Yasuhiro Shiraki

*Research Center for Advanced Science and Technology (RCAST), The University of Tokyo*

*4-6-1 Komaba, Meguro-ku, Tokyo 153, Japan*

*\*Hewlett-Packard Labs. Japan, 3-2-2 Sakado, Takatsu-ku, Kawasaki-shi, Kanagawa 213, Japan*

*\*\*Department of Electronics Engineering, University of Electro-Communications,*

*1-5-1 Chofugaoka, Chofu-shi, Tokyo 182, Japan*

We report on the lasing of InGaAs vertical-cavity surface-emitting lasers (VCSELs) fabricated on (411)A GaAs substrates under optical pulse excitation at room temperature.

MBE growth on non-(100) surfaces is now attracting much attention both from the points of view of device applications and scientific interests. In this experiment, (411)A GaAs substrates are employed since atomically flat heterointerfaces can be easily realized on these substrates<sup>1)</sup> and device applications including second harmonic generation (SHG) can be expected. The detailed VCSELs structure is shown in Fig.1. It consists of two AlAs/GaAs distributed Bragg reflector (DBR) mirrors sandwiching three 65Å In<sub>0.2</sub>Ga<sub>0.8</sub>As quantum wells with 1343Å GaAs barrier layers (2λ-cavity). The layer thicknesses in the AlAs/GaAs DBR mirrors were designed to be one-quarter of the room temperature lasing wavelength of 980nm.

The peak reflectivity and stop bandwidth around lasing wavelength of VCSELs on (411)A substrates were measured to be 99.6% and 99nm at room temperature.

Both VCSELs on (411)A and (100) substrates lased at 955nm and 967nm, respectively, at room temperature by optical pulse excitation at 860nm through the DBR mirror. Figure2 shows the number of photons from VCSELs as a function of the average input power in a logarithmic scale. The clear jump in the photon number definitely indicates lasing action. It is, therefore, seen that the threshold is 40mW and 60mW for VCSELs on (411)A and (100) substrates, respectively. In addition, the number of photons of VCSELs on (411)A substrates is seen to be larger in spontaneous region but smaller in stimulated region than that of VCSELs on (100) ones. These experimental results may reflect the higher reflectivity of AlAs/GaAs DBR mirrors and the improved optical gain and optical confinement in InGaAs/GaAs active regions of VCSELs on (411)A substrates.

Tel. 81-3-3481-4510 Fax 81-3-3481-4509 e-Mail hana@photonics.rcast.u-tokyo.ac.jp

## **Reference**

- 1) S. Shimomura et al. : Jpn. J. Appl. Phys. 32 (1993) L1728



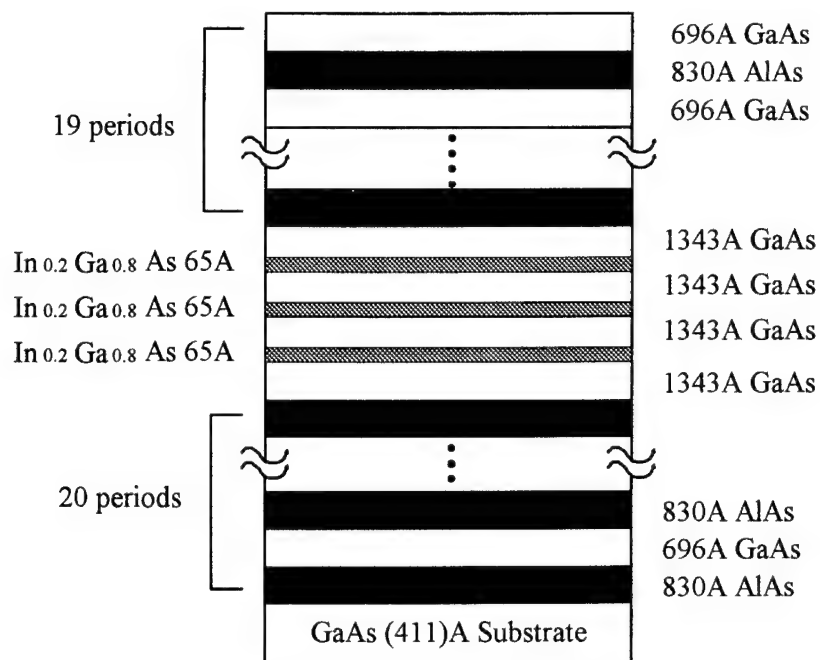


Figure 1. Layer structure used for vertical-cavity surface-emitting laser grown on (411)A GaAs substrates.

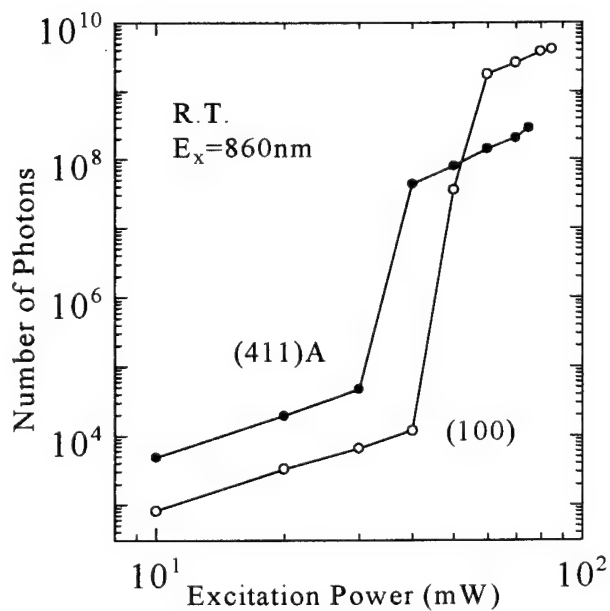


Figure 2. Number of Photons from vertical-cavity surface-emitting lasers as a function excitation power.

They were measured at the wavelength where lasing action occurred.

# Growth of Vertical Cavity Surface Emitting Laser Material on (311)B GaAs by MBE

D.E. Mars

Solid-State Technology Laboratory  
Hewlett-Packard Laboratories  
Palo Alto, California 94304

Y. Kaneko, S. Nakagawa, T. Takeuchi, and N. Yamada

Hewlett-Packard Laboratories, 3-2-2 Sakado, Takatsu, Kawasaki, Kanagawa 980, Japan

Nakagawa *et al.* previously reported on observing blue laser light by second harmonic generation (SHG) from a GaAs/ AlAs vertical cavity by optical pumping with an external laser.<sup>1</sup> The conversion efficiency can be significantly increased by imbedding the SHG layers within an electrically-pumped vertical cavity surface emitting laser (VCSEL). Calculations show that if the design wavelength is 980 nm, the VCSEL and SHG layers should produce on the order of 200-400  $\mu$ W of coherent optical power at twice the photon energy, or 490 nm. For SHG light normal to the surface, growth must be on substrate orientations other than {100} since the nonlinear optical coefficients are zero for {100} orientations. We grew on (311)B GaAs substrates for all of the work described here. The challenges for crystal growth include obtaining good material growth on (311)B, and maintaining a high degree of flux control necessary for highly reflective Distributed Bragg Reflector (DBR) mirror stacks and VCSEL's.

For the growth of VCSEL structures on (311)B we incorporated a multi-temperature growth scheme. High growth temperatures ( $> 650^\circ$  C) are necessary in the SHG and DBR layers but are incompatible with the InGaAs quantum well active regions in the VCSEL. Surface morphology and mirror reflectivity degraded significantly at low growth temperatures. In addition, from low temperature photoluminescence (PL) measurements we found a "forbidden" temperature range for the growth of the InGaAs between  $540^\circ$ - $560^\circ$  C. Active region growth temperatures in this range resulted in low intensity, broad PL and poor laser characteristics. At higher temperatures, In desorption is greatly increased, so that  $520^\circ$  C was selected as the optimal growth temperature. Even with non-optimal growth temperatures for the active region, the first reported VCSEL's on (311)B were fabricated with a pulsed  $J_{th} = 9 \text{ kA/cm}^2$  at  $-40^\circ$  C and  $28 \text{ kA/cm}^2$  at room temperature<sup>2</sup>. At the lower temperature, 10 nW of SHG blue light at 485 nm was detected under pulsed conditions and 2 nW was detected under CW conditions and was visible to the naked eye. When the growth temperature for the InGaAs was optimized, we measured broad area laser threshold current densities of  $< 500 \text{ A/cm}^2$ . Work is continuing to optimize the VCSEL growth and reduce the threshold current density.

---

<sup>1</sup> S. Nakagawa, N. Yamada, N. Mikoshiba, and D.E. Mars, Appl. Phys. Lett., 66 (17), p 2159, 24 April 1995.

<sup>2</sup> Y. Kaneko, S. Nakagawa, T. Takeuchi, D.E. Mars, N. Yamada, and n. Mikoshiba, Electr. Lett., 31, pp 805-806, 1995.

## Molecular Beam Epitaxy of AlGaAsSb system for 1.55 $\mu$ m Bragg mirrors

J.C. Harmand, A. Kohl

France Telecom/CNET Laboratoire de Bagneux

196 avenue Henri Ravera, BP 107, F 92225 Bagneux Cedex, France

Person to be contacted: J.C. Harmand

tel 33 1 42 31 75 09 / fax 33 1 42 53 76 32 / e-mail: harmand@bagneux.cnet.fr

The fabrication of vertical optical microcavities can be a key technology for a variety of photonic devices, including lasers, amplifiers, modulators and bistable switches. At the operating wavelength of 1.55 $\mu$ m, the AlAsSb/AlGaAsSb Bragg stacks on InP substrates appear as good candidates to build Distributed Bragg Reflectors (DBRs). The following advantages can be drawn: (i) lattice matching to InP (with a Sb composition close to 50%); (ii) transparency at 1.55 $\mu$ m wavelength (for Al compositions higher than 10%); (iii) last but not least, high refractive index contrast attainable. In spite of these advantages, only few attempts to realise these heterostructures have been reported up to now.

We have grown these materials on InP by elemental source molecular beam epitaxy. The group V sources are equipped with crackers so that dimers or tetramers can be produced. The control of group V composition in the  $\text{Al}_z\text{Ga}_{1-z}\text{As}_y\text{Sb}_{1-y}$  alloys appeared as complex. The dependance on the growth rate and on the Al/Ga ratio were evaluated. The effect of growth temperature and group V crackers temperatures were also investigated. Some of these results are presented in Fig.1 and 2.

Taking into account these results, we adjusted the growth conditions to get lattice matching for both  $\text{AlAs}_x\text{Sb}_{1-x}$  and  $\text{Al}_z\text{Ga}_{1-z}\text{As}_y\text{Sb}_{1-y}$  alloys, with constant incoming group V fluxes. Then, we have grown quarter wavelength DBRs at 500°C. A sample consisting of 15 pairs of  $\text{Al}_{0.13}\text{Ga}_{0.87}\text{As}_y\text{Sb}_{(1-y)}$  and  $\text{AlAs}_x\text{Sb}_{(1-x)}$  layers was grown (cross section shown in Fig.3). The photoluminescence of this sample is observed around 1.33 $\mu$ m at room temperature. This confirms the transparency of the stack at 1.55 $\mu$ m. The reflectivity is maximum at 1.58 $\mu$ m with a value over 0.98. The stop band is 210 nm wide. The refractive indices were estimated to be 3.11 for  $\text{AlAs}_x\text{Sb}_{(1-x)}$  and 3.65 for  $\text{Al}_{0.13}\text{Ga}_{0.87}\text{As}_y\text{Sb}_{(1-y)}$ . Increasing the number of pairs to 20 yielded a maximum reflectivity of 0.995, as shown in Fig.4. This is typically the value required for vertical cavity surface emitting lasers. Moreover, these 20 pairs represent a total thickness of less than 5  $\mu$ m. It is much less than the thickness of GaInAsP/InP or AlGaInAs/AlInAs distributed Bragg mirrors with comparable reflectivity. Besides the optical properties, we will report on n and p type doping of our heterostructures. This work shows that the AlAsSb/AlGaAsSb system is a good choice for epitaxial DBRs operating at 1.55 $\mu$ m.

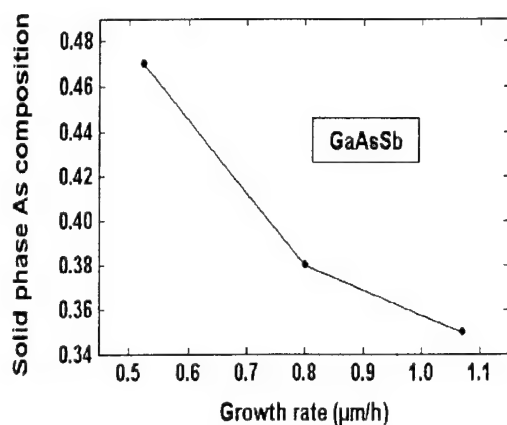


Fig.1: Influence of growth rate on the group V composition of GaAsSb.

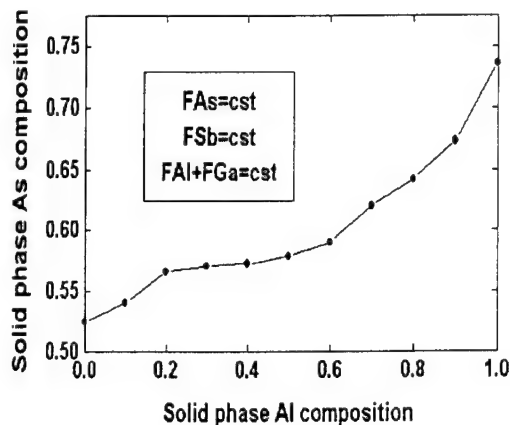


Fig.2: Influence of Al composition on the group V composition of AlGaAsSb.

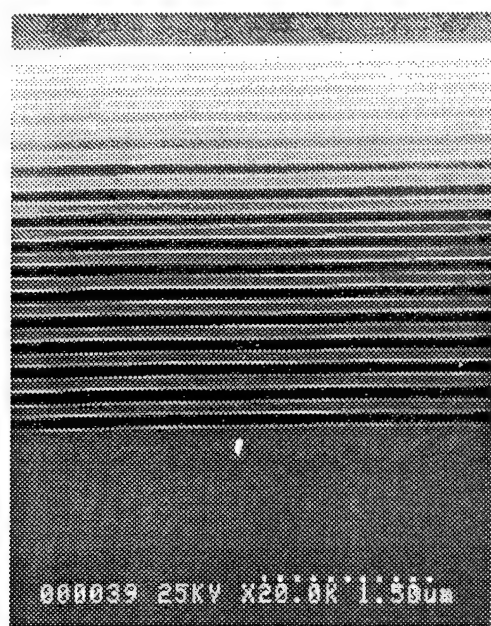


Fig.3. Scanning electron micrograph of the 15 periods  $Al_{0.13}Ga_{0.87}As_vSb_{(1-v)}/AlAs_xSb_{(1-x)}$  stack cross section.

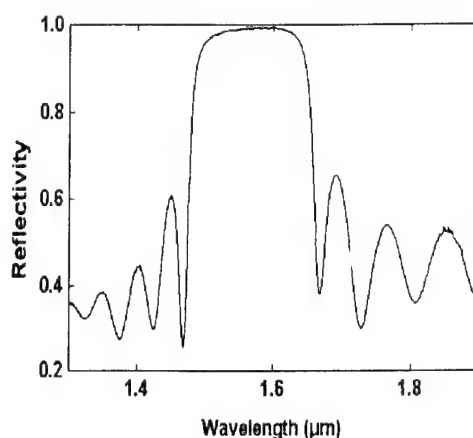


Fig.4. Spectral reflectivity of a 20 periods  $Al_{0.1}Ga_{0.9}As_vSb_{(1-v)}/AlAs_xSb_{(1-x)}$  distributed Bragg mirror. The reflectivity is 0.995 at  $1.58\mu m$

## 14. DEVICES AND QUANTUM WIRES

FRIDAY MORNING (SMOTHERS)

Session Chair: David Grider, Hughes Research Labs, Malibu, California

Co-Chair: Y. Ching Pao, Litton Solid State, Santa Clara, California

- 09:00 14.1 **MBE growth of quaternary InGaAlAs layers in InGaAs/InAlAs HBTs to improve device performance**  
T.R. Block, J. Cowles, L. Tran, M. Wojtowicz, A.K. Oki, and D.C. Streit  
TRW, Redondo Beach, California, USA.
- 09:20 14.2 **Improved hole transport properties of highly strained  $\text{In}_{0.35}\text{Ga}_{0.65}\text{As}$  channel double-modulation-doped structures grown by MBE on GaAs**  
M. Kudo, H. Matsumoto, T. Tanimoto, T. Mishima and I. Ohbu  
Central Research Laboratories, Hitachi Ltd., Tokyo, Japan.
- 09:40 14.3 **MBE growth of double-sided doped InAlAs/InGaAs HEMTs with an InAs layer inserted in the channel**  
M. Sexl, G. Böhm, D. Xu, H. Heiss, S. Kraus, G. Tränkle, and G. Weimann  
Walter-Schottky-Institut, Technische Universität München, Germany.
- 10:00 14.4 **Resonant tunnelling of holes in double barrier heterostructures grown by MBE on (110) oriented GaAs substrates**  
M. Henini, R.K. Hayden, T. Takamasu, N. Miura, L. Eaves, and G. Hill  
University of Nottingham, United Kingdom
- Break
- 10:40 14.5 **Molecular beam epitaxial growth of InGaAs/InGaAsP quantum wires on V-grooved InP substrates with (111) sidewalls**  
J. Wang, D.A. Thompson, B.J. Robinson and J.G. Simmons  
McMaster University, Hamilton, Ontario, Canada.
- 11:00 14.6 **Vertically stacked quantum wires fabricated by an in situ processing technique**  
M. López-López and Tomonori Ishikawa  
Optoelectronics Technology Research Laboratory, Tsukuba, Japan.
- 11:20 14.7 **UHV-AFM study of MBE-grown 10-nm scale ridge quantum wires**  
S. Koshiha, Ichiro Tanaka, Y. Nakamura, I. Kamiya, T. Someya, T. Ngo, and H. Sakaki, Quantum Transport Project, Tokyo, Japan.
- 11:40 14.8 **Improved GaAs/ $\text{Al}_{0.3}\text{Ga}_{0.7}\text{As}$  T-shaped quantum wires fabricated by glancing incidence MBE**  
N. Tomita, T. Kishi, M. Takekawa, S. Shimomura, K. Fujita, T. Watanabe, A. Adachi, and S. Hiyamizu, Osaka University, Japan.

# MBE Growth of Quaternary InGaAlAs Layers in InGaAs/InAlAs HBTs to Improve Device Performance

T.R. Block, J. Cowles, L. Tran, M. Wojtowicz, A.K. Oki, and D.C. Streit

TRW Electronics and Technology Division  
Redondo Beach, CA 90278

InAlAs/InGaAs HBTs grown on InP substrates can achieve excellent high-frequency performance. However, the use of InGaAs for the collector and base layers also results in relatively poor device characteristics including low breakdown and current gain due to the small InGaAs bandgap. Replacing one or both of these InGaAs layers with a quaternary InGaAlAs layer improves the device characteristics. We describe here the use of quaternary InGaAlAs layers of both constant and graded composition that when used in the collector or base layers results in substantial higher breakdown voltage and current gain.

HBT device wafers for this study were grown in Gen II modular MBE systems with all layers lattice-matched to (100) InP substrates. The HBT profiles used contain an  $n^+$  InGaAs subcollector layer followed by collector and base layers whose composition was varied as described below. All samples contained an 80 nm base layer doped with Be to  $3 \times 10^{19} \text{ cm}^{-3}$ , followed by an emitter composed of a compositionally-graded InGaAlAs base-emitter junction, an InAlAs emitter, and a heavily Si-doped InGaAs contact layer. HBT devices with  $1 \times 10 \text{ } \mu\text{m}^2$  emitters were fabricated and used for the profile comparisons described here.

The effects of InGaAlAs versus InGaAs collectors layers were studied using a set of wafers with a constant composition InGaAlAs layer for both the base and the collector. These wafers were compared to a set of wafers with InGaAlAs base and InGaAs collector layers. The InGaAlAs composition was chosen to have band gap energies 50 meV, 100 meV, and 200 meV greater than an InGaAs collector. The breakdown voltages  $BV_{cbo}$  and  $BV_{ceo}$  increased substantially from 15V to 23V and 7V to 17V, respectively, by using the InGaAlAs collector. The  $f_T$  was found to peak at a lower current density with higher Al composition. For comparison, we grew a collector structure which involved grading the InGaAlAs collector composition up from the InGaAs subcollector and back down to the InGaAs base. This structure required a higher Al composition layer to achieve similar breakdown results, but was capable of better RF performance for a given breakdown voltage.

The constant composition InGaAlAs layer for both the base and the collector was also found to increase the peak current gain  $\beta$  of the device from 40 to greater than 60. We attribute this mainly to a reduction in Auger recombination due to the larger band gap in the base. For comparison, we also grew a structure which involved compositionally grading the base layer to create a built-in-field to reduce the base transit time. This was found to increase the current gain substantially to 88. In all of these structures the use of an InGaAlAs layer increased the  $V_{be}$  of the devices as would be expected. In summary, we find that adding an InGaAlAs layer to the collector and/or base of an InGaAs/InAlAs HBT can be used to improve the device characteristics although with a tradeoff against other parameters.

# Improved hole transport properties of highly strained $\text{In}_{0.35}\text{Ga}_{0.65}\text{As}$ channel double-modulation-doped structures grown by MBE on GaAs

M. Kudo, H. Matsumoto, T. Tanimoto, T. Mishima and I. Ohbu  
Central Research Laboratory, Hitachi, Ltd., Kokubunji, Tokyo, Japan  
Phone: +81-423-23-1111 (ext. 3139), Fax: +81-423-27-7679  
e-mail: mkudo@crl.hitachi.co.jp

## **Abstract**

This paper presents results that show that the higher In content of highly strained  $\text{In}_{0.35}\text{Ga}_{0.65}\text{As}$  channel double-modulation-doped structures grown by molecular beam epitaxy significantly improves hole transport properties. Highly strained InGaAs channels have been shown to also have excellent electron transport properties. The high level of mobility of these structures combined with their high sheet hole concentration enabled us to make high performance p-FETs that have the potential for use in extremely high-efficiency push-pull power amplifiers.

Figure 1 shows the structures and schematic band diagrams of three types of p-type pseudomorphic InGaAs channel modulation-doped heterostructures. Sample #1 is a conventional single-modulation-doped (S-MOD) structure with a conventional In content of 0.2. Sample #2 is a S-MOD structure with a higher In content of 0.35. Sample #3 is a double-modulation-doped (D-MOD) structure, also with an In content of 0.35. The conditions for growing a highly strained  $\text{In}_{0.35}\text{Ga}_{0.65}\text{As}$  layer pseudomorphically on GaAs were optimized in our previous report [1].

Increasing the In content (from #1 to #2) increased mobility from  $237 \text{ cm}^2/\text{Vs}$  to  $256 \text{ cm}^2/\text{Vs}$  at room temperature as shown in Fig. 2. However, the higher In content meant that we had to reduce the channel thickness from 15 nm to 6 nm to avoid the generation of misfit dislocations. Since there was a stronger quantum size effect in the thinner channel layer, however, the sheet hole concentration increased only slightly despite the higher In content (Fig. 2). To obtain higher sheet hole concentration and high mobility at the same time, we used a D-MOD structure with an In content of 0.35 (#3). This structure provided both a high mobility of  $284 \text{ cm}^2/\text{Vs}$  and a high sheet hole concentration of  $1.84 \times 10^{12} \text{ cm}^{-2}$ . To our knowledge, this is the highest mobility ever reported for such a high sheet concentration in an AlGaAs/InGaAs modulation-doped structure. The In content and the quality of the channel were confirmed by photoluminescence (PL) measurement and high-resolution X-ray diffraction.

D-MODFET devices with a  $0.3\text{-}\mu\text{m}$  gate length and a  $20\text{-}\mu\text{m}$  gate width were fabricated using a conventional mesa isolation and gate recess process. Transconductance of  $118 \text{ mS/mm}$  was obtained, which is about 1.5 times that of S-MODFETs with an In content of 0.2.

The details of the growth procedure and the device performance will be given at the coming conference.

[1] M. Kudo, T. Mishima and M. Washima, J. Cryst. Growth **150**, 1236 (1995).

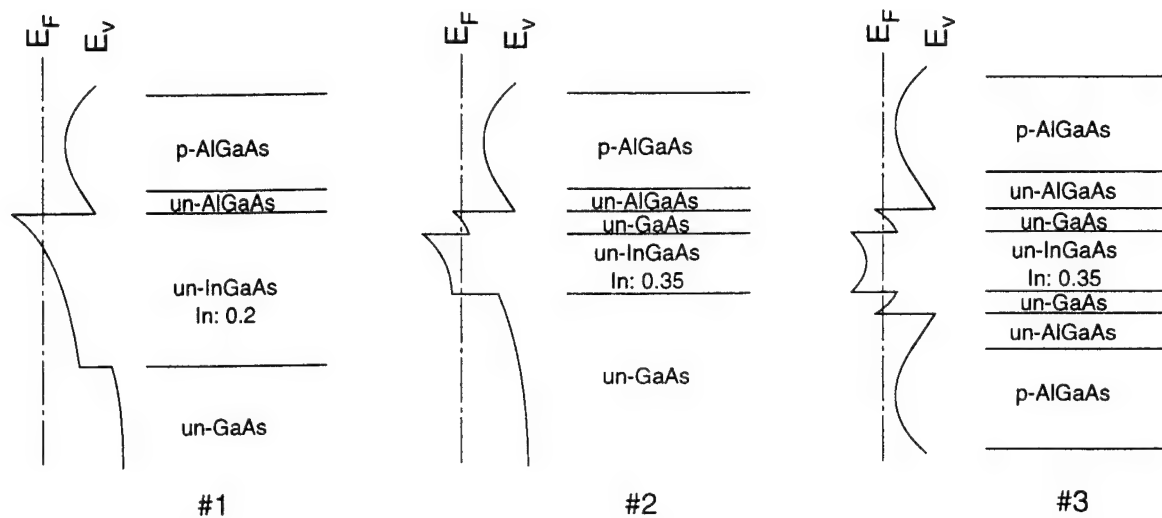


Fig. 1

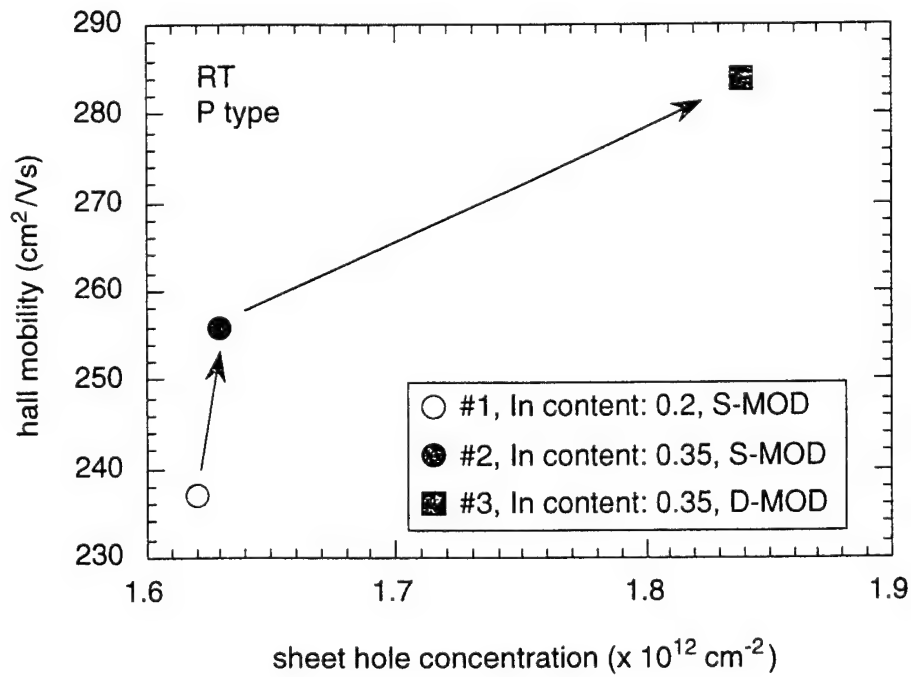


Fig. 2



## **MBE growth of double-sided doped InAlAs/InGaAs HEMTs with an InAs layer inserted in the channel**

M. Sexl, G. Böhm, D. Xu, H. HeiB, S. Kraus, G. Tränkle\*, and G. Weimann\*

Walter-Schottky-Institut, Technische Universität München, D-85748 Garching, Germany

Phone: #49 89 3209 2759, Fax: #49 89 320 6620, e-mail: mas@e26.physik.tu-muenchen.de

\* now at the Fraunhofer Institut für Angewandte Festkörperphysik, D-79108 Freiburg

InAlAs/InGaAs HEMT structures with an InAs layer inserted in the InGaAs channel were grown on InP-substrates by MBE. HEMTs with a gate length of 0.15  $\mu\text{m}$  showed very high transconductances and cut-off frequencies  $f_T$  in excess of 1230 mS/mm and 235 GHz, respectively.

The HEMT structures consisted of a 12 nm wide InGaAs channel, lattice matched to InP, in which a strained InAs layer was embedded. Si- $\delta$ -doping was used in both InAlAs barriers, with a spacer thickness of 5 nm and a donor concentration of  $5 \cdot 10^{12} \text{ cm}^{-2}$  and  $1.5 \cdot 10^{12} \text{ cm}^{-2}$  in the upper and the lower barrier. For samples grown at 470 °C the insertion of a 2 nm thick InAs layer in the channel raised the room temperature mobility to 10500  $\text{cm}^2/\text{Vs}$  compared to 8500  $\text{cm}^2/\text{Vs}$  in samples without an InAs layer. The optimized mobility increase was obtained for symmetrically centered InAs layers. For InAs thicknesses exceeding 3 nm, we observed a decrease in mobility, possibly due to beginning of lattice relaxation with misfit dislocations.

Growth at lower substrate temperatures of 420 °C obviously increased the critical thickness, thus allowing successful use of 4 nm InAs with very high resulting 77K and room temperature mobilities of 38400  $\text{cm}^2/\text{Vs}$  and 12500  $\text{cm}^2/\text{Vs}$ , respectively.

All these structures had a 2DEG carrier density around  $3.7 \cdot 10^{12} \text{ cm}^{-2}$ .

Having thus established that, under our growth conditions, 4 nm thick inserted InAs layers give optimized transport properties, we modified structures for device applications by i) increasing the  $\delta$ -doping concentrations to  $5.5 \cdot 10^{12} \text{ cm}^{-2}$  and  $2.75 \cdot 10^{12} \text{ cm}^{-2}$ , ii) increasing the Al-content in the barriers to 0.6 and iii) introducing an additional Si- $\delta$ -doping at the interface of the cap and supply layer. This resulted in i) 2DEG-densities of  $7.0 \cdot 10^{12} \text{ cm}^{-2}$ , ii) improved carrier confinement and breakdown voltages and iii) reduced source and drain resistances. HEMTs were fabricated from those modified layers.

MBE growth and characterization of the HEMT layers by X-ray diffraction and electrical transport measurements will be discussed, as well as device performance of short gate length HEMTs.

## Supporting material:

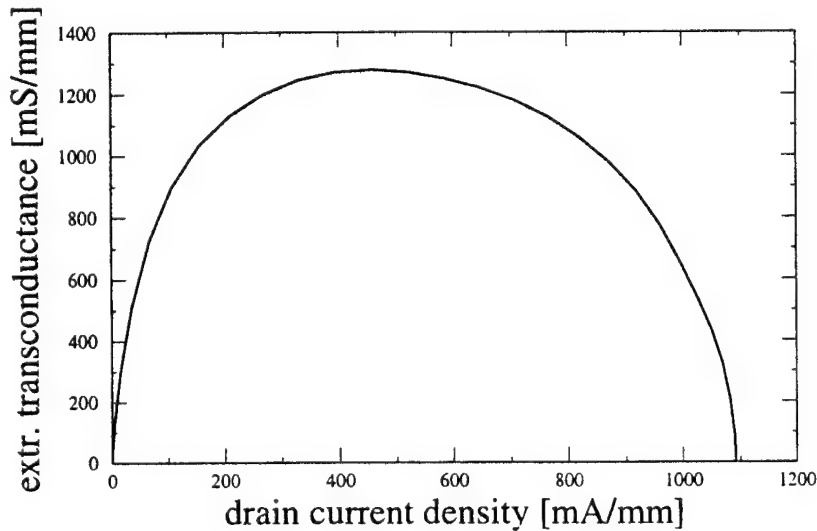
**MBE growth of double-sided doped InAlAs/InGaAs HEMTs  
with an InAs layer inserted in the channel**

Table: Mobility and 2DEG density of HEMT structures with different thicknesses and positions of an InAs layer, grown at substrate temperatures of 470 °C and 420 °C.

InAs [nm]	0	2.0	3.0	4.0	4.0
T <sub>Substrate</sub> [°C]	470	470	470	470	420
$\mu_{\text{Hall}}(300\text{K}) [\text{cm}^2/\text{Vs}]$ $n_{\text{Hall}}(300\text{K}) [10^{12}\text{cm}^{-2}]$	8500 3.74	10500 3.64	10300 3.96	6100 3.77	<b>12500</b> 3.72
$\mu_{\text{Hall}}(77\text{K}) [\text{cm}^2/\text{Vs}]$ $n_{\text{Hall}}(77\text{K}) [10^{12}\text{cm}^{-2}]$	19300 3.68	30200 3.46	27100 3.68	9100 3.58	38400 3.41

Position of InAs	middle of channel	near lower heterojunction	near upper heterojunction
InAs [nm]	2.0	2.0	2.0
T <sub>Substrate</sub> [°C]	470	470	470
$\mu_{\text{Hall}}(300\text{K}) [\text{cm}^2/\text{Vs}]$ $n_{\text{Hall}}(300\text{K}) [10^{12}\text{cm}^{-2}]$	10500 3.64	8000 3.90	9000 3.90
$\mu_{\text{Hall}}(77\text{K}) [\text{cm}^2/\text{Vs}]$ $n_{\text{Hall}}(77\text{K}) [10^{12}\text{cm}^{-2}]$	30200 3.46	17000 3.90	21000 3.50

Figure: InAlAs/InGaAs HEMTs with 4 nm InAs layer inserted in the InGaAs channel, extrinsic transconductance vs. drain current density at  $V_{\text{ds}} = 1\text{V}$ .



# Resonant Tunnelling of Holes in Double Barrier Heterostructures Grown by MBE on (110) Oriented GaAs Substrates

M.HENINI\*, R.K.HAYDEN#, T.TAKAMASU#, N.MIURA#, L.EAVES\*, and G.HILL&

\*Department of Physics, University of Nottingham, Nottingham NG7 2RD, U.K.

#ISSP, University of Tokyo, Roppongi, Minato-ku, Tokyo 106, Japan

&Department of Electronic and Electrical Engineering, University of Sheffield, S1 4DU, U.K.

**Abstract:** We report for the first time hole resonant tunnelling in Be-doped GaAs/AlAs double barrier quantum well structures grown by molecular beam epitaxy on the (110) GaAs surface. Although the heavy hole effective mass is large along [110] (0.71), very few resonances are observed in the current-voltage (I/V) characteristics as shown in the figures for a 200  $\mu\text{m}$  diameter mesa.

The structures were grown on semi-insulating (110)GaAs substrates misoriented  $6^\circ$  towards (111)A face using an Intevac GENII MBE system. The reason why we selected this misorientation is that good surface morphology could be achieved and that MBE layers grown on this (110) misoriented surface exhibit good electrical and optical properties without using low growth temperature (450-500  $^\circ\text{C}$ ), doubling the arsenic overpressure, and halving the gallium flux to 0.5 Monolayer/s needed on the exactly oriented (110) surface. The misorientation allows us to use a much higher growth temperature (560  $^\circ\text{C}$ ), standard As overpressure and Ga growth rate (one monolayer/s) without compromising the quality of the resonant tunnelling devices studied here, which are usually grown at 630  $^\circ\text{C}$  on the (100) surface. The growth was performed at a temperature of 560  $^\circ\text{C}$  with a growth rate of GaAs and AlAs of one monolayer/s and half monolayer/s, respectively, as measured by RHEED. The As/(Ga,Al) beam-equivalent pressure ratio determined by an ionisation gauge was  $\sim 12$ . After growth the epitaxial surfaces were examined using a Nomarski phase-contrast optical microscope and were found to be mirror smooth and nearly defect free.

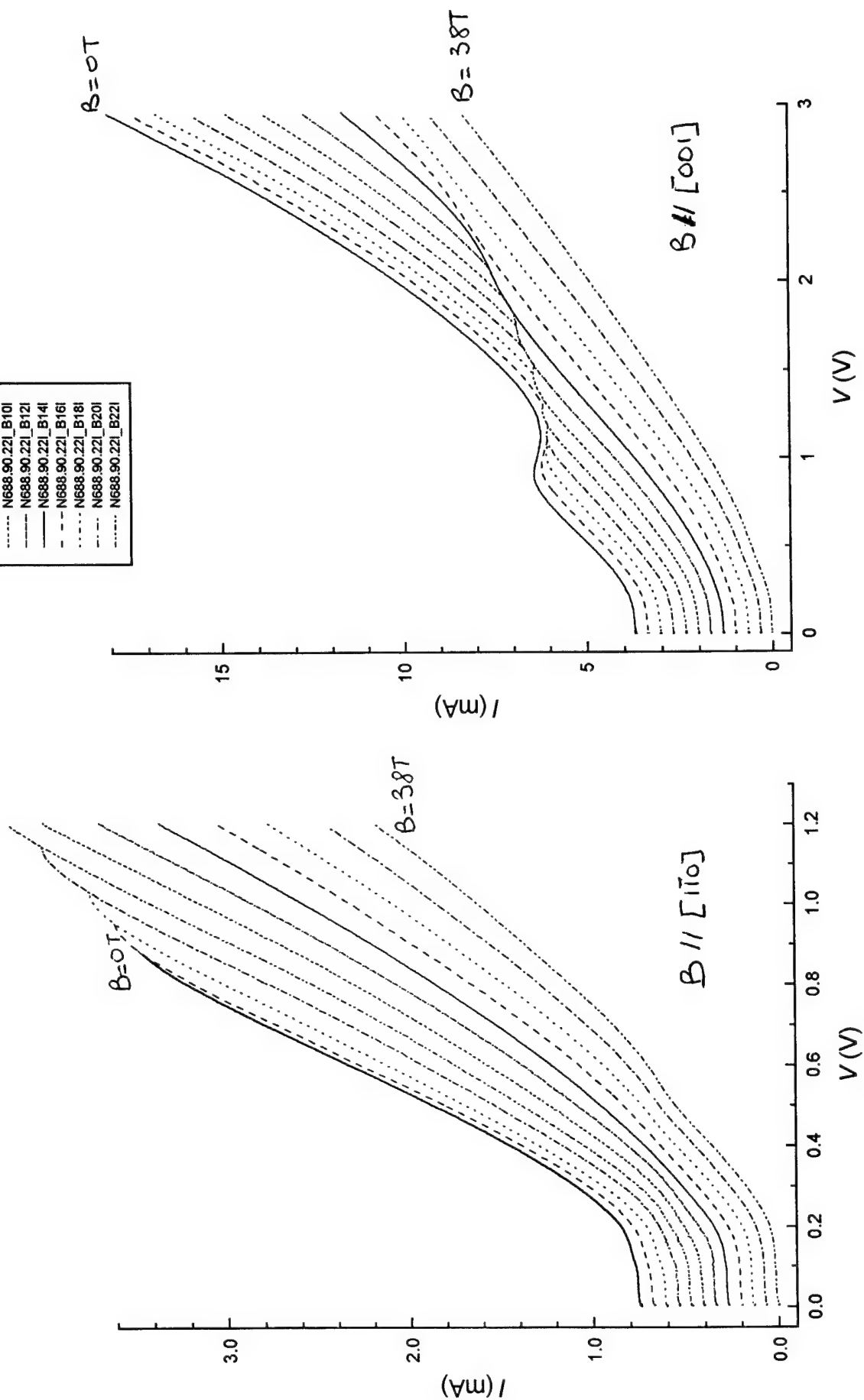
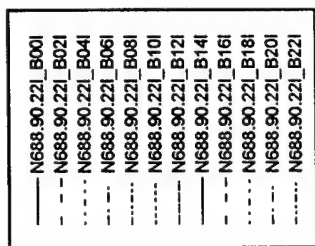
Magnetic fields up to 38 T applied parallel to the layer interfaces have been used to examine the anisotropy of the subbands that correspond to the resonant peaks in I(V). These are the first light hole and second heavy hole subbands. Tunnelling into the first subband is too weak to be observed. By comparing the effect of the magnetic on the voltage position of the peaks when  $B//[001]$  and  $B//[1,-1,0]$ , it can be seen that the anisotropy of the subbands is very small. This suggests that the large anisotropy shown in some calculations [1] only occurs in narrow quantum wells. In wider quantum wells (width  $> 3.0\text{nm}$ ), the anisotropy of the subbands is much smaller and only significant at large values of in-plane wavevector [2-3].

- [1] M.P.Young et al, J.Appl.Phys. **64**, 4609 (1988)
- [2] A.T.Meney, Superlatt.Microstruct. **11**, 31 (1992)
- [3] Z.Ikonic et al, Phys.Rev.B **46**, 4285 (1992)

Author to contact: Dr M.Henini

Tel/Fax: +44 (115) 951 5195/951 5180

e-mail: ppzmmh@ppn1.physics.nottingham.ac.uk



## **Molecular Beam Epitaxial Growth of InGaAs/InGaAsP Quantum Wires on V-grooved InP Substrates with (111) Sidewalls**

J. Wang\*, D.A. Thompson, B.J. Robinson and J.G. Simmons

Centre for Electrophotonic Materials and Devices and Dept. of Engineering Physics,  
McMaster University, Hamilton, Ontario L8S 4L7, CANADA.

Tel.: 905 525 9140 ext. 24936, Fax.: 905 527 8409, Email: g9326479@mcmail.cis.mcmaster.CA

Growth onto V-grooved substrates has been demonstrated to be one of most promising ways<sup>1</sup>, among various techniques, to make quantum wires (QWRs). QWR lasers with very low threshold currents have been grown onto V-grooved GaAs<sup>1,2</sup>. However, much less progress has been made on InP based materials, even though they are very important to telecommunication applications. To our knowledge, neither QWR laser structures nor InGaAs/InGaAsP QWRs have been successfully grown on V-grooved InP substrates. This is mainly due to a sidewall diffusive flux and increased incorporation of group III adatoms in the V-groove bottoms. Consequently, a planarization could develop as the growth of buffer and barrier layers proceeds, making QWR formation impossible. Also the differential migration of indium over gallium would result in strain development and possible relaxation generated defects. Recently, InGaAs/InP QWRs were reported on V-grooves with (111)A sidewalls<sup>3</sup>. For a laser structure, however, InGaAsP barrier or waveguiding layers with sufficient thicknesses have to be grown. Such InGaAsP layers and quantum well layers need to be defect-free and V-groove bottoms must be sharp before the growth of the quantum well. In this report, we describe our recent progress on InGaAs/InGaAsP QWRs grown on (111) V-grooved InP substrates.

The growth of InGaAsP on (111)A V-grooves results in a significant planarization, while that on (111)B V-grooves does not. Therefore, (111)B faceted V-grooves, wet-etched on (100) InP substrates, have been used for the QWR growth in this work. Structures containing an InP buffer, InGaAsP barrier layers and InGaAs quantum wells have been grown under optimized conditions using gas source molecular beam epitaxy. Transmission electron microscopy shows that all layers at V-groove bottoms are free of extended defects. Moreover, crescent-shaped InGaAs QWRs are formed with a very large thickness variation at the V-groove bottoms. The photoluminescence from the QWRs has been measured and spatially identified by using a selective etching technique. The QWR peaks have lower energy than those of the planar (100) and sidewall quantum wells. Lateral subband separations are calculated from the measured thickness variation and compared with photoluminescence results. Polarization has also been used to characterize the QWR photoluminescence. In addition, laser structures comprising such InGaAs/InGaAsP QWRs have been grown and are being analyzed optically and electrically.

### **References:**

1. E. Kapon, *Epitaxial Microstructure*, edited by A.C. Gossard, Academic Press, New York, 259 (1994)
2. S. Tiwari, G. D. Pettit, K.R. Milkove and F. Legoues, R.J. Davis and J.M. Woodall, *Appl. Phys. Lett.* **64**, 3536 (1994)
3. J. Wang, B.J. Robinson, D.A. Thompson and J.G. Simmons, *Appl. Phys. Lett.* **67** 1358 (1995)

\*. Corresponding author

## Vertically stacked quantum wires fabricated by an *in situ* processing technique

M. López-López<sup>†</sup> and Tomonori Ishikawa

Optoelectronics Technology Research Laboratory 5-5 Tohkodai, Tsukuba,  
Ibaraki 300-26, Japan.

During the fabrication process of nanostructures, in particular when dealing with III-V compound semiconductors, unintentional contamination of the processed surfaces must be minimized, since this would severely deteriorate the electrical and optical properties of the resulting structures. In this direction we have been developing a contamination-free processing technique called “*in situ* electron beam (EB) lithography”, in which all of the processes, including EB patterning, Cl<sub>2</sub> gas-etching, and epitaxial regrowth, are performed successively in an ultra-high-vacuum (UHV) environment. This process is performed in an UHV multichamber system which comprises seven chambers (Fig. 1); for sample loading, sample exchange, preheating, molecular beam epitaxy (MBE), surface treatments, analysis, and Cl<sub>2</sub> gas-etching. Samples can be transferred from one chamber to another through UHV tunnels without exposure to air. The top of the etching chamber is equipped with an EB gun, this chamber is also equipped with a gas-introduction system with a thin stainless-steel nozzle in order to supply O<sub>2</sub> gas to the sample surface along with EB irradiation.

In this work, using this technique we have fabricated vertically stacked structures consisting of two arrays of quantum wires. These structures were fabricated using the following steps (Fig. 2): (1) A clean GaAs surface was prepared by MBE on a GaAs (001) substrate. (2) In the etching chamber under an O<sub>2</sub> atmosphere, using a pattern generator, a 25 kV EB was raster scanned over the surface so as to selectively form a thin GaAs oxide layer by EB-stimulated oxidation. (3) Using the oxide layer as a mask, the pattern was transferred to GaAs by Cl<sub>2</sub> gas etching to define mesa stripes. (4) The sample was then transferred back to the MBE chamber in order to remove the oxide mask by thermal desorption in an As<sub>4</sub> flux. (5) By the regrowth of a GaAs layer, the mesa-top size was reduced to form narrow ridge structures. (6) The first array of wire structures was formed on the top of the ridges by the growth of an AlGaAs/GaAs quantum well. Subsequently, these wire structures were buried and the surface was flattened out by the growth of a 500nm thick GaAs layer. Then, the second array of wire structures was successively formed by a second pattern and regrowth process using steps (2) to (6).

The successful fabrication of the structures (Fig. 3), was confirmed by photoluminescence and cathodoluminescence (CL) measurements at 77K. It was found that the first array of wire structures emitted at a wavelength of 790nm, while the second array at 804nm (Fig. 4). These results show the flexibility and potential of *in situ* EB lithography for synthesizing vertically stacked structures.

<sup>†</sup>Present address: Departamento de Física, Centro de Investigación y de Estudios Avanzados del IPN, Apartado Postal 14-740, México 07000 D.F., México.

Tel: +52-5-747-70-00 ext. 4216, Fax: +52-5-747-70-96

e-mail: mlopez@fis.cinvestav.mx

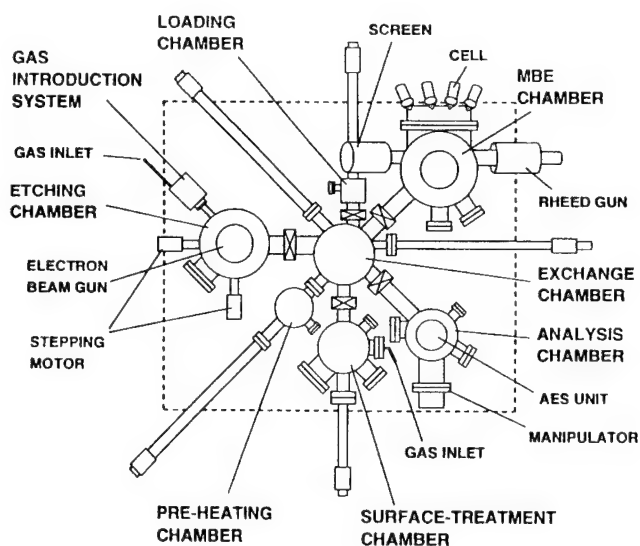


**Fig. 1** Schematic illustration of the UHV multichamber system used in this work.

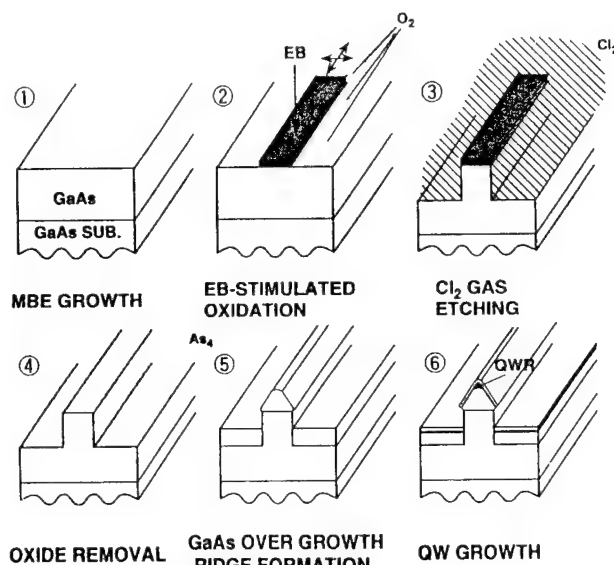


**Fig. 2** Process sequence of *in situ* patterning and regrowth used to define the first array of quantum wires. This first array of wire structures was buried in a 500nm thick GaAs layer. Then, the second array of wire structures was successively formed by a second pattern and regrowth process using steps (2) to (6).

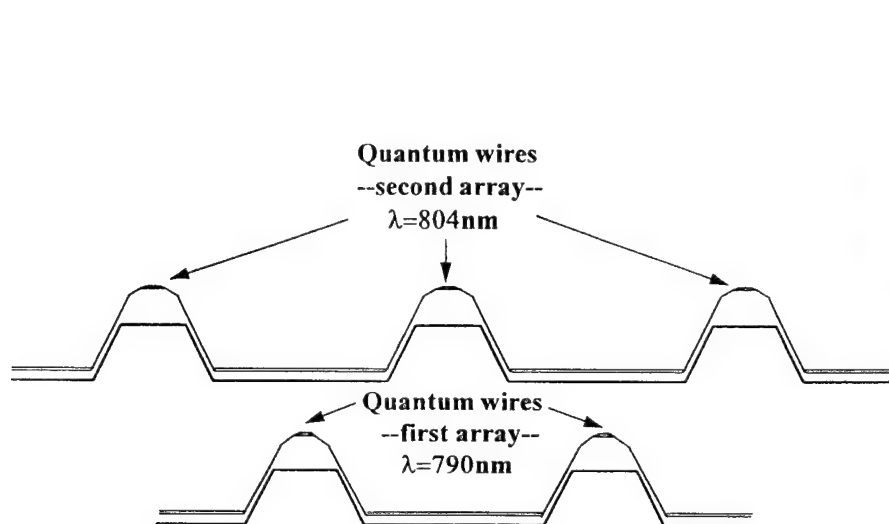
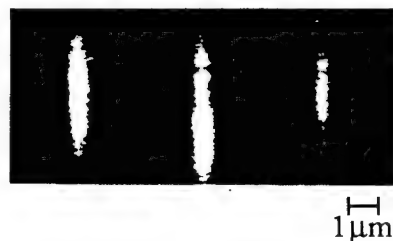


**Fig. 3** Schematic illustration of the vertically stacked structure consisting of two arrays of quantum wires.

second array of wires  
CL image ( $\lambda = 804\text{nm}$ )



first array of wires  
CL image ( $\lambda = 790\text{nm}$ )



**Fig. 4** Spatially resolved CL images showing the emission from the first ( $\lambda = 790\text{nm}$ ) and second ( $\lambda = 804\text{nm}$ ) array of wire structures.

# UHV-AFM Study of MBE-grown 10-nm Scale Ridge Quantum Wires

S. Koshiba\*, Ichiro Tanaka\*, Y. Nakamura\*,  
I. Kamiya\*, T. Someya\*\*, T. Ngo\*, and H. Sakaki\*\*\*

\* *Quantum Transition Project, JRDC, 4-6-7-4F Komaba, Meguro-ku, Tokyo 153, Japan*  
Tel: +81-3-3485-9434, FAX: +813-3460-9026,  
e-mail: koshiba @ kyokusho.rcast.u-tokyo.ac.jp.

\*\* *University of Tokyo, 4-6-1 Komaba, Meguro-ku, Tokyo 153, Japan*

We have earlier reported successful growth of 16 nm-wide ridge quantum wires (RQWIs) by MBE. Their lifetime of photoluminescence has shown a unique temperature dependence indicative of 1 dimensional excitons<sup>1)</sup>. For their device applications the structural uniformity and the width control of the wire are extremely important. In this work, we evaluate the shape of RQWIs with nm-scale resolution by using ultra-high-vacuum (UHV) AFM system which is connected to our MBE chamber. This MBE-AFM system provides us systematic and detailed information about the size and uniformity of ridges grown under different conditions. Previously we have shown that the ridge width  $W$  can be well controlled by adjusting the growth temperature ( $T_s$ )<sup>2)</sup>. However, variation of  $T_s$  affects not only on the width  $W$ , but also on the uniformity of ridges. For example, when  $T_s$  is lowered to 500°C, the ridge can be quite narrow ( $W < 10\text{nm}$ ), but its morphology degrades, probably due to the enhanced incorporation of Ga atoms on the side surface. Hence, a better growth condition for narrow and uniform ridges must be explored.

In this report, we investigate the effect of not only  $T_s$  but also that of As flux to show that a very sharp and uniform ridge structures ( $W < 10\text{ nm}$ ) can be obtained. Figure 1 is the width  $W$  of GaAs ridges measured as a function of  $T_s$ , for the MBE growth with low As flux (indicated as ●) and high As flux (as ○). Note that high As flux is effective in reducing  $W$  especially at high  $T_s$  ( $> 530^\circ\text{C}$ ), and  $W$  can be as narrow as 8 nm even at 540°C if high As flux is used. Figure 2(a) shows GaAs ridge structure measured right after the growth by UHV-AFM, which indicates a sharp and very uniform ridge can be grown at 530°C. Figure 2(b) shows that the height distribution or the roughness along the ridge is quite small within  $\pm 1\text{ nm}$  for the entire region ( $> 1\text{ }\mu\text{m}^2$ ) measured. The planes forming the ridge are almost as flat as the surface of GaAs grown on a (001) substrate grown under the optimum condition. Moreover, we have grown at 540°C a stack of three RQWIs consisting of 12 nm GaAs layers and 4 nm thick AlAs barrier layers on top of the ridge structure. Figure 3 is its cross sectional SEM micrograph where GaAs layers appear as bright layers and AlAs as dark and thin layers. Note that all three RQWIs have almost the same width and height, indicating that the shape of ridge grown under this condition is stable and reproducible. To conclude, we have demonstrated that very narrow and uniform RQWI structures, including the stack or coupled RQWIs can be grown by optimizing both the substrate temperature and the As pressure.

1. H. Akiyama, S. Koshiba, T. Someya, K. Wada, H. Noge, Y. Nakamura, T. Inoshita, A. Shimizu, and H. Sakaki, *Phys. Rev. Lett.* 72 (6), 924(1994)

2. S. Koshiba, T. Noda, H. Noge, Y. Nakamura, H. Ichinose, T. Shitara, D. D. Vvedensky, and H. Sakaki, *J Cryst. Growth* 150 332 (1995).



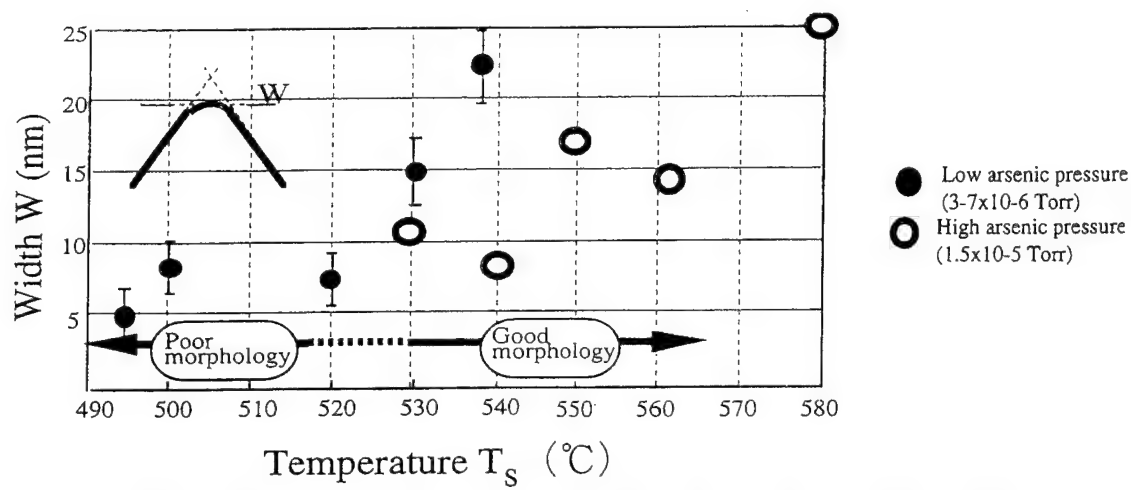


Figure 1. Measured widths of GaAs ridge as a function of  $T_s$ , which was taken at low As flux (indicated as open circle: ●) and high As flux (as solid circle : ○).

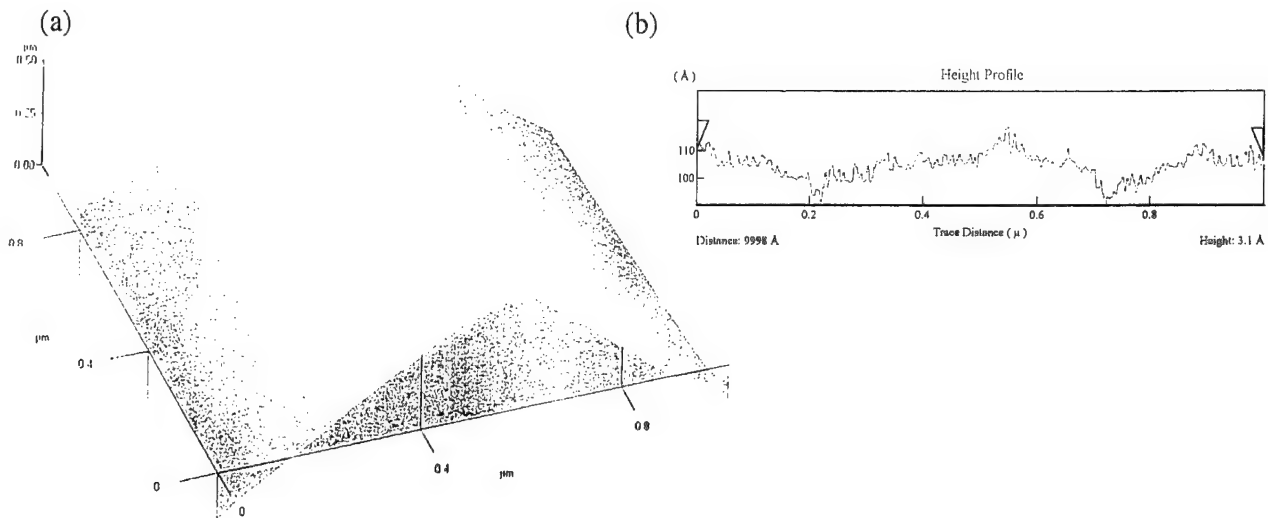


Figure 2. (a) a GaAs ridge structure measured by UHV-AFM which was grown at 560°C. (b) height distribution of this ridge structure along the ridge direction.



Figure 3. SEM micrograph of stacked ridge quantum wires.

# Improved GaAs / Al<sub>0.3</sub>Ga<sub>0.7</sub>As T-shaped quantum wires fabricated by glancing angle MBE

N. Tomita<sup>1</sup>, T. Kishi<sup>1</sup>, M. Takekawa<sup>1</sup>, S. Shimomura<sup>1</sup>,  
K. Fujita<sup>2</sup>, T. Watanabe<sup>2</sup>, A. Adachi<sup>3</sup> and S. Hiyamizu<sup>1</sup>

<sup>1</sup> Faculty of Engineering Science, Osaka University, Toyonaka, Osaka 560, Japan.

<sup>2</sup> ATR Optical and Radio Comm. Res. Labs., Soraku-gun, Kyoto 619-02, Japan.

<sup>3</sup> Nissin Electric Co. Ltd., Umezu-Takase-cho, Ukyo-ku, Kyoto 615, Japan.

Phone: +81-6-850-6457 Fax: +81-6-845-4632 E-mail: tomi@aquarius.mp.es.osaka-u.ac.jp

Glancing angle MBE (GA-MBE) on patterned substrates is one of the best methods for fabricating quantum wire (QWR) structures. In GA-MBE, the direction of Ga and Al beams with respect to the (100) substrate surface are arranged so that the preferentially formed (111)B facet is not directly exposed to the Ga and Al beams due to a self-shadowing effect as shown in Fig. 1 (a). Hence, the cross-section of a GaAs / Al<sub>0.3</sub>Ga<sub>0.7</sub>As multi-layer structure appears on the (111)B facet surface. T-shaped QWR (T-QWR) structures are fabricated by regrowing GaAs and Al<sub>0.3</sub>Ga<sub>0.7</sub>As layers on the (111)B facet by normal MBE [Fig. 1 (b)]<sup>1)</sup>. In this method, many QWRs arrays can be fabricated on (100) GaAs substrates, which is much convenient for device applications compared with the cleaved-edge T-QWRs<sup>2,3)</sup>. Cathodoluminescence (CL) was observed from the GaAs/Al<sub>0.3</sub>Ga<sub>0.7</sub>As T-QWR region at 78 K<sup>4)</sup>. Full-width-at-half-maximum (FWHM) of a CL peak from T-QWR fabricated by GA-MBE was 61 meV (78 K) in 1994<sup>1)</sup>. Recently, we could reduce this FWHM but the CL peak from the T-QWR was observed only as a slight shoulder next to the large CL peak from GaAs / Al<sub>0.3</sub>Ga<sub>0.7</sub>As QWs on (100) plane. In this paper, we report much improved CL spectrum from the GaAs / Al<sub>0.3</sub>Ga<sub>0.7</sub>As T-QWRs fabricated by GA-MBE, which shows a very small FWHM of a CL peak (9 meV at 78K). This FWHM is almost comparable with those (10 meV<sup>2)</sup>, 4 - 7 meV<sup>3)</sup>) of cleaved-edge T-QWRs.

First, a GaAs / Al<sub>0.3</sub>Ga<sub>0.7</sub>As MQW (6.6 nm / 17 nm, 5 periods) and an Al<sub>0.3</sub>Ga<sub>0.7</sub>As barrier layer (43 nm) were grown on a GaAs / Al<sub>0.3</sub>Ga<sub>0.7</sub>As (87 nm / 4.3 nm, 20 period) buffer layer on reverse-mesa etched (100) GaAs substrate by GA-MBE ( $T_s = 570^\circ\text{C}$ ,  $V/\text{III}=25$ ). Second, a GaAs / Al<sub>0.3</sub>Ga<sub>0.7</sub>As (7.3 nm / 51 nm) QW and a 12 nm-thick GaAs were overgrown on the (111)B facet and (100) plane ( $T_s = 630^\circ\text{C}$ ,  $V/\text{III}=10$ ) in a normal MBE mode with rotating the substrate at 60 rpm. Fig. 2 shows the cross-sectional SEM image of the grown structure. A CL spectrum (78 K) from the QWs and T-QWRs is shown in Fig. 3. Peaks at 787 nm and 795 nm come from the MQW on (100) plane and on the QW on the (111)B facet, respectively. Luminescence from the T-QWRs is observed at 803 nm. This peak energy (1.544 eV) is 31 meV lower than that of the MQW on (100) plane and is 15 meV lower than that of the QW on the (111)B facet plane. FWHM of the T-QWRs peak is 12 meV. The minimum FWHM of this peak observed is 9 meV which was obtained with decreasing the CL excitation intensity of electron beam. This value is almost comparable to those (10 meV<sup>2)</sup>, 4-7 meV<sup>3)</sup>) of the cleaved-edge T-QWRs.

## References

- 1) S. Shimomura et al. , Solid-State Electron., **37**, 597 (1994)
- 2) L. Pfeiffer et al. , J. Cryst. Growth, **127**, 849 (1993)
- 3) T. Someya et al., Phys. Rev. Lett. **74**, 3664 (1995)
- 4) N. Tomita et al. , submitted to J. Vac. Sci. Technology B (1996)

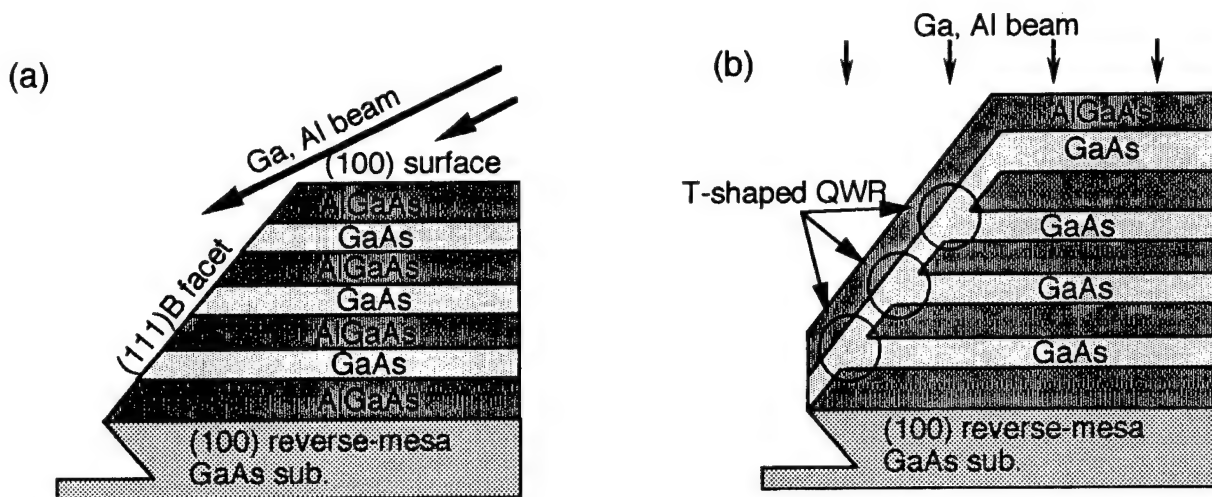


Fig.1 GaAs/AlGaAs T-QWRs grown by GA-MBE and overgrowth on the (111)B facet. Ga and Al beams are so inclined that these beams do not impinge directly into the (111)B facet, due to a self-shadowing effect (no substrate rotation, GA-MBE mode) (a). Cross-section of GaAs / AlGaAs T-QWR are fabricated by overgrowing GaAs QW and AlGaAs barrier layers on the (111)B facet with rotating the substrate (normal MBE mode) (b).

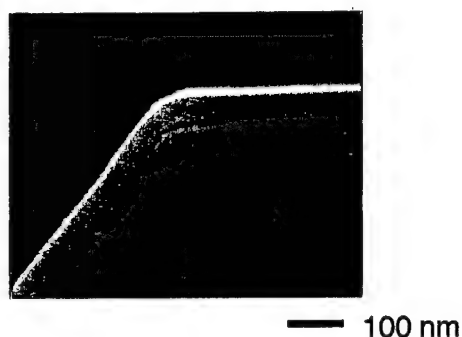


Fig. 2 Cross-sectional SEM image of the sample

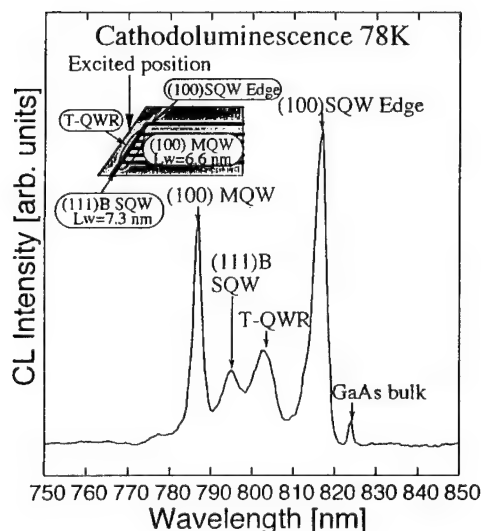


Fig. 3 CL spectrum (78 K) observed when the (111)B facet region is excited by the electron beam

## 15. LASERS AND DETECTORS

FRIDAY MORNING (ELKINS)

Session Chair: Jim Harris, Stanford University, Palo Alto, California

C-Chair: Y.M. Houn, Hewlett-Packard Laboratories, Palo Alto, California

- 09:00 15.1 **Low threshold current 1.3  $\mu\text{m}$  InAsP/InGaAsP lasers grown by gas-source molecular beam epitaxy,**  
P. Thiagarajan, G.E. Giudice, H. Temkin, and G.Y. Robinson  
Colorado State University, USA
- 09:20 15.2 **High temperature (Ga)InAsP / high band gap GaInAsP barriers 1.3  $\mu\text{m}$  SL - MQW lasers grown by gas source MBE**  
Ph. Pagnod-Rossiaux, F. Gaborit, N. Tschertner L. Roux, C. Starck, B. Fernier  
Alcatel-Alsthom Recherche, Marcoussis, France
- 09:40 15.3 **CBE of 1.55  $\mu\text{m}$  (GaIn)(AsP) lasers for monolithic integration**  
A. Nutsch, H. Kratzer, B. Tränkle, G. Weimann  
Walter Schottky Institut, Garching, Germany
- 10:00 15.4 **MOMBE growth of highly tensile-strained InGaAsP MQWs and their applications to 1.3  $\mu\text{m}$  wavelength low-threshold current lasers**  
H. Sugiura, M. Ogasawara, M. Mitsuhashi, N. Yamamoto, and M. Itoh  
NTT Opto-electronics Laboratories, Atugi, Japan.
- Break
- 10:40 15.5 **MBE grown mid-infrared type-II quantum well lasers**  
Chih-Hsiang Lin, P.C. Chang, Rui Q. Yang, S.J. Murry, D. Zhang, S.S. Pei,  
University of Houston, J.I. Malin, J.R. Meyer, C.L. Felix, J.R. Lindle, L. Goldberg,  
C.A. Hoffman, F.J., Bartoli, NRL, USA
- 11:00 15.6 **Wavelength modulator structures with soft optical confinement grown by the epitaxial shadow mask (ESM) MBE-technique**  
S. Malzer, M. Kneissl, U. Hilburger, R. Mayer, P. Kiesel, and G.H. Döhler  
Universität Erlangen-Nürnberg, Germany
- 11:20 15.7 **A new p-type compressively strained layer InGaAs-AlGaAs-GaAs miniband transport quantum well infrared photodetector for long wavelength infrared detection,** Sheng S. Li, J. Chu, and Pin Ho  
University of Florida, USA
- 11:40 15.8 **Large array of GaAs modulators and detectors flip-chip solder bonded to silicon CMOS using InGaP as the selective etch stop for GaAs substrate removal,** J.M. Kuo, Y.C. Wang, K.W. Goossen, L.M.F. Chirovsky, S.P. Hui, B.T. Tseng, J. Walker, A.L. Lentine, Lucent Technologies, USA.

## Low Threshold Current 1.3- $\mu\text{m}$ InAsP/InGaAsP Lasers Grown by Gas-Source Molecular Beam Epitaxy

P. Thiagarajan, G.E. Giudice, H. Temkin, and G.Y. Robinson\*  
*Department of Electrical Engineering, Colorado State University,  
Fort Collins, Colorado 80523, USA*

Lasers operating at 1.3  $\mu\text{m}$  are essential components in optical fiber communication systems and optical interconnect systems. For semiconductor lasers operating at 1.3  $\mu\text{m}$ , separate confinement heterostructure multiple quantum well (SCH-MQW) lasers using compressively strained InAsP wells with either lattice-matched or strained InGaAsP barriers grown on InP have been demonstrated to have superior high temperature and output power performance over the commonly used InGaAsP/InGaAsP SCH-MQW lasers [1,2]. We have recently reported on the optimization of the growth conditions for high quality 1.3  $\mu\text{m}$  InAsP/InGaAsP SCH-MQW lasers by gas source-molecular beam epitaxy (GSMBE) [3]. Here we report on InAsP/InGaAsP SCH-MQW lasers for 1.3  $\mu\text{m}$  emission grown by GSMBE with very low threshold currents of 1.1 mA at 20°C and 6.1 mA at 100°C. To our knowledge, these are the lowest threshold currents yet reported for any InGaAsP lasers grown by GSMBE.

InAsP/InGaAsP heterostructures were grown on (100) *n*-type InP substrates using conventional effusion cells to provide In and Ga atomic fluxes, and thermally cracked AsH<sub>3</sub> and PH<sub>3</sub> for As<sub>2</sub> and P<sub>2</sub> molecular beams. The laser structures consisted of a 1- $\mu\text{m}$  *n*-type InP cladding layer ( $1 \times 10^{18} \text{ cm}^{-3}$ ), the active region, a 1.5- $\mu\text{m}$  *p*-type InP cladding layer ( $7 \times 10^{17} \text{ cm}^{-3}$ ), and finally a 0.2- $\mu\text{m}$  *p*-type InGaAs contact layer ( $2 \times 10^{19} \text{ cm}^{-3}$ ). The active region consisted of six wells of InAs<sub>0.45</sub>P<sub>0.55</sub>, 4.5-nm thick, with 15-nm InGaAsP barriers with band gap emission of 1.15  $\mu\text{m}$ , and 110-nm InGaAsP separate confinement layers. The InP cladding layers were grown at 480°C, while the active region was grown at the optimum GSMBE temperature of 430°C [3]. Buried heterostructure lasers were fabricated from the GSMBE wafers with an InP *p-n-i-n* current blocking structure using MOCVD, and the laser facets were coated with SiO<sub>2</sub>/Si.

The threshold current was measured as a function of laser cavity length (*L*) and facet reflectivities (*R*<sub>1</sub> and *R*<sub>2</sub>) at 20°C. With uncoated facets (*R*<sub>1</sub>/*R*<sub>2</sub>=29%/29%), the threshold current was 5.0 mA for *L*=250 $\mu\text{m}$ . For one facet coated (29%/95%) the minimum threshold current was 3.0 mA at *L*=125 $\mu\text{m}$ , and with high reflectivity coatings on both facets (85%/95%) the threshold dropped to 1.1 mA. The internal quantum efficiency  $\eta_i$  and the internal loss  $\alpha_i$  were found to be 10.5 cm<sup>-1</sup> and 70%, respectively. The logarithmic gain approximation was found to accurately predict the dependence of threshold current on *L* and *R*<sub>1</sub>/*R*<sub>2</sub>.

In order to increase the output power, anti-reflection coatings for the front facet (*R*<sub>1</sub> = 10%) and high reflection coating for the rear facet (*R*<sub>2</sub> = 95%) were used. A maximum output power of 49 mW and 65 mW were measured at 20°C for *L*=250 $\mu\text{m}$  and 750 $\mu\text{m}$ , respectively. The maximum output powers decreased to 4 mW and 15 mW at 90°C. The highest slope efficiency at 20°C was measured to be 0.49 mA/mW for *L*=250 $\mu\text{m}$ . Even at these high operating powers and temperatures, no catastrophic failure of the lasers was observed.

---

[1] M. Yamamoto et al., IEEE J. Quantum Electron. QE-30,554 (1994).

[2] H. Ohashi et al., Electron. Lett., 31, 556 (1995).

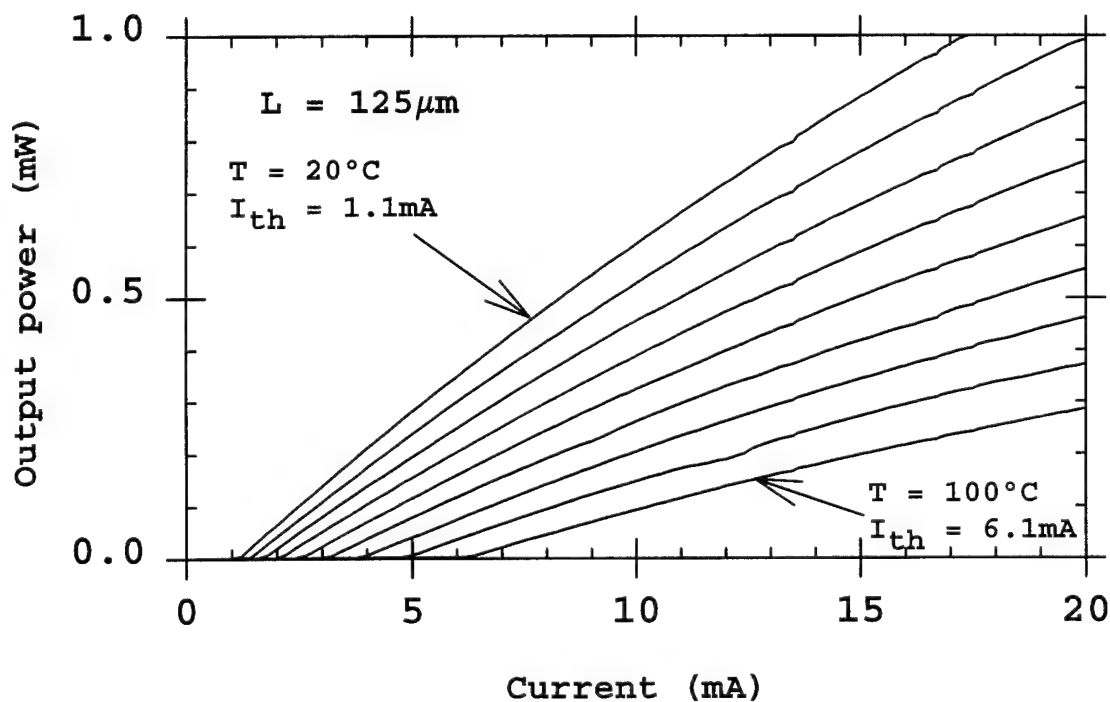
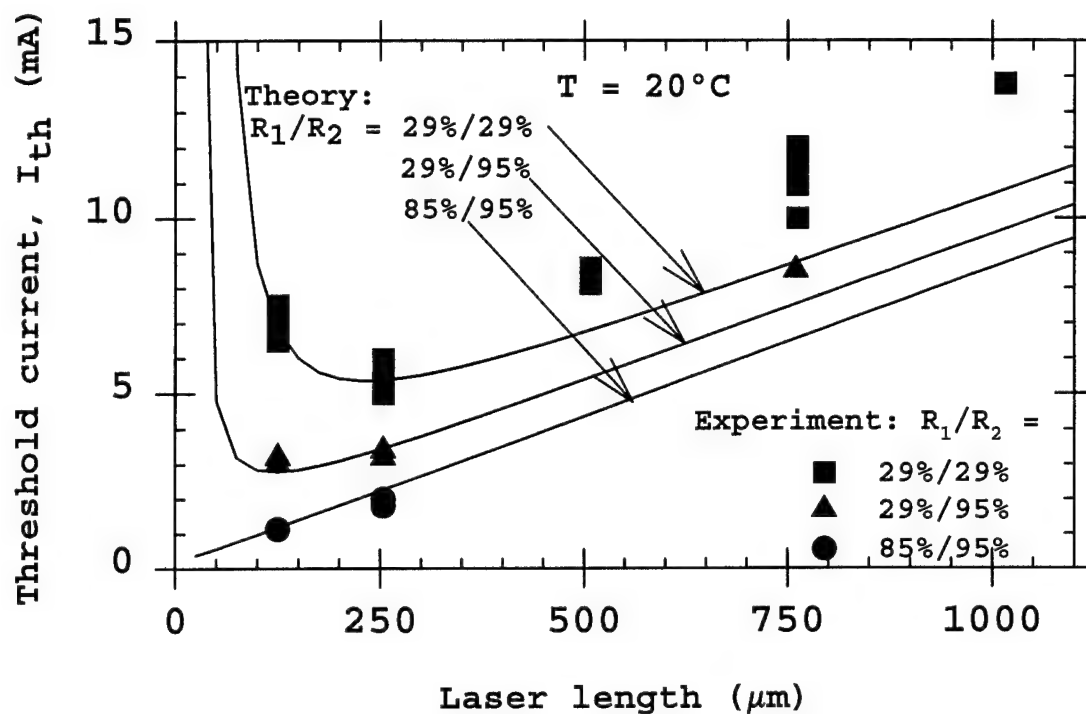
[3] P. Thiagarajan et al., Appl. Phys. Lett. 67, 3676 (1995).

\* Office: (970) 491-6575; Fax: (970) 491-2249; E-mail: Gary@lance.ColoState.edu

Attachment for

P.Thiagarajan et al.

"Low threshold current 1.3 $\mu$ m InAsP/InGaAsP lasers grown by gas source molecular beam epitaxy"



## High temperature (Ga)InAsP/ high band gap GaInAsP barriers 1.3 $\mu\text{m}$ SL- MQW lasers grown by Gas Source MBE.

Ph. Pagnod-Rossiaux, F. Gaborit, N. Tschertner, L. Roux, C. Starck, B. Fernier  
Alcatel-Alsthom Recherche, route de Nozay, F 91460 Marcoussis - France  
Tel. :33-1-64.49.11.28; Fax :33-1-64.49.17.85  
e-mail :Philippe.Pagnod@aar.alcatel-alsthom.fr

Low cost, high temperature 1.3  $\mu\text{m}$  lasers are key components for FTTH applications. In the GaInAsP/InP system, Auger recombination and carrier leakage in the SCH layers, resulting in low characteristic temperatures  $T_0$  (40-50 K), have been identified to limit high temperature performances of the devices [1],[2]. Those effects can be reduced by introduction of strain and by increasing the band gap of the barrier or confinement layers [3] respectively in MQW-SCH laser structures.

We present an experimental analysis of the dependance of  $T_0$  values on strain and barrier band gap. Laser structures, with a nearly constant confinement factor, consisting of 6 compressively strained (Ga)InAsP QW's with high band gap GaInAsP barriers embeded in lattice-matched GaInAsP optical confinement layers have been grown by GS-MBE. The composition of the wells is adjusted to let their strain range from 0.6 to 1.4 %. Tensile strain is introduced in the barriers of the InAsP structures (samples 3 to 6) to compensate for the high strain (1.4 %) necessary to reach emission at 1.3  $\mu\text{m}$ . The high quality of the tensile/compressive MQW structures grown by GS-MBE at low temperature (470  $^{\circ}\text{C}$ ) are demonstrated by XRD and PL spectra. The details of the structures are depicted in table 1. The samples have been processed as 100  $\mu\text{m}$  wide broad area lasers. Their characteristics as a function of length have been analysed at temperatures up to 80  $^{\circ}\text{C}$ .

Low  $J_{\text{th}}$  at 20  $^{\circ}\text{C}$ , ranging from 420 to 560  $\text{Acm}^{-2}$  for 1200  $\mu\text{m}$  long devices, are measured on samples 1 to 5 (Fig.1). Threshold current densities per well for infinite length ( $J_0$ ), as well as internal losses and quantum efficiencies, at 20  $^{\circ}\text{C}$  and 80  $^{\circ}\text{C}$  are reported in table 2. Low internal losses of 6 to 11  $\text{cm}^{-1}$  are calculated up to 80  $^{\circ}\text{C}$ . Such values demonstrate the high quality of the active material.

Average characteristic temperatures for 300 and 1200  $\mu\text{m}$  long lasers range from 50 to 80 K and from 60 to 110 K respectively, depending on the barrier band gap. A variation of  $T_0$  with respect to calculated electrons escape energy is seen on figure 2. The strain level in the wells seems to be of minor influence on the  $T_0$  values, as shown from samples 1 to 4. However, together with the increase of  $T_0$ , an increase of threshold current densities is observed (sample 6). This can be explained by a poor or non uniform injection of carriers in the QW's as the barrier band gap is increased.

In summary, high barrier band gap, compressively strained MQW 1.3  $\mu\text{m}$  broad area lasers have been grown by GS-MBE and characterized in the 20 - 80  $^{\circ}\text{C}$  temperature range. These results show that the optimization of a high temperature laser is a trade-off between low  $J_{\text{th}}$  at room temperature and large  $T_0$ .

- [1] Seki et al., APL 67(8), 1054-1056, 1995
- [2] Bernussi et al., APL 66(1), 67-69, 1995
- [3] Oohashi et al., Electr. Lett. 31(7), 556-557, 1995

Sample	Well				Barrier				
	Lw (nm)	Xw	Yw	$\epsilon$ (%)	Lb (nm)	Xb	Yb	$\epsilon$ (%)	Gap ( $\mu\text{m}$ )
1	8.1	0.2	0.62	0.6	10.2	0.11	0.25	0,03	1.10
2	8.4	0.105	0.54	1.0	8.4	0.105	0.25	0,06	1.05
3	8.0	0	0.43	1.38	8.1	0.19	0.35	-0,2	1.10
4	8.4	0	0.43	1.38	8.4	0.19	0.29	-0,4	1.08
5	8.4	0	0.4	1.28	8.4	0.19	0.18	-0,8	1.02
6	8.5	0	0.44	1.41	8.1	0.105	0.08	-0,5	0.96

Table 1: Composition parameters of the studied structures. Xw and Xb refer to the Ga content in wells and barriers respectively.

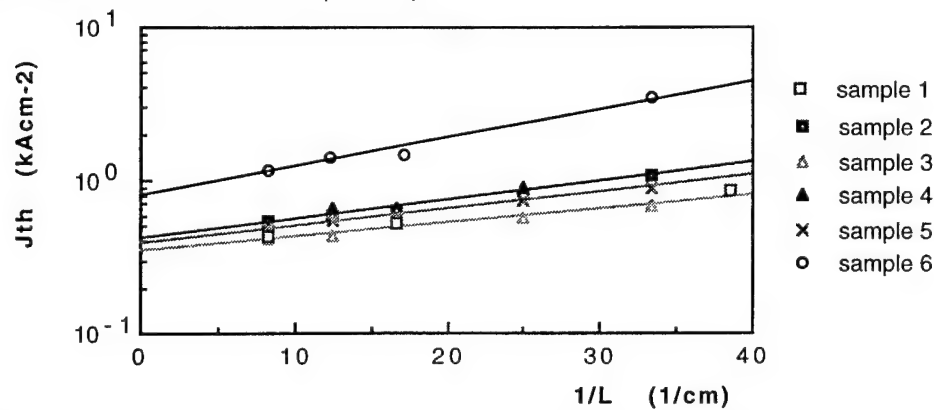


Fig.1: Threshold current densities at 20 °C, as a function of inverse cavity length.

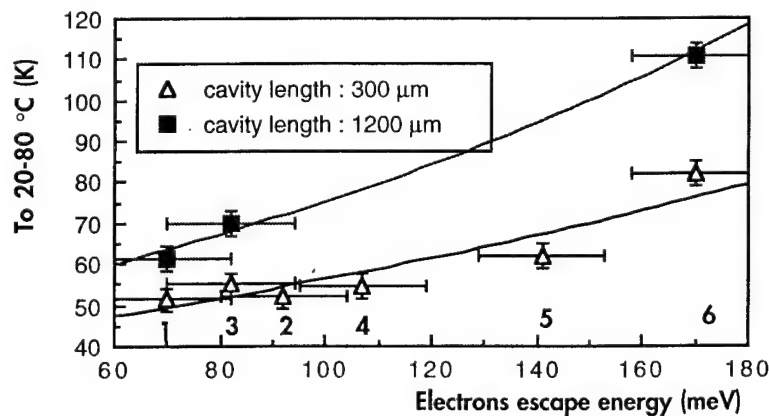


Fig.2: Characteristic temperature between 20 and 80 °C as a function of the electron escape energy (well to barrier conduction band offset - 1st quantized electron energy).

Sample	20 °C			80 °C		
	Jo (Acm-2)	$\alpha$ (cm-1)	$\eta$	Jo (Acm-2)	$\alpha$ (cm-1)	$\eta$
2	71	5.6	0.73	155	7.9	0.49
3	57	8.7	0.93	125	11	0.52
5	64	6.8	0.90	143	8.9	0.62
6	134	-	-	217	-	-

Table 2: Average characteristic parameters Jo,  $\alpha_{\text{int}}$  ( $\alpha$ ) and  $\eta_{\text{int}}$  ( $\eta$ ) of broad area lasers at 20 and 80 °C.



# CBE of 1.55 $\mu\text{m}$ (GaIn)(AsP) lasers for monolithic integration

A. Nutsch, H. Kratzer, B. Torabi, G. Tränkle\*, G. Weimann\*

Walter Schottky Institut, Am Coulombwall, D - 58748 Garching, Germany

Phone: 49 89 3209 - 2787, Fax: 49 89 3206 620, e-mail: [arn@e26.physik.tu-muenchen.de](mailto:arn@e26.physik.tu-muenchen.de)

\*Fraunhofer - Institut für Angewandte Festkörperphysik, Tullastr. 72, D - 79108 Freiburg

The monolithic integration of photonic devices with different structures requires selective epitaxy. Chemical beam epitaxy is well suited due to its mask selective growth without reactions in the gas phase. We have grown embedded laser structures in grooves in InP substrates, which were etched by ECR - RIE using  $\text{CH}_2/\text{H}_2$  with  $\text{Si}_3\text{N}_4$  masks, both, for etching and selective growth.

Our laser structures consisted of compressively strained ternary or quaternary MQWs, quaternary barriers ( $\lambda = 1.2 \mu\text{m}$ ) and confinement layers ( $\lambda = 1.1 \mu\text{m}$ ). Best crystal quality for quaternary GaInAsP was obtained at a rather high growth temperature of  $543^\circ\text{C}$ , which was used for all composites. The  $\text{V}/\text{III}_{\text{BEP}}$  - ratio, on the other hand, was individually adjusted for the various composites, allowing growth without any interruptions. Long wavelength GaInAsP used for the wells ( $\lambda = 1.6 \mu\text{m}$ ) required a low  $\text{V}/\text{III}_{\text{BEP}}$  ratio of 3. The  $1.2 \mu\text{m}$  barriers and the  $1.1 \mu\text{m}$  SCH layers were grown with high ratios of 8.5 or 10.5, respectively. The high quality of our layers required a very close control of these  $\text{V}/\text{III}_{\text{BEP}}$  - ratios (see figure 2).

Laser structures grown on planar InP wafers and processed to metal clad ridge waveguide (MCRW) lasers, showed low threshold current densities of  $78 \text{ A}/\text{cm}^2$  per well for six ternary wells. Quaternary wells with increased strain, using the identical well width of 5 nm, resulted in reduced values of  $j_{\text{th}\infty} = 68 \text{ A}/\text{cm}^2$ .

Ternary laser structures were selectively grown into grooves in the  $\text{Si}_3\text{N}_4$  masked InP - substrates. Epitaxial growth with the usual growth rate of  $1.4 \mu\text{m}/\text{h}$  yielded in a strong faceting. Reducing the growth rate to  $0.4 \mu\text{m}/\text{h}$  and simultaneously increasing the  $\text{V}/\text{III}_{\text{BEP}}$  - ratio in the n - InP cladding layer (figure 1) resulted in planar growth without marked edge distortions. Once planar growth had been established, we grew the laser structure using the above standard conditions, maintaining nearly planar growth (figure 1). Threshold currents of 40 mA were measured for selectively grown stripe lasers in  $4 \mu\text{m}$  wide grooves (cavity length  $530 \mu\text{m}$ ), being only slightly higher than those of 'planar' MCRW lasers of comparable length. No change in composition of the ternary core was found for lasers in  $7 \mu\text{m}$  and  $30 \mu\text{m}$  wide grooves compared to lasers on planar substrates. Quantum wells grown in narrow  $4 \mu\text{m}$  wide grooves, on the other hand, showed a redshift of 30 nm in wavelength.

# CBE of 1.55 $\mu\text{m}$ (GaIn)(AsP) lasers for monolithic integration

Nutsch et al.:

Supporting Material:

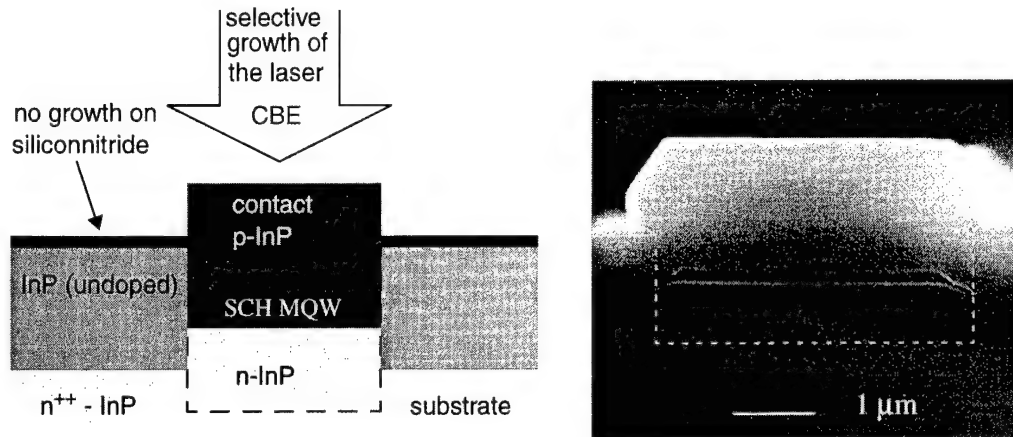


Fig. 1: Selective epitaxy was used to embed ternary Lasers into grooves in InP substrates. The SEM picture shows a cleaved facet.

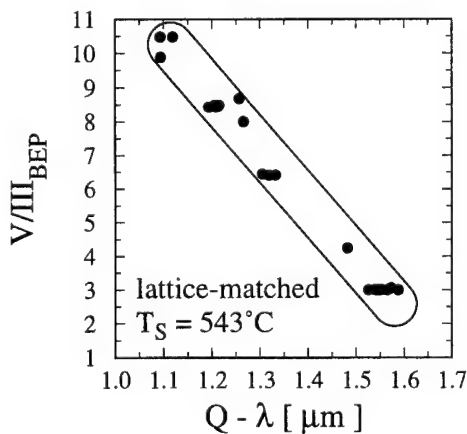


Fig. 2: High quality GaInAsP layers we obtained at  $T_S = 543^\circ\text{C}$  when the  $V/\text{III}_{\text{BEP}}$  ratio is controlled closely in a narrow window. With increasing Ga and As contents the  $V/\text{III}_{\text{BEP}}$  - ratio has to be lowered.

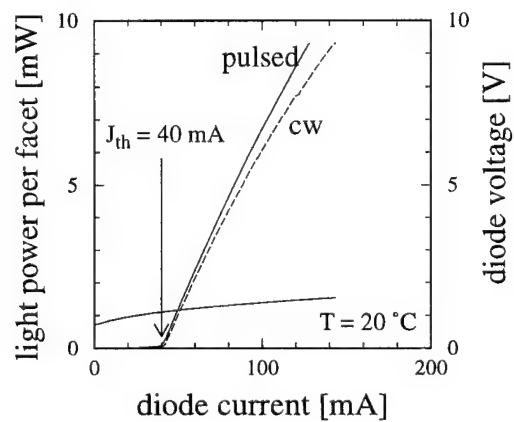


Fig. 3: Light current characteristics of a (GaIn)(AsP) laser embedded selectively in an InP groove. The threshold current is 40 mA for cw or pulsed operation, respectively.

## MOMBE growth of highly tensile-strained InGaAsP MQWs and their applications to 1.3- $\mu\text{m}$ wavelength low-threshold current lasers

H. Sugiura\*, M. Ogasawara, M. Mitsuhashi, N. Yamamoto, and M. Itoh  
NTT Opto-electronics Laboratories  
3-1, Morinosato Wakamiya Atugi, 243-01, Japan  
FAX: 81-462-40-4301  
TEL: 81-462-40-3252  
e-mail: sugiura@aecl.ntt.jp

This paper demonstrates that InGaAsP MQWs with six layers having as much as 1.8% tensile strain can be grown by using MOMBE and a strain-compensation technique. The threshold current density,  $J_{th}$ , of the lasers decreases with increase in strain value; the minimum  $J_{th}$  obtained was 0.6 kA/cm<sup>2</sup> at 1.3% strain.

It has been predicted that, theoretically, tensile-strained InGaAsP MQW lasers emitting at 1.3  $\mu\text{m}$  wavelength should perform better than compressive ones in such aspects as low threshold current and high resonance frequency. In order to extract the laser benefits, the well layers must have more than 1% strain and be more than 100 Å thick. This speculated performance, however, has not yet been achieved owing to the difficulty of growing wells of such high strain and thickness using MOCVD. We have solved this problem by using MOMBE, which permits growth of MQWs at a temperature 100°C lower than that used in MOCVD.

To get an overview of this strain compensation effect, we studied the critical conditions over which the PL intensities of MQWs decrease due to misfit dislocation generation. We grew MQWs composed of six pairs of an InGaAsP ( $\lambda=1.5 \mu\text{m}$  wavelength) well layer and an InGaAsP barrier layer ( $\lambda=1.1 \mu\text{m}$ ) at 520°C. The well and barrier thicknesses ( $L_w$  and  $L_b$ ) were kept at 100 and 150 Å, respectively. We varied the well layer tensile strain  $\epsilon_w$  from 0.5 to 1.8% and the barrier compressive strain  $\epsilon_b$  from 0.2 to 0.6%. Our systematic study of strain compensation revealed that PL intensities deteriorated drastically when the net strain  $e^*$ , i.e.,  $e^* = (\epsilon_w L_w + \epsilon_b L_b) / (L_w + L_b)$  exceeded 0.4% independent of the  $\epsilon_w$  values. The critical thicknesses determined at each net strain were several times greater than the values calculated using the Matthews formula. This fact had been proved also in our previous study on compressive-strained InAsP MQWs grown by MOMBE. Thus, low-temperature growth makes possible an increase in the critical thickness for either tensile or compressive strain, allowing the growth of the MQWs with a tensile strain as high as 1.8%.

The MQWs were characterized using cross-sectional TEM and low-temperature PL measurement. No dislocations were observed in the lattice image photos. The TEM in the  $g = [100]$  direction indicated that the MQWs have well-defined interfaces. The TEM for  $g = [110]$ , however, revealed a quasi-periodic pattern in the lateral direction in the well layers. The FWHM of the PL peak at 9 K increased with increase in strain, registering 20 meV at 1.3% strain. The  $[110]$  TEM and PL results strongly suggest that the well layers were affected by spinodal-like decomposition.

The MQWs were processed into broad area lasers with cavity lengths of 300  $\mu\text{m}$ . All the lasers operated in TM mode. At a fixed strain value of 1.45%, the threshold current density  $J_{th}$  decreased progressively from well number 2 to 6. At a fixed well number of six, the  $J_{th}$  value decreased with increase in the strain from 0.5 to 1.3% but it slightly increased for 1.45-1.8% range. The minimum  $J_{th}$  was 0.6 kA/cm<sup>2</sup> at 1.3%. This value is the smallest ever reported for tensile-strained MQW lasers.

Growth at low temperature is effective in improving the performance of strain-limited devices. The subject of increasing critical thickness is attractive for further academic study.

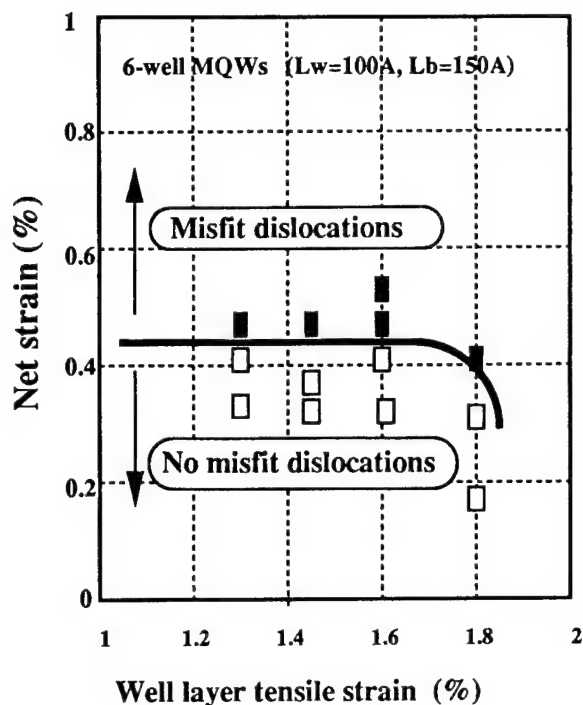


**Fig. 1** Plot of net strain against well layer tensile strain. At net strains over 0.4%, the MQW PL intensities are reduced drastically due to generation of misfit dislocations.

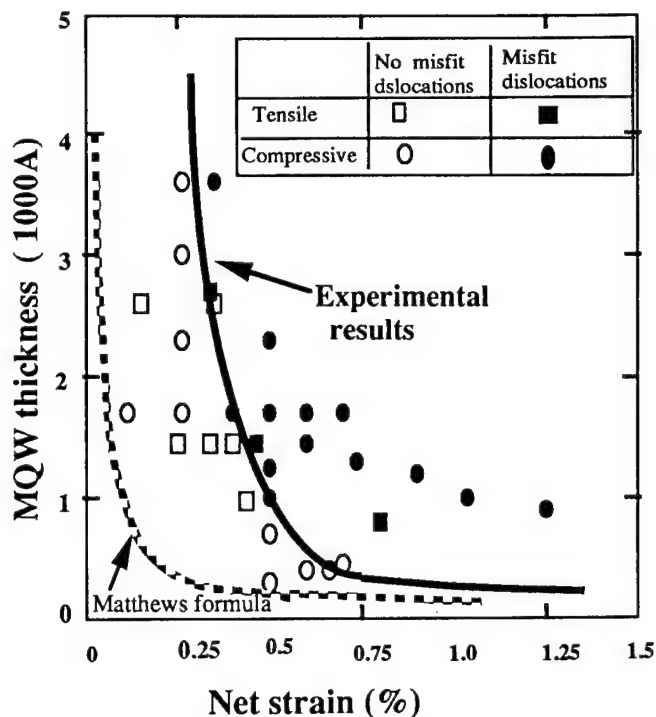


**Fig. 2** Map of MQWs for various total thicknesses and net strains, showing generation or absence of misfit dislocations. Solid curve: experimentally determined thier relation; broken line: relations calculated using the Matthews formula.

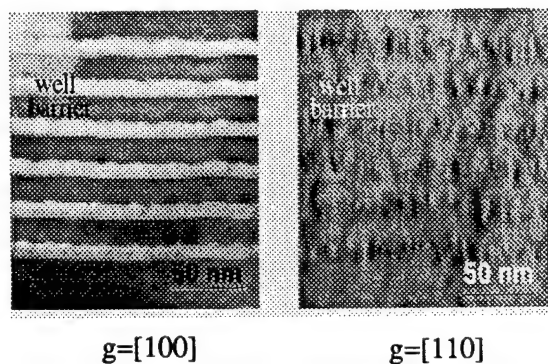


**Fig. 3** TEM photographs taken in the  $g = [100]$  (left) and  $[110]$  (right) directions for the 1.3% strained MQWs. The well-barrier interfaces are well defined in the  $[100]$  direction. The quasi-periodic pattern in  $[110]$  direction implies lateral composition modulation in the well layers due to spinodal decomposition.

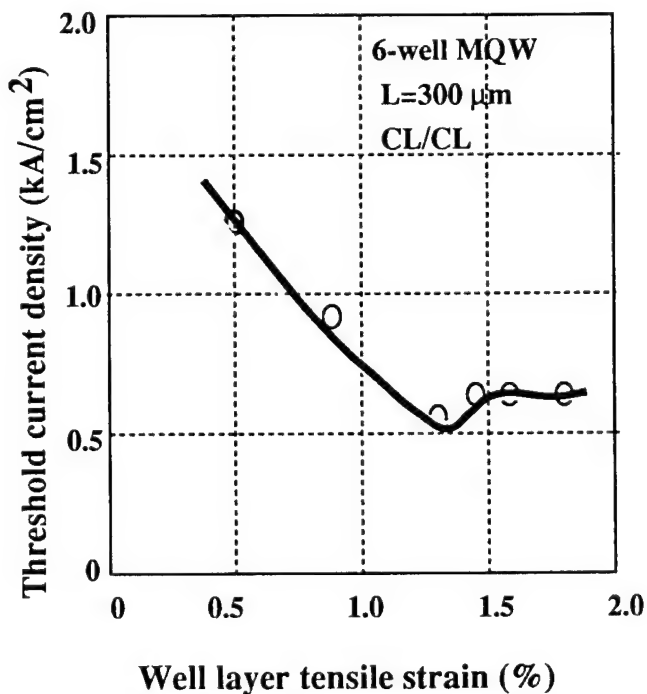


**Fig. 4** Relation between the threshold current density  $J_{th}$  and well layer tensile strain.  $J_{th}$  decreases with increase in strain, to a minimum  $J_{th}$  of 0.6 kA/cm<sup>2</sup> at 1.3% strain.

## MBE Grown Mid-Infrared Type-II Quantum-Well Lasers

Chih-Hsiang Lin, P. C. Chang, Rui Q. Yang, S. J. Murry, D. Zhang, and S. S. Pei  
Space Vacuum Epitaxy Center, University of Houston, Houston, TX 77204-5507  
Tel: (713) 743-3621, Fax: (713) 747-7724, E-mail: CHLin@uh.edu

J. I. Malin, J. R. Meyer, C. L. Felix, J. R. Lindle, L. Goldberg, C. A. Hoffman, and F. J. Bartoli  
Code 5600, Naval Research Laboratory, Washington, DC 20375

We have investigated mid-infrared lasers based on type-II InAs/InGaSb/InAs/AlSb quantum well (QW) and type-II quantum cascade (QC) configurations. Here, we will discuss the MBE growth of these type-II lasers. The optimal MBE growth temperature is from 380 °C to 470 °C for InAs, and is above 500 °C for AlSb. Since the InAs and InGaSb layers in active region act as wells, and AlSb layers act as barriers, the QW active region was grown at 440 °C to optimize the material qualities of the InAs and InGaSb layers. The AlSb cladding layers and GaSb buffer layer were grown at 510 °C. During growth, the InGaSb layers in the active region and the AlSb cladding layers displayed excellent  $1\times 3$  RHEED patterns, while the InAs layers exhibited  $1\times 2$  patterns with a V/III beam-equivalent pressure ratio of 10. However, the RHEED patterns for the AlSb barriers in the active region were not as good, probably because the growth temperature was lower than the optimal value for that material. From the double crystal X-ray spectra of test samples, the background As in GaSb was less than 0.2% with the As cell at the growth temperature and the As shutter closed, and the Sb background in InAs was less than 0.4%. However, from the TEM results for laser samples, there was some Sb floating into the InAs layers. We will discuss the effects of substrate temperature and growth interruptions on the interface quality and the floating of Sb into the InAs layers. The growth rates and compositions were calibrated to within  $\pm 2\%$  using RHEED on non-rotating InAs and GaAs samples.

Type-II QW lasers were grown in a Riber 32 MBE system on p-type GaSb substrates using traditional As<sub>4</sub> and Sb<sub>4</sub> effusion cells. Pulsed operation was obtained for optically pumped 3.3- $\mu\text{m}$  lasers up to 297 K and 4.06- $\mu\text{m}$  lasers up to 285 K. The active region of the 4.06- $\mu\text{m}$  lasers was composed of 35 periods of undoped InAs/In<sub>0.3</sub>Ga<sub>0.7</sub>Sb/InAs/AlSb (21 Å/31 Å/21 Å/43 Å) QWs, which were lattice-matched to the AlSb cladding layers. Figure 1 shows the peak output power at 210, 240, and 270 K vs. pumping intensity. Figure 2 show the threshold pumping intensity as a function of temperature. The characteristic temperature  $T_0$  of these lasers was 96 K for temperatures less than 170 K, and was 35 K for temperatures between 170 K and 270 K. For temperatures less than 170 K, the recombination lifetime at threshold  $\tau_{\text{th}}$  had a nearly constant value of 2 ns, suggesting that Shockley-Read recombination dominated in that range, and was responsible for the larger  $T_0$ . For temperatures higher than 170 K,  $\tau_{\text{th}}$  decreased in a manner consistent with the Auger process. The maximum peak output power per facet with a 500  $\mu\text{m}$  cavity length was 650 mW at 81 K and about 200 mW at 170 K. In this talk, we will also discuss theoretical analysis of lasers based on a type-II quantum cascade configuration, as shown in Figure 3.

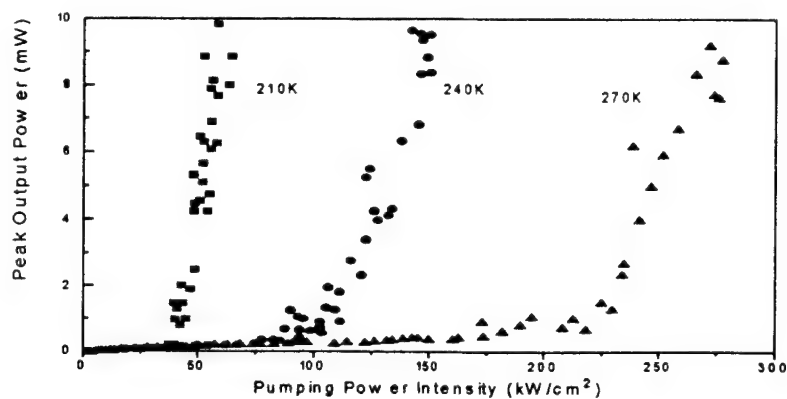


Figure 1. Peak output power at 210, 240, and 270 K vs. pumping intensity.

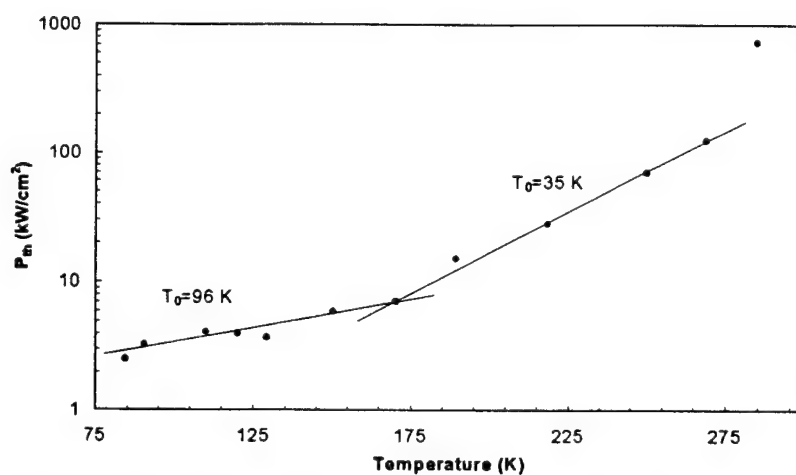


Figure 2. Threshold pumping intensity as a function of temperature.

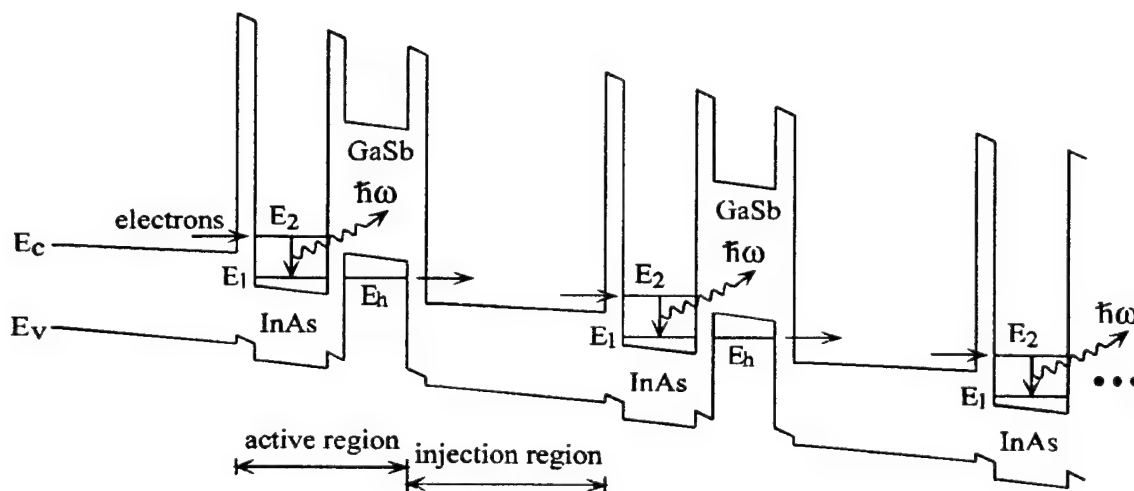


Figure 3. Schematic drawing of a type-II quantum cascade laser.

# Waveguide Modulator Structures with Soft Optical Confinement grown by the Epitaxial Shadow Mask (ESM) MBE-Technique"

*S. Malzer, M. Kneissl, U. Hilburger, R. Mayer, P. Kiesel, and G.H. Döhler*

Institut für Technische Physik, Universität Erlangen-Nürnberg,

Erwin-Rommel-Str. 1, D-91058 Erlangen, Germany

phone: 49 9131 85 7254

fax: 49 9131 85 7293

e-mail: malzer@physik.uni-erlangen.de

Excellent selective n- and p-contacts to highly doped and closely adjacent layers in n-i-p-i doping superlattices can be fabricated using the epitaxial shadow mask molecular beam epitaxy (ESM-MBE) [1]. With this method the growth within the window of a GaAs/AlGaAs mask obtained by selective wet chemical etching is controlled by the geometrical aspect of the effusion cells relative to the substrate. Selectivity of the contacts can be achieved even with continuously rotated substrate by "flash doping" the layers. In this case the shutter action of the doping cells has to be synchronized with the rotation of the substrate. It has been demonstrated that light detection and modulation with high contrast ratios over a broad wavelength range and at low voltage swings can be achieved. Whereas these devices had been designed for light penetration perpendicular to the active layers we now demonstrate first results of using ESM-MBE for the *in-situ* fabrication of waveguide structures, including waveguide modulators.. As-grown AlGaAs/GaAs p-i-n waveguide structures (see Fig. 1) exhibit soft lateral optical confinement because of the smooth decrease of the thickness towards the edges of the structure. Furthermore, the capacitance of the device is reduced due to the selective doping of the structure. As a result, only the center region of the device contributes to the capacitance which makes higher RC-time constants possible. We demonstrate first results on ESM-MBE grown waveguide and waveguide modulator structures. The modulator shown in Fig. 2 exhibits a modulation contrast of more than 30 dB (for a 900  $\mu\text{m}$  long device) for reasonably low voltage swings. Propagation losses are fairly low in this structure ( $< 11$  dB/cm) and mainly due to free carrier absorption in the waveguide region.

[1] K.H. Gulden et al., Appl. Phys. Lett. **62**, 3180 (1993)

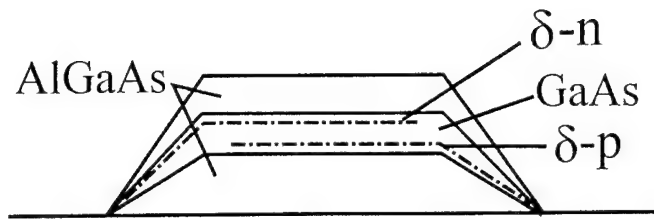
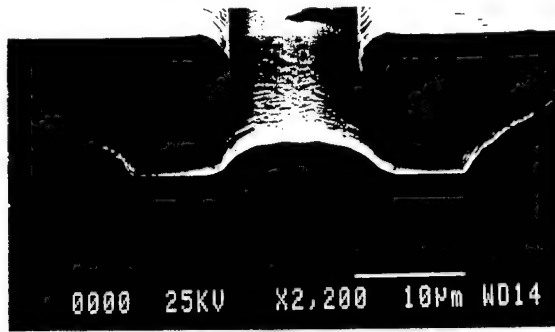


Fig. 1: Scanning electron microscope (SEM) photograph and cross-section of a ESM-MBE grown GaAs/AlGaAs p-i-n waveguide structure.

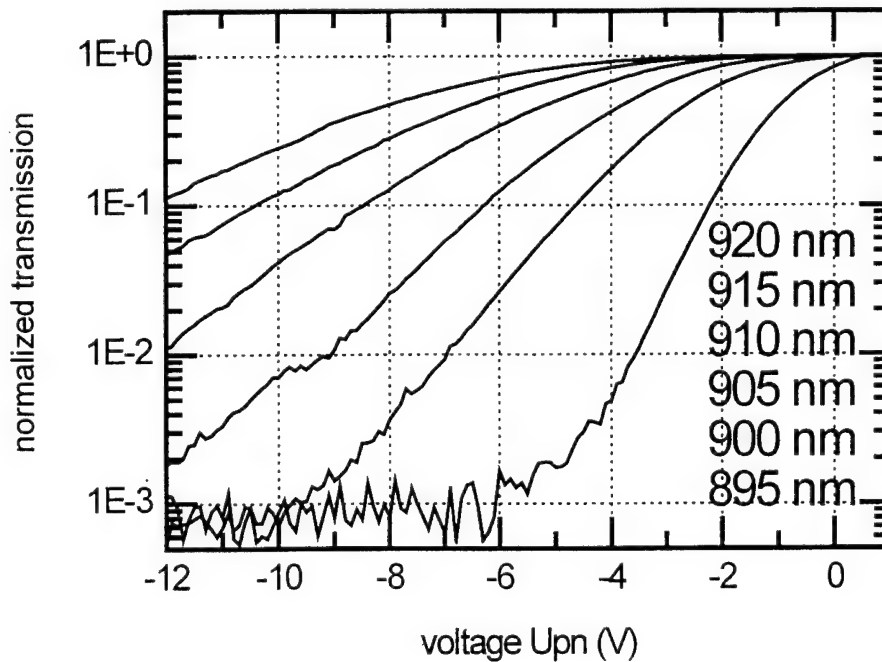


Fig.2: Transmission changes for different wavelengths in a 900  $\mu\text{m}$  long waveguide structure grown by the ESM-MBE technique. A switching contrast of more than 30 dB has been achieved.



# A New P-Type Compressively Strained Layer InGaAs/AlGaAs/GaAs Miniband Transport Quantum Well Infrared Photodetector for Long Wavelength Infrared Detection

Sheng S. Li and J. Chu  
Dept. of Electrical & Computer Engineering  
University of Florida  
Gainesville, FL 32611-6200  
Tel/Fax: 352-392-4937  
E-mail: Shengli@eng.ufl.edu

Pin Ho  
Lockheed Martin Electronics Laboratory  
Syracuse, NY 13221

III-V semiconductor quantum well infrared photodetectors (QWIPs) based on intersubband transition schemes for detection in the 3-5  $\mu\text{m}$  (MWIR) and 8-14  $\mu\text{m}$  (LWIR) atmospheric spectral windows have been extensively investigated in recent years[1-2]. However, most of the works reported are based on n-type QWIPs grown by MBE technique, which require metal or dielectric grating to couple normal incidence IR radiation into the quantum wells. Recently, we have reported two normal incidence p-type strained layer QWIPs using InGaAs/GaAs InGaAs/InAlAs material systems, which showed significant enhancement in intersubband optical absorption and reduction of the dark current in these devices. [3-4] In this work we report a new normal incidence p-type compressively strained layer bound-to-miniband (BTM) transition InGaAs/GaAs/AlGaAs QWIP for LWIR detection. The Be-doped InGaAs/GaAs/AlGaAs BTM QWIP was grown on semi-insulating (100) GaAs with 20 periods of 9.0 nm InGaAs quantum well and 2.7 nm GaAs/2.0 nm AlGaAs (10 periods) superlattice barrier layer. The detector exhibits a detection peak at 10.4  $\mu\text{m}$  with a full width half maximum spectral bandwidth that extends from 9 to 12  $\mu\text{m}$  and a measured peak responsivity of 28 mA/W at  $T = 65$  K and  $V_b = 3$  V. The device is under background limited performance (BLIP) for  $T \leq 40$  K and  $V_b \leq 2$  V. The schematic energy band diagram for this QWIP structure is shown in figure 1 along with an illustration of intersubband transition. Figure 2(a) shows the measured dark I-V characteristics as a function of applied bias and temperature, with the 300 K background photocurrent superimposed. Figure 2(b) illustrates the responsivity as a function of incident radiation wavelength at  $T = 40$  K and  $V_b = 2$  V. Results of a two-color p-type strained layer InGaAs/AlGaAs stacked QWIP for MWIR and LWIR two band detection will also be depicted in this paper.

## References:

1. B. F. Levine, J. Appl. Phys., **74**(8), R1 (1993).
2. L. S. Yu, S. S. Li, and P. Ho, Appl. Phys. Lett., **59**, 2712 (1991).
2. Y. H. Wang, J. Chu, S. S. Li, and P. Ho, J. Appl. Phys., **76**(10), 6009 (1994).
3. J. Chu, S. S. Li, Y. H. Wang, and P. Ho, ECS Proc. **95-28**, 126 (1995).

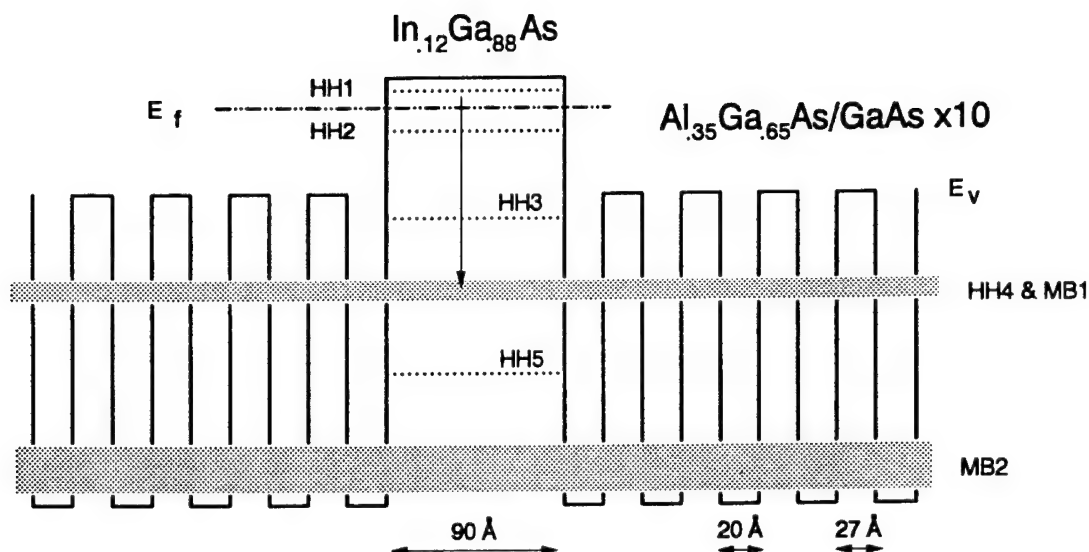


Figure 1. Schematic Energy Band Diagram and Intersubband Transition.

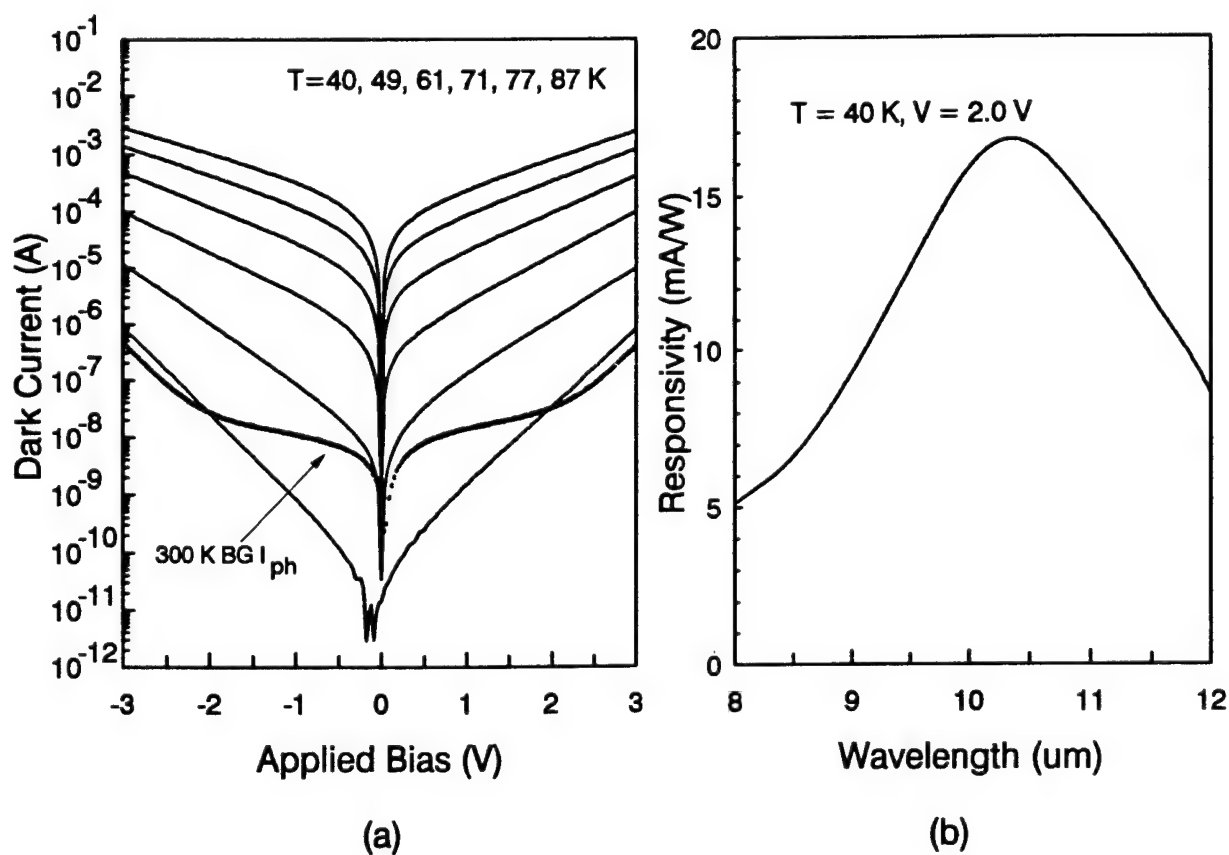


Figure 2. (a) Dark I-V and (b) Responsivity of the p-type CSL QWIP.

## Large Array of GaAs Modulators and Detectors Flip-Chip Solder Bonded to Silicon CMOS using InGaP as the Selective Etch Stop for GaAs Substrate Removal

J. M. Kuo<sup>1,\*</sup>, Y. C. Wang<sup>1,5</sup>, K. W. Goossen<sup>2</sup>, L. M. F. Chirovsky<sup>1</sup>, S. P. Hui<sup>1</sup>, B. T. Tseng<sup>1</sup>, J. Walker<sup>2</sup>, A. L. Lentine<sup>3</sup>, R. E. Leibenguth<sup>4</sup>, G. Livescu<sup>1</sup>, W. Y. Jan<sup>2</sup>, J. E. Cunningham<sup>2</sup>, L. A. D'Asaro<sup>1</sup>, D. Dahringer<sup>1</sup>, D. Kossives<sup>1</sup>, D. D. Bacon<sup>1</sup>, R. L. Morrison<sup>3</sup>, R. A. Novotny<sup>3</sup>, D. B. Buchholz<sup>3</sup>

Lucent Technologies

[1] Murray Hill, NJ 07974, [2] Holmdel, NJ 07733, [3] Naperville, IL 60566, [4] Breinigsville, PA 18031

\* Tel: (908) 582-3416, FAX: (908) 582-3901, E-mail: jmkuo@physics.att.com

W. E. Mayo

[5] Department of Mechanics and Materials Science, Rutgers University, Piscataway, NJ 08855

The integration of III-V optical interconnections onto silicon VLSI has attracted considerable effort recently, because it can alleviate the communication bottleneck that exists in today's large electronic switching and computing systems. A particular attractive approach is to integrate the III-V optical detectors and modulators as the surface normal optical input and output (I/O) devices directly onto the silicon electronic circuitry. The flip-chip solder bump bonding technique offers a promising solution to achieve this goal.

Recently, flip-chip solder bump bonding of GaAs/AlGaAs MQW detector/modulator diodes on silicon IC's has been demonstrated by Goossen et. al.<sup>1</sup> In that process, after flip-chip bonding, the GaAs substrate was removed with a selective etch to provide optical access to the individual diodes. A 1.5  $\mu\text{m}$  thick  $\text{Al}_{0.3}\text{Ga}_{0.7}\text{As}$  was used as the etch stop for substrate removal where the GaAs substrate was etched away by a jet etcher with a 1:100  $\text{NH}_4\text{OH}:\text{H}_2\text{O}_2$  etchant. The low etching selectivity between GaAs and  $\text{Al}_{0.3}\text{Ga}_{0.7}\text{As}$  limited the size of the GaAs chip for successful substrate removal. In this talk, we present the integration of a large (64x68) GaAs/AlGaAs modulators/detectors array to a silicon CMOS chip, using flip-chip solder bump bonding techniques together with a new concomitant GaAs substrate removal method which solve the problems. The circuit, which consists of an array of 16x1 switching nodes, has 4096 optical detectors and 256 optical modulators and over 140K silicon CMOS transistors. The physical size of the GaAs detector/modulator chip is 6.2 mm x 6.2 mm. The capability of removing such a relatively large area of GaAs substrate cleanly and uniformly is attributed to the introduction of a new  $\text{In}_{0.49}\text{Ga}_{0.51}\text{P}$  selective etch stop layer in the epilayer structure. The presence of the  $\text{In}_{0.49}\text{Ga}_{0.51}\text{P}$  selective etch stop layer has no detrimental effect on the performance of the GaAs/AlGaAs optical detector/modulator diodes as compared to the best performance of an otherwise identical structure with an  $\text{Al}_{0.3}\text{Ga}_{0.7}\text{As}$  etch stop. The uniformity of the epitaxial growth and fabrication process is demonstrated through the virtually identical photocurrents measured from the center to the edge of a 2" wafer. All but 2 of the 4352 multiple quantum well diodes generate photocurrent in response to light. Switching nodes have been tested at data rates above 400 Mb/s per channel. System operation from 155Mb/s-208 Mb/s has been demonstrated using this chip.

1. K. W. Goossen et. al., IEEE Photon. Technol. Lett. 7, 360 (1995).

## POSTER SESSION P1. III-V GROWTH ISSUES

**P1.1 Control of chemical composition and energy bandgap in  $\text{Ga}_x\text{In}_{1-x-y}\text{Al}_y\text{As}$  on InP during molecular beam epitaxy**, J.M. Schneider, J.-T. Pietralla, J. Ziegler, and H. Heinecke, University of Ulm, Germany

**P1.2 Growth and transformation of InAs/InP ultra-thin layers obtained by chemical beam epitaxy**, N. Lebouché-Girard, A. Rudra and E. Kapon, Ecole Polytechnique Fédérale de Lausanne, Switzerland

**P1.3 The growth of AlGaAs-InGaAs quantum well structures: first observation of critical interdependent effects utilizing a design of experiments approach**, Robert N. Bicknell-Tassius, Kyeong Lee, April Brown, Georgianna Dagnall, and Gary May, Georgia Institute of Technology, Atlanta, Georgia, USA

**P1.4 Properties of InAs thin films grown on (100)-oriented GaAs substrate with various tilted angles and directions**, Masaki Yamamoto, Tatsuro Iwabuchi, Takashi Ito, Takashi Yoshida, Hideaki Imai, Toshiro Isoya, and Ichiro Shibasaki, Asahi Kasei Electronics Co., Ltd., Fuji, Shizuoka, Japan

**P1.5 Carbon doping and delta doping in GaAs/AlGaAs for DBR applications**, T.B. Joyce and T.J. Bullough, The University of Liverpool, England, United Kingdom

**P1.6 Modulated beam studies of kinetics in GaAs (001) etching using  $\text{AsBr}_3$** , J. Zhang, O.P. Naji, P. Steans, P. Tejedor, T. Kaneko, T.S. Jones, and B.A. Joyce, Imperial College of Science, Technology and Medicine, London, England, United Kingdom

**P1.7 Stoichiometric low temperature (SLT) MBE GaAs and related compounds: structural, electrical and optical properties**, M. Missous and S. O'Hagan, UMIST, England, United Kingdom

**P1.8 Molecular beam epitaxial growth of bicrystalline metallic lateral superlattices**, Magali Sussiau, Frédéric Nguyen-Van-Dau, Pierre Galtier and A. Schuhl, Thomson CSF-LCR, Orsay, France

**P1.9 Passivation of misfit dislocations by atomic hydrogen irradiation**, M. Yokozeki, H. Yonezu, T. Tsuji, K.J. Lee, Y. Fujimoto and N. Ohshima, Toyohashi University of Technology, Japan

**P1.10 Morphology of MBE grown InAs films studied by atomic force microscope**, Y. Wang, Y.N. Sheng, Weikun Ge, Jiannong Wang, and L.L. Chang, Hong Kong University of Science & Technology, Japan

**P1.11 Carbon doping of molecular beam epitaxial GaAs (111) films using carbon tetrabromide**, D.H. Tomich, N.Y. Li and C.W. Tu, University of California, San Diego, USA

**P1.12 Formation of an n-GaAs/n-GaAs regrowth interface without carrier depletion using electron cyclotron resonance hydrogen plasma**, Takaki Niwa, Naoki Furuhashi, and Tadashi Maeda, NEC Corporation, Ibaraki, Japan

**P1.13 Continuously graded buffers for InGaAs/GaAs structures grown on GaAs**, A. Bosacchi, A.C. De Riccardis, S. Franchi, C. Ferrari, S. Gennari, L. Lazzarini, L. Nasi, and G. Salvati, Padova University, Italy

**P1.14 Growth dynamics of InGaAs/GaAs by MBE**, Françoise Fournier, April S. Brown, Carrie A. Carter-Coman, Robert A. Metzger, Alan Doolittle, Nan Marie Jokerst and Robert Bicknell-Tassius, Georgia Institute of Technology, Atlanta, Georgia, USA

**P1.15 Transient surface state during the CBE growth of GaAs**, T. Farrell, D. Hill, T.B. Joyce, T. J. Bullough and P. Weightman, The University of Liverpool, England, United Kingdom

**P1.16 MBE&E: MBE and/or etch**, K.R. Evans, J.E. Ehret, E.N. Taylor, C.R. Jones, D. Via, and R. Kaspi, Wright State University, Dayton, Ohio, USA

**P1.17 Effect of GaAs substrate properties on optical bandgap thermometry**, S.R. Johnson and T. Tiedje, University of British Columbia, Vancouver, British Columbia, Canada

**P1.18 Organized growth of GaAs/AlAs lateral superlattices on vicinal surfaces: where are the limits?**, F. Laruelle, F. Lelarge, F. Petit, T. Mélin and A. Cavanna, Laboratoire de Microstructures et de Microélectronique, Bagneux Cedex, France

**P1.19 Formation of multi-atomic steps and a novel n-AlGaAs/GaAs heterojunctions on a vicinal (111)B substrate by MBE and anisotropic transport of 2D electrons**, Y. Nakamura, S. Koshiba, and H. Sakaki, University of Tokyo, Japan

**P1.20 Be redistribution in InGaAs and InP grown by gas source molecular beam epitaxy**, Teruo Mozume, Kazuhiko Hosomi, Hitachi, Ltd., Tokyo, Japan

**P1.21 A Monte Carlo study of gallium desorption kinetics during MBE of (100)-GaAs/AlGaAs heterostructures**, K. Mahalingam, D. L. Dorsey, K. R. Evans, R. Venkatasubramanian, Wright Patterson Air Force Base, Ohio, USA

**P1.22 High temperature surface cleaning of AlGaAs without as flux for MBE regrowth**, K. Iizuka, K. Matsumaru, T. Suzuki, Y. Takahira, T. Nishioka, and H. Okamoto, Nippon Institute of Technology, Saitama, Japan

**P1.23 Evolution of short- and long-range order during Si incorporation on GaAs(100) observed by RAS and RHEED during MBE**, L. Däweritz, K. Stahrenberg, P. Schützendübe, J.-Th. Zettler, W. Richter, K. H. Ploog, Paul-Drude-Institut für Festkörperelektronik, Berlin, Germany

**P1.24 Evidence for mass exchange between 2- and 3- dimensional surface features during evolution of coherent strained 3D InAs islands on GaAs(100)**, T.R. Ramachandran, N.P. Kobayashi, W. Yu, P. Chen, and A. Madhukar, University of Southern California, Los Angeles, California, USA

**P1.25 MBE growth of two-dimensional electron gases on (110) GaAs**, C. B. Sørensen, H. Gislason and J.M. Hvam, University of Copenhagen, Denmark

**P1.26 Heuristic Rules for Group IV dopant site selection in III-V compounds**, R. Venkatasubramanian, Donald L. Dorsey, K. Mahalingam, University of Nevada, Las Vegas, Nevada, USA

**P1.27 Spreading of Si by surface segregation in  $\delta$ -doping of MBE grown  $\text{In}_{0.53}\text{Ga}_{0.47}\text{As}$** , E. Skuras, B. Vögele, A.R. Long, M.C. Holland, E.A. Johnson, C.R. Stanley, University of Glasgow, United Kingdom

**P1.28 Growth and physics of strongly coupled ultra high mobility p-type double quantum wells showing correlated  $\nu=1$  quantum hall and insulating states**, M. Henini, R.J. Hyndman, T. Ihn, B.L. Gallagher, P.J. Rodgers, J.R. Middleton, J. Chauhan and T.J. Foster, University of Nottingham, United Kingdom

**P1.29 Growth temperature-dependent conduction-type inversion of C-doped InGaAs grown by chemical beam epitaxy**, Jeong-Rae Ro, Sung-Bock Kim, Seong-Ju Park, and El-Hang Lee, Kwangju Institute of Science and Technology, Korea

**P1.30 Growth and Characterization of  $\text{In}_x\text{Ga}_{1-x}\text{As}$  ( $x \geq 0.65$ ) heterostructures on GaAs by molecular beam epitaxy using  $\text{In}_x(\text{AlGa})_{1-x}\text{As}$  graded buffer**, S.M. Wang, C. Karlsson, N. Rorsman, M. Bergh, E. Olsson, H. Zirath and T.G. Andersson, Chalmers University of Technology, Göteborg, Sweden

**P1.31 2D-limitations when increasing the Si-concentration from delta-doping to thin Si-layers in GaAs**, T.G. Anderson, NTT Basic Research Laboratories, Atsugi-shi, Kanagawa 243-1, Japan

**P1.32 The building up of terrace and atomic periodicity by MBE growth on (001) vicinal surfaces**, F. LeLarge, Z.Z. Wang, F. Laruelle, and B. Etienne, Laboratoire de Microstructures et de Microelectronique, C.N.R.S., Bagneux Cedex, France.

## Control of chemical composition and energy bandgap in $\text{Ga}_x\text{In}_{1-x-y}\text{Al}_y\text{As}$ on InP during molecular beam epitaxy

J.M. Schneider, J.-T. Pietralla, J. Ziegler and H. Heinecke

Department of Semiconductor Physics, University of Ulm, D-89069 Ulm, Germany

Tel: +49-731-502-6101 Fax: +49-731-502-6108 e-mail: heinecke@sunrise.e-technik.uni-ulm.de

Although  $\text{Ga}_x\text{In}_{1-x-y}\text{Al}_y\text{As}$  has become an attractive material for photonic device applications a significant scatter in the data of the energy bandgap  $E_g$  on the material composition is reported. For the quaternary material lattice matched to InP a linear interpolation between the ternary compounds  $\text{Ga}_{0.47}\text{In}_{0.53}\text{As}$  and  $\text{Al}_{0.48}\text{In}_{0.52}\text{As}$  with rising Aluminium content  $y$  is observed for the photoluminescence (PL) both at room temperature (RT) and at 4.2 K [e.g. 1,2]. On the other hand a bowing relationship for  $E_g$  with rising  $y$  is described [e.g. 3,4]. In addition for the energy bandgap of  $\text{Ga}_x\text{In}_{1-x}\text{As}$  and  $\text{Al}_y\text{In}_{1-y}\text{As}$  various data are reported.

A target of this investigation was to produce by molecular beam epitaxy (MBE) well defined  $\text{Ga}_x\text{In}_{1-x-y}\text{Al}_y\text{As}$  samples concerning the chemical composition and then to evaluate the energy bandgap by PL.

Hence we started first of all a systematic study of the optical properties of these ternaries and quaternaries grown on InP by solid source MBE. We have optimized the growth parameters to obtain high optical quality for both  $\text{Ga}_x\text{In}_{1-x}\text{As}$  [5] and  $\text{Al}_y\text{In}_{1-y}\text{As}$ , respectively. These results formed the basis and the reference for the growth of  $\text{Ga}_x\text{In}_{1-x-y}\text{Al}_y\text{As}$  on InP. The quaternary layers are produced by the *simultaneous growth of the ternaries*  $\text{Ga}_x\text{In}_{1-x}\text{As}$  (with growth rate  $r_1$ ) and  $\text{Al}_y\text{In}_{1-y}\text{As}$  ( $r_2$ ) using two Indium cells, one Gallium and one Aluminium cell. The growth rates are evaluated by high accuracy (0.3 %) layer thickness measurements. The chemical composition of the  $\text{Ga}_x\text{In}_{1-x-y}\text{Al}_y\text{As}$  layer is then determined by the ratio of the ternary growth rates ( $r_1/r_2$ ). The linear superposition of the ternary rates with a predictable composition of the quaternary layer is expected if the growth is performed below the Indium desorption region ( $T \leq 520^\circ\text{C}$ ).

We calculated the ( $\text{Al}_{0.48}\text{In}_{0.52}\text{As}$ ) fraction  $z = r_2/(r_1+r_2)$  in the quaternary layers which corresponds to  $y$  via  $y = 0.48 \cdot z$  ( $0 \leq z \leq 1 \Leftrightarrow 0 \leq y \leq 0.48$ ). The  $\text{Ga}_x\text{In}_{1-x-y}\text{Al}_y\text{As}$  layers are characterized by low temperature (4.2 K) as well as by RT-PL. High Resolution X-Ray Diffraction measurements are only used to control the linear superposition of  $\Delta d/d$  of both ternaries. Fig. 1 and 2 show the energy of the maximum PL intensity  $E_{g,PL}$  versus  $z$  in the quaternary layer for RT and 4.2 K. For both temperatures we find a linear dependence of the PL maximum on  $z$ . The data at 4.2 K are slightly shifted towards higher energies compared to the linear relationship found by Kopf et al. [1]. Our calculated linear fit for the quaternary data points is almost identical with the linear interpolation between our  $\text{Ga}_{0.47}\text{In}_{0.53}\text{As}$  and  $\text{Al}_{0.48}\text{In}_{0.52}\text{As}$  data.

On the basis of these results an equation system for the precise composition  $x, y$  of the quaternary layer in dependence of the maximum of the PL intensity and the lattice mismatch  $\Delta d/d$  was worked out. This knowledge was used to adjust the composition of quaternary layers for the growth of 1.55  $\mu\text{m}$  laser structures.

- [1] R.F. Kopf, H.P. Wei, A.P. Perley, G. Livescu, Appl. Phys. Lett. 60 (1992) 2386
- [2] T. Fujii, Y. Nakata, Y. Sugiyama, S. Hiyamizu, Jpn. J. Appl. Phys. 25 (1986) L254
- [3] J. Böhrer, A. Krost, D.B. Bimberg, Appl. Phys. Lett. 63 (1993) 1918
- [4] D. Olego, T.Y. Chang, E. Siiberg, E.A. Caridi, A. Pinczuk, Appl. Phys. Lett. 41 (1982) 476
- [5] M. Popp, M. Schiefele, M. Hurich, M. Wachter, J.M. Schneider, B. Marheineke, H. Heinecke, J. Cryst. Growth 150 (1995) 528

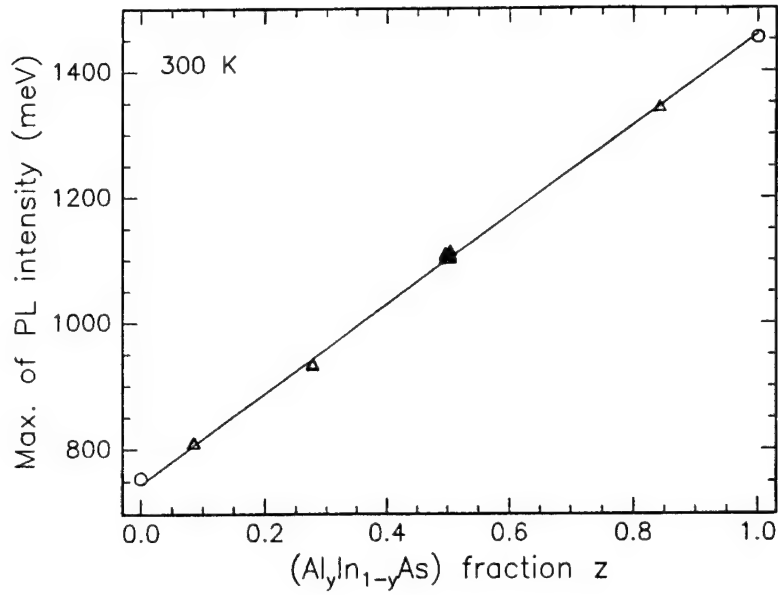


Fig.1: Maximum of the PL intensity at room temperature plotted vs. the (Al<sub>0.48</sub>In<sub>0.52</sub>As) fraction  $z = r_2/(r_1+r_2)$  in the quaternary layer.

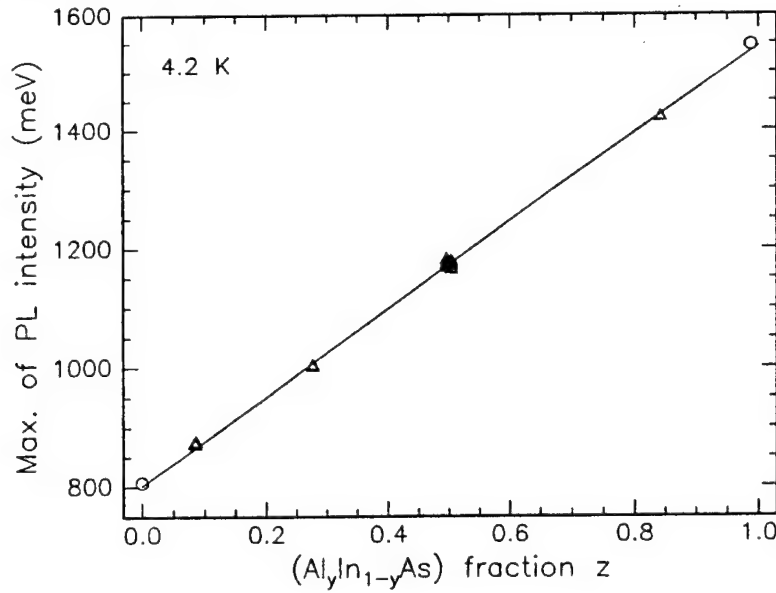


Fig.2: Maximum of the PL intensity at 4.2 K plotted vs. z.

Equation 1:  $x$  and  $y$  in  $\text{Ga}_x\text{In}_{1-x-y}\text{Al}_y\text{As}$  as function of  $\Delta d/d$  and  $E_{g,PL}$ .  $A, B, C$  are fit parameters worked out from the data of Fig 1 or 2.

$$x = \frac{E_{g,PL}(T) - A + (A - C) \cdot y}{B - A}$$

$$y = \frac{0.5 \cdot a_{InP} \left( \frac{\Delta d}{d} \right)_{exp} - \frac{(a_{GaAs} - a_{InAs})(E_{g,PL}(T) - A)}{B - A} - a_{InAs} + a_{InP}}{(A - C)(a_{GaAs} - a_{InAs}) + a_{AlAs} - a_{InAs}}$$

# Growth and transformation of InAs/InP ultra-thin layers obtained by Chemical Beam Epitaxy

N. Lebouché-Girard, A. Rudra and E. Kapon

Institut de Micro et Optoélectronique, Ecole Polytechnique Fédérale de Lausanne,  
CH-1015 Lausanne, Switzerland  
phone: 41 21 693 39 89, fax: 41 21 693 54 90, email: Rudra@eldp.epfl.ch

We have observed by Atomic Force Microscopy (AFM) the surface of InP and InAs/InP epilayers grown by Chemical Beam Epitaxy using trimethylindium, arsine and phosphine. We show the influence of the substrate miscut and the InAs layer thickness on the surface structure and its evolution under arsine anneal.

A 500nm thick InP buffer layer was grown at  $1\mu\text{m/h}$  at  $520^\circ\text{C}$  on exactly (100) oriented InP substrates as well as on substrates with slight misorientations ( $0.2, 0.4, 0.6, 0.8^\circ$ ) towards (111)A. The growth was followed by a 5' phosphine anneal. On the exactly oriented substrate, an atomically smooth surface with large terraces was obtained, while an array of steps oriented along  $\langle 1-10 \rangle$  was observed on the misoriented substrates, typical of a step flow growth mode. Step bunching was observed only on the substrate with a  $0.8^\circ$  miscut.

In a first set of experiments, one and two monolayers thick InAs layers were grown on an InP buffer obtained on an exactly oriented substrate. The layer was then annealed under cracked arsine. In all cases, the surface presents a high density of elongated tridimensional boxes. With increasing anneal time, the island size increases and their density decreases through coalescence. Fig. 1 shows the surface obtained after a 1mn arsine anneal of a 2 ml thick InAs layer. The box density is about  $6 \cdot 10^9 \text{ cm}^{-2}$  and their average length, width and height are 1150Å, 620 Å and 30Å respectively. This is understood as follows: while it is possible to grow a 2 monolayers thick InAs layer on InP in a quasi-bidimensional mode, the resulting film is in a metastable state, due to the lattice mismatch (3.5%) between InAs and InP. Annealing under  $\text{As}_2$  induces the formation of tridimensional structures. This is consistent with the RHEED observations reported previously, as well as with the photoluminescence spectra of ultra-thin InAs/InP quantum wells obtained with different growth interruptions [1].

In a second set of experiments, submonolayer InAs films were simultaneously deposited on an exactly oriented sample as well as on a sample with a  $0.8^\circ$  miscut. On the exactly oriented substrate, there is no dot formation. The 0.3ml film can be distinguished from the InP buffer background as it is composed of bidimensional islands which are typical on an incomplete layer (fig. 2). The situation is strikingly different on the misoriented surface, where dots are formed on the multiple steps which behave as preferential migration sites. These dots have an average width of 380Å and an average height of 27Å (fig. 3). When the InAs layer thickness is increased, the islands elongate along the steps, forming small segments which eventually merge into wires when the InAs layer thickness exceeds 0.6 ml (fig. 4).

[1] J.F. Carlin, R. Houdré, A. Rudra and M. Illegems, Appl. Phys. Lett. Vol.59, No. 23, 1991



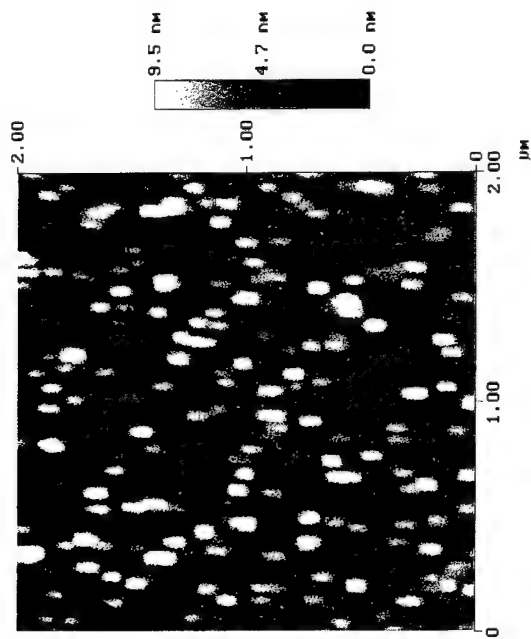


Fig. 1 : AFM image of a 2 ml thick InAs film after  $\text{As}_2$  anneal (exactly oriented substrate)

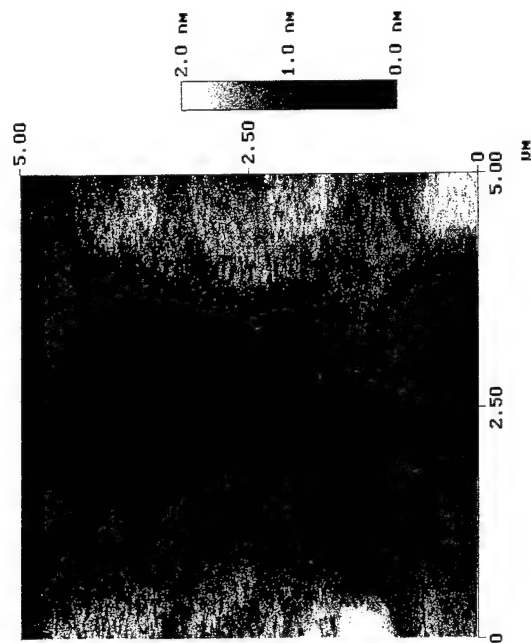


Fig. 2 : AFM image of a 0.3 ml InAs film after  $\text{As}_2$  anneal (exactly oriented substrate)

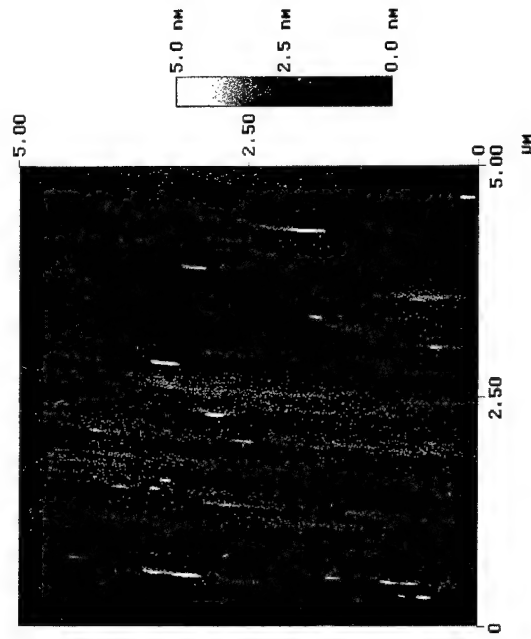


Fig. 3 : AFM image of a 0.3 ml thick InAs film after a 1'  $\text{As}_2$  anneal ( $0.8^\circ$  off substrate)

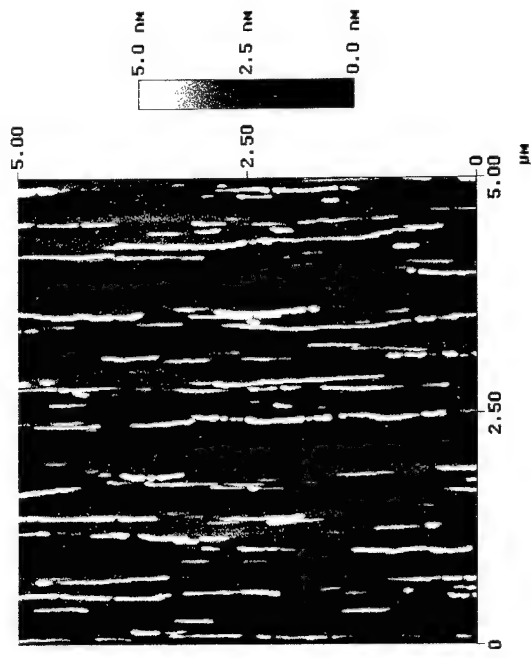


Fig. 4: AFM image of a 0.6 ml InAs film after a 1'  $\text{As}_2$  anneal ( $0.8^\circ$  off substrate)

## The Growth of AlGaAs-InGaAs Quantum Well Structures: First Observation of Critical Interdependent Effects Utilizing a Design of Experiments Approach

Robert N Bicknell-Tassius\*, Kyeong Lee, April Brown, Georgianna Dagnall, and Gary May  
School of Electrical Engineering and Computer Science

Georgia Tech Research Institute\*

Georgia Institute of Technology

Atlanta, GA 30332-0250

(P: (404) 894-9885, F: (404) 894-0222, email:rb91@prism.gatech.edu)

The traditional approach to determining relationships between growth conditions and material properties has rested on the standard experimental approach- varying one factor while holding the others constant. This technique does not effectively allow the observation of important interactions in device structures, for example, growing high quality AlGaAs requires high substrate temperature, unless other parameters are important, such as the minimization of dopant diffusion, which require low substrate temperature.

We have utilized Design of Experiment (DOE) (Resolution IV,  $2^{6-2}$  fractional factorial experiments with 16 trials) techniques to ascertain important interactions in AlGaAs-InGaAs single quantum well structures. *We observe interactions which have never been quantified before. In addition, we show, for the first time, the importance of effective oxide removal techniques for the growth of high quality structures.* These results clearly show that the optimum growth conditions are interdependent.

We varied the following factors for the sixteen runs: oxide removal temperature (etched substrates) from 580°C to 650°C; oxide removal time from 30 to 300 s; AlGaAs substrate temperature from 580°C to 630°C; InGaAs substrate temperature from 450°C to 520°C; As<sub>4</sub> by a factor of two; and heterostructure interrupt time from 30 to 90s. It is important to note that the oxide removal was complete as determined by RHEED observations for all of the temperature and time conditions.

We measured the defect density, AlGaAs structural and optical quality, and InGaAs optical quality by photoluminescence and double crystal X-Ray diffraction, and utilized SIMS to measure profiles of constituents and contaminants, such as oxygen and carbon. The chosen factors all affect the data, and large variations in materials properties were observed, for example, the defect density varied by one order of magnitude, the AlGaAs PL FWHM (full width at half maximum) varied by a factor of six, the AlGaAs X-Ray FWHM varied by a factor of two, and the InGaAs PL FWHM varied by a factor of six.

Some examples of determined effects are summarized. All of the factors were significant for the defect density. The AlGaAs quality (both X-Ray and PL) were most significantly affected by the oxide removal conditions. The InGaAs quantum well PL was most significantly affected by the InGaAs growth temperature and As<sub>4</sub> overpressure, as is expected. Important interactions between oxide removal conditions, AlGaAs growth conditions and InGaAs growth conditions are quantified. The interpretation of these interactions are upheld by the large variations in oxygen at the substrate-epitaxial film interface, in the AlGaAs, and in the quantum well. These interactions show that each effect is interrelated, for example to minimize the InGaAs PL FWHM, use a high AlGaAs substrate temperature if the oxide removal temperature is low, or a low AlGaAs growth temperature if the oxide removal temperature is high.

In summary, we have observed and quantified significant interactions in the growth of AlGaAs-InGaAs quantum well structures. We show that the DOE approach is an efficient means for optimizing growth conditions for a given device structure. In addition, we quantify, for the first time, important interactions between oxygen and AlGaAs and InGaAs growth conditions.

# Properties of InAs thin films grown on (100)-oriented GaAs substrate with various tilted angles and directions

Masaki Yamamoto, Tatsuro Iwabuchi, Takashi Ito, Takashi Yoshida,

Hideaki Imai\*, Toshiro Isoya, Ichiro Shibasaki\*

Asahi Kasei Electronics Co., Ltd.

Asahi Chemical Industry Co., Ltd.\*

2-1, Samejima, Fuji-city, Shizuoka 416, JAPAN

Tel: +81-545-62-3400 Fax: +81-545-62-3419

e-mail: a7410212@ut.asahi-kasei.co.jp

## Introduction

InAs thin film is promising material for magnetic sensor such as Hall elements because of high sensitivity and wide operation temperature. We studied InAs Hall elements fabricated from epitaxially grown InAs thin film on (100)-GaAs substrate by MBE<sup>1)</sup>. By doping n-type Si impurities, InAs thin films have both high electron mobility and electrical properties with small temperature dependence, which are important for magnetic sensor<sup>2)</sup>. For this purpose, we grew Si-doped InAs thin films on (100)-GaAs surface with various tilted angles and directions.

In this paper, we studied the dependence of surface morphologies and sheet carrier density of epitaxially grown InAs thin film on (100)-GaAs substrate with various tilted direction and tilted angle of misorientation, and also studied a relation between the tilted directions and one of the device properties i.e. offset voltage of Hall elements. We found a strong dependence of the offset voltage to the tilted direction of the GaAs substrate at definite misorientation direction. This results were applied to fabrication of practical InAs Hall elements by MBE process.

## Experiments and Results

InAs thin films were grown on semi-insulating (100)-GaAs substrate with 2° off with various tilted directions shown in Fig.1, thus, tilted toward [0-10] (named A-direction shown in Fig.1), toward [00-1] (D-direction), toward [0-1-1] (E-direction), and toward [01-1] (H-direction), under the standard growth condition. The substrate temperature is around 480°C and the growth rate is approximately 1.0  $\mu$ m/hour.

The Nomarski interference microscope photographs of surface morphologies of InAs thin films are shown in Fig. 3. The structures of surface morphologies of InAs thin films were different for the tilted directions of (100)-GaAs surface. The difference of surface morphologies is observed for two similar directions at the same misorientation such as A-direction and D-direction, where these two tilted directions are at right angle each other. Fig. 4 shows the difference of properties of the InAs thin films with various tilted angles and directions. The electron density and mobility depend on tilted directions from (100)-GaAs surface. The InAs thin film grown on (100)-GaAs surface with no misorientation is the largest electron density and highest mobility.

The offset voltage is important for Hall elements. We measured the offset voltage of InAs Hall elements with symmetrical cross pattern shown in Fig.2. As shown in Table 1, the smallest offset voltage was observed for the (100)-GaAs surface with E-direction.

Our Si-doped InAs Hall element, which has already been commercially available, is one of the successful MBE applications. It is found that the characteristics of the InAs Hall elements is dependent on the tilted angles and directions of the GaAs substrate. These results are important for fabrication of practical InAs Hall elements.

## References

- 1) I. Shibasaki, Y. Kanayama, K. Nagase, T. Ito, F. Ichimori, T. Yoshida, K. Harada, Digest of Technical Papers, Transducers'91, p. 1069 (1991)
- 2) T. Iwabuchi, T. Ito, M. Yamamoto, K. Sako, Y. Kanayama, K. Nagase, T. Yoshida, F. Ichimori, I. Shibasaki, J. Crystal Growth, 150, 1302 (1995)

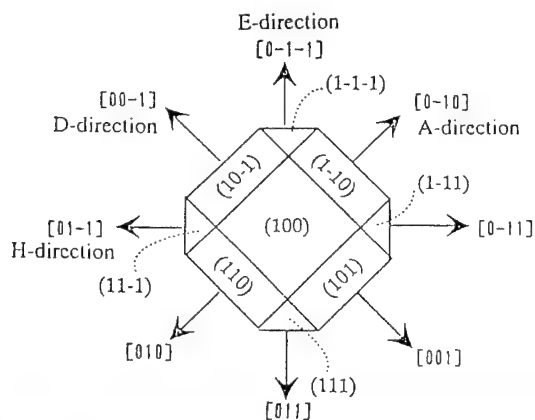


Fig.1 The various tilted directions of misorientation

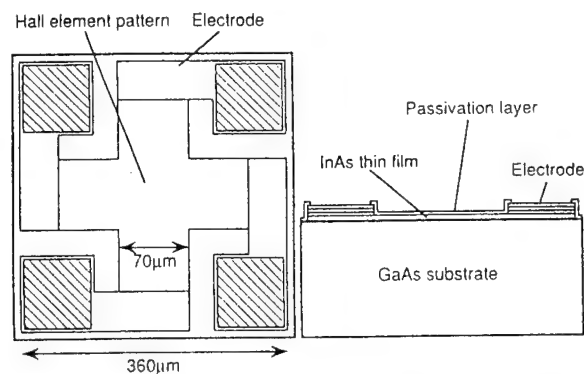


Fig.2 Structure of the InAs Hall element chip

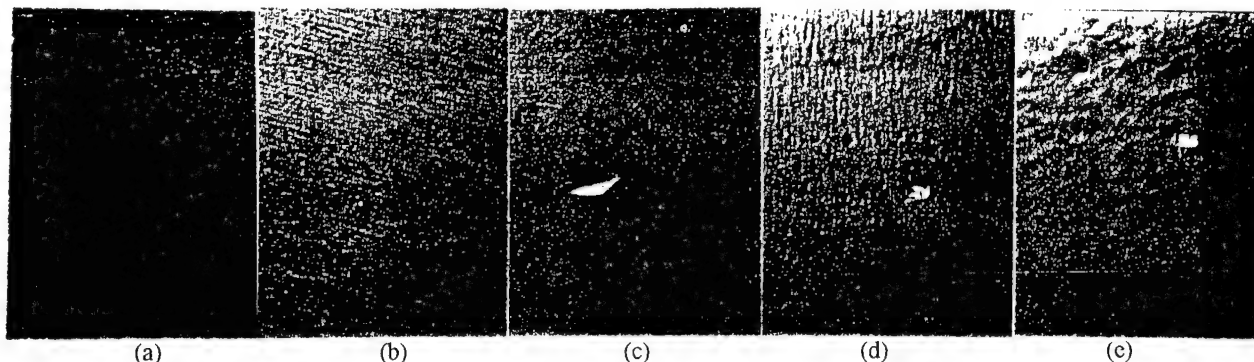


Fig.3 The Nomarski interference microscope photographs of surface morphologies of InAs thin films grown on (100)-oriented GaAs with various tiled directions (a) toward  $[0-10]$ , (b) toward  $[00-1]$ , (c) toward  $[0-1-1]$ , (d) toward  $[01-1]$  and (e) no misorientation

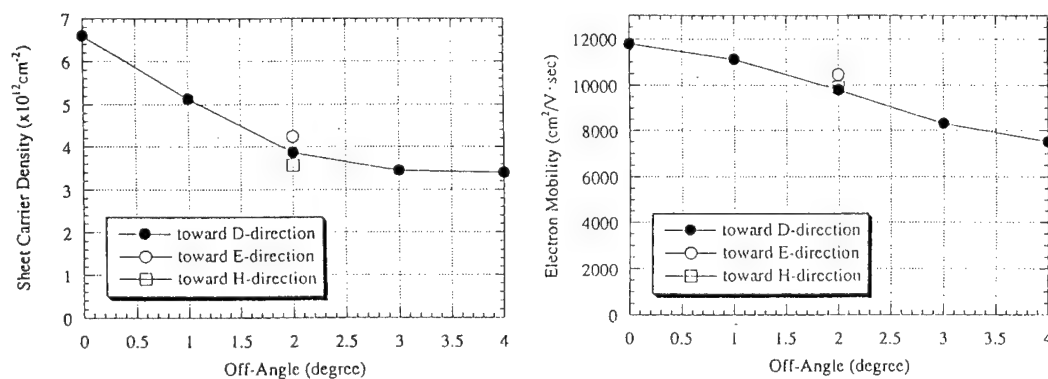


Fig.4 Properties of InAs thin films grown on GaAs substrates with various tilted angles and tilted directions of misorientation by MBE

Table.1 The offset voltage of Hall elements fabricated from the InAs thin films grown on (100)-oriented GaAs substrate with various tilted directions

The tilted direction of misorientation	Offset voltage $V_u$ Ave. $\pm \sigma$ (mV/Vin=3V)
$[0-10]$ (A-direction)	$-5.20 \pm 0.96$
$[00-1]$ (D-direction)	$5.55 \pm 0.99$
$[0-1-1]$ (E-direction)	$-0.03 \pm 0.68$
$[01-1]$ (H-direction)	$0.01 \pm 1.28$
no misorientation	$-0.12 \pm 1.58$

# Carbon Doping and Delta Doping in GaAs/AlGaAs for DBR Applications

T B Joyce and T J Bullough

Department of Materials Science and Engineering

The University of Liverpool

LIVERPOOL L69 3BX United Kingdom

Tel (44)151 794 5369 Fax (44)151 794 4675 email tjoyce@liv.ac.uk or timbull@liv.ac.uk

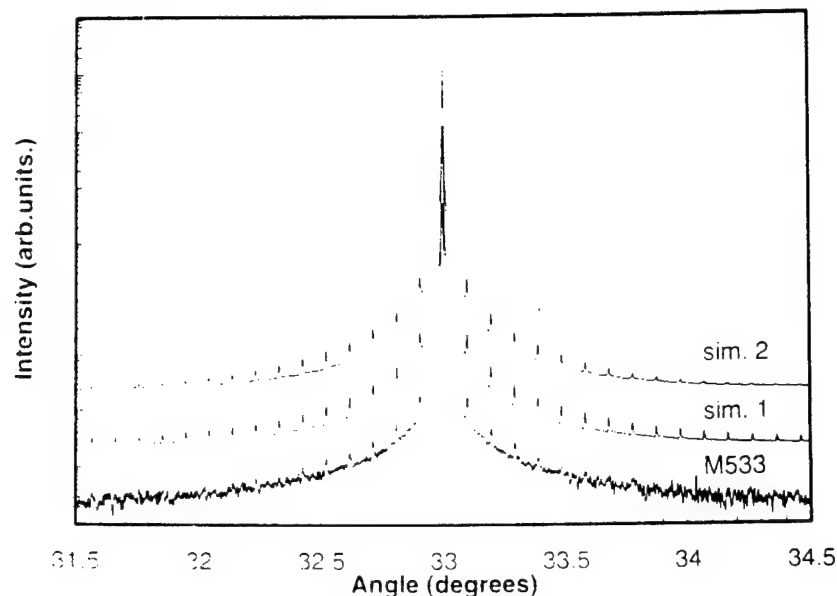
Carbon is well established as a p-type dopant in GaAs for the manufacture of devices such as heterojunction bipolar transistors because of its low diffusivity combined with the high doping levels possible by standard epitaxial techniques. Carbon doping and delta-doping of Al(Ga)As is of current interest for application to distributed Bragg reflectors (DBRs) in vertical cavity surface emitting lasers (VCSELs) in order to reduce the series resistance of the p-type DBR. We describe the CBE growth of C-doped GaAs, AlGaAs and AlAs using CBr<sub>4</sub> as a dopant, the characterisation of C incorporation in homogeneously and  $\delta$ -doped layers and the use of C-doping in DBRs.

DBR stacks consist of alternate layers of two semiconductor materials with different refractive indices (such as AlGaAs and AlAs). For VCSEL applications they must have low resistivities as they form the electrical contacts to the laser. However, a uniformly highly doped DBR will have too high an optical absorption. Low resistivity can be achieved by periodic doping of the DBRs, with a higher doping level at the heterojunctions. This can be achieved using graded dopant profiles or by  $\delta$ -doping.

CBE offers excellent control of both doping and layer composition in such structures, in particular the direct flux control available using vapour sources simplifies the growth of graded interfaces and the use of CBr<sub>4</sub> allows well controlled C-doping and  $\delta$ -doping. GaAs layers grown by CBE at Liverpool have been carbon doped with 100% electrical activity at up to  $5 \times 10^{20} \text{ cm}^{-3}$  using CBr<sub>4</sub>. Carbon doped GaAs was found to be free of impurities such as  $\text{As}_2\text{O}$  (seen when a C-strip doping source was used in MBE) or  $\text{H-CAs}$  (seen in MOVPE material). At very high doping levels ( $[\text{C}] > 10^{20} \text{ cm}^{-3}$ ) there is a reduction in the GaAs growth rate due to etching of the GaAs by Br species arising from the decomposition of CBr<sub>4</sub>.

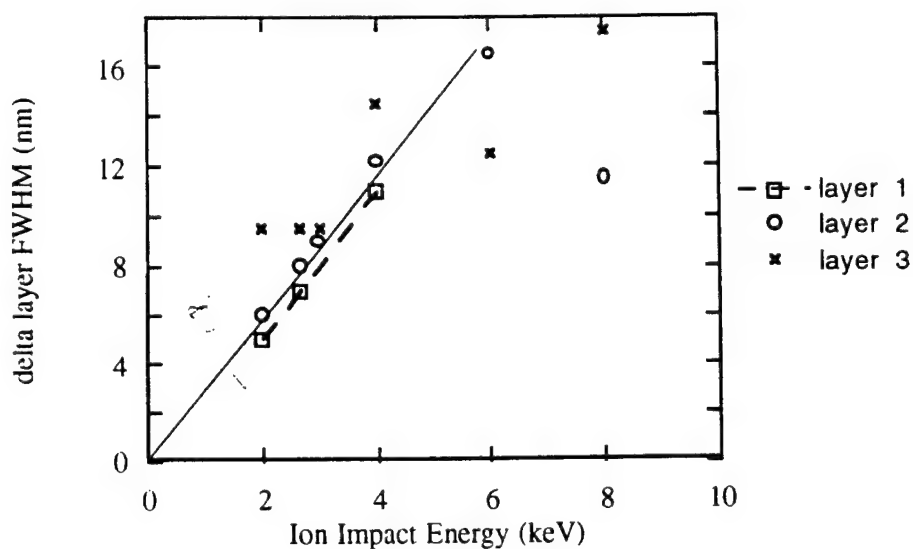
C  $\delta$ -doping superlattices comprising 50 carbon  $\delta$ -layers separated by 50nm GaAs spacers were grown with and without an interruption in the TEGa flux during the formation of the carbon delta layer. Simulation of HRXRD profiles shows that the areal carbon concentration in the  $\delta$ -doped layers is  $1.5 \times 10^{13} \text{ cm}^{-2}$  with a thickness of  $\leq 5 \text{ \AA}$  in samples with a 2-3 sec growth interrupt. This spatial resolution is a factor of 5-10 better than the limits of electrochemical capacitance voltage (ECV) profiling or secondary ion mass spectrometry. IR absorption spectra show a  $\text{C}_{\text{As}}$  concentration of  $1.1 \times 10^{13} \text{ cm}^{-2}$  per  $\delta$ -layer, in agreement with Hall and ECV measurements of  $N_{\text{A}}$ .

## HRXRD



Measured and simulated HRXRD profiles for a structure containing 50 C- $\delta$ -layers separated by 50nm GaAs spacer layers. The simulation labelled sim1 was obtained using a rectangular doping profile with an areal carbon concentration of  $1.5 \times 10^{13} \text{cm}^{-2}$  and a thickness of 5Å. Reducing the width to one monolayer (2.8Å) with the same areal C concentration gave an equally good fit while increasing the width to 10Å gave a worse fit. A good fit to the data can also be obtained using a triangular doping profile with a FWHM of 10Å (sim2), increasing the FWHM gives a worse fit to the data.

## SIMS



SIMS shows a FWHM of about 50Å for the  $\delta$ -doped layers described above because depth resolution is limited by ion beam induced atomic mixing effects. These effects increase with ion beam energy and with profiled depth. The figure shows the influence of ion impact energy on the measured FWHM of the three topmost  $\delta$ -layers of a sample. Extrapolating the data set from a series of profiles (at energies of 2 - 8 keV) to zero impact energy suggests that the actual FWHM is less than 1nm.

## Modulated beam studies of kinetics in GaAs (001) etching using AsBr<sub>3</sub>

**J. Zhang**, O.P. Naji, P. Steans, P. Tejedor, T. Kaneko, T.S. Jones and B.A. Joyce

IRC for Semiconductor Materials, Blackett Laboratory, Imperial College of Science, Technology and Medicine, Prince Consort Road, London SW7 2BZ, U.K.

Tel: +44 171 594 6672, Fax: +44 171 594 6685, E-mail: jing.zhang@ic.ac.uk

In-situ etching of GaAs (001) using AsCl<sub>3</sub> or AsBr<sub>3</sub> has been shown to occur in a layer by layer mode[1,2] as observed using the RHEED intensity oscillation technique. While supply rate limited and reaction rate limited regimes have been established, the kinetics and reaction pathways leading to the etching process remain unknown. In this paper, we present the first modulated beam mass spectrometry (MBMS) study of the etching process and identify the reaction products and the rate determining step in the reaction rate limited regime.

The MBMS technique allows unambiguous identification of reaction products by distinguishing species originating from the surface from those present in the background of the system. This technique, in conjunction with Fourier analysis, can be used for the determination of orders of reaction and surface lifetimes. Using modulation of the species leaving the surface, GaBr is identified as the main etching product over the whole range of temperature for which etching occurs, whilst GaBr<sub>2</sub> and GaBr<sub>3</sub> are not observed. These findings are similar to results obtained by Su et al.[3] using HCl as an etchant. Using modulation of the incident AsBr<sub>3</sub>, the "surface lifetime" of GaBr in the reaction limited regime has been determined to be of the order of milliseconds. Fourier analysis of these results eliminates any second order dependence of the etching on the supply rate of AsBr<sub>3</sub>. The lifetime of the GaBr signal reduces to a much shorter value (below the resolution of the instrument) in the supply rate limited regime. In contrast, the lifetimes of the AsBr and AsBr<sub>2</sub> signals remain short over the whole range of temperature where the signals are present. These experiments indicate that the rate limiting process is not the decomposition of AsBr<sub>3</sub>. In conjunction with previous etching rate measurements using RHEED, the rate limiting step in the reaction limited regime is shown to be a process involving the desorption of GaBr. A reaction pathway is proposed based on these observations.

[1] W.T. Tsang, T.H. Chiu and R.M. Kapre, *App. Phys. Lett.* **63** (1993) 3500

[2] T. Kaneko, P. Smilaure and B.A. Joyce, *Phys. Rev. Lett.* **74** (1995) 3289

[3] C. Su, Z.G. Dai, W. Luo, D.H. Sun, M.F. Vernon and B.E. Bent, *Surf. Sci.* **312** (1994) 181

**Stoichiometric Low Temperature (SLT) MBE GaAs and related compounds:  
structural, electrical and optical properties**

**M. Missous and S. O'Hagan,  
Department Of Electrical Engineering and Electronics, UMIST, PO Box 88,  
Manchester M80 1QD, England, UK  
Tel : +44 161 2004797  
FAX: +44 161 2004770  
Abstract:**

When MBE GaAs is grown at around 200 °C (compared to the normal 580-600 °C) while preserving the high temperature growth conditions, layers are produced manifesting a remarkable set of structural, electrical and optical properties. As grown, LT GaAs, as it is commonly referred to, has an excess of As, contains a high concentration of point defects making it impossible to dope, displays hopping band conductivity and shows virtually no luminescence. The statistics of defects responsible for the above properties are as follows :

- i)  $\sim 10^{20} \text{ cm}^{-3}$  As interstitial
- ii)  $\sim 10^{19} \text{ cm}^{-3}$  As<sub>Ga</sub> anti-sites
- iii)  $\sim 5 \times 10^{18} \text{ cm}^{-3}$  Ga vacancies

The materials thus produced is highly non-stoichiometric. It is also clear from the concentrations of point defects above that the materials is defects controlled. A question that arises is whether this non-stoichiometry is inevitable by virtue of the low growth temperature used ( as has been commonly assumed ) or it is in fact controllable.

We have shown and demonstrated that LT GaAs need not be associated with non-stoichiometry. By careful control of the arsenic beam supply during the growth of GaAs and  $\text{Al}_{0.42}\text{Ga}_{0.58}\text{As}$  at low temperatures (  $\sim 200^\circ\text{C}$  ), very strong and sustained Reflection High Energy Electron Diffraction (RHEED) oscillations have been observed. Both the period and intensity of the RHEED oscillations are shown to be a strong function of the arsenic overpressure with the former increasing with increasing arsenic supply, reflecting a decrease in the number of atoms taking part in the 2 dimensional (2D) growth mode, and the latter decreasing with increasing arsenic supply, reflecting the creation of a barrier to 2D growth by the excess arsenic. Under exact stoichiometric conditions, the quality of the GaAs and AlGaAs is comparable to those grown at high temperatures. It is therefore surmised that non-stoichiometry in low temperature grown GaAs can be overcome leading to the growth of Stoichiometric Low Temperature (SLT) materials possessing properties similar to those of conventional, high temperature grown layers.

Under these conditions, material in which total defect concentrations of less than  $10^{17} \text{ cm}^{-3}$  in GaAs and  $10^{16} \text{ cm}^{-3}$  in  $\text{In}_{0.53}\text{Ga}_{0.47}\text{As}$  (lattice matched to InP), well below the huge  $10^{20} \text{ cm}^{-3}$  that is normally obtained in conventional LT materials can be achieved therefore demonstrating that high quality II-V compounds can in effect be grown at extremely low temperatures. We have observed and demonstrated the following :

- 1) Establishment and control of Stoichiometry via RHEED oscillations.
- 2) Controlled doping from  $10^{17}$  to  $10^{19} \text{ cm}^{-3}$  in GaAs and from  $10^{16}$  to  $\sim 5 \times 10^{19} \text{ cm}^{-3}$  in  $\text{In}_{0.53}\text{Ga}_{0.47}\text{As}$
- 3) Quantum Well Luminescence in GaAs-AlGaAs and  $\text{In}_{0.53}\text{Ga}_{0.47}\text{As-In}_{0.52}\text{Al}_{0.48}\text{As}$  (lattice matched to InP) structures grown at 200 °C..
- 4) State of the art  $\text{In}_{0.53}\text{Ga}_{0.47}\text{As-In}_{0.52}\text{Al}_{0.48}\text{As}$  HEMTs grown at 200 °C including Double doped HEMTs



## MOLECULAR BEAM EPITAXIAL GROWTH OF BICRYSTALLINE METALLIC LATERAL SUPERLATTICES

Magali Sussiau, Frédéric Nguyen-Van-Dau, Pierre Galtier and A. Schuhl  
UMR 137, Thomson CSF - LCR, Domaine de Corbeville, 91404 Orsay, France.

Molecular Beam Epitaxy has been used to grow bicrystalline metallic lateral superlattices on top of vicinal Si(111) substrates misoriented towards [11-2] which were thermally pre-treated in order to activate the step bunching phenomena. Indeed, it is known that when cooling down such a substrate from  $\approx 900^\circ\text{C}$ , steps prefer to bunch away from  $7\times 7$  reconstructed terraces, leading to up to  $800\text{\AA}$ -wide flat reconstructed terraces separated by bunches of up to 25 monoatomic steps <sup>1</sup>.

Metallic layers were grown on such substrates with typical stack  $\text{Cu}_{50}\text{\AA}/(\text{FeNi or Co})_{100}\text{\AA}/\text{Pd}_{15}\text{\AA}$ . Transmission Electron Microscopy (TEM) experiments were carried out in cross section with a zone axis parallel to the steps direction. They indicate that two epitaxial relationship coexist in these samples, namely :

Metal (111) [11-2] // Si (111) [1-10] (ER1)

Metal (111) [11-2] // Si (101) [1-10] (ER2)

Moreover, dark field TEM observations revealed that ER1 occurs on top of the terraces while ER2 occurs on top of step bunched regions. The resulting metallic layers thus exhibit a pseudo-periodic lateral variation of their crystalline orientation and can be considered as bicrystalline metallic lateral superlattices.

By varying the initial thermal treatment of the substrate, we were able to increase the lateral modulation period of the starting surface topology. Similar samples grown on such substrates exhibit an increase of their lateral pseudo-period. But moreover, by carefully analysing the metal/Si interface, we show that a minimum number of steps bunched is necessary for the ER2 relationship to appear. This threshold is evaluated to 12-13 monoatomic steps.

All these samples exhibit an in-plane uniaxial magnetic anisotropy with the easy axis parallel to the step direction. The anisotropy field appear to be inversely proportional to the lateral pseudo-period. Finally, magnetoresistance measurements surprisingly reveal a single magnetic domain behaviour with a magnetization reversal by rotation.

<sup>1</sup> E.D. Williams et al., Surf. Sci., **294**, 219 (1993) and references therein.

### Contact and Presenting author :

NGUYEN VAN DAU Frédéric

Institution : THOMSON CSF - LCR

Department : UMR 137

Domaine de Corbeville 91404 ORSAY Cedex FRANCE

Phone : +33 1 69 33 90 92

Fax : +33 1 69 33 07 40

E-mail : VANDAU@LCR.THOMSON.FR

## Passivation of misfit dislocations by atomic hydrogen irradiation

M. Yokozeki, H. Yonezu, T. Tsuji, K. J. Lee, Y. Fujimoto and N. Ohshima

Department of Electrical and Electronic Engineering, Toyohashi University of Technology,

1-1 Hibarigaoka, Tempaku-cho, Toyohashi 441, Aichi, Japan

Tel : (+81) 532-44-6747, Fax : (+81) 532-44-6757

The degradation of LED and LD is caused by threading and misfit dislocations. We have reported that the threading dislocation density was effectively reduced by inserting multi-strained short-period superlattices (SSPSs) in the highly lattice mismatched heteroepitaxy. However, misfit dislocations remain at the heterointerfaces. Thus, we have investigated the passivation effect of misfit dislocations using atomic hydrogen irradiation.

An  $(\text{InAs})_1(\text{GaAs})_4$  SSPS was grown on the GaAs(001) substrate at a growth temperature of 350 °C. The misfit dislocation density can be controlled by varying the period of the SSPS. The atomic hydrogen was irradiated during the growth and cooling process. Figure 1 illustrates the schematic drawing of the sample structure. The atomic hydrogen was generated with a W filament heated up to about 1800 °C. The pressure of hydrogen was kept at  $3 \times 10^{-5}$  Torr. The electric characteristic and the nature of misfit dislocations were evaluated by electron beam induced-current (EBIC) and transmission electron microscopy (TEM) observations, respectively.

Figure 2 shows the plain-view TEM image of the  $(\text{InAs})_1(\text{GaAs})_4$  SSPS with 45 periods taken under  $g_{220}$  diffraction. The misfit dislocations, propagating in parallel to the heterointerface along the  $\langle 110 \rangle$  directions, were observed. Most of misfit dislocations were clarified to be the  $60^\circ$  type dislocation from the criterion of  $g \cdot b = 0$ .

The EBIC images are shown in Fig. 3. The dark line density was remarkably decreased by atomic hydrogen irradiation during the growth and cooling process rather than only cooling process, as shown in Figs. 3(a) and (b). On the contrary, it was not reduced by molecular hydrogen irradiation during the growth and cooling processes and no irradiation, as shown in Figs. 3(c) and (d). This means that the passivation of misfit dislocations was proceeded by atomic hydrogen irradiation during the growth and cooling process. Moreover, it was found that the  $\beta$ -type dislocations propagated  $[110]$  direction were effectively passivated, compared with the  $\alpha$ -type dislocations propagated  $[\bar{1}10]$  direction. It could be caused by the fact that the bonding force of As-H is stronger than the one of Ga-H.

In conclusion, it was clarified that the misfit dislocations can be passivated by atomic hydrogen irradiation during the growth and cooling processes and the passivation of the  $\beta$ -type dislocations is more effectively proceeded than that of the  $\alpha$ -type dislocations.

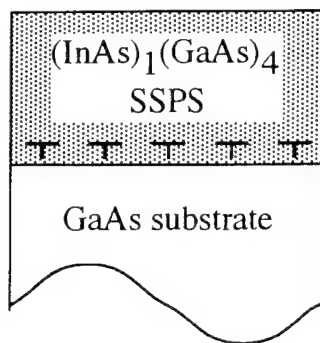


Fig.1 Schematic drawing of the sample structure

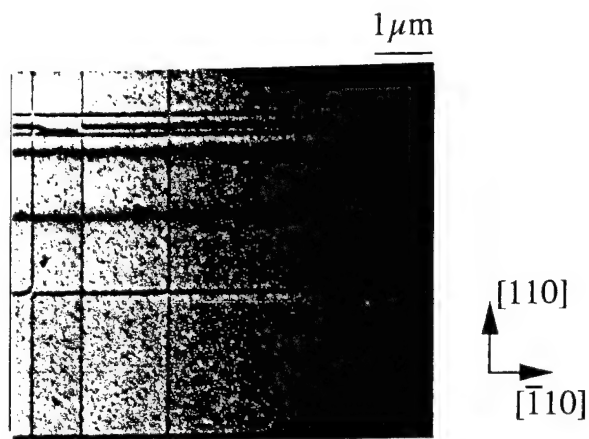


Fig. 2 A plain-view TEM image of the  $(\text{InAs})_1(\text{GaAs})_4$  SSPS with 45 periods taken under  $g_{220}$  diffraction. The misfit dislocations, propagating in parallel to the hetero-interface along the  $\langle 110 \rangle$  directions, were observed. Most of misfit dislocations were  $60^\circ$  type dislocation.

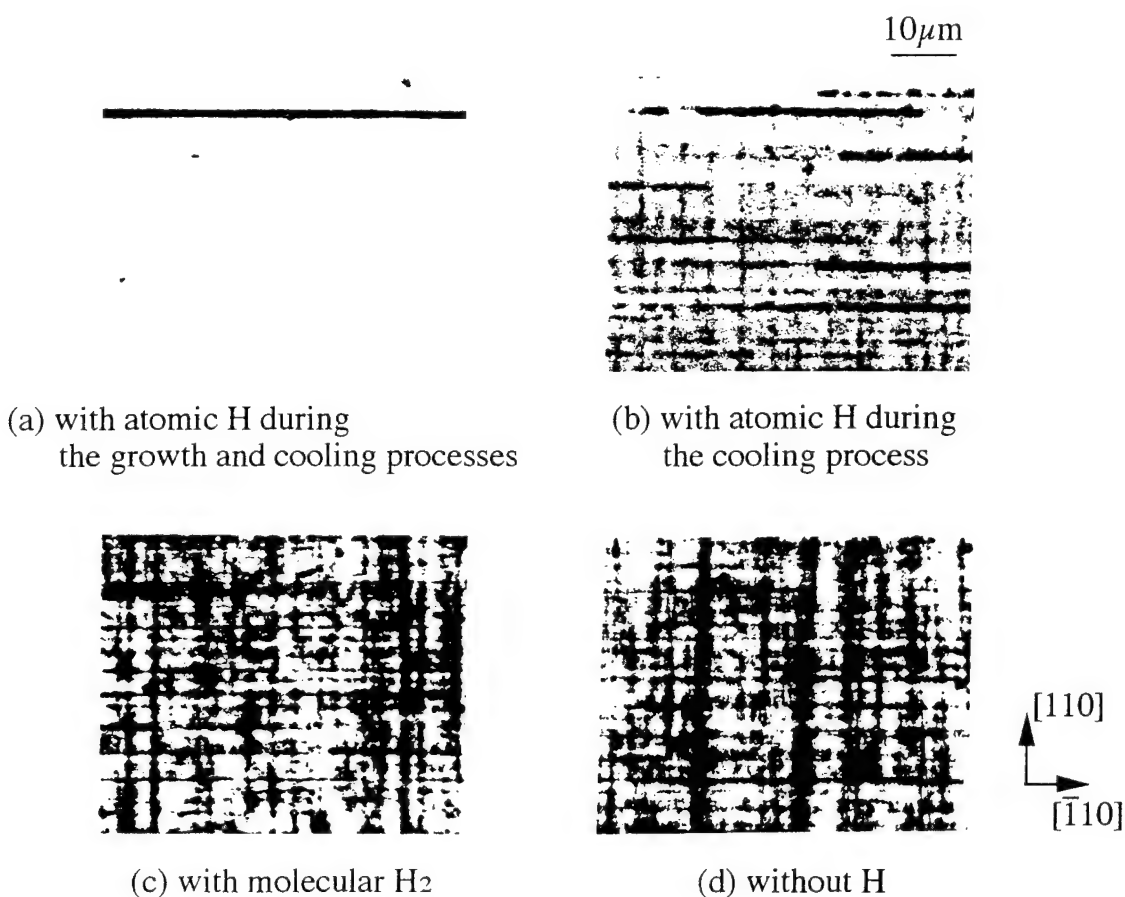


Fig. 3 EBIC images of  $(\text{InAs})_1(\text{GaAs})_4$  SSPS-on-GaAs(001). The dark line density was remarkably decreased by atomic hydrogen irradiation during the growth and cooling process rather than only cooling process, as shown in Figs. 3(a) and (b). On the contrary, the density was not reduced by molecular and no hydrogen irradiation, as shown in Fig. 3(c) and (d).

## **Morphology of MBE Grown InAs Films Studied by Atomic Force Microscope**

Y. Wang, Y. N. Sheng, Weikun Ge, Jiannong Wang, and L. L. Chang  
Department of Physics, the Hong Kong University of Science & Technology, Clear Water Bay, Kowloon, Hong Kong

Jie Xie  
The Materials Characterization & Preparation Center, the Hong Kong University of Science & Technology, Clear Water Bay, Kowloon, Hong Kong

The morphology of MBE grown InAs films grown on GaAs (100) substrates has been studied by atomic force microscope (AFM). These samples were grown on both (100) and  $2^\circ$  off toward (111)A oriented GaAs substrates. The samples consist of a 200 nm GaSb buffer layer grown at  $500^\circ\text{C}$ , a 20 nm InAs layer grown at  $430^\circ\text{C}$ , and an 1  $\mu\text{m}$  InAs layer grown either at  $510^\circ\text{C}$  or at  $430^\circ\text{C}$ . Strong RHEED intensity oscillations were observed after the 1  $\mu\text{m}$  InAs layer grown at  $510^\circ\text{C}$ . However, these oscillations were absent for samples grown at  $430^\circ\text{C}$ , even after 5 minutes annealing at  $480^\circ\text{C}$ .

The AFM measurements were conducted under ambient conditions. Although a native oxide layer has been formed, which is believed to be 4~5 nm thick, the monolayer steps and terraces remain clearly observable. The sample grown on (100) substrates show very large differences in surface morphology for different growth temperatures. For samples grown at  $510^\circ\text{C}$ , surfaces are quite smooth. However, in comparison with the samples grown at  $510^\circ\text{C}$ , the surfaces of samples grown at  $430^\circ\text{C}$  are rough and with a relatively high density of deep pits (more than 200 nm in depth) surrounded by terraces (about 40 nm high). These differences can be explained on the bases of: 1) insufficient and anisotropic In diffusions due to the energy barrier at the step edges, and 2) step pinning by surface defects, such as absorbed chemical impurities. The samples grown on  $2^\circ$  off (100) oriented substrates, both at  $510^\circ\text{C}$  and  $430^\circ\text{C}$ , show similar features in morphology. The surfaces for samples grown at both temperatures exhibit narrow step width as a result of the high step density provided by the misorientation.

Please contact Yuqi, Wang at: Tel.: (852)-23587495; Fax: (852)23581652; e-mail: phyuqi@usthk.ust.hk

## Carbon doping of molecular beam epitaxial GaAs{111} films using carbon tetrabromide

D.H. Tomich, N.Y. Li and C.W. Tu

*Department of Electrical and Computer Engineering*

*University of California, San Diego, La Jolla, CA 92093-0407*

E-mail: dtomich@ucsd.edu, FAX: (619) 534-2486, Phone: (619) 534-3014

Carbon, because of its low diffusion coefficient is an attractive replacement for the more commonly used beryllium and zinc as a p-type dopant in GaAs. Carbon tetrabromide has been reported<sup>1</sup> to have a high incorporation rate with carrier concentrations greater than  $1.0 \times 10^{20} \text{ cm}^{-3}$  in GaAs(001). Currently, the {111} faces of III-V compounds have attracted considerable interest for device applications. MESFET's fabricated on (111)B oriented GaAs wafers are free from the one-direction ([110] or [1-10]) gate arrangement of MESFET's on GaAs(001) since the space charge generated by piezoelectricity is canceled on the (111) face<sup>2</sup>. It is also known that the threshold current of GaAs/AlGaAs quantum well lasers can be lowered by using the (111) face<sup>3</sup>. Silicon can exhibit either donor or acceptor characteristics depending on the occupation site and it has been shown to be an n-type dopant in MBE grown GaAs(001) and (111)B films but a p-type dopant in MBE grown GaAs(111)A films. To our knowledge there has been no report on carbon doping in GaAs(111)A or (111)B. Therefore, it is interesting to study carbon doping the these growth directions.

Carbon doping studies have been performed at substrate temperatures and arsenic overpressures known to give good electrical characteristics and specular surfaces for homoepitaxial growth on GaAs(111)A and GaAs(111)B faces. The surfaces have been characterized with atomic force microscopy to assure consistent growth conditions and show step flow growth in all cases. Hall measurements of mobility and carrier concentrations have been performed. Carbon incorporation into films grown on both the A and B faces has been found to be p-type with efficient incorporation similar to that found in MBE grown GaAs on the (001) face. Photoluminescence results will also be reported.

This work is partially supported by the U.S. Air Force Wright Laboratory

1. P.J. Lemonias, et.al. J. Vac. Sci. Technol. B **12**(2), 1190 (1994).
2. K. Ueno, et.al. Technical Dig. of Int. Electron Device Meet. (IEEE, New York, 1988) 864.
3. T. Hayakawa, et.al. Jpn. J. Appl. Phys. **26**, L302 (1987)

# Formation of an n-GaAs/n-GaAs regrowth interface without carrier depletion using Electron Cyclotron Resonance hydrogen plasma

Takaki Niwa, Naoki Furuhashi, and Tadashi Maeda

Microelectronics Research Laboratories, NEC Corporation

34 Miyukigaoka, Tsukuba, Ibaraki, 305 Japan

Fax: +81-298-50-1107, Phone: +81-298-50-1522, E-mail: niwa@uhl.cl.nec.co.jp

This paper reports on the formation of a GaAs MBE regrowth interface without carrier depletion and contaminants using Electron Cyclotron Resonance (ECR) hydrogen plasma. To get a carrier-depletion-free interface, we have investigated the mechanism of removing contaminants such as Si, O, and C. SIMS shows that Si and O contaminants come from the sputtering of the quartz liner in the ECR chamber during the treatment, and these can be reduced to a level below the SIMS detection limit by lowering the hydrogen pressure to below  $10^{-3}$  Torr. TDS analysis reveals that C contaminant is removed through transformation into  $\text{CH}_3$  at substrate temperatures above  $400^\circ\text{C}$ . Furthermore, RHEED observation and C-V measurement indicate that ECR damage is eliminated at  $500^\circ\text{C}$ . Based on these results, we have produced an undamaged and contaminant-free regrowth interface for the first time.

Contaminants such as C, Si, and O adsorbed on the GaAs surface when the surface is exposed to air cause serious problems such as high contact resistance at the regrowth interface [1] or unstable device performance in GaAs FETs [2]. Previous works reported that C contaminant was removed by using ECR hydrogen plasma, but that Si and O contaminants were not effectively removed [3]. Therefore,  $\text{Cl}_2$  gas etching was necessary after the hydrogen plasma to remove these contaminants [4]. However, this treatment is difficult to apply to microscopic device-fabrication processes because  $\text{Cl}_2$  gas excessively etches the surface being treated.

Experiments were performed in the UHV ECR chamber connected to the MBE chamber by a transfer module. The samples were exposed to air for one month, after  $8 \times 10^{16} \text{ cm}^{-3}$  Si-doped GaAs had been grown by MBE. The sample surface was cleaned by the hydrogen plasma in the ECR chamber without any other treatments, followed by  $8 \times 10^{16} \text{ cm}^{-3}$  Si-doped GaAs regrown by MBE. The plasma treatment time was 20 minutes and microwave power was 200 W. SIMS shows that Si and O contaminants are produced by sputtering of the quartz liner during plasma treatment, and these are suppressed by lowering the hydrogen pressure to below  $10^{-3}$  Torr. At  $6.5 \times 10^{-4}$  Torr, Si and O contaminants are removed to a level below the SIMS detection limit. The C contaminant is hardly removed at all simply by lowering the hydrogen pressure, but is removed to a level below the SIMS detection limit at a substrate temperature of  $400^\circ\text{C}$ . TDS analysis shows that this is because a C atom on the GaAs surface reacting with hydrogen plasma produces  $\text{CH}_3$ , which can be removed from the GaAs surface at a substrate temperature of  $400^\circ\text{C}$ , according to the following equation:  $\text{C}_{(\text{adsorption})} + 3 \text{H}^* \rightarrow \text{CH}_3_{(\text{adsorption})} \rightarrow \text{CH}_3_{(\text{gas})}$  at  $400^\circ\text{C}$

However, this substrate temperature is not sufficient to achieve a carrier-depletion-free interface. The RHEED pattern after plasma treatment at a substrate temperature of  $430^\circ\text{C}$  is spotty, which indicates a rough surface. On the other hand, at  $500^\circ\text{C}$ , a streaky  $\text{C}(4 \times 4)$  RHEED pattern is observed, which proves there is little structural damage at the treatment surface. C-V measurement shows that the carrier at the regrowth interface is heavily depleted when the plasma treatment is performed at a substrate temperature of  $430^\circ\text{C}$ . This depletion indicates the existence of ECR damage related to the structural damage of the surface because the acceptor concentration calculated from the C-V profile is twice as high as the C concentration predicted from the analysis using the resolution function of SIMS. At  $500^\circ\text{C}$ , the carrier profile is flat near the n-GaAs/n-GaAs regrowth interface, which proves there is little ECR damage.

In conclusion, we have demonstrated the elimination of carrier depletion and contaminants at the GaAs regrowth interface by using hydrogen plasma. This technique will improve the electrical performance of devices with GaAs regrowth interfaces.

[1] J. Saito et al., J. Appl. Phys. **58**, 806 (1990)

[2] K. Kasahara et al., Solid State Elec. **38**(6), 1221 (1995)

[3] N. Kondo et al., Jpn. J. Appl. Phys. **33**(1B), L91 (1994) [4] M. Hong et al., Appl. Phys. Lett. **62**(21), 2658 (1993)

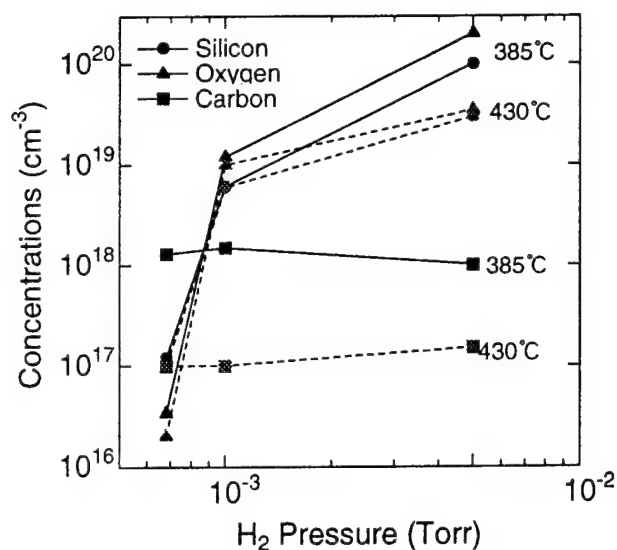


Fig. 1 Dependence of contaminant concentrations at regrowth interface on hydrogen pressure during plasma treatment. Contaminant concentrations were estimated by SIMS.

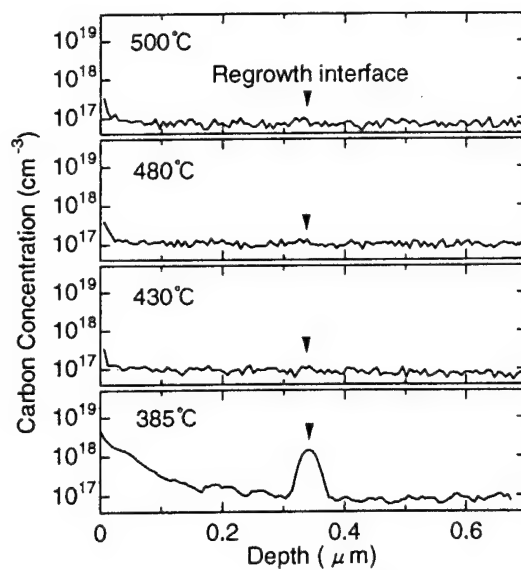


Fig. 2 SIMS profiles for a carbon contaminant near the regrowth interface cleaned by hydrogen plasma at various temperatures.

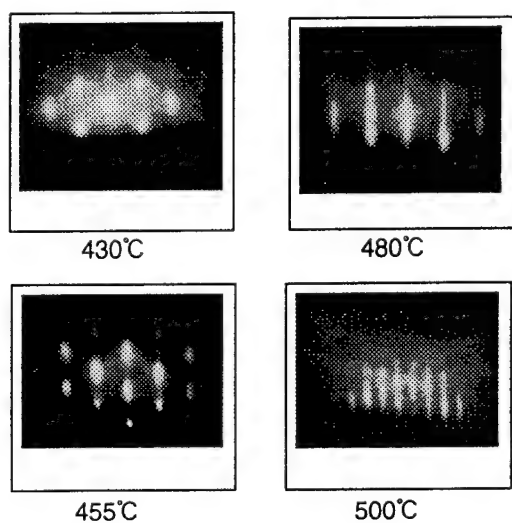


Fig. 3 RHEED patterns of GaAs surface at room temperature after hydrogen plasma treatment.

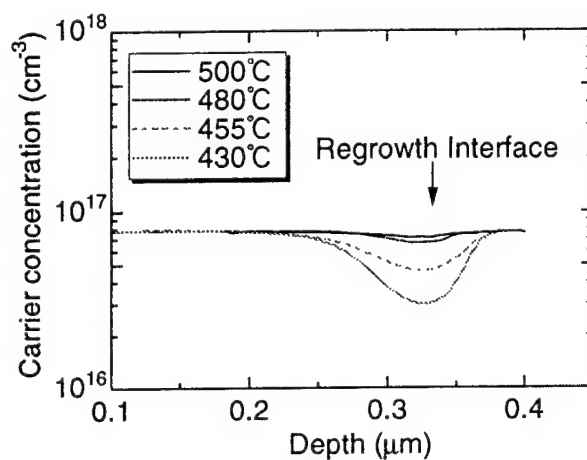


Fig. 4 C-V profile near n-GaAs/n-GaAs regrowth interface.

# Continuously graded buffers for InGaAs/GaAs structures grown on GaAs

A Bosacchi, AC De Riccardis, S Franchi\*, C Ferrari, S Gennari, L Lazzarini, L Nasi, G Salviati  
CNR - MASPEC Institute, Via Chiavari 18a, I-43100 Parma, Italy

AV Drigo and F Romanato  
INFN - Physics Department of Padova University, Via Marzolo 8, I-35131 Padova, Italy

In lattice-mismatched InGaAs structures grown on GaAs substrates, buffer layers are used to reduce the propagation of threading dislocations (TD) towards the active parts of devices, to confine misfit dislocations (MD) close to substrates and to prevent the onset of 3D nucleation. Different models [1-3] concur to give the following picture: Step-graded or continuously graded buffer structures with increasing lattice parameter can be divided in two regions, the topmost of which is strained and void of MDs, that, instead, are confined in the fully-relaxed, lowest one. The strain profile depends only on the composition profile; therefore, compressive, tensile and null strain can be predetermined in structures grown on top of buffers; this can be of great interest for engineering the electronic bands of the structures. Moreover, by designing the composition profiles of buffers it is possible to change: i) the thicknesses of the MD-free parts of buffers and ii) the MD concentrations and their profiles in the relaxed parts.

The aim of this work is to study how: i) design parameters of continuously graded buffers and ii) their growth conditions affect the properties of buffers and of MQWs grown on top of them.

The MBE growth of the  $\text{In}_x\text{Ga}_{1-x}\text{As}$  buffers has been carried out at temperatures ranging from 400 °C to 500 °C, using both  $\text{As}_2$  and  $\text{As}_4$  molecular beams; the MQWs, instead, have been prepared by ALMBE at 400 °C. The buffers have compositions with: i) linear, ii) square-root and iii) parabolic (with the maximum at the top of the buffer) dependences on the distance from substrates. The compositions are graded up to values of 0.41, 0.39 and 0.38 (for linear, square-root and parabolic grades, respectively) in 3000 nm. These values have been calculated so that MQWs with mean compositions  $x=0.34$  (consisting of 30  $\text{In}_{0.5}\text{Ga}_{0.5}\text{As}$  (75 Å) and GaAs (35 Å) layers) are, on the whole, fully unstrained on all the types of buffers. This approach is different from that generally used, where compositions are graded up to the mean compositions of the MQWs, thus leaving them under compressive strain. The experimental results have been obtained by the concomitant use of XTEM, HRXRD, AFM and PL. As for the effect of grading types, we observe by XTEM that non-linear buffers as compared to the linear ones have: i) wider MD-free parts and ii) higher MD concentrations near the substrates, in regions where the composition gradients are higher. Moreover, non-linear buffers are more effective in preventing the propagation of TDs into the MQWs. Both HRXRD and XTEM show that the MQWs have much better structural properties when they are grown at low temperatures using  $\text{As}_2$ . This is also confirmed by the observation the MQWs grown under these conditions and with linear buffers have a much brighter PL, which can be also observed at room temperature (at 1.3  $\mu\text{m}$ ). The use of low temperatures and  $\text{As}_2$  is also beneficial for the reduction of surface cross-hatching, which may have a rms roughness as low as 4 nm for linear buffers. The above results will be discussed in the framework of the current understanding of strain relaxation mechanisms.

- [1] J Tersoff, Appl. Phys. Lett. **62**, 693 (1993)
- [2] A Sacedón, F González-Sanz, E Calleja, E Muñoz, SI Molina, FJ Pacheco, D Araújo, R García, M Lourenço, Z Yang, P Kidd and D Dunstan, Appl. Phys. Lett. **66**, 3334 (1995)
- [3] G Salviati, C Ferrari, L Lazzarini, S Franchi, A Bosacchi, F Taiariol, M Mazzer, C Zanotti-Fregonara, F Romanato, and AV Drigo, Int Phys Conf Series **146**, 337 (1995)

\* tel: +39-521-269209, fax: +39-521-269206, e-mail: franchi@prmasp.bo.cnr.it



**Continuously graded buffers for InGaAs/GaAs structures grown on GaAs**  
A Bosacchi, AC De Riccardis, S Franchi, C Ferrari, S Gennari, L Lazzarini, L Nasi, G Salviati,  
AV Drigo and F Romanato

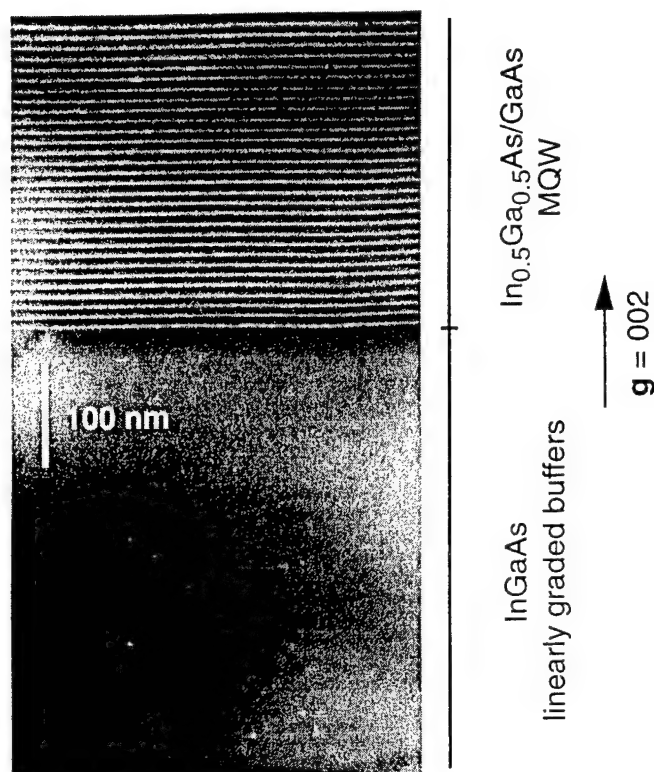


Fig. 1. Bright field,  $g=002$  type, (110) oriented XTEM micrograph of a  $\text{In}_{0.5}\text{Ga}_{0.5}\text{As}/\text{GaAs}$  MQW (with mean composition  $x=0.34$ ) grown on top of a linearly graded  $\text{In}_x\text{Ga}_{1-x}\text{As}$  buffer ( $0 < x < 0.41$ ). The buffer and the MQW were grown by MBE and ALMBE, respectively, at  $400^\circ\text{C}$  with a  $\text{As}_2$  beam. Underneath the MQW structure, a  $\sim 400$  nm thick part of the buffer is MD-free.

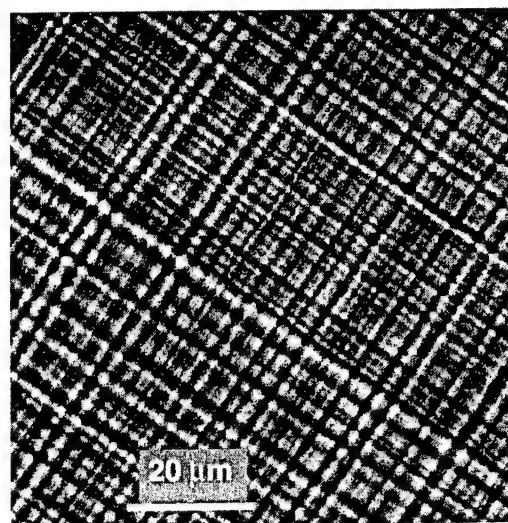
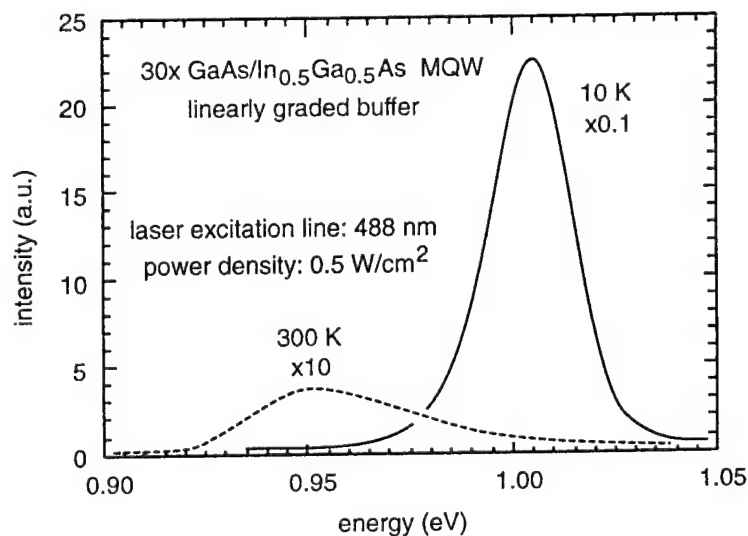


Fig. 2. AFM micrograph of the surface of a  $\text{In}_{0.5}\text{Ga}_{0.5}\text{As}/\text{GaAs}$  MQW (with mean composition  $x=0.34$ ) grown on top of a linearly graded  $\text{In}_x\text{Ga}_{1-x}\text{As}$  buffer ( $0 < x < 0.41$ ). The buffer and the MQW were grown by MBE and ALMBE, respectively, at  $400^\circ\text{C}$  with a  $\text{As}_2$  beam. The surface roughness (along the (110) directions) has a rms value of 4 nm and a period of  $\sim 2 \mu\text{m}$ .

Fig. 3 Photoluminescence spectra of a MQW consisting of 30 QWs of  $\text{GaAs}/\text{In}_{0.5}\text{Ga}_{0.5}\text{As}$  ( $35\text{\AA}/75\text{\AA}$ ) grown by ALMBE at  $400^\circ\text{C}$  with  $\text{As}_2$  on a linearly graded  $\text{In}_x\text{Ga}_{1-x}\text{As}$   $3 \mu\text{m}$  thick buffer layer ( $0 \leq x \leq 0.41$ ). The 21 meV FWHM at 10 K and the  $1.3 \mu\text{m}$  room temperature emission at low excitation power point to a very high optical quality of the structure. The spectral resolution is 0.5 meV.



## Growth Dynamics of InGaAs/GaAs by MBE

Françoise Fournier, April S. Brown, Carrie A. Carter-Coman, Robert A. Metzger, Alan Doolittle,  
Nan Marie Jokerst and Robert Bicknell-Tassius\*

School of Electrical and Computer Engineering / Microelectronics Research Center  
Georgia Institute of Technology  
791 Atlantic Drive NW  
Atlanta, GA 30332-0269

\*Georgia Tech Research Institute

Office Phone and fax numbers : (404) 894-5252, (404) 894-5028  
e-mail: [fournier@prodiga.mirc.gatech.edu](mailto:fournier@prodiga.mirc.gatech.edu)

The InGaAs/GaAs materials system has numerous important device applications. In addition, the strained system can be used for producing quantum confined structures. The control of surface segregation effects is critical for all of these applications, thus the improved understanding of growth kinetics, and, in particular, the interplay between surface segregation and desorption is important. We have also recently introduced the new concept of Strain Modulated Epitaxy (SME)<sup>1</sup>. In this approach, we utilize bottom-patterned compliant substrates to laterally modulate strain-dependent growth kinetics. An improved understanding of the dynamics of InGaAs growth on GaAs is required to effectively exploit this concept.

Desorption Mass Spectrometry (DMS) is a well known technique for measuring and quantifying segregation and desorption effects. Various studies<sup>2,3</sup> report the observation of different desorption mechanisms from DMS studies. In these studies, the desorption flux is attributed to different mechanisms, in one case, desorption from InGaAs; and, in the other, from an indium segregated layer.

We have performed an extensive DMS study of InGaAs growth on GaAs. For our experiments, the mass spectrometer is positioned in direct line-of-sight of the growing surface in a Riber-2300 MBE machine. We have recorded desorption curves as a function of substrate temperature (510-630°C), indium composition (5-22%), V/III beam equivalent pressure ratio (16, 36), arsenic species (As<sub>2</sub> and As<sub>4</sub>), and growth rate (0.4-0.9 µm/hr). Growth sequences were composed of twenty-five seconds of InGaAs deposition, followed by five minutes of GaAs after a growth interruption, in order to bury the InGaAs layer and smooth the surface.

We clearly observe two indium desorption mechanisms in the DMS indium signal as a function of time. The relative magnitude of each of the mechanisms depends critically on growth conditions, in particular V/III ratio and substrate temperature. The activation energy for one of the mechanisms can be obtained by fitting the appropriate part of the desorption decay curve. For most cases, the activation energy is around 1.3 eV, comparable to reported values<sup>4,5</sup> near 1.5 eV. However, the indium sticking coefficient varies dramatically with the growth parameters. This study clarifies the interpretation of DMS for understanding the growth kinetics of InGaAs on GaAs and addresses some of the discrepancies in the observed dependences of segregation and desorption on growth conditions. We also will discuss these results in the context of our SME approach to the lateral control of materials properties.

### References

- <sup>1</sup>C.A. Carter, A.S. Brown, R.Bicknell-Tassuis, N.M. Jokerst, F.Fournier, and D.E. Dawson, presented at the North American Conference on molecular Beam Epitaxy, 1995.
- <sup>2</sup>K.R.Evans, C.E. Stutz, E. N. Taylor, and J.E. Ehret, J.Vac.Sci.Technol. B9(4), Jul/Aug 1991
- <sup>3</sup>Y.C.Kao, F.G. Celii, and H. Y. Liu, J.Vac.Sci.Technol. B11(3), May/Jun 1993
- <sup>4</sup>K.R.Evans, R.Kaspi, J.E.Ehret, M.Skowronski, J.Vac.Sci.Technol.B13(4), Jul/Aug 1995
- <sup>5</sup>C.T.Foxon and B.A. Joyce, J.Crystal Growth 44(1978), 75

## Transient Surface State during the CBE Growth of GaAs

T. Farrell, D. Hill, T.B. Joyce, T.J. Bullough and P. Weightman\*

Department of Materials Science and Engineering  
\*Interdisciplinary Research Centre in Surface Science  
The University of Liverpool, PO Box 147  
LIVERPOOL L69 3BX England

Tel: (44) 151 494 5369 Fax: (44) 151 794 4675 email trevorf@liv.ac.uk

We report the occurrence of a transient surface state during the initial stages of CBE GaAs(001) growth. The state was detected in real-time reflectance anisotropy (RAS) growth monitoring. At low growth rates, less than  $1\mu\text{m}/\text{hour}$ , beam equivalent pressure (BEP) of triethylgallium (TEG)  $< 2.5 \times 10^{-5}$  mbar, the RAS signal changed from its pre-growth value under arsenic stabilisation at the growth temperature to its "during growth" value upon admission of the TEG, with the now familiar monolayer oscillations, figure 1. At higher triethylgallium BEPs the RAS trace was characterised by a pause and/or minima (depending on the growth temperature) during the transition from the pre-growth to during-growth conditions, and the disappearance of the monolayer oscillations. This structure in the RAS trace is indicative of a transient surface state. Figure 2 shows the minima in the RAS traces for high BEPs when the growth temperature was  $535^{\circ}\text{C}$ . As the group III BEP is increased, the transient state lasts for a longer period. Also clearly visible in figure 2 are oscillations in the RAS trace during the transient with a period independent of the group III BEP and shorter than the time for monolayer growth at the prevailing BEP. The structure in the RAS traces occurred at similar RAS values at the lower growth temperature of  $510^{\circ}\text{C}$  and although it is approached from a different direction (the pre-growth RAS value at these temperatures is strongly influenced by the surface reconstruction[1]) the subsequent RAS traces exhibit similar features to those occurring in the RAS traces for the higher temperature, figure 3. The effect of increasing the group V BEP is to shorten the time over which the transient state exists, figure 4. Transients in RAS monitored OMCVD growth and interrupted MBE growth of GaAs(001) have previously been reported by Aspnes[2] and discussed in terms of a Ga stabilised reconstruction (MBE) and dissociation kinetics of trimethylgallium (OMCVD). Although our CBE surface transients could indicate the temporary existence of a Ga stabilised reconstruction during the initial stages of growth, the absence of monolayer oscillations and the transient state oscillatory behaviour suggest that it is more likely to be due to the dissociation kinetics of the TEG molecule and this forms the basis for the discussion of the results.

- [1] I. Kamiya, D.E. Aspnes, L.T. Florez and J.P. Harbison, Phys. Rev. **B46** (1992) pp 15894-15904
- [2] D.E. Aspnes, IEEE Journal of Quantum Electronics, **25**, (1989), pp 1056-1063

Figure 1 RAS traces of GaAs growth at low Gp III BEP and high V/III ratio

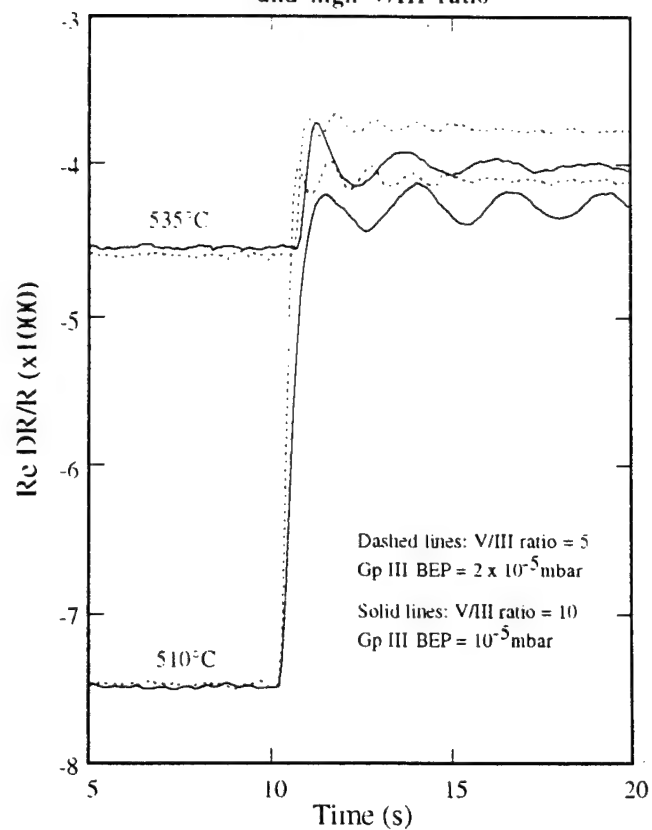


Figure 2 Dependence of the surface transient state on precursor pressure

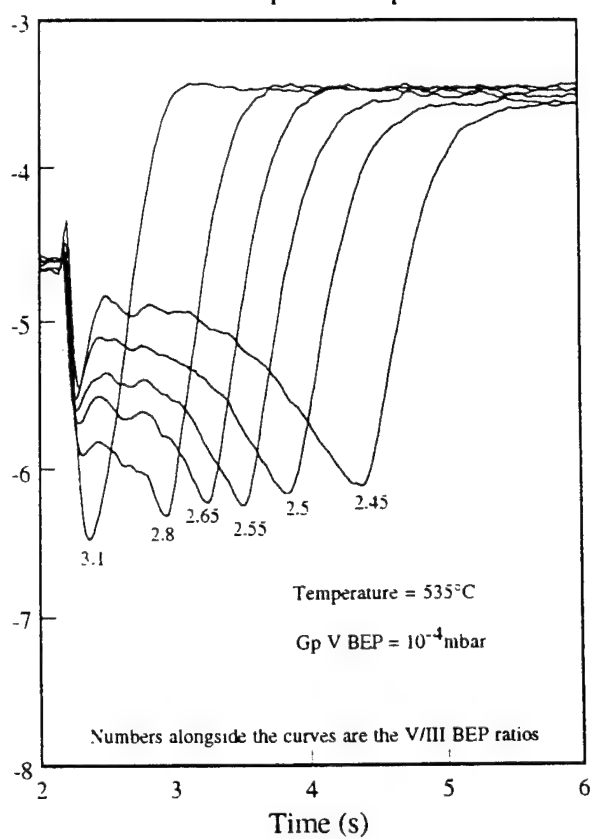


Figure 3 RAS trace of the transient surface state for different precursor pressures and temperatures

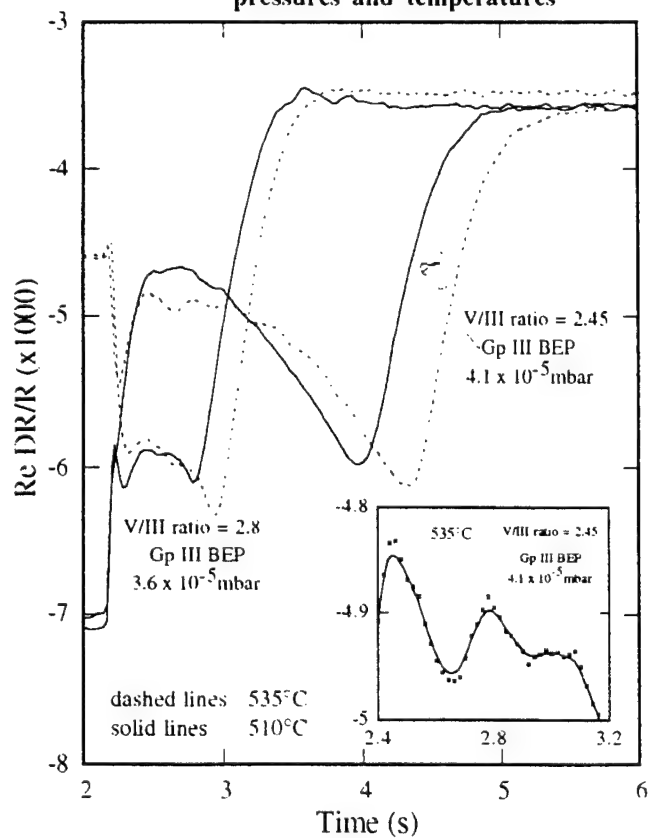
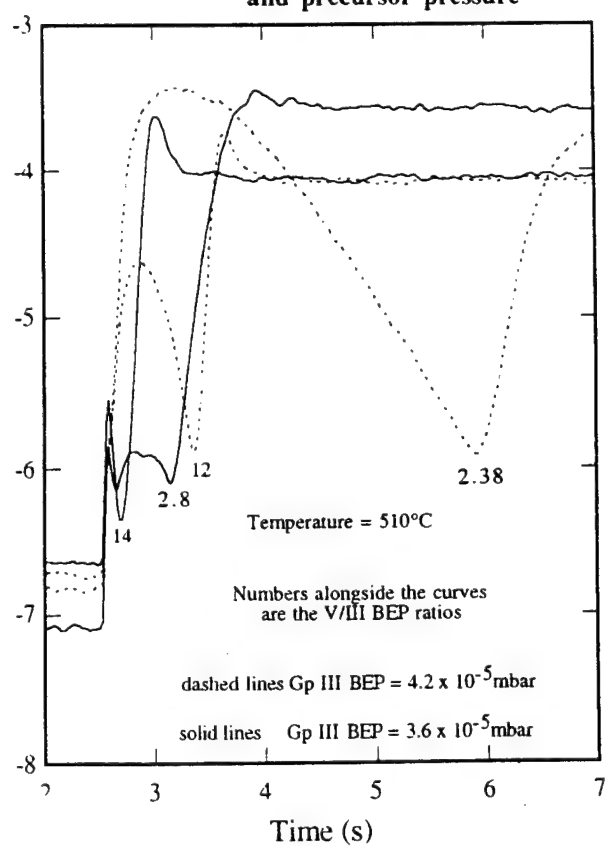


Figure 4 Surface transient state and precursor pressure



# MBE&E: MBE and/or Etch

K. R. Evans<sup>1</sup>, J. E. Ehret<sup>1</sup>, E. N. Taylor<sup>1</sup>, C. R. Jones<sup>2</sup>, D. Via<sup>2</sup>, and R. Kaspi<sup>2</sup>

<sup>1</sup>Wright Laboratory (WL/ELDM), Wright-Patterson Air Force Base, Ohio 45433-7323

<sup>2</sup>University Research Center, Wright State University, Dayton, Ohio 45435

The conventional approach to heterostructure growth by molecular beam epitaxy (MBE) involves a scheduled sequence of deposition steps and sometimes also growth interrupts. We present a logical extension of conventional MBE by adding controlled etch steps to the growth schedule. Controlled etching is accomplished by conventional temperature-programmed desorption (TPD), which is implemented as a completely automated subroutine in the computerized growth schedule. This new growth approach, which we term MBE and/or Etch, or MBE&E, significantly extends the capabilities of the MBE growth process.

For example, MBE-grown InGaAs/(Al,Ga)As interfaces are known to be graded over up to 10 monolayers, due to surface segregation of In atoms during growth. Since the composition profile at both top and bottom heterointerfaces closely mimics the time evolution of the surface segregated In population (Q) during growth, the direct control of Q would provide the ability to produce more truly "square" interfaces. (Kinetic limitation of In surface segregation is not practical due to the severe conditions required to realize it.) Fortunately, MBE&E provides for direct control of Q by selectively populating Q, via appropriate In deposition steps at the bottom interface, and selectively depopulating Q, via thermal etch steps at the top interface.<sup>1</sup> This approach results in a much more square quantum well, as was recently been corroborated by x-ray diffraction analysis and high resolution TEM imaging measurements.<sup>2</sup> Figure 1 shows a typical In and Ga TPD spectrum for a 45 monolayer thick pseudomorphic In<sub>0.22</sub>Ga<sub>0.78</sub>As film grown on an AlAs buffer on GaAs (001). The first In peak is due to thermal desorption of surface segregated In, while the second In and the only Ga peak are due to dissociation of the underlying InGaAs lattice. A similar approach has been used to produce GaAsSb/GaAs interfaces which are much more square than previously obtained.<sup>3</sup> Indeed, the utility of this technique is quite general since the bulk and surface compositions differ for all alloys, and it is the surface-enriched component which generally can be selectively removed via thermal desorption.

The growth of GaN by gas source MBE has suffered from low growth rates due in part to limited available fluxes of active nitrogen species. The ability to determine the surface Ga accumulation rate in-situ provides a valuable tool for optimizing growth conditions. In Figure 2 we show how Ga TPD spectra quickly indicate how certain growth conditions can give rise to significant Ga surface accumulation - in this case low growth temperature and/or low NH<sub>3</sub> flux.

A most exciting application of MBE&E is for quantum wire or dot fabrication. As schematically shown in Figure 3, quantum well structures which have been patterned with refractory or dielectric are then reloaded into the MBE chamber, where the exposed barrier and well regions are thermally etched; then the barrier is (re)grown to produce quantum wires or dots. Excellent lateral heterointerface properties are expected because the etch/regrow steps are performed sequentially in-situ. We will report on the progress of this recently initiated effort.

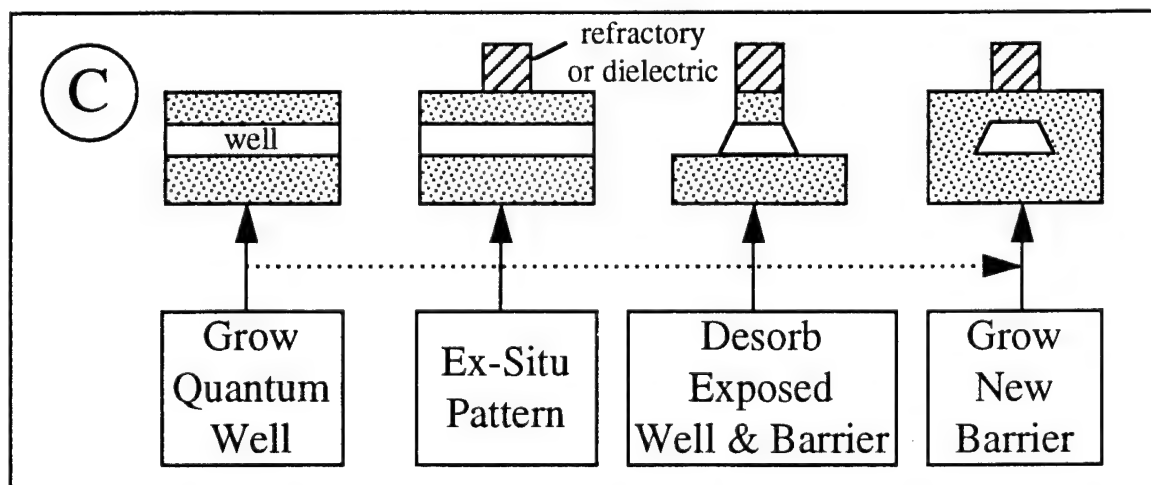
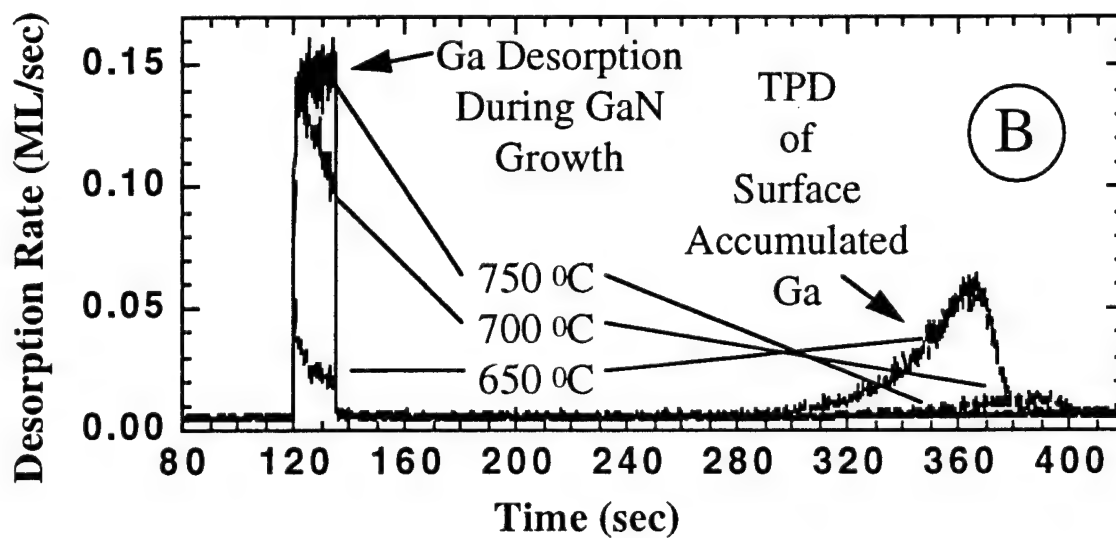
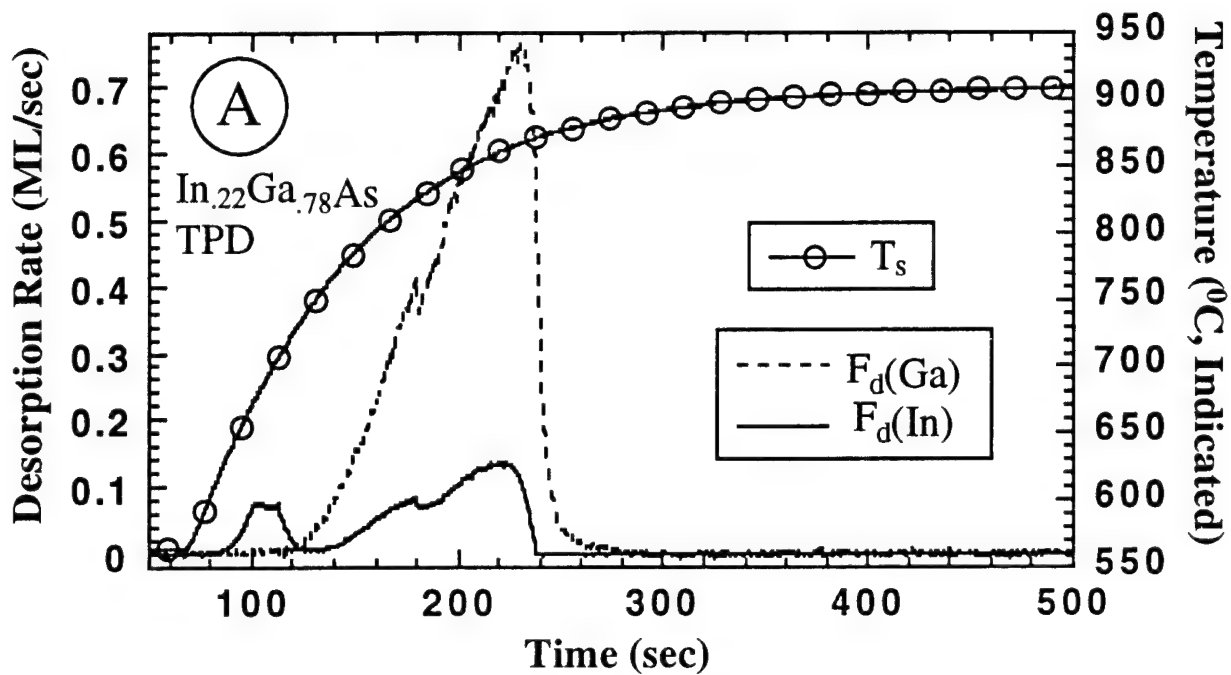
In summary, incorporation of TPD analysis as an integral subroutine in the MBE growth schedule enables rapid growth condition optimization, advanced heterointerface profile engineering, and the potential for high quality quantum dot and wire fabrication. These and other applications of MBE&E will be discussed in detail.

**Acknowledgments:** The authors thank C. Huang, L. Kyle, and C. Litton for technical support. Authors RK and CRJ were supported by US Air Force Contract # F33615-95-C-1765. This work was partially supported by the US Air Force Office of Scientific Research (AFOSR).

<sup>1</sup>K. R. Evans, et al., J. Vac. Sci. Tech. B 13, 1820 (1995).

<sup>2</sup>J. McCaffrey and Z. Wasilewski, private communication.

<sup>3</sup>R. Kaspi and K. Evans, to be published.



## Effect of GaAs Substrate Properties on Optical Bandgap Thermometry

S. R. Johnson\* and T. Tiedje

Advanced Materials and Process Engineering Laboratory,  
Departments of Physics and Electrical Engineering,  
University of British Columbia, Vancouver, BC, V6T 1Z4

Optical bandgap thermometry is a convenient method for measuring substrate temperature during epitaxial growth of III-V compound semiconductors that overcomes some of the limitations of thermocouples and pyrometers[1-4]. However changes in doping, substrate thickness, and back surface texture can have an appreciable effect on the optical absorptance in the vicinity of the bandgap and hence must be accounted for in order to obtain accurate temperature measurements by bandgap thermometry. Changes in these parameters can easily produce temperature errors that exceed the sensitivity of the measurement technique (0.5 °C in a typical situation). One solution is to calibrate the bandgap thermometer for each batch of substrates. However calibrations are time consuming and typically require access to a separate furnace as they are difficult to carry out in conventional thin film growth reactors.

In practice the substrate temperature is inferred from the spectral position of various critical points in the optical transmission or diffuse reflectance spectra, such as the inflection point or the knee (maximum of the first and the second derivatives respectively). In this work, information on the temperature dependent shape of the absorption edge in GaAs [5] is used to determine the effect on the critical points of: variations in substrate thickness, doping, back surface texture, deposited thin films, the width of the Urbach tail, and changes in the residual absorption below the bandgap. These effects are modeled for both transmission and diffuse reflectance, the two most commonly used optical configurations in bandgap thermometry. For example, for materials such as GaAs that exhibit the Urbach behavior, where the absorption edge is exponential in energy and has been measured as a function of temperature [5], an expression can be obtained for the position of the knee (relative to the bandgap energy) as a function of substrate thickness, which for GaAs is given by  $-[8.8 + \ln(d)]E_o(T)$  where  $d$  is the thickness of the substrate in units of mm and  $E_o(T)$  is the width of the absorption edge.

Bandgap thermometry is also sensitive to thin film interference during the growth of wide bandgap epilayers, which can cause the apparent temperature to oscillate. An algorithm is presented that uses the width of the knee in the spectrum to correct the position of the knee for the interference oscillations. This algorithm is suitable for real-time applications as the information needed to correct the knee position is obtained from the spectrum itself. The correction procedure is tested on temperature data taken during growth of AlGaAs on GaAs, at constant substrate heater power. The interference oscillations in the deposited thin film produced apparent rms temperature oscillations of about 1.5 °C at 570 °C which were reduced to about 0.7 C after correction.

\*Present address: Center for Solid State Electronics Research, Arizona State University, Tempe, AZ

- [1] S. R. Johnson, C. Lavoie, M. K. Nissen, T. Tiedje, US Patent No. 5,388,909 (1995).
- [2] T. P. Pearsall, S. R. Saban, J. Booth, B. T. Beard, and S. R. Johnson, Rev. Sci. Instrum. **66**, 4977 (1995).
- [3] J. A. Roth, T. J. DeLyon, and M. E. Adel, Mat. Res. Soc. Symp. Proc. **324**, 353 (1994).
- [4] D. M. Kirillov and R. A. Powell, US Patent No. 5,118,200 (1992).
- [5] S. R. Johnson and T. Tiedje, J. Appl. Phys. **78**, 5609 (1995).

Shane Johnson  
Center for Solid State Electronics Research  
Arizona State University  
Box 876206  
Tempe, AZ 85287-6206

Office: 602-965-2565  
Fax: 602-965-8118  
Email: shane.johnson@asu.edu



ORGANIZED GROWTH OF GaAs/AlAs LATERAL SUPERLATTICES  
ON VICINAL SURFACES : WHERE ARE THE LIMITS?

F. Laruelle, F. Lelarge, F. Petit, T. Mélin and A. Cavanna

Laboratoire de Microstructures et de Microélectronique (L2M), C.N.R.S.,  
B.P. 107, 92225 Bagneux Cedex, France.

Tel : + 33 1 42 31 73 30. Fax : + 33 1 42 31 73 78. E-mail : francois.laruelle@bagneux.cnet.fr

We have already discussed the MBE growth optimization of GaAs/AlAs Lateral Superlattice (LSL) on vicinal surfaces to get new electronic properties typical of strongly modulated Electronic Systems (ES) [1]. Lateral organization of GaAs and AlAs by atomic steps in LSL is incomplete due to the strong atomic vertical exchange of Ga and Al [2]. We address here limits and growth issues to the realization of One Dimensional (1D) multiple quantum wires with negligible lateral tunnel coupling. This requires LSLs with larger periodicities or with higher Al content to increase the potential over confinement energy ratio.

One objection against growing on substrates with very low misorientation angles  $\alpha$  of  $0.2^\circ$ – $0.3^\circ$  is that the LSL tilt angle  $\beta$  would always be large since it goes as  $\arctan(\epsilon/\alpha)$  where  $\epsilon$ , expressed in Monolayers (ML), is the error to the ideal unity surface coverage by the LSL layers. We show the LSL tilt is *not* a critical issue when electronic properties are concerned. Since the potential amplitude scales with  $N\epsilon$  and not  $\beta$ , where  $N$  is the LSL thickness in ML, the flux control is *not* ten times more stringent on  $0.2^\circ$  than on  $2^\circ$  surfaces with this respect! The surface coverage needs to be controlled with an accuracy only better than  $1/N$  where  $N$  is usually less than 100. The flux *stability* however is much more critical to maintain a constant coverage throughout the LSL growth typically during 30–60 min. The Ga flux stability is determined by very accurate RHEED oscillation measurements for 40 min. . It is improved by a factor three using a two filaments Ga cell ( $3\sigma$  statistic fluctuations of only 0.2%) compared to single filament one (0.6%) provided that three hours have elapsed after outgassing the Ga cell. If the tilt is not a problem, we show that surface migration of adatoms is a severe matter. Although the RHEED pattern exhibits a split specular spot indicative of a well defined step periodicity even on MBE grown GaAs  $0.2^\circ$  misoriented surfaces, AFM scans reveal that step edges are rough for misorientation smaller than  $0.3^\circ$  because of a too short migration length of Ga adatoms.

Increasing the LSL average Al content  $x_{av}$  leads to a much higher potential modulation since transport, optics and TEM indicate that the Ga/Al lateral separation increases with  $x_{av}$ . The modulation doping is less efficient since the effective barrier height between the doped  $Al_{0.33}Ga_{0.67}As$  and the LSL decreases. We show that 1D ES exhibit at low temperature new electronic features specific of a 1D potential owing to the low disorder. The absence of magneto-resistance along the step edges and the presence of a sharp Fermi edge singularity show that electrons at the Fermi level are not sensitive to the step edge roughness. We therefore qualify LSL lateral interfaces as pseudo-smooth according to the classification used for quantum wells interfaces.

[1] B. Etienne, F. Laruelle, J. Bloch, L. Sfaxi and F. Lelarge, J. Cryst. Growth **150**, 336 (1995).

[2] B. Etienne and F. Laruelle, J. Cryst. Growth **127**, 1056 (1993).



# Formation of Multi-atomic Steps and a Novel n-AlGaAs/GaAs Heterojunctions on a Vicinal (111)B Substrate by MBE and Anisotropic Transport of 2D electrons

Y. Nakamura, S. Koshiba, and H. Sakaki

RCAST, University of Tokyo, 4-6-1 Komaba, Meguro-ku, Tokyo 153, Japan and  
Quantum Transition Project, JRDC, 4-7-6 Komaba, Meguro-ku, Tokyo 153, Japan  
tel:81-3-3481-4464, fax:81-3-3466-8308, e-mail:nakamura@kyokusho.rcast.u-tokyo.ac.jp

Recently, the use of multi-atomic step structures for the fabrication of quantum wire (QWR) and planar superlattice (PSL) has been attempted <sup>1, 2</sup>. We report on the growth and transport properties of novel n-AlGaAs/GaAs heterojunctions prepared on a vicinal (111)B GaAs substrate, where multi-atomic steps are formed with the average period of 20~30nm. We show that the electrical conductance  $G_{\perp}$  across the steps is far lower than that  $G_{\parallel}$  along the steps. This anisotropy is found to increase when the Fermi energy or temperature is lowered. These results indicate that the electron motion is blocked by some potential barriers perpendicular to the steps, whereas their motion along the steps is almost free.

A 0.6  $\mu\text{m}$ -thick GaAs layer was grown by MBE at 590  $^{\circ}\text{C}$  on a vicinal (111)B substrate inclined  $2^{\circ}$  toward  $[\bar{1}\bar{1}0]$ . The growth rate was  $\sim 0.25\mu\text{m/hr}$  and the  $\text{As}_4/\text{Ga}$  flux ratio of beam equivalent pressure was 77. Figures 1 (a) and (b) show, respectively, the image of the GaAs surface taken by the atomic force microscopy (AFM) and its spectrum. Note that quasi-periodic step structures are formed with the average period of 22nm. Even more regular steps are achievable by raising the  $\text{As}_4$  flux by factor of two. A selectively doped n-AlGaAs layer with a 20nm-thick spacer layer was grown on this corrugated GaAs surface as illustrated in Fig. 1 (c). Two types of FETs with Hall-bars were prepared so that the current is either perpendicular to or parallel to the steps (See Fig. 2 (a) and (b)).

The drain current  $I_d$  of two samples was measured at 18K as functions of the gate voltage  $V_g$ . The result for the drain voltage  $V_d$  of 0.1V is shown in Fig. 2 (c). The current  $I_{d\parallel}$  or conductance  $G_{\parallel}$  ( $=I_d/0.1\text{V}$ ) parallel to the steps increases almost linearly with  $V_g$  for  $V_g \geq -2\text{V}$ , whereas the  $I_{d\perp}$  or  $G_{\perp}$  perpendicular to the steps is virtually zero for  $V_g \leq -0.5\text{V}$ . The ratio  $G_{\parallel}/G_{\perp}$  is 140 even at gate voltage  $V_g=0\text{V}$ . This anisotropy was found to decrease when temperature  $T$  is raised as shown in Fig. 3. The observed  $T$  dependence of  $I_{d\perp}$  suggests that the transport is via thermally activated process over some potential barriers. In contrast,  $I_{d\parallel}$  parallel to the steps seems to have a character of an ordinary 2DEG. Moreover, we found that  $I_{d\perp}-V_d$  relation show negative differential resistance as shown in Fig. 4. These results indicate that the electronic motion parallel to the steps is smooth but that perpendicular to them is almost forbidden by some potential barriers.

In summary, we have grown by MBE a novel n-AlGaAs/GaAs heterojunction on a vicinal (111)B GaAs substrate and found that multi-atomic step structures at the heterojunction influence electron transport substantially.

We thank Dr. Ichiro Tanaka and Dr. Metzner for their very useful discussions, and Professor Shiraki and Mr. Usami for the help in AFM observation.

<sup>1</sup> R. Nötzel, L. Däweritz, N. N. Ledentsov, and K. Ploog, *Surf. Sci.* **267**, 209 (1992).

<sup>2</sup> R. Nötzel, D. Eissler, and K. Ploog, *J. Crystal Growth* **127**, 1068 (1993).

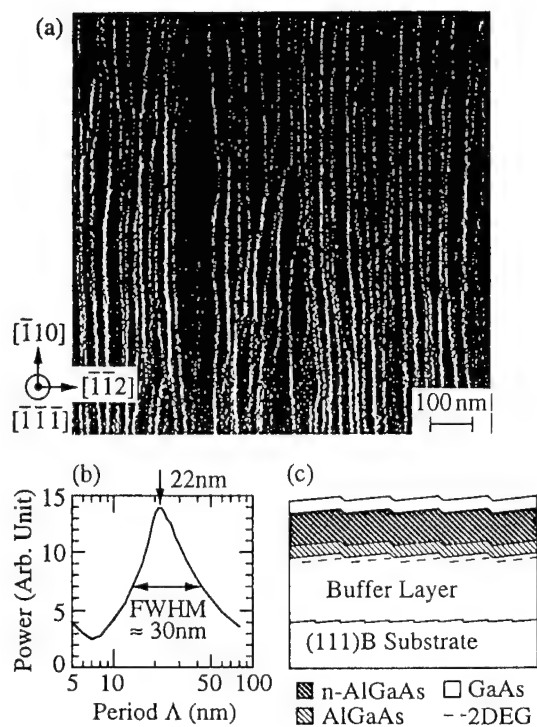


Fig. 1 The AFM image of a GaAs layer grown on a vicinal (111)B surface (a), the spectrum of the surface (b), and the cross-section of the heterojunction (c).

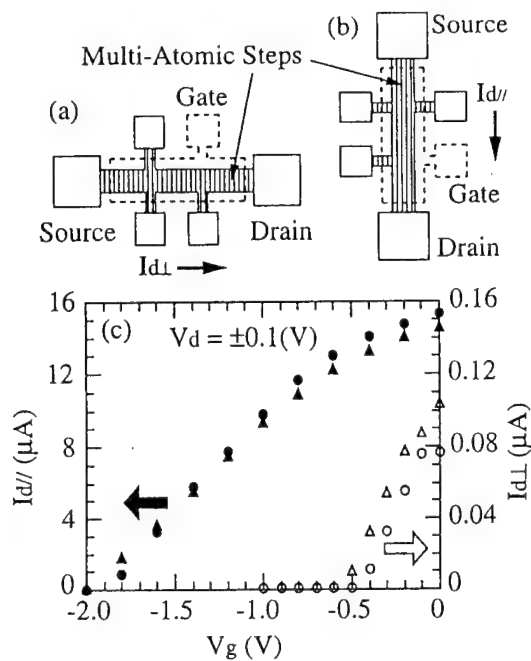


Fig. 2 Two FETs in (a) and (b). The current  $I_{d//}$  and the  $I_{d\perp}$  (c). Circles and triangles are data points for the drain voltage  $V_d$  of +0.1V and -0.1V, respectively.

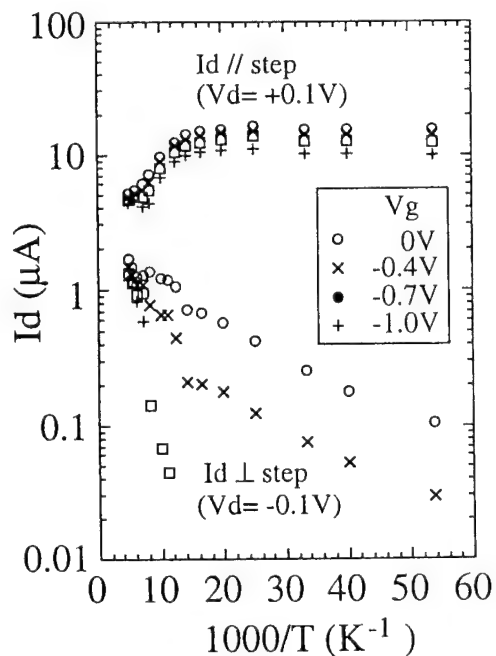


Fig. 3 The temperature dependence of current  $I_{d//}$  and  $I_{d\perp}$  with a parameter of  $V_g$ .

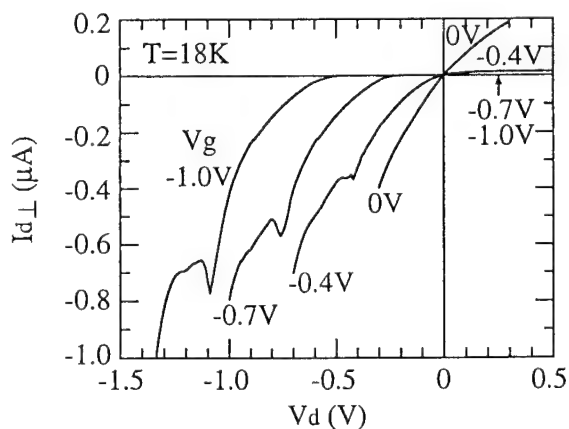


Fig. 4 The current  $I_{d\perp}$  flowing perpendicular to the steps.

## **Be redistribution in InGaAs and InP grown by gas source molecular beam epitaxy**

**Teruo Mozume, Kazuhiko Hosomi**

*Central Research Laboratory, Hitachi, Ltd., Kokubunji, Tokyo 185, Japan*

Phone: +81-423-23-1111

Fax: +81-423-27-7821

e-mail: mozume@crl.hitachi.co.jp

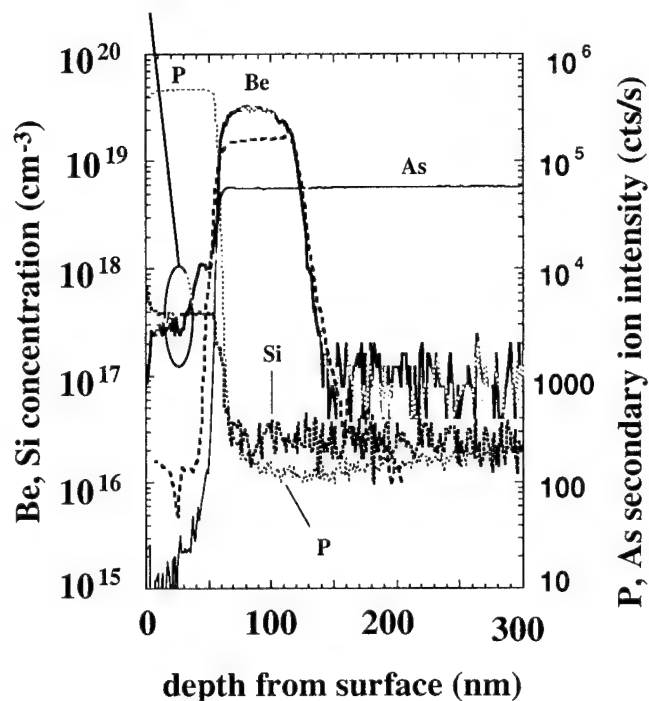
To achieve the full potential of heterojunction bipolar transistors (HBTs) in terms of the high-speed performance, rigorous control of doping profiles in the base region is necessary. Specifically, device performance can be improved through heavy p-type doping of the transistor base region to reduce base resistance while maintaining narrow abrupt base-doping profiles to keep the minority-carrier transit time through this region short. For the acceptor-doped base layer, beryllium is the conventional dopant used in molecular beam epitaxy (MBE) because of its high doping efficiency, good hole transport properties, and acceptable diffusion rate at moderate doping levels. However, for doping levels in the  $10^{19} \text{ cm}^{-3}$  range, it has been reported that concentration-dependent diffusion becomes a significant problem under typical MBE growth conditions and the presence of nearby n-type layers, as in an HBT structure, increases the amount of diffusion.

Although Be diffusion in GaAs/AlGaAs has been extensively studied and has been found to be based on the substitutional-interstitial diffusion (SID) mechanism, there are few reports on Be redistribution in InGaAs/InP and the mechanism of this redistribution has been described as rather complex.

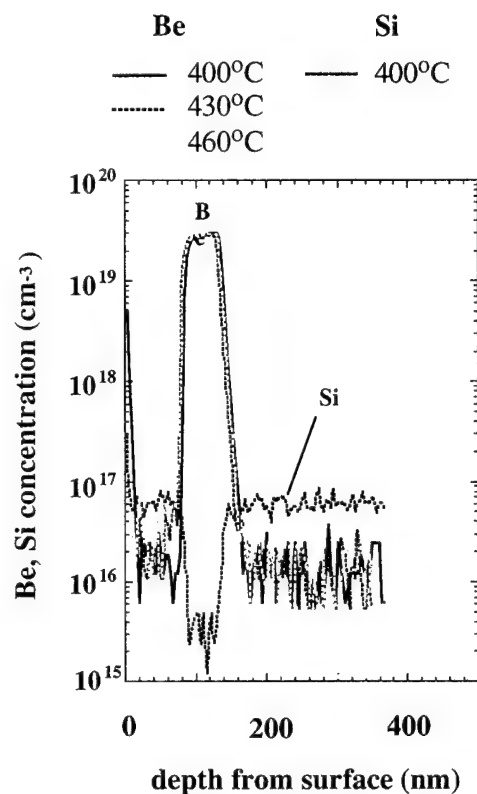
To gain a better understanding of the processes involved in Be redistribution, we have investigated the effects of growth temperature, group V flux, and n-type doping concentrations in nearby layers by studying secondary ion mass spectrometry (SIMS) depth profiles. InGaAs and InP layers were grown by gas source molecular beam epitaxy (GSMBE) using Ga and In as group-III growth species and 100% AsH<sub>3</sub> and PH<sub>3</sub> as group-V growth species.

We found that extended use of high-concentration Be doping causes Be deposition even when the Be shutter is closed, and this unintentional Be doping causes significant Be redistribution into the InP-layer grown next. When the Be temperature was lowered by 200°C to about 650°C before and after the Be doping layers were grown, the SIMS profiles of InGaAs and InP showed negligible dependence on growth temperature, AsH<sub>3</sub>/PH<sub>3</sub> flow rate, or n-type doping levels ranging from  $7 \times 10^{17}$  to  $4 \times 10^{19} \text{ cm}^{-3}$  in the nearby layer. In InGaAs/InP heterostructures, however Be profiles spread wider as the PH<sub>3</sub> flow rate increased, which is inconsistent with the previously proposed SID mechanism.

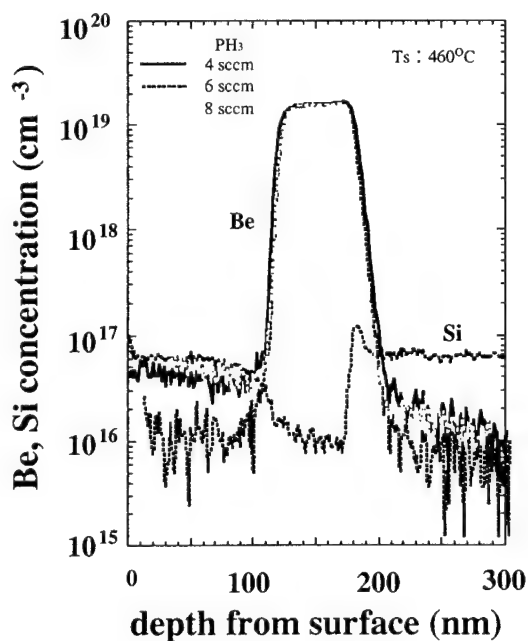
Be temperature was kept constant throughout growth



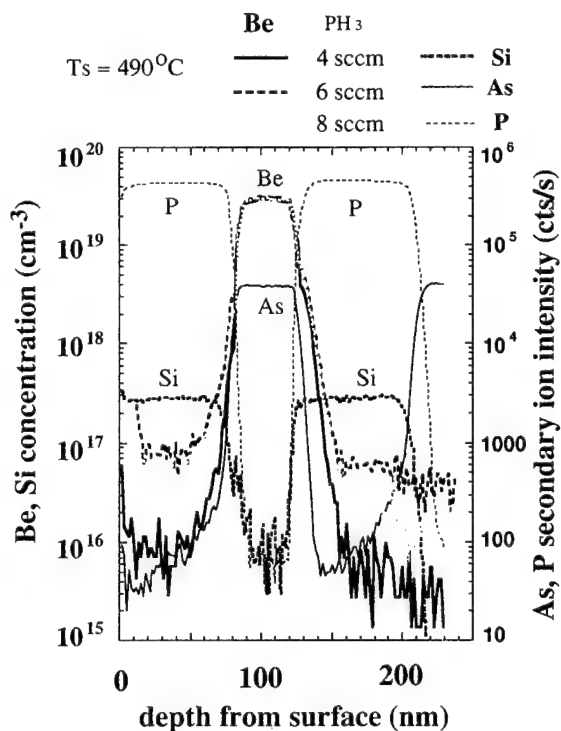
Be temperature profile dependence of Be profiles in InGaAs/InP heterostructures



Growth temperature dependence of Be profiles in InGaAs



Phosphine flow-rate dependence of Be profiles in InP



Phosphine flow-rate dependence of Be profiles in InGaAs/InP heterostructures  
AsH<sub>3</sub> : 6 sccm

## A Monte Carlo Study of Gallium Desorption Kinetics during MBE of (100)-GaAs/AlGaAs Heterostructures

K. Mahalingam and D. L. Dorsey  
Wright Laboratory  
Materials Directorate (WL/MLPO)  
Wright Patterson AFB, OH 45433-7707

K. R. Evans  
Wright Laboratory,  
Solid State Electronics Directorate (WL/AADP)  
Wright Patterson AFB, OH 45433-7323

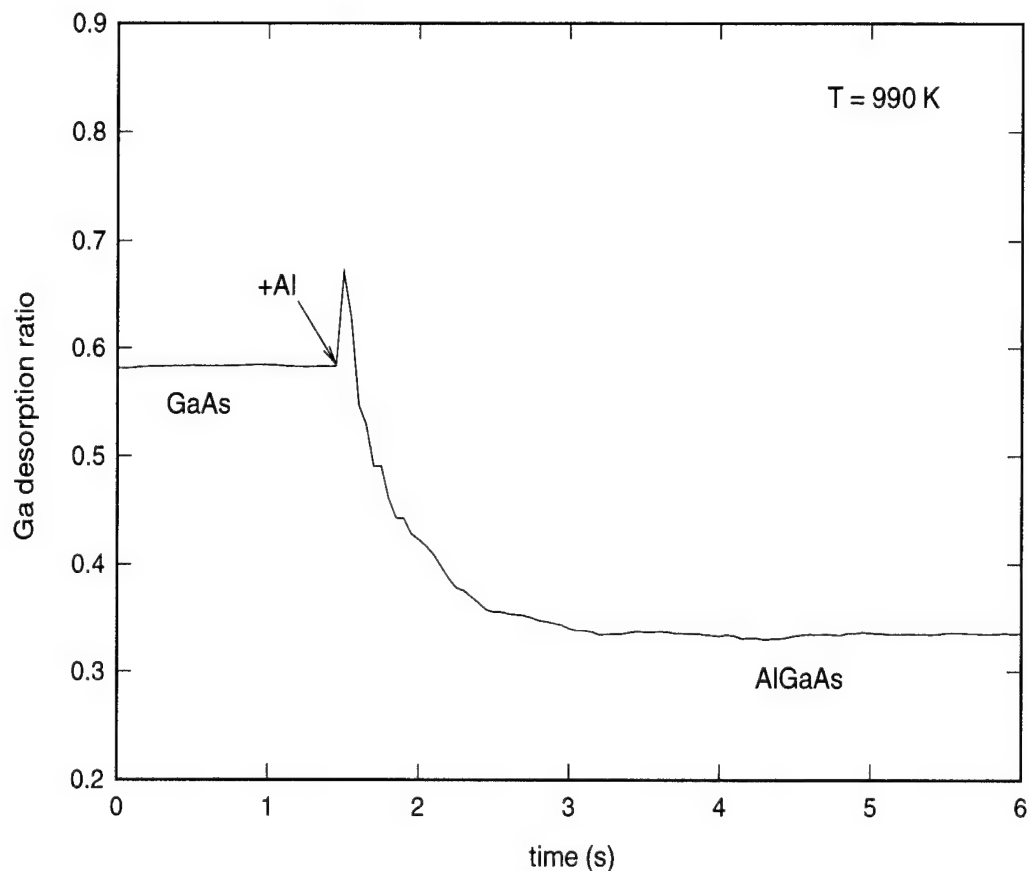
R. Venkatasubramanian  
Department of Electrical Engineering  
University of Nevada  
Las Vegas, NV 89154

Molecular beam epitaxy (MBE) of GaAs/Al<sub>x</sub>Ga<sub>(1-x)</sub>As heterostructures is often performed at substrate temperatures where considerable Ga desorption is observed. In-situ desorption mass spectrometry studies by Evans et. al [1] have shown that the time evolution of the Ga desorption rate during heterointerface formation differs significantly at the AlGaAs-on-GaAs and GaAs-on-AlGaAs interfaces, resulting in significant grading of the AlGaAs-on-GaAs interface. In this study we develop a Monte Carlo simulation model for MBE of GaAs/AlGaAs heterostructures wherein a surface Al-Ga exchange reaction is included as a kinetic mechanism in order to explain the observed Ga desorption behavior. Simulations were performed for growth temperatures in the range of 650-720°C, with flux conditions and growth rates the same as that reported in the experimental studies [1]. The desorption rates of the individual species and the Al/Ga concentration profiles (during growth of AlGaAs) were obtained as a function of growth time. The results from these simulations show that the experimentally observed transients in Ga desorption rate at AlGaAs-on-GaAs heterointerface are well described in terms of two independent mechanisms: (1) the surface Al-Ga exchange mechanism and (2) the competition for site occupation between Al and Ga, arising due to difference in Al-Ga and Ga-Ga interaction strengths. Further details on the role of surface stoichiometry and the influence of V/III flux ratio on Ga desorption behavior will be presented. The dependence of activation energy for Ga desorption on Al concentration and V/III flux ratios will also be examined.

1. K. R. Evans, C. E. Stutz, E. N. Taylor and J. E. Ehret, J. Vac. Sci. Technol. **B9**, 2427 (1991).

## SUPPORTING DATA

K. Mahalingam, D. L. Dorsey, K. R. Evans, and R. Venkatasubramainam, "A Monte Carlo Study of Gallium Desorption During MBE of (100)-GaAs/AlGaAs Heterostructures"



Plot showing Ga desorption ratio versus time predicted from a model which includes a Al-Ga surface exchange mechanism and a site competition mechanism for Al and Ga. This model is able to reproduce the transient in Ga desorption ratio during growth of AlGaAs on GaAs, observed experimentally by Evans et al. [1]. While the sharp rise in Ga desorption ratio upon opening of the Al shutter is well described by both the surface exchange and site competition mechanisms, the reduction in Ga desorption ratio during growth of AlGaAs is explained only by the site competition mechanism.

## High Temperature Surface Cleaning of AlGaAs without As Flux for MBE Regrowth

K. Iizuka, K. Matsumaru, T. Suzuki, Y. Takahira\*, T. Nishioka\* and H. Okamoto\*

Nippon Institute of Technology

4-1 Gakuendai, Miyashiro, Minami-Saitama, Saitama 345, JAPAN

TEL: +81-480-34-4111, FAX: +81-480-34-2941, e-mail: iizuka@nit.ac.jp

\* Chiba University, Faculty of Engineering

1-33 Yayoi-cho, Inage-ku, Chiba 263, JAPAN

A novel high temperature surface cleaning method for GaAs substrate was proposed [1], which was very successful in MBE regrowth for fabricating an epilayer necessary for a DFB laser diode [2]. This cleaning was carried out in the preparation chamber at a temperature as high as 575°C without As flux. Surface contamination was completely removed, and furthermore the cleaned surface maintained mirror-like smoothness. So, direct growth of high quality GaAs/AlGaAs QW structure without any buffer layer on such surface was possible. In this study, this method is extended to the cleaning of an AlGaAs epilayer surface which was exposed to the atmosphere. Quality of the cleaned surface was examined by RHEED, AES, QMS, SIMS and AFM. GaAs/AlGaAs QW structures were grown over the surface and their PL spectrum was also examined.

An AlGaAs (Al composition  $x=0.3\sim0.4$ ) epilayer surface was immersed in the deionized water and some oxide was formed on it. After then, the wafer was undergone by heat treatment at 650°C without As flux in the preparation chamber. QMS exhibits that the amount of sublimation of Ga, Al and As from the surface decreases drastically in the case of  $x$  greater than 0.3. Figure 1 shows RHEED pattern and AES spectrum of the AlGaAs surface after cleaning. Although the surface looks mirror-like by naked eye inspection, RHEED shows a spot pattern. AFM indicates that the root mean square of the surface roughness is much smaller as compared to that of the cleaned GaAs surface, and independent of the cleaning temperature as shown in Fig.2. AES shows that oxygen remains on the surface suggesting the  $Al_2O_3$  formation during the air exposure or under the thermal cleaning of the surface, but carbon was completely removed from the surface.

An epilayer with 500nm GaAs buffer layer followed by SQWs composed of GaAs QWs 3, 4.5, 7 and 15nm thick separated by AlGaAs 50nm thick barriers was grown on the cleaned AlGaAs surface with growth temperature at 670°C. In Fig.3, well defined PL spectrum was measured at 300K, which was in contrast to the epilayer grown on the surface cleaned by the conventional method (a flush annealing under As environment at 690°C), which often gave rougher surface and broad PL spectrum. In the present regrowth, thickness of the buffer layer is critical, and at least 100nm is necessary for intense PL as shown in Fig.4. It can be reduced up to 25nm if the starting epilayer surface is an AlGaAs covered with a thin GaAs passivation layer.

[1] K. Iizuka, K. Matsumaru, T. Suzuki, H. Hirose, K. Suzuki, H. Okamoto, J. Cryst. Growth, 150 (1995) 13.

[2] Y. Takahira, T. Usami and Y. Matsushima, to be presented at Optoelectronic Conf., 1996.

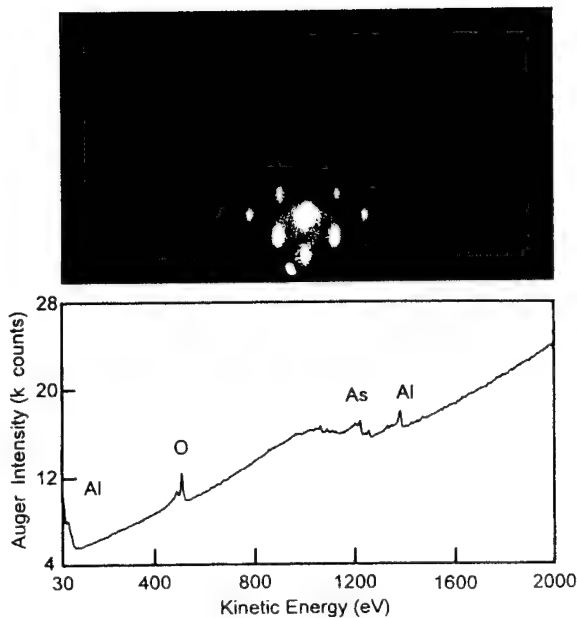


Fig.1 RHEED pattern and AES spectrum of AlGaAs surface which was treated at 650°C without As flux.

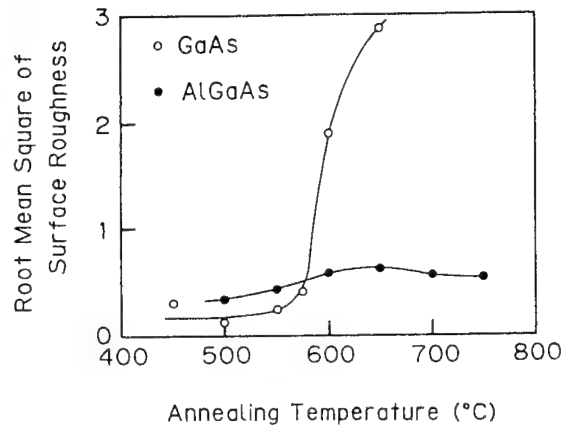


Fig.2 Annealing temperature dependence of the root mean square of the surface roughness in AFM image.

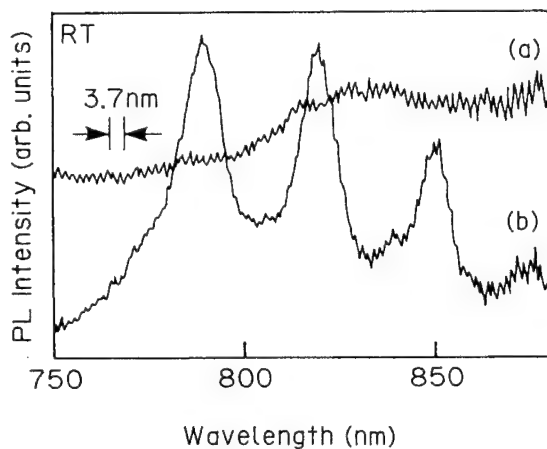


Fig.3 PL spectra from the stacked SQWs on treated AlGaAs with 500nm thick AlGaAs buffer layer.

- (a) treated by conventional method.
- (b) treated by high temperature surface cleaning method.

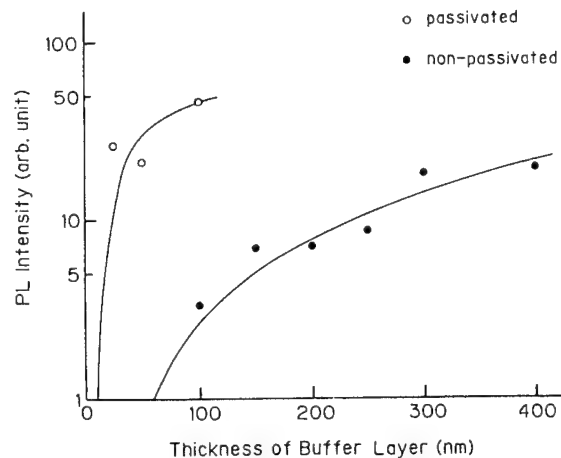


Fig.4 PL intensity from SQW on treated AlGaAs surface which was passivated (open circle) or non-passivated (solid circle) as a function of thickness of regrown AlGaAs buffer layer.



## Evolution of short- and long-range order during Si incorporation on GaAs(001) observed by RAS and RHEED during MBE

L. Däweritz<sup>1</sup>, K. Stahrenberg<sup>2</sup>, P. Schützendübe<sup>1</sup>, J.-Th. Zettler<sup>2</sup>, W. Richter<sup>2</sup>, K.H. Ploog<sup>1</sup>

<sup>1</sup> Paul-Drude-Institut für Festkörperelektronik, Hausvogteiplatz 5-7, D-10117 Berlin, Germany

<sup>2</sup> Institut für Festkörperphysik, Technische Universität Berlin, D-10623, Berlin, Germany

Tel.: (49-30)203 77 359, Fax: (49-30) 203 77 201, daeweritz@pdi.wias-berlin.de

We have studied the atomic processes during Si deposition on the singular GaAs(001) surface and on the vicinal surface with 2° misorientation toward (111)Ga at enhanced adatom mobility (substrate temperature 590 °C, As<sub>4</sub> beam equivalent pressure 1x10<sup>-6</sup> Torr, pulsed Si supply). In a narrow parameter range (close to the phase transition between an As- and metal-rich surface) we find characteristic differences between the singular and the vicinal surfaces regarding the evolution of the short-range order (local chemical composition) as well as of the long-range order monitored by reflectance anisotropy spectroscopy (RAS) and reflection high-energy electron diffraction (RHEED).

As shown in Fig. 1 for the vicinal surface, the RAS spectrum of the initial (2 x 4) reconstructed surface is dominated by the transition at 2.6 eV which is assigned to the As dimers with  $[\bar{1}10]$  bonding direction. During deposition of 0.3 ML Si the whole spectrum is shifted to a lower level and a clear minimum at 2 eV due to Ga dimers with  $[110]$  bonding direction appears, as expected for the evolution of a metal (Ga, Si)-rich surface. The clear 2.6 eV peak due to the As dimers persists, however. Recordings of fractional-order RHEED beams evidence a *phase separation* into differently reconstructed domains. The behaviour of the fractional-order RHEED beams as well as of the RAS spectra for coverages above 0.3 ML Si can be understood by the re-adsorption of As dimers after a certain completion of the first Si layer followed by the formation of a Si double layer with 90° rotation of adsorbed As dimers. The drop in the high-energy part of the RAS spectrum indicates an increased surface roughness at medium Si coverages.

The pulsating behaviour of the RAS signal recorded at a photon energy of 2.6 eV during pulsed Si supply (Fig. 2a) reveals that both on the singular and on the vicinal surface ordering processes occur with a destruction of As dimers during the pulse and their partial reformation after the pulse. There are, however, clear differences in the RAS transients for the two surfaces with minima at ~ 0.3 ML and ~ 0.6 ML Si, respectively, that are discussed in terms of a different re-adsorption of As dimers as a consequence of a different long-range order of the incorporated Si. The rapid change in the specular beam RHEED intensity (Fig. 2b) after deposition of ~ 0.1 ML Si on the vicinal surface is typical for a system with rapid changes in strain and structure (reconstruction, steps). Therefore, we conclude that the phase separation into metal- and As-rich domains is much stronger on the vicinal surface due to an accumulation of Si atoms in the near-step-edge region.

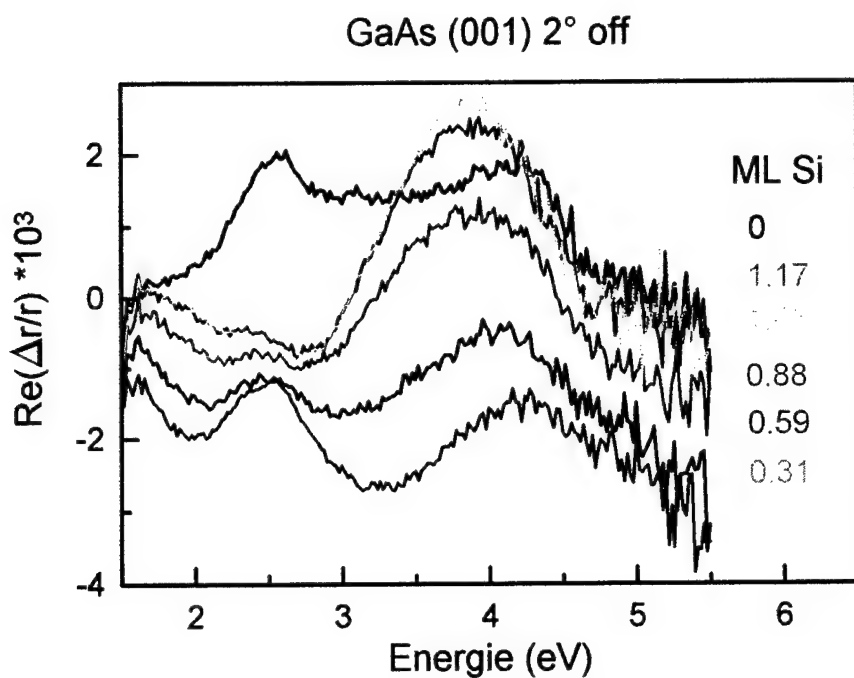


Fig. 1. RAS spectra of the vicinal GaAs(001) surface taken during Si deposition.

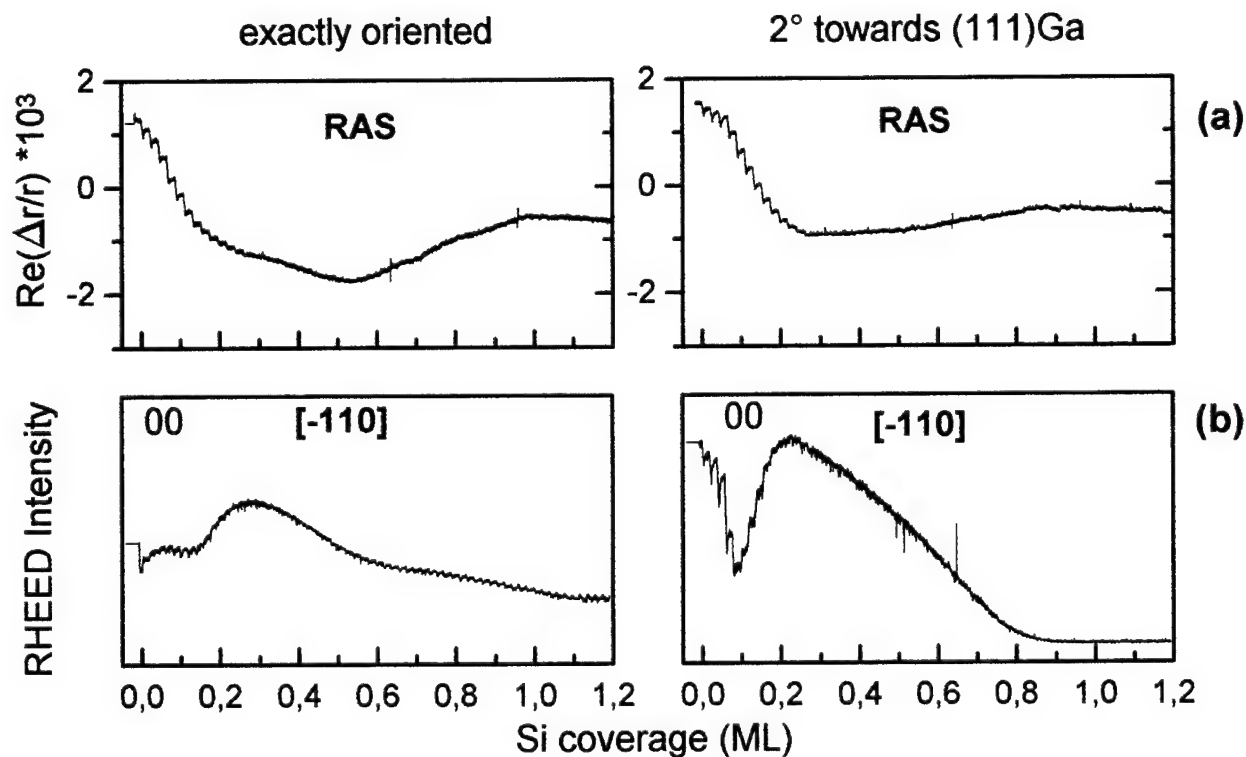


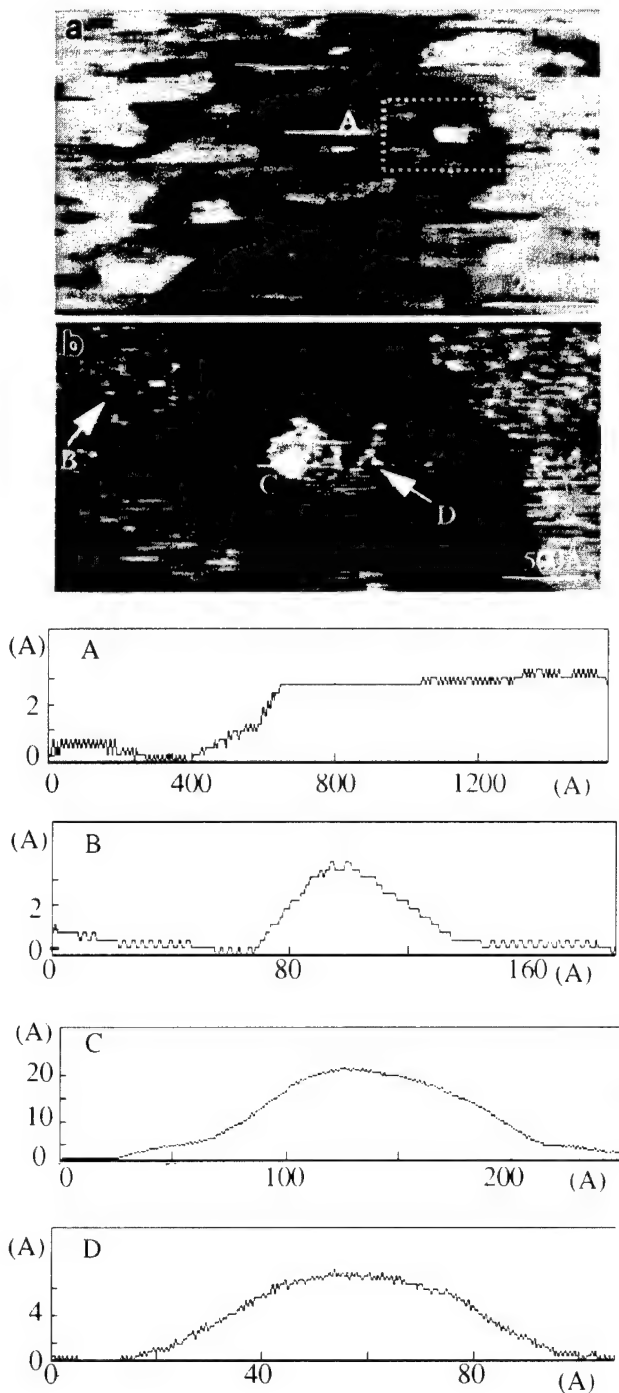
Fig. 2. RAS transients (a) and recordings of the specular beam RHEED intensity (b) for Si deposition on singular and vicinal GaAs(001).

## EVIDENCE FOR MASS EXCHANGE BETWEEN 2- AND 3-DIMENSIONAL SURFACE FEATURES DURING EVOLUTION OF COHERENT STRAINED 3D InAs ISLANDS ON GaAs(001)

T. R. Ramachandran, N. P. Kobayashi, W. Yu, P. Chen, and A. Madhukar  
Photonic Materials and Devices Laboratory, Departments of Materials Science and Physics,  
University of Southern California, Los Angeles, CA 90089-0241, U.S.A.  
TEL: 213-740-4325; FAX: 213-740-4333; E-mail: trr@photonics.usc.edu

The formation and evolution of *coherent*, three-dimensional (3D) strained InAs islands on GaAs(001) during MBE growth is examined via *in-situ* ultra high vacuum combined scanning tunneling microscope (STM) and atomic force microscope (AFM). The STM images show, for the first time, that the formation of the 3D InAs islands on GaAs(001) from an initial two-dimensional (2D) morphology is mediated by a pathway of *coexisting* 2D clusters (1 monolayer high, 10-200nm lateral size), *quasi*-3D clusters (2-4 monolayers high, ~10-50nm lateral size) and 3D islands (>4 monolayers high, 10-20nm lateral size). AFM images reveal that the evolution of the 3D islands exhibits an initial dramatic increase in their average lateral size and dispersion, followed by a subsequent reduction in the average lateral size and narrowing of the dispersion over a very small (<0.08ML) increment in the InAs delivery. This behavior is found to be accompanied by a remarkable exchange of InAs material between the 2D large clusters and the 3D features that involves the breakup of, or rearrangement of mass within, the largest 3D islands formed at the earliest stage. To examine a possible origin for this effect, we have investigated the potential role of stress build-up at island edges with increasing lateral size for low aspect ratios, as observed. To this end, we have chosen the vehicle of Ge islands on Si due to the well tested nature of their Stillinger-Weber potentials. Molecular dynamics simulations with upto  $10^6$  particles have been carried out and the atomically-resolved stress components calculated for the first time. The results show that the stress fields at the 3D island edges can significantly weaken the binding energy of adatoms at island edges with increasing size. The simulations also show that the surface stress modifies the diffusion energy barrier for adatoms at sites along the most probable diffusion channel between two adjacent islands in a manner that may favor the migration of adatoms towards the smaller 3D island. Together, the STM/AFM observations and the simulations thus reveal that the influence of the emerging strain fields on the adatom migration and island-edge attachment/detachment kinetics can account for both, island average size reduction and narrowing in size dispersion (i.e. the tendency for size equalization).

Work supported by the U.S. AFOSR and ONR.



#### UHV STM images of $\sim 1.57\text{ML}$ InAs on GaAs(001):

In panel (a) the irregular features in the background (one such feature is marked A) are clusters that are one monolayer high with respect to the immediately surrounding area. Depending on the chemical nature of the underlying atomic plane these features would be either 2D clusters or quasi-3D clusters. Panel (b) is a higher resolution scan of the boxed area in panel (a). The feature marked B refers to a small lateral-size cluster that is one monolayer high with respect to the immediately surrounding area while D refers to a quasi-3D cluster (height 2-4 monolayers). The "bright dot" (marked C) is a 3D island. The cross-sectional profiles of each of the above marked features A-D are shown below panel (b).

## MBE growth of two-dimensional electron gases on (110) GaAs

C.B. Sørensen<sup>1</sup>, H. Gislason<sup>2</sup> and J.M. Hvam<sup>2</sup>

<sup>1</sup>Niels Bohr Institute, Ørsted Laboratory, University of Copenhagen, Universitetsparken 5  
DK 2100 Copenhagen Ø, Denmark,

Phone: +45 35 32 04 00, Fax: +45 35 32 04 60, E-MAIL: cbs@fys.ku.dk

<sup>2</sup>Mikroelektronik Centret, The Technical University of Denmark, bld. 345 East,  
DK-2800 Lyngby, Denmark

The growth of high-quality two-dimensional electron gases (2DEG's) on the (110) surface of GaAs, has in recent years attracted an increased interest. This is mainly motivated by the growth of one-dimensional structures by MBE cleaved edge overgrowth (CEO) [1].

The optimal growth conditions for the (110) surface are a high V/III flux ratio and a low substrate temperature. These conditions compensate for the low incorporation coefficient of the As to the non-polar (110) surface. An additional improvement in the quality of the grown layers can be achieved by using As<sub>2</sub> instead of As<sub>4</sub> [2,3]. It turns out, however, that the (110) growth is very sensitive to small changes in the substrate temperature. To find the optimum temperature, we characterize the growth as a function of substrate temperature in the temperature range 440 - 595 °C. A series of samples were grown with a fixed layer structure of a GaAs buffer layer and a 2DEG. The quality of the growth is characterized by the transport properties of the 2DEG's and by low-temperature photoluminescence (PL) characterization of the GaAs buffer layer. Also, we discuss the (110) surface morphology as a function of substrate temperature.

Measurements of mobility and carrier density show, that the highest mobility is obtained in a narrow temperature window around an optimum temperature of 470 °C ± 5 °C. At temperatures lower than this the mobility and carrier density drops drastically, until the samples become insulating below 440 °C. In the temperature range 480-520 °C the mobility and carrier density change only slightly. At high temperatures (>540 °C) the mobility drops to a low value, whereas the carrier concentration stays virtually unchanged.

The drastic change in the 2DEG mobility and carrier density for the substrate temperatures below 470 °C is found to be correlated with the PL of the GaAs buffer layer. The PL spectra, which were recorded at 4 K using a HeNe excitation (632.8 nm, 4 W/cm<sup>2</sup>), change remarkable when comparing the sample grown at 480 °C to the one grown at 460 °C. The spectrum of the sample grown at 480 °C is dominated by the n=1 free exciton emission from the GaAs buffer layer with a 15 times higher intensity than the carbon impurity related emission. On the contrary, the spectrum from the sample grown at 460 °C is dominated by the carbon related luminescence. These results indicate, that an increased incorporation of impurities at the lowest substrate temperatures is reducing the mobility and the carrier density.

The surface morphology is smooth for the samples grown at substrate temperatures below 470 °C, while the surfaces of the samples grown in the 480 -520 °C temperature range display a very slight amount of "orange peel" on the scale of ≈1 μm. However, going to the high temperatures (>540 °C) a clear faceting on the surface is observed, indicating a Ga-rich growth as reported before by several other groups. The limiting factor on the 2DEG mobility, in this case, is the roughness of the GaAs/AlGaAs interface.

- [1] L. Pfeiffer, K.W. West, H.L. Stormer, J.P. Eisenstein, K.W. Baldwin, D. Gershoni and J. Spector, Appl. Phys. Lett. **56**, 1697 (1990)
- [2] C.B. Sørensen, H. Gislason, D. Birkedal and J.M. Hvam, Microelectronics Journal, **26**, 767 (1995)
- [3] M.C.Holland, A.H. Kean and C.R. Stanley, J. Cryst. Growth, **150**, 455 (1995)

# Heuristic Rules for Group IV Dopant Site Selection in III-V Compounds,

R. Venkatasubramanian

Department of Electrical and Computer Engineering, University of Nevada, Las  
Vegas, Las Vegas, NV 89154.

Donald L. Dorsey

Air Force Wright Laboratory, WL/MLPO, Wright Patterson AFB, OH  
45433-7707

K. Mahalingam, Systran Corporation, Dayton, OH 45432

## Abstract

The use of column IV dopants in III-V compounds is of great interest because they are easy to handle and in the case of *Si*, readily available in most MBE chambers. It should be noted all column dopants are amphoteric in all III-V compounds. An element which is predominantly a donor in one material may act as an acceptor in another material depending on its size relative to the cation and anion, the substrate orientation during growth and other growth conditions. In this work, we present rules for predicting group IV dopant site selection in III-V compounds. These rules take into account the relative covalent radii of the atoms, types and relative numbers of surface dangling bonds available and the anion to cation flux ratio. Preliminary predictions show excellent agreement with available experimental data of *GaAs*, *AlAs*, *InSb*, *GaSb*, *AlSb* and their compounds grown on substrates of various orientations and under various growth conditions.

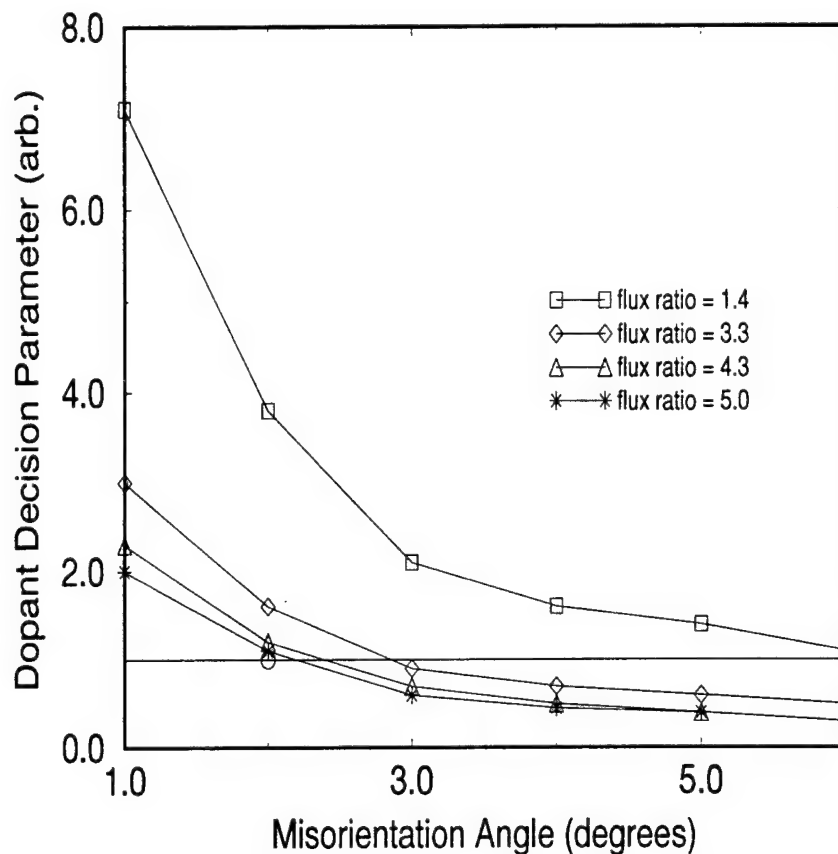
*Contact Author:* R. Venkatasubramanian

*Address:* Department of Electrical Engineering

University of Nevada, Las Vegas, Las Vegas, NV 89154-4026

*Phone:* (702) 895 1094 *Fax:* (702) 895 4075

*email:* venkat@unlv.edu



Figure, Dopant decision parameter in *GaAs* and *AlAs* versus misorientation angle from (111)A plane towards the (100) plane for various flux ratios. The dopant decision parameter is defined as the anion to cation (atom) flux ratio and the anion to cation site ratio. When the dopant decision parameter is greater than unity, there are more cation sites available for *Si* and hence the material will be n-type. When the dopant decision parameter is less than unity, there are more anion sites available for *Si* and hence the material will be p-type.

# Spreading of Si by Surface Segregation in $\delta$ -doping of MBE Grown $\text{In}_{0.53}\text{Ga}_{0.47}\text{As}$

E. Skuras, B. Vögele, A. R. Long, M. C. Holland, E. A. Johnson<sup>1</sup>, C. R. Stanley<sup>§</sup>

University of Glasgow, Glasgow, G12 8QQ, U.K.

<sup>§</sup>Tel.: ++44-(0)141-330-4798; Fax: ++44-(0)141-330-6002; email: C.Stanley@elec.gla.ac.uk

A study of Si  $\delta$ -doping in  $\text{In}_{0.53}\text{Ga}_{0.47}\text{As}$  grown on InP by MBE has been reported recently<sup>1,2</sup>. 1.2 K Shubnikov-de Haas (SdH) measurements and self-consistent calculations<sup>3</sup>, which treat the doping profile width as a fitting parameter, were used to assess the extent of dopant spreading as a function of substrate temperature ( $T_s$ ). This indicated that near-ideal confinement of the Si to the  $\delta$ -doped plane is achieved at  $T_s \leq 470^\circ\text{C}$ , a reduction of only  $50^\circ\text{C}$  from the typical InGaAs growth temperature of  $\approx 520^\circ\text{C}$  where spreading of the Si dopants in excess of 30 monolayers (ML) occurs. The work has now been extended by growing structures designed to show that dopant spreading is explained by surface segregation rather than diffusion.

The diagrams in fig. 1 illustrate the growth temperatures for a series of samples grown at  $1.0\text{ }\mu\text{m/hr}$  on Fe-InP(100) with an  $\text{As}_2$  flux of  $\approx 1.9 \times 10^{15}\text{ molecules cm}^{-2}\text{ s}^{-1}$ . The Ga and In fluxes were calibrated by RHEED intensity oscillations to ensure lattice-matching while the Si furnace temperature was established from both low magnetic field Hall and high magnetic field SdH measurements of the free electron density in a large number of uniformly doped GaAs and  $\text{In}_{0.53}\text{Ga}_{0.47}\text{As}$  layers.

1.2 K SdH measurements were performed in the dark using a 13 T magnet on Hall bars with a 3:1 length to width ratio. Magneto-resistance data were numerically differentiated, expressed in reciprocal magnetic field and frequency analysed by fast Fourier transform (FFT) techniques. The peak positions ( $\nu_i$ ) in the FFT spectra were converted into sub-band densities  $n_i$  through the expression  $n_i = 2e\nu_i/h$  where  $e$  is the electronic charge and  $h$  is Planck's constant. The degree of dopant spreading is related to the  $n_{i=0}/n_{i=1}$  ratio<sup>1,2</sup>.

The amplitude spectra for two  $\delta$ -doped samples with areal Si densities  $n_{\text{Si}}$  of  $4 \times 10^{12}\text{ cm}^{-2}$  (B535 and B610) are shown in fig. 2. The spreading in B535 is estimated to extend 32-36 ML away from the intended plane while it is negligible in B610. The implication here is that little diffusion of Si occurs during the 30 min the wafer is held at  $520^\circ\text{C}$  for the growth of the  $0.5\text{ }\mu\text{m}$  un-InGaAs layer after  $\delta$ -doping at  $470^\circ\text{C}$ . To distinguish between the two mechanisms possibly responsible for dopant spreading at  $T_s \geq 470^\circ\text{C}$ , samples (fig. 1(c)) with  $n_{\text{Si}} = 3 \times 10^{12}\text{ cm}^{-2}$  were grown with the following temperature cycles:

B684;  $0.5\text{ }\mu\text{m}$  un-InGaAs and  $\delta$ -doping with both  $T_1$  and  $T_\delta$  at  $520^\circ\text{C}$ , a pause to lower  $T_s$  to  $470^\circ\text{C}$ , and then growth of a further  $0.5\text{ }\mu\text{m}$  un-InGaAs with  $T_2 = 470^\circ\text{C}$ .

B685;  $0.5\text{ }\mu\text{m}$  un-InGaAs and  $\delta$ -doping with  $T_1$  and  $T_\delta$  at  $470^\circ\text{C}$ , a pause to raise  $T_s$  to  $520^\circ\text{C}$ , and then growth of the remaining  $0.5\text{ }\mu\text{m}$  un-InGaAs layer with  $T_2 = 520^\circ\text{C}$ .

The amplitude spectra for B684 and B685 are shown in fig. 3. Analysis of this data confirms that spreading in B684 is negligible while that in B685 amounts to  $\approx 40$  ML. These results from layers grown with novel procedures and supplemented by data from a wide variety of other  $\delta$ - and slab-doped InGaAs structures will be presented as strong evidence for surface segregation as the cause for spreading of Si  $\delta$ -doped layers in InGaAs grown in excess of  $470^\circ\text{C}$ .

## References

- [1] M. McElhinney, E. Skuras, B. Vögele, M. C. Holland, A. R. Long, C. R. Stanley, E. A. Johnson, *Appl. Phys. Lett.*, 68, 940 (1996).
- [2] M. McElhinney, E. Skuras, S. N. Holmes, E. A. Johnson, A. R. Long, C. R. Stanley, *J. Crystal Growth* 150, 266 (1995).
- [3] E. A. Johnson and A. MacKinnon, *Semicond. Sci. Technol.* 5, S189 (1990).

<sup>1</sup>Blackett Laboratory, Imperial College, London, SW7 2BZ, U.K.



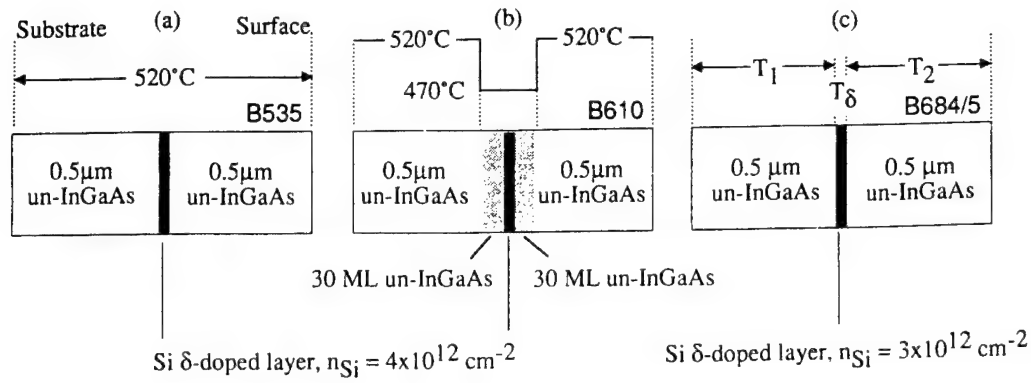


Fig. 1: (a) B535,  $\delta$ -doped structure grown entirely at 520 °C: (b) B610, 0.5  $\mu\text{m}$  undoped InGaAs grown at 520 °C, 30 ML -  $\delta$ -doping - 30 ML deposited at 470 °C, 0.5  $\mu\text{m}$  undoped InGaAs grown at 520 °C: (c) B684,  $T_1$  and  $T_\delta$  both set to 520 °C,  $T_2 = 470$  °C; B685,  $T_1$  and  $T_\delta$  both set to 470 °C,  $T_2 = 520$  °C.

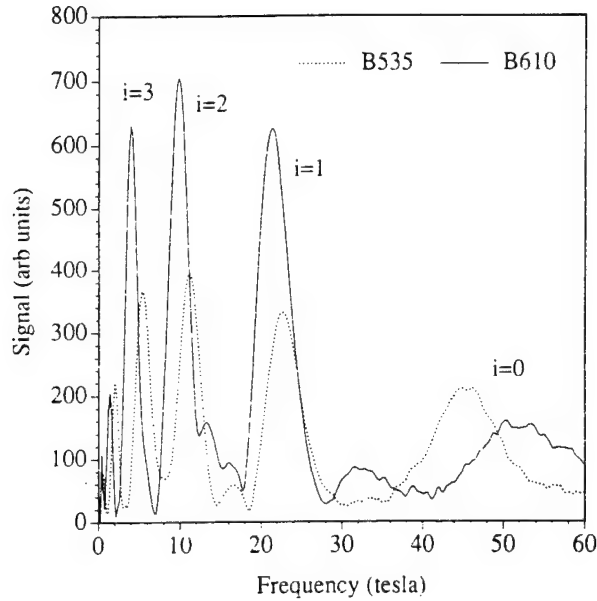


Fig. 2: The amplitude spectra for two  $\delta$ -doped samples with areal Si densities of  $4 \times 10^{12} \text{ cm}^{-2}$  grown at 520 °C (B535) and 470 °C (B610). The higher frequency of the  $i=0$  peak for B610 represents a larger electron concentration  $n_0$  in its lowest occupied sub-band compared with the value of  $n_0$  for B535. The resultant reductions in  $n_i$  ( $i \geq 1$ ) for B610 are reflected in a shift to lower frequencies of the  $i \geq 1$  peaks and an increase in the sub-band ratio  $n_{i=0}/n_{i=1}$  compared with the corresponding values for B535. The spreading in B535 is estimated between 32-36 ML.

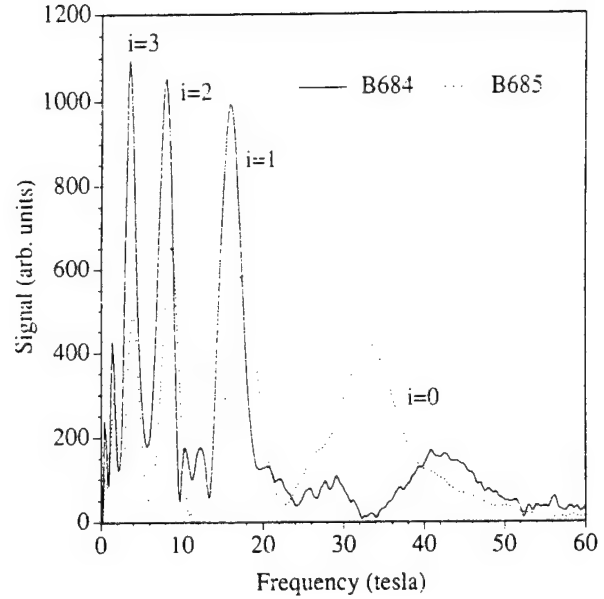


Fig. 3: The amplitude spectra for B684 and B685,  $\delta$ -doped samples with areal Si densities of  $3 \times 10^{12} \text{ cm}^{-2}$ . The tighter confinement of dopant atoms in B684 is again reflected through the higher frequency of the  $i=0$  peak compared with that of B685, and a shift to low frequency for the  $i \geq 1$  peaks. The spreading in B685 is  $\approx 40$  ML.

# GROWTH AND PHYSICS OF STRONGLY COUPLED ULTRA HIGH MOBILITY P-TYPE DOUBLE QUANTUM WELLS SHOWING CORRELATED $\nu=1$ QUANTUM HALL AND INSULATING STATES

M. Henini, R. J. Hyndman, T. Ihn, B. L. Gallagher, P. J. Rodgers, J. R. Middleton,  
J. Chauhan and T. J. Foster

Department of Physics, University of Nottingham, Nottingham NG7 2RD

Here we report on the MBE growth of p-type double quantum wells on the (311)A GaAs surface using silicon as the acceptor. Similar procedures to those we have developed to produce high quality single heterojunctions<sup>1</sup> are used. The As<sub>4</sub> beam was generated using a Varian cracker cell which was filled with arsenic from Preussag (6N's purity arsenic lumps). Both the total carrier density and the relative number of holes in the two wells are tuned by use of both front and back gates. At very low temperature (100 mK) hole mobilities exceeding  $400,000 \text{ cm}^2 \text{V}^{-1} \text{s}^{-1}$  at a carrier concentration of  $1.5\text{-}2.3 \times 10^{11} \text{ cm}^{-2}$  have been obtained. This hole mobility is the highest ever observed in p-type double quantum wells. We will describe the preparation procedures of the MBE equipment and the growth conditions used to grow these samples.

The high hole mass leads to weak tunnelling even at small layer separation and the calculated symmetric/antisymmetric energy gap is  $\leq 50 \text{ mK}$ . We observe strong quantum Hall  $\nu = 1$  states with gap energies of  $\sim 100 \times \Delta_{\text{SAS}}$  when the densities are balanced. The states at  $\nu = 3, 5, 7, \dots$  are all absent. This is direct and unambiguous proof of the existence of a correlated bilayer  $\nu = 1$  state in the limit of weak tunnelling. The state systematically weakens with increasing total carrier density and is destroyed as the layer separation in units of magnetic length,  $d/l_B$ , approaches  $\sim 1.8$ , in good agreement with theory. The state is found only to exist below a critical temperature  $T^*$ , below which it shows activated behaviour.  $T^*$  also tends to zero as  $d/l_B$  approaches  $\sim 1.8$ . This behaviour is consistent with the predicted finite temperature phase transition for the correlated state. The agreement between different samples is very good, indicating that disorder does not play a major rôle in these high quality samples.

At the lowest densities a direct transition from the  $\nu = 1$  quantum Hall state into an activated insulating state occurs followed by a re-entrance of the fractional quantum Hall state at  $\nu = 2/3$  ( $1/3$  filling factor in each well). In single layer hole gases, insulating behaviour for  $\nu < 2/5$  followed by a re-entrance of the  $1/3$  state has been shown to be consistent with Wigner crystallisation stabilised by Landau level mixing<sup>2,3</sup>. Recent theoretical studies [4,5] of the possibility of bi-layer wigner states have show that the interlayer Coulombic interaction will stabilise the Wigner state when the layers have the same density. In our samples we are able to study the effects of unbalancing the densities of the two wells while keeping the total density constant. Doing so we find that the insulating state has the expected behaviour being strongest at balance and rapidly weakening with unbalance. This provides strong evidence for the role of interlayer interaction in stabilising the insulating state.

1. M. Henini et al; Appl. Phys. Lett. **65**, 2054 (1995).
2. B. L. Gallagher et al; Physica B **211**, 417 (1995).
3. H. C. Manoharan and M. Shayegan; Phys. Rev. B **50**, 17662 (1994).
4. L. Zheng and H. A. Fertig Phys. Rev. B **52**, 12282 (1995)
5. S. Narasimhan and T-L. Ho Phys. Rev. B **52**, 12291 (1995)

Author to contact: Dr M. Henini

Tel/Fax: +44 115 951 5195/951 5180

e-mail: ppzmmh@ppn1.physics.nottingham.ac.uk

P1.28

# Growth Temperature-Dependent Conduction-type Inversion of C-doped InGaAs Grown by Chemical Beam Epitaxy

JEONG-RAE RO<sup>1,\*</sup>, Sung-Bock Kim<sup>1</sup>, Seong-Ju Park<sup>1,2</sup>, and El-Hang Lee<sup>1</sup>

<sup>1</sup>Electronics and Telecommunications Research Institute, Taejeon 305-600, Korea

<sup>2</sup>Kwangju Institute of Science and Technology, Kwangju 506-303, Korea

We report, for the first time, the growth temperature-dependent conduction-type transition of carbon-doped InGaAs on GaAs grown by chemical beam epitaxy(CBE) using trimethylindium(TMIn), trimethylgallium(TMGa), triethylgallium(TEGa), arsine(AsH<sub>3</sub>) and unprec cracked monoethylarsine(MEAs). Carbon(C) has been increasingly used as a p-type dopant for GaAs, and InGaAs in MBE, MOCVD and MOMBE because it offers a much lower diffusion coefficient than those of the conventionally used p-type dopants such as Be and Zn. However, carbon doping in InGaAs is found less controllable than in GaAs because of amphoteric nature of carbon in InGaAs. For instance, InGaAs layers grown by MOMBE and MBE show p- to n-type conversion with increasing indium composition. Up to now, p-type InGaAs was obtained only when TMGa together with solid In and solid As, CCl<sub>4</sub>, or CBr<sub>4</sub> was used for C dopant sources. However, in our previous work, p-type carbon-doped InGaAs was successfully grown at low growth temperature by CBE using unprec cracked MEAs, TEGa and TMIn[1]. In this study, we further investigated the effect of hydride gases and V/III ratios on the temperature dependent type inversion of C-doped InGaAs epilayers.

Figure 1 shows the growth temperature-dependent carrier concentration of InGaAs layers obtained from van der Pauw method. The hole concentrations of InGaAs using MEAs, TEGa, and TMIn decreased with increasing growth temperature and the conductivity type changed from p to n around 450°C. The growth temperature-dependent change of conductivity type of InGaAs was also observed with prec cracked arsine, TEGa, and TMIn. These results suggest that the amphoteric nature of carbon is critically dependent on the growth temperature and that the lattice site of carbon can be changed in the InGaAs material system, showing temperature-dependent type inversion. Figure 2 shows the dependence of the indium composition in InGaAs layer on the growth temperature. Unlike the MOMBE-grown samples[2], severe temperature-dependent variations of the indium composition were not observed in CBE-grown InGaAs using unprec cracked MEAs. These results indicate that the inversion of conductivity type with increasing growth temperature as shown in fig. 1 does not result from the variation of indium composition. Figure 3 shows the dependence of carrier concentration of InGaAs epilayers on V/III ratio obtained at the growth temperature of 400°C. All samples grown under the conditions of various V/III ratios and low growth temperature show p-type conduction. Therefore, the growth temperature-dependent conduction type is not attributed to the influence of V/III ratio.

In summary, we report the growth temperature-dependent conduction-type transition of C-doped InGaAs on GaAs grown by CBE using various source materials. To the best of our knowledge, no work has been known to report on the growth temperature-dependent conduction-type inversion of carbon-doped InGaAs. In this talk, the carbon incorporation behavior in InGaAs will be discussed in detail, using the result on the growth temperature, V/III ratio, In composition, and surface morphology.

[1] J. R. Ro, S. J. Park, S. B. Kim, and E. H. Lee, *J. Cryst. Growth*, *in press*.

[2] E. Tokumitsu, J. Shirakashi, M. Qi, T. Yamada, S. Nozaki, M. Konagai, and K. Takahashi, *J. Cryst. Growth*, **120**, 301 (1992).

\* Corresponding author :

Address : Research Dept., ETRI, Yusong P. O. Box. 106, Taejeon 305-600, Korea.

Tel. +82-42-860-6021 Fax. +82-42-860-5033 E-mail. rjr@idea.etri.re.kr

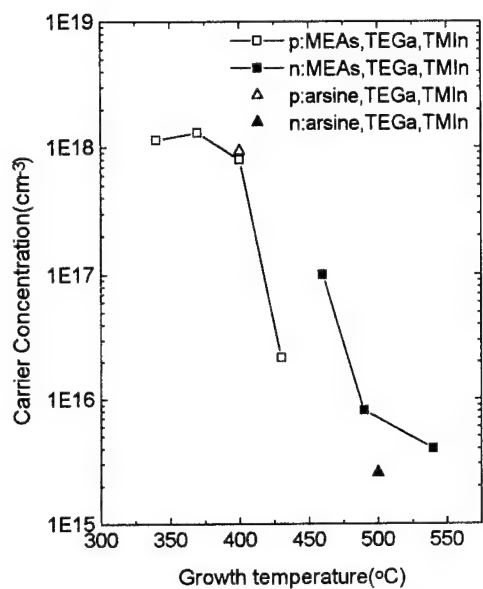


Fig. 1. Dependence of conduction type and carrier concentration in InGaAs on growth temperature. (V/III=10)

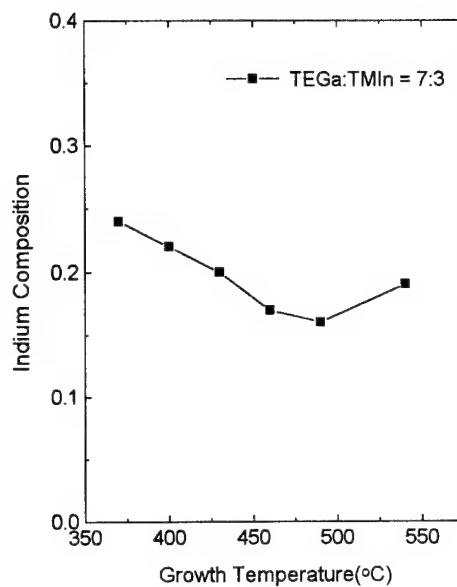


Fig. 2. Effect of growth temperature on the indium composition. (V/III=10)

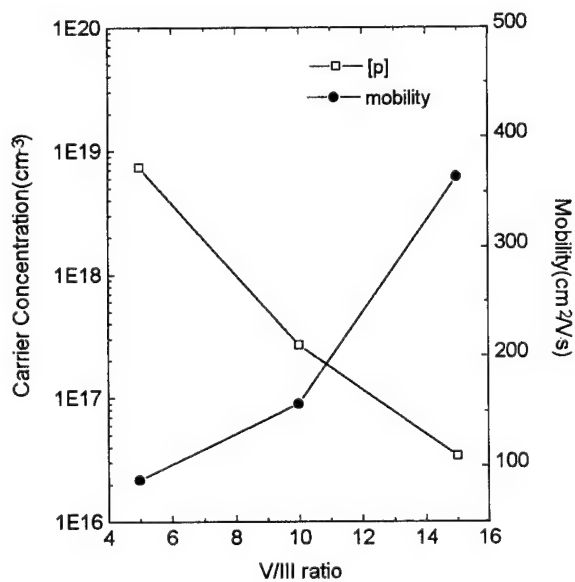


Fig. 3. Dependence of carrier concentration in InGaAs on the V/III ratio. (T=400°C)

# Growth and Characterization of $\text{In}_x\text{Ga}_{1-x}\text{As}$ ( $x \geq 0.65$ ) Heterostructures on GaAs by Molecular Beam Epitaxy Using $\text{In}_x(\text{AlGa})_{1-x}\text{As}$ Graded Buffer

S. M. Wang, C. Karlsson, N. Rorsman, M. Bergh\*, E. Olsson\*\*,  
H. Zirath and T. G. Andersson\*\*

Department of Microwave Technology

\*Department of Solid State Electronics

\*\*Department of Physics

Chalmers University of Technology

S-41296 Göteborg, Sweden

## Abstract

$\text{In}_x(\text{AlGa})_{1-x}\text{As}$  graded buffer has been previously used to grow high quality  $\text{In}_x\text{Ga}_{1-x}\text{As}$  bulk layers and related device structures on GaAs by molecular beam epitaxy (MBE) with  $x$  up to mainly 0.5. This grading technique can be used to provide a metamorphic "substrate" with tunable lattice constant between GaAs and InAs. In this paper we report MBE growth of  $\text{In}_x\text{Ga}_{1-x}\text{As}$  ( $x \geq 0.65$ ) and  $\text{In}_x\text{Ga}_{1-x}\text{As}/\text{InAlAs}$  ( $x \geq 0.7$ ) modulation doped heterostructures on GaAs using linearly graded  $\text{In}_x(\text{AlGa})_{1-x}\text{As}$  buffer and study influence of the graded buffer and the growth conditions on material quality. For a grading slope of 3.2% (lattice mismatch)/ $\mu\text{m}$ , transmission electron microscopy demonstrated that most dislocations were blocked in the graded buffer leaving clean upper layers with a very low threading dislocation density. As compared with InAs bulk layers directly grown on GaAs, electron mobility was higher in the InAs with graded buffer and was not affected by increasing the grading slope up to 6%/ $\mu\text{m}$ . Replace of Ga by Al in the graded buffer reduced background carrier concentration but did not decrease electron mobility significantly. Double crystal X-ray diffraction revealed that InGaAs bulk layers grown on the graded buffer had larger tilting angle and residual strain than those without grading. Surface morphology highly depended on the growth temperature and the root-mean-square values of 2 nm were measured by atomic force microscopy in samples grown at low temperature. Modulation doped heterostructures with  $x=0.7$  to 1 in the channel have been successfully grown on GaAs. Electron mobility of  $1.37 \cdot 10^4 \text{ cm}^2/\text{Vs}$  with a carrier density of  $1.9 \cdot 10^{12} \text{ cm}^{-2}$  was obtained at 300 K.

Contact: Dr. S. M. Wang  
Department of Microwave Technology  
Chalmers University of Technology  
S-41296 Göteborg, Sweden  
Tel. +46-31-7721896 Fax. +46-31-164513  
e-mail: Shumin@ep.chalmers.se

## 2D-limitations when increasing the Si-concentration from $\delta$ -doping to thin Si-layers in GaAs

T.G. Andersson, J.V. Thordson and G. Swenson

*Department of Physics, Chalmers University of Technology and Göteborg University*

*S-412 96 GÖTEBORG, Sweden*

Fax: +(46) 31 772 3385, e-mail: f4bta@fy.chalmers.se

The free carrier concentration in 2D structures,  $n_{2D}$ , as a result of  $\delta$ -doping is usually desired to be as high as possible, typically  $n_{2D} \geq 1 \times 10^{12} \text{ cm}^{-2}$  for device applications. An ideal  $\delta$ -doping at this level is above the corresponding doping concentration in each atomic plan for 3D-doping giving maximum carrier concentration,  $n_{3D}^{\text{max}}$ . In reality there are deviations from an ideal 2D-system due to generation of defects and outdiffusion of Si-atoms from the  $\delta$ -plane to the neighboring crystal planes. These defects reduce the free carrier concentration. Physical reasons for limitations in  $n_{2D}$  after  $\delta$ -doping have been studied with reference to the corresponding doping/carrier concentrations in bulk. Thin Si layers were grown by MBE on GaAs at a medium temperature, 500 °C, and covered with a 0.1  $\mu\text{m}$  thick cap layer. The silicon atoms were deposited from the dopant cell with the arsenic shutter opened. Conductivity was studied by Hall effect and the concentration by SIMS. The Si thickness ranged from low  $\delta$ -doping concentrations,  $\sim 1.4 \times 10^{11} \text{ cm}^{-2}$  up to several ML thick films. The confining potential shape and the wave functions were calculated from a self consistent solution of the Schrödinger and Poisson equations. At low doping concentrations,  $n_{2D} < 1 \times 10^{11} \text{ cm}^{-2}$ , the V-shaped  $\delta$ -potential is shallow,  $< 10 \text{ meV}$ . Therefore the well is emptied even in a weak internal electric field, e.g. close to a surface or interface. The free carrier concentration increased with doping concentration but was limited to  $5 \times 10^{12} \text{ cm}^{-2}$ . This value dropped somewhat and saturated with further sub-ML coverage from 0.1 ML and up. In contrast, the electron mobility was fairly constant up to 1 ML. Films with 1 to 3 MLs of Si were strained and provided good RHEED patterns from both Si and the cap layer. There was only limited diffusion of Si atoms into the GaAs. Relaxation occurred between 3 and 4 monolayers, giving enhanced diffusion of Si atoms into the cap layer. The relaxed Si layer provided a high defect density with reduced crystal quality in the cap layer. At 4 MLs the Si film was relaxed and non-conducting.

We analysed the width of the concentration profile,  $\Delta_t$ , as a result of diffusion of Si-atoms from the doping plane. There is a strong relation between  $\Delta_t$  and both growth temperature and doping concentration. It is known that growth at 400 °C gives nearly ideal  $\delta$ -layer but this temperature is generally too low for device materials. Using SIMS we found  $\Delta_t \sim 60 \text{ Å}$  at 500 °C which is an upper limit since it is close to the instrumental depth resolution. In Fig. 1, the  $\delta$ -layer thickness is plotted as a function of growth temperature. The width is analysed and compared with experiments when a fraction,  $f$ , of the Si-atoms migrate to the next atomic plane. In this way a concentration profile is generated to describe the real Si-distribution. The solid

line is the calculated width for thermally activated migration. Above 410 °C the experimental data at high concentrations,  $[Si] \sim (4-7) \times 10^{13} \text{ cm}^{-2}$ , are limited by a maximum thickness,  $\Delta_t^{\max}$ , given by the relation  $\Delta_t^{\max} = 0.172 \cdot \exp(1.236 \cdot 10^{-2} \cdot T) (\text{\AA})$  for  $T$  in °C (upper dashed line). As shown there is also a strong dependence of the thickness with doping especially for high temperatures indicating a lower limit of  $\Delta_t$  to 60 - 100 Å in the range 590 - 650 °C for low doping concentrations,  $[Si] \sim (3-4) \times 10^{12} \text{ cm}^{-2}$ .

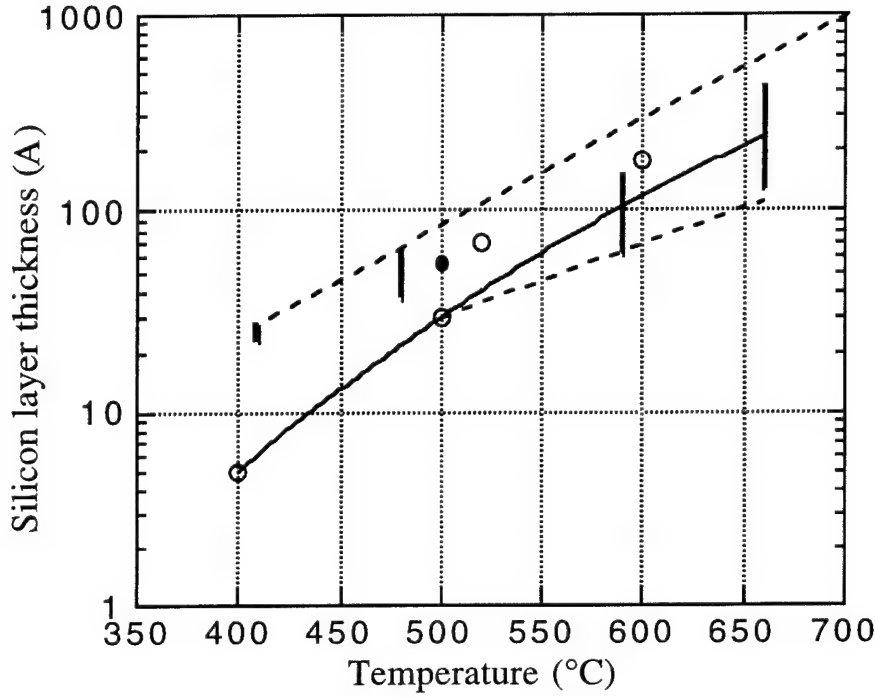


Fig. 1. The Si delta-doping layer thickness as a function of growth/annealing temperature. The thickness is higher for higher doping concentrations and the difference is more pronounced for higher temperatures.

In the ideal situation the diffusion is an atomic movement from plane-to-plane, i.e. between  $Si_{Ga}$ -sites involving intermediate interstitial or  $Si_{As}$ -sites. At 500 °C the diffusion constant,  $D$ , is of the order  $10^{-18} \text{ cm}^2/\text{s}$ . The total time,  $t$ , to grow the Si layer plus the 100 nm GaAs cap layer is typically  $(3-10) \times 10^3$  seconds. Then the diffusion length,  $L = \sqrt{D \cdot t}$ , is 10 - 20 Å giving a slightly larger total layer thickness, which is in good agreement with estimated widths of 30 - 50 Å. The thickness of the  $\delta$ -layer will in turn influence the potential profile, the potential width and the extension of the  $i$ :th wave function,  $\Delta_{\Psi_i}$ , characterising subband  $i$ . These concepts are analysed by calculations.

# THE BUILDING UP OF TERRACE AND ATOMIC PERIODICITY BY MBE GROWTH ON (001) GaAs VICINAL SURFACES

F. Lelarge, Z.Z. Wang, F. Laruelle and B. Etienne  
*Laboratoire de Microstructures et de Microélectronique, C.N.R.S.,  
B.P. 107, 92225 Bagneux Cedex, France.  
Fax: +33 1 42 31 73 78, email: francois.lelarge@bagneux.cnet.fr*

Organized growth on vicinal surfaces appears as a good way to realize, in a single technological step, high quality 1D GaAs/AlAs quantum structures with novel properties [1–2]. This requires to keep a surface with a nearly periodic arrangement of the monomolecular Ga terminated steps during MBE growth. In previous works by others, near field microscopy (AFM or STM) of vicinal GaAs (001) has shown regular step arrangement for weak misorientation ( $0.3^\circ$ ) but step bunching occurred on  $1^\circ$  and  $2^\circ$  misoriented samples. In this work, we study the morphology of such vicinal surfaces ( $0.2^\circ$  to  $2^\circ$ ) by AFM as a function of the growth conditions. The measurements are performed outside the MBE system and our entire scanning unit is placed in a plexi-glass glove box purged with pure nitrogen gas.

Optimizing growth conditions, we are able to obtain a periodic array of steps for terrace length below 40 nm. Because the post-growth oxydation limits the lateral resolution (4 nm), kinks on step edges are not resolved. The terrace width distributions exhibit a pronounced peak close to the nominal terrace periodicity (misorientation accuracy  $\pm 0.1^\circ$ ). These distributions obey to a Gaussian law with a nearly linear relationship between the standard deviation and the mean value of the Gaussian ( $\sigma = 0.23 \langle L \rangle$ ). These results are very similar to vicinal Si (111) where it was founded  $\sigma = 0.25 \langle L \rangle$  [3]. We consider several equilibrium models based on: i) straight noninteracting steps, ii) single step meandering between fixed walls, iii) terrace-step-kink (TSK) model to take into account only entropic repulsion, iv) entropic and energetic step-step repulsion. An energetic repulsion with a  $L^{-2}$  decay as in the last model is needed to explain the Gaussian law. The close similarity with Si is really surprising if we consider the conditions used ( $T=900^\circ\text{C}$  and cooling in few hours) which are far away from ours ( $T=600^\circ\text{C}$  and growth rate of 0.2 ML/s). Moreover, in our case, the growth is necessary to get a periodic step array so that it is obvious that kinetics should also be important. A 2D Monte-Carlo simulation has been developed in order to investigate the role of the surface anisotropy (binding energy and diffusion) and of the Schwoebel barrier in the building up of the step periodicity.

Such simulation allows also the study of the kinetics required for the group III atom lateral ordering during the heteroepitaxy of GaAs/AlAs structures. Indeed, an AlGaAs alloy with an in-plane periodic modulation of its Al composition is obtained [1]. It can be written :  $x_{\text{Al}}(y) = x \{ 1 + \lambda_{\text{at}}(x) \cos(2\pi y/L) + \dots \}$  where  $y$  is in the direction orthogonal to the steps, i.e. along [110],  $x$  is the mean alloy composition,  $L$  is the terrace length ( $L=16\text{--}32$  nm here) and  $\lambda_{\text{at}}(x)$  is called the atomic ordering parameter. This quantity has been measured, in our MBE grown structures, by TEM ( $\lambda_{\text{at}} \sim 0.3$  for  $x=0.5$ ) or by low temperature optical and transport measurements ( $\lambda_{\text{at}} \sim 0.25\text{--}0.15$  for  $x=0.1\text{--}0.05$ ). It cannot be explained by a model ignoring the in-plane kinetics of the Al adatoms as proposed by Lorke [4], resulting from an instantaneous atomic exchange: the predicted values are then too small by a factor of 3 (for  $x=0.1$ ) or 4 (for  $x=0.05$ ).

- [1] J. Bloch, U. Bockelmann and F. Laruelle, *Europhys. Lett.*, **28**, 501 (1994).
- [2] B. Etienne, F. Laruelle, J. Bloch, L. Sfaxi and F. Lelarge, *J. Cryst. Growth* **150**, 336 (1995).
- [3] X.S. Wang, J.L. Goldberg, N.C. Bartelt, T.L. Einstein and E. D. Williams, *Phys. Rev. Lett*, **65**, 2430 (1990).
- [4] A. Lorke, in *Low Dimensional Structures Prepared by Epitaxial Growth or Regrowth on Patterned Substrates*, ed. by K. Eberl, P.M. Petroff and P. Demeester, Kluwer Academic Publishers (1995) 139.



**POSTER SESSION P2. II-VI AND GROUP IV GROWTH ISSUES.**

**P2.1 Growth and characterization of  $\text{In}_2\text{Se}_3$  epitaxial films by molecular beam epitaxy**, Tamotsu Okamoto, Akira Yamada and Makoto Konagai, Tokyo Institute of Technology, Japan

**P2.2 Ellipsometric determination of CdZnTe preparation for HgCdTe MBE growth**, J.D. Benson, A.B. Cornfield, M. Martinka, and J.H. Dinan, J.A. Woollam Co. Inc., Lincoln, Nebraska, USA

**P2.3 Epitaxy of a new diluted magnetic semiconductor based on GaAs**, A. Shen, H. Ohno, F. Matsukura, Y. Sugawara, and S. Kanno, Tohoku University, Sendai, Japan

**P2.4 Effects of strain on the growth and properties of  $\text{CuInSe}_2$  epitaxial films**, S. Niki, P.J. Fons, T. Kurafuji, A. Yamada, H. Oyanagi, W. Bi and C.W. Tu, Electrotechnical Laboratory, Ibaraki, Japan

**P2.5 Preparation of high-quality  $\text{CuInSe}_2$  and  $\text{CuGaSe}_2$  epitaxial films by an in-situ annealing technique**, Bae-Heng Tseng, Song-Bin Lin, Gin-Lern Gu and Sing-Chu Lai, National Sun Yat-Sen University, Kaohsiung, Taiwan-R.O.C.

**P2.6 Spiral growth and improved nucleation of PbTe on  $\text{BaF}_2$  (111)**, A.Y. Ueta, G. Springholz, N. Frank and G. Bauer, Johannes Kepler Universität, Linz, Austria

**P2.7 Control of the (100) and (111) CdMnTe/CdTe MBE growth on (100) GaAs substrates**, M. Yano, K. Koike, T. Furusho and M. Kimata, Osaka Institute of Technology, Japan

**P2.8 Investigation of the optical and structural properties of MBE grown ZnSe/GaAs heterostructures**, J. Luyo, Edgar López-Luna, M. Meléndez-Lira, I. Hernández-Calderón, O. de Melo-Pereira, P. Díaz-Arencibia, R. León, J. Fuentes, H. Sitter, CINVESTAV, México, D.F.

**P2.9 Elastic and plastic deformation in the low mismatched heteroepitaxial system  $\text{Cd}_x\text{Hg}_{1-x}\text{Te}/\text{Cd}_{1-x}\text{Zn}_x\text{Te}$** , T. Colin, T. Skauli, S. Løvold, Norwegian Defence Research Establishment, Kjeller, Norway

**P2.10 ZnSe homoepitaxial growth on solid-phase recrystallized substrates**, E. Tournié, P. Brunet, C. Ongaretto, C. Morhain, and J.-P. Faurie, Centre National de la Recherche Scientifique, (CRHEA/CNRS), Antipolis, France

**P2.11 MBE growth of n-type ZnSe and ZnS using ethylchloride as a dopant**, Takashi Yasuda, Bao-Ping Zhang, and Yusaburo Segawa, The Institute of Physical and Chemical Research (RIKEN), Sendai, Japan

**P2.12 Growth of mechanism of II-VI compound semiconductors by molecular beam epitaxy**, Hiroyuki Okuyama, Takayuki Kawasumi, Akira Ishibashi, Masao Ikeda, Sony Corporation Research Center, Yokohama, Japan

**P2.13 Hydrogen sulfide treatment of GaAs substrate and its effect on initial stage of ZnSe growth**, Jun Suda, Ryuji Tokutome, Yoichi Kawakami, Shizuo Fujita and Shigeo Fujita, Kyoto University, Japan

**P2.14 Homogeneous and  $\delta$ -doped ZnS:Mn for flat panel displays grown by MBE**, S. Schön, T. Yang, M. Chaichimansour, W. Park, B.K. Wagner, and C.J. Summers, Georgia Institute of Technology, Atlanta, Georgia, USA

**P2.15 Tuning of ZnSe-GaAs band discontinuities in heterojunction diodes**, V. Pellegrini, M. Börger, F. Beltram, M. Lazzarino, J.J. Paggel, L. Sorba, S. Rubini, and A. Franciosi, University of Minnesota, Minneapolis, Minnesota, USA

**P2.16 Molecular beam epitaxial growth of ZnSe(111) films on GaAs(111)B substrates and nitrogen doping**, N. Matsumura, T. Matsuoka, H. Shimakawa and J. Saraie, Kyoto Institute of Technology, Japan

**P2.17 Interface structure of CdTe/Si**, S. Sivananthan, N.D. Browning, C.H. Grein, S. Rujirawat, T. Almeida, J.P. Faurie, R. Sporken, D.J. Willis, C.Y. Tsen, and David J. Smith, University of Illinois, Chicago, Illinois, USA

- P2.18 Molecular beam epitaxial growth of  $\text{ZnSe}$ ,  $\text{ZnS}_x\text{Se}_{1-x}$  and  $\text{ZnS}_x\text{Se}_{1-x}$  and  $\text{Zn}_{1-y}\text{Mn}_y\text{S}_x\text{S}_{1-x}$  layers on GaAs substrates studies of interface structures and control of alloy compositions**, Y.P. Chen, C.C. Kim, S.-C. Y. Tsen, David J. Smith, and S. Sivananthan, University of Illinois, Chicago, Illinois, USA
- P2.19 P-type doping of beryllium-chalcogenides grown by molecular beam epitaxy**, H.J. Lugauer, F. Fischer, T. Litz, J. Laubender, A. Weingärtner, A. Waag, T. Gerhard, U. Zehnder, L. Worschech, W. Ossau, G. Landwehr, C. Becker, and J. Geurts, Universität Würzburg, Germany
- P2.20 Molecular beam epitaxy of beryllium telluride**, Xiao-Chuan Zhou and Wiley P. Kirk, Texas A&M University, College Station, Texas, USA
- P2.21 A study of MBE growth and thermal annealing of p-type long wavelength  $\text{HgCdTe}$** , L. He, J.R. Yang, S.L. Wang, S.P. Guo, M.F. Yu, X.Q. Chen, W. Z. Fang, Y.M. Qiao, Q.Y. Zhang, R.J. Ding, and T.L. Xin, Shanghai Institute of Technical Physics, People's Republic of China
- P2.22 Blue-light emission from  $\text{ZnSTe}$ -based EL devices**, J. Mao, I.K. Sou, Z. Yang, K.S. Wong, G.K.L. Wong, Hong Kong University of Science & Technology, Clear Water Bay, Hong Kong
- P2.23 Nitrogen doping of Te based 2-6 compounds**, S. Tatarenko, T. Baron, A. Arnoult, J. Cibert, M. Grun, A. Haury, A. Wasiela, and K. Saminadayar, DRFMC/SP2M/PSC, Grenoble Cedex, France
- P2.24 Room temperature continuous wave operation of  $\text{ZnSe}$  based blue-green laser diode grown by molecular beam epitaxy**, Moon-Deock Kim, Hae-Sung Park, Bong-Jin Kim, Jeong-Keun Ji, Eun-Soon Oh, Sang-Dong Lee, Tae-Il Kim, Samsung Advanced Institute of Technology, Suwon, Korea
- P2.25 Large-mismatch heteroepitaxy of  $\text{InSb}$  on Si substrates using fluoride buffer layers**, W.K. Liu, X.M. Fang, J. Winesett, Weiluan Ma, Xuemei Zhang, M.B. Santos and P.J. McCann, University of Oklahoma, Norman, Oklahoma, USA
- P2.26 Fabrication of flexible single crystal semiconductor heterostructures**, M.H. Na, J. Haetty, H.C. Chang, H. Luo and A. Petrou, State University of New York at Buffalo, New York, USA
- P2.27 MBE growth of  $\text{PbSe}/\text{CaF}_2/\text{Si}(111)$  heterostructures**, P.J. McCann, X.M. Fang, W.K. Liu, B.N. Strecker, and M.B. Santos, University of Oklahoma, Norman Oklahoma, USA
- P2.28 Low temperature epitaxy of Si on hydrogen-terminated Si (001) using thermal and energetic beams**, M.E. Taylor, D. L. Capewell, M.V. Ramana Murty, D.G. Goodwin, and H.A. Atwater, California Institute of Technology, Pasadena, California, USA
- P2.29 Faceting of sidewalls in selectively grown epitaxial layers on  $\text{SiO}_2$ -masked Si substrates**, Qi Xiang, Shaozhong Li, Dawen Wang and Kang L. Wang, University of California, Los Angeles, California, USA
- P2.30 Enhancement of substitutional carbon incorporation in hydrogen-mediated pseudomorphic growth of strained alloy layers in  $\text{Si}(001)$** , G. Lippert, H.J. Osten, P. Zaumseil, Myeongcheol Kim, Institute for Semiconductor Physics, Frankfurt, Germany
- P2.31 New hydrogen desorption kinetics from vicinal  $\text{Si}(001)$  surfaces observed by RAS**, J. Zhang, A.K. Lees, A.G. Taylor, M.H. Xie, B.A. Joyce, Z. Sobiesierksi, and D.I. Westwood, Imperial College of Science, Technology and Medicine, London, United Kingdom
- P2.32 Reduction of  $\text{SiGe}$  heterointerface mixing by atomic hydrogen irradiation during MBE and its mechanism**, Kiyokazu Nakagawa, Yoshinobu Kimura and Masanobu Miyao, Hitachi Ltd., Tokyo, Japan
- P2.33 Control of composition and crystallinity in the molecular beam epitaxy of strain-compensated  $\text{Si}_{1-x}\text{Ge}_x\text{C}_y$  alloys on Si**, E.T. Croke, A.T. Hunter, C.C. Ahn, T. Laursen, A.E. Bair, D.J. Smith and J.W. Mayer, Hughes Research Laboratories, Inc. Malibu, California, USA
- P2.34 Stratified suspension of highly order Si nanoparticles in  $\text{SiO}_2$  created by Si MBE with oxygen co-implantation**, Yukari Ishikawa, N. Shibata, S. Fukatsu, The University of Tokyo, Tokyo, Japan

**P2.35 Reduction of defect density in mismatched SiGe/Si by low temperature Si buffer layers**, K. Linder, F. Zhang, P. Bhattacharya, University of Michigan, Ann Arbor, Michigan, USA

**P2.36 Hybrid MBE growth and mobility limited factors of n-channel Si/SiGe modulation-doped systems**, A. Yutani and Y. Shiraki, The University of Tokyo, Tokyo, Japan

**P2.37 Effects of hydrogen on Si(001) growth dynamics during GSMBE from disilane**, Kazuki Mizushima and Dimitri D. Vvedensky, Imperial College, London, United Kingdom

**P2.38 Visible light emission from MBE-grown Si/SiO<sub>2</sub> superlattices**, S.V. Novikov, J. Sinkkonen and S.V. Gastev, Helsinki University of Technology, Finland

**P2.39 Luminescence study on Ge islands as stressors on Si<sub>1-x</sub>Ge<sub>x</sub>/Si quantum well**, E. S. Kim, N. Usami, and Y. Shiraki, The University of Tokyo, Tokyo, Japan

**P2.40 The growth and luminescence of SiGe dots**, H. Chen, X.G. Xie, W. Q. Cheng, Q. Huang, J. M. Zhou, Chinese Academy of Sciences, Beijing.

**P2.41 Direct MBE growth of GE quantum dots on Si**, V.A. Markov, A.I. Nikiforov, N.V. Nomerotsky, E.M. Trukhanov, V.I. Varlamov, Russian Academy of Sciences, Novosibirsk, Russian

**P2.42 Photoluminescence study of Si/SiGe multiple quantum wells grown by MBE**, D. Grützmacher, R. Hartmann, U. Gennser, E. Müller, A. Dommann, Micro- and Nanostructures Laboratory, Villigen-PSI, Switzerland

**P2.43 Surface-stabilized MBE-growth of SiC on SiC(001)**, A. Fissel, K. Pfennighaus, U. Kaiser, M. Wendt, B. Schröter and W. Richter, Friedrich-Schiller-Universität Jena, Germany

**P2.44 Growth and Characterization of lattice-matched HgSe**, L. Parthier, Institut für Physik Humboldt-Universität zu Berlin, Germany

# Growth and Characterization of $\text{In}_2\text{Se}_3$ Epitaxial Films by Molecular Beam Epitaxy

Tamotsu Okamoto, Akira Yamada\* and Makoto Konagai\*

*Research Center for Quantum Effect Electronics, Tokyo Institute of Technology*

*\*Department of Electrical and Electronic Engineering, Tokyo Institute of Technology*

*2-12-1, O-okayama, Meguro-ku, Tokyo 152, JAPAN*

*Tel +81-3-5734-2662 Fax +81-3-5734-2897 E-mail: okamoto@pe.titech.ac.jp*

III<sub>2</sub>-VI<sub>3</sub> compound semiconductors such as  $\text{Ga}_2\text{Se}_3$  have a defect zincblende structure, in which 1/3 of cation sites are vacant. Up until now, we investigated the molecular beam epitaxial (MBE) growth of  $\text{Ga}_2\text{Se}_3$  films on (001)GaAs and (001)GaP substrates, and it was found that a spontaneous superlattice was formed and that unique properties such as large optical anisotropy were shown by the ordering of Ga vacancies in  $\text{Ga}_2\text{Se}_3$  films. On the other hand,  $\text{In}_2\text{Se}_3$  has two types of crystal structure different from  $\text{Ga}_2\text{Se}_3$ , i.e., layered structure ( $\alpha$ -phase) and defect wurtzite structure ( $\gamma$ -phase). In this paper, we will report the epitaxial growth of  $\text{In}_2\text{Se}_3$  films on (001)GaAs substrates by MBE and the excitonic emission in the epitaxial  $\text{In}_2\text{Se}_3$  films for the first time.

First of all, we investigated the effects of VI/III ratio and growth temperature on crystal structure. At the growth temperature of 500°C, spot pattern associated with zincblende structure was observed in the RHEED patterns of the  $\text{In}_2\text{Se}_3$  films with VI/III ratio of 5 to 30. Furthermore, in Raman spectra of the films, a peak located at 108 $\text{cm}^{-1}$  was observed. These results suggest that  $\alpha$ - $\text{In}_2\text{Se}_3$  epitaxial films with layered structure based on zincblende structure were obtained on (001)GaAs substrates. From cross-sectional SEM images, c-axis of  $\alpha$ - $\text{In}_2\text{Se}_3$  was found to be normal to the  $[\bar{1}11]$  and  $[1\bar{1}1]$  direction of (001)GaAs. On the other hand, in the film with VI/III ratio of 90, spot pattern was not observed by RHEED measurement, and a peak located at 151 $\text{cm}^{-1}$  was observed in the Raman spectra. These results indicate that polycrystalline  $\gamma$ - $\text{In}_2\text{Se}_3$  film was obtained under Se-rich condition. Furthermore, similar results were observed at the growth temperature of 540°C with VI/III ratio of 10, suggesting that polycrystalline  $\gamma$ - $\text{In}_2\text{Se}_3$  film was obtained at high growth temperature.

Furthermore, we investigated the optical properties of the  $\text{In}_2\text{Se}_3$  films by PL measurement at 4.2K. A sharp peak located at 578.9nm (2.14eV) was observed in the epitaxial  $\text{In}_2\text{Se}_3$  films. This peak was also observed in the polycrystalline  $\gamma$ - $\text{In}_2\text{Se}_3$  films. From comparison between PL spectra and wavelength dependence of photoconductivity in the polycrystalline  $\gamma$ - $\text{In}_2\text{Se}_3$  film on glass, the peak located at 578.9nm was found to be excitonic emission. This is the first report on the excitonic emission in the  $\text{In}_2\text{Se}_3$  films. In the layered structure, carriers are confined by van der Waals gaps. Therefore, we expect that  $\text{In}_2\text{Se}_3/\text{Ga}_2\text{Se}_3$  superlattice exhibits quasi-one dimensional properties.



## Ellipsometric determination of CdZnTe preparation for HgCdTe MBE Growth

J.D. Benson\*, A.B. Cornfeld, M. Martinka, and J.H. Dinan

Night Vision and Electronics Sensors Directorate, Ft Belvoir, Va.

B. Johs, P. He, and John A. Woollam

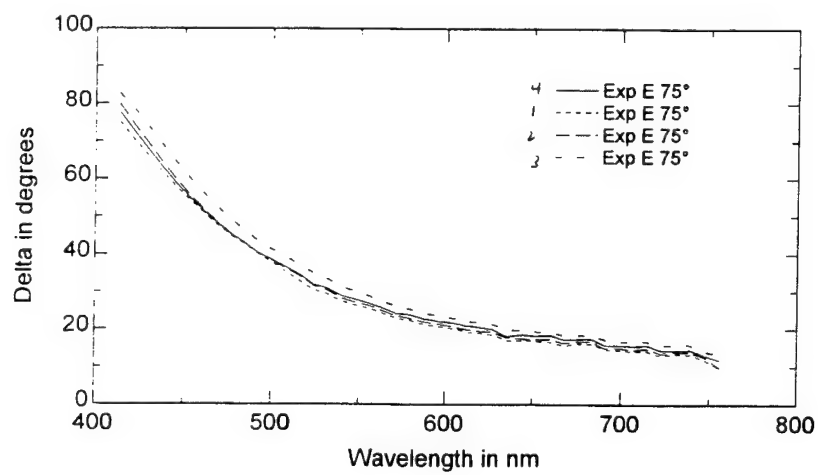
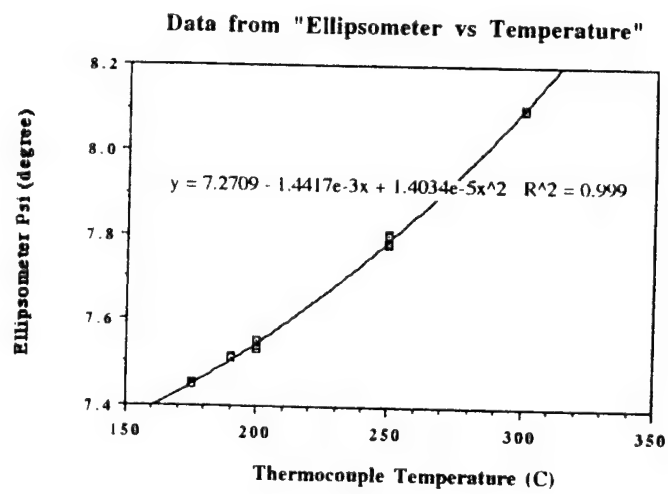
J.A. Woollam Co. Inc., Lincoln Ne.

An in-situ spectroscopic ellipsometer has been equipped on a molecular beam epitaxy system to improve control of HgCdTe growth. Ellipsometry is a widely used technique to determine semiconductor thin film growth parameters. It is a highly sensitive, non destructive technique. Real time analysis is now possible since the advent of personal computers. Using this device, in-situ analysis of composition, growth rate, and surface cleanliness have been monitored in our HgCdTe MBE system.<sup>i</sup> In this work analysis of the surface preparation and oxide desorption from a CdZnTe wafer was determined. As part of an initial investigation, the variation in ellipsometric parameters as a function of substrate temperature was determined. Shown in figure 1 is the variation of Psi (at 416.3 nm) as a function of substrate temperature as determined by the thermocouple. From this figure it is seen that the ellipsometer can determine substrate temperature with a precision of 2.5°C. To determine surface roughness and chemical make-up for a chemically cleaned (211)B CdZnTe wafer, reflection high energy electron diffraction and Auger are combined with the in-situ ellipsometric analysis. These three surface sensitive techniques were performed on the substrate as installed and after heating to 340°C under vacuum. The combined analysis indicates that the substrate was brought into the MBE system slightly tellurium rich and with an oxide. As the wafer was heated to 340°C, the oxide desorbed and the tellurium concentration decreased. Figure 2 shows Delta as a function of wavelength for the (211)B CdZnTe wafer 1) as installed in MBE system, 2) heated to 200 °C with tellurium desorption, 3) heated to 340 °C with oxide desorption, 4) at 200 °C ready for HgCdTe MBE growth..

---

\* J. David Benson, AMSEL-RD-NV-ITT, 10221 Burbeck Rd., Ft Belvoir VA. 22060-5806, 703-704-1711, fax 703-704-1705, e-mail dbenson@nvl.army.mil

<sup>i</sup> J.D. Benson, A.B. Cornfeld, M. Martinka, K.M. Singly, Z. Derzko, P.J. Shorten, J.H. Dinan, P.R. Boyd, F.C. Wolfgram, B. Johs, P. He, J.A. Woollam, "In -situ spectroscopic ellipsometry of HgCdTe", To be published in J. of Electronic Materials.



## Epitaxy of a new diluted magnetic semiconductor based on GaAs

A. Shen, H. Ohno\*, F. Matsukura, Y. Sugawara, and S. Kanno

Research Institute of Electrical Communication, Tohoku University, Sendai 980-77, Japan

Phone/Fax: +81-22-217-5555, e-mail: shen@riec.tohoku.ac.jp

\*Also with Research Development Corporation of Japan (JRDC)

A. Oiwa, A. Endo, S. Katsumoto, and Y. Iye

Institute of Solid State Physics, University of Tokyo, Tokyo 106, Japan

We report here the successful preparation of a new diluted magnetic semiconductor (DMS), (Ga,Mn)As, which is based on the most well understood and extensively used III-V compound, GaAs. Magnetization measurements revealed the presence of ferromagnetic order in the (Ga,Mn)As films at low temperatures.

The (Ga,Mn)As films were grown by solid-source molecular-beam epitaxy (MBE) on semi-insulating (001) GaAs substrates using elemental Ga, Mn and As as source materials. No intentional doping was employed throughout the growth procedure. Growth rate of 0.6-0.8  $\mu\text{m/h}$  was used with Mn content,  $x$ , varying from 0.015 to 0.07, which was calibrated by electron probe micro-analysis (EPMA) measurement results on (In,Mn)As layers grown using the same MBE machine. All the (Ga,Mn)As layers were grown under As-stabilized condition at a substrate temperature,  $T_s$ , of 250°C.

Reflection high energy electron diffraction (RHEED) was used to monitor the surface reconstruction throughout the growth procedure. The surface reconstruction of GaAs grown at high temperature was (2x4) (during and after growth), which changed to c(4x4) when  $T_s$  was lowered to 480-520°C and remained the c(4x4) below (after growth). No surface reconstruction was observed for GaAs grown at 250°C. The surface reconstruction of the (Ga,Mn)As was (1x2). No indication of formation of MnAs clusters was observed.

X-ray diffraction measurements showed that the lattice constant of (Ga,Mn)As increases linearly with  $x$ , and the extrapolated lattice constants for GaAs and MnAs are in good agreement with the known GaAs value and the MnAs value extrapolated from the InMnAs, suggesting that all the Mn atoms were incorporated in the zinc-blende alloy.

Magnetization measurements done by a SQUID magnetometer on the sample with  $x=0.035$  showed the presence of a ferromagnetic order in the (Ga,Mn)As films at low temperatures; the Curie temperature,  $T_c$ , was 60K. Magnetotransport measurements showed that anomalous Hall effect dominates the transport properties of the samples at low temperatures. The highest  $T_c$  obtained so far is nearly 100K for the sample with  $x=0.043$ .



## EFFECTS OF STRAIN ON THE GROWTH AND PROPERTIES OF $\text{CuInSe}_2$ EPITAXIAL FILMS

**S. Niki, P. J. Fons, T. Kurafuji, A. Yamada, H. Oyanagi,  
W. Bi\* and C. W. Tu\***

Electrotechnical Laboratory, 1-1-4 Umezono, Tsukuba, Ibaraki 305, Japan

(phone) 81-298-58-5610 (FAX) 81-298-58-5615 (e-mail) s.niki@etlrips.etl.go.jp

\*Depart. of Elect. and Comp. Engin., Univ. of California at San Diego, La Jolla, CA 92093, U. S. A.

$\text{CuInSe}_2$  (CIS) has emerged as a promising material for thin film high-efficiency solar cells. While various growth techniques have been investigated, more detailed material information is required for further improving the performance of CIS-based solar cells. Several authors have reported on the growth and structural analysis of CIS epitaxial layers heteroepitaxially grown on various substrates such as GaAs, Si, GaP, for the purpose of studying the intrinsic properties of CIS<sup>1)</sup>. However, the control of point defects critical to the understanding of intrinsic optical and electrical properties of the CIS films is not satisfactory and the epitaxial growth mechanism is not well understood.

In this work, focus has been on the growth of high quality CIS epitaxial films based upon the understanding of strain effects on growth mode and defect formation. CIS epitaxial films with a range of growth parameters have been grown by solid-source molecular beam epitaxy on both GaAs (001) (CIS/GaAs) and *pseudo* lattice-matched InGaAs substrates (CIS/InGaAs) by controlling both the substrate surface and lattice mismatch. Film properties have been characterized primarily by reflection high energy electron diffraction (RHEED), high resolution X-ray diffraction (HRXRD), transmission electron microscopy (TEM) as well as low temperature photoluminescence (PL) spectroscopy.

The S-passivated (2x1) GaAs surface has been used for the growth of CIS films; epitaxial growth with the c-axis normal to the substrate has been demonstrated. RHEED patterns obtained from Cu-rich films showed a (1x3) reconstruction which was streaky along the  $[1\bar{1}0]$  direction and wavy along the three-fold  $[1\bar{1}0]$  direction, while In-rich films showed a spotty (1x1) pattern with large number of twins on {112} planes. TEM and HRXRD analysis on Cu-rich CIS indicated the formation of a chalcopyrite  $\text{CuInGaSe}_2$  layer in the vicinity of the CIS/GaAs interface caused by strain-induced interdiffusion of Ga (In) into CIS (GaAs), and also the existence of a Stranski-Krastanov like growth mode at the beginning of the epitaxial growth. Cu-rich films showed sharp and distinct PL emissions, making possible the assignment of their radiative recombination processes<sup>2)</sup>, however the emissions due to defect levels were still dominant possibly due to the large lattice mismatch of  $\Delta a/a \sim 2.2\%$  between CIS and GaAs.

*Pseudo* lattice-matched InGaAs substrates with  $\Delta a/a \sim 0.2\%$  at RT have also been used for growth of CIS films. Significant reduction of residual strain and improved surface roughness in comparison with CIS/GaAs have been achieved, and the above mentioned strain-driven interdiffusion did not take place. Electrical properties of the films improved markedly with mobilities as high as  $100 \text{ cm}^2/\text{V}\cdot\text{sec}$  and hole concentrations of as low as  $1 \times 10^{17} \text{ cm}^{-3}$ . Free exciton emissions of  $E_{X1}$  ( $\sim 1.040 \text{ eV}$ ) and  $E_{X2}$  ( $\sim 1.045 \text{ eV}$ ) were predominantly observed in the PL spectra (2K) for the first time, and the defect-related emissions dominant in the PL spectra of CIS/GaAs became negligibly small in the PL spectra of CIS/InGaAs. Above results suggested the growth of CIS epitaxial films suitable for device applications, and also implied that the CIS-based solar cells can be further improved by optimizing the matching in lattice parameters.

### REFERENCES

- 1) For example, A. N. Tiwari et al., Appl. Phys. Lett. 65, 2299 (1994). 2) S. Niki et al., Appl. Phys. Lett. 67, 1289 (1995).

## Supplemental information

EFFECTS OF STRAIN ON THE GROWTH AND  
PROPERTIES OF  $\text{CuInSe}_2$  EPITAXIAL FILMS

S. Niki, P. J. Fons, T. Kurafuji, A. Yamada, H. Oyanagi, W. G. Bi\* and C. W. Tu\*

Electrotechnical Laboratory, 1-1-4 Umezono, Tsukuba, Ibaraki 305, Japan

(phone) 81-298-58-5610 (FAX) 81-298-58-5615 (e-mail) s.niki@etlrips.etl.go.jp

\*Department of Electrical and Computer Engineering,

Univ. of California at San Diego, La Jolla, CA 92093, U. S. A.

Control of defects is considered to be one of the key issues to be addressed for further improving the  $\text{CuInSe}_2$  (CIS)-based solar cells. Intrinsic defects in CIS have been characterized by various defect-sensitive techniques, however considerable discrepancies still exist in their assignment and interpretation partly due to the lack of high quality material. In this work, focus has been on the growth of high quality CIS epitaxial films based upon the understanding of the effects of strain on growth mode and film quality, and CIS films have been grown on GaAs (CIS/GaAs) and on *pseudo* lattice matched InGaAs substrates (CIS/InGaAs).

Fig. 1 shows 2D reciprocal X-ray intensity area mapping of Cu-rich CIS on GaAs (001). A peak with the same in-plane lattice constant as CIS clearly appeared between CIS and GaAs. Another 2D mapping using the same sample in the vicinity of CIS (309) reflection suggested chalcopyrite structure, and the evaluation of strain using elasticity theory and secondary ion mass spectroscopic analysis suggested the formation of chalcopyrite  $\text{CuInGaSe}_2$  in the vicinity of CIS/GaAs interface. Since CIS/InGaAs with  $\Delta a/a \sim 0.2\%$  at RT did not show such a peak, such interdiffusion is associated with misfit strain between CIS and GaAs.

Fig. 2 shows the low temperature photoluminescence spectra of CIS/GaAs and CIS/InGaAs. Free exciton-related emissions of  $E_{X1}$  ( $\sim 1.040\text{eV}$ ) and  $E_{X2}$  ( $\sim 1.045\text{eV}$ ) were predominantly observed in the PL spectra (2K), while the defect-related emissions were dominant in the PL spectra of CIS/GaAs. This is the first observation of dominant free exciton emissions from CIS films, indicating the growth of high quality CIS epitaxial films suitable for device applications.

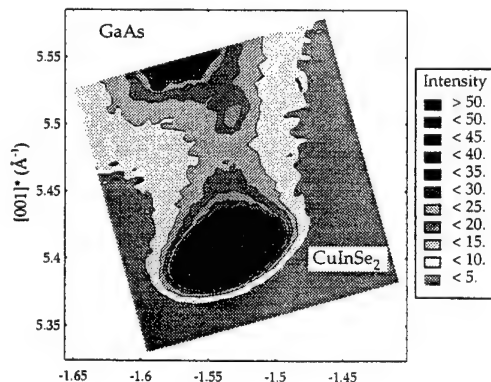


Fig. 1 shows two-dimensional reciprocal X-ray intensity area mapping of Cu-rich CIS grown on GaAs (001)

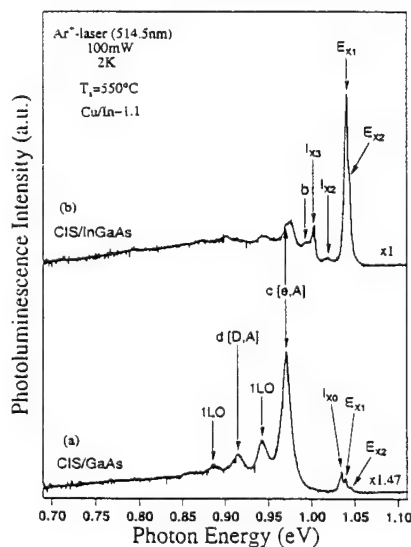


Fig. 2 low temperature photoluminescence spectra of CIS (a) on GaAs (001) (b) on InGaAs substrate.

## **Preparation of high-quality CuInSe<sub>2</sub> and CuGaSe<sub>2</sub> epitaxial films by an in-situ annealing technique**

Bae-Heng Tseng, Song-Bin Lin, Gin-Lern Gu, and Sing-Chu Lai

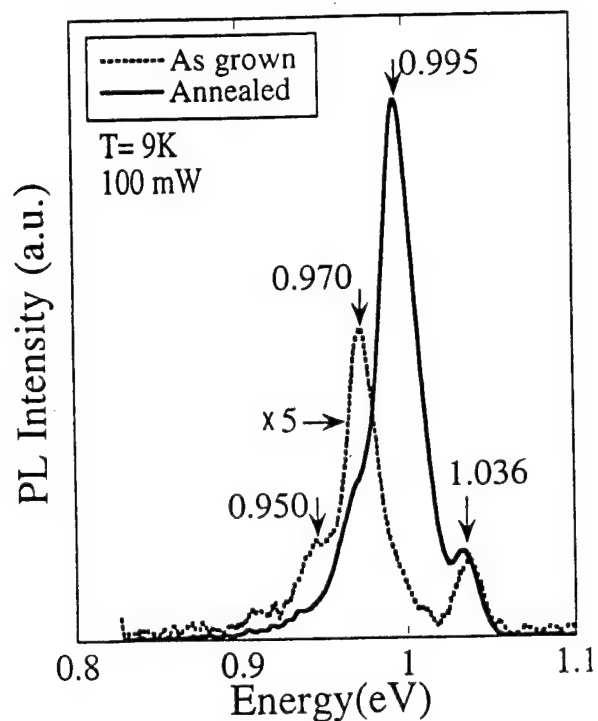
Institute of Materials Science and Engineering, National Sun Yat-Sen University,  
Kaohsiung 804, Taiwan-R.O.C.

( Tel: +886-7-282-1516; FAX: +886-7-521-1690; e-mail: baeheng@mail.nsysu.edu.tw )

I-III-VI<sub>2</sub> compounds have found applications in solar cells and non-linear optics. The bandgaps of these materials have a range as wide as their II-VI analogues. The capability to grow high-quality epitaxial films may help the development of new devices. In this work, we demonstrate that an in-situ annealing technique may improve the optical and electrical properties of CuInSe<sub>2</sub> and CuGaSe<sub>2</sub> epitaxial films. We believe that the same technique will be successfully applied to other I-III-VI<sub>2</sub> compounds.

Thin films of CuInSe<sub>2</sub> and CuGaSe<sub>2</sub> were grown on (001)GaAs substrates by molecular beam epitaxy (MBE). Thermal annealing was conducted in the MBE chamber immediately after film deposition in the presence of a Se-beam flux. This process brings the film to chemical equilibrium. The equilibrium state is determined by the annealing temperature and the Se overpressure. We found a slight increase in the Se content but no significant change in the atomic ratio of cations after annealing. Typically, an anneal at 400°C for 60 min is adequate for a CuInSe<sub>2</sub> film. For CuGaSe<sub>2</sub> films, a higher annealing temperature at 470°C should be used since the bonding strength associated with Ga atoms is stronger than that with In atoms.

The luminescence properties of the films were studied by photoluminescence (PL) spectroscopy. Figure 1 shows the PL spectra of a slightly In-rich CuInSe<sub>2</sub> film before and after annealing. A dramatic increase in the PL intensity and a change in the distribution of intrinsic defects in CuInSe<sub>2</sub> are noted. A similar result is found in the CuGaSe<sub>2</sub> films, see Fig. 2. In addition, Hall measurements show an increase in the carrier mobility and a decrease in the degree of compensation in annealed films. The TEM examinations, which show a complete elimination of anti-phase domains (the anti-phase domain boundary is actually a plane of anti-site defects) and a dramatic reduction in the dislocation density in annealed films, give evidences that the improvement in the film properties is mainly due to the refinement of defect structures after annealing.



0.950 eV:  $\text{In}_{\text{Cu}}$ (donor) to  $\text{Cu}_{\text{In}}$ (acceptor) transition  
 0.970 eV:  $\text{In}_{\text{Cu}}$ (donor) to  $\text{V}_{\text{Cu}}$ (acceptor) transition  
 0.995 eV: Conduction band (CB) to  $\text{V}_{\text{Cu}}$ (acceptor) transition  
 1.036 eV: Excitonic transition

Fig. 1 PL spectra of a slightly In-rich  $\text{CuInSe}_2$  film before and after annealing.

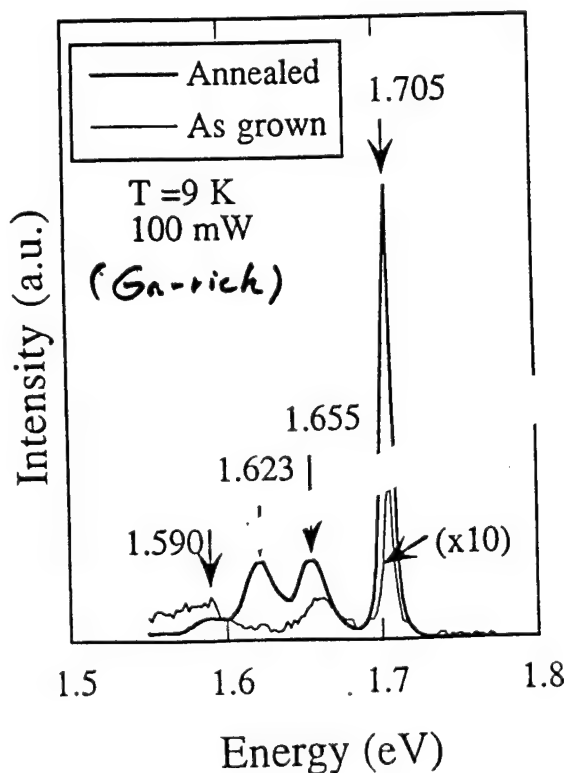


Fig. 2 PL spectra of a slightly Ga-rich  $\text{CuGaSe}_2$  film before and after annealing.

## Spiral Growth and improved Nucleation of PbTe on BaF<sub>2</sub> (111)

A. Y. Ueta, G. Springholz, N. Frank and G. Bauer,

*Institut für Halbleiterphysik, Johannes Kepler Universität, A-4040 Linz, Austria*

BaF<sub>2</sub> (111) has proven to be the most suitable substrate for MBE growth of narrow band gap IV-VI semiconductor compounds. Not only falls its lattice-constant of 6.200 Å within the range of that of the lead salt compounds, but also its thermal expansion coefficient is very well matched, in contrast to the common GaAs or Si substrates. In addition, BaF<sub>2</sub> is insulating and optically transparent in a very wide spectral region. However, because of the CaF<sub>2</sub> crystal structure, the natural (111) cleavage plane of BaF<sub>2</sub> that determines the substrate orientation is opposed to the preferred (100) growth direction of the lead salts. Therefore, heteroepitaxial growth always starts in a 3D Vollmer-Weber growth mode where isolated pyramids are formed, coalescing only after deposition of several 1000 Å of PbTe. In addition, a high density of misfit and threading dislocations is formed due to the 4.2% lattice-mismatch between PbTe and BaF<sub>2</sub>. As a consequence, thick buffers have to be grown on the BaF<sub>2</sub> substrates in order to achieve the high structural perfection and good electronic properties required for IV-VI compound heterostructures.

In this work, we present a systematic study of nucleation and growth of PbTe on BaF<sub>2</sub> (111) using *in situ* RHEED and UHV scanning tunneling microscopy (STM) and ex situ atomic force microscopy (AFM), and the structural and electronic properties of the epitaxial layers were studied by high resolution x-ray diffraction and Hall effect measurements. It is shown, that by the use of a very thin EuTe nucleation layer of only 1-2 monolayers in thickness, which serves as a template, the coalescence of the 3D PbTe islands on BaF<sub>2</sub> can be drastically enhanced so that already after 200 Å layer thickness a completely uniform 2D overlayer is formed. This improved nucleation is explained by the formation of a high density of nucleation sites on the BaF<sub>2</sub> substrate by the EuTe template. On these layers, UHV-STM reveals a high density of threading dislocations penetrating through the surface. As the layer thickness increases, however, the number of threading dislocations drastically decreases due to annihilation processes and larger and larger growth spirals are formed around the residual threading dislocations. In this process, the threading dislocation density determined quantitatively by STM drops from initially 10<sup>9</sup> cm<sup>-2</sup> to less than 3 x 10<sup>6</sup> cm<sup>-2</sup> at PbTe layer thickness of 5 µm, and at the same time the 4 K electron mobility increases from 10<sup>4</sup> cm<sup>2</sup>/Vs at 1000 Å to up to 2.6x10<sup>6</sup> cm<sup>2</sup>/Vs. Surprisingly, even very thin PbTe layers are essentially completely relaxed and x-ray diffraction indicates a remarkably high structural perfection. Not only do finite thickness oscillations appear for layer thicknesses of 500 Å, but even more triple axis omega scans exhibit an extremely narrow coherent scattering peak on a broad diffuse background. In fact, the width of the coherent part of the peak is as small as 15 arcsec. Thus, in spite of the large 4.2% lattice-mismatch, the PbTe layer is almost completely decoupled from the underlying BaF<sub>2</sub> and thus acts as a virtual substrate for subsequent IV-VI epitaxial layers.

Contact: Dr. G. Springholz, Institut für Halbleiterphysik, Universität Linz  
Altenbergerstr. 69, A-4040 Linz, Austria Tel.: ++43-732-2468-9602,  
FAX: ++43-732-2468-650 e-mail: G.Springholz@hlphys.uni-linz.ac.at

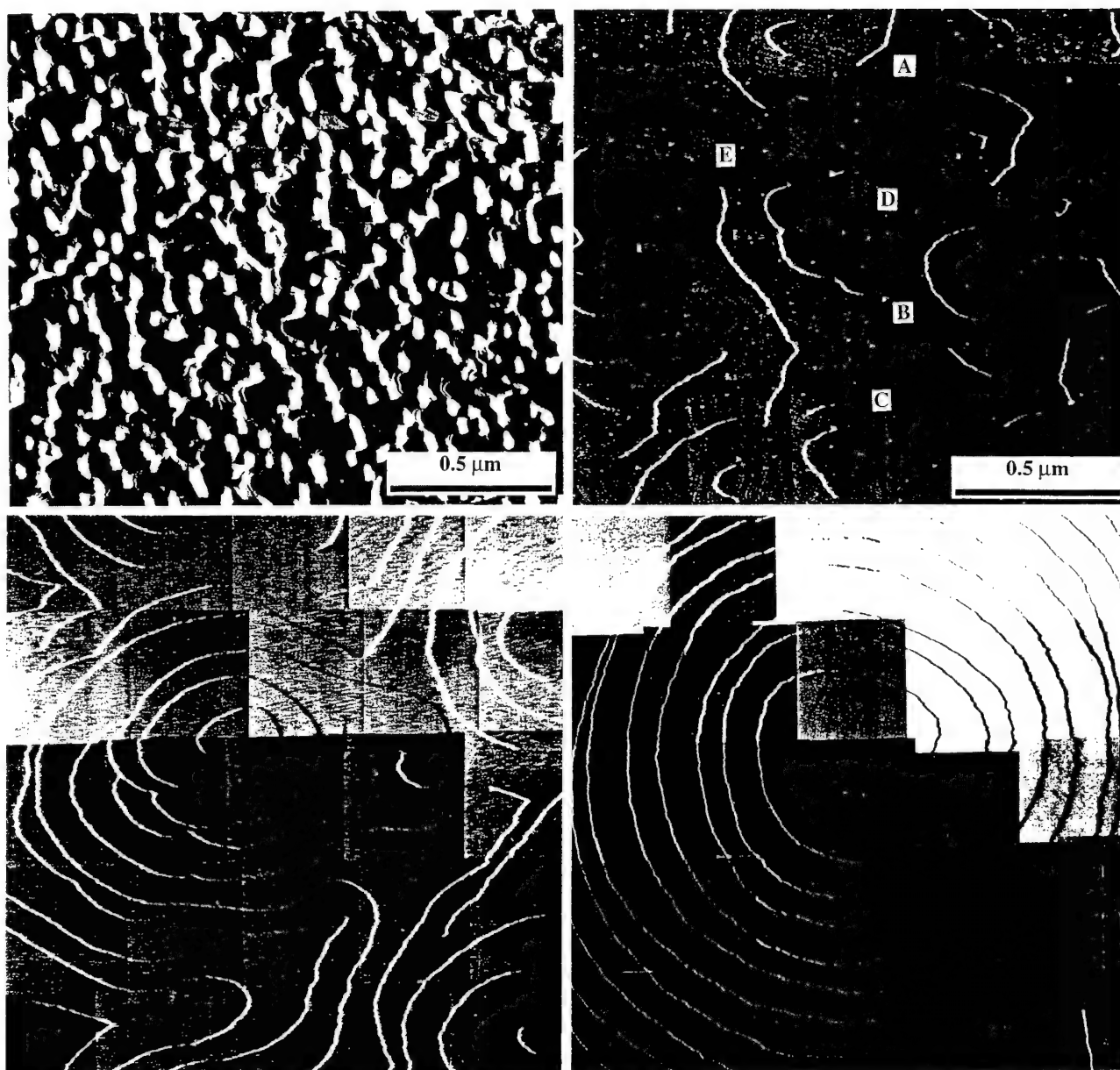


**Figure 1:** Scanning tunneling microscopy images of PbTe epitaxial layers of 170, 600, 5000 and 3  $\mu\text{m}$  layer thickness (top left to bottom right, respectively) grown on  $\text{BaF}_2$  (111) using a novel template technique. The height of all the steps is exactly one monolayer in height (1 ML = 3.8  $\text{\AA}$ ). During continued PbTe deposition, the number of threading dislocations observed by STM drops by 2 orders of magnitude and as a consequence larger and larger growth spirals are formed with diameters of up to 30  $\mu\text{m}$  and at the same time the 4K electron mobility increases by about the same order of magnitude to values of up to  $2.6 \times 10^6 \text{ cm}^2/\text{Vs}$  for layer of several  $\mu\text{m}$  in thickness.

## Control of the (100) and (111) CdMnTe/CdTe MBE Growth on (100) GaAs Substrates

\*M. Yano, \*K. Koike, \*T. Furushou and \*\*M. Kimata

\*New Materials Research Center, Osaka Institute of Technology

Asahi-ku Ohmiya, Osaka 535, Japan

Phone: +81-6-954-4313, Fax: +81-6-957-2136, E-mail: yano@elc.oit.ac.jp

\*\*School of Science and Engineering, Waseda University

Shinjuku-ku Ohkubo, Tokyo 169, Japan

In order to understand the interaction between the magnetic ions and the conduction electrons in quantum structures, CdMnTe/CdTe is a promising candidate since the CdMnTe barrier is a typical diluted magnetic semiconductor nearly lattice matched to CdTe. Many efforts have been devoted for the molecular beam epitaxial (MBE) growth of the CdMnTe/CdTe films. High quality films, however, were limited for the samples on lattice matched substrates such as CdTe and CdZnTe although many works have been done to use GaAs substrate. The major problem of the GaAs substrate comes from the large lattice mismatching to the CdMnTe/CdTe. It has been known that both orientations of (100) and (111) are possible for the CdMnTe/CdTe films on the (100) GaAs substrate. Recently, these two orientations have become controllable by choosing the growth condition. To obtain high quality films, however, understanding is still insufficient for both cases of the (100) and (111) growth. In this paper, we report the MBE growth of the CdMnTe/CdTe films on the (100) GaAs substrates and discuss the quality focusing on the crystallographic and optical properties.

We used solid source MBE apparatus equipped with a reflection high energy electron diffraction (RHEED) system. The source materials were CdTe, Cd, Te and Mn. After removing the GaAs surface oxide at 580°C, the substrate temperature was once increased to 600°C and then decreased to around 300°C to start the irradiation of the CdTe beam. The CdTe film became (111) orientation when the GaAs surface was kept free from any beams until the start of the growth. On the other hand, it became (100) orientation when the substrate had been irradiated by the Te beam at 600°C. The (100) CdTe also appeared regardless to the Te beam irradiation when the native oxide of the GaAs substrate was removed incompletely. Note that the lattice constants in the [011] and [0-11] directions of (100) CdTe are about 14% larger than those of (100) GaAs substrates, and that the lattice constant in the [-211] direction of (111) CdTe closely agree with the [011] of (100) GaAs whereas that of the [0-11] direction is 14% larger than that of the substrates.

We monitored the CdTe growth by the RHEED and analyzed the change of lattice constants with the thickness. This measurement indicated that the coherent growth of the (100) CdTe was limited within the initial several monolayers due to the large lattice mismatch. When the film thickness exceeded the critical thickness, we observed a rapid relaxation of the strained structure. After several hundred nanometers growth, however, the film was still compressed by the substrate although 85% of the lattice mismatch had been accommodated within the initial several ten nanometers. In the case of the (111) growth, on the other hand, the CdTe layer was lattice matched in the [-211] direction although its strain in the [0-11] direction still remained after the several hundred nanometer growth. These results were supported by the Raman scattering data that their LO phonon peaks shifted towards higher energy side due to the compressive strain.

Our MBE condition was optimized by analyzing the surface composition during the growth. To analyze the surface composition, we measured the change of reconstruction pattern by the pulsed irradiation of Cd and Te beams. This measurement revealed that the desorption of Cd and Te adatoms had respective activation energies of 3.0 and 0.87 eV on the CdTe surface, i.e., the CdTe surface during growth was Cd rich at low temperatures and it turned to be Te rich above 330°C. This means that the growing surface is nearly stoichiometric at 330°C. The film surface became flat under the stoichiometric condition. Defect density in the film also became the lowest, which was shown by the photoluminescence measurement.

On top of the flat CdTe buffer layer, we started the CdMnTe growth by adding Mn and Te beams. A RHEED oscillation measurement showed that the incorporation ratio of the Mn adatoms was nearly unity although those of Cd and Te atoms decreased to zero around at 380°C. The RHEED oscillation technique was also used to grow CdMnTe/CdTe superlattices by controlling the Mn composition and the thickness of the CdMnTe layer. The details of the superlattice quality will be discussed at the conference in relation to the growth conditions.



# INVESTIGATION OF THE OPTICAL AND STRUCTURAL PROPERTIES OF MBE GROWN ZnSe/GaAs HETEROSTRUCTURES $\square$

J. Luyo, Edgar López-Luna, M. Meléndez-Lira, I. Hernández-Calderón  
*Physics Department, CINVESTAV, Apdo. Postal 14-740, 07000, México, D.F.*

O. de Melo-Pereira, P. Díaz-Arencibia, R. León, J. Fuentes

<sup>+</sup>*Faculty of Physics, University of Havana, Cuba*

H. Sitter

*Institut für Experimentalphysik, Universität Linz, Austria*

The commercial application of green-blue emission lasers, based on quantum wells of ZnSe related compounds, cannot be accomplished yet due to the short life-time of the devices caused by the generation of defects during operation. Some of the intrinsic defects are originated by the lattice mismatch between the commonly used substrate, GaAs(100) and the buffer layer of ZnSe, and also between the quantum well material,  $\text{Zn}_{1-x}\text{Cd}_x\text{Se}$ , and the barrier material. Here, we report our results on the growth of ZnSe/GaAs(100) heterostructures by molecular beam epitaxy (MBE) and their characterization by optical, structural and surface sensitive methods.

The optical properties of the heterostructures were characterized by photoluminescence (PL), photoreflectance (PR), and Raman (RS) spectroscopies. The structural properties were investigated *in-situ* by reflection high energy electron diffraction (RHEED) and afterwards by high resolution X-ray diffraction (HRXRD). The surface of the substrates prior and after growth and of the film surface were investigated by Auger electron spectroscopy (AES). The results of the different experiments indicated in a consistent manner that the films and interfaces grown at 325 °C presented a very high crystalline quality. Analysis of the intensities and lineshape of the LO and TO phonons of the GaAs substrate and of the ZnSe films indicated a ZnSe critical thickness of around 0.2  $\mu\text{m}$ , in consistency with the HRXRD results. The appearance of the TO in GaAs for films near the critical thickness can be correlated with imperfections produced by the appearance of dislocations. Comparison of PR and PL spectra excited with photons of larger and lower energy than the band gap of ZnSe allowed to identify characteristic features of the ZnSe/GaAs interface and their behavior with substrate temperature and thickness of the films. Direct evidence of the presence of stress in the substrate is exhibited in the PL spectra. The analysis of Franz-Keldysh oscillations in the PR spectra allowed us to characterize the built-in interfacial electric field. The results of the different experiments are correlated and explained in terms of the structural properties of the heterostructures.

$\square$ Partially supported by CONACyT, Mexico.

Author for correspondence:

Prof. Isaac Hernández-Calderón  
Physics Department  
CINVESTAV  
Apdo. Postal 14-740  
07000 México, D.F.  
MEXICO  
ihernand@fis.cinvestav.mx

Ph. (52-5)747-7000 x 4203  
Fax (52-5)747-7096

(Poster session preferred)



## Elastic and plastic deformation in the low mismatched heteroepitaxial system $\text{Cd}_x\text{Hg}_{1-x}\text{Te} / \text{Cd}_{1-y}\text{Zn}_y\text{Te}$ .

T. COLIN\*, T. SKAULI, S. LØVOLD

Norwegian Defence Research Establishment - Division for Electronics

PO Box 25

N-2007 KJELLER - NORWAY

### Abstract

The knowledge of relaxation mechanisms in a semiconductor material is important in device design unless devices are limited to naturally unstrained homoepitaxial structures. In the case of epitaxial structures used for infrared detection, the required device thickness (around  $10\mu\text{m}$  for detection in the second transparency window of the atmosphere) is well above the critical thickness if the lattice mismatch with its substrate exceeds  $2 \cdot 10^{-4}$ . Therefore these structures are often grown on  $\text{Cd}_{1-y}\text{Zn}_y\text{Te}$  (CZT) where the Zinc concentration can be, in principle, adjusted to get perfect lattice matching to any composition in  $\text{Cd}_x\text{Hg}_{1-x}\text{Te}$  (CMT). However a perfect lattice matching can be difficult to achieve in practice<sup>1,2</sup>. This problem can be particularly drastic on the large-area CZT substrates now commercially available. The mechanism and extent of strain relaxation need therefore to be addressed. This is the goal of this presentation.

The elastic and plastic deformation of epitaxial layers of  $\text{Cd}_x\text{Hg}_{1-x}\text{Te}$  ( $0.2 < x < 0.5$ ) grown by Molecular Beam Epitaxy on  $\text{Cd}_{1-y}\text{Zn}_y\text{Te}$  ( $0.02 < y < 0.04$ ) have been studied by X-ray diffraction. The mostly used method for determination of the relaxation state is based on diffraction peak separation measurement between substrate and epilayer. It is unapplicable in the low mismatched heteroepitaxial systems. This arises because, when the epilayer starts to release the elastic strain related to the pseudomorphic growth, its thickness is comparable to the probing depth of X-rays therefore impeding clear observation of the substrate diffraction peak. In addition, overlapping of the diffraction peaks for small elastic deformation hinders its correct observation. By mapping the substrate lattice parameter before growth, both these problems can be overcome. The experimental study has been performed on uniform Cadmium Mercury Telluride (CMT) layers grown on Cadmium Zinc Telluride (CZT) substrates with varying Zinc concentration. It is therefore possible, within each sample, to clearly identify the different deformation regimes (elastic deformation in the regions of small lattice mismatch, plastic deformation in the regions with larger mismatch).

This study allowed us to confirm that there is only one relaxation mechanism in the heteroepitaxial system CMT/CZT. As previously reported by other workers<sup>1,4</sup>, there is an apparent dissymmetry in relaxation of tensile strain and relaxation of compressive strain (see Figure 1). These results have been successfully modeled in the frame of a preexisting model based on energetic considerations<sup>3</sup>. This model has been adapted to the growth on low symmetry growth planes as (211). Technologically important parameters like the energy of formation of misfit dislocation and differential thermal expansion coefficients have been determined from this study. Specific aspects of relaxation on high index planes will also be commented.

---

\* Tel : (47) 63 80 73 33 - Fax : (47) 63 80 72 12 - e-mail : Thierry.Colin@ffi.no

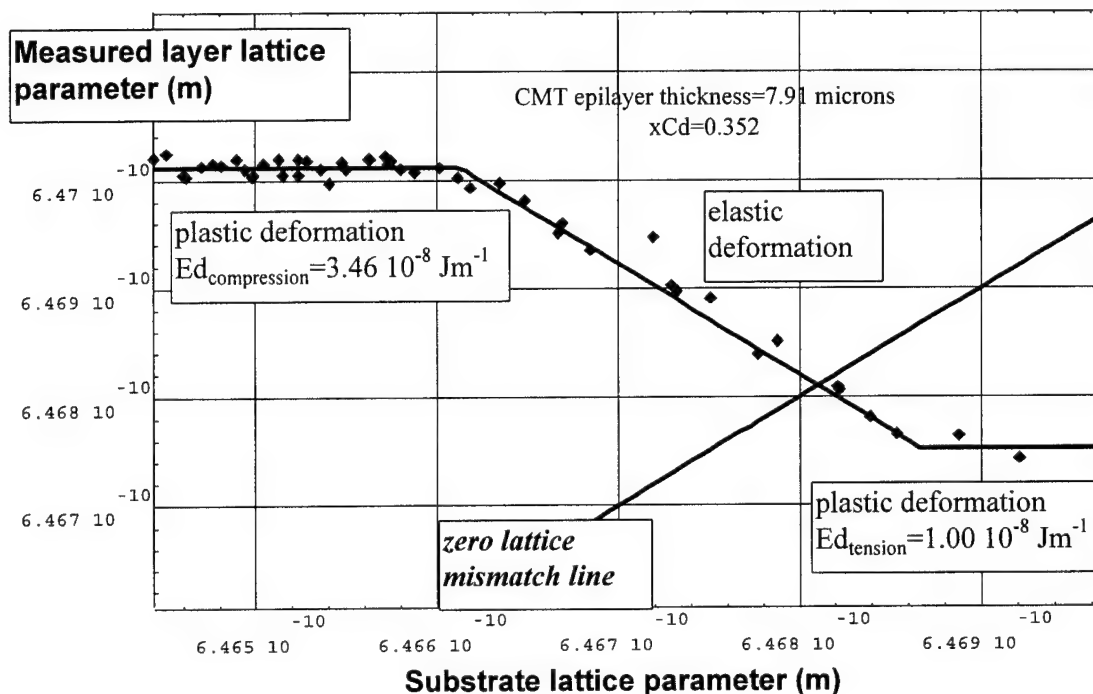


**Figure 1:** Evolution of the CMT epilayer lattice parameter perpendicular to the (211) growth plane as a function of the underlying CZT substrate lattice parameter. The measured data (dots) can be easily modeled (thick lines) and show very clearly the transition between elastic and plastic deformation both in compressively and tensively strained material. The indicated  $E_d$  parameters are the apparent linear energy of formation of misfit dislocations required to model the strain relaxation in the two plastic deformation regions.

## References

- [1] S.P. Tobin, F.T.J. Smith, P.W. Norton, J. Wu, M. Dudley, D. Di Marzio, L.G. Casagrande  
J. Electron. Mat., 24 (9), (1995), 1189
- [2] T. Skauli, T. Colin, S. Løvold  
to be published.
- [3] C. Fontaine, J.P. Gaillard, S. Magli, A. Million, J. Piagnet  
Appl. Phys. Lett. 50 (14), (1987), 903
- [4] L. Sugiura, K. Shigenaka, F. Nakata, K. Hirahara  
J. Cryst. Growth 145, (1994), 547

## **ZnSe homoepitaxial growth on solid-phase recrystallized substrates**

E. Tournié,<sup>1</sup> P. Brunet, C. Ongaretto, C. Morhain, and J.-P. Faurie

*Centre de Recherche sur l'Hétéro-Epitaxie et ses Applications, Centre National de la Recherche Scientifique, (CRHEA/CNRS), F-06560 Valbonne- Sophia Antipolis (France).*

R. Triboulet, and J.O. Ndad

*Laboratoire de Physique des Solides de Bellevue, Centre National de la Recherche Scientifique, (LPSB/CNRS), F-92195 Meudon (France).*

Blue-green light emitting devices based on ZnSe heterostructures have been up to now implemented mainly on GaAs substrates because of the lack of high-quality ZnSe single crystals. However, the heteropolar II-VI / III-V interface is the seed for structural defects which are believed to be the main cause for the short lifetime of light-emitting and laser diodes. Therefore, it appeared necessary to evaluate the possibility to produce high-quality ZnSe single crystals and to develop the epitaxial growth of ZnSe and related materials on such crystals. In this work, we have studied the MBE-homoepitaxy of ZnSe on single crystals grown by solid-phase recrystallisation.

We have first characterized the as-grown ZnSe single crystals to assess their suitability as substrates. The linewidth of the (004) X-ray rocking curves lies in the 15-20 arcsec range. The low-temperature photoluminescence (PL) spectra are dominated by bound-exciton (BE) lines and the deep-level emission is 5 orders of magnitude weaker than the near-band edge (NBE) emission. PL reveals the absence of Cu which is a usual contaminant of ZnSe bulk material and a fast-diffusing impurity during epitaxial overgrowth. These substrates are thus of the highest quality achievable at present time.

We then have investigated the *ex situ* as well as *in situ* preparations of the substrate surface before MBE growth. Both steps appear to be very critical in order to obtain a correct nucleation of ZnSe on ZnSe. A proper polishing procedure allows to reproducibly obtain a two-dimensional (2D) RHEED pattern already when introducing the sample in the growth chamber at room temperature, even without any impinging flux. When heating the substrate under a Se or a Zn flux, very clear (3x1) or faint c(2x2) reconstructions, respectively, emerge above ~400 °C. In both cases, the reconstructions do not evolve, neither when heating further up to substrate degradation which occurs near 550 °C, nor when cooling down to the growth temperature near 300 °C.

When starting the growth on a Se-treated surface, the RHEED pattern invariably turns spotty for a few monolayers (MLs). On the contrary, on a Zn-treated surface the growth starts in a 2D-mode with an immediate improvement of the RHEED pattern. In both cases usual reconstructions, *i.e.* (2x1) or c(2x2) or a mixture of both depending on the Se/Zn flux ratio, appear during growth. Particularly interesting in our context is the comparison of the RHEED patterns when growing ZnSe on GaAs or ZnSe substrates. In fact, in the latter case the streaks are much thinner than in the former. In addition, many more oscillations of the specular spot are detected. This reveals a higher structural quality of the growing surface.

Finally, the PL properties of the samples are dominated by the NBE emission revealing a high purity. However, we will show that they are strongly influenced by the *in situ* pre-growth treatment.

---

<sup>1</sup> Tel: +33 / 93.95.42.23, fax: +33 / 93.95.83.61, e-mail: et@crhea1.unice.fr

MBE Growth of n-type ZnSe and ZnS  
Using Ethylchloride as a Dopant  
Takashi Yasuda, Bao-Ping Zhang, and Yusaburo Segawa

Photodynamics Research Center (PDC)  
The Institute of Physical and Chemical Research (RIKEN)  
19-1399 Koeji, Nagamachi, Aoba-ku, Sendai 980, Japan  
Phone: +81-22-228-2012, FAX: +81-22-228-2010  
e-mail: tyasuda@postman.riken.go.jp

Recent progress on p- and n-type conductivity control of ZnSe-based II-VI compounds has facilitated the use of these compounds in blue-green laser applications. Nitrogen gas activated by an RF plasma cell is found to be an efficient p-type dopant which can be introduced into the growth chamber through a variable leak valve. The dopant gas can be separated completely with the vacuum chamber, which is a great advantage in maintaining MBE chamber. A solid source of zinc chloride ( $\text{ZnCl}_2$ ), which is evaporated by a conventional K-cell in the vacuum chamber is extensively used as an n-type dopant. Although  $\text{ZnCl}_2$  is known to be an efficient n-type dopant for ZnSe, the relatively high vapor pressure of this source material limits the highest baking temperature of the chamber to about  $100^\circ\text{C}$ , because the diffusion of  $\text{ZnCl}_2$  in the MBE chamber causes considerable contamination to the other sources. Therefore, much attention must be paid when utilizing  $\text{ZnCl}_2$  during MBE growth.

In this study, we used an alternative n-type dopant source of ethylchloride ( $\text{EtCl}$ ). This is a liquid source with high vapor pressure at room temperature and can be introduced into the chamber through a variable leak valve. The use of  $\text{EtCl}$  makes it possible to place the dopant source outside of the growth chamber separated by the valve, which enables baking at higher temperature. In addition,  $\text{EtCl}$  can be easily baked out due to its high vapor pressure. This new design also gives us an opportunity to maintain the dopant source and the vacuum chamber separately.

The samples were grown by conventional MBE using Zn, Se, and S as sources. The growth was performed between  $150^\circ\text{C}$  and  $250^\circ\text{C}$ . The equivalent beam pressure ratio (VI/II) was kept at 3 to 5 during growth. The  $\text{EtCl}$  beam pressure was controlled by a variable leak valve, monitored by an ion gauge. The  $\text{EtCl}$  beam went through the vent line before the doping started, and then was switched to the MBE chamber by the computer controlled valve operation. This switching procedure prevents inadvertent introduction of  $\text{EtCl}$  into the MBE chamber.

When we increased the  $\text{EtCl}$  beam pressure from  $2.0 \times 10^{-7}$  torr to  $5.0 \times 10^{-6}$  torr, the carrier concentrations of ZnSe samples increased linearly from  $7.9 \times 10^{16} \text{ cm}^{-3}$  to  $1.4 \times 10^{18} \text{ cm}^{-3}$ . Therefore, it seems to be easy to control the carrier concentration precisely using this new dopant source. Low-temperature photoluminescence spectra of these samples exhibit dominant excitonic emission, but there is a weak deep emission, such as self-activated emission, resulting in the low compensation ratio in these samples. The Cl-doping into ZnS will be discussed as well using  $\text{EtCl}$  as a dopant.

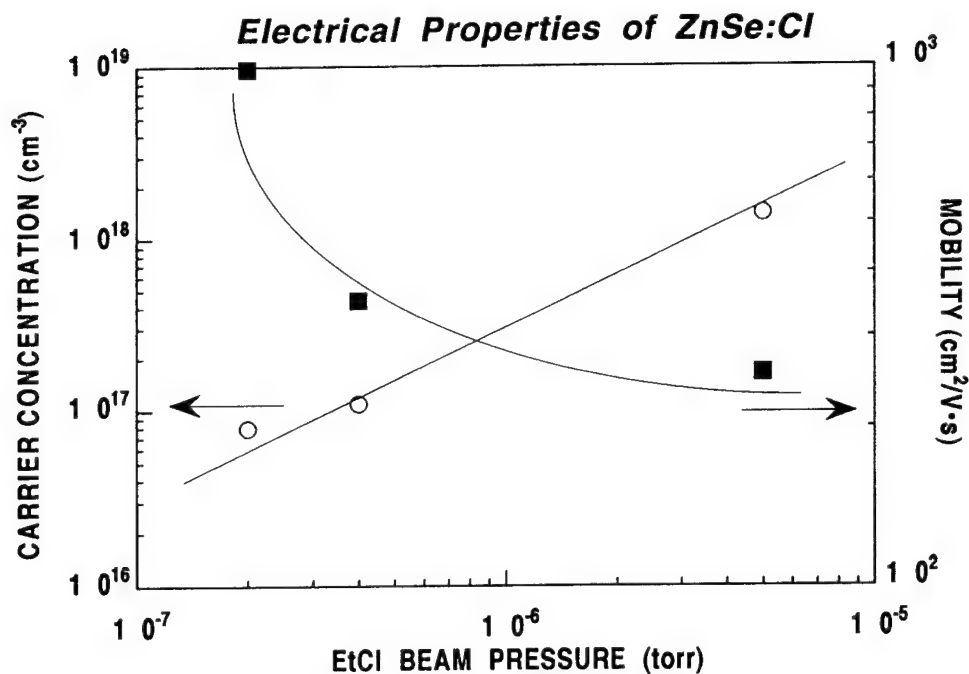


Fig. 1 EtCl beam pressure dependence of carrier concentration and mobility of ZnSe:Cl.

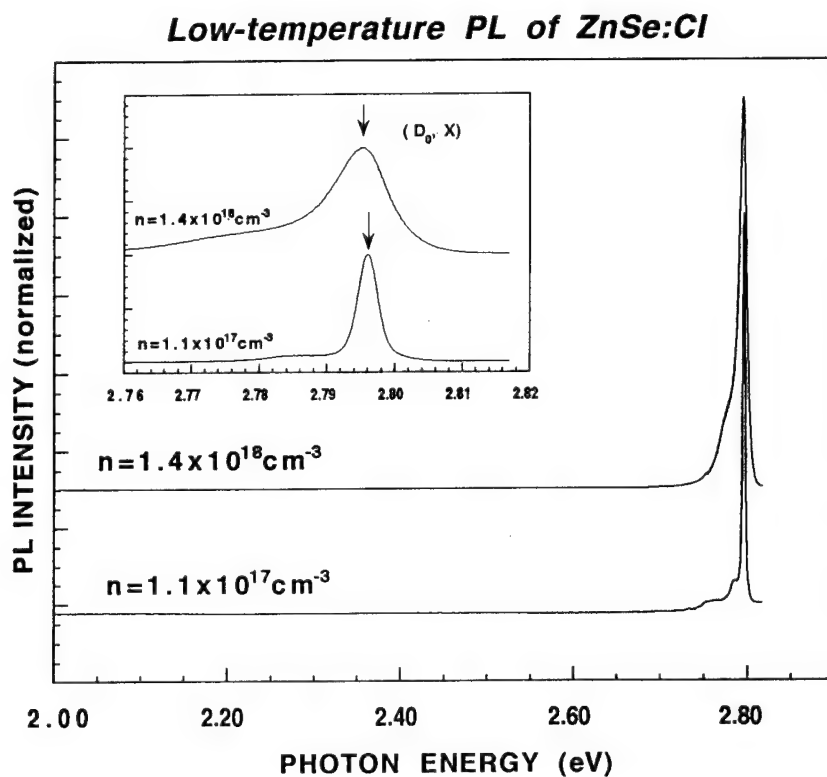


Fig.2 Low-temperature PL of ZnSe: Cl with different carrier concentrations of  $1.4 \times 10^{18} \text{ cm}^{-3}$  (upper spectrum) and  $1.1 \times 10^{17} \text{ cm}^{-3}$  (lower spectrum). The samples were excited by a He-Cd laser at about 2K.

# Growth Mechanism of II-VI Compound Semiconductors by Molecular Beam Epitaxy

*Hiroyuki Okuyama, Takayuki Kawasumi, Akira Ishibashi, Masao Ikeda*

*Sony Corporation Research Center, Fujitsuka 174, Hodogaya, Yokohama 240, Japan*

*TEL: +81-45-353-6832, FAX: +81-45-353-6905, E-mail : hokuyama@src.sony.co.jp*

The growth mechanism of II-VI semiconductors by molecular beam epitaxy (MBE) is discussed and a basic theory which can also be applied to other compound semiconductors is proposed. The mole fraction and the growth rate of ZnMgSSe were measured and they are explained by the theory, in which the desorption rate of adatoms from the surface covered with group II elements (surface II) is different from the surface covered with group VI elements (surface VI) and the adatoms easily move between surface II and surface VI. The theory is expressed by the following equations when the growth temperature is about 275C, temperature at which II-VI devices are normally fabricated. Samples were fabricated by MBE in which conventional solid Zn, Mg, Se sources were used and a valved cracking cell was used as the S source (cracking zone: 250C). From the experimental data, the maximum sticking coefficient of S is decreased with increasing the cracking temperature. The subscript *c* means the cation element and the subscript of *a* means the anion element.

$$k_c J_c - (D_{2c} \theta_2 + D_{6c} \theta_6) n_c - p_c n_c \theta_6 = 0 \quad (1)$$

$$k_a J_a - (D_{2a} \theta_2 + D_{6a} \theta_6) n_a^\gamma - p_a n_a \theta_2 = 0 \quad (2)$$

where  $n_i$  is the density of adatoms,  $J_i$  is the flux intensity,  $D_{2i}$  and  $D_{6i}$  are the desorption rates of adatoms on surface II and VI, respectively,  $p_i$  is the constant of adatom incorporation,  $k_i$  is the maximum sticking coefficient of cracked source. If the flux is not cracked or heated,  $k_i=1$ . When *i* shows the anion,  $i=a$  and  $\gamma>1$  because the anion flux is a cluster flux and it is expected to decompose into atoms or smaller clusters to form the adatom species. In this calculation we used  $\gamma=2$  because it is difficult to determine  $\gamma$ . The sum of the coverage of surface II and surface VI is 1.

$$\theta_2 + \theta_6 = 1 \quad (3)$$

When the surface II coverage is 0.5, both  $c(2 \times 2)$  and  $(2 \times 1)$  patterns of RHHED are expected to be observed. The growth rate, *g*, and the mole fractions, *x* and *y*, of  $Zn_{1-x}Mg_xS_ySe_{1-y}$  are expressed by the following equations.

$$g = p_{Zn} n_{Zn} \theta_6 + p_{Mg} n_{Mg} \theta_6 = p_{Se} n_{Se} \theta_2 + p_S n_S \theta_2 \quad (4)$$

$$x = p_{Mg} n_{Mg} / (p_{Mg} n_{Mg} + p_{Zn} n_{Zn}) \quad (5)$$

$$y = p_S n_S / (p_S n_S + p_{Se} n_{Se}) \quad (6)$$

This theory can explain the experimental value by adjusting parameters. The adjusted parameters are listed in fig. 1. The parameter of adatom incorporation is defined to be 1 and the desorption of cations (anions) on surface VI (II) is disregarded because this adsorption is like chemi-sorption. From fig. 1, the desorption rate of Zn on surface II is 50 times larger than that of Mg, which corresponds to the difference between the vapor pressures. The maximum sticking coefficient of S is not 1 because S flux was cracked and has the excess energy to evaporate. The desorption of Se is low when the surface is in the stoichiometric condition in which both  $c(2 \times 2)$  and  $(2 \times 1)$  patterns were observed by RHHED. Figures 2, 3 and 4 show the Zn, S and Se flux intensity dependence of the mole fractions and the growth rate of ZnMgSSe. The experimental values are almost successfully explained by this theory and adjusted 5 parameters. We can apply this theory to other compound semiconductors.

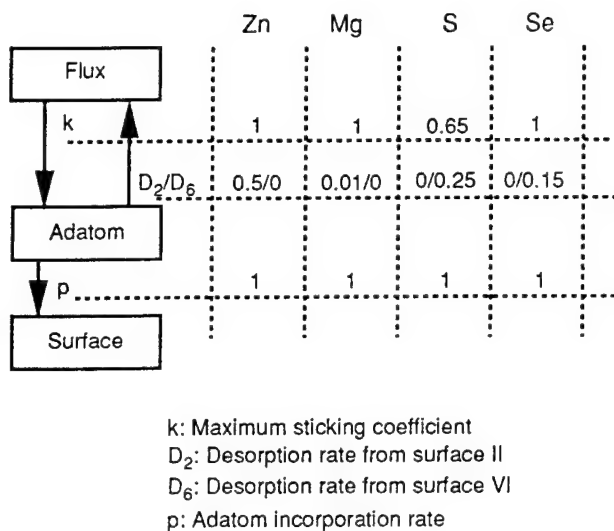


Figure 1 Adjusted parameters in eq. (1) - (6).

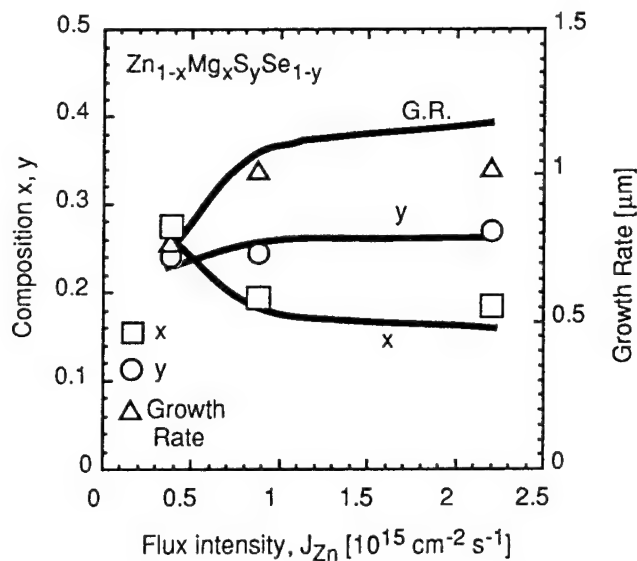


Figure 2 Zn flux intensity dependence of the mole fraction and the growth rate of experimental values (symbol) and calculated ones (curve) of ZnMgSSe.  $J_{Mg}$ ,  $J_S$ ,  $J_{Se}$  are 0.12, 0.19, 0.53 [ $10^{15} \text{ cm}^{-2} \text{ s}^{-1}$ ], respectively.

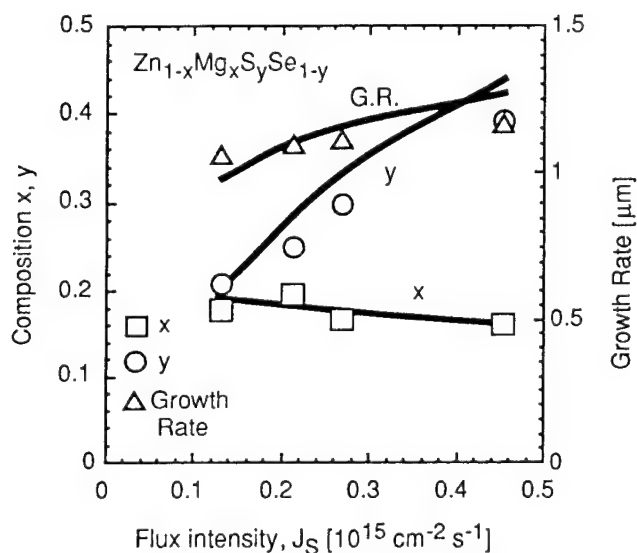


Figure 3 S flux intensity dependence of the mole fraction and the growth rate of experimental values (symbol) and calculated ones (curve) of ZnMgSSe.  $J_{Zn}$ ,  $J_{Mg}$ ,  $J_{Se}$  are 0.88, 0.13, 0.53 [ $10^{15} \text{ cm}^{-2} \text{ s}^{-1}$ ], respectively.

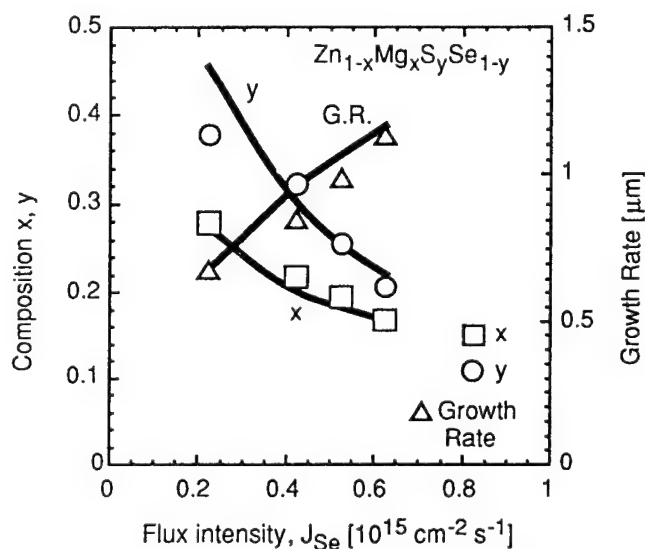


Figure 4 Se flux intensity dependence of the mole fraction and the growth rate of experimental values (symbol) and calculated ones (curve) of ZnMgSSe.  $J_{Zn}$ ,  $J_{Mg}$ ,  $J_S$  are 0.88, 0.12, 0.19 [ $10^{15} \text{ cm}^{-2} \text{ s}^{-1}$ ], respectively.

# Hydrogen sulfide treatment of GaAs substrate and its effect on initial stage of ZnSe growth

Jun Suda, Ryuji Tokutome, Yoichi Kawakami, Shizuo Fujita and Shigeo Fujita  
*Dep. of Electronic Science and Engineering, Kyoto Univ., Kyoto 606-01, Japan*  
Tel: +81-75-753-5357 / Fax: +81-75-753-5898 / E-mail: suda@kuee.kyoto-u.ac.jp

The control of GaAs substrate surface is essentially important for ZnSe/GaAs heteroepitaxy. So far, thermal etching without arsenic overpressure has generally been employed, but high vapor pressure of arsenic easily makes a Ga-rich surface, which is found to obstruct two dimensional (2D) nucleation of ZnSe. For one solution, a two chamber MBE system is used to grow a GaAs epitaxial buffer layer, and the (4 x 3) surface has brought very high quality ZnSe-based epilayers. On the other hand, many different surface treatment techniques have been proposed as other approaches to control the surface. We have reported that (NH<sub>4</sub>)<sub>2</sub>S<sub>x</sub> treatment of GaAs is effective for MOMBE growth of ZnSe. But recently it is revealed that the substrate surface is rough due to etching by the (NH<sub>4</sub>)<sub>2</sub>S<sub>x</sub>. In this paper, we report *in situ* H<sub>2</sub>S treatment of GaAs, with the characterization of the surface by RHEED and AFM observation, and show the effect of this technique on initial stage of ZnSe MBE growth.

The treatment is done under H<sub>2</sub>S environment at the pressure of 10<sup>-8</sup> Torr. Substrates used in this experiment are (100) oriented GaAs. After the etching process, the substrates were mounted onto a molybdenum-block using indium.

Figure 1 is the evolution of RHEED patterns with the increase of substrate temperature in H<sub>2</sub>S environment. Below 500 °C, a halo pattern is observed. Then, faint streaks appeared. At about 590 °C, the intensity of streaks dramatically increases and an arrow head pattern is observed as shown in fig. 1(a). The surface oxide layer is thought to be desorped at this temperature. After a few seconds, the RHEED pattern changes to (4 x 3) reconstruction with very intense streaks and Laue zone reflection as shown in fig. 1(b). If the substrate temperature further increases, the RHEED pattern changes into (2 x 6) reconstruction with arrow head-like streaks as shown in fig. 1(c).

Figure 2 is AFM images observed in the air. As shown in fig. 2(b), the surface which exhibited (4 x 3) reconstruction is atomically flat. Monolayer steps can be observed. It is consistent with the observation of Laue zone reflection in the RHEED pattern.

Figure 3 shows RHEED specular spot intensity just after starting the growth of ZnSe on GaAs (4 x 3) surface obtained by the H<sub>2</sub>S treatment. Very clear intensity oscillation is observed over 40 cycles onto H<sub>2</sub>S treated GaAs surface, showing 2D nucleation of ZnSe. To the best of our knowledge, this is the first observation of 2D initial growth of ZnSe onto GaAs substrates without GaAs epitaxial buffer layers. We believe that the H<sub>2</sub>S treatment makes it possible to control the initial stage of ZnSe growth for good quality layers without GaAs buffer layers.



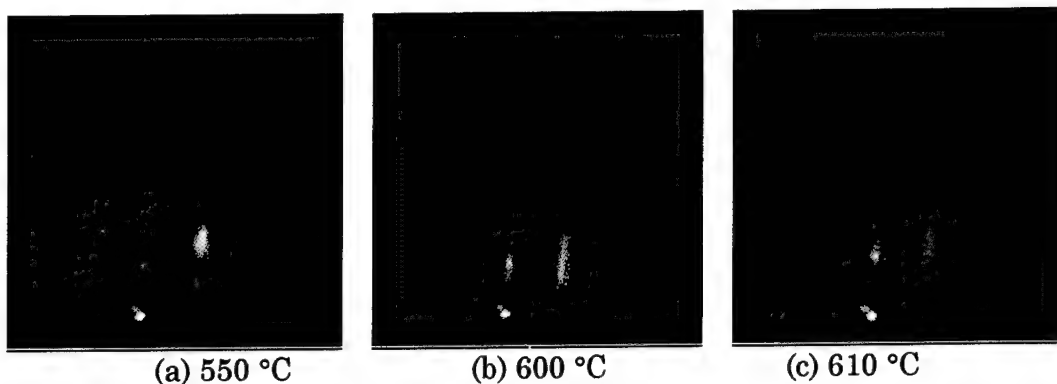


Figure 1. Evolution of RHEED patterns with the increase of substrate temperature in  $\text{H}_2\text{S}$  environment. (a) arrow head-like streaks, (b) sharp streaks with  $(4 \times 3)$  reconstruction and Laue zone reflection and (c) arrow head-like streaks with  $(4 \times 6)$  reconstruction.

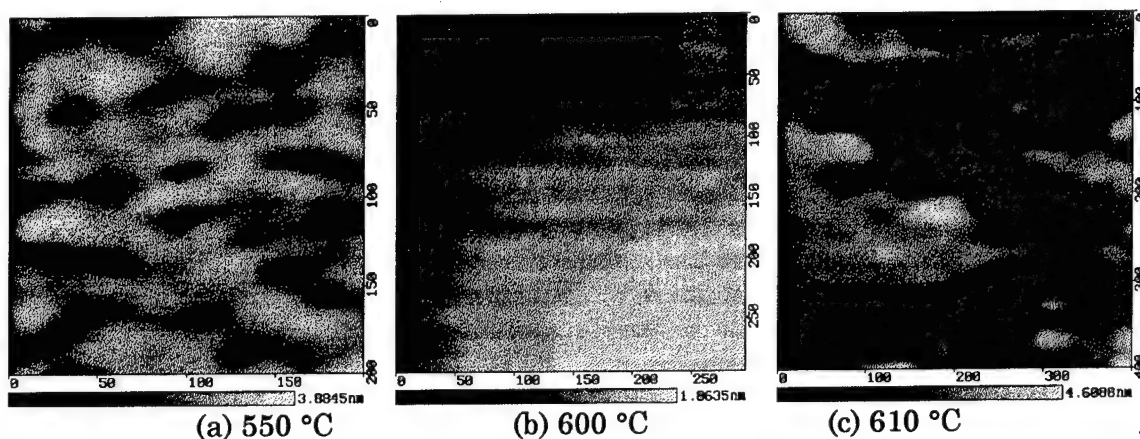


Figure 2. AFM images observed in the air. (a) wavy surface developed along  $[110]$  direction. (b) atomically flat surface and (c) atomically flat but composed of small domains.

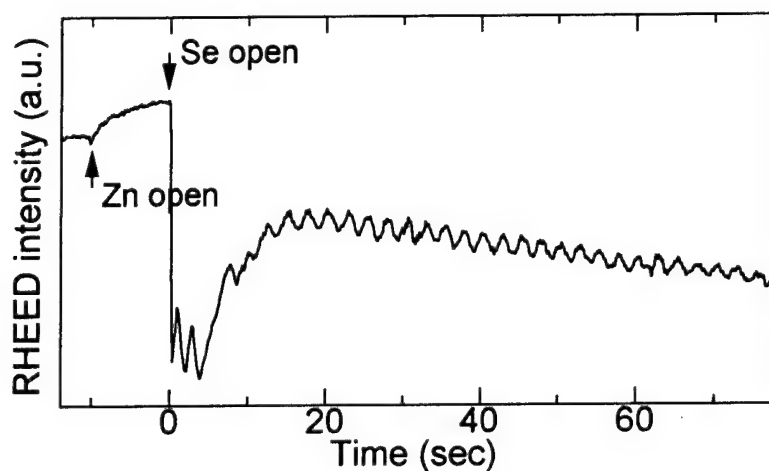


Figure 3. Intensity oscillations of RHEED specular spot for the growth of ZnSe on  $\text{H}_2\text{S}$  treated  $(4 \times 3)$  GaAs surface. Clear intensity oscillation is observed just after starting the growth.

## **HOMOGENEOUS AND $\delta$ -DOPED ZnS:Mn FOR FLAT PANEL DISPLAYS GROWN BY MBE**

S. Schön, T. Yang, M. Chaichimansour, W. Park, B.K. Wagner and C.J. Summers  
Phosphor Technology Center of Excellence, Manufacturing Research Center  
Georgia Institute of Technology, Atlanta, GA 30332-0560  
Tel: (404) 894-0109 Fax: (404) 894-5073  
e-mail: chris.summers@gtri.gatech.edu

The wide bandgap compound semiconductor ZnS has many applications in optoelectronic devices. Manganese doped ZnS is used to fabricate ac- and dc-based electroluminescent flat panel display devices. The luminescent intensity strongly depends on the crystallinity and growth method of the ZnS thin film and the nature of the luminescence center, its coordination in the crystal lattice and its concentration.

ZnS:Mn thin films were grown by molecular beam epitaxy (MBE) and gas source MBE (GSMBE) on GaAs(100), glass/ITO and glass/ITO/dielectric stacks using a solid ZnS source and a novel sulfur precursor, t-BuSH, to supply an excess sulfur flux. This was found to improve the film quality by decreasing the number of sulfur vacancies. Substrate temperatures varied from 174 to 200°C. Homogeneous doping was carried out at different flux ratios  $F_{\text{ZnS}}/F_{\text{Mn}}$  using a Mn solid source. The linear dependence of the Mn concentration determined by SIMS on the flux ratio shown in figure 1 points to complete incorporation of Mn in the host ZnS.

Delta-doping technique is expected to confine the excitation energy transfer within separate 2-dimensional planes and therefore to suppress the 3-dimensional coupling between Mn ions and non-radiative defects which cause luminescence quenching. We have already showed that Mn delta-doped ZnS grown by chemical beam epitaxy (CBE) exhibited much brighter luminescence than the homogeneously doped ZnS using the same Mn flux which indicates that the luminescence efficiency has been greatly enhanced by delta-doping.<sup>1</sup> This delta-doping process was carried out by depositing only Mn for a time period of 50s several times during the thin film deposition. Figure 2 presents a depth profile of a nine times delta-doped sample. A Mn diffusion of more than 10nm to each side of the layer was observed. Calculations of the diffusion behavior of Mn in thin ZnS films will be presented.

As shown in Figure 3, low temperature photoluminescence (PL) studies showed bright band edge emission from undoped ZnS films, including free and bound excitons. The narrow linewidth and high intensity indicate high optical quality. Both the homogeneously and delta Mn doped ZnS films showed the characteristic orange luminescence and enhanced luminescence intensity was observed from delta-doped samples.

<sup>1</sup> W. Tong, T. K. Tran, W. Park, S. Schön, B. K. Wagner, and C. J. Summers, in Proceedings of the First International Conference on the Science and Technology of Display Phosphors, 1995

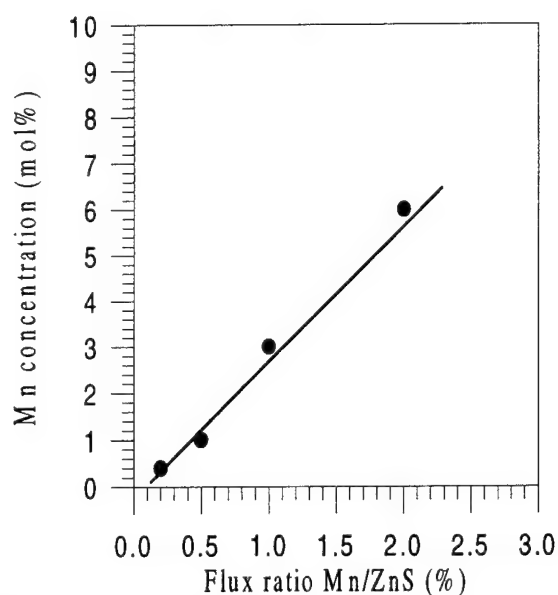


Fig. 1: Mn concentration in the film depending on flux ratio Mn/ZnS during growth.

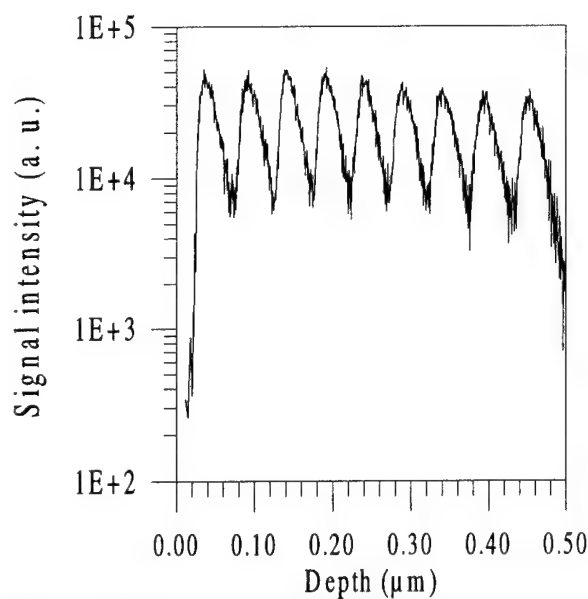


Fig. 2: SIMS depth profile of a nine times delta-doped ZnS:Mn.

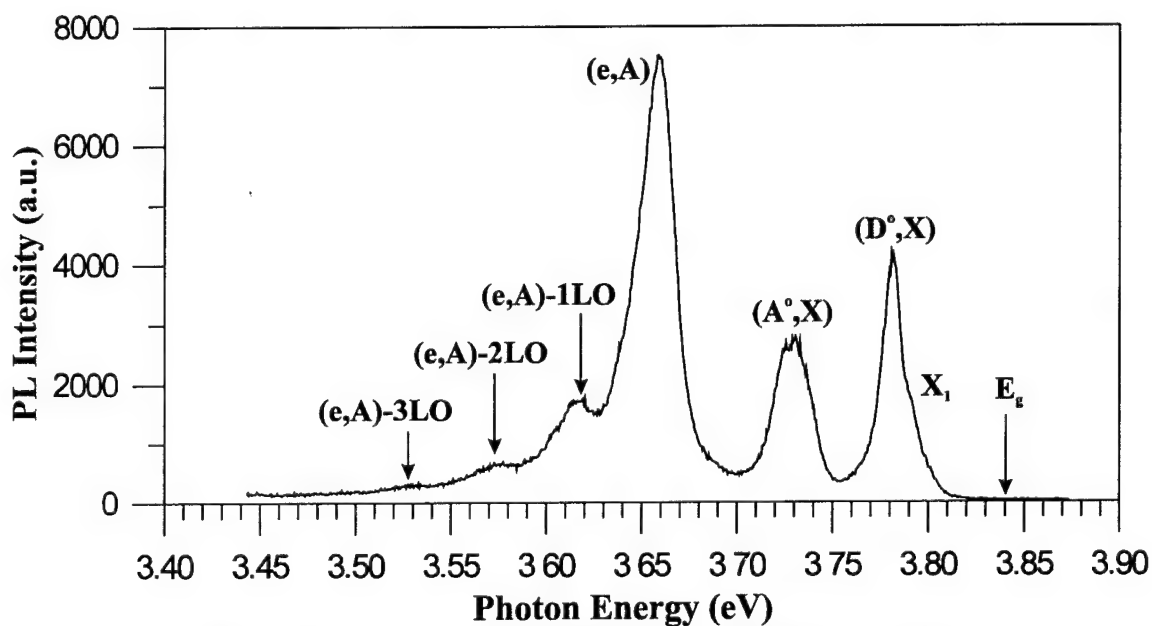


Fig. 3: Photoluminescence Spectrum of ZnS/GaAs at 10K

## TUNING OF ZnSe-GaAs BAND DISCONTINUITIES IN HETEROJUNCTION DIODES

V. Pellegrini,<sup>a</sup> M. Börger,<sup>a</sup> F. Beltram,<sup>a,b</sup> M. Lazzarino,<sup>b</sup> J.J. Paggel,<sup>b</sup>  
L. Sorba,<sup>b</sup> S. Rubini,<sup>b</sup> and A. Franciosi<sup>b,c</sup> \*

<sup>a</sup> *Scuola Normale Superiore, P.za dei Cavalieri 7, 56126 Pisa, Italy*

<sup>b</sup> *Laboratorio Nazionale TASC-INFM, Area di Ricerca,  
Padriciano 99, 34012 Trieste, Italy*

<sup>c</sup> *Department of Chemical Engineering and Materials Science  
University of Minnesota, Minneapolis, MN 55455*

The possibility of tuning the band offset in semiconductor heterojunctions would have an important impact on the optimization of optoelectronic devices. Recent photoemission studies of ZnSe/GaAs(001) heterojunctions [1] - crucial elements of blue lasers - have shown that the band offsets depend on the local interface composition. This, in turn, can be controlled acting on the Zn/Se flux ratio employed during the early stages of growth by molecular beam epitaxy (MBE). Photoemission studies of the band offsets, however, are limited to the analysis of the early stages of heterostructure formation (overlayer thickness  $\sim 1.5$ - $3.0$  nm). A major open question is if the metastable interface configurations responsible for offset tuning can be incorporated in functional devices [2].

We performed low-temperature transport measurement of the conduction band offsets in ZnSe/GaAs(100) heterojunction diodes as a function of interface composition. The key result is that the changes in band alignment observed earlier by photoemission in the thin overlayer samples survive the following stages of device fabrication and processing, and can be observed in fully functional devices. In fact, we report here what is, to our knowledge, the first verification of a locally engineered band offset in a fully functional device by transport methods.

The diodes were grown by MBE in a system which includes interconnected chambers for the growth of II-VI and III-V semiconductors. The diodes included a 500 nm p-GaAs buffer, a 500 nm p-Al<sub>x</sub>Ga<sub>1-x</sub>As graded layer with  $x$  varying from  $x=0$  to  $x=0.2$ , a 500 nm Al<sub>0.2</sub>Ga<sub>0.8</sub>As  $p=4 \times 10^{16} \text{cm}^{-3}$ , a 10 nm GaAs  $p=4 \times 10^{16} \text{cm}^{-3}$  layer in which the carrier were selected photoinjected to avoid hot electrons effects, and a 500 nm thick Cl-doped ZnSe ( $n=4 \times 10^{16} \text{cm}^{-3}$ ) layer. Different Zn/Se initial flux ratios were employed to fabricate the II-VI/III-V interfaces with different local compositions. The conduction band offset in the corresponding n-ZnSe/p-GaAs heterojunctions, buried well below the photoemission sampling depth, was determined from measurement of the low-temperature tunneling current [3] of photoinjected carriers.

We found conduction band offsets as high as 0.751 eV for Se-rich interfaces and as low as 0.261 eV for Zn-rich interfaces. The resulting 0.5-eV tuning range of the band offset is the largest ever reported for a functional solid state device. The corresponding valence band offsets, estimated from the bulk bandgap difference, were in good agreement with photoemission results from thin-overlayer samples.

\*Work supported in part by ARO under grants DAAH04-93-G-0319 and DAAH04-93-G-0206.

- [1] R. Nicolini, L. Vanzetti, Guido Mula, G. Bratina, L. Sorba, A. Franciosi, M. Peressi, S. Baroni, R. Resta, A. Baldereschi, J.E. Angelo, and W.W. Gerberich, *Phys. Rev. Lett.* **72**, 294 (1994); A. Bonanni, L. Vanzetti, L. Sorba, A. Franciosi, M. Lomascolo, P. Prete, and R. Cingolani, *Appl. Phys. Lett.* **66**, 1092 (1995).
- [2] E. Pelve', F. Beltram, C.G. Bethea, B.F. Levine, V.O. Shen, S.J. Hsieh, and R.R. Abbott, *J. Appl. Phys.* **66**, 5656 (1989).

Corresponding author: A. Franciosi, Department of Chemical Engineering and Materials Science, University of Minnesota, 421 Washington Ave SE, Minneapolis, MN 55455. Ph. (612)625-4540; FAX: (612)626-7246; e-mail: FQX6439@VX.CIS.UMN.EDU

# MOLECULAR BEAM EPITAXIAL GROWTH OF ZnSe(111) FILMS ON GaAs(111)B SUBSTRATES AND NITROGEN DOPING

N.Matsumura, T.Matsuoka, H.Shimakawa and J.Saraie

*Department of Electronics and Information Science, Faculty of Engineering and Design,*

*Kyoto Institute of Technology, Matsugasaki, Kyoto 606, Japan*

Tel: +81-75-724-7434, FAX: +81-75-724-7400, e-mail: matsumur@dj.kit.ac.jp

In the molecular beam epitaxial (MBE) growth of ZnSe related compound semiconductors on GaAs substrates, (100) surface has been usually used and other surfaces such as (111) surface were hardly used [1]. However, there is an attractive feature of (111) growth, that is, optical properties of strained-layer superlattice structure are modified by piezoelectric effect and new optoelectronic devices are expected [2,3]. Another interest is the impurity doping to ZnSe(111) surface because the numbers of chemical bond of Zn and Se on (111) surface are different from those on (100) surface. In this paper, the properties of ZnSe(111) films grown on GaAs(111)B substrates by MBE and the results of nitrogen doping were reported.

The substrates used were Cr-O doped just-oriented and  $10^\circ$ -misoriented GaAs(111)B substrates toward [100] direction. For comparison just-oriented GaAs(100) substrates were also used. The substrates were thermally etched prior to the growth without As beam irradiation at  $580^\circ\text{C}$  for 2 min. The growth temperature was  $340^\circ\text{C}$ . 6N-Zn and -Se were used as source materials. Nitrogen was used as a p-type dopant from a plasma cell. The plasma power was varied from 0 to 100 W. The epilayers were characterized by surface morphology, reflection high energy electron diffraction (RHEED), X-ray diffraction, photoluminescence (PL) and capacitance-voltage (C-V) measurement.

The epilayers grown on GaAs(111)B substrates showed mirror-like surface but were revealed to consist of twins from RHEED observation. PL spectra of undoped epilayers showed defect-related Y-line and deep emissions with weak exciton emissions (Fig. 1), but these emissions were suppressed in N-doped epilayers (Fig. 2).

The PL spectrum of the N-doped ZnSe(111) epilayer at 50 W (Fig. 2) showed deep-donor and acceptor pair ( $D^dAP$ ) emissions while that of the ZnSe(100) epilayer grown under the same growth condition showed combination of the acceptor bound exciton ( $I_1^s$ ) and the shallow-donor and acceptor pair ( $D^sAP$ ) emission with weak  $D^dAP$  emission, which suggests the increase in nitrogen incorporation in ZnSe(111) epilayers. The net acceptor concentration of ZnSe(111) epilayers will be measured. The origin of the twins and the doping character will be discussed.

## References

- [1] N.Matsumura, K.Maemura, T.Mori and J.Saraie, Jpn.J.Appl.Phys. **34**(1995)L1114.
- [2] D.L.Smith and C.Mailhot, Phys.Rev. **58**(1987)1264.
- [3] K.W.Goossen, E.A.Caridi, T.Y.Cheng, J.B.Stark and D.B.A.Miller, Appl.Phys.Lett. **56**(1990)715.

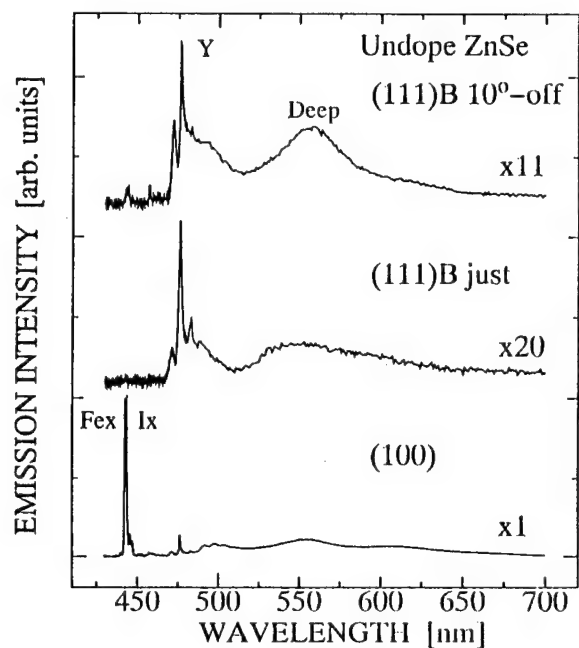


Fig. 1 PL spectra of undoped ZnSe(111) and (100) epilayers grown on GaAs(111)B and (100) substrates, respectively.

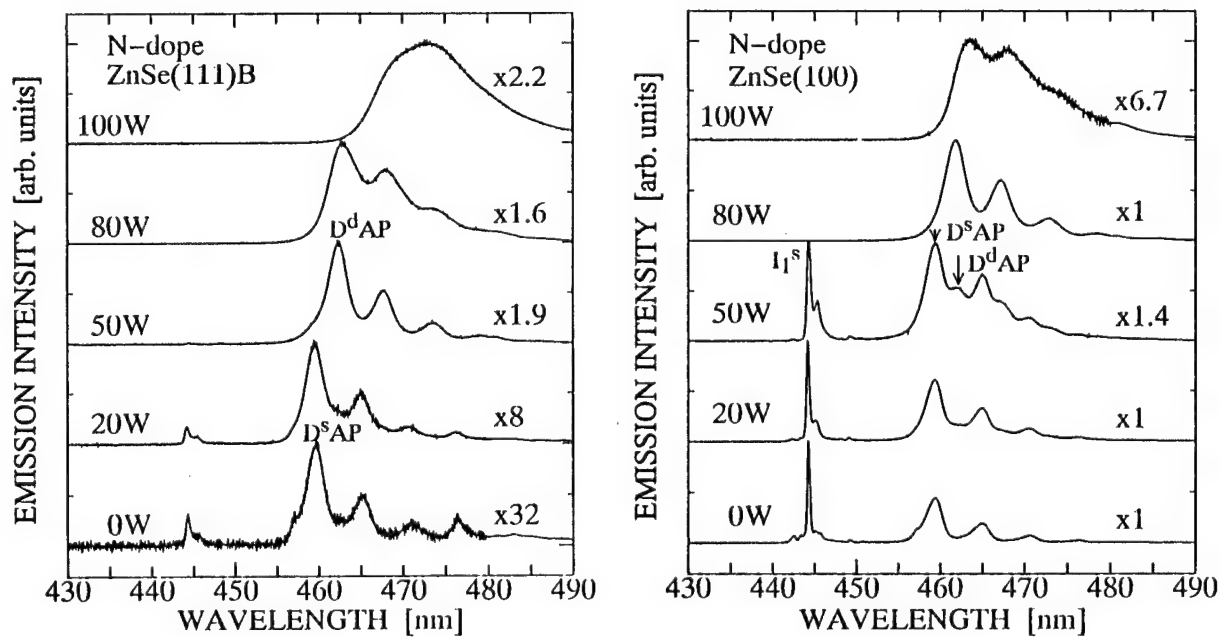


Fig. 2 PL spectra of N-doped ZnSe(111) and (100) epilayers grown on GaAs(111)B and (100) substrates, respectively.

## Interface structure of CdTe/Si

S.Sivananthan, N.D.Browning, C.H. Grein, S. Rujirawat, T.Almeida, J.P. Faurie, R.Sporcken, D.J.Willis, C.Y. Tsen, and David J. Smith

Microphysics Laboratory, Department of Physics, University of Illinois, Chicago, IL 60607-7059, USA

Department of Physics and Astronomy and Center for Solid State Science, Arizona State University, Tempe, AZ 85287-1504, USA

The epitaxial growth of dissimilar materials is motivated by both scientific and technological interests, perhaps the most obvious of which is the lack of suitable substrates to carry out homoepitaxy. This is currently the case for high  $T_c$  materials, widegap semiconductors etc. Another approach to homoepitaxy is to use alternative substrates or compliant substrates. In this regard we have studied the MBE growth of CdTe on Si. There is great interest in the heteroepitaxial growth of CdTe, in particular because CdTe could be used for soft x-ray detectors and also as a substrate for the growth of HgCdTe for infrared detectors. The growth of high quality material on Si substrates will lead to the fabrication of very large, truly monolithic focal plane arrays. In this work we have carefully studied the interface formation of CdTe/Si. This study not only provides information regarding the microscopic mechanism for the formation of the CdTe/Si interface, but also can shed light on the understanding of the other compliant substrate.

The interface structure was studied by varying the MBE growth initiation parameters to modify the interfacial layer. The structural aspects of the CdTe/Si interface have been studied extensively by both high-resolution transmission electron microscopy (TEM) and scanning transmission electron microscopy (STEM). The TEM micrographs reveal that the film-substrate interface is coherent over large areas. Similar results have been obtained from STEM using the incoherent Z-contrast imaging technique. This latter technique generates an atomic-resolution image in which intensity is proportional to the local composition. For the CdTe film, this feature allows Te to be identified as the terminating plane in the film. Furthermore, the image contrast strongly suggests the presence of Te in the first few top layers of the Si substrate. This result is confirmed by atomic-resolution electron energy loss spectroscopy (EELS). Using the characteristic core-loss features in the energy loss spectrum, a compositional profile of the interface can be obtained. In this case Cd, is found to be contained only in the CdTe layer, whereas Te has diffused 2-3 atomic planes into the silicon. While it is difficult to characterize a structure only 2 atomic planes thick by composition, the relative intensities and crystal spacings do suggest that a  $\text{Si}_2\text{Te}_3$  compound is formed at the interface. This identification is at least partly confirmed by the decomposition of the interface into  $\text{SiO}_2$  over time, a feature common in  $\text{Si}_2\text{Te}_3$ . These results are consistent with the initial predeposition of Te flux prior to CdTe deposition and with observations by RHEED. The growth experiments show that the formation of the appropriate interface is critical for the growth of high quality MBE CdTe on Si. This was further confirmed by the x-ray photon spectroscopic studies. Furthermore, ab-initio total energy calculations performed on SiTe in a variety of crystal structures suggest that bond bending energies in SiTe are weaker than in bulk Si, consistent with the observed coherent interface.

Our results show that the mismatch strain is absorbed mostly by the interfacial layer, allowing the CdTe to assume its natural lattice parameter at the interface itself. This is equivalent to a compliant substrate in which the strain related to the lattice mismatch is accommodated by the substrate/interfacial compound rather than by the epitaxial layer. These results from the MBE growth, XPS, and electron microscopy will be presented to establish a theoretical model for the interfacial structure of the CdTe/Si interface.



# MOLECULAR BEAM EPITAXIAL GROWTH OF $\text{ZnSe}$ , $\text{ZnS}_x\text{Se}_{1-x}$ and $\text{Zn}_{1-y}\text{Mn}_y\text{S}_x\text{Se}_{1-x}$ LAYERS ON GaAs SUBSTRATES: STUDIES OF INTERFACE STRUCTURES AND CONTROL OF ALLOY COMPOSITIONS

Y. P. Chen<sup>a</sup>, C. C. Kim<sup>a</sup>, S.-C. Y. Tsen<sup>b</sup>, David J. Smith<sup>b</sup> and S. Sivananthan<sup>a</sup>

<sup>a</sup> University of Illinois at Chicago, Department of Physics, Microphysics Laboratory, Chicago, IL 60607-7059

<sup>b</sup> Center for Solid State Science and Department of Physics and Astronomy, Arizona State University, Tempe, AZ 85287-1704

After successfully growing zinc-blende MnS layers on GaAs substrates<sup>1</sup>, we have systematically studied growth of  $\text{ZnSe}$ ,  $\text{ZnS}_x\text{Se}_{1-x}$  and  $\text{Zn}_{1-y}\text{Mn}_y\text{S}_x\text{Se}_{1-x}$  layers on GaAs(100) substrates by molecular beam epitaxy. Our studies focus on the understanding of the ZnSe/GaAs interface and its correlation to the initial growth modes and the control of S and/or Mn composition for  $\text{ZnS}_x\text{Se}_{1-x}$  and  $\text{Zn}_{1-y}\text{Mn}_y\text{S}_x\text{Se}_{1-x}$  alloys with lattice constants matching that of the GaAs substrate. Initial growth of ZnSe and the interface formation between ZnSe and GaAs were assessed *in-situ* by Reflection High Energy Electron Diffraction (RHEED) and X-ray Photoemission Spectroscopy (XPS). The interface structures were also studied by Transmission Electron Microscopy (TEM). The results confirm that the initial growth modes play an important role in interface formation and, thus, the layer quality of ZnSe. Very smooth interfaces of ZnSe/GaAs were obtained when GaAs substrates were exposed to Zn before the Se flux in contrast to the rough interfaces of the layers obtained with exposure of GaAs substrates to Se flux first. X-ray Double-Crystal Rocking Curve measurements were used to determine the quality of the grown layers. The full width at half maximum (FWHM) of the X-ray rocking curve of the best ZnSe layer was as low as 27 arcsec. The alloy compositions of  $\text{ZnS}_x\text{Se}_{1-x}$  and  $\text{Zn}_{1-y}\text{Mn}_y\text{S}_x\text{Se}_{1-x}$  layers were determined by X-ray diffraction and spectroscopic ellipsometry, the latter of which measures the energy gap and optical properties of the grown layers. The energy gap for quaternary  $\text{Zn}_{1-y}\text{Mn}_y\text{S}_x\text{Se}_{1-x}$  layers varied from 2.7 eV to 3.2 eV paving the way for good optical confinement in a laser structure. We will also present our studies on the optimization of growth conditions for a laser structure so that each layer, having the desired band gap and optical properties, is closely lattice matched to the GaAs substrate.

<sup>1</sup> B.J. Skromme, Y. Zhang, D. J. Smith and S. Sivananthan, Appl. Phys. Lett. **67**, 2690 (1995).

Contact Author: Y. P. Chen  
Address: The University of Illinois at Chicago  
Department of Physics (M/C 273)  
845 W. Taylor, Room# 2236 SES  
Chicago, IL 60607-7059  
Telephone: 312-413-0041  
FAX: 312-996-9016  
E-mail: ychen@uic.edu



# P-type Doping of Beryllium-Chalcogenides Grown by Molecular Beam Epitaxy

H.-J.Lugauer\*, F.Fischer, T.Litz, J.Laubender, A.Weingärtner, A.Waag, T.Gerhard,  
U.Zehnder, L.Worschech, W.Ossau, and G.Landwehr

*Physikalisches Institut der Universität Würzburg, Am Hubland, D-97074 Würzburg, Germany*

C.Becker and J.Geurts

*I. Physikalisches Institut der RWTH Aachen, P.O. Box, D-52056 Aachen, Germany*

## Abstract

A sufficiently high p-type doping of Zn(SSe) and ZnMg(SSe) ternaries and quaternaries is still one major problem preventing the production of pure blue or violet laser diodes which are working at room temperature under continuous-wave operation. With increasing band gap energy, the maximum hole concentration is decreasing rapidly, the mechanism for that behavior is still under discussion.

In this contribution we present an alternative approach for the p-type doping of wide gap II-VI-semiconductors. We have grown Be-chalcogenides by molecular beam epitaxy (MBE) on GaAs substrates. BeTe and BeSe have a smaller lattice constant than GaAs, therefore Be containing compounds such as (BeMg)Te, (BeZn)Se or (BeMgZn)Se are very promising alternatives to the sulfur containing ternaries and quaternaries mentioned above.

We show results on the p-type doping of such layers grown using a modified nitrogen plasma source, which also allows to use solid group V materials (e.g. arsenic) to be cracked in the plasma discharge. The p-type dopability of BeTe:N as determined by the means of van-der-Pauw measurements and FIR-spectroscopy lies in the same order of magnitude compared to that of ZnTe, free hole concentrations  $N_A - N_D$  of more than  $1 \times 10^{19} \text{ cm}^{-3}$  have been measured. By adding for example Mg or Mn, still highly p-type layers are obtained which are fully lattice matched to GaAs. Furthermore, the small lattice mismatch of BeTe to GaAs allows to grow highly p-type BeTe/ZnSe strained superlattices with an average lattice constant matched to that of GaAs. In addition, we will also compare the dopability of (BeZn)Se and (BeMgZn)Se ternaries and quaternaries to that of their S-containing counterparts.

To demonstrate the potential of this material system, we have fabricated (BeMgZn)Se/(BeZn)Se SQW- and MQW-LED's on p-GaAs which all show a bright, deep blue emission at a low onset voltage and lifetimes of several 100 hours at current densities of more than  $50 \text{ A/cm}^2$ . One reason for the low operating voltage is that the valence band of BeTe is aligned rather well with that of GaAs, and together with the high p-type dopability of BeTe a low resistive transition from GaAs to ZnSe via a BeTe/ZnSe pseudograding is possible.

---

\*Corresponding author.

Address: Universität Würzburg, Experimentelle Physik III/MBE, Am Hubland, D-97074 Würzburg, Germany  
Tel. ++49 (0)931 888-5757, Fax. -5142, e-mail: lugauer@physik.uni-wuerzburg.de

## **Molecular Beam Epitaxy of Beryllium Telluride**

Xiao-Chuan Zhou and Wiley P. Kirk  
Texas A&M University, NanoFAB Center  
Engineering-Physics Building, College Station, TX 77845-4242

Beryllium telluride (BeTe) was epitaxially grown, for the first time, on GaAs substrate by using MBE method. This work is the beginning of a study in a group of barely explored Be-VI wide-bandgap semiconductors, including BeS, BeSe, and BeTe, which have lattice constants ranging from 4.86 Å to 5.63 Å and bandgaps ranging from 6.1 eV to 2.7 eV. In contrast with other II-VI compound semiconductors, such as ZnS and ZnSe, Be-VI materials are of highly covalent (or low ionic) chemical bonds in nature. Consequently, they are highly stable in zincblende structure.

Using an empirical method, we found all three Be-VI materials to be of high stacking fault energies in the range of 49 meV/atom to 64 meV/atom. As comparison, ZnS, ZnSe and GaAs have stacking fault energies of 5 meV/atom, 11 meV/atom, and 47 meV/atom, respectively. Therefore by using Be-VI materials, we have the opportunity to growth II-VI epitaxial layers, either lattice matched to GaAs or to Si, of low stacking fault density.

In this presentation, we report our initial results on the growth of BeTe on GaAs(100) substrate. Pure Be and Te were used as the source materials. Substrate temperature and beam flux ratio were varied in wide ranges in order to find a suitable growth window. RHEED and X-ray diffraction were used for in-situ surface and ex-situ crystallinity characterizations.

Preferred form of presentation: Oral

Contact person: Xiao-Chuan Zhou  
Texas A&M University  
NanoFAB Center, Eng./Phys. Bldg.  
College Station, TX 77843-4242  
Tel: 409-845-7843  
Fax: 409-845-2590  
E-mail: zhou@nanofab.tamu.edu

## A Study of MBE Growth and Thermal Annealing of p-type Long Wavelength HgCdTe

L. He<sup>a)</sup>, J.R. Yang, S.L. Wang, S.P. Guo, M.F. Yu, X.Q. Chen, W.Z. Fang, and Y.M. Qiao

Q.Y. Zhang, R.J. Ding, and T.L. Xin

Research Center for Epitaxial Semiconductor Materials, National Laboratory for Infrared Physics

Shanghai Institute of Technical Physics, Chinese Academy of Sciences

420 Zhong Shan Bei Yi Rd., Shanghai 200083, People's Rep. of China

<sup>a)</sup>phone: (021)6542 0850, Fax: (021)6324 8028, e-mail: lihe@fudan.ihep.ac.cn

Molecular beam epitaxy (MBE) technique for HgCdTe growth has been shown to be a flexible technology for the manufacturing of infrared detectors. In this paper, we report our recent results on MBE growth and thermal annealing of Hg-vacancy doped p-type LW HgCdTe epilayers.

HgCdTe epilayers were grown on GaAs (211)B substrates in a Riber 32P MBE system. To improve the uniformity of the epilayers, the substrate holder was rotated during the growth. The growth temperature for HgCdTe was kept to be constant at  $183^{\circ}\text{C} \pm 2^{\circ}\text{C}$ , measured by an infrared pyrometer which was carefully calibrated before growth.

The surface morphology of HgCdTe epilayers are essentially featureless, despite of a few void-like features orientated from the treatment of substrate surfaces. EPD values were in a range of  $6\text{--}8 \times 10^6 \text{ cm}^{-2}$  revealed by using a standard etchant. The epilayers showed excellent uniformity in both composition and thickness. Fig.1(a) and (b) show an example of typical uniformity of a HgCdTe epilayer in a 2 inches diameter geometry. The standard deviation (STDDEV) in x value is 0.00041, with a STDDEV in thickness of  $0.238 \mu\text{m}$ . To our knowledge, this is the best result ever been reported. Fig.2 shows the compositional reproducibility of LW samples in a run to run scheme. An average x value of 0.23 was obtained with a STDDEV of 0.01.

The as-grown samples were n-type. In order to convert the electrical conduction type to appropriate values of p-type suitable for FPAs application, we developed a new flexible thermal annealing technique which allows us to raise the annealing yield as well as control ability of electrical parameters. Tab.1 shows Hall measurement results with a *Van de Paul* geometry at 77 K for some of the annealed samples. The samples for the measurement were cut into pieces of  $15 \times 15 \text{ mm}^2$  size, with 4 small electrodes (approximately  $800 \mu\text{m}$  in diameter) to minimize the errors introduced by the geometry effects. It is found that the hole concentration can be reproduced well in the required range of  $1\text{--}2 \times 10^{16} \text{ cm}^{-3}$  for samples with an x value of 0.21-0.33. The very high hole mobility reflects the high material quality obtained.

To conform the material quality, small scale  $32 \times 32$  FPAs were fabricated by using Boron implantation into a p-type HgCdTe epilayer. An example of thermal image of a pair of pliers is shown in Fig.3. The x value of HgCdTe for this device is 0.24. The preliminary results showed that the average detectivity  $D^*_\lambda$  was approximately  $1\text{--}2 \times 10^{10} \text{ cm}^2/\text{Hz}/\text{W}$ . It is believed that the device performance can be further improved by using lattice-matched ZnCdTe substrates for HgCdTe epitaxy.

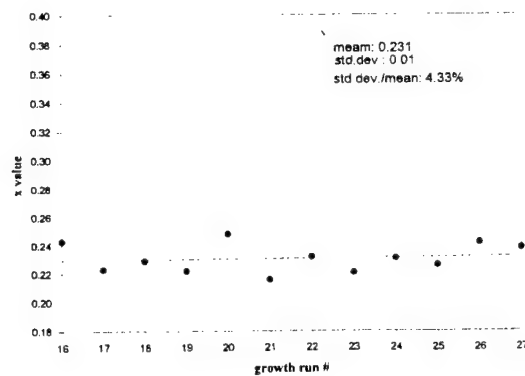
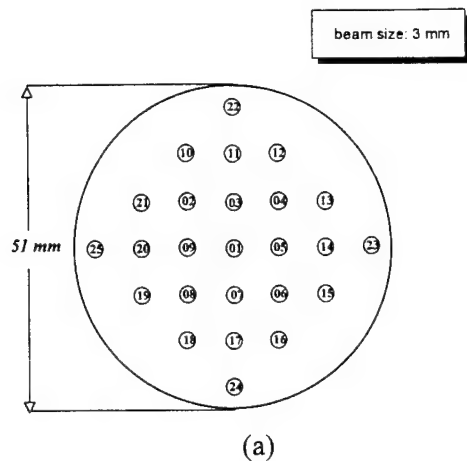


Fig.2 Reproducibility of x values in a run to run scheme.

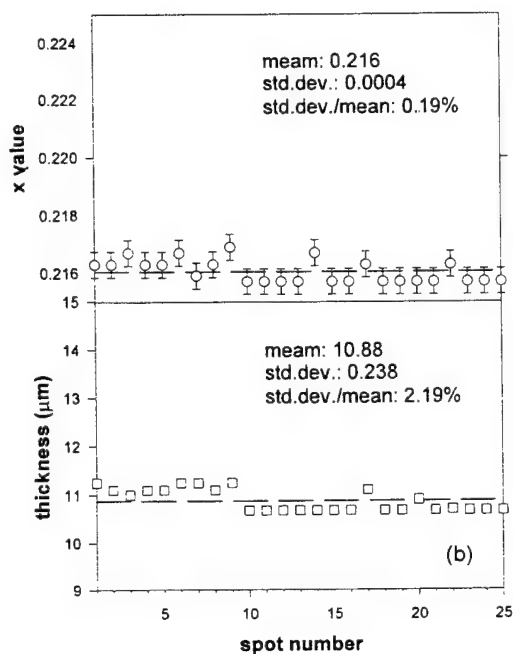


Fig.1. An example of composition and thickness uniformity of MBE-grown 2 inches HgCdTe, with (a) the sampling matrix for infrared transmission measurements using a Fourier transform spectrometer, and (b) x value and thickness distributions.

Tab.1 Electrical Properties of p-type annealed samples measured at 77 K

sample No.	concentration ( $\text{cm}^{-3}$ )	mobility ( $\text{cm}^2/\text{Vs}$ )	x value
g09	$1.67 \times 10^{16}$	653.0	0.234
g10	$1.86 \times 10^{16}$	852.9	0.214
g15	$1.25 \times 10^{16}$	1160.0	0.223
g16	$1.14 \times 10^{16}$	866.0	0.222
g18	$1.01 \times 10^{16}$	795.0	0.221
g19	$1.48 \times 10^{16}$	696.8	0.231
g21	$1.13 \times 10^{16}$	687.2	0.240
g22	$1.57 \times 10^{16}$	690.1	0.238

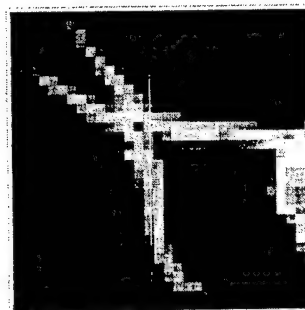


Fig.3. A 32x32 PFA thermal image of a room-temperature object .

## Blue-light emission from ZnSTe-based EL devices

J. Mao, I.K. Sou, Z. Yang, K.S. Wong, G.K.L. Wong

Department of Physics, Hong Kong University of Science & Technology  
Clear Water Bay, Hong Kong  
Tel: 852-2358-7514  
Fax: 852-2358-1652  
Email: PHIKSOU@USTHK.UST.HK

Recently, Jan Schetzina et al<sup>(1)</sup> of North Carolina State University reported the operation of a super bright green LED using structures based on ZnSeTe alloy quantum wells. The internal quantum efficiency of these LED's is measured to be even higher than that of GaN-based LED's. The high efficiency of light emission from ZnSeTe alloy is attributed to the large difference in the electronegativity of Te (2.1) and Se (2.4), which results in efficient trapped-exciton recombination at Te isoelectronic hole traps. Soon after, we reported the first successful MBE growth of  $\text{ZnS}_{1-x}\text{Te}_x$  system, a relatively unexplored II-VI alloy<sup>(2)</sup>. Very strong photoluminescence was observed in samples with  $x$  between 1 to 6%, probably as a result of the larger difference in electronegativity between Te (2.1) and S (2.5). The color of emitted light can be tuned from deep-blue to yellow by adjusting Te concentration. Room-temperature external quantum efficiency of about 4% has been achieved on epilayers as thin as 1000 Å. ZnSTe alloy enjoys the advantage that at 3% Te concentration, the alloy is perfectly lattice-matched with Si substrate. It also seems to have stronger thermal-mechanical strengths (due to alloy hardening effect) than those of ZnSe compound. Quite recently, we successfully demonstrated n-type doping of this alloy system using incorporation of Al during MBE growth<sup>(3)</sup>. Electron carrier concentration as high as  $2 \times 10^{19} \text{ cm}^{-3}$  has been achieved.

In this work, we report the characteristics of light emission from various ZnSTe-based EL (electroluminescence) structures. In our earlier studies, structures of Au/undoped-ZnSTe/ $n^+$ -GaAs or  $p^+$ -Si substrates are used. EL from these structures are weak and kinetic EL (flying bright spots) patterns are observed under microscope. Photoluminescence measurements on these EL cells as a function of increasing bias indicate that even though the luminescence spectrum is unshifted, a significant monotonous decrease in the intensity occurs at high biases. Field-induced quenching of bound-carriers at Te traps seems to be responsible for these observed characteristics. Following our success in n-doping ZnSTe alloy, we fabricated EL cells using various ZnSTe:Al-based structures. In contrast to the observations on earlier structures, blue EL from these structures is much stronger and uniformly distributed across the entire cell. No kinetic pattern was observed. The difference comes from the fact that field quenching effect on Te traps in n-type ZnSTe:Al layer is significantly reduced since the bias is not applied to this conducting layer. I-V measurements on these structures seem to indicate that blue EL results from localized states in the active layer that are impact-excited by hot-carriers injected from the Au/II-VI schottky barrier. Details of the I-V characteristics and the spectral analysis of EL will be discussed. The development in this work is an important step towards the realization of ZnSTe-based optoelectronic devices that can be integrated on Si substrate. Of course, p-n homojunction LED should be more efficient. Studies on p-type doping in ZnSTe alloy are underway in our lab.

### References

- (1) Yu, Z., Hughes, W.C., Roland, W.H., Boney, C., Cook, J.W., Jr., Schetzina, J.F., Cantwell, G., Harsch, W.C., Appl. Phys. Lett. 66, 115 (1995).
- (2) Sou, I.K., Wong, K.S., Wong, Z.Y., Yang, H., Wong, G.K.L., Appl. Phys. Lett. 66, 1919 (1995).
- (3) Sou, I.K., Yang, Z., Mao, J., Ma, Z.H., Tong, K.W., Wong, G.K.L., ICPS XXIII, 1996, abstract (submitted).

## NITROGEN DOPING OF Te BASED 2-6COMPOUNDS

S. Tatarenko\*, T. Baron\*, A. Arnoult\*, J. Cibert\*, M. Grun, A. Haury, A. Wasiela, and K. Saminadayar\*\*

*\*Laboratoire de Spectrométrie Physique, CNRS et Université Joseph Fourier - Grenoble, BP 87, 38402 St Martin d'Hères Cedex, France.*

*\*\*DRFMC/SP2M/PSC, CEA Grenoble, 38054 Grenoble Cedex9, France*

The p type doping with nitrogen of CdTe, ZnTe, CdZnTe, ZnMgTe, CdMgTe and the quaternary alloy CdZnMgTe as well as the doping of the related heterostructures have been investigated in details. Experimentally, two types of nitrogen plasma sources have been used : DC glow and electron cyclotron resonance(ECR).

Concerning ZnTe(001) the most relevant points can be summarized as follows: doping levels as high as  $10^{20} \text{ cm}^{-3}$  are achieved; the acceptor ionization energy is deduced from Hall measurements and photoluminescence spectra to be  $53.4 \pm 1 \text{ meV}$ ; the length of the Zn-N bond is estimated, from X-Ray diffraction measurements performed on modulation doped layers, to be  $2.16 \pm 0.05 \text{ \AA}$ .

Concerning CdTe(001) doping levels of  $8 \cdot 10^{17} \text{ cm}^{-3}$  have been obtained by using the ECR plasma source and a low growth temperature. An acceptor ionization energy of  $57 \pm 2 \text{ meV}$  is found for nitrogen in CdTe. A strong diffusion of the nitrogen in the modulation heavily doped layers is confirmed.

In the case of the CdZnTe and ZnMgTe alloys a systematic decrease of the doping efficiency is observed as far as the Zn content decreases. However the effects associated to the increase of Cd or Mg concentrations are not the same. As a matter of fact, it is deduced from SIMS measurements or nuclear reaction analysis that the introduction of Cd decreases the nitrogen concentration while the introduction of Mg increases significantly the amount of nitrogen incorporated in the layer demonstrating the great affinity between Mg and N. In the same way an increase of the nitrogen content with Mg concentration is observed in CdMgTe alloys. In addition the doping of CdZnMgTe (22%Mg and 7%Zn) has been studied. By using low growth temperature ( $240^\circ\text{C}$ ) doping levels as high as  $5 \cdot 10^{17} \text{ cm}^{-3}$  have been achieved giving rise to layers showing excellent optical properties. The doping level decreases dramatically when increasing the growth temperature.

Following the studies on the doping of the thick layers, the nitrogen doping of heterostructures has been realized. In the present communication the electrical and structural properties of CdTe/CdZnMgTe multiquantumwells doped in the barriers will be discussed with more emphasis. X-Ray diffraction analyses conclude to the absence of a significant interdiffusion between the wells and the barriers when the structure is grown at low temperature( $240^\circ\text{C}$ ) while an interdiffusion correlated to the simultaneous presence of Mg and N is observed at higher temperature ( $300^\circ\text{C}$ ). Furthermore, for layers grown at  $240^\circ\text{C}$ , Capacitance Voltage profiles confirms the localisation of the nitrogen atoms in the barriers and the transfer of holes across the spacing layer into the quantum wells due to the significant valence band offset in the CdTe/MgTe system. This structures have allowed the optical study of the 2D holes gas and of charged excitons ( $X^+$ ).

As a conclusion of the previous studies, a model combining the local strain induced in the lattice by the presence of nitrogen, the strength of the bonds between Te and metal and the possible formation of  $\text{A}_3\text{N}_2$  nitrides is proposed to explain the differences observed in the doping efficiency for the different tellurides.

**contact :** S.Tatarenko, DRFMC/SP2M/PSC, CEA Grenoble, 38054 Grenoble Cedex 9, France  
tel : 33 76 88 34 95, fax : 33 76 88 50 97, e-mail : [statarenko@cea.fr](mailto:statarenko@cea.fr)

## Room temperature continuous wave operation of ZnSe based blue-green laser diode grown by molecular beam epitaxy

Moon-Deock Kim, Hae-Sung Park, Bong-Jin Kim, Jeong-Keun Ji, Eun-Soon Oh, Sang-Dong Lee, Tae-Il Kim

*Photonics Semiconductor Lab., Materials & Devices Research Center, Samsung Advanced Institute of Technology, P.O. Box 111, Suwon, Korea 440-600*  
TEL +82-2-331-280-9131, FAX +82-331-280-9357, E-mail mdkim@saitgw.sait.samsung.co.kr

Much effort has been devoted in recent years to studies on wide-gap II-VI semiconductor heterostructures to realize blue-green laser diodes(LDs). Several groups have by now demonstrated room temperature continuous wave(CW) operation of devices with emission at or near 520 nm using essentially identical structures.[1-3] This structure consists of a both ZnMgSSe and ZnSSe lattice-matched to GaAs, cladding and guiding layers respectively, with a compressively strained ZnCdSe QW, ZnSSe graded, and ZnSe/ZnTe superlattice p-type contact. In this letter, we describe CW operation of a blue-green LD at room temperature.

The LD structure shown in Fig.1 was grown on a (100) silicon doped GaAs substrate using molecular beam epitaxy(MBE) at a growth temperature of 280°C. The designed bandgap energies of the ZnCdSe and the ZnMgSSe are 2.53 and 2.96 eV at 11 K respectively. The bandgap energy difference between the active and cladding layers is thus 0.43eV at 11 K. Gain-guided lasers were fabricated. The p-ZnSe/ZnTe superlattice ohmic layer was chemically etched off with a remaining 7  $\mu\text{m}$ -wide mesa stripe region. An insulating layer was deposited on the open stripe region for reduction of the current path. Pd/Pt/Au multilayer metal was evaporated as a p-electrode on the p-type ZnTe top layer. Au/Ge metal serves as an n-electrode to the n-GaAs substrate. The wafer was cleaved into 800  $\mu\text{m}$  stripes, on whose facets high reflectivity coating was made. The reflectivities were 70 % for the front and 95 % for the rear facet. The strips were then cleaved into 800  $\mu\text{m}$  width pellets.

Figure 2 shows the light output against injection current(L-I) characteristics of the laser diode at room temperature(296 K) measured under continuous and pulsed-current conditions. The threshold current( $I_{th}$ ) under continuous current is 50 mA corresponding to a threshold current density  $J_{th}$  of 890 A/cm<sup>2</sup>. The voltage at lasing threshold is 9 V. The emission spectra taken at room temperature are shown in Fig. 3. The Stimulated emission is observed at wavelengths of 524 nm under pulsed operation and 526 nm under pulsed and continuous operation, respectively.

In conclusion, we achieved the CW operation of blue-green laser diodes at room temperature with the emission wavelength of 526 nm. A threshold current of 50 mA was obtained under CW operation from the ZnCdSe/ZnSSe/ZnMgSSe SQW-SCH structure.

### References

- [1] C. T. Walker, J. M. DePuydt, M. A. Haase, J. Qiu and H. Cheng, Physica B **185**, 27(1993).
- [2] N. Nakayama, S. Itoh, T. Ohata, K. Nakano, H. Okuyama, M. Ozawa, A. Ishibashi,

M. Ikeda, and Y. Mori, Electron. Lett. 29,1488(1993).

- [3] A. Salokatve, H. Jeon, J. Ding, M. Hovinen, A. V. Nurmikko, D. C. Grillo, L. He, J. Han, Y. Fan, M. Ringle, R. L. Gunshor, G. C. Hua and N. Otsuka, Electron Lett. 29,2192(1993).

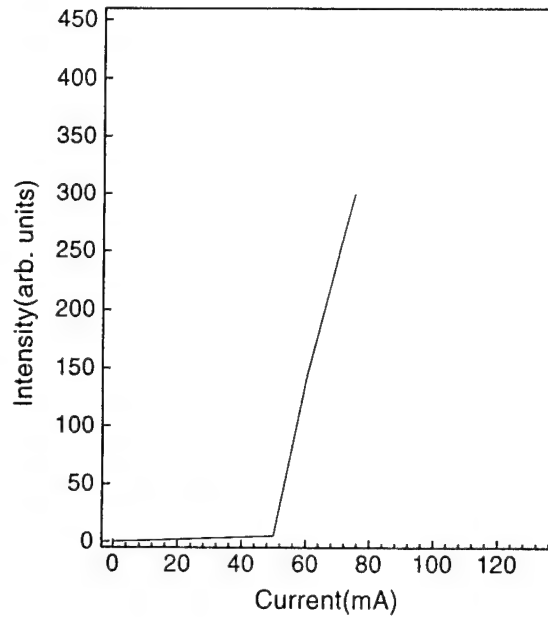
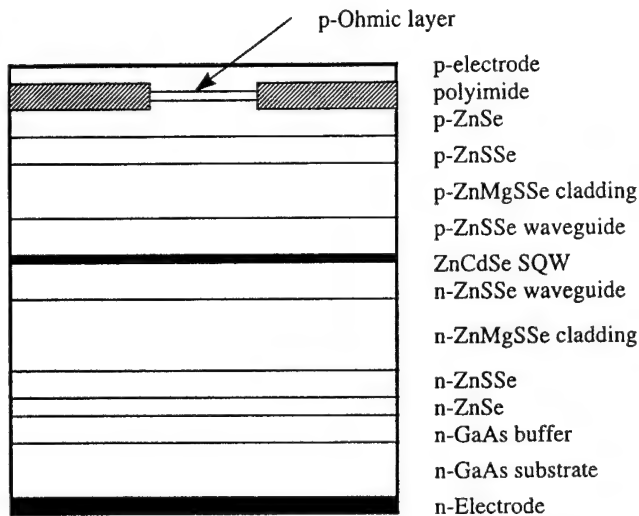


Fig. 1. Schematic structure of ZnCdSe/ZnSSe/ZnMgSSe SQW-SCH laser diode.

Fig. 2. L-I characteristics under continuous current operation of ZnCdSe/ZnSSe/ZnMgSSe laser diode at room temperature.

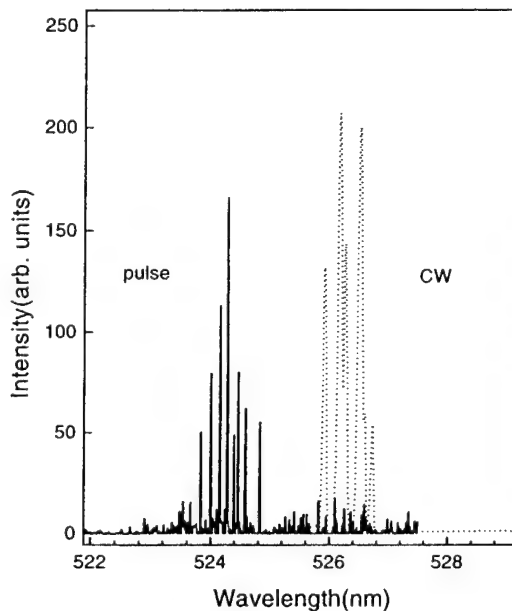


Fig. 3. Emission spectra of ZnCdSe/ZnSSe/ZnMgSSe SQW-SCH laser diode operating under pulsed and continuous wave.



## Large-mismatch Heteroepitaxy of InSb on Si Substrates using Fluoride Buffer Layers

W. K. Liu<sup>1\*</sup>, X. M. Fang<sup>2</sup>, J. Winesett<sup>1</sup>, Weiluan Ma<sup>1</sup>, Xuemei Zhang<sup>1</sup>, M.B. Santos<sup>1</sup> and P. J. McCann<sup>2</sup>

1. Department of Physics and Astronomy and Laboratory for Electronic Properties of Materials

2. School of Electrical Engineering and Laboratory for Electronic Properties of Materials

University of Oklahoma, Norman, OK 73019

Mature IC technology and the availability of low-cost, rugged and large-area wafers have made Si the most attractive substrate material for semiconductor thin film growth. With the advance in MBE technology, heteroepitaxy on Si with lattice mismatch as large as 20% has been achieved. InSb has the smallest bandgap, highest intrinsic electron mobility and lowest electron effective mass of all binary III-V compounds. Monolithic integration of InSb devices on Si substrates thus offers potential in high-speed microelectronics as well as in IR detector array fabrication. Compared to GaAs/Si (~14% mismatch) and CdTe/Si (~19% mismatch) heteroepitaxy, very little has been reported on the growth of InSb on Si. Group IIa fluoride layers have been widely used as buffers for the growth of PbSe and CdTe (lattice-matched to InSb) on Si. The ~19% lattice mismatch between InSb and Si can be reduced through graded layers of CaF<sub>2</sub> and BaF<sub>2</sub>.

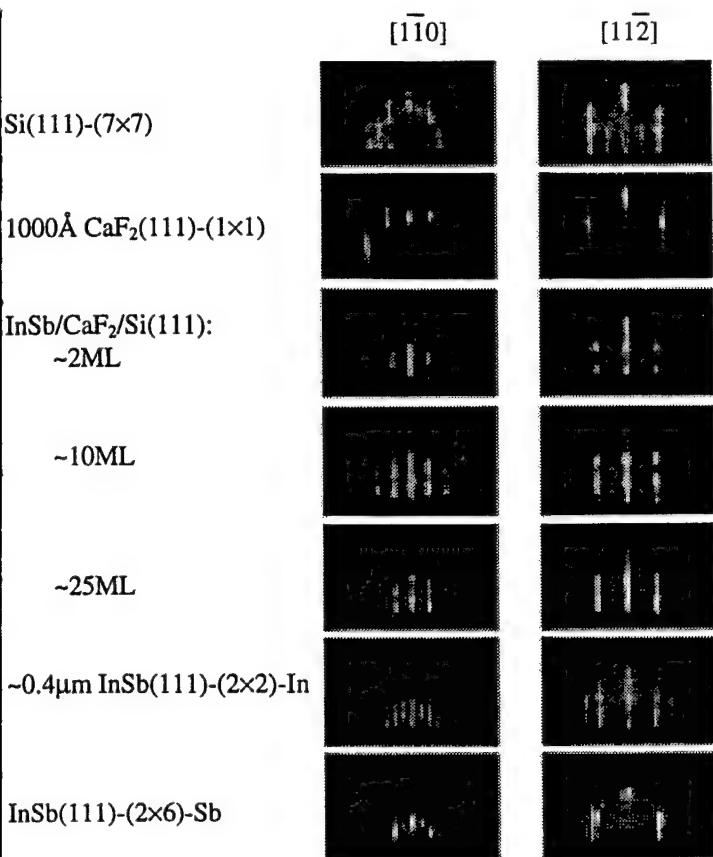
We report the results of initial attempts to grow large lattice-mismatched InSb/Si structures using group IIa fluoride buffer layers. Substrate temperatures in the range of 300-400°C were used and MBE growth was initiated by opening the In and Sb shutters simultaneously, producing In-terminated InSb(111)-A surfaces on Si(111) substrates. High structural quality was confirmed by reflection high-energy electron diffraction and electron channeling. Electron mobility of ~55,000 cm<sup>2</sup>/Vs and a density of ~2×10<sup>16</sup> cm<sup>-3</sup> were measured at room temperature for an 8μm-thick InSb layer grown on CaF<sub>2</sub>/Si(111). On CaF<sub>2</sub>/Si(001) substrates, InSb grew in the (111)-A orientation with two domains 90° apart and exhibited inferior electrical and structural properties compared to structures grown on (111) substrates. In-situ XPS and SEM data will also be included.

This work is supported by NSF grant no. ECS-9410015.

\* phone: (405) 325-3961

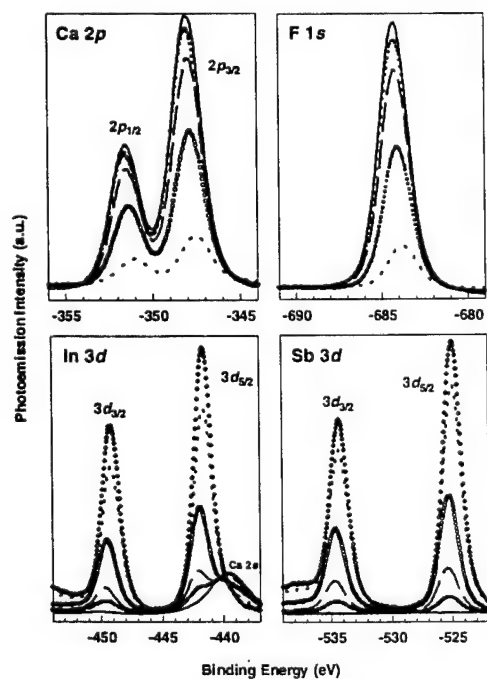
fax: (405) 325-7557

email: wliu@phyast.nhn.uoknor.edu

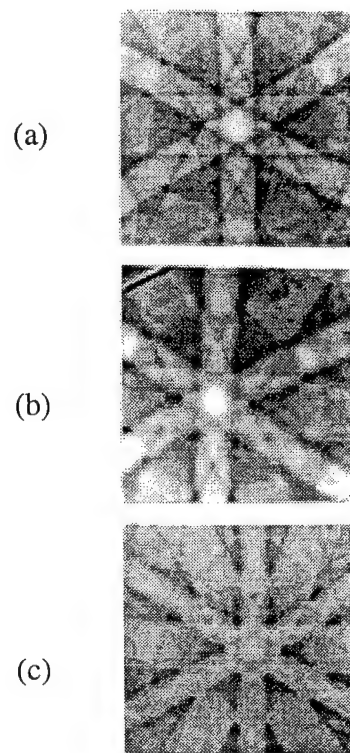


Evolution of RHEED patterns during the growth of InSb/CaF<sub>2</sub>/Si(111)

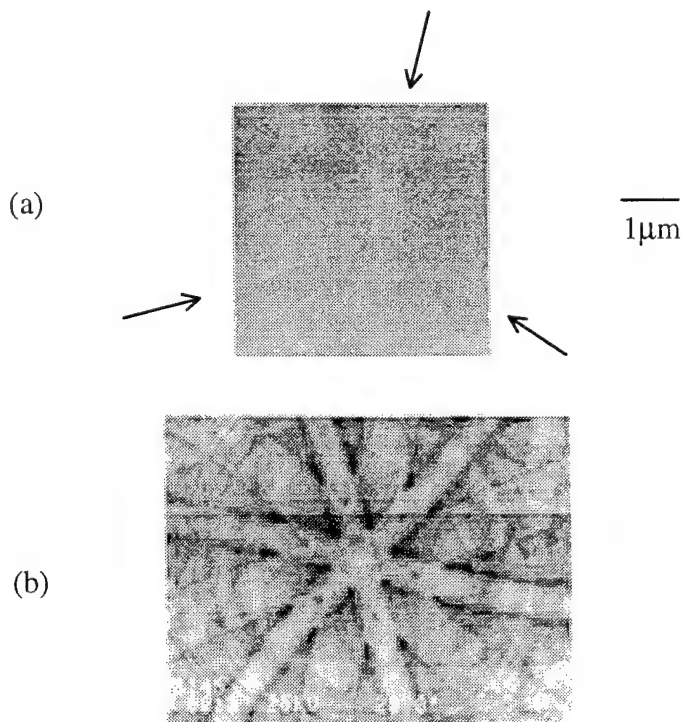
— 1000Å CaF<sub>2</sub>, ○ ~1ML, --- ~2ML, □ ~7ML, ··· ~25ML, ◇ ~100ML InSb



XPS spectra taken at various stages during the growth of InSb/CaF<sub>2</sub>/Si(111)



ECP showing the replication of 6-fold symmetry in (a) Si(111) substrate, (b) ~1000Å CaF<sub>2</sub>/Si(111) and (c) 8μm thick InSb/CaF<sub>2</sub>/Si(111)



(a) SEM micrograph of a 13μm InSb/BaF<sub>2</sub>/CaF<sub>2</sub>/Si(111) film revealing shallow triangular steps believed to be related to {100}<110>-type glide steps and (b) Corresponding ECP pattern showing the presence of (111)-related 6-fold symmetry.

## Fabrication of Flexible Single Crystal Semiconductor Heterostructures

M.H. Na, J. Haetty, H.C. Chang, H. Luo, and A. Petrou

Department of Physics, State University of New York at Buffalo, Buffalo, NY 14260

Flexible materials, amorphous materials (e.g., amorphous Si) using flexible substrates and flexible polymeric materials have been studied because of the vast possibilities they present for solar cell and optoelectronic applications. However, to our knowledge, there has been no successful attempt in producing single crystal heterostructures on flexible substrates. The difficulty lies in the lack of flexible substrates with crystal structures compatible with epitaxial growth of conventional semiconductors (i.e., Si, Ge, III-Vs and II-VIs). In this study, flexible single crystal semiconductors--which combine the flexibility and the high quality of single crystal structures--have been produced by reversing the conventional procedure. Rather than growing epitaxial semiconductors on flexible substrates, the flexible substrates are formed on the surface of samples, grown by molecular beam epitaxy (MBE), an approach which greatly reduces the level of difficulty. Once the original growth substrate (e.g., GaAs) is removed by mechanical polishing and chemical etching, the MBE-grown single crystal structure will be left on the flexible substrate.

The flexibility of a film depends strongly on its thickness. A sketch of the cross section of a tube of radius  $R$ , formed by bending a film of thickness  $d$ , is shown in Fig. 1. The strain  $\Delta a/a$  at the inside and the outside surface are given approximately by  $-d/2R$  and  $d/2R$ , respectively. For a  $1\text{ }\mu\text{m}$  thick layer (typical for MBE-grown samples), a tube with a radius of  $1\text{ mm}$  corresponds only to a maximum strain of  $0.01\%$ , which is far less than the lattice mismatch in many semiconductor heterostructures and can be tolerated by many material systems.

Two types of samples have been successfully fabricated using flexible In (conducting) and silicone (transparent) films as the substrates. All samples were prepared from ZnSe- and ZnTe-based heterostructures; the study is being currently extended to GaAs/AlGaAs heterostructures. Highly selective etching solutions enabled us to fabricate large area samples ( $1\text{ cm} \times 1\text{ cm}$ ), which is only limited by the samples grown so far for this purpose.

Photoluminescence (PL) and transmission measurements were used to examine the quality of the flexible samples. The PL peak from the ground state transition of the quantum wells (ZnSe/ZnCdSe), taken at  $T = 10\text{ K}$ , is shown in Fig. 2. The PL peak from a sample with an In film as the substrate is compared with that from the sample on the original GaAs substrate. Without involving quantitative studies of the spectra, it should be pointed out that not only is there no obvious degradation of the PL signal in the flexible sample, but a clear narrowing of the PL peak can also be seen instead. The PL peak narrowing in the flexible sample indicates that the effect of strain from the original GaAs substrate is eliminated with the removal of the substrate, which improves the overall quality of the optical signal. This is the most important criterion for the feasibility of the approach at this stage.

It should be pointed out that the advantage of this method is that the entire procedure does not introduce any difficulty beyond current technologies for commercial applications.

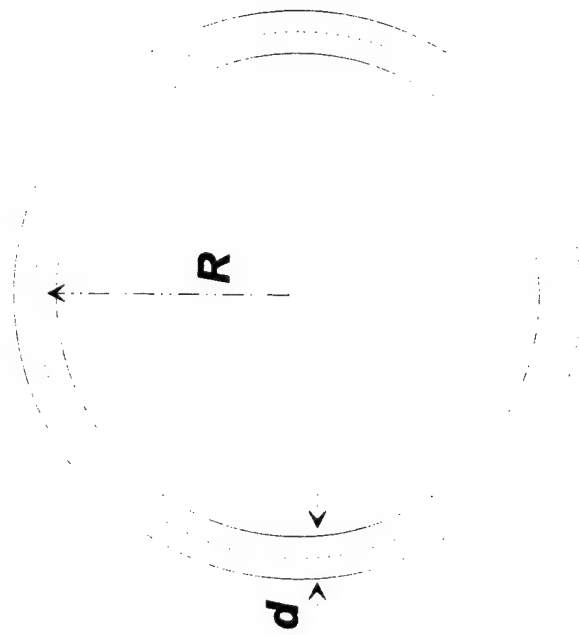


**Figure 2.** Schematic diagram of the cross section of a tube of radius  $R$  made of epilayer of thickness  $d$ .

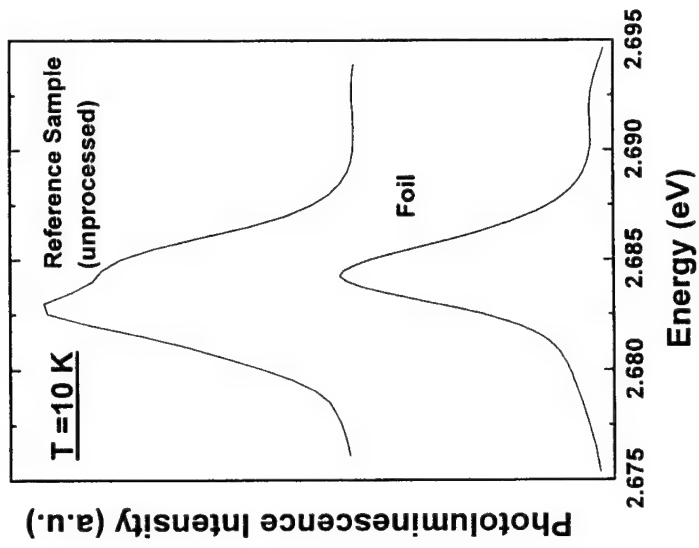


**Figure 1.** PL peak corresponding to the ground state transition in the ZnSe/ZnCdSe quantum wells, both from the flexible sample and the unprocessed reference sample.

## MBE Growth of PbSe/CaF<sub>2</sub>/Si(111) Heterostructures

P.J. McCann<sup>1\*</sup>, X.M. Fang<sup>1</sup>, W.K. Liu<sup>2</sup>, B.N. Strecker<sup>1</sup> and M.B. Santos<sup>2</sup>

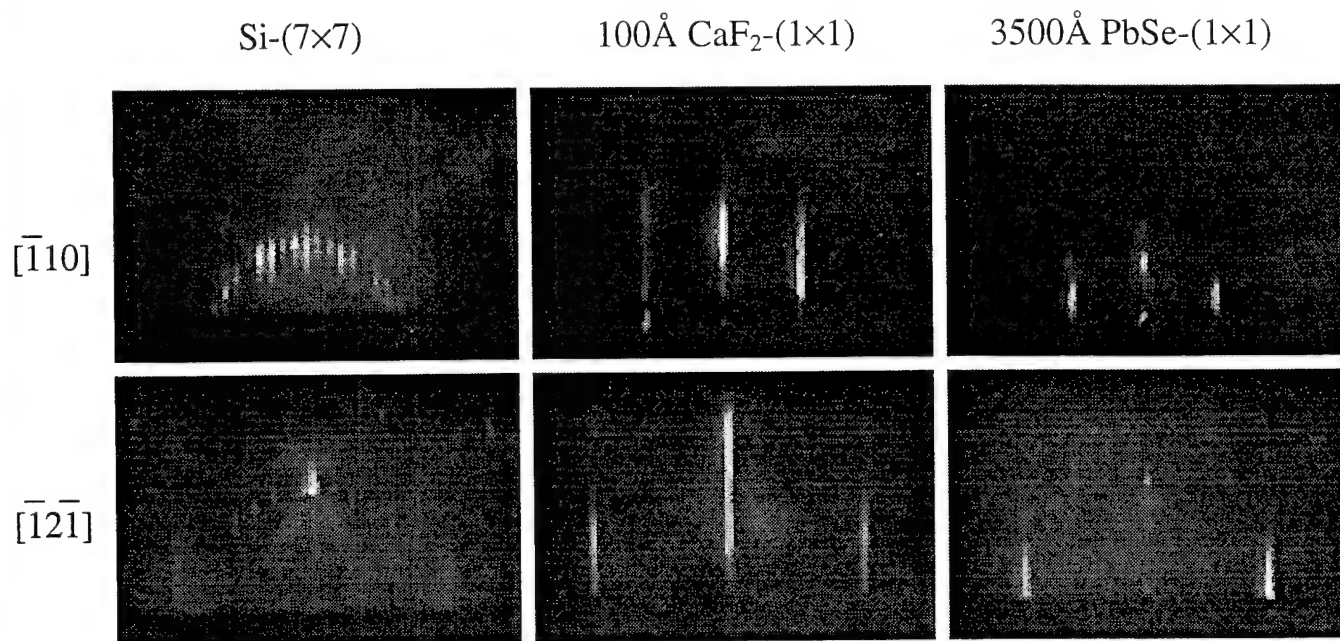
1. School of Electrical Engineering and Laboratory for Electronic Properties of Materials, University of Oklahoma, Norman, OK 73019
2. Department of Physics and Astronomy and Laboratory for Electronic Properties of Materials, University of Oklahoma, Norman, OK 73019

Epitaxial growth of high quality PbSe/CaF<sub>2</sub>/Si(111) heterostructures is an important new materials technology for fabricating infrared detector arrays and tunable diode lasers. Epitaxial growth of CaF<sub>2</sub> on Si commonly employs a high-temperature (>850°C) oxide desorption step. This high Si preparation temperature precludes good CaF<sub>2</sub> epitaxy in a chamber that is also used for PbSe growth since residual Se vapor from previous PbSe growth can cause Si surface contamination. To avoid this problem, CaF<sub>2</sub> and PbSe growths are usually carried out in separate vacuum chambers.

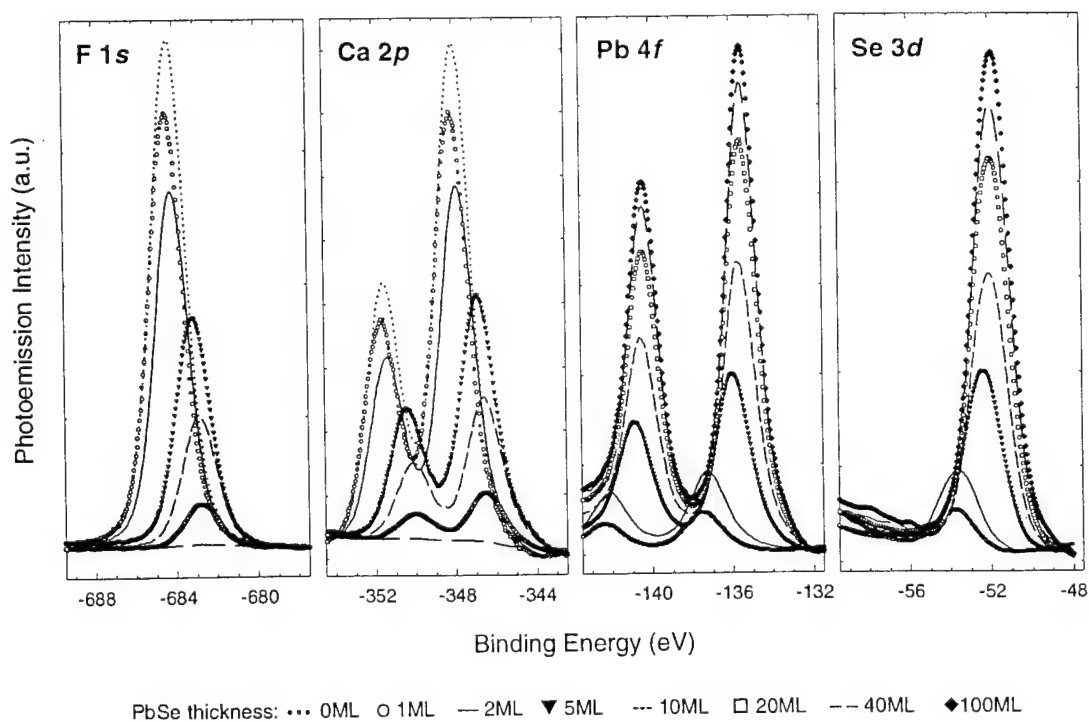
We present results for successful epitaxial growth of PbSe/CaF<sub>2</sub>/Si(111) heterostructures using just one growth chamber of a molecular beam epitaxy system. Following the Shiraki procedure, three-inch diameter Si(111) wafers were passivated with hydrogen by dipping in an HF:H<sub>2</sub>O (1:10 in volume) solution. We show that high quality single crystalline CaF<sub>2</sub> can be grown on Si(111) after the passivating hydrogen layer is removed at ~520°C. This reduction in the Si preparation temperature appears to be sufficient to eliminate problems associated with a Se background. Further epitaxial growth of PbSe can thus be carried out on the CaF<sub>2</sub>/Si(111) in the same growth chamber. High structural quality of PbSe was confirmed by sharp (1×1) streaks in the RHEED pattern and smooth surfaces revealed by SEM and Nomarski microscopy. The PbSe epilayers show mobilities of  $1-2 \times 10^4 \text{ cm}^2 \text{ V}^{-1} \text{ s}^{-1}$  and carrier concentrations of  $3-4 \times 10^{17} \text{ cm}^{-3}$  at 77K. The PbSe/CaF<sub>2</sub> interface has also been characterized by using x-ray photoelectron spectroscopy. Ca 2p, F 1s, Pb 4f and Se 3d peaks all show marked chemical shifts as a function of PbSe surface coverage, suggesting that the interface consists of both Pb - F and Ca - Se bonds.

This work is supported by NSF EPSCoR under Cooperative Agreements OSR-9108771 and OSR-9550478.

\*phone: 405-325-4288 fax: 405-325-7066 email: mccann@mailhost.ecn.uoknor.edu



RHEED patterns observed during the growth of PbSe/CaF<sub>2</sub>/Si(111)



XPS spectra taken at various stages during the growth of PbSe on CaF<sub>2</sub>/Si(111)

M.E. Taylor  
California Institute of Technology 128-95  
Pasadena, CA 91125

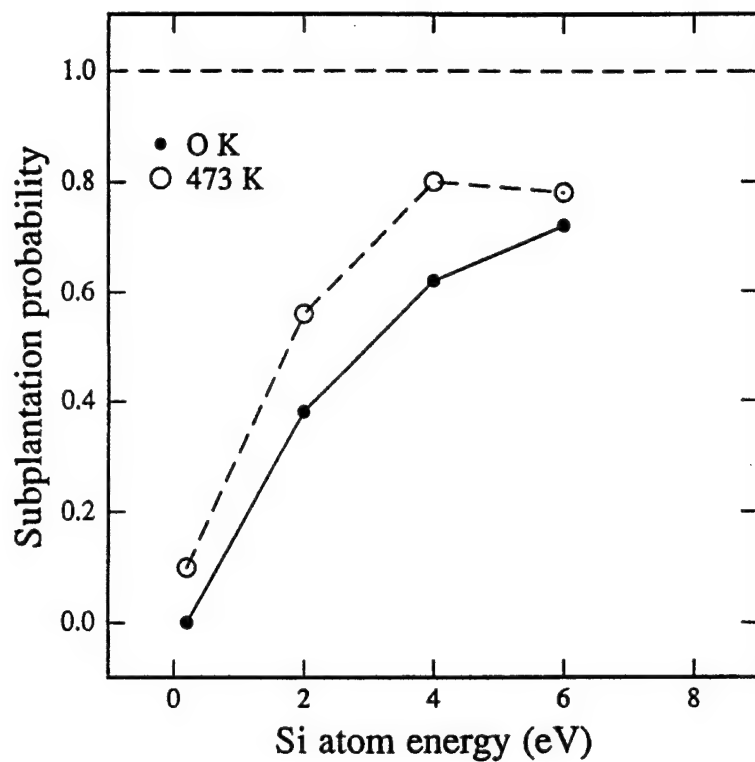
Phone: (818) 395-3826  
FAX: (818) 795-7258  
Email: [maggie@daedalus.caltech.edu](mailto:maggie@daedalus.caltech.edu)

### **Low Temperature Epitaxy of Si on Hydrogen-Terminated Si (001) Using Thermal and Energetic Beams**

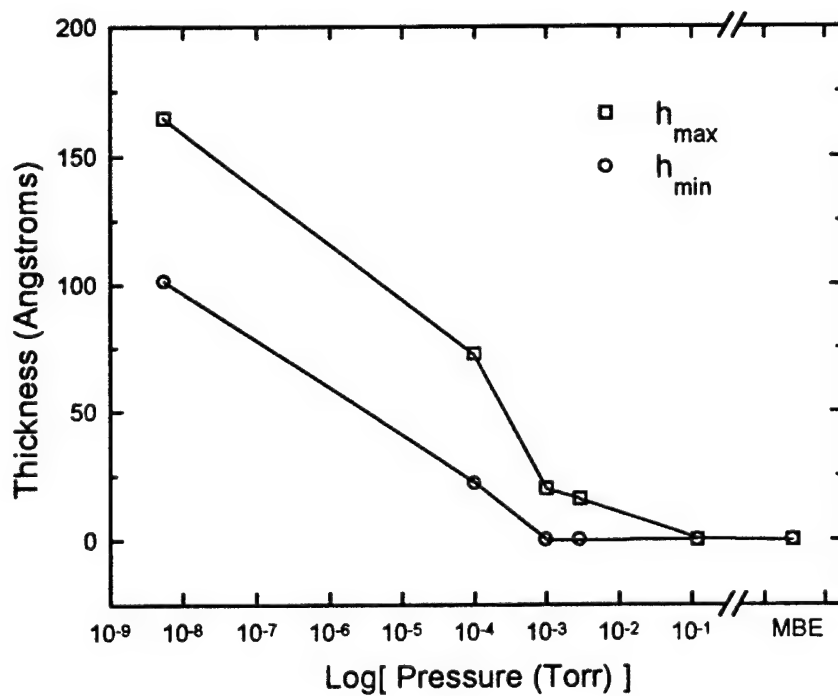
M.E. Taylor, D.L. Capewell, M.V. Ramana Murty, D.G. Goodwin, and H.A. Atwater, California Institute of Technology, Pasadena, CA 91125

Low temperature ( $T < 370^\circ\text{C}$ ) molecular beam epitaxy on Si (001) leads to a crystal-to-amorphous transition at a finite epitaxial thickness  $h_{\text{epi}}$ . To date, the intrinsic mechanisms for this have not been fully elucidated; however it is clear that adsorbed hydrogen, even at very low coverages, can profoundly affect the crystal-to-amorphous transition. We demonstrate here both (i) that Si epitaxy is possible as low as  $T = 200^\circ\text{C}$  on the hydrogen-saturated (1x1) Si(001) dihydride surface by a "subplantation" mechanism using an incident Si energy of 12 eV and (ii) this enables the crystal-to-amorphous transition to be investigated.

Growth of Si on dihydride-terminated (1x1) Si(001) by conventional molecular beam epitaxy results in an immediate crystal-to-amorphous transition ( $h_{\text{epi}} = 0$ ). Nonetheless, molecular dynamics simulations predict that epitaxial Si can be grown on dihydride-terminated (1x1) Si(001) through a "subplantation" process when energetic ( $> 4$  eV) Si atoms are incorporated in the first subsurface layer, causing segregation of the dihydride-terminated surface Si atoms. Previous work indicates that laser ablation of Si into vacuum at an energy density of  $3.0 \text{ J/cm}^2$  produces a Si energy distribution that peaks at approximately 12 eV and has a low energy tail. If an Ar background gas is introduced, the Si energy distribution becomes bimodal, with a high energy peak at approximately 12 eV, and a second peak at a lower energy. As the gas pressure is increased, the low energy peak decreases in energy and increases in size relative to the high energy peak. At very high gas pressures, the energy distribution becomes essentially identical to that for conventional molecular beam epitaxy. Epitaxial Si films were grown on dihydride-terminated (1x1) Si(001) at  $200^\circ\text{C}$  by ultrahigh vacuum pulsed laser deposition at an energy density of  $3.0 \text{ J/cm}^2$  and reflection high energy electron diffraction was used to identify the crystal-to-amorphous transition. Backfilling the chamber with ultrapure Ar at pressures ranging between  $1 \times 10^{-4}$  Torr and  $1.2 \times 10^{-1}$  Torr enabled the Si atom mean energy to be varied from 12 eV to thermal energies. Cross-sectional transmission electron microscopy was used to measure epitaxial thickness as a function of pressure, and indicated that pressures of  $1 \times 10^{-3}$  Torr or higher lead to a dramatic reduction in  $h_{\text{epi}}$ , suggesting that a reduction in the mean Si atom energy to below about 4 eV leads to a decreased subplantation efficiency. Ion probe measurements and Direct Simulation Monte Carlo simulations for Si atom energy distributions will be reported as well. Finally, the variation of  $h_{\text{epi}}$  with substrate temperature for pulsed laser deposition in vacuum is similar in microstructural evolution (i.e., development of (111) facets and large-amplitude surface roughness) to that seen for molecular beam epitaxy, but pulsed laser deposition yields a larger  $h_{\text{epi}}$  at a given temperature than for molecular beam epitaxy. This suggests that growth by pulsed laser deposition does not fundamentally alter the overall kinetics of low temperature Si (001) epitaxy, but does enable effects of hydrogen adsorbates to be distinguished from surface roughening in the crystal-to-amorphous transition, and further indicates that the crystal-to-amorphous transition is directly related to development of (111) facets during low temperature epitaxy.



Subplantation probability as a function of energy for Si atoms incident on a Si(001) surface as predicted by molecular dynamics simulations.



Minimum and maximum epitaxial thicknesses obtained from Si films grown by pulsed laser deposition at  $3.0 \text{ J/cm}^2$  on dihydride-terminated Si(001) at  $200^\circ\text{C}$ .



## **Faceting of Sidewalls in Selectively grown epitaxial layers on SiO<sub>2</sub>-masked Si Substrates**

**Qi Xiang<sup>\*</sup>, Shaozhong Li, Dawen Wang, and Kang L. Wang**

Device research Laboratory, Department of Electrical Engineering,  
University of California, Los Angeles, Los Angeles, California 90095-1594

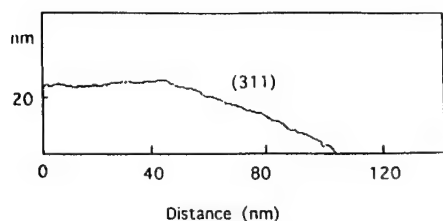
**Greg U'Ren and Mark Goorsky**

Department of Materials Science and Engineering,  
University of California, Los Angeles, Los Angeles, California 90095-1594

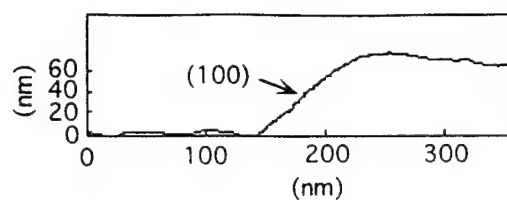
Selective epitaxial growth (SEG) of Si and SiGe is a promising technique for fabrication of Si-based nanostructures such as quantum wires and dots, and scaled down deep submicron devices in a very large scale integrated (VLSI) circuit. For SEG in small windows, facet formation and competition are important issues. The understanding of facet formation and competition will provide better control of SEG nanometer scale mesa shapes which are crucial for many practical applications. In this paper, facet formation and competition in SEG of Si on SiO<sub>2</sub>-masked Si substrates in gas source molecular beam epitaxy (GSMBE) were studied experimentally and theoretically. Experimentally, SEG in windows with different alignments on differently orientated substrates were performed in GSMBE using disilane. Substrate orientations studied include (100), (110) and (111). Window alignments studied include pattern sides along <110> on (100), along <110> and <100> on (110) and along <110> on (111). Sidewall faceting including facet formation, competition and evolution during SEG growth were investigated. For SEG mesas in windows aligned along [110] on (100) substrates, sidewall faceting from the initial (311) to (111) was observed (Fig.1). For SEG mesas in windows aligned along [110] and [100] on (110) substrates, (311) and (111) sidewall facets were observed on the baseline of [100], and (100) sidewalls on the baseline of [110] (Fig.2). As one of the important factors leading to faceting in SEG, growth rate anisotropy among different orientation surfaces of (100), (110), (111) and (311) for different growth conditions was studied. Results are shown in Fig.3. Bulk growth rate anisotropy plays an important role in faceting and the data obtained are essential for modeling. As a fundamental phenomenon related to faceting in SEG, the inter-facet mass transport during SEG growth of Si was also studied. Mass accumulation around the edge of the SEG mesa top surface due to the inter-facet migration from the sidewalls to the top surface was observed (Fig.1 and Fig.2). For different window alignments, obvious differences in mass accumulation were observed and are believed to be due to different surface energies and growth rates among different facets. The effects of mass transport on growth rate anisotropy among facets, the sidewall facet evolution, and the window size dependence of the effective growth rate of the SEG mesa height, were also investigated. Theoretically, a model based on total free energy and surface migration was developed for modeling the facet formation, competition and evolution. Both the inter-facet and intra-facet surface migration processes were taken into account in the model. The simulation results explain our experimental observations and provide an improved understanding of the facet growth on patterned substrates.

---

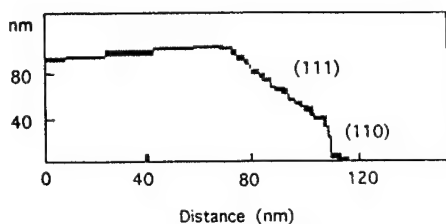
<sup>\*</sup> Contact person. Address: Device research Laboratory, Department of Electrical Engineering, University of California, Los Angeles, Los Angeles, California 90095-1594. Telephone: (310) 206-0207. Fax: (310) 206-8495. E-mail: xiang@ee.ucla.edu



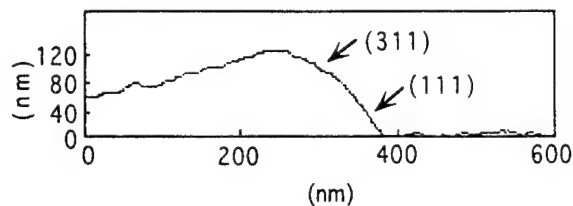
(a)



(a)



(b)



(b)

**Figure 1.** AFM line analyses for edges of a SEG mesa aligned along  $[110]$  on a  $(100)$  substrate. (a) a thin mesa showing a  $(311)$  sidewall facet formed. (b) a thick mesa showing a tilt  $(111)$  and a vertical  $(110)$  sidewall facet formed.

**Figure 2.** AFM line analyses for edges of a SEG mesa grown on a  $(110)$  substrate. (a) a mesa edge along  $[110]$  direction, showing a  $(100)$  sidewall facet formed. (b) a mesa edge along  $[100]$  direction, showing a  $(311)$  (upper part) and  $(111)$  (lower part) sidewall facets formed.

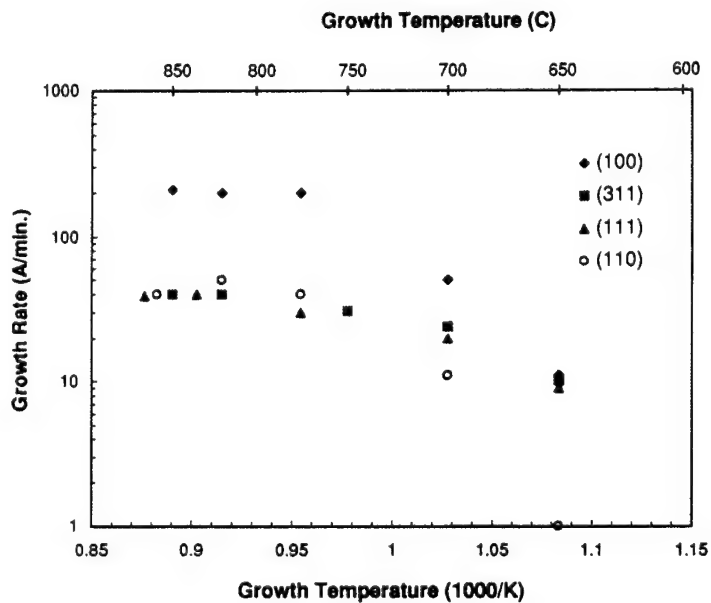


**Figure 3.** Growth rate anisotropy among substrates with different orientations of  $(100)$ ,  $(311)$ ,  $(111)$  and  $(110)$  for a disilane flow rate of 3 sccm.

## Enhancement of Substitutional Carbon Incorporation in Hydrogen-mediated Pseudomorphic Growth of Strained Alloy Layers on Si(001)

G. Lippert, H.J. Osten, P. Zaumseil, Myeongcheol Kim

Institute for Semiconductor Physics, PO Box 409, D-15204 Frankfurt (O), GERMANY,

☎ + 49 335 5625 403/ fax + 49 335 5625 300 ; e-mail: lippert@ihp-ffo.de

One of the critical challenges for further development and applications of strained C containing heterostructures is the ability to incorporate the carbon atoms solely in substitutional positions, which has a large impact on electrical and optical properties of these layers. An understanding of the factors limiting substitutional carbon incorporation is helpful in fabrication of nonequilibrium materials, such as  $\text{Si}_{1-y}\text{C}_y$  or  $\text{Si}_{1-x-y}\text{Ge}_x\text{C}_y$  layers grown heteroepitaxially on Si(001) substrates. We show that the interstitial to substitutional carbon ratio is strongly influenced by the growth conditions, such as growth temperature and Si growth rate.

The incorporation behavior can be well described by first order kinetics. Both reduction in growth temperature and increase of the overall growth rate leads to an increase of the substitutional to interstitial carbon ratio. However, these can also cause some deterioration in crystal quality. Angle-resolved x-ray photoelectron spectroscopy investigations were performed on these layers *in-vacuo*. It yields growth temperature dependent segregation effects for carbon atoms, existing in Si-C interstitial complexes and/or silicon carbide nanoparticles.

Strategies to change the surface kinetics seem to be necessary to shift the window for a high substitutional to interstitial carbon ratio to process conditions suitable for good epitaxial quality. It is known that the presence of a so-called surfactant atoms on the surface during growth can drastically alter the growth kinetics.

We report about application of hydrogen as a surfactant during growth of  $\text{Si}_{1-y}\text{C}_y$  and  $\text{Si}_{1-x-y}\text{Ge}_x\text{C}_y$ . Atomic hydrogen was supplied during MBE growth using an rf source. The epitaxial layers were grown at a hydrogen pressure above  $10^{-5}$  mbar. Epitaxial layers could be achieved under such conditions.

We found a significant enhancement of the amount of substitutionally incorporated carbon atoms in hydrogen-mediated growth compared to commonly used MBE growth. The influence of growth temperature on the carbon incorporation is reduced using hydrogen.

Finally, the influence of atomic and molecular hydrogen on the carbon incorporation will be compared.

## New hydrogen desorption kinetics from vicinal Si(001) surfaces observed by RAS

**J. ZHANG**, A.K. Lees, A.G Taylor, M.H. Xie, B.A. Joyce, Z. Sobiesierksi\* and D.I. Westwood\*

IRC for Semiconductor Materials, Blackett Laboratory, Imperial College of Science, Technology and Medicine, Prince Consort Road, London SW7 2BZ, UK.  
Tel: +44 171 594 6672; Fax: +44 171 594 6685; E-mail: jing.zhang@ic.ac.uk

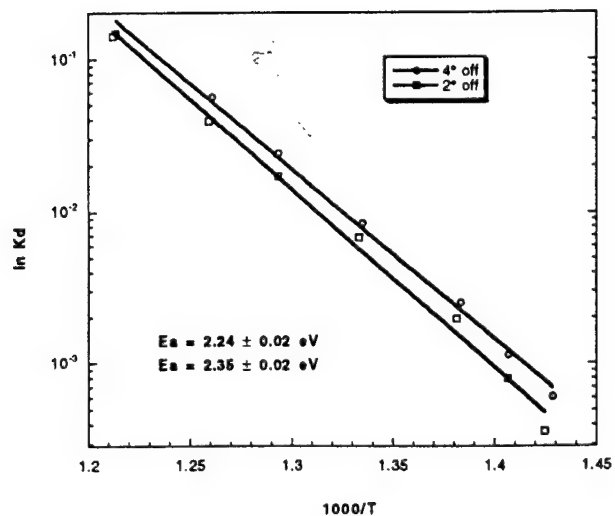
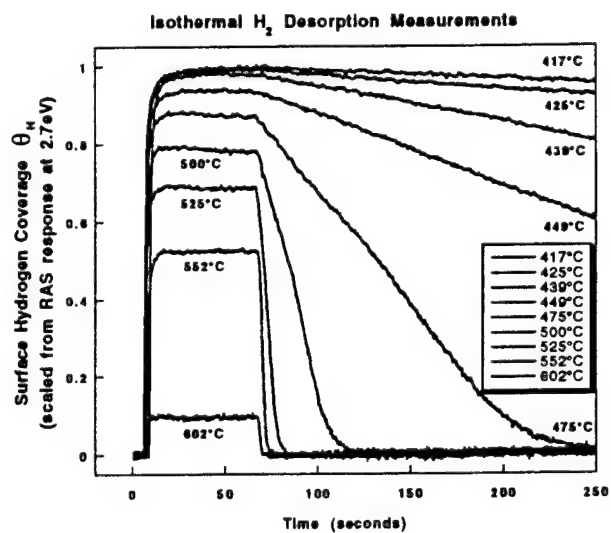
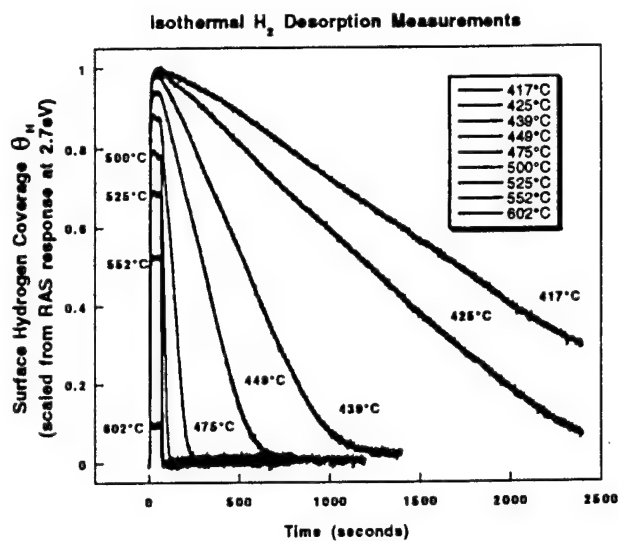
\*Department of Physics and Astronomy, University of Wales College of Cardiff, P.O. Box 913, Cardiff CF2 3YB, UK

Reflection anisotropy (difference) spectroscopy (RAS) has recently been applied to study of vicinal Si surfaces[1] and growth dynamics in gas source molecular beam epitaxy (GSMBE) of Si and SiGe alloys[2,3]. The dependence of RA on changes in the electronic configuration of the Si dimers on the (001) surface induced by adsorbates make it possible to monitor *in situ* the chemical processes taking place on the Si (001) surface during GSMBE. Using vicinal (001) surfaces misoriented towards the nearest (111) plane, we have investigated the effect of surface hydrogen generated from atomic hydrogen, silane and disilane on the RAS. The changes in the RAS spectra induced by adsorption are shown to be independent of the source gases. The symmetry of the surface was established as 2x1 corresponding to the monohydride phase.

RA response at 2.7eV was used to monitor dynamic changes in the coverage of surface hydrogen. This response was compared with TPD measurements in the literature and shown to be linearly dependent to the surface hydrogen coverage. Isothermal desorption measurements of hydrogen from vicinal Si(001) surfaces were made. The coverage exhibits a linear decrease with respect to time at high coverage and temperature. This implies zeroth order desorption kinetics in contrast to the widely accepted first order results obtained mostly from singular (001) surfaces. The zeroth order kinetics are explained in terms of desorption via a precursor state with the rate limiting step being the desorption from such state. For the zeroth order behaviour to be sustained over a range of coverages, the population in the precursor state must remain constant. This can occur if the density of precursor state is significantly smaller than the surface hydrogen population. We propose that this precursor state is associated with steps and remains saturated over a range of surface hydrogen coverage. For this to occur, transport of hydrogen from terraces to the precursor state can not be the rate limiting step. Hence, surface migration/diffusion is a much faster process than desorption as predicted by first principles calculations reported in the literature.

The model has significant implications on the growth of Si/SiGe in GSMBE with respect to growth rate and Ge surface segregation. These are discussed within the framework of the proposed model.

- [1] T. Yasuda, L. Mantese, U. Rossow and D.E. Aspnes, Phys. Rev. Lett. **74**, (1995), 3431.
- [2] A.R. Turner, M.E. Pemble, J.M. Fernandez, B.A. Joyce, J. Zhang and A.G. Taylor, Phys. Rev. Lett. **74**, (1995), 3213.
- [3] J. Zhang, A.G. Taylor, A.K. Lees, J.M. Fernandez, B.A. Joyce, D. Raisbeck, N. Shukla and M.E. Pemble, Phys. Rev. B. Scheduled for publication in April 15th issue.



## **Reduction of SiGe Heterointerface Mixing by Atomic Hydrogen Irradiation during MBE and its Mechanism**

Kiyokazu Nakagawa, Yoshinobu Kimura and Masanobu Miyao  
Central Research Laboratory, Hitachi, Ltd., Kokubunji, Tokyo 185, Japan  
Tel: +81-423-23-1111 Fax: +81-423-27-7722 e-mail: k-nakaga@crl.hitachi.co.jp

Surface segregation is a phenomenon in which Ge segregates to the epitaxial surface during MBE growth, and atomic hydrogen irradiation during MBE growth can reduce this phenomenon. To reveal the mechanism of both the phenomenon and the hydrogen irradiation effect, we have investigated the dependence of the phenomenon with and without atomic hydrogen irradiation on the Si growth rate, substrate orientation, and the substrate temperature.

We carried out Si deposition with an e-gun evaporator, and used an effusion cell for Ge deposition. The atomic hydrogen was formed by applying RF power to a gas cell. The surface concentration of Ge atoms segregated on the overgrown Si surfaces was measured using x-ray photoelectron spectroscopy.

The segregated Ge concentrations were plotted as a function of the Si deposited thickness with and without hydrogen irradiation (Fig. 1). As we reported previously, the segregated Ge concentration does not depend exponentially on the Si growth thickness and a second-order reaction as well as a first-order reaction is necessary to describe the Ge segregation phenomenon in Si. Atomic hydrogen does not affect the first-order reaction but does affect the second-order reaction. In addition, the decrease in the segregation when the Si growth rate increases from 0.1 nm/s to 0.3 nm/s (Fig. 2), means that the jumping rate for surface segregation is comparable with the Si growth rate.

The segregation length is defined as the Si deposition thickness at which the Ge surface concentration becomes 0.1 ML (1/10 of the initial Ge concentration) at a Si growth rate of 0.1 nm/s. The segregation phenomenon does not monotonically increase with the growth temperature; it forms a peak with and without hydrogen irradiation (Fig. 3). The segregation length on Si(100) is larger than that on Si(111). The atomic hydrogen irradiation reduced the Ge surface segregation. As the growth temperature decreased, the crystal quality deteriorated and the segregation length became constant. The temperature at which the segregation length became constant is 50°C higher when hydrogen irradiation was used, regardless of the substrate orientations.

These results are explained as follows. The difference in the segregation lengths with Si(100) and Si(111) substrates is due to a difference in the number of exchange paths with different substrates. In the low temperature range, however, the number of paths becomes the same due to the deterioration of crystal quality. The atomic hydrogen irradiation does not change the potential of the two-energy-state model, but it changes the probability of the second-order reaction occurring. As a result, the segregation is reduced.

We estimated the jumping rate of Ge atoms by using the experimental results related to the growth rate. We were able to show that a simulation based on a model, in which hydrogen modifies the probability of the second-order reaction rather than the energy, can reproduce the experimental results (Fig. 4).

# Reduction of SiGe Heterointerface Mixing by Atomic Hydrogen Irradiation and its Mechanism

Kiyokazu Nakagawa, Yoshinobu Kimura and Masanobu Miyao

Central Research Laboratory, Hitachi, Ltd., Kokubunji, Tokyo 185, Japan

Tel: +81-423-23-1111 Fax: +81-423-27-7722 e-mail: k-nakaga@crl.hitachi.co.jp

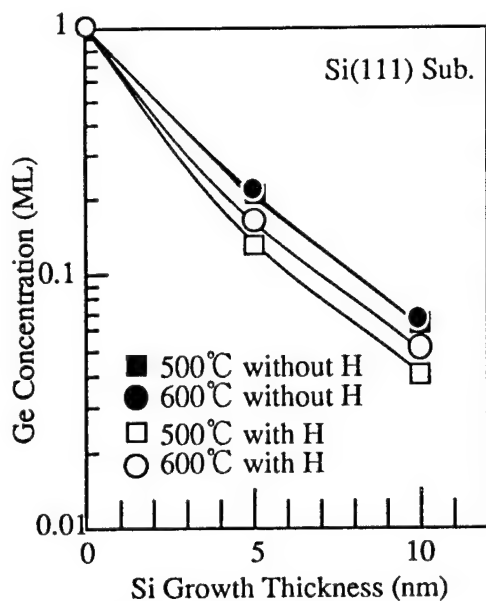


Fig. 1 Segregated Ge concentration as a function of Si overgrowth thickness with and without atomic hydrogen irradiation.

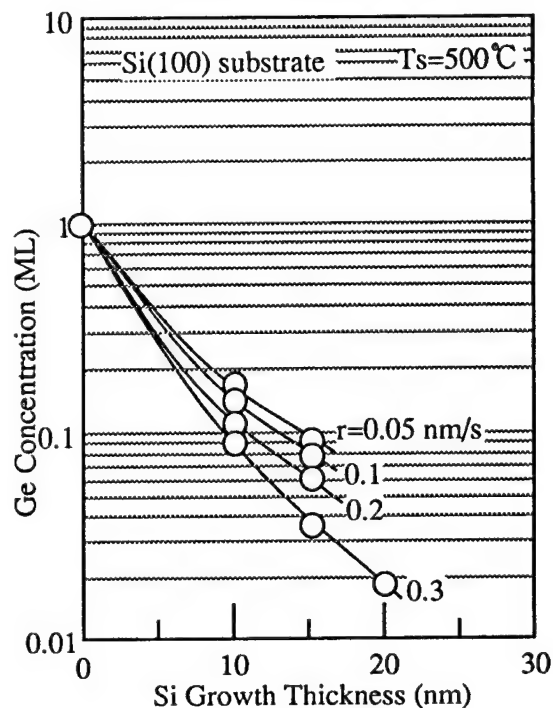


Fig. 2 Dependence of Surface Segregated Ge concentration on Si overgrowth rate.

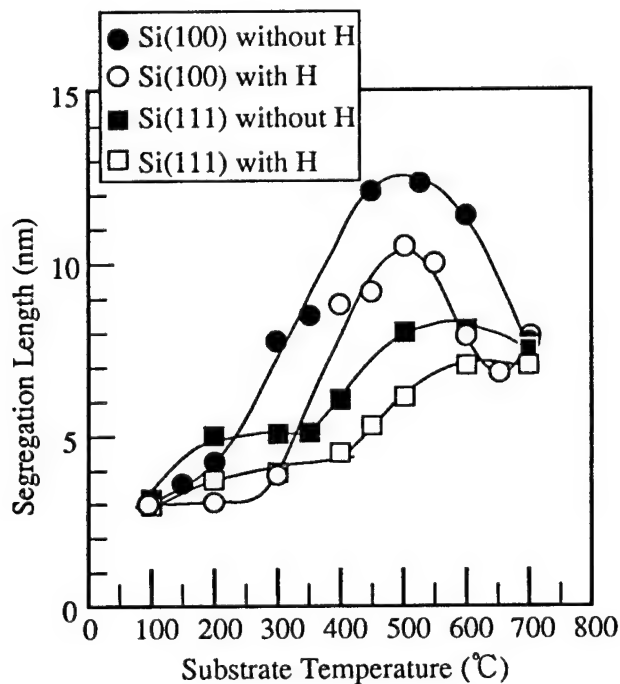


Fig. 3 Segregation length on Si(100) and Si(111) substrates with and without atomic hydrogen irradiation as a function of substrate temperature.

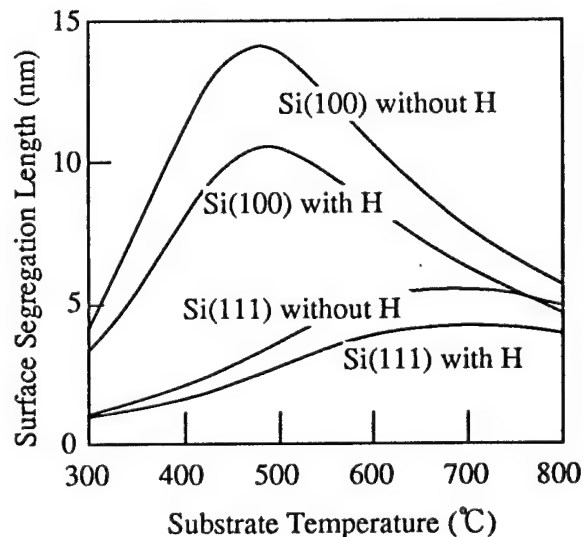


Fig. 4 Result of a simulation based on the two-state model. In the simulation, the decrease in the segregation lengths of Si(100) to Si(111) is due to fewer exchange paths along the bonds. The decrease in length caused by hydrogen irradiation is due to an increased incorporation ratio of Ge-Ge pairs into Si.



## Control of Composition and Crystallinity in the Molecular Beam Epitaxy of Strain-Compensated $\text{Si}_{1-x-y}\text{Ge}_x\text{C}_y$ Alloys on Si

E. T. Croke and A. T. Hunter, Hughes Research Laboratories, Inc.,  
Malibu, CA 90265; C. C. Ahn, California Institute of Technology,  
Pasadena, CA 91125; T. Laursen, A. E. Bair, D. J. Smith, and J. W.  
Mayer, Arizona State University, Tempe, AZ 85287.

Tel: 310-317-5546 FAX: 310-317-5485

email: croke@madmax.hrl.hac.com

The control of strain and electronic structure in Group IV heterostructures offers the potential for improving the compatibility of device structures fabricated from these materials and the processing environments currently available for Si. Alloys of Si, Ge, and C grown on Si are expected to provide enhanced flexibility in the design of such structures. While techniques to control the composition of films containing Si and Ge have been well established by both chemical vapor deposition (CVD) and molecular beam epitaxial (MBE) growth techniques, control of C composition in such films remains a subject of extensive study. For this work, we have demonstrated a mass-spectrometry-based approach to the control of carbon composition in  $\text{Si}_{1-y}\text{C}_y$  and  $\text{Si}_{1-x-y}\text{Ge}_x\text{C}_y$  alloys grown by MBE. We have performed extensive characterization of a wide range of structures with a variety of compositions. High-resolution x-ray diffraction (HRXRD), Rutherford Backscattering Spectroscopy (RBS), and Secondary Ion Mass Spectrometry (SIMS) were used to measure Ge and C concentration and Transmission Electron Microscopy (TEM), to determine the extent of defect formation.

The basic setup for our experiments consists of a Perkin-Elmer (Model 430S) Si MBE system, capable of codepositing Si, Ge, and C from electron beam evaporators onto heated Si substrates. Solid, high-purity graphite, inserted into the 40 cc hearth of one of the evaporators serves as the source of C. Tuned to amu 24 ( $\text{C}_2$ ), a residual gas analyzer (RGA) located directly above the carbon source, provides a quantitative measure of the carbon flux. The signal from the RGA is compared to a previously calibrated setpoint depending on the desired carbon flux and is used to control the power to the electron gun. A cutout in the C shutter allows the flux to be continually monitored regardless of whether the shutter is open or closed, eliminating transients that would otherwise occur as the shutter opens. A series of  $\text{Si}_{1-y}\text{C}_y/\text{Si}$  superlattices were grown at 450 °C and analyzed by HRXRD to determine C concentration as a function of RGA setpoint for a fixed Si flux, generating a calibration curve to be used for the growth of  $\text{Si}_{1-x-y}\text{Ge}_x\text{C}_y$  alloys.

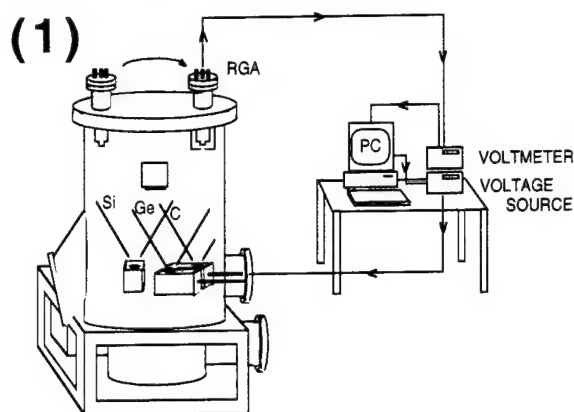
For carbon concentrations in excess of 1%, growth of  $\text{Si}_{1-y}\text{C}_y$  was found to produce a rough surface, as evidenced by spottiness in Reflection High-Energy Electron Diffraction (RHEED) patterns observed during growth. As long as the  $\text{Si}_{1-y}\text{C}_y$  layer thickness did not exceed a certain critical value found to be C concentration dependent, the subsequent Si layers smoothed the RHEED patterns and the structures remained relatively defect-free. At still higher concentrations and thicknesses, RHEED revealed evidence of twinning and the material became highly defective. For  $\text{Si}_{1-x-y}\text{Ge}_x\text{C}_y$  superlattices, the observed roughening and defect formation was found to occur at lower C concentrations. However, we were able to obtain high-quality samples with as much as 20% Ge and 0.4% C in the SiGeC layers. Decreasing the Ge content to around 10% was found to significantly improve the quality of the structures at higher concentrations of C. By growing a series of  $\text{Si}_{1-0.1-y}\text{Ge}_{0.1}\text{C}_y/\text{Si}$  superlattices, we showed that our method of controlling the carbon flux can be successfully used to produce high-quality, crystalline structures with strain configurations ranging from compressive, to lattice-matched, and then, finally, to tensile, as the carbon concentration increased from about 1 to 1.7% for about 10% Ge.

In conclusion, we have grown and characterized  $\text{Si}_{1-y}\text{C}_y/\text{Si}$  and  $\text{Si}_{1-x-y}\text{Ge}_x\text{C}_y/\text{Si}$  heterostructures through the use of a mass-spectrometry controlled electron beam source of carbon. The structures were determined to be of excellent quality within a certain range of Ge and C concentrations and layer thicknesses. HRXRD, TEM, RBS, and SIMS analytical techniques were used to evaluate the composition and crystallinity of the samples reported here.

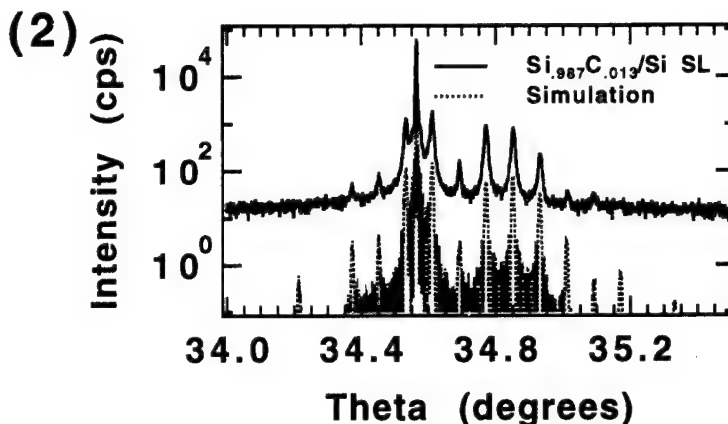


# Control of Composition and Crystallinity in the Molecular Beam Epitaxy of Strain-Compensated $\text{Si}_{1-x-y}\text{Ge}_x\text{C}_y$ Alloys on Si

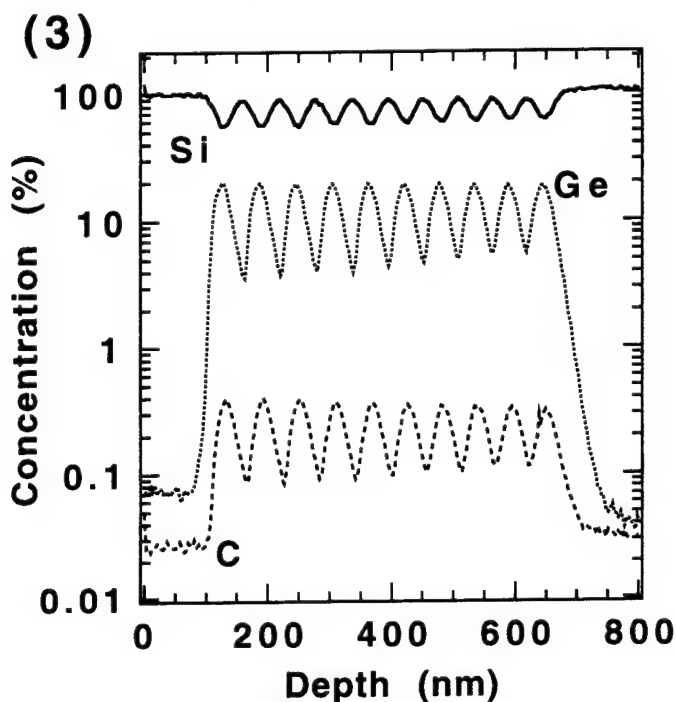
E. T. CROKE et al., Hughes Research Laboratories, Inc., 3011 Malibu Canyon Rd., Mail Stop RL63, Malibu, CA 90265



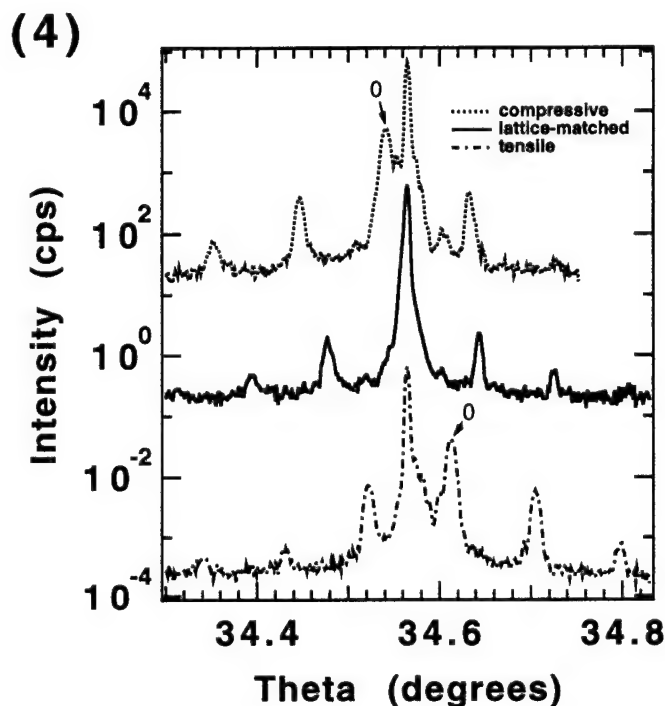
(1) Schematic diagram illustrating the mass-spectrometry-controlled approach to obtaining a stable, reproducible carbon flux. The residual gas analyzer (RGA) is located directly above an electron gun containing graphite. The signal from the RGA is used as a quantitative measure of the carbon flux and is used by a computer to control the power to the electron gun.



(2) High-resolution x-ray diffraction (HRXRD) spectrum taken from a 10-period, 280 Å  $\text{Si}_{0.987}\text{C}_{0.013}$  / 350 Å Si superlattice (SL). The data (solid curve) are shown to compare well with simulation (dotted curve). The sharpness of the superlattice peaks suggests that the carbon flux remains highly stable throughout the growth of the entire structure.



(3) SIMS profiles for Si, Ge, and C from a 10-period, 230 Å  $\text{Si}_{0.796}\text{Ge}_{0.200}\text{C}_{0.004}$  / 345 Å Si superlattice. The data show good delineation between layers and again, uniformity of composition throughout the structure.



(4) HRXRD spectra taken from three SiGeC/Si superlattices demonstrates the degree of flux control achievable using this method. For each sample, the Ge concentration in the SiGeC layers was held fixed while the carbon concentration was allowed to vary through the lattice-matched condition.

## Stratified suspension of highly ordered Si nanoparticles in SiO<sub>2</sub> created by Si MBE with oxygen co-implantation

Yukari Ishikawa, and N. Shibata  
Japan Fine Ceramics Center,  
2-4-1 Mutsuno, Atsuta-ku, Nagoya 456, Japan

S. Fukatsu  
Department of Pure and Applied Sciences,  
The University of Tokyo, 3-8-1 Komaba, Meguro-ku, Tokyo 153, Japan,  
Tel: +81-3-5454-6754; Fax: +81-3-5454-4311; E-mail: fkatz@srv.bme.rcast.u-tokyo.ac.jp

Establishing a realistic device made of Si and allied compounds is a cornerstone issue in the field of optoelectronics. Recently, dielectric suspensions of Si and Ge fine structures of nano-dimensions have attracted much interest due to their unique optical properties. In particular, visible light emission capability of Si nanoparticles in SiO<sub>2</sub> at room temperature holds promise in the context of efficient Si-based light emitter fabrication.

The problems encountered when dealing with Si nanoparticles in SiO<sub>2</sub> fabricated by conventional techniques such as laser ablation, gas-evaporation, co-sputtering, and Si implantation are (1) the dispersive character of nanoparticles that are randomly distributed in SiO<sub>2</sub> without preference of crystal orientation and (2) the meager controllability over the particle dimensions. Clearly, in the perspective of futuristic optoelectronic applications, it is strongly desired to develop a technique which allows to establish an ordered arrangement and to control the feature size so that one might make most of the potential of these nanoparticles.

In this paper, a novel architecture of Si nanoparticle system is described by using Si MBE hybridized with multiple oxygen co-implantation. The growth was performed on a clean Si(100) by repeating the unit period, viz. deposition of Si, oxygen ion implantation, and in situ annealing. Si nanoparticles are formed during the annealing step. Transmission electron microscopy was performed to assess the details of nanoparticle environment.

The Si nanoparticles created this way offer the solution to the above problems. (1) is readily solved by the followings; (a) Nanoparticles are highly oriented and the preferred crystalline axis is oriented to the substrate normal, [100]. This also means that nanoparticles are grown without epitaxy disruption on Si(100); (b) Nanoparticles are arranged in the form of alternating Si, SiO<sub>2</sub> slabs. On the other hand, the problem (2) is removed since (a) the particle dimension statistics for the width and height were characterized by a log-normal distribution with the identical mean value, 21nm, and variance, 1.5nm, and (b) the initial Si thickness clearly puts the ceiling over the particle height, thus facilitating size control.

Besides these, an almost perfect crystallinity of Si nanoparticles was confirmed by lattice imaging and diffraction analysis. On the other hand, the morphologies of Si nanoparticles turned out to be a nearly isotropic polygon significantly faceted with (100) and (111) planes as opposed to the thermodynamically stable crystal morphology of Si, i.e., icosidodecahedron having only the (111) and (311) facets. This seems to invoke the revision of the conventionally accepted scenario of particle formation dynamics.

Furthermore visible green band luminescence was clearly observed at room temperature for Si nanoparticles with dimensions approaching the quantum confinement regime.

---

Contact author:

S. Fukatsu  
Department of Pure and Applied Sciences,  
The University of Tokyo, 3-8-1 Komaba, Meguro-ku, Tokyo 153, Japan,  
Tel: +81-3-5454-6754; Fax: +81-3-5454-4311, E-mail: fkatz@srv.bme.rcast.u-tokyo.ac.jp

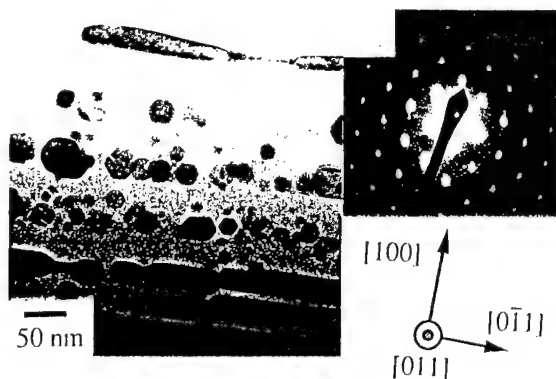


FIG. 1. Stratified SiO<sub>2</sub> suspension of highly oriented Si nanoparticles. Dark contrast corresponds to Si. Left: Cross section TEM. Right: Selective diffraction of a nanoparticle. Note the ordered crystalline arrangement of nanoparticles.

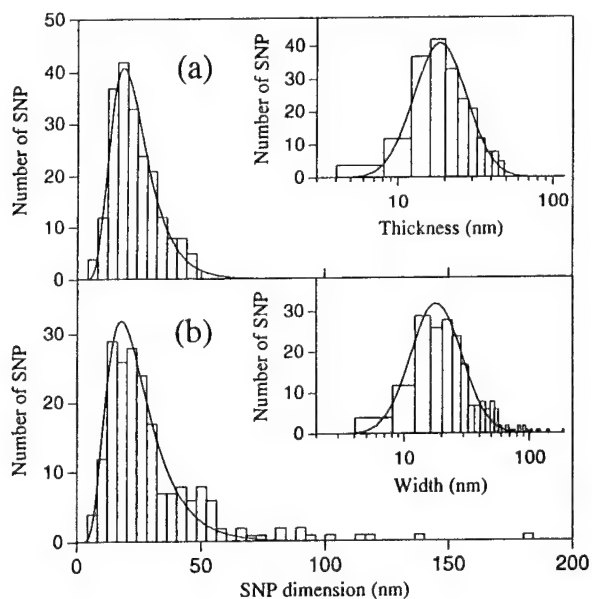


FIG. 2. Log-normal distribution of nanoparticle dimension. The insets are the semilog plots. Upper: Height. Lower: Width. Note the close similarity between the two distributions, and the ceiling over the height.

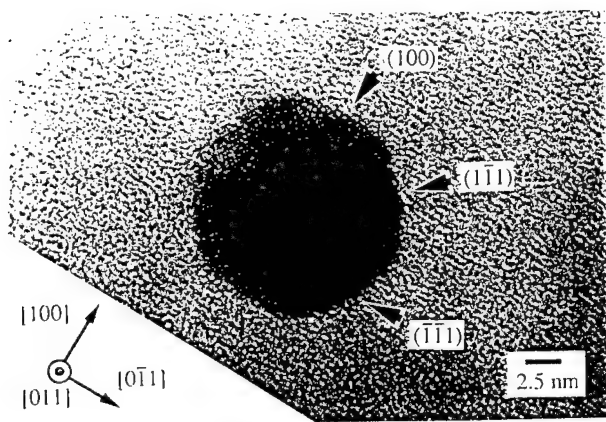


FIG. 3. Higher magnification of a Si nanoparticle of  $d \approx 14$  nm. Note the (100) and (111) facets appear as opposed to thermodynamically allowed crystal structure having only (111) and (311) facets.

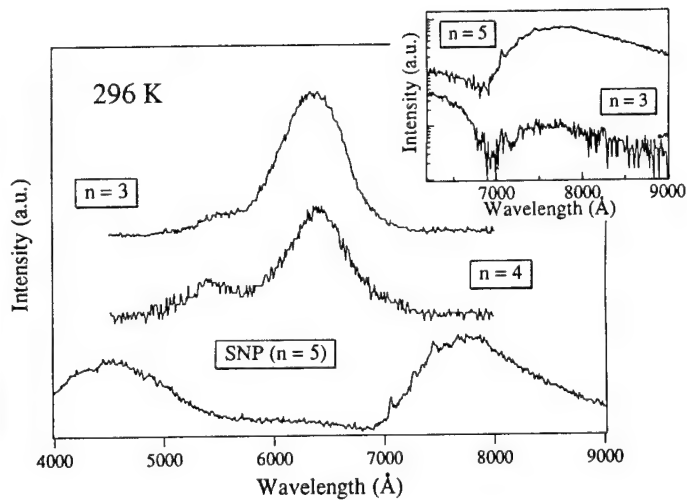


FIG. 4. Room temperature photoluminescence spectra of Si nanoparticles (bottom). The upper traces are luminescence of Si slab embedded in SiO<sub>2</sub>.

## Reduction of defect density in mismatched SiGe/Si by low temperature Si Buffer Layers

K. Linder, F. Zhang, P. Bhattacharya  
Solid State Electronics Laboratory

Department of Electrical Engineering and Computer Science

University of Michigan, Ann Arbor, MI, 48109-2122 USA

email: pkb@eecs.umich.edu

FAX: (313) 763-9324

Ph: (313) 763-6678

SiGe/Si heterostructures have gained considerable attention for both electronic and optoelectronic applications due to their compatibility with existing Si technology. While most current applications incorporate low Ge composition alloys, the exploitation of Ge-rich alloys ( $x \geq 0.4$ ) would greatly enhance device performance. Theoretically, Ge-rich alloys would be excellent for high performance heterojunction bipolar transistors (HBTs) due to an improvement in the carrier transport properties<sup>1</sup>. Producing relaxed, defect free Ge-rich alloys have been difficult due to the 4% mismatch between Si and Ge. In the present study, several types of buffer layers have been examined to reduce the threading dislocation density in SiGe grown by molecular beam epitaxy (MBE). These include multiple superlattice structures as well as a graded step layer structures. In most cases, it seems that it is energetically favorable for the dislocation to propagate into the growing layer and multiply, in spite of the "dislocation filters". On the other hand, a new technique, using a thin low temperature (LT) Si buffer layer, reduces dislocation propagation by a significant amount.

The experimental samples, typically 1  $\mu\text{m}$  thick  $\text{Si}_{0.4}\text{Ge}_{0.6}$ , were grown on (001)Si at a substrate temperature of 570°C by MBE using disilane and solid Ge as sources. The dislocations formed at the interface were characterized by cross-sectional transmission electron microscopy (XTEM). The defect densities were also determined from analysis of XTEM data. In the SiGe epitaxial layers grown over single or multiple Si/SiGe strained layer superlattice buffers (average composition same as the SiGe layer) it was found that as the number of SLS regions increased, the dislocation density decreased. The best reduction observed was by a factor of 10. Epitaxial layer with step graded buffer layers were also characterized for their effectiveness in dislocation bending. These buffer layers were also effective in reducing the dislocation density to some extent but the improvement was small. With both types of buffer layers, the dislocation densities were still too high for any practical device application ( $\sim 10^7 \text{ cm}^{-2}$ ). Also, the structures would be too thick for well defined lithography.

The best results, in terms of defect reduction, were obtained with a new buffer layer. A thin layer of Si ( $\sim 1000 \text{ \AA}$ ) was grown at low temperature ( $\leq 500^\circ\text{C}$ ) on the substrate with the disilane cracked at 600°C. A 0.5  $\mu\text{m}$  SiGe layer was then grown under normal growth conditions. It was seen from XTEM that the high density of defects produced in the low temperature buffer were mostly contained in it or bent into the substrate, thus producing an almost defect-free active layer (maximum defect density  $\sim 10^4 \text{ cm}^{-2}$ ). The mechanism for the defect trapping is being investigated. It appears that the LT buffer energetically favors the dislocations to propagate to the wafer edge. The epitaxial layers have been characterized by X-ray and Raman measurements. Results from ongoing experiments with high Ge-containing HBTs will be presented as well.

### References

1. J. M. Hinckley, and J. Singh, J. Appl. Phys. 94, 76 (4192).

Work supported by AFOSR under Grant F49620-95-0013

# Hybrid MBE growth and mobility limiting factors of *n*-channel Si/SiGe modulation-doped systems

A.Yutani and Y.Shiraki

Research Center for Advanced Science and Technology, The University of Tokyo

4-6-1 Komaba, Meguro-Ku, Tokyo 153 JAPAN

Tel. +81-3-3481-4430 Fax. +81-3-3481-4509

e-mail: yutani@photonics.rcast.u-tokyo.ac.jp

We present here performances of strained Si/relaxed SiGe modulation-doped (MOD) structures grown by *hybrid MBE growth*, *i.e.* a combination of gas-source MBE (GSMBE) and solid-source MBE (SSMBE), and discuss mobility limiting factors in strained Si channels.

Schematic structure of the samples grown here is shown in Fig. 1. Since GSMBE gives rise to better crystal quality than SSMBE and SSMBE is good for controlling doping concentration, buffer, channel and spacer layers of the MOD structure were grown by GSMBE, and supply and cap layers were by SSMBE in order to obtain high performances. After GSMBE growth, wafers were transferred in the air to the SSMBE chamber. Figure 2 shows the RHEED patterns before and after cleaning in ultra high vacuum at 700°C for two minutes. Clear  $2\times 1$  structures observed after the cleaning indicate that the transfer in the air does not bring serious contamination even on SiGe surfaces.

Transport properties of the samples grown by this method were examined in van der Pauw or Hall bridge geometries by varying the silicon channel layer thickness,  $W$ , from 200Å to 13Å. Figures 3 and 4 show the temperature dependence of the mobility and the carrier density, respectively. In the 200Å sample, mobility up to  $50000\text{cm}^2/\text{Vs}$  is achieved at 25K and the mobility is seen to monotonically decrease with decreasing  $W$ . Back-gating measurement revealed that the Fermi velocity limits the mobility in cases of  $W \geq 53\text{Å}$  which is characteristic of MOD systems. However, it is seen that samples with narrower channels show mobility-decrease at low temperatures and, moreover, their mobility was found to be strongly dependent on the channel thickness. This suggests that the mobility is governed by the interface roughness and its temperature dependence was well represented by the theory<sup>1</sup>.

In extremely narrower samples, a drastic drop of the Hall voltage was observed. Temperature dependence of the conductivity of these samples did not obey the activation type but well followed the power law with  $1/3$  which is characteristic of two-dimensional variable range hopping (2D-VRH) conduction. This may come from the localization due to well width fluctuation which causes big variation in energy levels in the case of very thin wells.

---

<sup>1</sup>H. Sakaki *et al.* : Appl. Phys. Lett. 51 1934 (1987)

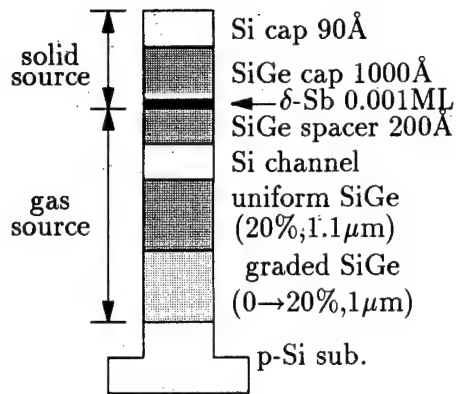
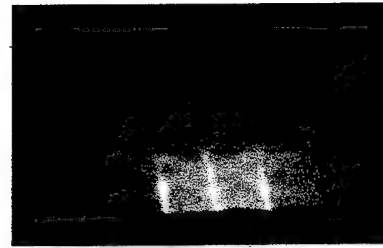


**Figure 1:** Sample structure with the hybrid MBE technique. Buffer, channel and spacer layers are grown by gas-source MBE; supply and cap layers are by solid-source MBE.



(a)



(b)

**Figure 2:** RHEED images of (a) just after loading to the solid-source MBE; (b) after 700°C, two minutes thermal cleaning.

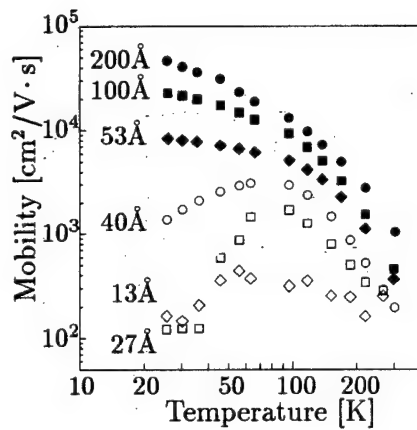


**Figure 3:** Temperature dependence of the samples grown by the present technique with varied channel width  $W$ . In  $W=200\text{Å}$  sample mobility up to  $\sim 50000\text{cm}^2/\text{Vs}$  is achieved at 25K.

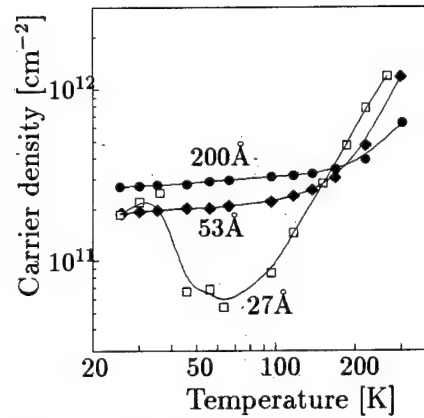


**Figure 4:** Temperature dependence of the samples. For simplicity characteristics of 200Å, 53Å and 27Å samples are shown. Characteristics of 100Å, 40Å and 13Å samples are similar to 200Å, 53Å and 27Å samples, respectively.

# Effects of Hydrogen on Si(001) Growth Dynamics during GSMBE from Disilane

Kazuki Mizushima<sup>†</sup> and Dimitri D. Vvedensky

*The Blackett Laboratory, Imperial College, London SW7 2BZ, United Kingdom*

Pavel Šmilauer

*HRLZ, KFA Jülich, 52425 Jülich, Germany*

Andrew Zangwill

*School of Physics, Georgia Institute of Technology, Atlanta, Georgia 30332*

Jing Zhang and Bruce A. Joyce

*Interdisciplinary Research Centre for Semiconductor Materials,  
Imperial College, London SW7 2BZ, United Kingdom*

The effects of hydrogen on Si(001) growth dynamics during gas-source molecular-beam epitaxy (GSMBE) from disilane are investigated by simulations using a kinetic Monte Carlo model. The growth dynamics are modeled with four species, i.e. Si, H, SiH<sub>2</sub> and SiH<sub>3</sub>, and includes the dissociative adsorption of two SiH<sub>3</sub> species from Si<sub>2</sub>H<sub>6</sub>, decomposition pathways of SiH<sub>3</sub> and SiH<sub>2</sub>, desorption of hydrogen, anisotropic diffusion of each species, different sticking energies for A and B (single-atomic-height) step edges, and the effects of dimerization. Hydrogen desorption is assumed to occur preferentially at step edges, based on recent reflectance anisotropy (RA) measurements [1].

We have investigated the effects of hydrogen coverage on growth rate, the oscillations of the reflection high-energy electron diffraction (RHEED) intensity and the RA signal, and the morphological differences of the growing surface in comparison with that of a solid-source (no hydrogen) MBE model. Oscillations of the RA signal, which are explained by the change of relative domain coverage during layer-by-layer growth [2], are well reproduced by the model and the detailed features of the oscillations and their differences from RHEED oscillations are investigated. The hydrogen-induced creation of small high-density islands at lower temperatures [3] is also investigated.

<sup>†</sup> Permanent address: Advanced Technology Research Laboratories, Mitsubishi Materials Corporation, 1-297 Kitabukuro-cho, Omiya, Saitama 330, Japan

[1] J. Zhang et al., to be published.

[2] A.R. Turner et al., Phys. Rev. Lett. **74**, 3213 (1995); J. Zhang et al., to be published.

[3] J.E. Vasek et al., Phys Rev B **51**, 17207 (1995).

Contact:

D.D. Vvedensky, The Blackett Laboratory, Imperial College, London SW7 2BZ, UK

Tel: +44-171-594-7573;

Fax: +44-171-823-7451;

email: d.vvedensky@ic.ac.uk



## Visible light emission from MBE-grown Si/SiO<sub>2</sub> superlattices

S.V.Novikov<sup>a\*</sup>, J.Sinkkonen<sup>a</sup> and S.V.Gastev<sup>b</sup>

<sup>a</sup>Electron Physics Laboratory, Helsinki University of  
Technology, FIN-02150, Finland

<sup>b</sup>A.F.Ioffe Physico-Technical Institute  
St.-Petersburg 194021, Russia

Si based light-emitting materials are very attractive for different devices applications. Such materials could then be incorporated into the device required by the optoelectronic industry using well-known Si processing technology. Unfortunately, silicon has indirect band gap, which prevents efficient electron-photon energy conversion. Interest in the possibility of light emission from silicon was increased a few years ago with the discovery of the bright luminescence from the electrochemically etched porous silicon<sup>1</sup>. Recently the luminescence from Si/SiO<sub>2</sub> superlattices, grown by *ex situ* oxidation of thin Si layers was reported<sup>2</sup>.

Here we report the fabrication of fully *in situ* molecular-beam epitaxy (MBE) grown Si/SiO<sub>2</sub> superlattices, which have luminescence in the visible range.

The Si/SiO<sub>2</sub> superlattices were grown in VG Semicon V80M MBE system at room temperature on p-type (100) Si wafers after Shiraki<sup>3</sup> chemical treatment without removing of the native oxide at the high temperature for prevention of the roughness increasing. Thin amorphous Si films with thickness 1.5-4.0 nm were deposited using e-beam evaporation. During deposition, the samples were exposed under H-atoms beam for passivating the traps in the silicon. Si layers were oxidized using RF plasma source with O<sub>2</sub> inlet. The thickness of the SiO<sub>2</sub> was 1 nm. This procedure was repeated until necessary superlattice periods were completed.

The room temperature photoluminescence (PL) spectrums of the superlattices were measured using Ar laser excitation. We have observed the visible to near-infrared photoluminescence of the samples at the range 1.7-2.1 eV with a full peak width at half maximum about 0.5 eV. The energy position of the PL peaks depends on the thickness of the Si layer and shifts to higher energy when the thickness is decreasing. This data corresponds to the quantum confinement of the Si energy band structure.

### References:

1. L.T.Canham Appl.Phys.Lett. 57, 1046-1048 (1990).
2. Z.H.Lu, D.J.Lockwood and J.-M.Baribeau, Nature 378, 258-260 (1995).
3. A.Ishizaka and Y.Shiraki J.Electrochem. Sci and Techn. 150, 966-971 (1986).

---

\*Corresponding author. Laboratory of Electron Physics,  
Helsinki University of Technology, Otakaari 7A SF-02150  
Espoo 15, Finland; FAX +358-0-460-224; Tel +358-0-451-2329;  
E-mail: novikov@elfys4.hut.fi.



## **Luminescence study on Ge islands as stressors on Si<sub>1-x</sub>Ge<sub>x</sub>/Si quantum well**

E. S. Kim, N. Usami, and Y. Shiraki

*Research Center for Advanced Science and Technology (RCAST),*

*The University of Tokyo, 4-6-1 Komaba, Meguro-ku, Tokyo 153, Japan*

Tel: +81-3-3481-4510, FAX: +81-3-3481-4509

We report new photoluminescence (PL) induced by self-assembled Ge islands that act as stressors on Si<sub>1-x</sub>Ge<sub>x</sub>/Si quantum well (QW).

Samples were grown by gas source molecular beam epitaxy on (100)-oriented p-type Si wafers using disilane and germane as source substances. A 4000 Å Si buffer was grown, followed by a 34 Å strained Si<sub>0.82</sub>Ge<sub>0.18</sub> QW at 740 °C. After growth of a Si spacer of 300 Å, a pure Ge top layer was grown at 700 °C. The Ge coverage was varied in the range of 2 monolayers (ML) to 15 ML.

Above 3.3 ML of the Ge coverage, new peaks were observed in the PL spectra at the lower energy than the peaks of the QW without Ge layers (Fig. 1). At the same time, the onset of the formation of Ge islands was observed at 3.3 ML of the Ge layer by atomic force microscopy (AFM) measurements (Fig. 3). The new peaks are, therefore, ascribed to the strain effects by the Ge islands. The self-assembled Ge islands may generate local strain to induce lateral bandgap modulation in underlying SiGe QW, which gives rise to the new peaks. The redshift was found to be increased up to 3.7 ML, however at 4.1 ML, the amount of the redshift was suddenly decreased and the peak position was maintained constantly despite the further increase of the Ge coverage (Fig. 2).

This dependence of PL on the Ge coverage is unexpected and interesting to be explained. The redshift at the early stages comes from the increase in the elastic deformation due to evolution of the Ge islands, but the sudden change around 4 ML is hardly explained. The interactions among the Ge islands may be one of possible explanations. That is, the Ge islands tend to conglomerate as seen in Fig. 2 and the interaction or superposition of strain effects of individual islands may be taken into account to decrease the strain field around the islands. More detailed studies are necessary to clarify the mechanism.

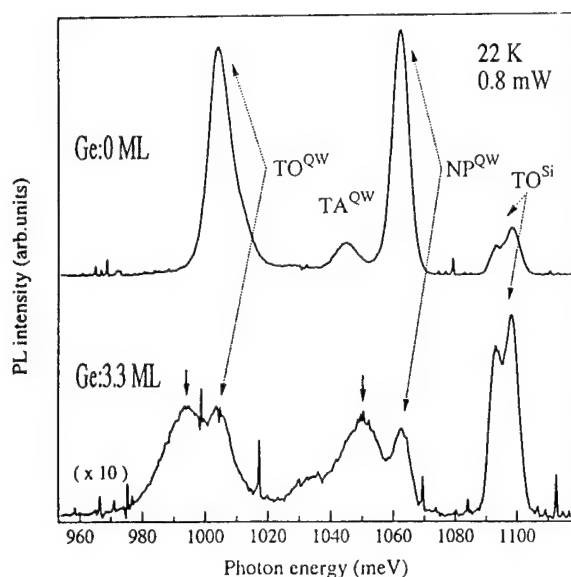


Fig.1 PL spectra of samples with 3.3 ML of Ge coverage and without Ge. Arrows indicate new peaks from quantum-dot-like structures induced by the Ge islands

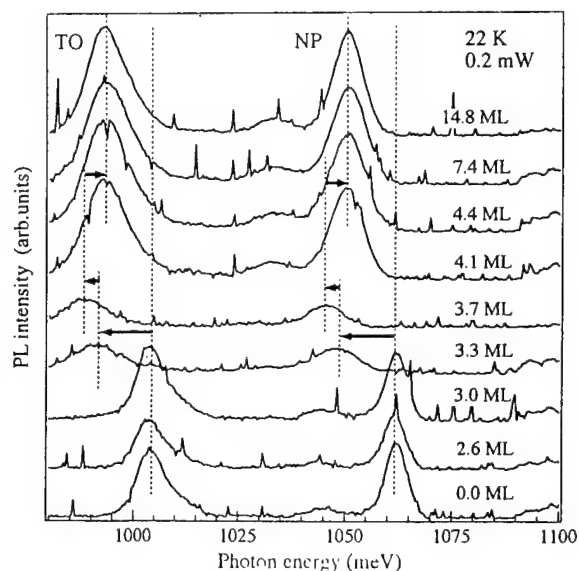
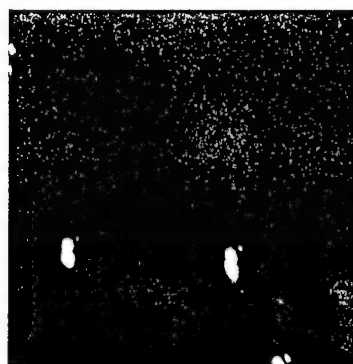


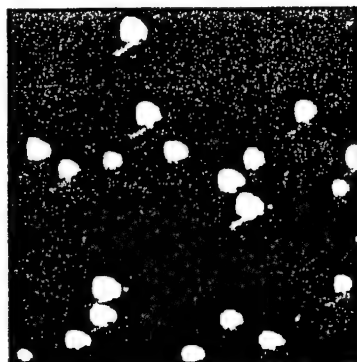
Fig.2 Shift of the PL peaks with increase of the Ge coverage. At 3.3 ML of Ge coverage the peaks begin to be shifted to lower energy side. The shift is more increased at 3.7 ML, however at 4.1 ML is returned to higher energy side.



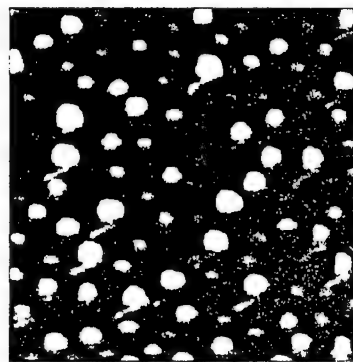
3.0 ML



3.3 ML



4.1 ML



14.8 ML

Fig.3 AFM images of the surface morphology of Ge layer at various Ge coverage . The images are  $2 \times 2 \mu\text{m}^2$

# The growth and luminescence of SiGe dots

H. Chen, X. G. Xie, W. Q. Cheng, Q. Huang, J. M. Zhou

Institute of Physics, Chinese Academy of Sciences, Beijing 100080, China  
Fax: (86)-010-2562605, Tel.: (86)-010-2551205, e-mail: XGXie@aphy02.iphy.ac.CN

It is found that the SiGe alloy self-organizes into uniform quantum dots embedded in the Si layer during the growth of a strained Si(8MLs)/Ge(4MLs) short period superlattice on a Si(001) substrate at the temperature of 800°C by molecular beam epitaxy. The dynamical process of the formation of the SiGe quantum dots was investigated by reflection high energy electron diffraction in situ. Transmission electron microscopy was used to confirm the existence of the quantum dots and estimate their spatial distribution. The planar-view TEM image reveals an array of well-ordered dots on the (001) plane. The size of the dots is about 100nm, and the separation between two dots is about 300nm. The surprising alignment of the dots suggests a strong positional correction during the formation process. The formation mechanism and composition of the dots is clarified by the (004) dark field image of cross-section sample. The dots are found to be composed of SiGe islands with a diameter of 100nm, embedded in a Si matrix with a thickness of about 20nm. The difference between our structure and the quantum dots formation from one SiGe layer is that our structure is much higher. The formation of the quantum dots may be understood by considering the complex interplay among the lattice strain, surface energy, surface migration and stress transport.

It is interesting to find that only one PL peak appears at the wavelength of 995nm, corresponding to the energy 1.24eV, which is higher than the indirect band-gap (1.15eV at 80K) of Si. By increasing the temperature from 80K to 300K, photoluminescence peak of the quantum dots shifts to a lower energy, and the intensity decrease by two orders of magnitude as expected. We also found that the PL intensity of quantum dots is two orders of magnitude higher than that of SiGe/Si quantum wells at 80K. Taking into account of the filling factor, that is the coverage of the SiGe containing quantum dots structure, the luminescence of dots seems to exceed that of the quantum well by more than three orders of magnitude. From these results of the photoluminescence measurement, we confirm that the PL peak from the quantum dots is the NP peak and the TO peak from quantum dots does not exist. The position of PL peak from quantum dots is higher than the indirect band gap from  $\Gamma_v$  to  $X_c$  of Si, so the exciton in the quantum dots can not be confined in the indirect band gap of Si, and the phenomenon can not be interpreted as quantum confinement and the zone-folding folding. This is a novel phenomenon different from reports before.

Although it is difficult to understand the phenomenon at present, strain induced interface ordering due to islanding is very unusual phenomenon in itself, with important implication for device application, and will therefore be the topic of further investigations. We therefore expect a lot of experimental and theory work to this, opening a wide field for investigation.

## DIRECT MBE GROWTH OF GE QUANTUM DOTS ON SI

Markov V.A., Nikiforov A.I, Nomerotsky N.V., Trukhanov E.M,  
Varlamov V.I.

Institute of Semiconductor Physics, Russian Academy of Sciences,  
13 Lavrentyev Prospekt, 630090 Novosibirsk, Russia  
FAX: (383-2)-35-75-02; E-mail: markov@isph.nsk.su

The transformation of Ge film to three-dimensional (3d-) Ge islands during MBE on Si(001) and (111) have been used as a basic idea to fabricate nanostructures with quantum dots. As the Ge film grows up to 1 nm thick the RHEED-oscillations disappeared due to 3d-islands formation. Transmission electron microscopy (TEM) images of islanded films were obtained. The plane sizes of the 3d-islands were founded to increase with increasing Ge growth temperature from 12 nm for 300C to 20 nm for 400C. The average height of the islands estimated from cross section TEM images is about 3.0 nm. Strain relaxation in the films was performed by substrate deformation around 3d-islands without misfit dislocation introduction. For tunneling experiments the Ge islands are located between two potential barriers formed by the Si layers 6-12 nm thick. Effects of Coulomb blockade and hole's resonance tunneling through the discrete energy levels in the quantum dots were observed.

Corresponding author:  
Nikiforov Alexandr  
Institute of Semiconductor Physics  
Russian Academy of Sciences  
13 Lavrentyev Prospekt  
630090 Novosibirsk  
Russia

FAX: (383-2)-35-75-02  
E-mail:nikif@isph.nsk.su

## Photoluminescence study of Si/SiGe multiple quantum wells grown by MBE

D. Grützmacher, R. Hartmann, U. Gennser, E. Müller, A. Dommann<sup>\*</sup>

*Paul-Scherrer-Institute, Micro- and Nanostructure Laboratory, CH-5232 Villigen-PSI, Switzerland*

*<sup>\*</sup>Neutechnikum Buchs, Laboratory for Vacuumtechnology, CH-9470 Buchs, Switzerland*

Si/SiGe multiple quantum wells (MQW) with Ge concentrations ranging from 10-30% have been deposited by MBE at temperatures ranging from 500-750°C at a rate of 0.1 nm/s. Both, Si and Ge, were evaporated by e-guns. High resistive ( $\rho > 420\Omega/\text{cm}$ ) as well as heavily Boron doped ( $\rho < 0.1\Omega/\text{cm}$ ) Si (100) substrates have been used for deposition. The main parameter varied during growth was the polarity and the strength of the applied bias voltage to the substrate. Before the evaporation started a bias voltage ranging from +1500 to -1500 V was applied to the substrate. A positive bias during growth will collect secondary electrons from the e-gun evaporation at the substrate, whereas positively charged Si and Ge ions are repelled. Without bias the substrate might charge up during e-gun evaporation by secondary electrons leading to an acceleration of ions to the substrate. This effect is enhanced by applying a negative substrate bias. In this study we analyse the impact of this ion bombardment during growth on the structural and optical properties of Si/SiGe quantum well structures.

After growth the quantum well structures were treated by rapid thermal annealing (RTA) processes in the temperature range from 750 to 950°C. The RTA was carried out in  $\text{N}_2/\text{H}_2$  (4%) gas mixtures as well as in pure  $\text{N}_2$ . The samples were analysed before and after the RTA treatment by low temperature photoluminescence (4K), transmission electron microscopy (TEM) and x-ray diffractometry.

MQW samples grown with a positive bias of +1500V at the substrate showed phonon resolved band-edge exciton luminescence even for samples grown at low temperatures on high resistive substrates. Subsequent RTA steps lead to an increase in intensity and a narrowing of the linewidth of the PL peaks. Moreover, a significant blue shift of about 20-30 meV was observed, which is attributed to Ge outdiffusion into the Si barriers. In contrast, samples grown without or a negative bias showed no phonon resolved luminescence before RTA processing. Instead broad luminescence in the range from 0.75 to 1 eV was observed. However, also in this case RTA lead to phonon resolved band-edge luminescence with narrow peaks. Remarkably, only a very small blue shift of the PL spectra with increasing RTA temperatures is detected, indicating a reduced outdiffusion of Ge. This observation is made independently of the Ge concentration in the quantum wells. Furthermore the gas ambient during RTA, pure  $\text{N}_2$  or  $\text{N}_2/\text{H}_2$  gas mixture, had no effect on the lineshape or the intensity of the PL spectra, indicating that solely temperature induced structural changes can be made responsible for the variation of the PL spectra caused by RTA.

Using careful analysis by x-ray diffraction and TEM the structural changes were analysed. First results indicate that ion induced local stacking faults might be responsible for the broad band PL. Local stacking faults are found predominantly in the SiGe layers, which may be due to the higher mass of Ge atoms.

contact author: Dr. Detlev Grützmacher  
Micro- and Nanostructures Laboratory  
CH-5252 Villigen-PSI, Switzerland

Tel: (+41) 56 310 3751  
Fax: (+41) 56 310 2646  
e-mail: gruetzmacher@psi.ch

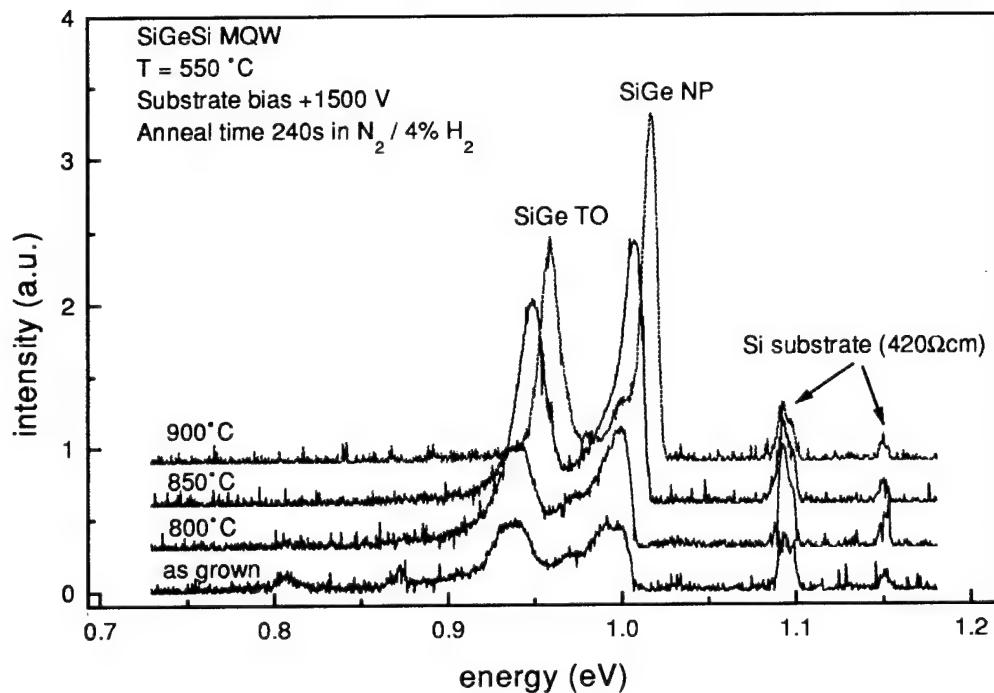


Fig. 1: Photoluminescence (4K) spectra of a  $\text{Si}_{0.76}\text{Ge}_{0.24}/\text{Si}$  multiple quantum well grown with an applied bias of +1500V to substrate. The figure compares the spectrum of the as grown MQW with those observed after rapid thermal annealing at 800, 850 and 950°C.

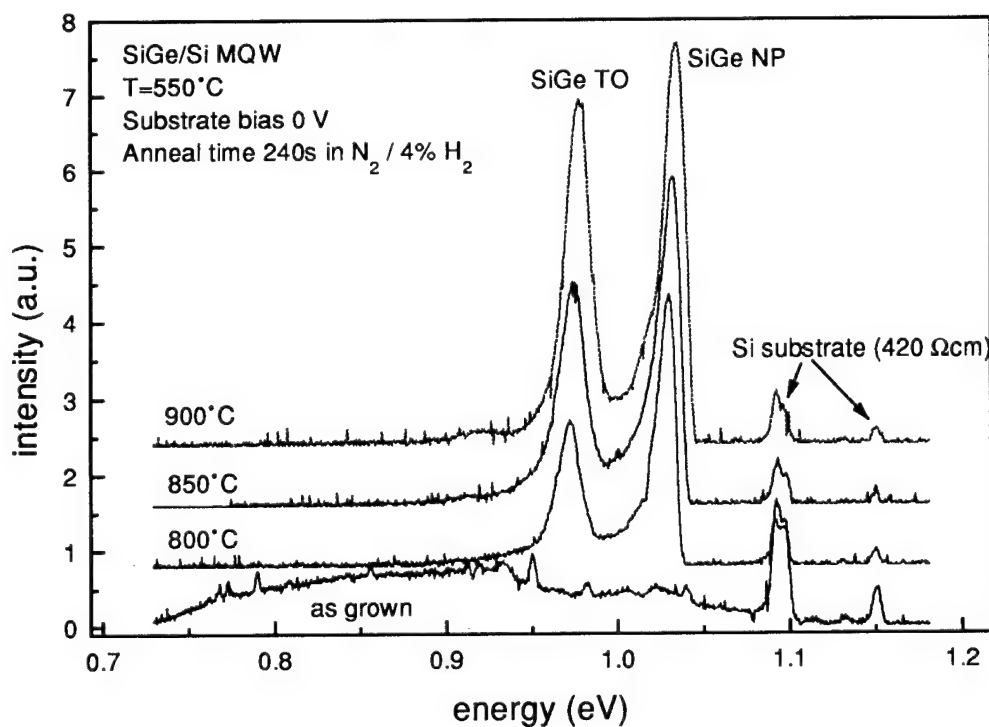


Fig.2: Photoluminescence (4K) spectra of a  $\text{Si}_{0.83}\text{Ge}_{0.17}/\text{Si}$  MQW grown without substrate bias and annealed at same conditions as the sample shown in Fig.1.

### **SURFACE-STABILIZED MBE-GROWTH OF SiC ON SiC(0001)**

**A. Fissel<sup>a</sup>, K. Pfennighaus<sup>a</sup>, U. Kaiser<sup>a</sup>, M. Wendt<sup>b</sup>, B. Schröter<sup>a</sup> and W. Richter<sup>a</sup>,** <sup>a</sup>Institut für Festkörperphysik, Friedrich-Schiller-Universität Jena, Max-Wien-Platz 1, D-07743 Jena; <sup>b</sup>Institut für Hochtechnologie, PF100239, D-07702 Jena, , Germany

SiC is an interesting and relatively new semiconductor material. One of the most interesting properties of SiC is the occurrence of different structures (polytypes) in this material with different physical properties. The only cubic polytype, 3C, for example, has a band gap of about 2.2 eV, whereas one of the hexagonal polytypes, 4H, has a gap of about 3.1 eV. Therefore, it may be possible to synthesize new materials, such as heterostructures and superlattices, with controllable band gap or other new interesting properties, only by a different stacking of atomic SiC layers. In this context, epitaxial films of SiC are of interest.

Especially during the last few years MBE has attracted more interest in SiC epitaxy because of the lower deposition temperatures (< 1400 °C) and the clean growth ambient. Moreover, the deposition process can be controlled within an atomic layer range necessary to grow definite layer structures.

In this subject, we report our new results in the growth of epitaxial SiC films by solid-source MBE. The films were grown on SiC(0001) between 900 and 1100°C, where Si and C were evaporated separately by means of electron beam guns, by an continuous deposition and using an alternate supply of Si and C, controlled to an atomic level by surface superstructures. The MBE growth mode, surface morphology and structure were investigated by *in situ* RHEED, *ex situ* AFM in air, SEM and by TEM.

In general, results show that the growth mode is strongly influenced on the surface stoichiometry. In case of Si-stabilized surface, showing 3-fold superstructures, films grow layer-by-layer via two-dimensional nucleation even at relative low temperatures (<1000°C). This may be a result of significant influence of exchange between Si and C, rather than from a higher carbon mobility.

Differences concerning the film structure were found to be dependent on the deposition mode indicating a different nucleation. Whereas in the case of continuous deposition the films consist of a mixture of the cubic and hexagonal polytypes, films grown by an alternating supply were dominantly of hexagonal SiC. We will present results of our deposition experiments using different surface superstructures. Moreover, the stabilization of surface superstructures during the growth by alternating supply enhances the layer-by-layer growth. Consequently, we assume that the nucleation conditions are strongly influenced by the surface superstructure, and, therefore, heterosystems of SiC polytypes may be obtainable using different surface phases.

*This work was supported by the Sonderforschungsbereich 196 (project A03) of the Deutsche Forschungsgemeinschaft.*

\* Corresponding author  
Phone: +49-3641-635914  
Fax: +49-3641-635738  
Mail: P5ANFI@CNVE.RZ.UNI-JENA.DE

# GROWTH AND CHARACTERIZATION OF LATTICE-MATCHED HgSe

L. Parthier\*, H. Wißmann, S. Luther, G. Machel, M. v. Ortenberg

*Institut für Physik, Humboldt-Universität zu Berlin, Invalidenstrasse 110,  
10115 Berlin, Germany, FAX: +49 30 2803329*

Mercury selenide is a semiconductor with interesting magnetic-optical properties. In technical applications undoped HgSe is used as p-contact for blue ZnSe-based devices /1, 2/. The special modification of Iron-doped HgSe is characterized by a donor level pinned to the Fermi energy ( $N_{Fe} \geq 5 \times 10^{18} \text{ cm}^{-3}$ ) resulting in an extremely high carrier mobility especially favourable for low dimensional structures. Also in combination with  $\text{Hg}_{1-x}\text{Mn}_x\text{Se}$  layers ( $x \leq 2\%$ ) a spin superlattice can be produced /3/. Up to now only few molecular beam epitaxial (MBE) grown HgSe-structures have been reported, however /4/. For these epitaxially grown HgSe layers ZnTe-buffers on GaAs substrates were used. However, the large lattice mismatch ( $\Delta a/a = -7.4\%$ ) requires a thick buffer layer ( $> 2 \mu\text{m}$ ) to reduce the high defect density generated at the interface.

We report here on two fundamental improvements for the epitaxial growth of HgSe-based heterostructures. The first step is very simple but obvious, we replace the GaAs substrate by GaSb. In this way we reduce the lattice mismatch drastically ( $\Delta a/a = -0.11\%$ ) and a smaller thickness of the buffer layer is sufficient, but the strain in the layer remains compressive which is unfavourable for the strain relaxation. The second step is the complete fitting of the buffer to HgSe by introduction of the ternary layer  $\text{ZnTe}_{1-x}\text{Se}_x$ . By spatial variation of the Se content from  $0.016 \leq x \leq 0.041$  the buffer layer can be fully matched to both the GaSb substrate and the HgSe layer, corresponding to a change of the misfit from  $+0.2\%$  up to zero in relation to HgSe. Only tensile strain is expected in this case /5/. For an optimized heterostructure we have to consider the large difference of the thermal expansion coefficients ( $\alpha_{\text{ZnTe}} = 8.19 \times 10^{-6} \text{ K}^{-1}$ ,  $\alpha_{\text{HgSe}} = 1.48 \times 10^{-6} \text{ K}^{-1}$ ).

The  $\text{ZnTe}_{1-x}\text{Se}_x$  buffer layers were grown at  $330^\circ\text{C}$ , the HgSe layer at  $90^\circ\text{C}$  with a Hg/Se beam pressure ratio of about 110. A HgSe-heterostructure with 200 nm thickness on a  $1 \mu\text{m}$  thick  $\text{ZnTe}_{0.972}\text{Se}_{0.028}$  buffer was grown completely pseudomorphic on a GaSb substrate, which is demonstrated by the corresponding full widths at half maximum (FWHM) of 150 arcsec and 60 arcsec, respectively, in the rocking curve. The corresponding relaxation states R are determined to 1% and 5%, respectively. A 180 nm HgSe layer grown on a 145 nm  $\text{ZnTe}_{1-x}\text{Se}_x$  buffer layer shows *pendellösung* thickness fringes indicating the high crystalline perfection of the structures, and has a FWHM of 84 arcsec with R near zero (0.05%). This value is to our knowledge one of the best reported so far. The properties of HgSe in dependence of the buffer layer will be discussed in detail.

The carrier concentration and the mobility are calculated from Shubnikov-de-Haas oscillations in high magnetic fields up to 12 Tesla. The best samples have a high mobility up to  $2.1 \times 10^6 \text{ cm}^2/\text{Vs}$  with a carrier concentration of  $1.0 \times 10^{17} \text{ cm}^{-3}$  at 4.2 K.

/1/ J. Ren, DB. Eason et al., J. Crystal Growth **138** (1994).

/2/ S. Einfeldt, H. Heinke et al., J. Crystal Growth **138** (1994) 471.

/3/ M. v. Ortenberg, Advance in Solid State Physics, **31** (1991) 261.

/4/ Th. Widmer, D. Schikora et al., Semicond. Sci. Technol. **10** (1995) 1264.

/5/ H. Wißmann, L. Parthier et al., 3rd European Symp. "X-Ray Topography and High Resolution Diffraction", Palermo, 22. - 24. April 1996.

\* Corresponding author, E-Mail: parthier@physik.hu-berlin.de



POSTER SESSION P3.

PATTERNED GROWTH, ANTIMONIDES, PHOSPHIDES, AND NITRIDES.

**P3.1 Fabrication and cathodoluminescence study of interacting 3D confined GaAs volumes and isolated GaAs quantum boxes prepared via one step *in-situ* MBE growth on non-planar patterned GaAs (001) substrates**, A. Konkar, H.T. Lin, D.H. Rich, P. Chen and A. Madhukar, University of Southern California, Los Angeles, California, USA

**P3.2 Manipulating InAs island sizes with chemical beam epitaxy growth on GaAs patterns**, Mark S. Miller, Søren Jeppesen, Anders Petersson, Ivan Maximov, Bernhard Kowalski, and Lars Samuelson  
Lund University, Sweden

**P3.3 High density GaAs/(GaAs)<sub>2</sub>(AlAs)<sub>2</sub> quantum wires naturally formed on (775)B-oriented GaAs substrate by MBE**, M. Higashiwaki, M. Yamamoto, S. Shimomura, A. Adachi and S. Hiyamizu  
Osaka University, Japan

**P3.4 Vertically aligned self-assembled InGaAs quantum dots layers on (311)A/B and (100)GaAs substrates**, P.P. González-Borrero, D.I. Lubyshev, E. Marega Jr., and P. Basmaji  
Instituto de Física de São Carlos-Universidade de São Paulo, Brazil

**P3.5 The use of Si as p-type dopant in Al<sub>0.33</sub>Ga<sub>0.67</sub>As grown by molecular beam epitaxy on (111)A, (211)A and (311)A GaAs surfaces**, M. Henini, N. Galbiati, E. Grilli, M. Guzzi, and L. Pavesi  
University of Nottingham, United Kingdom

**P3.6 Patterned growth on GaAs (311)A substrates**, Richard Nötzel, Johann Menniger, Manfred Ramsteiner, Achim Trampert, Hans-Peter Schönherr, Lutz Däweritz, and Klaus H. Ploog  
Paul-Drude-Institut für Festkörperelektronik, Berlin, Germany

**P3.7 Selective area MOMBE etching of III-V semiconductors using TDMAAs and TDMASb**, K. Yamamoto, H. Asahi, T. Hayashi, K. Hidaka and S. Gonda, Osaka University, Japan

**P3.8 Photoluminescence spectra of shadow masked multiple quantum wells**, S. Sopitpan, P. Cheewatas, S. Thainoi, S. Rattanathamman, and S. Panyakeow, Chulalongkorn University, Bangkok, Thailand

**P3.9 Indium antimonide doped with manganese grown by molecular beam epitaxy**, D. L. Partin, J. Heremans, C.M. Thrush, General Motors Research and Development Center, Warren, Michigan, USA

**P3.10 Molecular beam epitaxial growth of high electron mobility InAs/AlGaAsSb deep quantum well structures**, Naohiro Kuze, Hiromasa Goto, Masahiro Matsui, Ichiro Shibasaki, Hiroyuki Sakaki  
Asahi Chemical Industry Co. Ltd., Shizuoka, Japan

**P3.11 MBE growth and characterization of high quality strained InGaAsSb/AlGaAsSb quantum well structures**, A. Z. Li, Y.L. Zheng, Y. Zhao, G. T. Cheng and W. Z. Shen, Chinese Academy of Sciences, Shanghai

**P3.12 MBE growth of GaInAsSb p/n junction diodes for thermophotovoltaic applications**, Parvez N. Uppal, Greg Charache, Paul Baldasaro, Brian Campbell, Stefan Svensson, David Gill  
Lockheed Martin Sanders, Nashua, New Hampshire, USA

**P3.13 Molecular beam epitaxial growth of Ga<sub>1-x</sub>In<sub>x</sub>Sb on GaAs substrates**, J.H. Roslund, O. Zsebök, G. Swenson and T.G. Andersson, Chalmers University of Technology and Göteborg University, Gothenburg, Sweden

**P3.14 *In-Situ* STM study of GaSb and AlSb (001) surface reconstructions**, P.M. Thibado, B.R. Bennett, B.V. Shanabrook and L.J. Whitman, Naval Research Laboratory, Washington, DC, USA

**P3.15 Stranski-Krastanov growth of InSb and GaSb on GaAs: structure of the wetting layers**, B.R. Bennett, B.V. Shanabrook, P.M. Thibado, L.J. Whitman, and R. Magno  
Naval Research Laboratory, Washington D.C., USA

**P3.16 Zinc blende structure GaN grown by radio frequency plasma assisted molecular beam epitaxy,** J.W. Han, H.D. Cho, K.S. Eom, C.B. Kim, N.H. Ko, S.H. Park, T.W. Kang, C.H. Hong, D.H. Kim, Sejong University, Seoul, Korea

**P3.18 Initial growth stage of GaN on Si substrate by alternating source supply using dimethylhydrazine,** Akihiro Hashimoto, Yoshitaka Aiba, Takanori Motizuki, Mitugu Ohkubo and Akio Yamamoto, Fukui University, Japan

**P3.19 Relation between surface reconstruction transitions and growth kinetics of zincblende (001) GaN,** Oliver Brandt, Hui Yang Akira Yamada, and Klaus H. Ploog, Paul-Drude-Institut für Festkörperelektronik, Berlin, Germany

**P3.20 Surface crystal-structure of a GaN film as an in-situ mask using MOMBE,** Seikoh Yoshida and Masahiro Sasaki, Optoelectro. Technolo. Research Laboratory, Ibaraki, Japan

**P3.21 DC-plasma source for nitrogen activation in MBE of GaN,** G.D. Kipshidze, S.V. Drozdov, V.B. Lebedev, S.V. Novikov, L.V. Sharonova, A. Ya. Shik, V.N. Jmerik, V.M. Kuznetsov, A.V. Andrianov, A.M. Gurevich, N.N. Zinov'ev, C. T. Foxon, and T.S. Cheng, Ioffe Physical-Technical Institute, St. Petersburg, Russia

**P3.22 Gas source molecular beam epitaxy of cubic GaN/GaAs (001) using hydrazine,** S.A. Nikishin, G.A. Seryogin and H. Temkin, Colorado State University, Ft. Collins, Colorado, USA

**P3.23 Cathodoluminescence of GaN films grown under Ga and N rich conditions by radio frequency-molecular beam epitaxy,** Sung Hwan Cho, Uitsu Tanaka, Takahiro Maruyama, Katsuhiro Akimoto, Hajime Okumura and Sadufumi Yoshida, University of Tsukuba, Ibaraki, Japan

**P3.24 Radiative decay in type-II GaP/AlP/GaP quantum wells,** S. Nagao, T. Fujimori, H. Gotoh, H. Fukushima, T. Takano, S. Koshihara, F. Minami, Mitsubishi Chemical Corporation, Ibaraki, Japan

**P3.25 Growth of epitaxial dysprosium phosphide/gallium arsenide heterostructures by MBE,** R.J. Hwu, L.P. Sadwick, P.P. Lee, M. Patel, H. Balasubramaniam, M. Nikols, P.C. Taylor, J. Viner, R.T. Lareau, and D.C. Streit, University of Utah, Salt Lake City, Utah, USA

**P3.26 CBE growth of InP, GaP, and GaInP using uncracked tertiarybutylbisdimethylaminophosphine - implications for conventional MBE,** L.P. Sadwick, and G.B. Stringfellow, and H.H. Ryu, T. Groshens, R.W. Gedridge Jr., R. T. Lareau, The University of Utah, Salt Lake City, Utah, USA

**P3.27 Real-time investigation of In surface segregation during chemical beam epitaxy of  $\text{In}_x\text{Ga}_{1-x}\text{P/GaAs}$  and  $\text{In}_x\text{Ga}_{1-x}\text{As/GaAs}$  heterostructures,** M. Mesrine, J. Massies, C. Deparis, N. Grandjean and E. Vanelle, Centre de Recherche sur l'Hétéro-Epitaxie et ses Applications, Valbonne, France

**P3.28 Molecular beam epitaxy of strain-compensated InGaAs/GaAsP quantum-well intersubband photodetectors,** K. Bacher and S. Massie, Quantum Epitaxial Designs, Inc. Bethlehem, Pennsylvania, USA

**P3.29 Self-organized quantum dot structures in strained  $(\text{GaP})_n(\text{InP})_m$  short period superlattices grown on GaAs (N11) by gas-source MBE,** S.J. Kim, H. Asahi, M. Takemoto, K. Asami and S. Gonda, Osaka University, Japan

**P3.30 Studies of thin GaN layers grown on sapphire using an RF-source,** T.G. Anderson, NTT Basic Research Laboratories, Atsugi-shi, Kanagawa 243-1, Japan.

**Fabrication and cathodoluminescence study of interacting 3D confined GaAs volumes and isolated GaAs quantum boxes prepared via one step *in-situ* MBE growth on non-planar patterned GaAs (001) substrates.**

A. Konkar, H.T. Lin, D.H. Rich, P. Chen, and A. Madhukar  
*Photonics Materials and Devices Laboratory, Department of Materials Science and Engineering, University of Southern California, Los Angeles, CA 90089-0241*  
Phone #: (213) 740 4325; Fax #: (213) 740 4333; email: madhukar@mizar.usc.edu

Fabrication of *three-dimensionally* quantum confined structures (i.e. quantum boxes) via purely growth controlled techniques is an attractive alternative to post-growth lithographic approaches as the latter are accompanied by potential damage and contamination. We report here the first time-resolved cathodoluminescence (CL) studies of carrier relaxation in three-dimensionally confined GaAs/AlGaAs volumes created via growth on non-planar patterned substrates utilizing the technique of substrate-encoded size-reducing epitaxy (SESRE) [1]. We have fabricated (i) interacting 3D confined GaAs volumes and 1D confined GaAs quantum wells (QW), and (ii) isolated GaAs QBs, both on the tops of <100> oriented square mesas on GaAs(001). The fabrication of isolated QBs via SESRE is a especially demanding task since the highly nonlinear nature of the intra- and inter-facet adatom migration lengths as a function of shrinking mesa size demands that precise amounts of the barrier and the well materials be deposited at exactly the correct stage of growth to form the desired QB. CL studies, time-resolved and under steady-state excitation, were carried out on the above mentioned structures to gain an understanding of the kinetics of carrier transport in these nanostructures.

For case (i), we grew structures containing 3D confined GaAs volumes with lateral dimensions  $\leq 1000$  Å and thicknesses of  $\sim (30 \text{ to } 100)$  Å on the (001) mesa tops and GaAs QWs with thicknesses of  $\sim (10 \text{ to } 40)$  Å on the {101} type sidewalls surrounding the (001) mesa top. Both, the mesa top 3D confined GaAs volumes and sidewall QWs, are separated by  $\sim (20 \text{ to } 100)$  Å thick AlGaAs barriers. Results from CL studies on one such mesa are shown in figs. 1 and 2. Figure 1 shows area-averaged CL spectrum from a region of  $1 \mu\text{m} \times 1 \mu\text{m}$  centered around the mesa top. Three strong identifiable peaks marked p1 (788 nm), p2 (798 nm) and p3 (806 nm) are observed. CL images taken at various wavelengths indicate that the emissions between 798 to 814 nm are localized to a region around the mesa top whereas emissions below 798 nm are predominantly from the sidewall region. Figure 2 shows results from *time-resolved* CL spectra from the same mesa. Significant carrier transfer from the thin GaAs QWs grown on the {101} sidewalls to the thicker 3D confined GaAs volumes on the (001) mesa top region is evidenced by the decrease in the p1 peak intensity and increase in the p3 intensity with time, for both, the onset (O1 to O6) and the decay (D1 to D5) time windows. The various channels through which such carrier transfer occurs will be discussed.

For case (ii), we have fabricated the isolated 3D confined GaAs volumes with varying dimensions: lateral size  $\sim 10$  nm to  $\sim 100$  nm and thickness of  $\sim 2$  nm to  $\sim 10$  nm. Shown in fig. 3 is a transmission electron microscope (TEM) image of one such isolated 3D confined GaAs volume surrounded by AlGaAs. The lateral size of the GaAs volume in this case is  $\sim 11$  nm and the height is  $\sim 2$  nm, well within the quantum confinement regime. Note the negligible GaAs growth on the {101} sidewalls resulting in good lateral confinement. Results from both steady-state excitation and time-resolved CL studies will be presented for such isolated GaAs quantum boxes.

This work was supported by ARO, ONR, AFOSR, and NSF (RIA-ECS).

References:

1. A. Konkar, K.C. Rajkumar, Q. Xie, P. Chen, A. Madhukar, H.T. Lin, and D.H. Rich, *J. Cryst. Growth* **150**, 311 (1995).

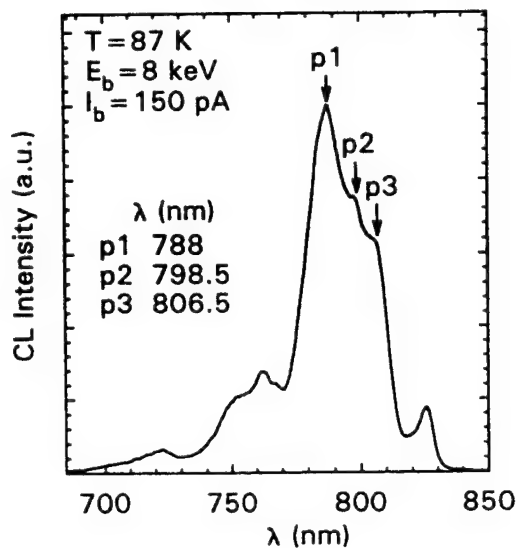


Fig. 1 Constant excitation area- averaged CL spectra from a  $1\mu\text{m} \times 1\mu\text{m}$  region centered around the mesa top.

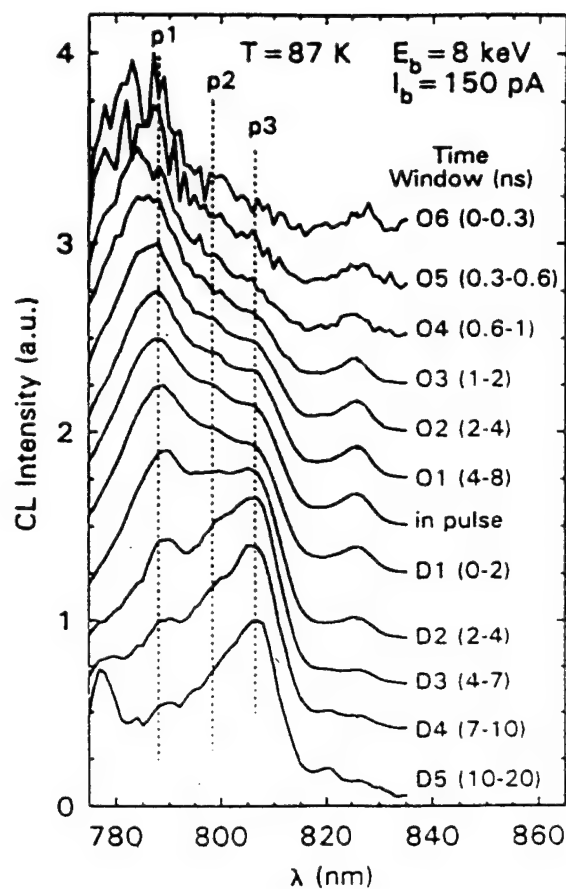


Fig. 2 Time delayed CL spectra with various onset (Oi) and decay (Di) time windows. All spectra are normalized to have about the same maximum peak height. Peak positions p1 - p3, corresponding to values determined from fig. 1 are indicated by the vertical dashed lines.

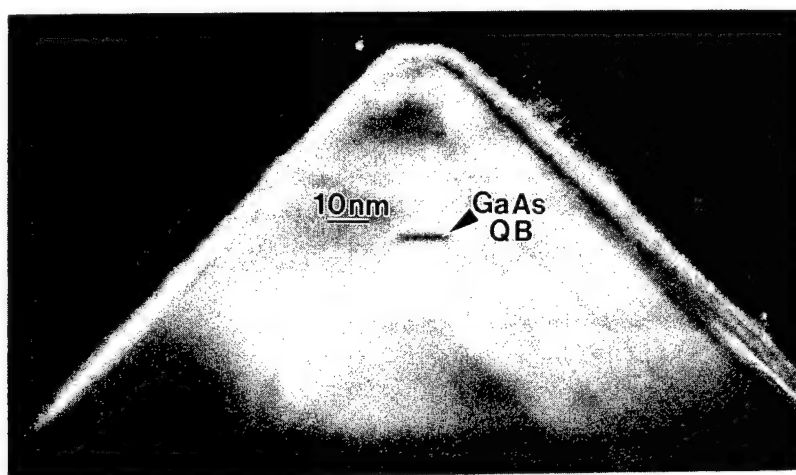


Fig. 3 (002) dark field TEM image of the mesa top showing isolated GaAs quantum box.

# Manipulating InAs island sizes with chemical beam epitaxy growth on GaAs patterns

Mark S. Miller, Søren Jeppesen, Anders Petersson, Ivan Maximov,  
Bernhard Kowalski, and Lars Samuelson

*Department of Solid State Physics, Lund University, 221 00 Lund, Sweden.*

Small InAs pyramids can form without dislocations during the initial stages of InAs growth on GaAs. The deep conduction-band potential-well of a pyramid in GaAs can contain only a single bound state [1]. The pyramids thus are excellent candidates for electronic-structure building-blocks if this bound state can be manipulated by manipulating the size, shape, or composition. The as-deposited islands are characterized by a distribution about a specific size, which is reflected in the electronic structure. For example, the PL peak energy can vary from 1.1 to 1.4 eV and the PL peak widths range from 30 to 100 meV [2]. While both peak energy and width can be varied, a given set of growth conditions determines the distribution parameters.

We have previously reported the selective placement and alignment of InAs islands in pattern features on GaAs substrates [3]. Strings of islands several  $\mu\text{m}$  long were assembled with a minimum center to center distance of 33 nm. Depositions on a fields of etched and overgrown holes showed the possibility of placing one or more islands in each hole. When capped with GaAs the islands in the patterns had the characteristic pyramid luminescence energies.

We demonstrate here the manipulation of island electronic structure by chemical beam epitaxy growth on patterned GaAs substrates. Specifically, we found that the luminescence energy changes with the pattern shape and orientation for a given set of growth conditions. For example, we deposited and capped islands on patterns consisting of concentric circular trenches. We then characterized the islands with cathodoluminescence, imaging the island luminescence at a particular energies. The images show that at different orientations along the circular arcs, the islands have different luminescence energies and, presumably, different sizes. We have also taken atomic force microscope images of uncapped islands on circles and correlated the island densities and alignments with the luminescence found around the circles.

- 
- [1] M. Grundmann, O. Stier, and D. Bimberg, *Phys. Rev. B* **52**, (1995).
  - [2] J. M. Gérard, in *Confined Electrons and Photons New Physics and Applications* E. Burnstein and C. Weisbuch, Eds. (Plenum Press, New York and London 1995) pp. 357.
  - [3] S. Jeppesen, M. Miller, D. Hessman, B. Kowalski, I. Maximov, and L. Samuelson, *Appl. Phys. Lett.* in press, 15 April (1996).

## AFM of InAs pyramids in GaAs trenches

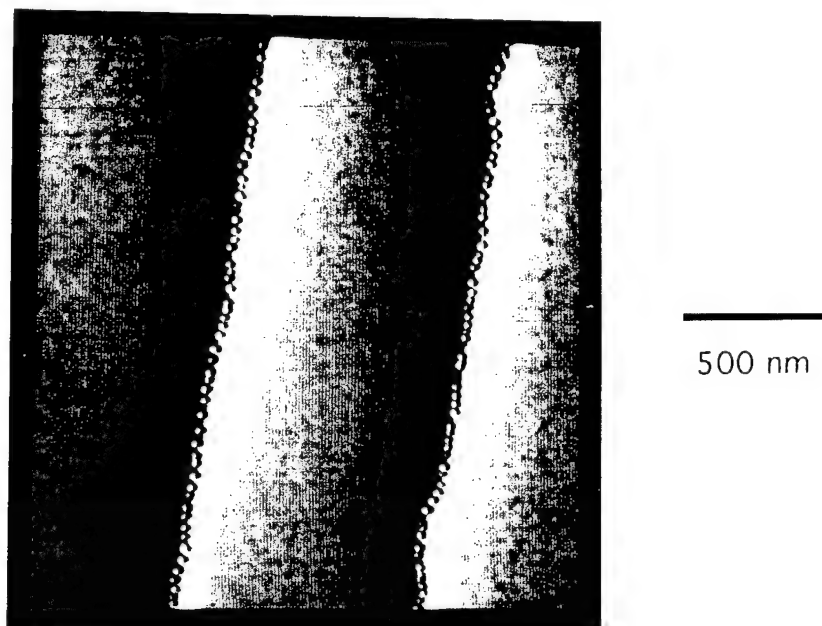


**Figure 1.** AFM image of InAs islands in GaAs trench running parallel to [110]. The trenches are 160 nm broad and 10 nm deep. In this "shaded" image, illumination from the left is simulated.

## Cathodoluminescence imaging of capped InAs pyramids in circular GaAs trenches

58A1-3.BLD 1.3684 eV 1mV

58A1-4.BLD 1.4317 eV 5mV

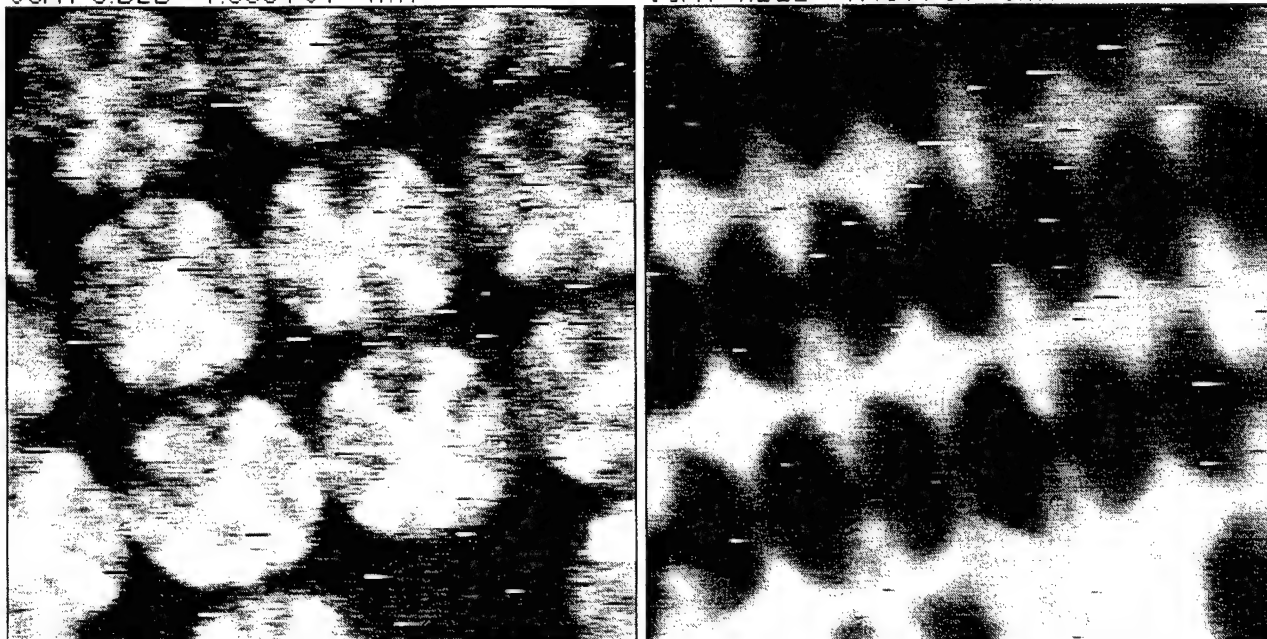


**Figure 2.** Cathodoluminescence images of InAs islands in concentric GaAs trenches. The outer diameter of each set of 6 concentric circles is 12  $\mu\text{m}$ . The image at left is taken with island luminescence at an energy of 1.37 eV. Note the preferred angles for islands at this energy. Other energies have other angles. The image at right is taken with wetting layer luminescence at 1.43 eV.

# High density GaAs/(GaAs)<sub>2</sub>(AlAs)<sub>2</sub> quantum wires naturally formed on (775)B-oriented GaAs substrate by MBE

M. Higashiwaki<sup>1</sup>, M. Yamamoto<sup>1</sup>, S. Shimomura<sup>1</sup>, A. Adachi<sup>2</sup> and S. Hiyamizu<sup>1</sup>

<sup>1</sup>*Faculty of Engineering Science, Osaka University, Toyonaka, Osaka 560, Japan*

<sup>2</sup>*Nissin Electric Co. Ltd., Umezu-takase-cho, Ukyo-ku, Kyoto 615, Japan*

Phone: +81-6-850-6457, Fax: +81-6-845-4632, E-mail: higashi@d310.mp.es.osaka-u.ac.jp

QWR structures have very interesting properties from view points of new physical phenomena and device application. We have reported that GaAs/AlAs QWRs are formed in a GaAs/AlAs quantum well (QW) with a regularly corrugated AlAs on GaAs interface and a flat GaAs on AlAs interface grown on (775)B-oriented GaAs substrates by MBE (Fig. 1).<sup>1)</sup> Lateral period and vertical amplitude of the interface corrugation were 12 nm and 1.2 nm, respectively. Photoluminescence (PL) from the GaAs/AlAs QW with well width  $L_w = 3.3$  nm (QWRs) showed polarization anisotropy  $\{P = (I_{||} - I_{\perp}) / (I_{||} + I_{\perp})\}$  of 0.11 at 4.2 K<sup>1)</sup>. If the GaAs well layer becomes thinner, lateral confinement of carriers by the interface corrugation becomes more effective. In the GaAs/AlAs QW system, however,  $L_w$  is limited to about 3 nm because of the *X-point* of an AlAs barrier layer. In order to avoid this problem, we used (GaAs)<sub>2</sub>(AlAs)<sub>2</sub> barrier to make a narrower QWs. In this paper, we report QWRs formed in a GaAs/(GaAs)<sub>2</sub>(AlAs)<sub>2</sub> QWs with a reduced well width of  $L_w = 2.1$  nm on a (775)B GaAs substrate, which show much improved polarization anisotropy  $P = 0.21$ . This value is almost comparable with the highest polarization anisotropy reported for QWRs. Furthermore, density of the QWRs on (775)B substrate is  $8 \times 10^5$  QWRs/cm, which is the highest ever obtained.

The GaAs/(GaAs)<sub>2</sub>(AlAs)<sub>2</sub> QWs structure with corrugated interfaces was grown on a (775)B GaAs substrate (Fig. 2). A buffer layer, barrier layers, and a GaAs cap layer were grown at  $T_s = 580^\circ\text{C}$ , and GaAs well layers with well widths of  $L_w = 2.1, 3.0, 4.2, 6.6, 12$  nm were grown at  $T_s = 640^\circ\text{C}$ . Because the surface corrugation of GaAs layer on (775)B substrate is observed at  $T_s = 640^\circ\text{C}$ , and is not observed at  $T_s = 580^\circ\text{C}$ . V/III pressure ratio was 7 (11.2) for GaAs (AlAs), and growth rates were 1  $\mu\text{m/h}$  for both GaAs and AlAs layers.

Polarized PL spectra (14 K) from the GaAs/(GaAs)<sub>2</sub>(AlAs)<sub>2</sub> QWs (QWRs) is shown in Fig. 3. With decreasing  $L_w$  from 12 nm to 2.1 nm, the polarization anisotropy  $P$  of PL monotonously increases from 0.01 to 0.21. The value of  $P = 0.21$  is about 2-times larger than that (0.11) from the previous GaAs/AlAs QWRs. This result indicates that the one-dimensional confinement of carriers is much enhanced by reducing the thickness of a GaAs well in GaAs/(GaAs)<sub>2</sub>(AlAs)<sub>2</sub> QWs on (775)B GaAs substrate. Full-width-at-half-maximum of PL peak from the QWRs is 30 meV.

## Reference

- 1) M. Higashiwaki et al., to be published in Jpn. J. Appl. Phys. (1996).



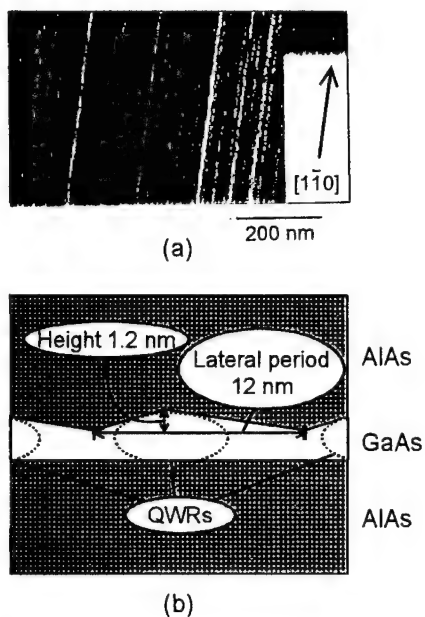


Fig. 1 : (a) AFM image of a GaAs surface of GaAs/AIAs QWRs grown on (775)B GaAs substrate.  
(b) Schematic illustration of the QWRs of the  $(\bar{1}10)$  cross-section.

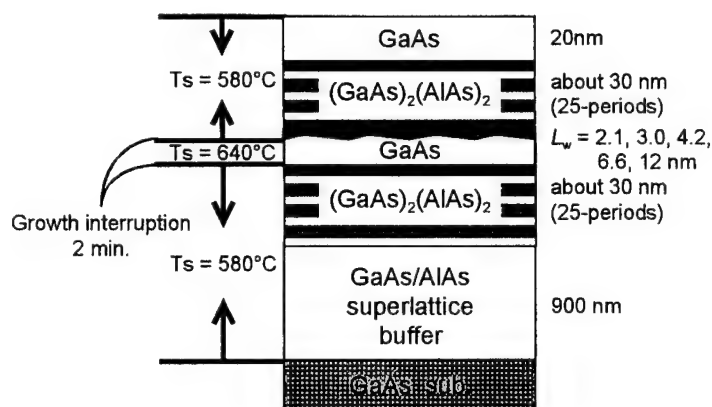


Fig. 2 : GaAs/(GaAs)<sub>2</sub>(AlAs)<sub>2</sub> QWRs (QWRs) structure grown on (775)B GaAs substrate.

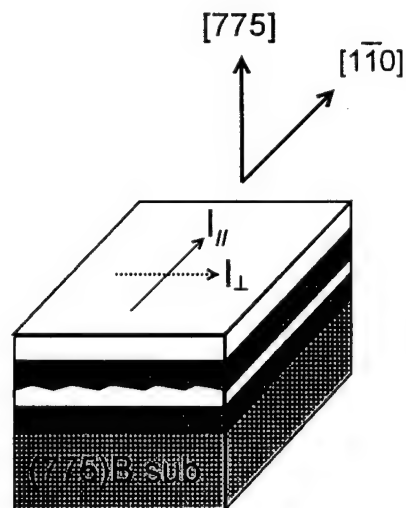
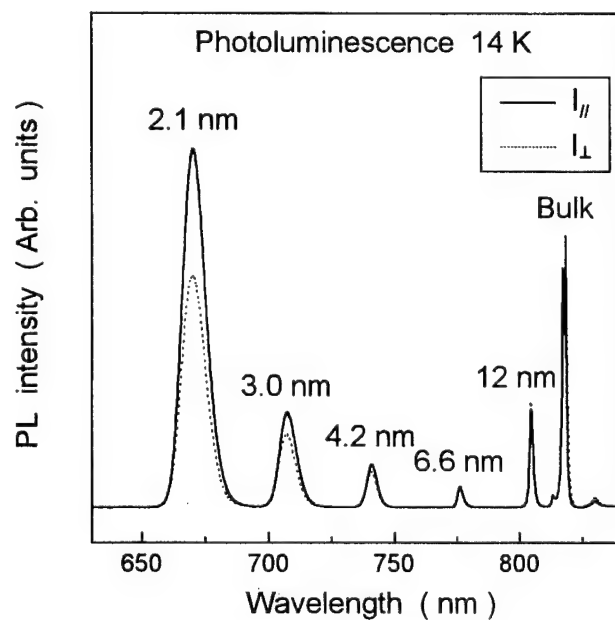


Fig. 3 : Polarized PL spectra from GaAs/(GaAs)<sub>2</sub>(AlAs)<sub>2</sub> QWRs grown on (775)B GaAs substrate.



# **Vertically Aligned Self-assembled InGaAs Quantum Dots Layers on (311)A/B and (100) GaAs Substrates**

P.P. González-Borrero, D.I. Lubyshev, E. Marega Jr., and P. Basmaji

Instituto de Física de São Carlos-Universidade de São Paulo  
CP 369, CEP 13560-970, São Carlos, SP, Brazil

Vertically self-organized growth of InAs islands separated by GaAs spacer layer has been reported in molecular-beam epitaxy (MBE) on (100) GaAs substrates<sup>1</sup>.

In this work, we present substrate orientation effects on optical properties of vertically stacking  $\text{In}_{0.5}\text{Ga}_{0.5}\text{As}$  layers grown by MBE on (311)A/B and reference (100) GaAs substrates mounted on the same substrate holder. The structure consists of a 80 nm GaAs/AlAs (2nm/2nm) superlattice grown at 600 °C, followed by a 0.5  $\mu\text{m}$  GaAs buffer layer. After that, the substrate temperature was lowered to 500 °C and 6 monolayers (ML) of  $\text{In}_{0.5}\text{Ga}_{0.5}\text{As}$  were deposited for (100) plane. Then, GaAs spacer layers were deposited at the same temperature. Growth interruption during 3 min. before and after  $\text{In}_{0.5}\text{Ga}_{0.5}\text{As}$  deposition, was carried out. In order to provide the vertical collinearity of the islands, this combination of 6 ML  $\text{In}_{0.5}\text{Ga}_{0.5}\text{As}$  and GaAs spacer layer was repeated 10 times. To complete the structure, a 50 nm GaAs cap layer was deposited. Samples were grown for different GaAs spacer thickness. The spacer thickness variation shows influence in PL spectra for all planes. Difference on peak shape, peak position, amplitude and integral luminescence has been observed for all surfaces. These differences suggest that the In migration on the spacer layer caused by the strain fields induced in the spacer layer by the islands buried below, is different in the three surfaces. Vertical electronic coupling between QD is confirmed by photoluminescence (PL) temperature dependence. Low temperature PL measurements indicate the presence of non-vertically aligned  $\text{In}_{0.5}\text{Ga}_{0.5}\text{As}$  QD principally on (311) surfaces.

## **Reference:**

1. Qianghua Xie et al., Phys. Rev. Lett. **75**, 2542 (1995)

(contact person: P. Basmaji, IFSC-USP, CP 369, São Carlos, SP, Brazil;

Fax: (55) (16) -(2723616) or -(2749206); e-mail: Pierre@ifqsc.sc.usp.br)

**The Use of Si as p-Type Dopant in  $\text{Al}_{0.33}\text{Ga}_{0.67}\text{As}$   
Grown by Molecular Beam Epitaxy  
on (111)A, (211)A and (311)A GaAs Surfaces**

M.HENINI<sup>@</sup>, N.GALBIATI<sup>\*</sup>, E.GRILLI<sup>\*</sup>, M.GUZZI<sup>\*</sup>, and L.PAVESI<sup>#</sup>

<sup>@</sup>Department of Physics, University of Nottingham, Nottingham NG7 2RD, UK.

<sup>\*</sup>Department of Physics, University of Milan, Via Celoria 16, I-20133 Milan, Italy.

<sup>#</sup>Department of Physics, University of Trento, Via Sommarive 14, I-38050 Povo, Italy

**Abstract:** The possibility of exploiting in device manufacturing the amphoteric character of the Si impurity in GaAs by simply using different planes has recently attracted great interest. It has been demonstrated that under identical growth conditions Si incorporates preferentially as a donor for growth on (N11)B and as an acceptor on (N11)A surfaces (N=1,2,3). However, Si is mainly a donor when the growth is on the conventional (100) plane. Here, a systematic study of Si-doped  $\text{Al}_{0.33}\text{Ga}_{0.67}\text{As}$  grown on (111)A, (211)A, and (311)A GaAs surfaces by molecular beam epitaxy is reported. The conditions in which the samples have been grown are optimal for the (311)A planes which are also similar to those of (100). This choice was made in view of devices grown on patterned substrates in which the n-doped AlGaAs is grown on the (100) substrate orientation. Thus the attention has been devoted to the surface orientations that give a p-type doping.

The samples were grown simultaneously under the same conditions so as to render them comparable. The substrates temperature was 630°C, the growth rate 1.5  $\mu\text{m}/\text{hour}$ , and the  $\text{As}_4$  beam equivalent pressure  $1.2 \times 10^{-5}$  Torr. Both electrical and photoluminescence measurements have been carried out to investigate the physics of the Si incorporation. All the samples, studied for different Si concentrations, display p-type conductivity indicating that Si incorporates predominantly in the As sites. We found that the (111)A surfaces incorporate less carbon than the (211)A and the (311)A ones which need a higher Si flux before the presence of Si clearly manifests itself in the electrical and optical measurements. The samples grown on the (111)A planes showed a lower optical and morphological quality; however, this does not affect markedly the values of the Hall mobility, the free carrier concentration and the photoluminescence efficiency. The (311)A samples show the higher optical quality with shallow impurities related optical transitions, while the (211)A samples present both crystalline defects and shallow impurities. The obtained results are explained by a kinetic growth model in which the single to double dangling bonds ratio present on the different surfaces plays an important role in determining the impurities incorporation.

Author to contact: Dr M.Henini

Tel/Fax: +44 (115) 951 5195/951 5180

e-mail: ppzmmh@ppn1.physics.nottingham.ac.uk

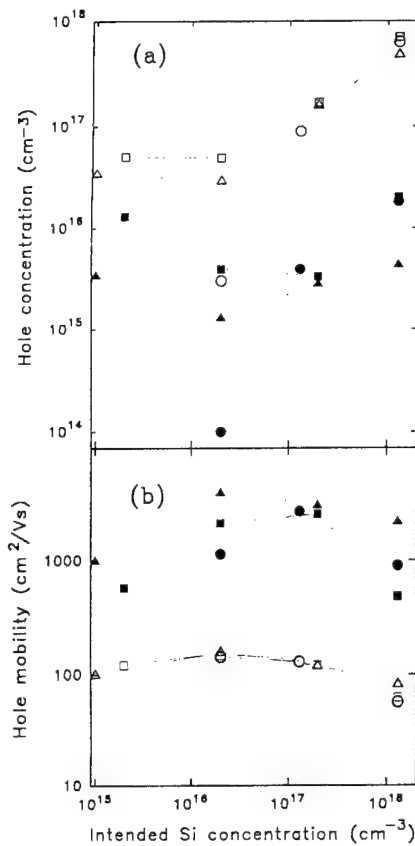


Fig. 1 - Free hole concentration (a) and hole mobility (b) as a function of the intended silicon concentration ( $N_i$ ) for (111)A (dots), (211)A (squares) and (311)A (triangles) samples. The filled and the open symbols refer to 77 K and 300 K data respectively. The (111)A sample with  $N_i = 1 \times 10^{15} \text{ cm}^{-3}$  is almost insulating, but still display a  $p$ -type conductivity. The lines through the data are only guide for the eyes.

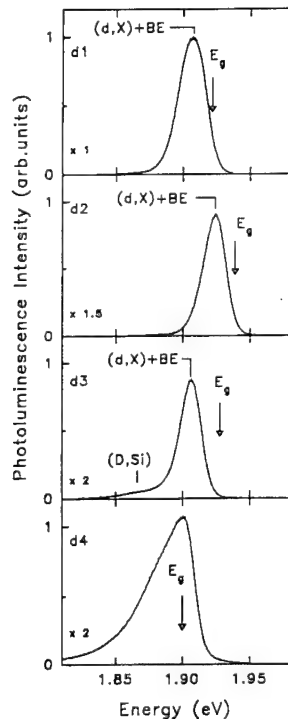


Fig. 3 - Photoluminescence spectra of the (211)A samples listed in Table I measured at 12 K. The PL was excited by the 488 nm laser line with a power density of  $20 \text{ W/cm}^2$ . The relative sensitivity factor is given on the left. The hollow arrows indicate the energy gap ( $E_g$ ) values. The labels on the spectra have the following meaning: BE, bound exciton; (d,X) defect bound exciton; (D,Si), donor to silicon acceptor pair transition.

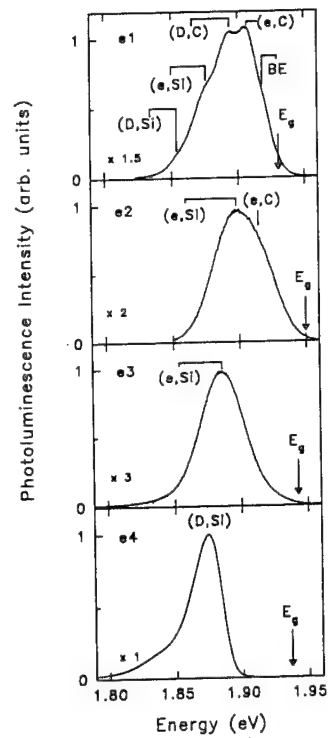


Fig. 2 - Photoluminescence spectra of the (311)A samples listed in Table I measured at 12 K. The PL was excited by the 488 nm laser line with a power density of  $20 \text{ W/cm}^2$ . The relative sensitivity factor is given on the left. The hollow arrows indicate the energy gap ( $E_g$ ) values. The labels on the spectra have the following meaning: BE, bound exciton; (e,C), free electron to carbon acceptor transition; (D,C), donor to carbon acceptor pair transition; (e,Si), free electron to silicon acceptor transition; (D,Si), donor to silicon acceptor pair transition.

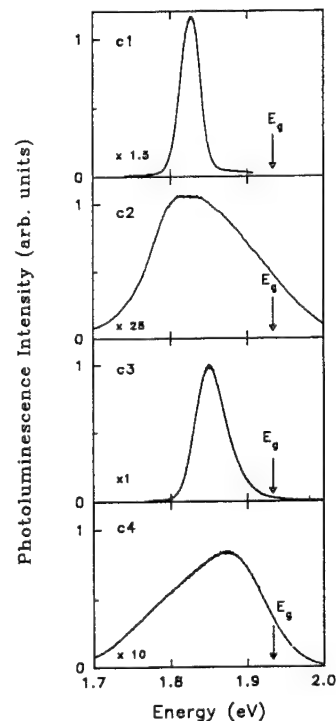


Fig. 4 - Photoluminescence spectra of the (111)A samples listed in Table I measured at 12 K. The PL was excited by the 488 nm laser line with a power density of  $20 \text{ W/cm}^2$ . The relative sensitivity factor is given on the left. The hollow arrows indicate the energy gap ( $E_g$ ) values (see text).

## Patterned Growth on GaAs (311)A Substrates

Richard Nötzel, Johann Menniger, Manfred Ramsteiner, Achim Trampert,  
Hans-Peter Schönherr, Lutz Däweritz, and Klaus H. Ploog

*Paul-Drude-Institut für Festkörperelektronik,  
Hausvogteiplatz 5-7, D-10117 Berlin, Germany*

*Tel.: +49 30 20377 523, Fax: +49 30 20377 201, e-mail: notzel@pdi.wias-berlin.de*

We investigate the MBE growth of  $\text{Al}_x\text{Ga}_{1-x}\text{As}$  on patterned GaAs (311)A substrates. As expected from the high crystallographic anisotropy of the (311) surface [1,2] the selectivity of growth qualitatively differs from that on the high-symmetry (100) and (111) planes (Fig. 1). This offers a new flexibility for the design of devices and quantum structures. The surface diffusion lengths of Ga atoms along the perpendicular [01-1] and [-233] directions are determined (Fig. 2). The conditions for obtaining smooth surface profiles are discussed.

For the mesa stripes oriented along [01-1] a fast growing facet close to a (3-1-1) plane is established after wet chemical etching. During growth a smooth convex curved surface profile develops enclosing thicker GaAs regions along the sidewall between thinner regions on the mesa top and bottom. The evolution of this unique surface profile due to the migration of Ga atoms from both sides toward the sidewall (opposite to the case of patterned GaAs (100) substrates) is investigated by TEM and CL. On the opposite side a slow growing (111) facet evolves. Only here roughening during growth is observed.

For mesa stripes oriented along [-233], two symmetric sidewalls close to {331} facets develop after wet etching. The growth rate on these facets is smaller compared to that on the mesa top and bottom resulting in surface profiles similar to those on patterned GaAs (100) substrates. However, no roughening of the growth front occurs.

The diffusion lengths of Ga atoms along [01-1] and [-233] are determined by AFM from the variation of the GaAs layer thickness close to the sidewalls of shallow square shaped mesas. The diffusion lengths are 0.3-0.5  $\mu\text{m}$  along [01-1] and 1-1.5  $\mu\text{m}$  along [-233]. Hence, smooth surface profiles are obtained for either a slow growing facet together with the larger diffusion length parallel to the edge or a fast growing sidewall with the larger diffusion length perpendicular to the step. This is essential for choosing the optimum pattern alignment on arbitrarily oriented substrates. The anisotropy of the diffusion length is, however, comparable to that on (100) surfaces. This suggests that the highly anisotropic microscopic surface corrugation along [-233] [1] additionally stabilizes the respective growth fronts on patterned GaAs (311)A substrates. Finally, the formation of the fast growing sidewall is applied to steps with heights down to 10 nm to produce very uniform quantum wire-like heterostructures.

[1] R. Nötzel, N. Ledentsov, L. Däweritz, M. Hohenstein, and K. Ploog, *Phys. Rev. Lett.* **67**, 3812 (1991).

[2] R. Nötzel, J. Temmyo, and T. Tamamura, *Nature* **369**, 131 (1994).

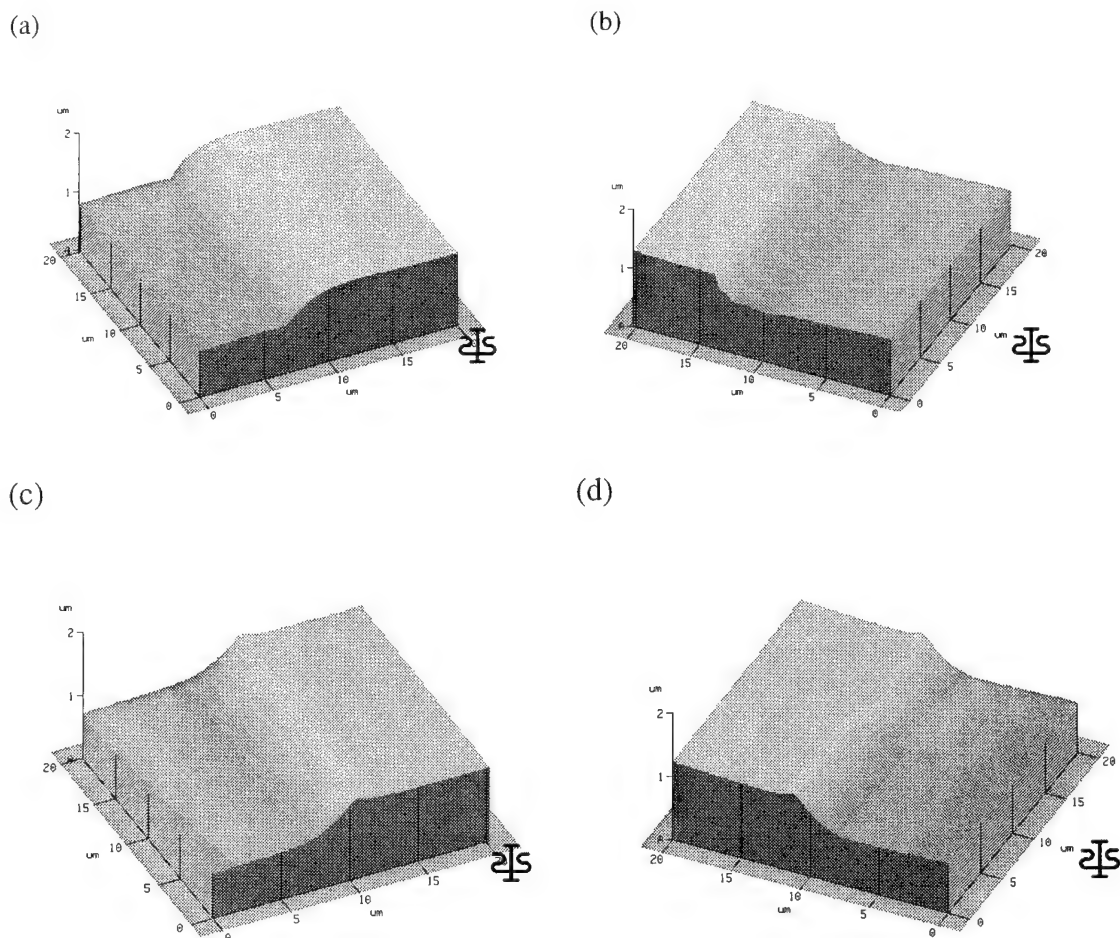


Fig. 1. AFM images of the edges of the 400 nm high steps along  $[01-1]$  (a) fast growing sidewall and (b) slow growing sidewall. (c), (d) AFM images of the steps along  $[-233]$ .

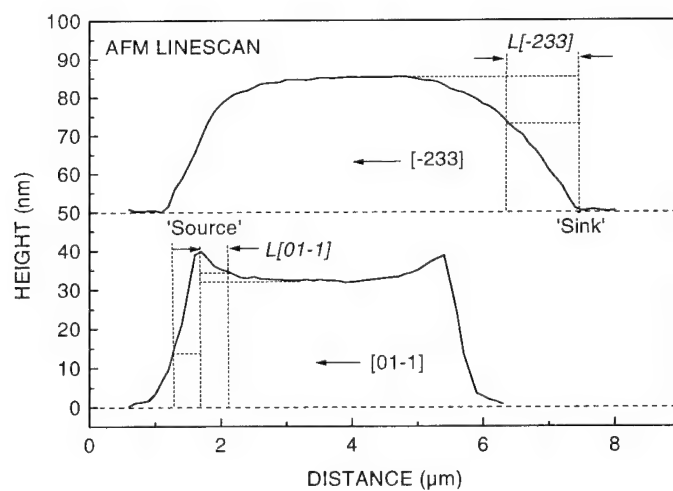


Fig. 2. AFM linescans across shallow square shaped mesas along  $[01-1]$  and  $[-233]$ .

## Selective Area MOMBE Etching of III-V semiconductors using TDMAAs and TDMASb

K. Yamamoto, H. Asahi, T. Hayashi, K. Hidaka and S. Gonda  
The Institute of Scientific and Industrial Research, Osaka University  
8-1, Mihogaoka, Ibaraki, Osaka 567, Japan  
Tel:+81-6-879-8406; Fax:+81-6-879-8509; e-mail:yama21@sanken.osaka-u.ac.jp

Selective area etching and regrowth in the same vacuum chamber are emerging as a very promising technique for fabricating nanoscale structures, since the optical and electrical properties are affected by contamination due to air exposure or surface residues. For this purpose, MOMBE is a useful method because both processes can be conducted in the same vacuum chamber. As precursor, trisdimethylaminoarsenic  $\{\text{As}[\text{N}(\text{CH}_3)_2]_3\}$ , was proved to be useful in the growth of arsenides [1]. Recently, we found that non-precracked TDMAAs etches GaAs [2] and the etching proceeds in the layer by layer mode [3]. Therefore, TDMAAs is a promising candidate for the precursor of etching in addition to the growth of GaAs.

In this paper, we investigate the MOMBE growth and etching of GaAs. Fig. 1 shows the dependence of growth and etching rates on TEGa flux. The periods of RHEED intensity oscillation by etching became long with the increase of TEGa flux below 0.2 SCCM. At more than 0.2 SCCM, the oscillation occurred again, indicating that the growth of GaAs exceeds the etching. After 2  $\mu\text{m}$  etching, the mirror-like surfaces were obtained especially at low  $T_{\text{sub}}$  (Fig.2) although the surface migration of group III is insufficient. This improvement of surface morphology at low  $T_{\text{sub}}$  may be due to the formation of many small vacancies or islands followed by the preferentially removing of these atoms by etching process[4].

Selective area etching using TDMAAs was performed on the partly  $\text{SiO}_2$  masked GaAs substrate. Fig. 3 shows the typical cross-sectional SEM photographs of the etched substrate with  $\text{SiO}_2$  stripe mask aligned along the  $[011]$  and  $[0\bar{1}1]$  directions. It was found that the etched shapes depended on both stripe mask orientation and  $T_{\text{sub}}$ , while they were almost independent of TDMAAs flow rate and of stripe window width. Under high  $T_{\text{sub}}$  region, vertical side walls were obtained for both directions. This results from the difference of etching rates on side walls, e.g. (111), (011) and (411), formed by etching. That is, the etching rates of (100), (411) and (111) became close with the increasing of  $T_{\text{sub}}$ , leading to the vertically etching.

In the conference, we will discuss the detailed relation between etching condition and etched shape. We also present the data on selective etching by using TDMASb.

- [1] C.R. Abernathy, P.W. Wisk, S.J. Pearton, F. Ren, D.A. Bohling and G.T. Muhr, J. Cryst. Growth 124 (1992) 64.
- [2] H. Asahi, X.F. Liu, K. Inoue, D. Marx, K. Asami, K. Miki and S. Gonda, J. Cryst. Growth 145 (1994) 668.
- [3] A.B. Villafior, H. Asahi, D. Marx, K. Miki, K. Yamamoto and S. Gonda, J. Cryst. Growth 150 (1995) 638.
- [4] T. Kaneko, P. Smilauer, B.A. Joyce, T. Kawamura and D.D. Vvedensky, Phys. Rev. Lett. 74 (1995) 3289.

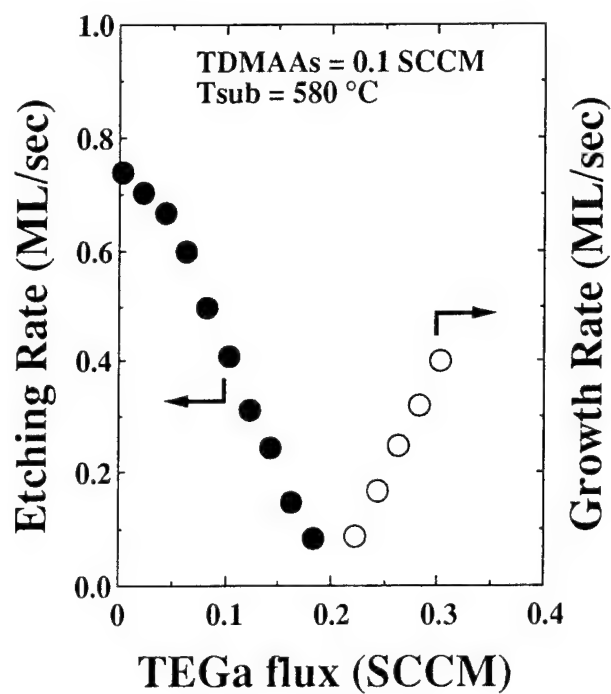


Fig. 1 Etching/Growth rates of GaAs as a function of TEGa flux.



Fig. 2 SEM photograph of GaAs surface etched by TDMAAs at  $T_{sub} = 450\text{ }^{\circ}\text{C}$

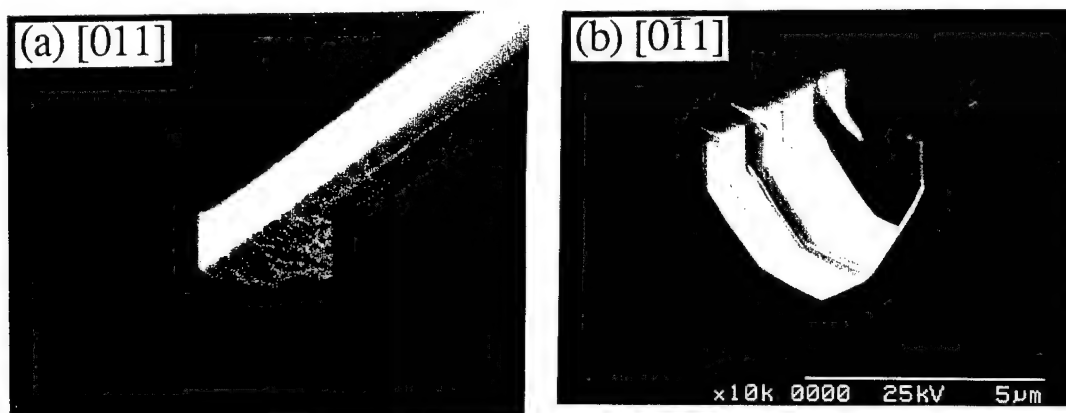


Fig. 3 Cross-sectional SEM view of GaAs etched by TDMAAs on partly  $\text{SiO}_2$  masked substrates with stripes aligned along the  $[011]$  and  $[0\bar{1}1]$  directions.

# Photoluminescence Spectra of Shadow Masked Multiple Quantum Wells

S. Sopitpan, P. Cheewatas, S. Thainoi, S. Rattanathammapan, and S. Panyakeow

Semiconductor Devices Research Laboratory,

Chulalongkorn University,

Bangkok 10330, Thailand

Tel. +66-2-218-6524

Fax +66-2-251-8991

email : fengdkg@chulkn.car.chula.ac.th

## Abstract

Lines of local epitaxy of GaAs/GaAlAs multiple quantum wells with linewidth of  $5\text{ }\mu\text{m}$  and line separation of  $250\text{ }\mu\text{m}$  were fabricated by Molecular Beam Epitaxy (MBE) using shadow mask technique. Photoluminescence measurement at 10 K was performed by using an argon laser with cylinder lens producing focussing line for the excitation. The focussed line of laser beam was  $\sim 100\text{ }\mu\text{m}$  and could be aligned to the stripes of MQW. The photoluminescence spectrum characteristics reflect the quantum well structure as well as the crystal quality of shadow masked epitaxial layers. The photoluminescence shows twin PL peaks at 756 and 773 nm with nearly equal intensity when the exciting beam lined parallel to the stripes of MQW. Similar result was obtained at perpendicular configuration but it shows better separation of the twin PL peaks. It is observed that each PL peak was strong and sharp comparable to those from conventional MQW samples. The spectral FWHM was 15 nm. This experimental data indicated that MBE grown MQW through shadow mask is feasible for further device fabrication.



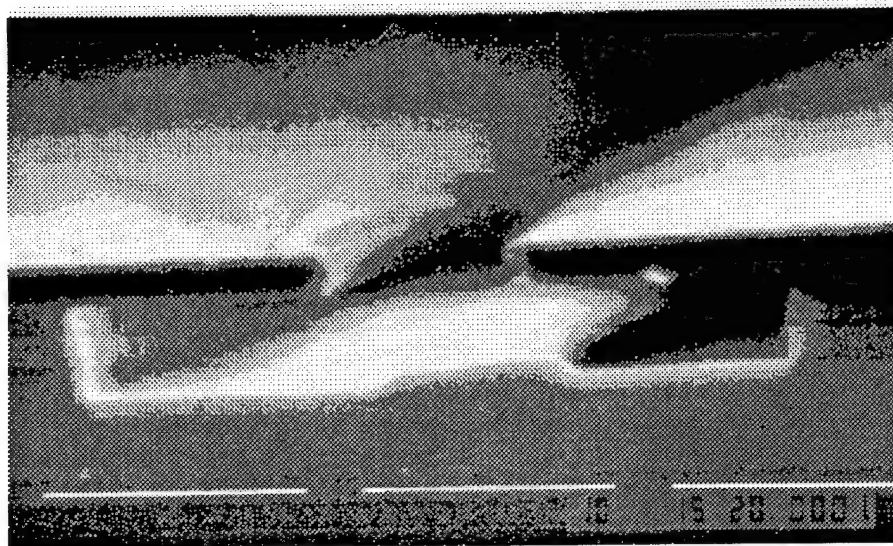


Fig.1 SEM of shadow masked MQW stripes

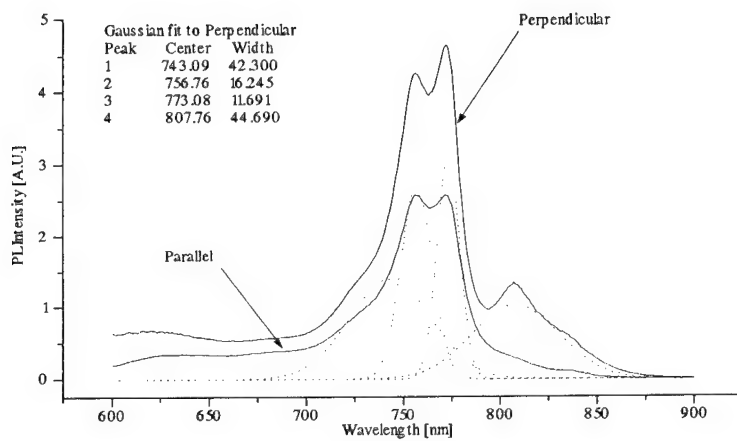


Fig.2 PL spectrum of MQW stripes

## **Indium Antimonide Doped with Manganese Grown by Molecular Beam Epitaxy**

**D.L. Partin, J. Heremans, C.M. Thrush**

**Physics and Physical Chemistry Department**

**General Motors Research & Development Center**

**Warren, MI 48090-9055**

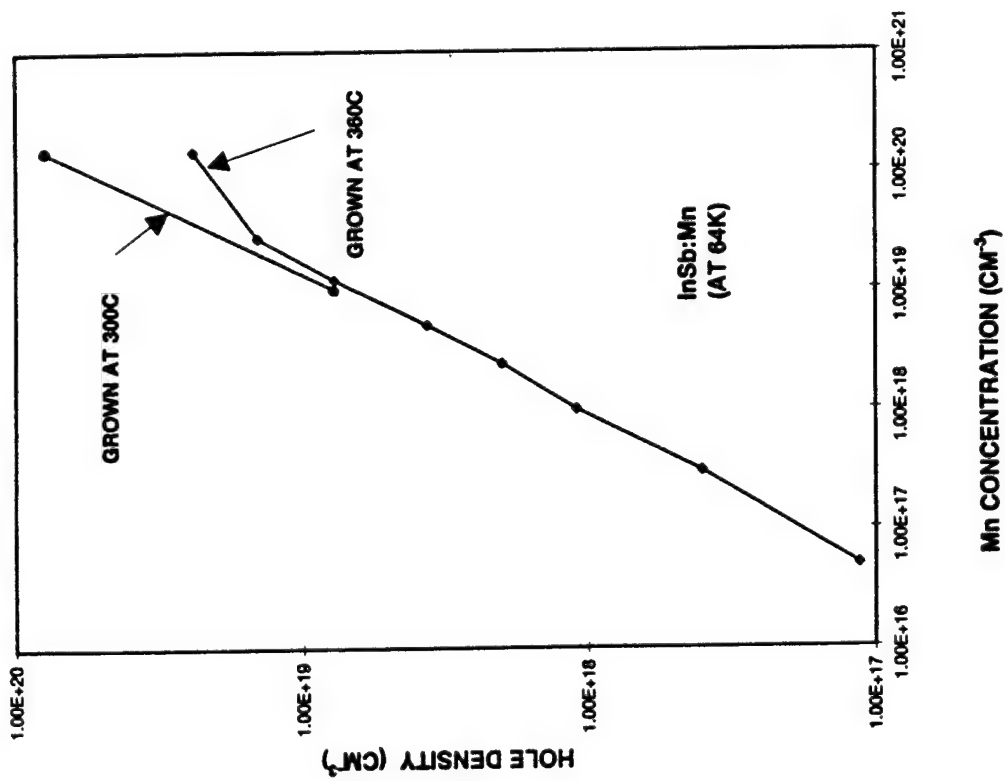
**PHONE: 810-986-0645, FAX:810-986-3091**

**E-MAIL: DPARTIN@CMSA.GMR.COM**

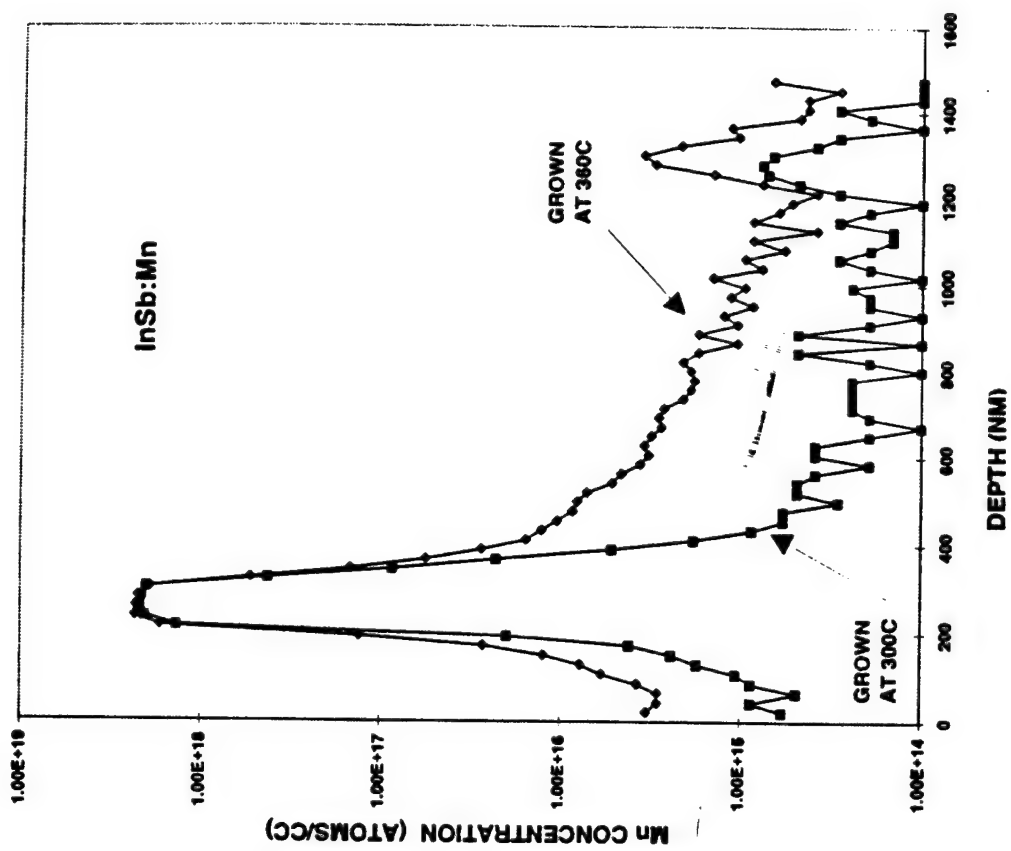
### **ABSTRACT**

Indium antimonide is of interest for infrared detecting and emitting devices and for magnetic field sensors. In this study, indium antimonide doped with manganese and grown by molecular beam epitaxy was investigated. For films grown at 360°C, the hole density at 64K is proportional to the manganese concentration to the power 0.80 up to  $N_{Mn} \approx 5 \times 10^{19} \text{ cm}^{-3}$ , above which saturation occurs. Reducing the growth temperature to 300°C improves dopant efficiency at manganese concentrations of  $\approx 10^{20} \text{ cm}^{-3}$ . Secondary Ion Mass Spectroscopy (SIMS) was used to show that the incorporation of manganese is proportional to the manganese flux during growth over a wide range of manganese concentrations. Auger electron spectroscopy studies showed that there is no substantial surface segregation. Heavily manganese doped samples exhibited a negative magnetoresistance at helium temperatures. Lightly manganese doped samples have transport dominated by electrons at temperatures below 35K due to hole freezeout and again by electrons at high temperatures due to intrinsic carriers. Additional SIMS studies showed that manganese diffusion is appreciable in indium antimonide at 360°C.

MANGANESE CONCENTRATION VS HOLE DENSITY



DEPTH PROFILE OF Mn VS GROWTH TEMPERATURE



# Molecular beam epitaxial growth of high electron mobility

## InAs/AlGaAsSb deep quantum well structures

Naohiro Kuze <sup>a,\*</sup>, Hiromasa Goto <sup>a</sup>, Masahiro Matsui <sup>a</sup>, Ichiro Shibasaki <sup>a</sup>, Hiroyuki Sakaki <sup>b</sup>

<sup>a</sup> Central Laboratory, Asahi Chemical Industry Co., Ltd., 2-1 Samejima, Fuji, Shizuoka, 416, Japan

Phone+81-545-62-3121 Fax+81-545-62-3089 \*email: a8212678@ut.asahi-kasei.co.jp

<sup>b</sup> RCAST, The University of Tokyo, 4-6-1 Komaba, Meguro, Tokyo, 153, Japan

We have investigated InAs deep quantum well structures (InAs DQWs) made from InAs/AlGaAsSb materials. This material system is of interest for its high electron mobility and large conduction band offset at the InAs/AlGaAsSb heterojunction. Bolognesi et al. [1] achieved high mobilities of 33000 cm<sup>2</sup>/Vs in the InAs/AlSb system, using a nucleation layer, buffer layers as thick as a few microns, smoothing superlattices and In-Sb like interface controls. However, the structure with AlSb layers are inadequate for reliable devices because AlSb is easily oxidized.

In our InAs DQWs, InAs layer is sandwiched between quaternary AlGaAsSb layer lattice-matched to InAs. InAs DQWs consist of four simple layers, including a submicron-thick AlGaAsSb buffer layer, as shown in Fig.1. During the growth of InAs DQWs, neither superlattices nor interface control are employed. We applied InAs DQWs to Hall sensors as a practical device and obtained good reliabilities [2]. In the present paper, we report that we have obtained high electron mobilities of more than 32000 cm<sup>2</sup>/Vs at room temperature by investigating the As<sub>4</sub>/Sb<sub>4</sub> beam-equivalent-pressure (BEP) ratio dependence of electrical and optical characteristics of InAs DQWs.

Fig.2 shows room temperature mobility for InAs/Al<sub>0.5</sub>Ga<sub>0.5</sub>AsSb DQWs as a function of As<sub>4</sub>/Sb<sub>4</sub> BEP ratio. We also observed good surface morphology of AlGaAsSb layer just before growing InAs layer by atomic force microscopy [3] and a strong photoluminescence (PL) peak ~ 1.2 eV of AlGaAsSb band-edge emission at 10K as shown in Fig.3. We determined optimum As<sub>4</sub>/Sb<sub>4</sub> BEP ratio of 6.5 for AlGaAsSb from the full width at half-maximum of PL peak (fig.4) and room temperature mobility results. InAs DQWs now routinely yield high electron mobility of more than 30000 cm<sup>2</sup>/Vs with sheet carrier densities of 1x10<sup>12</sup> cm<sup>-2</sup>.

**References** [1] C.R. Bolognesi, et al., J. Vac. Sci. Technol. B10 (1992) 877.

[2] N. Kuze, et al., J. Cryst. Growth 150 (1995) 1307.

[3] N. Kuze, et al., to be published in MRS Symp. Proc. D (Fall 1995).

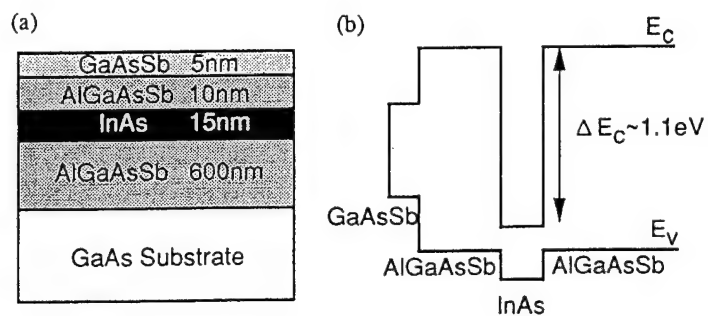


Fig. 1. (a) Schematic cross section and (b) energy band diagram of InAs/Al<sub>0.5</sub>Ga<sub>0.5</sub>AsSb DQWs.

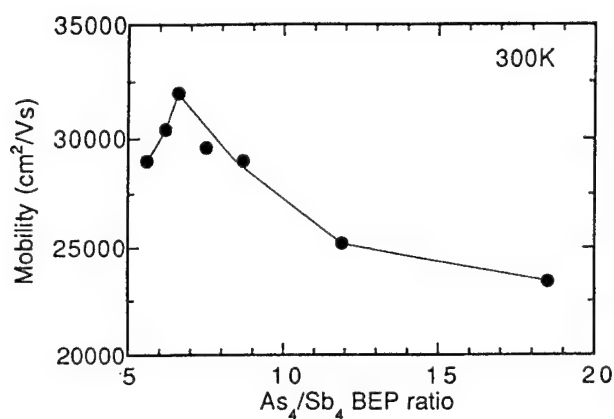


Fig. 2. Room temperature mobility for InAs DQWs as a function of As<sub>4</sub>/Sb<sub>4</sub> BEP ratio.

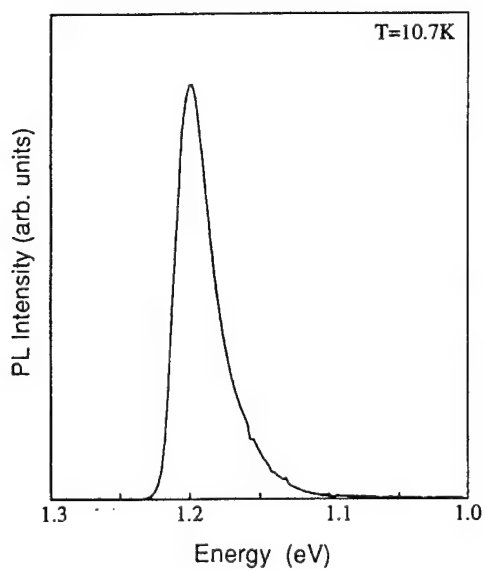


Fig. 3. Photoluminescence spectra of AlGaAsSb band-edge emission in InAs DQWs at 10.7K.

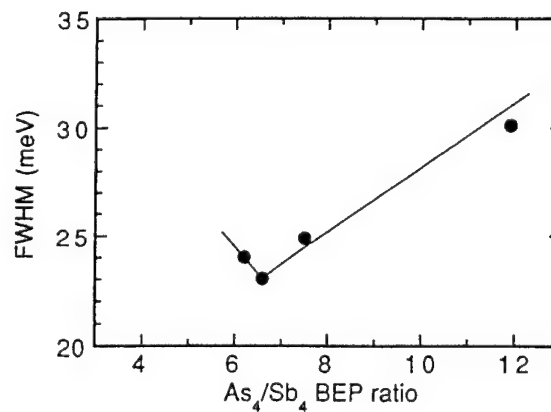


Fig. 4. The FWHM of the PL peak for AlGaAsSb as a function of As<sub>4</sub>/Sb<sub>4</sub> BEP ratio.

# **MBE Growth and Characterization of High Quality Strained InGaAsSb/AlGaAsSb Quantum Well Structures**

A. Z. Li, Y. L. Zheng, Y. Zhao, G. T. Cheng and W. Z. Shen

State Key Laboratory of Functional Materials for Informatics

Shanghai Institute of Metallurgy, Chinese Academy of Sciences, Shanghai 200050

Telephone: +86-21-62511070, FAX: +86-21-62513510, E-mail: azli@fudan.ihep.ac.cn

MBE growth and characterization of strained InGaAsSb/AlGaAsSb quantum wells on GaSb for basic study and 2 $\mu$ m mid infrared light source have been investigated. The optimization of MBE growth for antimony quaternary alloy quantum structures was studied and high quality of single and 20 periodic InGaAsSb/AlGaAsSb QWs on GaSb have been obtained. The MQW samples show FHMW as narrow as 9meV in photoluminescence spectra at 4K, several intersubband absorption peaks in low-temperature absorption measurement and -5 order satellites in double crystal X-ray rocking curve (DCXRC) and the SQW samples show the thermal ionization of exciton-phonon coupling, indicating a high quality MBE growth. Simulation on the DCXRC of the MQW structure was carried out fully first time to investigate the strain. The room-temperature lasing with stable low threshold current density ( $<900\text{A}/\text{cm}^2$ ) has been achieved by using InGaAsSb/AlGaAsSb MQWs as active layer and broad area stripe laser process.

\* Shanghai Institute of Optical and Fine Mechanics, Chinese Academy of Sciences

\*\* Shanghai Institute of Technical Physics, Chinese Academy of Sciences

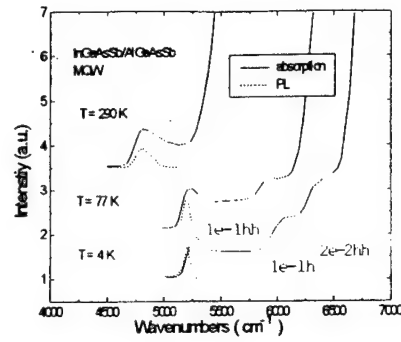


Fig 1. Infrared absorption and photoluminescence spectra of InGaAsSb/AlGaAsSb MQW at different temperature

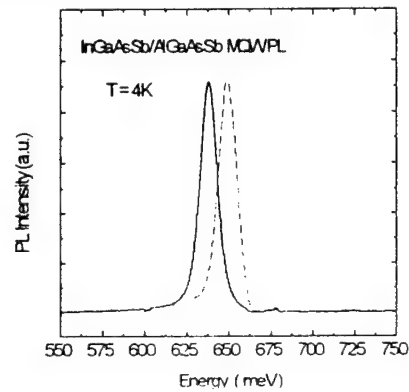


Fig 2. 4K photoluminescence spectra of InGaAsSb/AlGaAsSb MQW materials

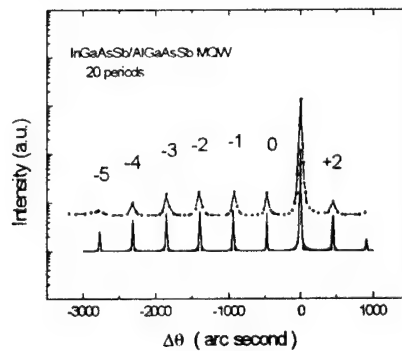


Fig 3. Experimental and simulation on the (400)  $\text{CuK}\alpha 1$  double crystal X-ray rocking curves of 20 periodic InGaAsSb/AlGaAsSb MQW

# MBE Growth of GaInAsSb p/n Junction Diodes for Thermophotovoltaic Applications

by

Parvez N. Uppal\*

Phone: (603)885-1016

Fax: (603)885-1074

Lockheed Martin Sanders, NHQ6-1551, 65 Spit Brook Road, Nashua, NH 03061

Greg Charache, Paul Baldasaro and Brian Campbell

Lockheed Martin, P.O. Box 1072, Schenectady, NY 12301

Stefan Svensson\*

ARL, AMSRL-PS-PB, 2800 Powder Mill Rd., Adelphi, MD 20783

David Gill\*

National Semiconductor, 10810 Guilford Rd., Suite 111, Annapolis Junction, MD 20701

## Abstract

This paper reports recent progress in the development of quaternary III-V thermophotovoltaic (TPV) devices based on MBE grown  $\text{Ga}_{1-x}\text{In}_x\text{As}_y\text{Sb}_{1-y}$ . TPV is of interest for a variety of Civilian, Military and Space applications. Previous investigators have found that a TPV approach offers significant potential for improved efficiency, when compared with thermoelectric technology. The objective of this work is to develop a TPV cell which is "tunable" to the emission spectrum of a heated blackbody, at temperatures in the range of 1200 - 1473 K. One aspect of this "tuning" is to match the band gap,  $E_{\text{gap}}$ , of the photovoltaic device to the peak output of the heat source. An advantage of the quaternary III-V semiconductor systems is that devices can be fabricated by molecular beam epitaxy on a suitable binary substrate, such as GaSb or InAs, and the band gap and lattice constant can be adjusted more or less independently, to match requirements. Quaternary cells, with band gap in the 0.5 to 0.72 eV range, have been fabricated and tested. For 0.54eV devices we obtained  $V_{\text{oc}} = 0.3$  V and  $I_{\text{sc}} = 1.5$  amperes/cm<sup>2</sup> under infrared illumination of a 1200K blackbody. Under high illumination levels the  $V_{\text{oc}}$  and  $I_{\text{sc}}$  ranged from 0.5 V at 3 amperes/cm<sup>2</sup> for 0.72eV devices to 0.31 V at 1.2 amperes/cm<sup>2</sup> for 0.5eV devices, indicating good PV device characteristics over the range of bandgaps. The diode ideality factor for 0.54eV devices ranged from 2.45 at low illumination indicating tunneling-dominated dark current, to 1.7 at high illumination intensity indicating recombination-generation dominated dark currents.

MBE growth of the quaternary alloys on GaSb or InAs substrates using non-indium bonded blocks led to wafer bending into concave and convex shapes depending upon a "positive" or "negative" mismatch, even a slight ~ 0.1% mismatch led to this bending. This indicates that the quaternary material "prefers" to bend rather than create dislocations to relax the strain. For the same composition ternary alloy (GaInSb) no such bending was observed even though the lattice mismatch was much larger. We believe this to be caused by the alloy hardening effect in the quaternary alloys, which makes it energetically harder for dislocations to propagate and instead the material deforms to relieve strain. This indicates that in the mixed arsenide-antimonide quaternaries strain relaxation proceeds differently as compared to the ternaries, and can have important device implications.

\*Work done while at Lockheed Martin Laboratories, Baltimore, MD 21227



# MOLECULAR BEAM EPITAXIAL GROWTH OF $\text{Ga}_{1-x}\text{In}_x\text{Sb}$ ON GaAs SUBSTRATES

J H Roslund, O Zsebök, G Swenson and T G Andersson

Department of Physics  
Chalmers University of Technology and Göteborg University  
S-412 96 Gothenburg, Sweden  
Telephone: +46 31 772 3327  
Facsimile: +46 31 772 3385  
e-mail: f4bjr@fy.chalmers.se

In this study growth by molecular beam epitaxy and structural characterisation of a series of  $\text{Ga}_{1-x}\text{In}_x\text{Sb}$  layers are reported. In recent years the  $\text{Ga}_{1-x}\text{In}_x\text{Sb}$  alloy has been suggested for use in a number of applications, but its growth has not been as thoroughly investigated as that of the corresponding arsenide,  $\text{In}_x\text{Ga}_{1-x}\text{As}$ . We have investigated the structural properties as the alloy composition varies in the full compositional range. The samples were 4  $\mu\text{m}$  thick  $\text{Ga}_{1-x}\text{In}_x\text{Sb}$  layers grown on semi-insulating GaAs substrates and characterised by reflection high-energy electron diffraction (RHEED), X-ray diffraction (XRD), secondary ion mass spectroscopy (SIMS), Hall-effect measurements, optical microscopy, scanning electron microscopy (SEM), surface profiling and Fourier transform photoluminescence (FTPL). The growth temperatures used were in the range 430–470 °C. The  $\text{Ga}_{1-x}\text{In}_x\text{Sb}$  was grown under a (1 $\times$ 3) RHEED reconstruction for  $x < 0.4$  and (2 $\times$ 3) for higher In fractions. Unintentionally doped samples had carrier concentrations below  $6 \times 10^{16} \text{ cm}^{-3}$  with a maximum at  $x = 0.5$ , where the conduction switched from  $p$ -type to  $n$ -type. The undoped GaSb and InSb binaries had high mobilities, 730 and 61 000  $\text{cm}^2/\text{Vs}$  at room temperature, respectively, indicating good structural quality. In the intermediate range XRD peaks were broadened and the sample surface unusually rough and scattered with square plateaux. No change in growth parameters was seen to substantially improve the quality here. However, a careful analysis of the XRD data revealed a weak tendency for XRD peaks to be narrower for low V-III ratios. For GaSb it was clear that a low V-III ratio gave a high mobility but lower photoluminescence intensity. The insertion of a 1  $\mu\text{m}$  thick InAs buffer layer caused the surface of  $\text{Ga}_{0.66}\text{In}_{0.34}\text{Sb}$  to change appearance and become more similar to  $\text{In}_x\text{Ga}_{1-x}\text{As}$  surfaces, indicating that the surface appearance is strongly affected by the initial part of the growth. SIMS showed that the alloy composition was uniform throughout the layers. Only samples with low In concentrations grown below 440 °C exhibited measureable photoluminescence. Growth started at 580 °C resulted in non-uniform alloy composition as verified by back-scattered electron imaging in SEM and energy-dispersive X-ray analysis. In summary,  $\text{Ga}_{1-x}\text{In}_x\text{Sb}$  can be grown with good structural quality, but with rougher surfaces and broader XRD peaks than  $\text{In}_x\text{Ga}_{1-x}\text{As}$ .

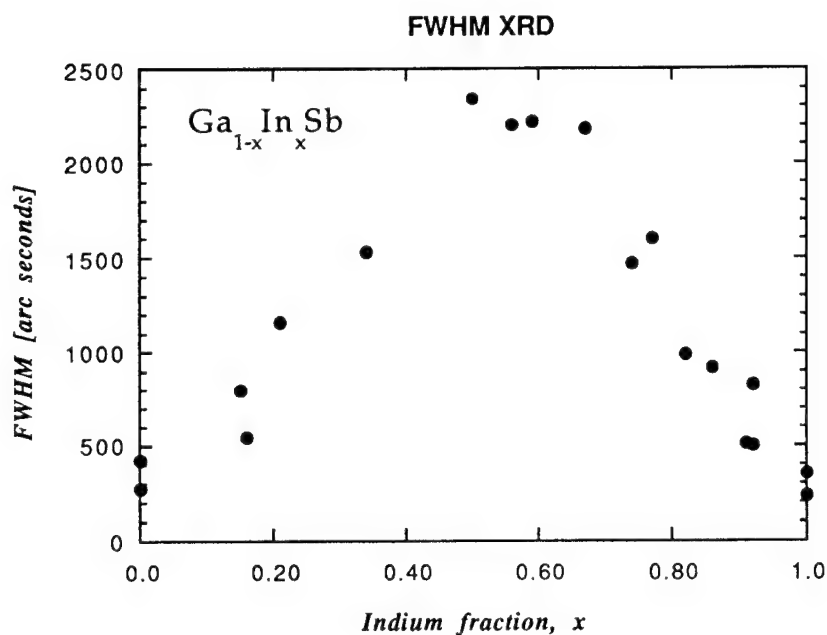


**Figure 1.** Full width at half maximum of the  $\text{Ga}_{1-x}\text{In}_x\text{Sb}$  peak in X-ray diffraction as a function of the In molar fraction  $x$ . The figure indicates that the broadening is related to disorder in the alloy.

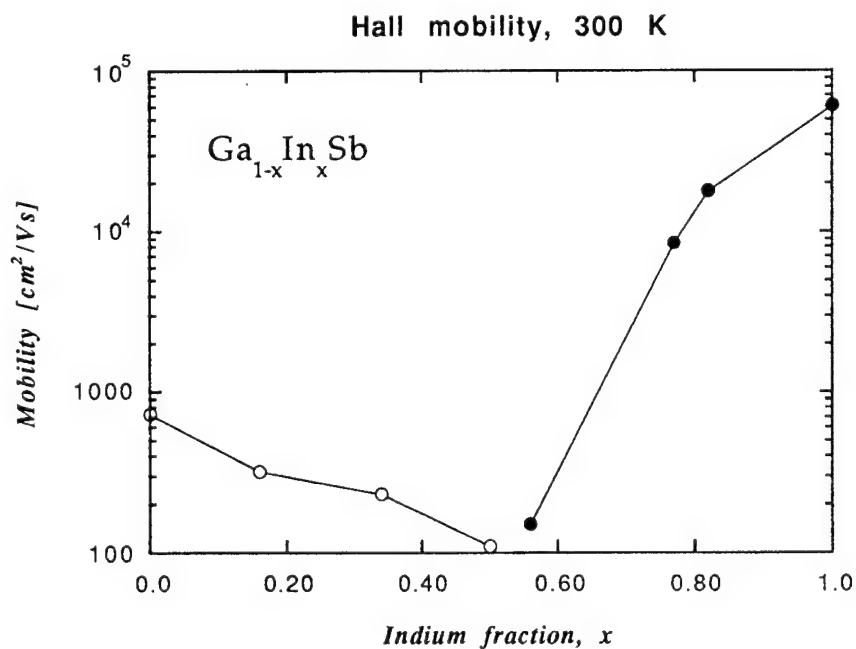


**Figure 2.** The hole (o) and electron (•) mobilities obtained from Hall effect measurements in the van der Pauw arrangement at 300 K. The lines are included as guides for the eye.

# ***In-Situ* STM Study of GaSb and AlSb (001) Surface Reconstructions<sup>1</sup>**

**P. M. Thibado, B. R. Bennett, B. V. Shanabrook, and L. J. Whitman**  
*Naval Research Laboratory, Washington, DC 20375*

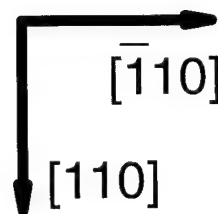
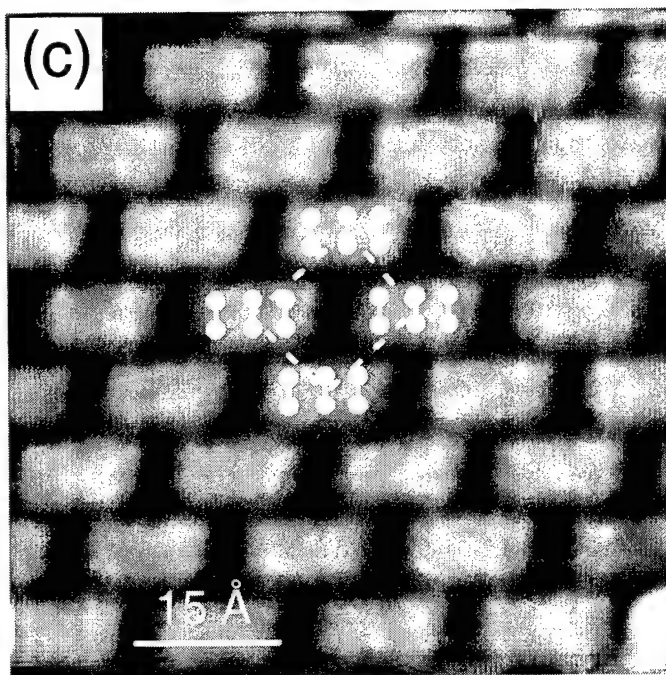
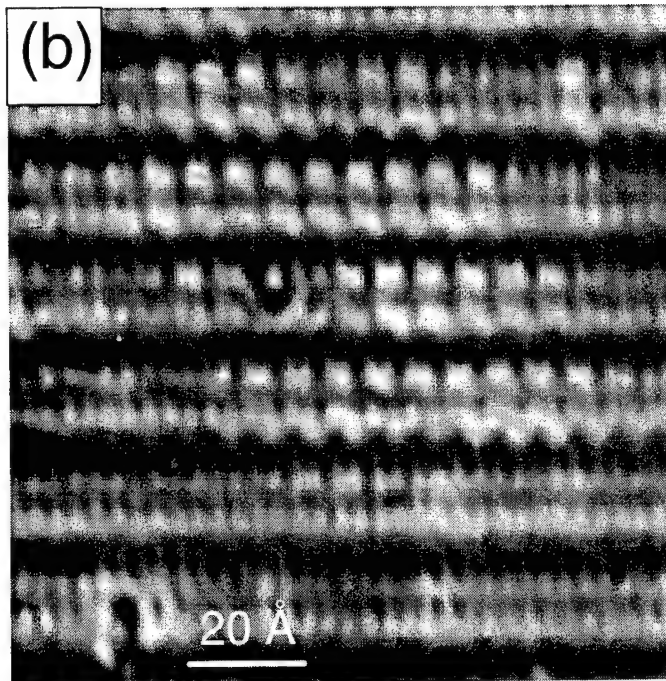
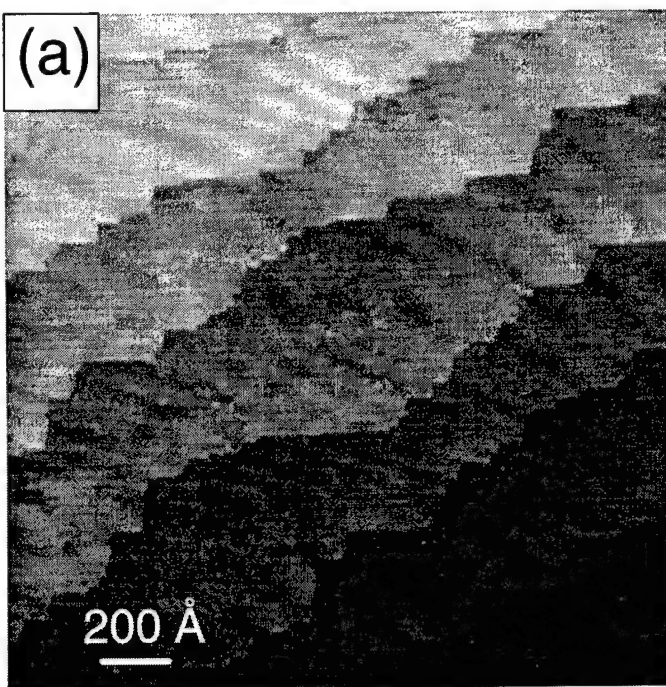
There is an extensive effort to develop novel high-speed and opto-electronic devices utilizing the "6.1 Å" family of III-V compound semiconductors, InAs, GaSb, and AlSb. In short-period heterostructures, the interfaces constitute a significant fraction of the total heterostructure volume, and therefore the structure and stoichiometry of the growth surface during interface formation is expected to have a significant impact on the ultimate device performance. Hence, the development of smooth, abrupt interfaces requires a fundamental understanding of the structure of the III-V(001) surface reconstructions. As part of our effort to determine the role of the growth-front surface reconstruction on heterostructure interfacial abruptness, we have investigated the atomic-scale structure of Sb-rich surface reconstructions on both GaSb and AlSb (001) surfaces with *in-situ* scanning tunneling microscopy (STM).

The surfaces were prepared by MBE at various substrate temperatures and Sb<sub>4</sub> fluxes while monitoring with RHEED, and then cooled to room temperature under no flux prior to STM study. Under a fixed Sb<sub>4</sub> flux, GaSb reconstructions observed with decreasing temperature are: (1×3), c(2×6), (1×5), and (2×5)/c(2×10), consistent with earlier observations. In contrast, only two reconstructions are observed on AlSb(001) under Sb-rich conditions: the previously observed (1×3), and a c(4×4) phase (to our knowledge not previously reported). It is surprising that at lower temperatures GaSb reconstructs to (n×5), since all other III-Sb and III-As compounds reconstruct to c(4×4). We believe the different GaSb structures arise from the excellent lattice match with crystalline Sb which minimizes the dimer-induced strain.

We have identified two surface reconstruction-related effects which can affect heterostructure interfacial abruptness: non-stoichiometric surface structure (III/V < 1) and reconstruction-related morphology. The (1×3), (1×5), and (2×5)/c(2×10) reconstructions of GaSb have 1.66, 1.80, and 2.2 layers of Sb on top of a Ga plane, respectively. Similarly, the (1×3) and c(4×4) reconstructions of AlSb have 1.66 and 1.75 layers of Sb on top of an Al plane, respectively. When another material (e.g. InAs) is grown on top of one of these surfaces during the fabrication of a heterostructure, the excess Sb (> 1 layer) may diffuse across the interface and thereby degrade the compositional abruptness. The reconstruction may affect the growth morphology by inducing anisotropy in the growth kinetics, leading to anisotropic roughness during non-equilibrium growth. In addition, terrace-edge shape may depend on the reconstruction during growth due to reconstruction-dependent kink energies. For example, we find that under certain growth conditions long, very straight terrace edges can be formed along the  $[\bar{1}10]$  direction. This result suggests that by appropriately miscutting the substrate very well-ordered quantum wires or tilted superlattices could be formed.

<sup>1</sup>Supported by the Office of Naval Research.

Contact author:	Paul M. Thibado	(202) 404-8845
	Code 6177	(202) 767-3321 (FAX)
	Naval Research Laboratory	pthibado@stm2.nrl.navy.mil
	Washington, DC 20375	



*In-situ* scanning tunneling microscopy (STM) images of MBE-grown GaSb and AlSb (001) surfaces. A GaSb buffer layer surface consisting of large, atomically smooth terraces ( $\sim 300$  Å wide) separated by monolayer-height ( $3$  Å) steps is shown in Fig. (a). Each terrace is displayed with a different gray level. Note the long, straight sections of the terrace edges (low kink density) in the  $[\bar{1}10]$  direction. A higher magnification image acquired on a single GaSb terrace reveals a mixed  $(1\times 5)$  and  $(2\times 5)/c(2\times 10)$  surface reconstruction as shown in Fig. (b). The dark horizontal rows spaced 5 unit cells apart ( $\sim 22$  Å) define the periodicity of the surface reconstruction in the  $[110]$  direction. A high-magnification image of an AlSb(001) surface with a  $c(4\times 4)$  reconstruction is shown in Fig. (c). The surface unit cell and several top layer Sb dimers are indicated.

# Stranski-Krastanov Growth of InSb and GaSb on GaAs: Structure of the Wetting Layers

B.R. Bennett, B.V. Shanabrook, P.M. Thibado, L.J. Whitman, and R. Magno  
Naval Research Laboratory, Washington, DC 20375-5347, U.S.A.

The Stranski-Krastanov (SK) or layer-plus-island growth mode in strained heteroepitaxy has been recognized for decades. Recently, there has been considerable interest in using SK growth to deposit self-assembled semiconductor quantum dots (QDs) in material systems including InAs/GaAs, InP/InGaP, and GaSb/GaAs. Although QDs with uniformities on the order of 10% are routinely achieved, many potential applications such as solid-state lasers require more uniform ensembles of QDs. Theoretical work suggests that the uniformity of QDs is related to the structure of the 2D wetting layer which forms first, but few experimental studies have been reported. In this work, we investigate the structure of wetting layers of GaSb/GaAs (mismatch = 7.8%) and InSb/GaAs (mismatch = 14.6%).

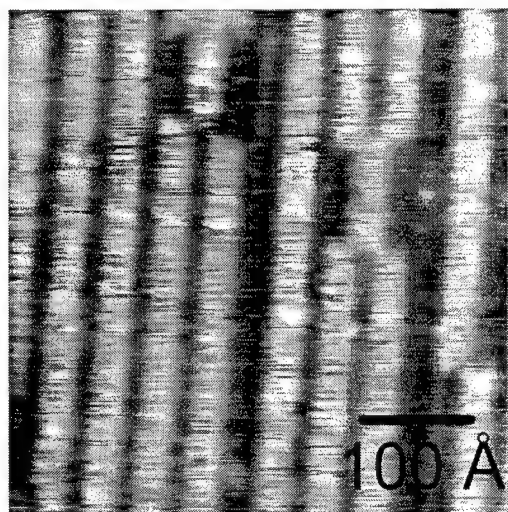
Experiments are carried out in an interconnected multi-chamber UHV facility that includes a III-V solid-source MBE and a surface analysis chamber with STM. First, a GaAs buffer layer is grown at 580°C on GaAs(001), using growth interrupts to achieve a smooth surface with  $\sim 5000$  Å wide terraces separated by monolayer-height (3 Å) steps. Then, a well-ordered (2x4) or c(4x4) reconstruction is prepared using appropriate adjustments of substrate temperature and As<sub>4</sub> flux. The temperature is lowered to 400-500°C and 1-4 monolayers (ML) of GaSb or InSb is deposited by migration-enhanced epitaxy while monitoring the RHEED pattern. Finally, the sample is transferred to the STM and imaged at room temperature.

As a first step to understanding (Ga,In)Sb growth, we exposed a GaAs-(2x4) surface to Sb<sub>4</sub>. The resulting RHEED pattern revealed a (2x8) reconstruction. This new reconstruction, which we believe results from the incorporation of Sb along with As on the surface, was examined by STM, confirming the 8 Å by 32 Å periodicity. Whereas well-ordered surfaces are observed for GaAs-(2x4), GaAs-c(4x4), and Sb:GaAs-(2x8) surfaces, both RHEED and STM reveal a disordered surface after the deposition of 1-2 ML GaSb. Specifically, a network of interconnected 2D island-like structures  $\sim 100$  Å in diameter is observed, with  $\leq 1$  ML-deep gaps between them. Quantum dots (QDs) are not present at these coverages. After deposition of 3-4 ML GaSb, QDs are present and the wetting layer structure is modified, with anisotropic ribbon-like structures 40-60 Å wide oriented along the  $[\bar{1}10]$  direction. For InSb on GaAs, a similar surface morphology (i.e. QDs and  $\sim 50$  Å-wide ribbons) is observed after growth of *only* 1.5-2.0 ML.

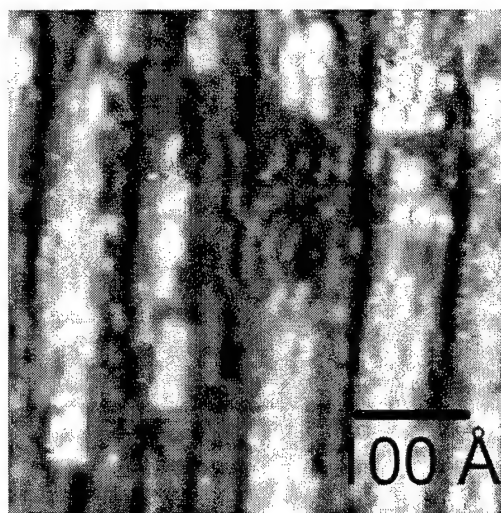
The traditional view of SK growth is that the initial deposition occurs as a continuous wetting layer. Our results, however, suggest a more complicated picture: a discontinuous morphology which arises from the combined effects of the relative surface energies (of the absorbates and substrate), and the mismatch-related strain (which is relieved by the vacancy lines). The anisotropy of the structures in the wetting layers does not appear to arise from kinetic limitations but, rather, is attributed to the direction-dependent strain associated with the dimer-based surface reconstructions.

Contact: Brian Bennett, Naval Research Laboratory, Code 6874, 4555 Overlook Avenue-SW, Washington, DC 20375-5347; phone: 202-767-3665; fax: 202-767-1165; email: bennett@bloch.nrl.navy.mil

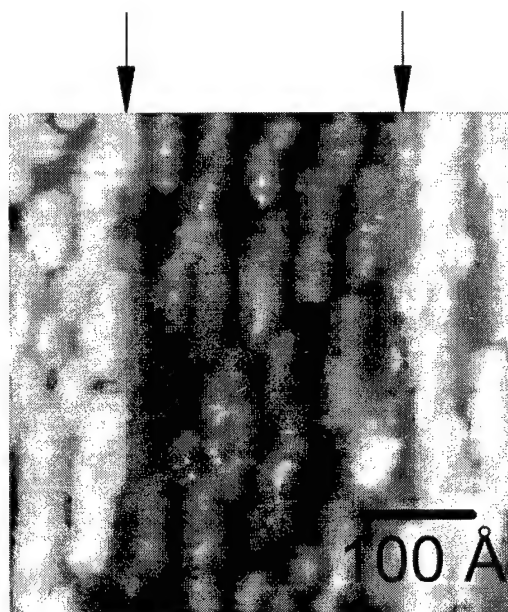




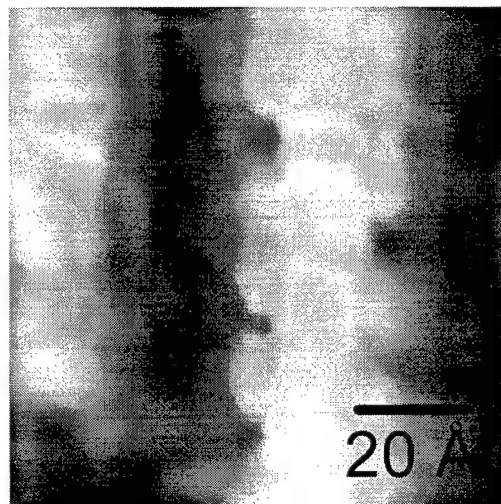
(a)  $\Delta z = 8 \text{ \AA}$



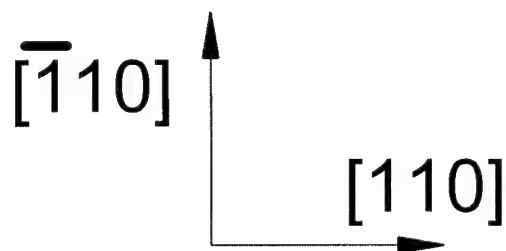
(b)  $\Delta z = 16 \text{ \AA}$



(c)  $\Delta z = 10 \text{ \AA}$



(d)  $\Delta z = 10 \text{ \AA}$



*In situ* scanning tunneling microscopy (STM) images of layers grown by MBE: (a) GaAs(001)-(2x4) surface exposed to  $\text{Sb}_4$ , resulting in a (2x8) reconstruction. (b) 3.5 ML GaSb/GaAs, note the ribbon-like structures along the  $[110]$  direction; quantum dots (not shown) were also observed. (c) 1.5 ML InSb/GaAs, note the elongated islands and monolayer-height terraces (indicated by arrows); quantum dots (not shown) were also observed. (d) Higher magnification image of (c), showing atomic structure. (B.R. Bennett, B.V. Shanabrook, P.M. Thibado, L.J. Whitman, and R. Magno, Naval Research Laboratory)

# Zinc Blende Structure GaN Grown by Radio Frequency Plasma Assisted Molecular Beam Epitaxy

J.W. Han

Department of Physics, Sejong university, Seoul 133-747, Korea

H.D. Cho, K.S. Eom, C.B. Kim, N.H. Ko, S.H. Park, T.W. Kang

Department of Physics, Dongguk university, Seoul 100-715, Korea

C.H. Hong, D.H. Kim

LG Electronics Research Center, Seoul 137-140, Korea

Recently, interest in the group-III nitride semiconductors has attracted because of their potential for the development of light emitting devices in the visible and UV spectral regions. Bulk single crystals or wafers are not yet available and the choice of adequate substrates for heteroepitaxy has been a nontrivial problem for experimentalists. Sapphire( $\text{Al}_2\text{O}_3$ ) is commonly used but its large misfit with respect to GaN(13.8%) has been a limiting factor in the quality of the grown epilayers. There have been several reports that the nitridation play an important role in the growth of GaN on  $\text{Al}_2\text{O}_3$  substrates. Most of films had a wurtzite phase. However, growing zinc blende GaN for the LD fabrication have been attracted and there have been reports using 3C-SiC substrates for the growth of zinc blende GaN.[1,2,3] Liu. et. al. reported that using 3C-SiC on Si substrate, the growth of zinc blende GaN was confirmed by in situ reflection high energy electron diffraction (RHEED), X-ray diffraction (XRD) and photoluminescence (PL).[4] In this study, before growing GaN on 3C-SiC coated (001) Si, we investigated how the nitridation has an influence on the growth of GaN films. As a results, we present high quality of undoped zinc blende GaN/3C-SiC coated (001) Si substrates using a molecular beam epitaxy in which the reactive nitrogen ion source is used 13.56 MHz radio frequency plasma radical source. The zinc blende nature of GaN films is confirmed by in situ RHEED, XRD and PL. From the RHEED ( $2\times 2$ ) streaky pattern, we are assured that the high quality zinc blende GaN films are grown. The XRD showed that (002) zinc blende GaN is observed near at  $2\theta=40.1^\circ$  and exhibited the full width at half maximum (FWHM) of about  $80\sim 85$  min. At 10 K, PL of the zinc blende GaN is dominated by band edge emission at 3.492 eV .

## Reference

1. D.E. Lacklison, J.W. Orton, I. Harrison, T.S. Cheng, L.C Jenkins, L.C. Foxon and S.E. Hooper, J. Appl. Phys. 78, 1838 (1995)
2. T. Sasaki and T. Matsuoka, J. Appl. Phys. 64, 4531 (1988)
3. Z. Sitar, L.L. Smith and R.F. Davis, J. Cryst. Growth, 141, 11 (1994)
4. H. Liu, A.C. Frenkel, J.G. Kim and R.M. Park, J. Appl. Phys. 74, 6124 (1993)

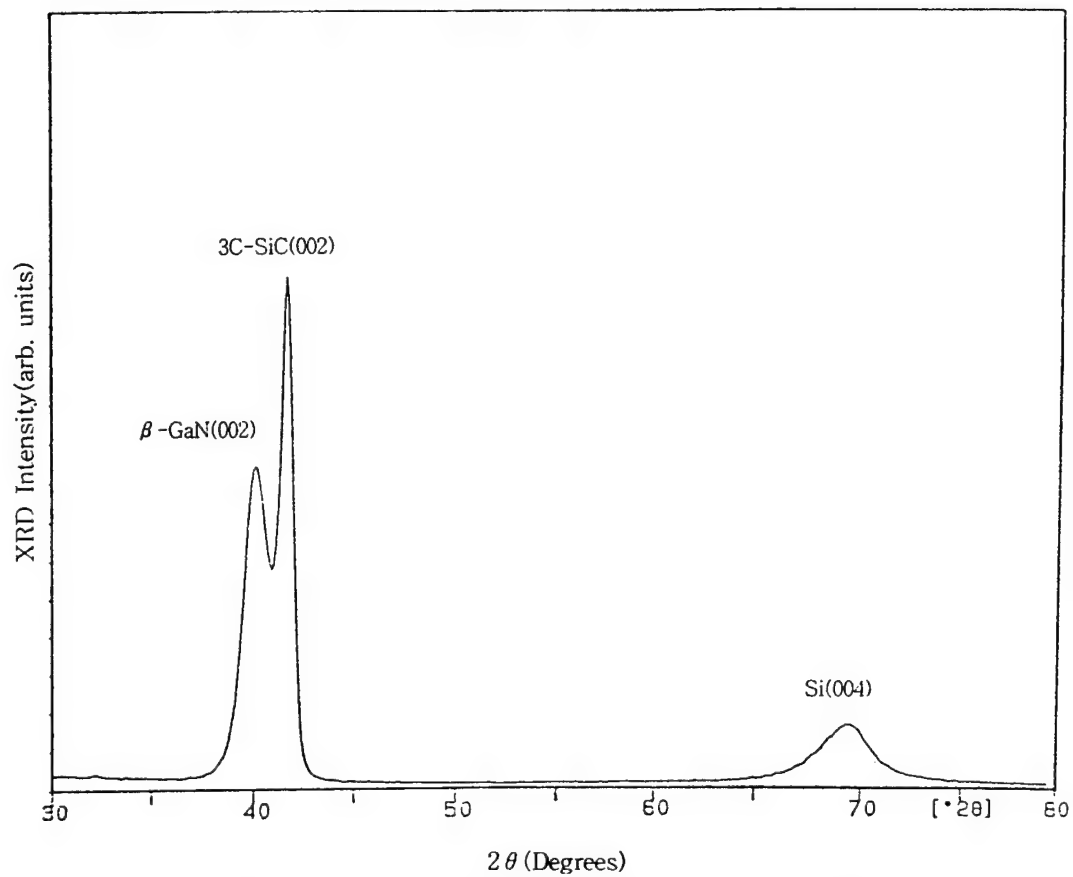


Fig 1. X-ray diffraction of GaN films grown at 600°C

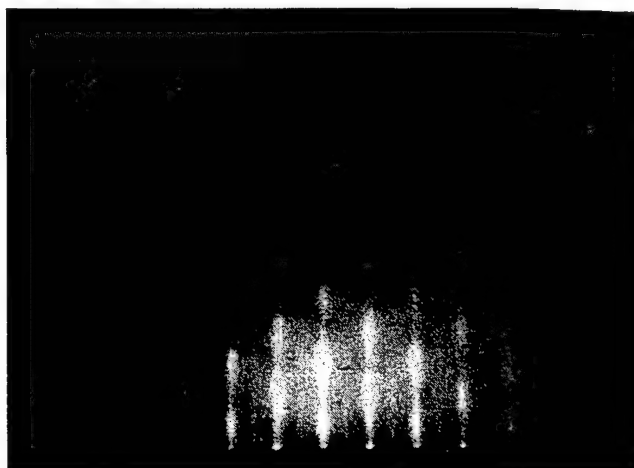


Fig. 2 RHEED (2×2) pattern of GaN films grown at 600°C



## Initial Growth Stage of GaN on Si Substrate by Alternating Source Supply Using Dimethyl-hydrazine

Akihiro Hashimoto, Yoshitaka Aiba, Takanori Motizuki, Mitugu Ohkubo and Akio Yamamoto  
Department of Electrical and Electronics Engineering  
Fukui University, Bunkyo 3-9-1, Fukui 910, Japan

Growth of III-V nitride compound semiconductor onto Si substrate offers very attractive potential to future optoelectronic devices onto silicon-based integrated circuits such as optoelectronics integrated circuits (OEIC).<sup>1)</sup> It is well known in the case of III-V compound semiconductors such as GaAs on Si that initial growth stage plays an important role in the following growth process and the crystal quality.<sup>2)</sup> Especially, the initial nitridation process of the Si substrates would prevent from the following normal epitaxial growth in the III-V nitride growth on Si and it needs to control of the nitridation in the initial stage to obtain the high quality III-V nitride films on Si.<sup>3)</sup> There are some possibilities to control the initial nitridation and/or growth stages such as using the low temperature buffer layer proposed by T. Lei et al.<sup>1)</sup> However, it is not yet enough to understand the initial nitridation process during the III-V nitride growth. As the clean Si surface that made in the ultra-high vacuum circumstances maybe considerable reactive, it strongly needs to find out the control parameters on the initial growth without nitridation. In this paper, we propose the alternatively source supply method using Ga and dimethyl-hydrazine (DMHy) to control the initial nitridation process of the Si substrates.

Nitridation experiments were carried out by the MOMBE system using trimethyl-gallium (TMG), metal Ga and DMHy. Si (111) n-type wafers, on which deposited about 0.5  $\mu\text{m}$  Si epitaxial layers with an annealing at 1000  $^{\circ}\text{C}$  after the depositions in the another Si-MBE system, were used as substrates and the beam-equivalent pressure of the DMHy gas was  $2 \times 10^{-6}$  torr. Alternatively source supply were carried out in the first step of the growth using the Ga sources and the DMHy by shutter controls. X-ray photoelectron spectroscopy (XPS) measurements were performed as the surface characterizations after the initial growth. Total thickness of the GaN films were control by the amounts of the supplied Ga atoms and were estimated about 40 monolayers (ML) typically as the cubic structure.

Figure 1 shows that  $\text{Si}_{2p}$  XPS spectra corresponded to the various initial growth conditions. The peaks of 99 eV, 102 eV and 103.4 eV correspond to the Si-Si, Si-O and Si-N bonds, respectively. It can be easily seen in the case of supplying only DMHy as shown in Fig. 1(a) that there is a strong peak at about 103 eV that is between the Si-N and the Si-O bonds. This peak may be due to the native oxide formed during the transfer from the Si-MBE to the MOMBE systems. Because the nitrogen related XPS signal at 398 eV can be also observed in the same wide-scanned spectra, so this result indicates that the Si surface partially covered with the Si-N bonds although the Si-O bonds of the native oxide films suppress the nitridation of the Si surfaces. In the cases of the 1 ML TMG supplying before the DMHy supply as shown in Figs. 1(b) and 1(c), the Si-N and the N peak intensities increase remarkably in contrast with the decrease of the Si-O peak intensities. The increases of the Si-N peak intensities are due to the removal effect of the native oxide films by the Ga beam irradiations with the progress of nitridation of the clean Si surfaces. The comparison between the spectra as shown in Figs. 1(b) and 1(c) also indicates that the following 40 ML GaN growth seems not to give the any effect to the initial Si-N surfaces. However, in the cases of the 10 ML Ga supplying, the apparently decreases of Si-N peak intensities are observed with vanishing of the Si-O peaks. The substrate temperature dependences of the Si-N peak intensity were also observed as shown in Figs 1(d) and 1(e), that is, in the case of the substrate temperature of 600  $^{\circ}\text{C}$ , the additional suppression of the Si-N peak intensity was observed in comparison with the case of the temperature of 500  $^{\circ}\text{C}$ . These results indicate that both the existence of the Ga atoms on the Si surfaces and the substrate temperature at the initial growth stage of the III-V nitrides films play an essential role in the suppression of the nitridation of the initial growth stages. This result was also supported by the XPS spectral behavior of nitrogen signals.

In conclusion, the alternating source supply of Ga and DMHy to control the initial nitridation stage were proposed. The analysis of the XPS spectra showed that the Ga atoms play an important role both in the removal of the Si native oxide films and the suppression of the nitride formation during the initial growth stages. It is expected that the alternative source supplying methods in the

initial growth stage of the III-V nitride on Si substrates is an useful one to grow the excellent lattice-mismatched heteroepitaxial layers of III-V nitride onto Si substrates.

#### References

- 1) T.Lei, M.Fanciulli, R.J.Molnar, T.D.Moustakas, R.J.Graham and J.Scanlon, Appl. Phys. Lett. **59**, 944 (1991).
- 2) A.Hashimoto, N.Sugiyama and M.Tamura, Jpn. J Appl. Phys. **30**, 3755 (1991).
- 3) A.Yamamoto, M.Tsujino, M.Ohkubo and A.Hashimoto, J. Cryst. Growth **137**, 415 (1994).

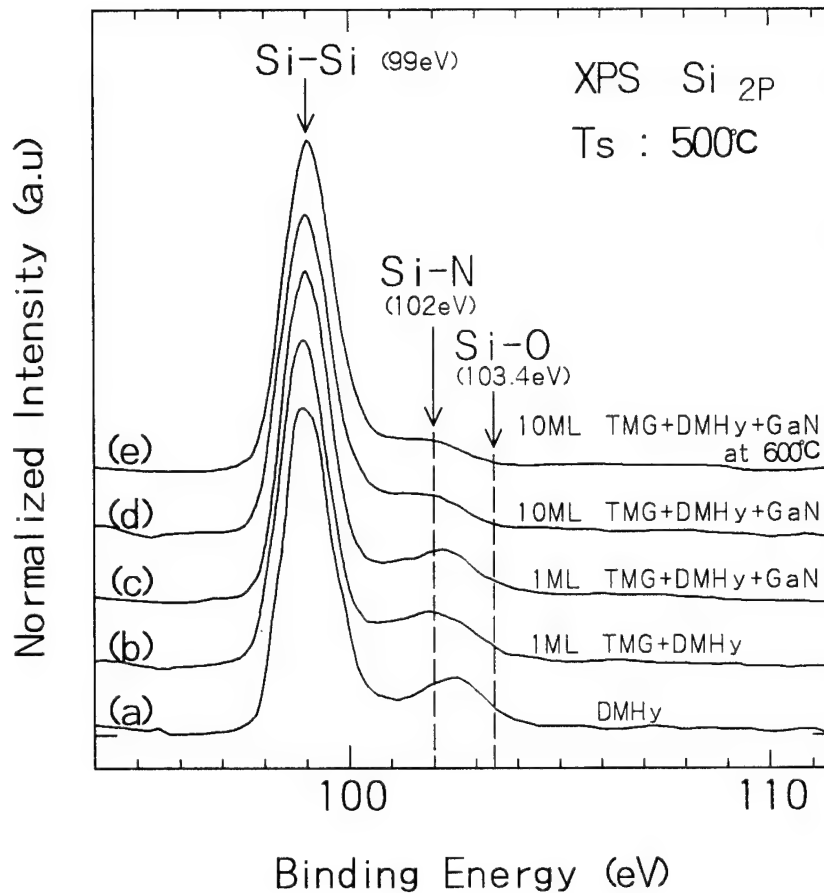


Fig. 1. Si<sub>2p</sub> XPS spectra corresponded to the various initial growth conditions.

# Relation between surface reconstruction transitions and growth kinetics of zincblende (001) GaN

Oliver Brandt\*, Hui Yang, Akira Yamada<sup>†</sup>, and Klaus H. Ploog

*Paul-Drude-Institut für Festkörperelektronik,  
Hausvogteiplatz 5-7, D-10117 Berlin, Germany*

We study, both experimentally and theoretically, the stability and the dynamics of the surface reconstructions of cubic GaN. The cubic GaN layers are grown by plasma-assisted molecular beam epitaxy on (001) GaAs. Reflection high-energy electron diffraction is used to monitor the transient behavior of the surface reconstruction upon the pulsed supply of either Ga or N at a given substrate temperature. The reconstructions observed are first phenomenologically classified on the basis of the experimentally determined surface coverage and symmetry. In addition to the N terminated (1×1) surface, a (2×2) and a c(2×2) reconstructed phase were observed which are linked to 0.5 monolayer (ML) and 1.0 ML of Ga coverage, respectively. The (2×2) reconstructed surface is distinguished among these in that it is the stable surface of cubic GaN in vacuum, while the (1×1) and c(2×2) surfaces are obtained only upon an impinging flux of either Ga or N onto the (2×2) surface. Once the supply of N/Ga ceases, the surface relaxes within a finite time towards the (2×2) reconstruction. The simplest explanation for this effect consists in the initial adsorption of either N or Ga, thus forming surface phases distinct in coverage and symmetry from the (2×2) surface phase, followed by the isothermal desorption of the species building up these phases. We develop a model of the adsorption-diffusion-desorption kinetics of Ga and N adatoms to quantitatively understand the dynamics of the surface reconstruction transitions. We thus obtain the Arrhenius parameters for the desorption of Ga and N. Our results show that all of the surfaces phases of GaN constitute kinetic barriers for the decomposition of GaN being of either energetic or entropic character depending on surface termination. The (2×2) reconstructed surface constitutes the rate-limiting barrier for the thermal decomposition of cubic GaN. The exceptional role of the (2×2) reconstructed surface is investigated theoretically by *ab initio* total-energy calculations. The high stability of the (2×2) reconstructed surface is found to result from a large relaxation of the Ga dimers towards the surface, which in turn leads to a high stiffness of this surface.

---

\*Author to whom correspondence should be addressed. Tel.: +49-30-20377-366; Fax.:+49-30-20377-366; E-mail: brandt@pdi.wias-berlin.de

<sup>†</sup>Permanent address: Tokyo Institute of Technology, 2-12-1 O-okayama, Meguro-ku, Tokyo 152, Japan.

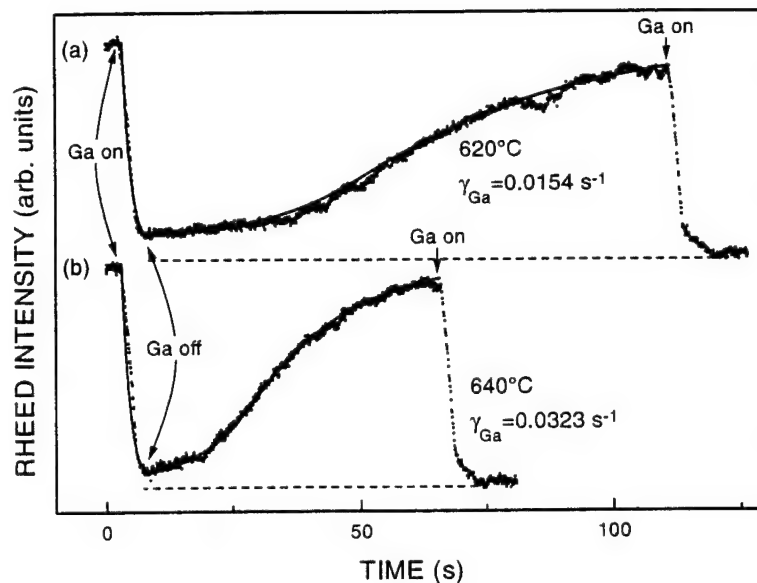


Fig. 1: RHEED intensity transient upon a 0.5 monolayer Ga dose at (a) 620°C and (b) 640°C. Solid squares represent experimental data, and solid lines show the best fit of our model. The dashed lines show the zero level which is defined by the half-order beam intensity equaling the background intensity. The time intervals of Ga supply are indicated in the figure, as well as the desorption rates deduced from the fits.

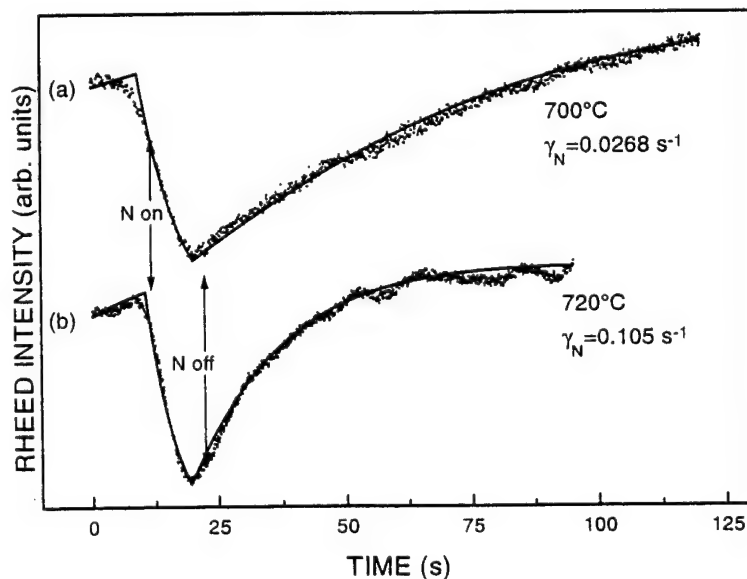


Fig. 2: RHEED intensity transient upon a 1.0 monolayer N dose at (a) 700°C and (b) 720°C. Solid squares represent experimental data, and solid lines show the best fit of our model. The time intervals of N supply are indicated in the figure, as well as the desorption rates deduced from the fits.

## Surface crystal-structure of a GaN film as an in-situ mask using MOMBE

Seikoh Yoshida<sup>1)</sup> and Masahiro Sasaki<sup>2)</sup>

Optoelectro. Technolo. Research Laboratory, 5-5 Tohkodai, Tsukuba, Ibaraki 300-26, Japan

1) Present address: The Furukawa Electric Co., Ltd. Yokohama R&D Laboratories, 2-4-3 Okano, Nishi-ku, Yokohama 220, Japan Tel:+81-45-311-1219, Fax:+81-45-322-6961, e-mail:seikoh@mrc\_mc.yokoken.furukawa.co.jp

2) Present address: Toshiba Research and Development Center, 1 Komukai-Toshiba-cho, Saiwai-ku, Kawasaki 210, Japan

We have studied an atomically thin GaN film as a mask for the in-situ selective area growth (SAG) of GaAs using metalorganic molecular beam epitaxy (MOMBE). The in-situ process means that all of the processes for SAG containing formation, patterning, and removal of the mask materials are performed in an ultrahigh vacuum (UHV) system. We have already reported that the GaAs growth selectivity as a mask of a cubic GaN surface on a GaAs (100) substrate to GaAs deposition using MOMBE strongly depends on the GaN formation conditions (substrate temperatures and source-gas pressures); that is, not all of the GaN surfaces formed act as good masks, but only single crystalline GaN surfaces showing streak-like reflection high-energy electron-diffraction (RHEED) patterns have strong selectivity as a mask. However, it has not yet been clarified whether or not hexagonal GaN formed on a GaAs (111)B substrate has high selectivity to GaAs deposition.

We examined atomically thin GaN film formation on GaAs (111)B in order to investigate whether GaN can be used as a mask for an in-situ process or not. Thin GaN films were formed on GaAs (111)B substrates with various surface structures. When the native oxide on the GaAs (111)B surface was removed using trisdimethylaminoarsine (TDMAAs) at 450°C, the RHEED pattern of GaAs (111)B showed a streaky (2x2) pattern. After that, a GaAs epitaxial layer was grown on the surface using trimethylgallium (TMG) and TDMAAs at 500°C. Atomically thin GaN was formed on the GaAs (111)B epitaxial layer at different substrate temperatures using a dimethylhydrazine ((CH<sub>3</sub>)<sub>2</sub>NNH<sub>2</sub>) as a nitrogen source gas. The formed GaN surfaces were exposed to TMG and As<sub>4</sub> at 430°C in order to investigate any growth suppression to GaAs on GaN surfaces. When a GaN surface, showing a streaky single GaN RHEED pattern, which was formed on GaAs (111)B was exposed to TMG and As<sub>4</sub> for more than 2 hours, the RHEED pattern was not changed. That is, GaAs polycrystals were not deposited on the surface. On the other hand, on other GaN surfaces showing RHEED pattern corresponding to polycrystal, the RHEED pattern changed within 30 minutes when the surfaces were exposed to TMG and As<sub>4</sub>. Based on these results, it was found that the GaAs growth suppression of a GaN surface showing a streaky RHEED pattern corresponding to flat and single GaN is highest.

It was thus confirmed that a single GaN film showing a streaky RHEED pattern formed on a GaAs (111)B substrate as well as GaAs (100) substrate has the highest growth suppression effect to GaAs deposition on the surface at 430°C although other GaN surfaces showed lower suppression effects.

## Supporting materials

### Relation between surface structures of GaN and the GaAs growth suppression period on the surfaces

RHEED	Amorphous	Polycrystalline	Single Hexagonal (Streak)	Single Cubic (Streak)
GaAs growth suppression period	<10min	30min	>2hrs	>3hrs



Photograph showing a streaky GaN RHEED pattern formed on a GaAs (111)B.

## DC-plasma source for nitrogen activation in MBE of GaN

G.D.Kipshidze, S.V.Drozhdov, V.B.Lebedev, S.V.Novikov, L.V.Sharonova,  
A.Ya.Shik, V.N.Jmerik, V.M.Kuznetsov, A.V.Andrianov, A.M.Gurevich, N.N.Zinov'ev,  
C.T.Foxon\* and T.S.Cheng\*

Ioffe Physical-Technical Institute, St.Petersburg, 194021, Russia

\*Department of Physics, University of Nottingham, Nottingham NG7 2RD, England

The group III-nitrides are being studied increasingly as promising materials for visible light emitting diodes and lasers for the blue/UV part of the spectrum. In MBE both gaseous and plasma-activated nitrogen sources are used. There are two basic methods of nitrogen plasma excitation - RF and ECR microwave activation of nitrogen.

In this paper we report on the first results of epitaxial growth of GaN layers on GaAs (001) substrates using a modified MBE system, equipped with elemental solid sources of group-III metals and DC-plasma source for nitrogen activation in configuration of reverse magnetron at ultra-low pressures. The properties of grown GaN layers are investigated using a variety of techniques including in-situ reflection high-energy electron diffraction (RHEED) and Auger electron spectroscopy (AES), ellipsometry and photoluminescence (PL).

The samples were grown using a modified MBE technique in a growth chamber equipped with the plasma source based on the neutral gas ionization and activation by discharge in crossed electrical (up to 4KV/cm) and magnetic fields (up to 0.1 T). The source was made in reverse magnetron configuration with a coaxial geometry of the electrodes and with a central anode. It was very important that the pumping speed of ion pump used in the MBE growth chamber is high; about 5000 liter/second in our case. This allowed us to use fluxes of nitrogen corresponding to a beam equivalent pressure (BEP) up to  $10^{-5}$  Torr and so to carry on all the GaN growth processes in a normal MBE pumping system configuration. This fluxes of nitrogen and electric and magnetic fields led to the condition of the closed Hall drift of the electrons on cycloidal trajectory and formation of a negative space charge of the electrons between cathode and anode, and as a result to activation of the nitrogen. The discharge in crossed ExB fields can be realized in different regimes. In this work most of the samples were grown under the "vacuum" regime in the source. The main specific feature of it is that in a wide pressure range (from  $10^{-12}$  up to  $10^{-3}$  Torr) the space energy spectrum and the electrons concentration are independent from gas pressure in the discharge chamber. This causes the linear dependence of output activated nitrogen flow on N pressure in the source.

PL and AES studies showed that thin GaN films can be grown on GaAs substrates by MBE equipped with a novel plasma source for nitrogen activation in configuration of reverse magnetron at ultra-low pressures. We have experimentally classified the impurity related radiative recombination as well as having found the value of forbidden gaps for GaN.

G.D.Kipshidze,  
Ioffe Physical-Technical Institute  
26 Politekhnicheskaya st.,  
St.Petersburg, 194021  
Russia

FAX: 7-812-2471017  
e-mail: [gela@shik.ioffe.rssi.ru](mailto:gela@shik.ioffe.rssi.ru)

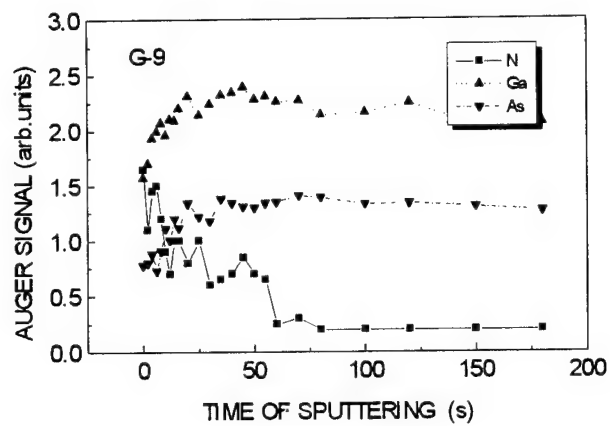


Fig.1 AES depth profiles of the grown GaN sample

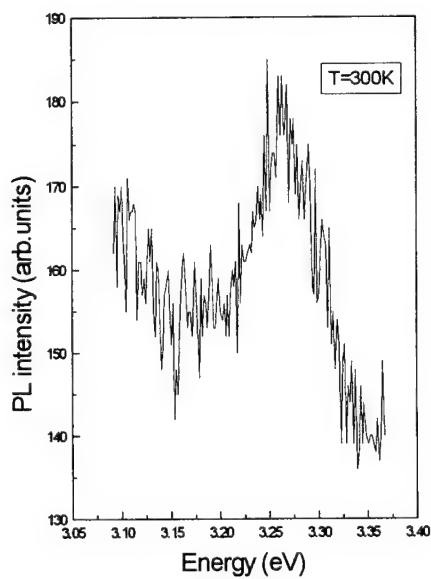


Fig.2 Near band gap PL spectra at 300 K of GaN sample



## Gas Source Molecular Beam Epitaxy of Cubic GaN/GaAs (001) Using Hydrazine.

S. A. Nikishin, G.A.Seryogin and H.Temkin,

*Electrical Engineering Department, Colorado State University, Ft. Collins, CO 80523  
tel.(970)-491-2060, FAX: (970)-2804, e-mail:sergei@lance.colostate.edu*

V. G. Antipov, S.S.Ruvimov, A.V.Merkulov  
*A.F.Ioffe Institute, St.Petersburg, 194021, Russia*

We report on the growth of GaN on (001) GaAs by gas-source molecular beam epitaxy (GSMBE) with hydrazine ( $N_2H_4$ ) as a source of nitrogen. The high reactivity of  $N_2H_4$  provides an attractive alternative to atomic N or  $NH_3$  in epitaxial growth of GaN [1]. We use a variety of *in-situ* analytical methods, reflection high-energy electron diffraction (RHEED), Auger electron spectroscopy (AES), and low energy electron diffraction (LEED) to examine the substrate and growth nucleation. Our results demonstrate that the initial stages of epitaxial growth of cubic GaN on GaAs are characterized by three-dimensional nucleation. The island size and the film morphology can be controlled by the active N flux, with highly uniform films obtained at a  $N_2H_4$ /Ga flux ratio of 1000. According to the transmission electron microscopy (TEM) data, the 10 nm thick layer of GaN adjacent to the substrate had a textured character. The characteristic defects revealed by TEM are the stacking faults and the interface steps. The height of the interface steps is clearly correlated with the measured surface roughness. An interface layer between GaAs and GaN, 0.32 nm thick, was also observed. The origin of this interface layer formation is likely to be related to the outdiffusion of As.

The RHEED results, supported by *ex-situ* atomic force microscopy (AFM) and TEM, show that for the growth at 550-600°C at a rate of 50-100 nm/hr, the initial dominant orientation of GaN islands is along the [110] direction. This orientation is preserved during the entire growth process. However, the surface morphology and the root-mean-square (RMS) surface roughness are strongly dependent on the  $N_2H_4$ /Ga flux ratio. The flux ratio at the substrate is estimated to vary from 70 to 1000. This results in a decrease of the average crystallite length from 94 nm to 27 nm, and the corresponding reduction in the RMS roughness from 11.4 nm to 1.8 nm, as expected from 3D nucleation. These results correlate well with the secondary ion mass spectroscopy profiles measured for thin GaN films. A significant increase in the GaN/GaAs interface width is attributed to increased roughness with decreasing  $N_2H_4$ /Ga flux ratio.

Under the optimized growth conditions a nitrogen stabilized (1×1) surface reconstruction can be obtained on GaN/GaAs. Smooth epitaxial layers with an RMS roughness as low as 1.8 nm have been obtained.

1. V.G.Antipov, A.S.Zubrilov, A.V.Merkulov, S.A.Nikishin, A.A.Sitnikova, M.V.Stepanov, S.I.Troshkov, V.P.Ulin, N.N.Faleev, *Semiconductors*, 29 (10), 946, 1995.

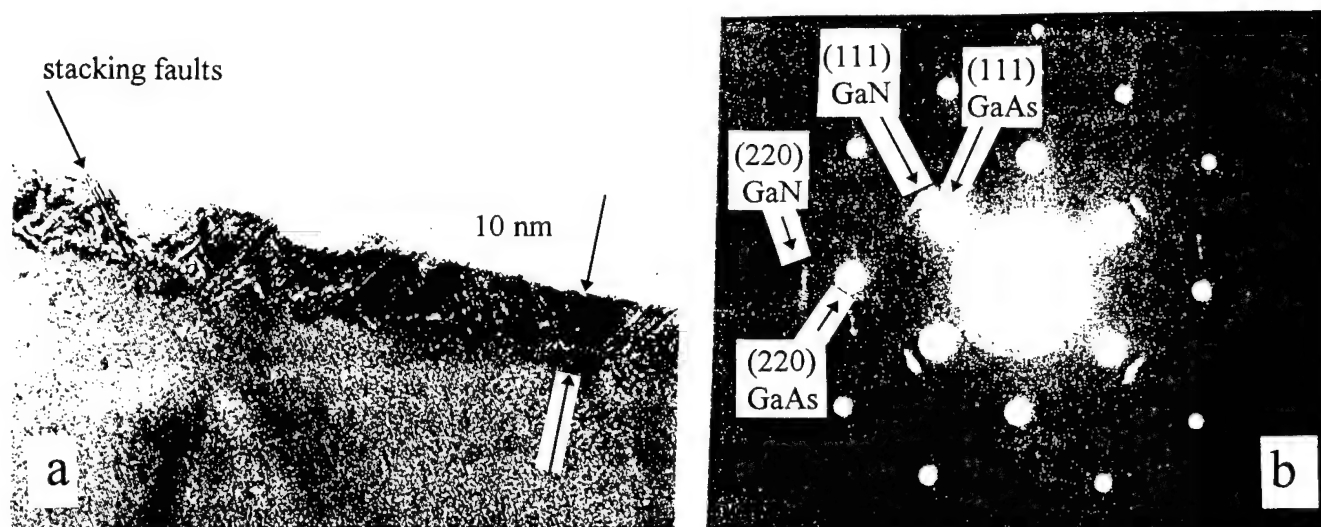


Fig.1. A  $[0\bar{1}1]$  cross-sectional image for GaN/GaAs (001) layer 10 nm thick (a) and corresponding electron diffraction pattern (b), showing cubic GaN structure.

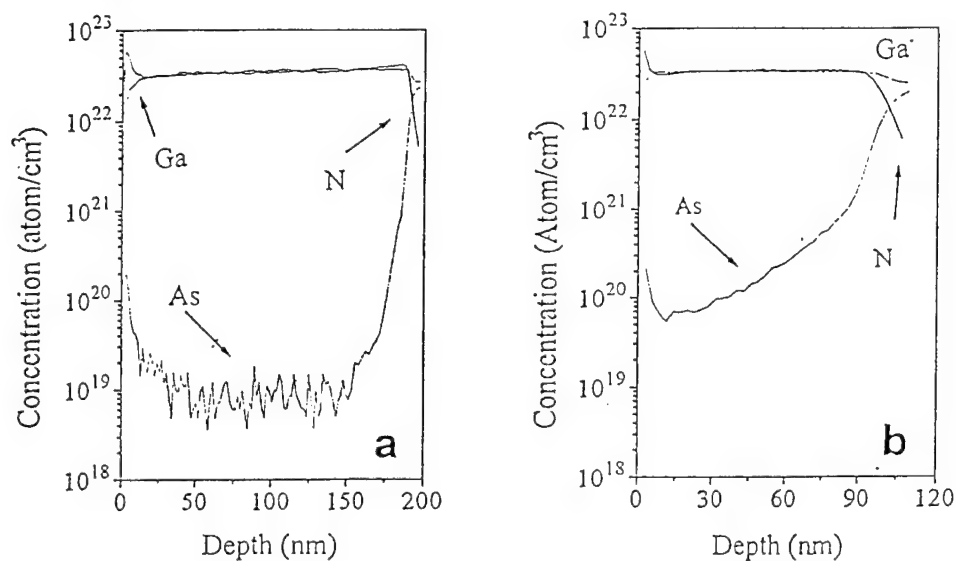


Fig. 2 SIMS profiles for samples of GaN/GaAs(001): a)  $\sim 180$  nm thick, RMS  $\sim 1.8$  nm,  $(N_2H_4/Ga) \sim 700$ ; b)  $\sim 100$  nm thick, RMS  $\sim 11.4$  nm,  $(N_2H_4/Ga) \sim 70$

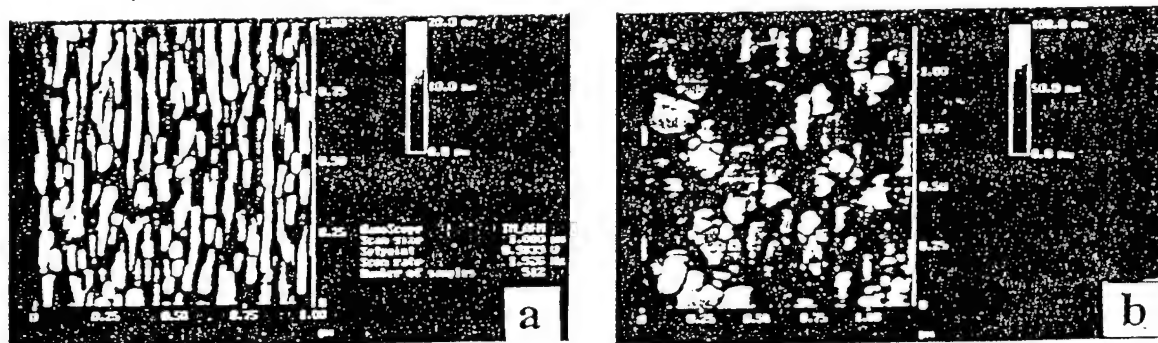


Fig.3. AFM images of  $\sim 150$  nm thick GaN layers grown at different  $N_2H_4/Ga$  flux ratios  
a)  $(N_2H_4/Ga) \sim 10^3$ ; b)  $(N_2H_4/Ga) \sim 70$ .

## **Cathodoluminescence of GaN films grown under Ga and N rich conditions by radio frequency-molecular beam epitaxy**

Sung Hwan CHO, Uitsu TANAKA, Takahiro MARUYAMA and Katsuhiro AKIMOTO  
Hajime OKUMURA\* and Sadufumi YOSHIDA\*

Institute of Materials Science, University of Tsukuba, 1-1-1 Tennodai, Tsukuba, Ibaraki 305, Japan, TEL:+81-298-6942, FAX:+81-298-7440

\*Electrotechnical Laboratory, 1-1-4 Umezono, Tsukuba, Ibaraki 305, Japan

Cathodoluminescence (CL) image and spectra of GaN films grown under various V/III ratio were measured at room temperature. It was found that the 300 K CL spectra of all samples were dominated by the near band-edge emission at 364 nm and the CL image at 364 nm significantly depend on V/III ratio, i.e., bright patch pattern with the diameter of about 4  $\mu\text{m}$  was observed in the film grown under Ga rich condition, on the other hand, the CL image grown under N rich conditions show quite uniform. The cause of the patch pattern may be due to the local variation of V/III ratio induced by a Ga micro segregation.

GaN films were grown on c-plane sapphire substrates under gallium and nitrogen rich conditions with radio-frequency molecular beam epitaxy (RF-MBE). Prior to the growth of GaN, the substrate surface was exposed to the nitrogen plasma for 20 min at 670 °C to form a thin AlN layer. Then, the GaN films were grown with substrate temperature of 700 °C, RF plasma power of 150 W, nitrogen flow rate of 0.4~4 sccm and Ga-cell temperature of 975 °C.

In the GaN films grown under the gallium rich condition, micro-structures like hillocks with the diameter of about 4  $\mu\text{m}$  were observed by scanning electron microscope (SEM). This region of hillocks show very strong emission intensity in CL spectra at 364 nm in comparison with smooth surface region.

When the V/III ratio increased, the hillocks disappeared in SEM image. However, the bright patch pattern with the diameter of about 2  $\mu\text{m}$  was still observed in CL image at 364 nm. In the GaN films grown under the nitrogen rich condition, flat and smooth surfaces were obtained and the any spatial variation in the CL image taken at 364 nm was not observed.

The bright patch pattern in the CL image may be formed by a Ga micro segregation where the crystal is Ga-rich and has high electron concentration due to N vacancy. It should be suggested that the nitrogen rich conditions are favourable to obtaining structurally and optically uniform films in RF-MBE.

# Radiative decay in type-II GaP/AlP/GaP quantum wells

S.Nagao, T.Fujimori, H.Gotoh

*Opto-electronics Laboratory, Mitsubishi Chemical Corporation, 1000, Higashimamiana, Ushiku, Ibaraki 300-12, Japan*

phone: +81-298-41-8220

FAX: +81-298-43-3796

e-mail: nagao@rc.m-kagaku.co.jp

H.Fukushima, T.Takano, S.Koshihara, F.Minami

*Department of Applied Physics, Tokyo Institute of Technology, Meguro-ku, Tokyo 152, Japan*

We have studied the optical properties of type-II GaP/AlP/GaP quantum wells (QW's) with different well widths which provide detailed information concerning the mechanisms of the radiative recombination. The GaP/AlP/GaP multiple QW structures were grown on GaP(001) substrates by gas source MBE using  $\text{PH}_3$  and elemental Ga and Al. Precise monolayer growth control was performed for the AlP well layers by means of in-situ monitoring of RHEED intensity oscillations.

At low temperatures, the PL spectra consists mainly of a no-phonon line. The decay of the no-phonon line is slow and nonexponential with lifetimes on the order of 1-100  $\mu\text{s}$ . The decay curves can be fit to a model which assumes that the radiative recombination occurs as the result of incoherent scattering due to disorder at the interface. The fit revealed that there are random and non-random contributions to the observed decay rates. The  $\Gamma$ -X mixing responsible for the no-phonon transition is assumed to be caused by the short range potential of the quantum wells along the z direction and fluctuations in the potential at the interfaces. The random processes are associated with the latter while non-random processes are associated with the former. We examined the dependence of the QW width on both random and non-random contributions to the radiation decay. The non-random/random contribution ratio increases with decreasing well width indicating the enhancement of the  $\Gamma$ -X mixing by the short range potential of the quantum wells as well as the increase of the penetration of the electron wave-function into the GaP barriers.

Furthermore, we refer to the radiation decay in sub-monolayer GaP/AlP/GaP QW's in comparison with that of QW's with thickness of several monolayers.

## Growth of Epitaxial Dysprosium Phosphide/Gallium Arsenide Heterostructures by MBE

### STUDENT PAPER

R.J. Hwu<sup>1</sup>, L.P. Sadwick<sup>1,2</sup>, P. P. Lee<sup>2</sup>, M. Patel<sup>1</sup>, H. Balasubramaniam<sup>1</sup>,  
M. Nikols<sup>2</sup>, P. C. Taylor<sup>3</sup>, J. Viner<sup>3</sup>, R.T. Lareau<sup>4</sup> and D.C. Streit<sup>5</sup>

<sup>1</sup>Dept. of Electrical Engineering, University of Utah, 3280 MEB, Salt Lake City, UT 84112

<sup>2</sup>Dept. of Materials Science, University of Utah, Salt Lake City, UT 84112

<sup>3</sup>Physics Dept., University of Utah, Salt Lake City, UT 84112

<sup>4</sup>Army Research Labs, Fort Monmouth, NJ 07703

<sup>5</sup>TRW, One Space Park, Redondo Beach, CA 90278

Details of the growth of epitaxial dysprosium phosphide (DyP) grown on gallium arsenide (GaAs) by gas source and conventional MBE will be presented. DyP is highly lattice matched to GaAs, with the room temperature mismatch being less than 0.01%. Custom-designed group V thermal cracker cells and group III high temperature effusion cells were used to grow DyP. High quality DyP epilayers, as determined by X-ray, SIMS. and TEM measurements, were obtained for growth temperatures ranging from 450 to 600°C at DyP growth rates of approximately 1  $\mu\text{m/hr}$ . The DyP growth dependence on substrate, cracker, and e-cell temperatures and V/III ratio will be presented.

The DyP epilayers are n-type with measured electron concentrations on the order of  $3 \text{ to } 4 \times 10^{20} \text{ cm}^{-3}$  with room temperature mobilities of 250 to 300  $\text{cm}^2/\text{Vs}$ . XPS results indicate that DyP is a semimetal. A consistent barrier height of 0.8 eV to GaAs is obtained from current versus voltage and capacitance versus voltage measurements.

Material and surface science properties of DyP/GaAs to be reported include Hall, two-theta and double-crystal X-ray diffraction spectra, SEM, TEM, SIMS, XPS, and Auger results. DyP/GaAs is stable in air with no apparent oxidation taking place, even after months of ambient exposure to untreated air. Detailed results of optical absorption including FTIR, photothermal deflection spectroscopy, and transmission studies coupled with variable temperature magnetotransport measurements will be presented.

**CBE Growth of InP, GaP, and GaInP using Uncracked  
Tertiarybutylbisdimethylaminophosphine - Implications for Conventional MBE**

L.P. Sadwick, and G.B. Stringfellow, and H.H. Ryu  
College of Engineering, The University of Utah, Salt Lake City, Utah 84112

T. Groshens and R.W. Gedridge, Jr.  
Naval Air Warfare Center Weapons Division, China Lake, CA 93555

R. T. Lareau  
Army Research Laboratories, Fort Monmouth, NJ 07703

Due to the allotropic nature and high vapor pressure of phosphorus (P), the growth of P-containing compounds by conventional MBE has historically been difficult. Recently, advances have been made in the design and operation of cracked valve sources. However, alternative approaches still need to be explored for the growth of P-containing compounds. We report the growth of indium phosphide (InP), gallium phosphide (GaP), and gallium indium phosphide (GaInP) by the chemical beam epitaxy (CBE) technique using a new experimental P precursor, tertiarybutylbisdimethylaminophosphine (TBBDMAP). TBBDMAP was specifically designed for use in the CBE growth of P-containing compounds. A potentially important advantage of TBBDMAP as compared to other P precursors is the ability to grow without thermally precracking. To the best of our knowledge this is the first report of the CBE growth of single crystalline layers of InP without precracking the group P source. The T<sub>50</sub> of TBBDMAP is approximately 425°C. InP was successfully grown with mirror-like morphology without P precursor precracking for substrate temperatures in the range of 450 to 520°C. All the samples were n-type with strong bound exciton photoluminescence (PL) was observed with only a relatively small impurity peak present even though the TBBDMAP is not of electronic grade purity. Depending on growth conditions, the unintentional doping ranged from mid 10<sup>16</sup> to low 10<sup>17</sup> cm<sup>-3</sup>; the main impurity detected by secondary ion mass spectroscopy (SIMS) was sulfur. Values of PL full width at half maximum were typically 10 meV at 16K. Results of a systematic study of the effects of growth temperature and V/III ratio for InP grown using TBBDMAP will be presented.

A discussion of the potential for growth using TBBDMAP in conventional MBE systems will be presented. The design of a TBBDMAP injector cell that can be readily incorporated into GSMBE and MBE systems and requires only a standard effusion cell port for gas entry will be described. Vacuum pumping requirements and contamination considerations when using TBBDMAP will also be addressed.

# Real-time investigation of In surface segregation during chemical beam epitaxy of $\text{In}_x\text{Ga}_{1-x}\text{P}/\text{GaAs}$ and $\text{In}_x\text{Ga}_{1-x}\text{As}/\text{GaAs}$ heterostructures

M. Mesrine, J. Massies, C. Deparis, N. Grandjean and E. Vanelle  
Centre de Recherche sur l'Hétéro-Epitaxie et ses Applications - CNRS  
Parc de Sophia Antipolis, rue Bernard Grégory - 06560 Valbonne (France)  
**Tel.:** (33) 93 95 42 14 **Fax.:** (33) 93 95 83 61 **e-mail:** jm@crheal.unice.fr

It is now recognized that surface segregation is a severe limitation to the building of perfectly abrupt III-V semiconductor interfaces. However, most of the available data is only concerned with the growth of  $\text{Ga}_x\text{In}_{1-x}\text{As}/\text{GaAs}$  by standard solid sources molecular beam epitaxy and only a few results have been reported for other III-V materials [1] as well as for different growth methods such as chemical beam epitaxy (CBE) [2-4]. Also only scarce reports concern real-time investigation during growth. In this communication we report on the study of In surface segregation during CBE growth of  $\text{GaInP}/\text{GaAs}$  and  $\text{GaInAs}/\text{GaAs}$  heterostructures. Owing to the peculiarities of the incorporation kinetics of triethylgallium used as Ga source, In segregation at both direct and inverse interfaces is evidenced in real-time by reflection high-energy electron diffraction via growth rate variation. Indeed, the growth rate transient at both interfaces (see for example Figs. 1a and 2b), which is not observed in the case of homoepitaxial growth (Figs. 1b and 2a), is the signature of surface segregation. This is well confirmed by the fact that the transient is eliminated when predepositing a certain amount of InP(InAs) on GaAs before the growth of GaInP(or GaInAs) (Fig. 1c). This amount corresponds to the equilibrium In surface concentration in the steady-state growth regime.

The determination of the amount of In which segregates for a given set of growth parameters and the layer-by-layer variation of the growth rate allow the deduction of the composition profiles through a simple segregation model [5].

- [1] J. M. Moison, F. Houzay, F. Barthe, J. M. Gerard, B. Jusserand, J. Massies and F. S. Turco-Sandroff, *J. Cryst. Growth* 111 (1991) 141 and references therein.
- [2] Y. Imura, K. Nagata, Y. Aoyagi and S. Namba, *J. Cryst. Growth* 105 (1990) 230.
- [3] H. S. Hansen, A. Bensaoula, S. Tougaard, J. Zborowski and A. Ignatiev, *J. Cryst. Growth* 116 (1992) 271.
- [4] J. P. Landesman, J. C. Garcia, J. Massies, G. Jezequel, P. Maurel, J.P. Hirtz and P. Alnot, *J. Vac. Sci. Technol.* b 10 (1992) 1761.
- [5] K. Muraki, S. Fukatsu, Y. Shiraki and R. Ito, *Appl. Phys. Lett.* 61 (1992) 557.

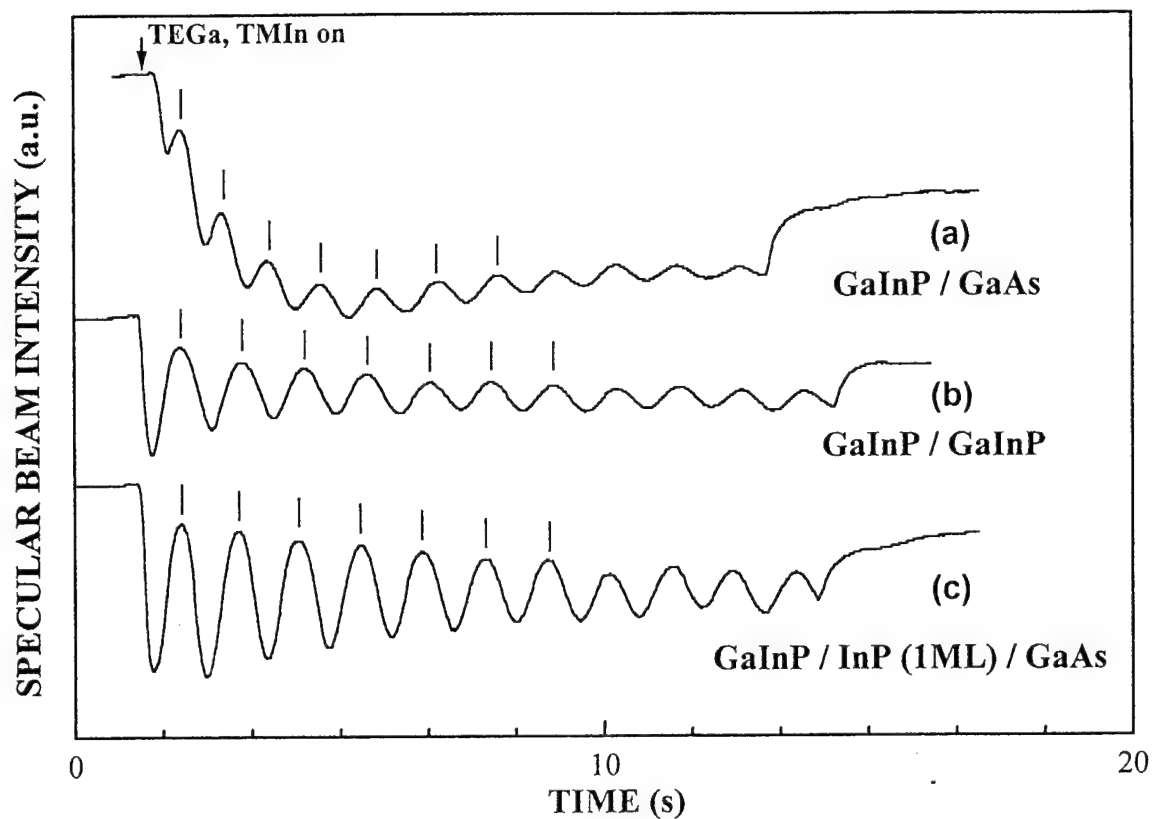


Fig. 1: Typical RHEED specular beam intensity oscillation of (a) GaInP on GaAs (b) GaInP on GaInP and (c) GaInP on 1monolayer (ML) of InP deposited on GaAs. Growth temperature 550°C.

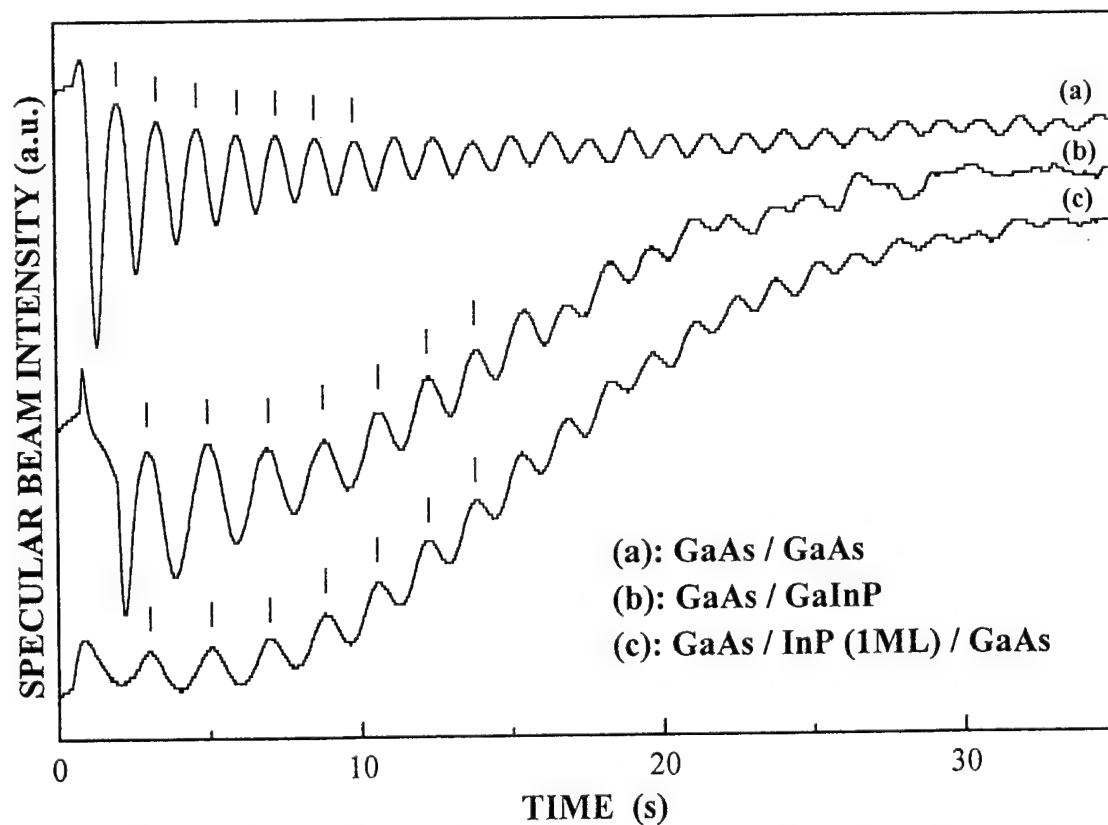


Fig 2: Typical RHEED specular beam intensity oscillation of (a) GaAs on GaAs; (b) GaAs on GaInP and (c) GaAs on 1ML of InP deposited on GaAs. Growth temperature 550° C.



# Molecular Beam Epitaxy of Strain-Compensated InGaAs/GaAsP Quantum-Well Intersubband Photodetectors

K. Bacher and S. Massie  
Quantum Epitaxial Designs, Inc.  
119 Technology Dr. Bethlehem, Pa 18015  
(610) 861-6930 (phone)  
(610) 861-5273 (FAX)

Quantum-Well Intersubband Photodetectors (QWIPs) are potentially important devices for mid- and long- infrared wavelengths ( $>4$  microns), especially for focal plane array and two-color applications. Current, state-of-the-art QWIPs for detecting light in the 8-10 micron range consist of multiple GaAs wells separated by  $\text{Al}_x\text{Ga}_{1-x}\text{As}$  barriers with  $x$ -values of 0.25 - 0.30. In order to reduce the aluminum content of the barriers or access shorter wavelengths, one must increase the depth of the quantum well by adding indium. Multiple InGaAs quantum wells, however, will tend to relax during growth because of the lattice mismatch with the GaAs substrate, leading to reduced device performance and pixel-to-pixel non-uniformity across a focal plane array.

For our application at 15 microns, we have addressed the problem of relaxation by incorporating a small percentage of phosphorous (from an InP effusion cell) into the GaAs barriers to compensate the strain of the InGaAs wells. In this way, we have been able to grow QWIP structures with 40 periods of 50 Å  $\text{In}_{0.2}\text{Ga}_{0.8}\text{As}$  quantum wells with 500 Å GaAsP barriers which exhibit no relaxation by high resolution x-ray diffraction measurements. X-ray measurements (Figure 1) and photoluminescence measurements demonstrate the excellent material quality obtained. Device results will be presented demonstrating the viability of this approach for fabricating high-performance QWIPs.

This work is supported by NASA under the administration of the Jet Propulsion Laboratories.

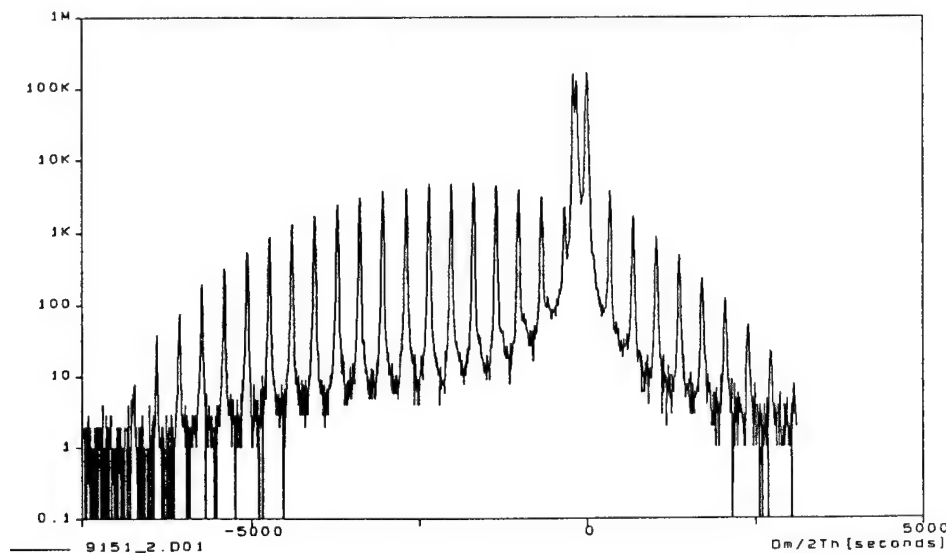


Figure 1: X-ray spectrum of strain-compensated QWIP.

# Self-organized quantum dot structures in strained $(\text{GaP})_n(\text{InP})_m$ short period superlattices grown on GaAs (N11) by gas-source MBE

S. J. Kim, H. Asahi, M. Takemoto, K. Asami and S. Gonda

The Institute of Scientific and Industrial Research, Osaka University  
8-1, Mihogaoka, Ibaraki, Osaka 567, Japan  
Tel. +81-6-879-8407, Fax. +81-6-879-8509, E-mail: asahi@sanken.osaka-u.ac.jp

Quantum wire/dot structures are gathering increasing interest for novel device applications and physical studies. Cheng et al. observed the growth-induced lateral periodic composition modulation in the strained  $(\text{GaP})_n(\text{InP})_n$  short period superlattices (SLs) grown on GaAs (100) substrate by gas source MBE (molecular beam epitaxy) and applied to the fabrication of quantum wires [1]. Recently, we have reported the substrate orientation dependence of lateral composition modulation and the self-organized formation of quantum dot structures in the  $(\text{GaP})_n(\text{InP})_n$  SLs grown by gas source MBE [2-3].

In this paper, we report on the monolayer number  $n$  and substrate orientation dependencies of the self-organized dot structures in the  $(\text{GaP})_n(\text{InP})_n$  SLs grown by gas source MBE.  $(\text{GaP})_n(\text{InP})_n$  SLs (thickness: 300 nm) were grown on GaAs (100), (211)A, (311)A, and (411)A substrates. Formed dot structures and their PL (photoluminescence) peak energies were greatly dependent on substrate orientation (N11) and monolayer number  $n$  due to lateral composition modulation or CuPt-type ordering.  $(\text{GaP})_1(\text{InP})_1$  SLs have no lateral composition modulation except for (100), and PL peak energies shifted toward lower energy as decreasing surface index  $N$ . At  $N=1$ , quasi-perfect CuPt-type ordering was observed.

Self-organized dot structures were formed in the  $(\text{GaP})_n(\text{InP})_n$  SLs grown on GaAs (N11)A by increasing  $n$ . TEM (transmission electron microscopy) images clearly showed that they have dot (columnar) structures with a size of about 10-20 nm (Fig. 1). The columnar structures are oriented along [211],  $\bar{[211]}$  and [100] directions for the SLs grown on (211)A, (311)A and (411)A substrates, respectively. This composition modulation is probably due to the interaction between the step structure on the surface and the island formation along the [0-11] direction, which is primarily determined by the direction of group-V dimer bonds related to the different surface energy and migration direction on the surface. These results suggest that the growth of  $(\text{GaP})_n(\text{InP})_n$  SLs on the GaAs (N11)A is promising to form a high density of quantum dot structures over  $\sim 10^{11} \text{ cm}^{-2}$ .

Quantum dot (QD) structures were fabricated by growing  $(\text{GaP})_n(\text{InP})_m$  SL (18 periods) /  $\text{In}_{0.49}\text{Ga}_{0.51}\text{P}$  (thickness = 20 nm) multilayers on GaAs (311)A and (411)A substrates. Cross-sectional TEM image clearly showed the QD structure formation with a lateral period of about 10 nm in both (01-1) and (011) (Fig. 2). From these QD structures PL emissions were observed (Fig. 3), where the PL peak energies were varied with the substrate orientation and multilayer structures. Temperature dependence of the PL peak energy showed an anomalous behavior in 125-170 K range (Fig. 4). Such behavior may be attributed to residual strain related to the existence of the ordered structure along the [311] growth direction in  $(\text{GaP})_2(\text{InP})_{2.5}$  SL regions. Anomalous temperature dependence was also observed for the  $(\text{GaP})_2(\text{InP})_2$  SLs grown on GaAs (311)A as well as for the SLs grown on other (N11) substrates.

In the conference, the detailed results on the self-organized structures in the  $(\text{GaP})_n(\text{InP})_n$  SLs and  $(\text{GaP})_n(\text{InP})_m$  SL/ $\text{In}_{0.49}\text{Ga}_{0.51}\text{P}$  QD structures are presented, and the growth mechanism will be also discussed.

## References

- [1] K.C.Hsieh, J.N.Baillargen and K.Y.Cheng: Appl.Phys.Lett. 57 (1990) 2244
- [2] S.J.Kim, H.Asahi, K.Asami, T.Ishibashi and S.Gonda: presented at 22nd Intern. Symp. on Compound Semiconductors, Korea, 1995, PF-26
- [3] S.J.Kim, H.Asahi, M. Takemoto, K.Asami, M. Takeuchi and S.Gonda: presented at 8th Intern. Confer. on Indium Phosphide and Related Materials, Germany, 1996, ThB 1-5

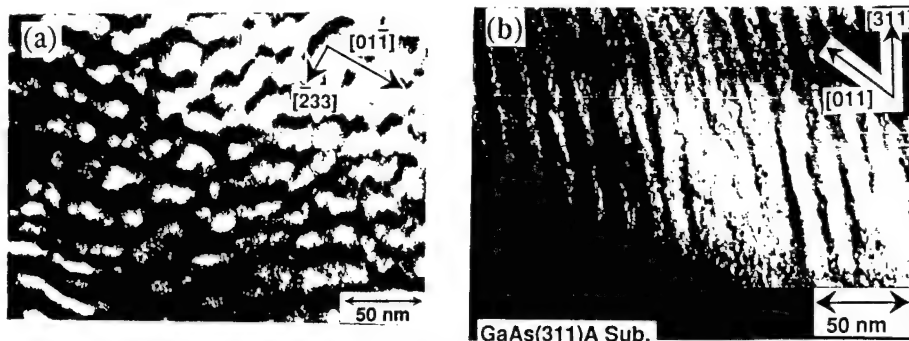


Fig. 1 TEM images for the  $(\text{GaP})_2(\text{InP})_2$  SLs grown on GaAs (311)A. (a) bright-field plan-view TEM image and (b)  $g=002$  dark-field cross-sectional TEM image for (01-1). The columnar structure ordering is oriented along the  $[211]$  direction.

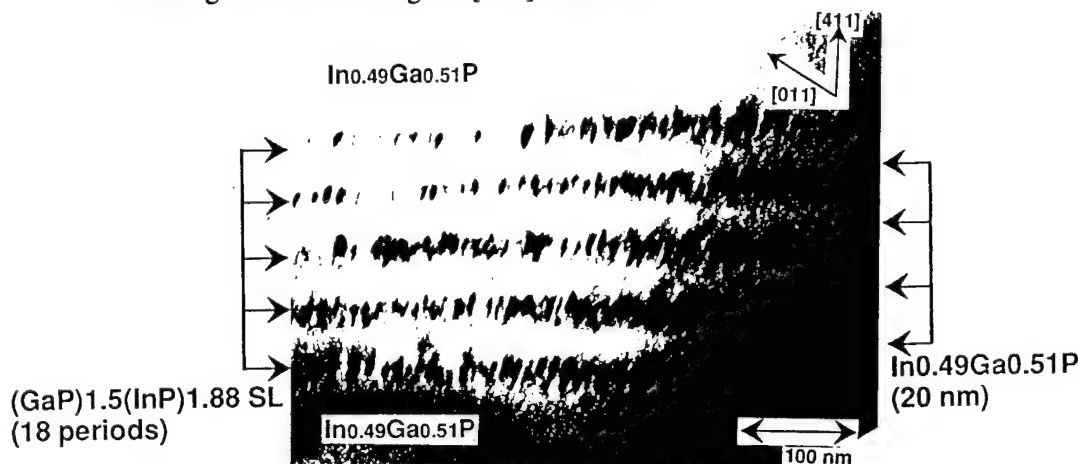


Fig. 2 (01-1) bright-field cross-sectional TEM image of the  $(\text{GaP})_{1.5}(\text{InP})_{1.88}$  SL/ $\text{In}_{0.49}\text{Ga}_{0.51}\text{P}$  quantum dot structure grown on GaAs(411)A. Both (011) and (01-1) cross-sectional TEM images showed the lateral composition modulation in the SL region.

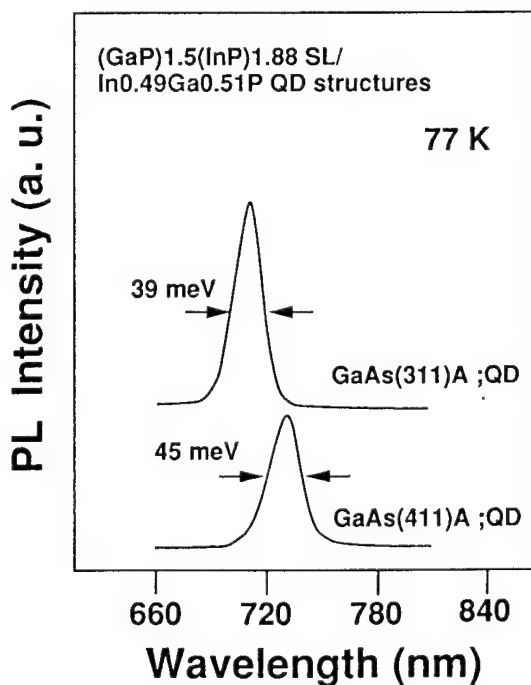


Fig. 3 77K PL spectra for the self-organized  $(\text{GaP})_{1.5}(\text{InP})_{1.88}$  SL/ $\text{In}_{0.49}\text{Ga}_{0.51}\text{P}$  quantum dot structures grown on (311)A and (411)A. P3.29

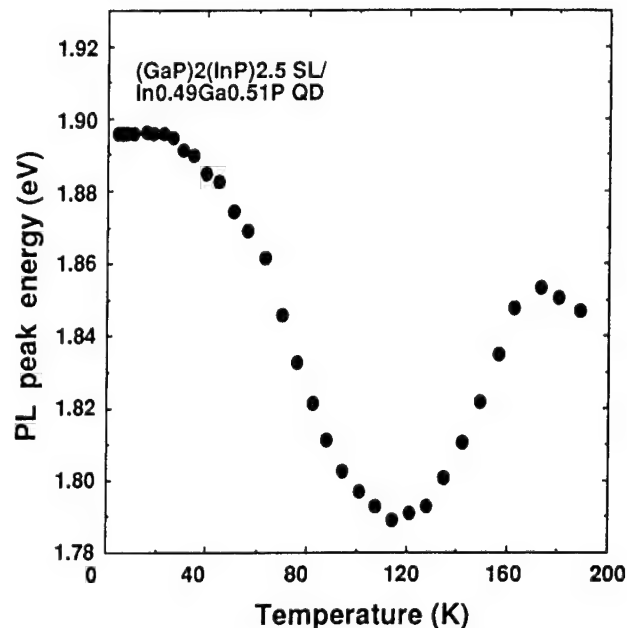


Fig. 4 Temperature dependence of PL peak energy for the  $(\text{GaP})_2(\text{InP})_{2.5}$  SL/ $\text{In}_{0.49}\text{Ga}_{0.51}\text{P}$  quantum dot structure grown on GaAs (311)A. Temperature dependence of PL peak energy shows an anomalous behavior in the range 125-170 K.

# Studies of Thin GaN Layers Grown on Sapphire using an RF-source

T G Andersson\*, K Nozawa and Y Horikoshi

NTT Basic Research Laboratories

3-1 Morinosato, Atsugi-shi, Kanagawa 243-1, Japan.

Fax: +(81) 462 40 4727, e-mail: thorvald@will.brl.ntt.jp

Thin layers of GaN were grown by MBE on sapphire (0001) using an RF-source and studied with reference to growth temperature and growth rate. Substrates were mounted In-free and their backside had a predeposited thin layer of Mo facing the heater filaments. Part of the substrate surface was masked in order to measure the film thickness after growth. A turbomolecular pump kept the N<sub>2</sub>-pressure at about  $2 \times 10^{-5}$  torr for an N<sub>2</sub>-flux of 0.5 sccm. Before growth, the substrate was thermally annealed under UHV-conditions. This was followed by deposition of a 50 nm thick AlN-layer grown in a two-step process at 500 and 600 °C. The GaAs growth rate on GaAs (001),  $r_{\text{GaAs}}$ , was used as reference. The GaN layers were inspected by optical microscopy, thicknesses were measured by a surface profiler, the structure by X-ray diffraction, surface morphology by SEM and AFM and the optical quality was studied by photoluminescence at 300 and 9 K using a He-Cd laser.

In the first part we studied the effect on the GaN growth rate and PL-emission by varying  $r_{\text{GaAs}}$  at 800 °C. Growth rate data are shown in Figure 1. In general the GaN growth rate,  $r_{\text{GaN}}$ , was considerably lower than that of GaAs mainly due to the crystallographic difference between the zincblende and wurtzite structures. Micrographs by SEM and AFM showed microcrystallites with sizes from ~ 30 to 300 nm. The value of  $r_{\text{GaN}}$  was higher than expected for the epitaxial wurtzite structure at a low growth rate,  $r_{\text{GaAs}} = 0.1 \mu\text{m/h}$ . For  $r_{\text{GaAs}} = 0.2 - 0.5 \mu\text{m/h}$  the GaN growth rate was found to be 45% of  $r_{\text{GaAs}}$  indicating a sticking coefficient of ~ 85%. Above this

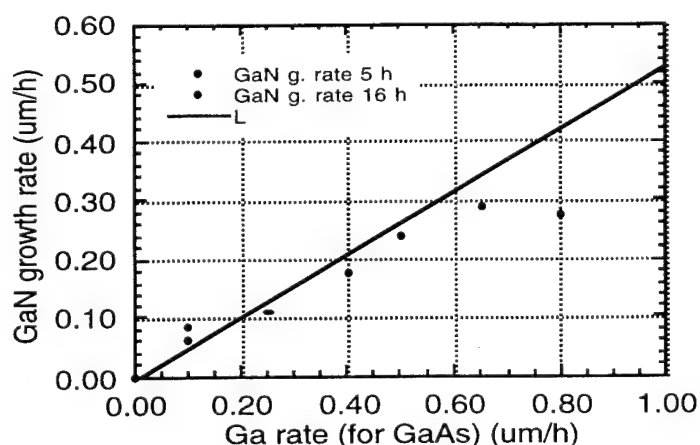


Figure 1.

range,  $r_{\text{GaN}}$  was independent of  $r_{\text{GaAs}}$  probably due to saturation in nitrogen/gallium supply. The intensity of the exciton related PL-peak at 3.475 eV varied strongly with growth rate (despite

increasing film thickness at constant growth time). The best GaN-layer quality was found at  $r_{\text{GaAs}} = 0.4 \mu\text{m/h}$ .

In the second series the effect of the growth temperature was addressed for a low growth rate,  $r_{\text{GaAs}} = 0.1 \mu\text{m/h}$ . Growth during 5 h provided layer thicknesses of approximately 300 nm. With increasing growth temperature the sticking coefficient for Ga ad-atoms declined. However, we could not establish a clear dependence of  $r_{\text{GaN}}$  on growth temperature in the range 700 - 800 °C for  $r_{\text{GaAs}} = 0.1 \mu\text{m/h}$ . X-ray analysis showed that the GaN peak FWHM declined from approximately 100 arcmin. at 600 °C to around 60 arcmin. at 730-790 °C while the buffer layer AlN peak width decreased from 100 arcmin. at 730 °C to 20 arcmin. at 815 °C. For growth temperatures above 800 °C only the AlN-peak was detected as the GaN growth rate was drastically reduced due to an increasing Ga desorption rate. For the given parameters, the results showed the existence of an optimum growth temperature rather than an improved layer quality with temperature. Growth at 785 °C gave the best film in terms of PL-intensity.

In general the PL-emission at ~2.2 eV was low, independent of the measurement temperature. In the near band gap region, five different peaks were observed, at 3.24 to 3.475 eV, with peak intensity depending on growth parameters. A peak at 3.42 eV, possibly related to defects as the films were rather thin, had higher intensity than the exciton related peak at 3.475 eV. In Figure 2 a PL-spectrum at 9 K having narrow peaks, is shown for a thick film (~ 1  $\mu\text{m}$ ) grown at 800 °C at  $r_{\text{GaAs}} = 0.1 \mu\text{m/h}$ .

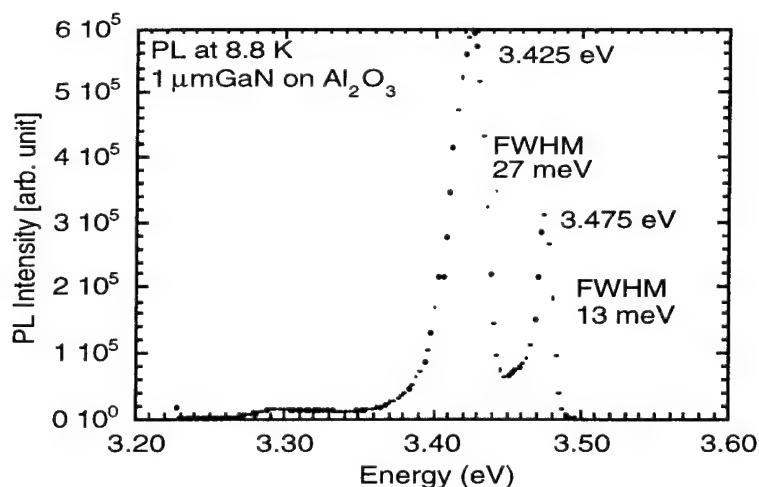


Figure 2.

In summary we studied thin GaN films on sapphire substrates. We found that variations in growth parameters such as growth temperature and growth rate largely influenced the film quality. Therefore high quality layers can be made only within a "parameter window". Since the X-ray peak width of the AlN strongly decreased with temperature the quality of the AlN buffer layer can influence the GaN-layer.

\* Permanent address, Department of Physics, Chalmers University of Technology and Göteborg University, S-412 96 Göteborg, Sweden.

## POSTER SESSION P4. CHARACTERIZATION, DEVICES, AND LASERS

**P4.1 Materials and device characteristics of  $\text{In}_y\text{Al}_{1-y}\text{As}/\text{In}_z\text{Al}_{1-z}\text{As}$  LCE-HEMTs on GaAs using low temperature MBE growth**, D.P. Docter, J.J. Brown, J. Speck and D.E. Grider, Hughes Research Laboratories, Malibu, California, USA

**P4.2 MBE growth and characterization of doped multiple quantum well avalanche photodiodes**, H.M. Menkara, R.N. Bicknell-Tassius, R. Benz II, and C.J. Summers, Georgia Tech Research Institute, Atlanta, Georgia, USA

**P4.3 Low dark current waveguide AlGaInAs/InP photodiodes using hybrid MBE and MOCVD growth**, K. Nishikata, H. Shimizu, K. Hiraiwa, S. Yoshida, N. Yamanaka, A. Kasukawa and M. Irikawa, The Furukawa Electric Co., Ltd. Yokohama, Japan

**P4.4 GaAs/AlAs resonant tunneling diodes with extremely flat interfaces grown on (411)A GaAs substrate by MBE**, K. Shinohara, K. Kasahara, S. Shimomura, A. Adachi, N. Sano and S. Hiyamizu, Osaka University, Japan

**P4.5 Molecular beam epitaxy of  $\text{Al}_{0.48}\text{In}_{0.52}\text{As}/\text{Ga}_{0.47}\text{In}_{0.53}\text{As}$  heterostructures on metamorphic  $\text{Al}_x\text{Ga}_{1-x}\text{In}_{1-y}\text{As}$  buffer layers**, M. Haupt, K. Köhler, P. Ganser, S. Emminger, S. Müller, and W. Rothmund, Fraunhofer-Institut für Angewandte Festkörperphysik, Freiburg, Germany

**P4.6 Designing delta-doped quantum well structures suitable for power FET applications**, J.M. Roberts, J.J. Harris, M. Hopkinson, C. Roberts, UCL, London, United Kingdom

**P4.7 High voltage gain, high breakdown voltage, and device linearity improvement by pseudomorphic FET with triple delta-doped channel**, Wen-Shiung Lour, Jiann-Ru Chen, and H.R. Chen, National Taiwan-Ocean University, Republic of China

**P4.8 Photoluminescence characterization of MBE grown AlGaAs/InGaAs/GaAs Pseudomorphic HEMTs**, M. Wojtowicz, D. Pascua, A.C. Han, T. R. Block, and D.C. Streit, TRW Electronics and Technology Division Redondo Beach, California, USA

**P4.9 Sub-40 $\mu\text{A}$  continuous-wave lasing in an oxidized vertical-cavity surface-emitting laser with dielectric mirrors**, D.L. Huffaker, L.A. Graham, H. Deng, D.G. Deppe, C. Lenox, and B.G. Streetman, The University of Texas at Austin, Texas, USA

**P4.10 Full gaseous source growth of separate confinement MQW 1.55  $\mu\text{m}$  laser structures in a production MOMBE**, M. Popp, H. Heinecke, University of Ulm, Germany

**P4.11 Improved electro-absorption properties in 1.3  $\mu\text{m}$  MQW waveguide modulators by modified doping profile**, X.B. Mei, K.K. Loi, W.S.C. Chang, and C.W. Tu, University of California, San Diego, California, USA

**P4.12 CBE growth of 850nm GaAs/AlGaAs quantum-well lasers**, T.J. Whitaker, P.D.J. Calcott, T. Martin, M.J. Kane, G.W. Smith, R.J. Balmer, and M. Houlton, DRA (Malvern) Worcestershire, United Kingdom

**P4.13 GSMBE growth and characterization of InGaAs/InP strained-layer MQWs in a P-i-N configuration**, Wang Xialiang, Sun Dianzhao, Kong Meiying, Hou Nun and Zen Yiping, Chinese Academy of Sciences, Beijing, China

**P4.14 Characterisation of bulk-GaInP and (GaAs/GaInP) p-i-n diode structures grown by solid-source MBE**, M. Hopkinson, J.P.R. David and R. Ghin, University of Sheffield, United Kingdom

**P4.15 Symmetric triangular-barrier optoelectronic switch (S-TOPS) by gas source MBE**, H. Sakata, Y. Nagao, and Y. Matsushima, KDD R&D Laboratories, Saitama, Japan

**P4.16 Al/GaAs/GaAs, AlGaAs/InGaAs multiple quantum wells and Si-doped p-type quantum well infrared photodetectors grown on (311)A GaAs**, Albert Chin, K. Lee, J. Chu, and S.S. Li, National Chiao Tung University, Hsinchu, Taiwan

**P4.17 CBE growth of tensile-strained GaAsP/GaAlAs quantum well heterostructures for laser application**, J.Ch. Garcia, A. Lebkiri, A. Fily, Ph. Collot, J. Massies, M. Leroux, Laboratoire Central de Recherches Thomson, Orsay, France

**P4.18 Strain compensation in highly carbon doped GaAs/AlAs distributed Bragg reflectors**, A. Mazuelas, R. Hey, M. Wassmer, and H.T. Grahn, Paul-Drude-Institut für Festkörperelektronik, Berlin, Germany

**P4.19 808nm high power laser grown by MBE through the control of Be diffusion and use of short-period superlattice**, Donghai Zhu, Zhanguo Wang, Jiben Liang, Bo Xu, Zhanping Zhu, Jun Zhang, Qian Gong, Shengying Li, Chinese Academy of Sciences, Beijing, P.R. China

**P4.20 GaAs quantum well islands form by sub-monolayer AlAs masking and thermal desorption**, Timothy A. Strand, R.L. Naone, L.A. Coldren, P.M. Petroff, and E.L. Hu, University of California, Santa Barbara, California, USA

**P4.21 Molecular-beam epitaxy of self-assembled InAs quantum dots on non-(100) oriented GaAs**, P.P. González-Borrero, E. Marega Jr., D.I. Lubyshev, E. Petitprez and P. Basmaji, Instituto de Física de São Carlos-Universidade de São Paulo, Brazil

**P4.22 InAs/GaAs self-organized quantum dots grown by ALMBE and MBE**, A. Bosacchi, P. Frigeri, S. Franchi, P. Allegri, and V. Avanzini, CNR-MASPEC Institute, Parma, Italy

**P4.23 Temperature-insensitive photoluminescence at high temperatures in GaInAs strained multiple quantum wire heterostructures**, D.E. Wohlert, S.T. Chou, and K.Y. Cheng, University of Illinois at Urbana-Champaign, Illinois, USA

**P4.24 Growth of GaInAsP quantum wire heterostructures using the strain-induced lateral-layer ordering process**, A.C. Chen, A.M. Moy, K.Y. Cheng, L.J. Chou and K.C. Hsieh, University of Illinois at Urbana-Champaign, Illinois, USA

**P4.25 Formation of self-aligned  $\text{In}_{0.5}\text{Ga}_{0.5}\text{As}$  quantum dots on GaAs by molecular beam epitaxy**, Jen-Inn Chyi, Tzer-En Nee, Ching-Ting Lee, Jia-Lin Shieh, and Jen-Wei Pan, National Central University Chung-Li, Taiwan, Republic of China

**P4.26 MBE growth and magnetotunnelling transport properties of a single GaAs/AlAs/GaAs barrier incorporating InAs quantum dots**, M. Henini, I.E. Itskevitch, T. Ihn, P. Moriarty, A. Nogaret, P.H. Beton, L. Eaves, P.C. Main, J.R. Middleton and J. Chauhan, University of Nottingham, UK

**P4.27 Luminescence anomaly in band gap tailored InGaAlAs quaternary alloy grown by MBE**, A. Ramam and S.J. Chua, National University of Singapore, Singapore

**P4.28 Determination of the aluminum content in  $\text{Al}_x\text{Ga}_{1-x}\text{As}$  layers: the final chapter**, Z.R. Wasilewski, M.M. Dion, D.J. Lockwood, P. Poole, R.W. Streater and A.J. SpringThorpe, National Research Council of Canada, Ottawa, Ontario, Canada

**P4.29 Non-destructive whole wafer well thickness measurements on ultra-high speed tunnelling structures by excitation photoluminescence**, P.D. Buckle, P. Dawson, M. Missous and W.S. Truscott, University of Manchester Institute of Science and Technology, Manchester, United Kingdom

**P4.30 The roles of substrate perfection and strain in channel layers of InP-based pseudomorphic high electron mobility transistors**, K.M. Matney and M.S. Goorsky, D.C. Streit, and T.R. Block, University of California, Los Angeles, California, USA

**P4.31 Scanning tunneling spectroscopy and first-principles investigation on GaAs(001)(2x6)-S surface formed by molecular beam epitaxy**, Shiro Tsukamoto, Takahisa Ohno, and Nobuyuki Koguchi, National Research Institute for Metals, Ibaraki, Japan



**P4.32 Growth mode induced surface morphology and its relation to optical and electrical properties of GaAs single quantum wells**, R. Hey, I. Gorbunova, M. Ramsteiner, U. Jahn, K. Friedland, L. Däweritz and K.H. Ploog, Paul-Drude-Institut für Festkörperelektronik, Berlin, Germany

**P4.33 Does scanning tunneling microscopy provide a realistic picture of the step array of vicinal GaAs(001) surfaces grown at high temperature?**, L. Däweritz, H. Nörenberg, P. Schützendübe, and K. Ploog, University of Oxford, United Kingdom

**P4.34 Photoluminescence of low temperature AlGaAs/GaAs multiple quantum wells**, W. Feng, F. Chen,, Q. Huang, and J.M. Zhou, Chinese Academy of Sciences, Beijing, People's Republic of China

**P4.35 Effects of morphology and strain on photoemission oscillations measured during the growth of resonant tunneling devices**. J.J. Zinck and D.H. Chow, Hughes Research Laboratories, Malibu, California

**P4.36 X ray fluorescence: a complementary in-situ MBE probe**, Joseph Pellegrino, National Institute of Standards and Technology, Gaithersburg, Maryland, USA

**P4.37 Substrate temperature change in III-V molecular beam epitaxy**, Keith R. Evans and J.E. Ehret, C.R. Jones and R. Kaspi, Wright Laboratory, Wright-Patterson Air Force Base, Ohio, USA

**P4.38 Reflectivity difference spectroscopy study on thin film ZnSe grown on GaAs by molecular beam epitaxy**, C.C. Kim, Y.P. Chen, M. Daraselia, S. Sivananthan, D.J. Smith, S.-C.Y. Tsen, Arizona State University, Tempe, Arizona, USA

**P4.39 Real-time monitoring of RHEED using digital signal processing techniques**, R.F. Kromann, R.N. Bicknell-Tassius, A.S. Brown and J.S. Dorsey, Georgia Institute of Technology, Atlanta, Georgia, USA

**P4.40 Concept of sensor simulator for real-time monitoring and control of molecular beam epitaxy growth**, J.J. Zhou, Y. Li, P. Thompson, D.L. Sato and H.P. Lee, University of California, Irvine, California, USA

**P4.41 In situ BEEM study of interfacial dislocations and point defects**, H. von Känel, T. Meyer, H. Sirringhaus, and Y.Y. Lee, Laboratorium für Festkörperphysik, Zurich, Germany

**P4.42 *in situ* STM characterisation of Ga<sup>+</sup> focused ion beam interactions with MBE grown GaAs(100)**, S.J. Brown, P.D. Rose, E.H. Linfield, D.A. Ritchie, G.A.C. Jones, University of Cambridge, United Kingdom



# Materials and Device Characteristics of $\text{In}_y\text{Al}_{1-y}\text{As}/\text{In}_z\text{Al}_{1-z}\text{As}$ LCE-HEMTs on GaAs Using Low Temperature MBE Growth

**D.P. Docter, J.J. Brown, J. Speck\*, and D.E. Grider**

Hughes Research Laboratories, 3011 Malibu Canyon Rd., Malibu, CA 90265

Tel: (310) 317-5736 FAX: (310) 317-5450

\*Materials Science Dept., University of California at Santa Barbara

Because of the attraction of using larger and lower cost substrates, there has been increasing interest in MBE growth of lattice mismatched  $\text{In}_{0.52}\text{Al}_{0.48}\text{As}/\text{In}_{0.53}\text{Ga}_{0.47}\text{As}$  High Electron Mobility Transistors (HEMTs) on GaAs substrates utilizing low temperature buffer layers to accommodate mismatch and limit propagation of misfit dislocations into the active HEMT device region. However, this approach need not be limited to the particular compositions (i.e.,  $y = 0.53$ ,  $z = 0.52$ ) lattice matched to InP, and it can be applied to  $\text{In}_z\text{Al}_{1-z}\text{As}/\text{In}_y\text{Ga}_{1-y}\text{As}$  HEMTs grown at other compositions which may offer significant advantages in device performance (e.g., improved breakdown voltages).

With this in mind, we have studied the material and device characteristics of lattice mismatched  $\text{In}_z\text{Al}_{1-z}\text{As}/\text{In}_y\text{Ga}_{1-y}\text{As}$  HEMTs grown on GaAs by MBE for compositions ranging from  $y, z = 0.30$  to  $0.50$ . Each of these heterostructures, referred to as Lattice Constant Engineered (LCE) HEMTs, utilizes a graded-composition low temperature (LT)  $\text{In}_z\text{Al}_{1-z}\text{As}$  buffer grown on GaAs with an active  $\text{In}_z\text{Al}_{1-z}\text{As}/\text{In}_y\text{Ga}_{1-y}\text{As}$  HEMT device structure grown on top at standard MBE growth temperatures.

Results from DCXRD, PL, TEM, and Hall mobility measurements on LCE-HEMT heterostructures all show that the graded LT- $\text{In}_z\text{Al}_{1-z}\text{As}$  buffer material effectively limits dislocation propagation into the high quality active HEMT structure on top. This effect may be due to point defects in the LT- $\text{In}_z\text{Al}_{1-z}\text{As}$  buffer that assist dislocation glide and annihilation. LCE-HEMTs with compositions from  $y, z = 0.30$  to  $0.50$  exhibit Hall mobilities from  $7630 \text{ cm}^2/\text{V-s}$  to  $10610 \text{ cm}^2/\text{V-s}$ , values which equal or exceed those of PHEMTs on GaAs and lattice matched HEMTs on InP, respectively. We will report on these and other materials characteristics which exhibit the expected dependence on the compositions of the  $\text{In}_z\text{Al}_{1-z}\text{As}/\text{In}_y\text{Ga}_{1-y}\text{As}$  LCE-HEMT structures.

We have fabricated  $0.25 \text{ }\mu\text{m}$  gate length  $\text{In}_z\text{Al}_{1-z}\text{As}/\text{In}_y\text{Ga}_{1-y}\text{As}$  LCE-HEMTs using heterostructures with compositions ranging from  $y, z = 0.30$  to  $0.50$ . These LCE-HEMTs exhibit very good DC and RF device characteristics. In particular,  $0.25 \text{ }\mu\text{m}$  LCE-HEMTs ( $y, z = 0.40$ ) exhibit a transconductance ( $G_m$ ) of  $616 \text{ mS/mm}$  and  $f_T = 75 \text{ GHz}$ . DC, RF, and power characteristics of these and other short gate length devices will be presented.

This work has been supported in part by AFOSR.

## **MBE Growth and Characterization of Doped Multiple Quantum Well Avalanche Photodiodes**

H. M. Menkara , R. N. Bicknell-Tassius, R. Benz, II and C. J. Summers

Advanced Materials Technology Division  
Georgia Tech Research Institute  
Atlanta, GA 30332-0861  
Office Phone and fax numbers: (404) 894-9885, (404) 894-4832  
e-mail: rb91@prism.gatech.edu

Extensive studies have been carried out on Multiple Quantum Well (MQW) structures because of their potential applications in avalanche photodiodes (APDs) and tunneling devices. The desire for high performance optical detectors has resulted in several proposed MQW APD structures using different material systems in an attempt to optimize their gain, noise, and bandwidth characteristics. In addition, the recent interest in the use of APDs in imaging systems has necessitated the development of devices with low levels of dark currents and high gains for low light applications.

In this study, we show how certain growth, processing and surface treatment techniques can be used to dramatically lower the dark current behavior of APDs by several orders of magnitude. The devices that were measured were volume- and delta-doped MQW APDs that were grown using Molecular Beam Epitaxy (MBE). All devices consisted of a 1  $\mu\text{m}$  Be-doped ( $3 \times 10^{18} \text{ cm}^{-3}$ )  $p^+$  top layer, and a 1  $\mu\text{m}$  Si-doped ( $3 \times 10^{18} \text{ cm}^{-3}$ )  $n^+$  back contact layer. In the volume-doped MQW devices, high electric fields were achieved in the narrow bandgap GaAs wells of the avalanche region through the introduction of 50 Å of highly doped ( $3.0 \times 10^{18} \text{ cm}^{-3}$ ) adjacent  $p^+$  and  $n^+$  layers. In the delta-doped APDs, this was accomplished using delta-doped  $p^+$  and  $n^+$  layers with a sheet charge density of  $1-5 \times 10^{12} \text{ cm}^{-2}$ , separated by undoped spacer layers ranging from 50 to 150 Å. Through careful dopant calibration, using multiple codoped samples, the devices could be grown such that they were essentially fully depleted as grown, even though doping levels in the avalanche region were in the low  $10^{18} \text{ cm}^{-3}$ .

After processing the devices into mesa diodes, various surface passivation treatments were investigated. These include both plasma ashing in an  $\text{O}_2$  plasma and sodium sulfide treatments. Through the application of such treatments, a decrease in the reverse bias dark current by as much as a factor of 1000 was achieved. Dark currents as low as 1 pA were obtained under zero bias. In some APDs, the dark currents increased to only 12 pA at 20% of breakdown. In addition, these devices exhibited extremely high gains which exceeded 35,000 in some APDs. In traditional APDs structures, the presence of high dark currents usually presents a limiting factor preventing the further increase in a device's photocurrent gain beyond avalanche breakdown. By being able to reduce the dark currents in, we were able to maintain dark current levels well below those of the photocurrents. This made it possible to achieve and sustain high levels of gains well beyond the onset of junction breakdown.

# Low Dark Current Waveguide AlGaInAs/ InP Photodiodes Using Hybrid MBE and MOCVD Growth

K. Nishikata, H. Shimizu, K. Hiraiwa, S. Yoshida, N. Yamanaka, A. Kasukawa and M. Irikawa

Yokohama R&D Laboratories, The Furukawa Electric Co., Ltd.

2-4-3 Okano, Nishi-ku, Yokohama 220, Japan

TEL: +81-45-311-1219, FAX: +81-45-322-6961, e-mail: knishi@mrc\_mc.yokoken.furukawa.co.jp

Waveguide photodiodes (WGPDs) have previously had high dark current ( $\geq 1$  nA) while the traditional surface-illuminated photodiode achieved superior low dark current (10 to 100 pA). The high dark current had been one of problems in the development of the WGPDs. To reduce the dark current in the WGPDs, it is essential that the high-crystalline quality for required thick layers is obtained and surface-leakage current, especially on the mesa-side of a ridge-stripe structure, is eliminated, because surface leakage on the mesa-side was a main source of the surface-leakage current.

In order to solve this problem, we optimized MBE-growth conditions and utilized hybrid-growth technique of MBE and MOCVD. The dark current of the WGPDs was 7 pA with one cleaved facet at the reverse bias voltage of -3V. This remarkably-reduced dark current indicates generation-recombination dominates the leakage and the surface-leakage component is eliminated.

Fig. 1 shows the schematic cross section of the WGPD. First, using MBE, an AlGaInAs absorption layer sandwiched by AlGaInAs optical confinement layers were grown. We optimized the MBE growth conditions of growth rate, V/III ratio and growth temperature ( $T_g$ ) to suppress small defects ( $4\text{ }\mu\text{m} \times 1\text{ }\mu\text{m}$ , the height of 20 nm) observed for the thick layer growth. Fig. 2 shows the defect density as a function of the  $T_g$ . The minimum of the defect density was observed at the  $T_g$  of  $460^\circ\text{C}$ . With the growth rate of  $1.0\text{ }\mu\text{m} / \text{hour}$ , the V/III ratio of 10 and the  $T_g$  of  $460^\circ\text{C}$ , we have successfully obtained high-crystalline quality of more than  $6\text{ }\mu\text{m}$  AlGaInAs layer. Second, we grew p-InP cladding and p-GaInAsP contact layers using MOCVD. The epitaxial layers were processed into WGPDs in which the junction were  $30\text{ }\mu\text{m}$ ,  $50\text{ }\mu\text{m}$  and  $100\text{ }\mu\text{m}$  long by  $19\text{ }\mu\text{m}$  wide.

Fig. 3 shows the dark current at the reverse voltage of -3V as a function of the absorption-stripe length. The dark current for devices with one cleaved facet were 7 pA, 10 pA and 16 pA with the stripe length of  $30\text{ }\mu\text{m}$ ,  $50\text{ }\mu\text{m}$  and  $100\text{ }\mu\text{m}$ , respectively. The diffusion current is estimated to be a few pA and the tunneling current is negligible at this low bias voltage. The dark current value at the stripe length of 0 indicates the leakage on the illumination surface. The increase with the stripe length consists of the leakage current originating from the generation-recombination and mesa-surface leakage components. These results with the small values indicate the generation-recombination component dominates and the surface leakage component is eliminated.

In summary, we optimized the MBE-growth conditions and utilized the hybrid-growth technique of MBE and MOCVD. As a result, we obtained WGPDs with low dark current which is 7 pA with one cleaved facet at the reverse bias voltage of -3V.

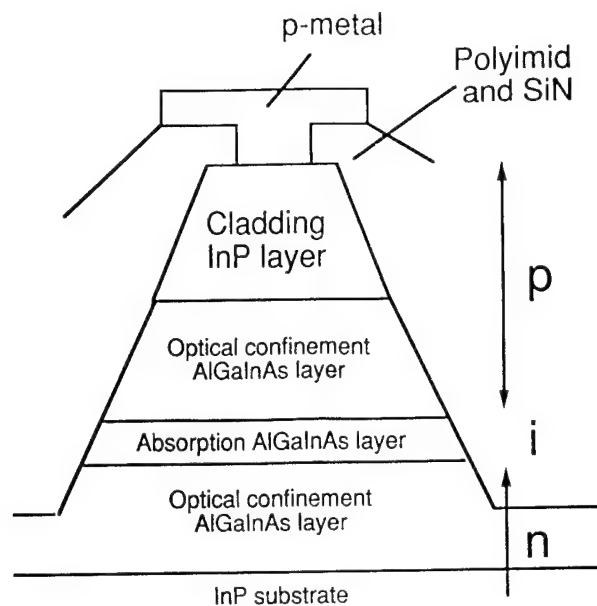


Fig.1 Schematic view of p-i-n waveguide photodiodes. An absorption layer and optical confinement layers of AlGaInAs were grown by MBE and a cladding layer of InP and a contact layer of GaInAsP were grown by MOCVD.

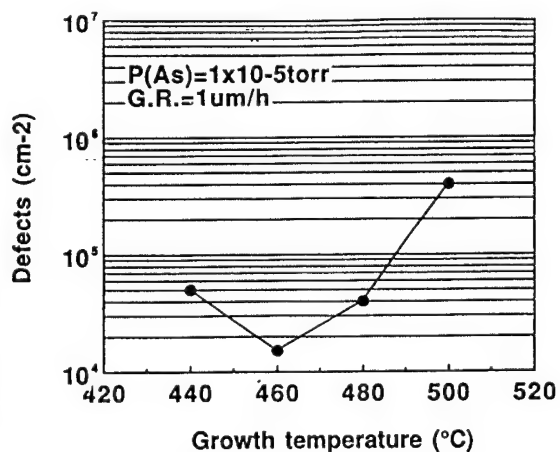


Fig.2 Defect density of 3μm AlGaInAs as a function of growth temperature.

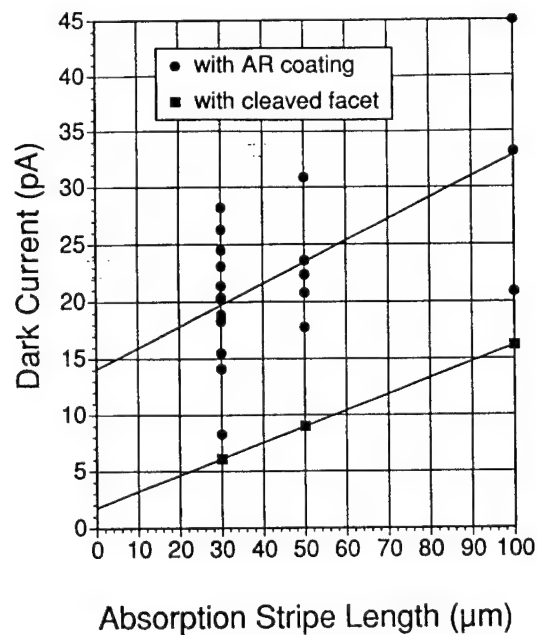


Fig.3 Dark current of the waveguide photodiodes at the reverse bias voltage of -3V.

# GaAs/AlAs resonant tunneling diodes with extremely flat interfaces grown on (411)A GaAs substrate by MBE

K. Shinohara<sup>1</sup>, K. Kasahara<sup>1</sup>, S. Shimomura<sup>1</sup>, A. Adachi<sup>2</sup>, N. Sano<sup>3</sup> and S. Hiyamizu<sup>1,4</sup>

<sup>1</sup> Faculty of Engineering Science, Osaka University, Toyonaka, Osaka 560, Japan

<sup>2</sup> R & D Division, Nissin Electric Co. Ltd., Umezū-Takase-cho, Ukyō-ku, Kyoto 615, Japan

<sup>3</sup> Faculty of Science, Kwansei Gakuin University, Nishinomiya, Hyogo 662, Japan

<sup>4</sup> Research Center for Extreme Materials, Osaka University, Toyonaka, Osaka 560, Japan

Phone: +81-6-850-6457, Fax: +81-6-845-4632, E-mail: shino@d310.mp.es.osaka-u.ac.jp

Atomically flat GaAs/AlGaAs interfaces over a macroscopic area have been desired for applications to quantum devices. It has been reported that GaAs/Al<sub>0.3</sub>Ga<sub>0.7</sub>As quantum wells (QWs) grown on (411)A GaAs substrates by MBE show extremely flat interfaces over a very large area (1 cm × 1 cm).<sup>1,2)</sup> Only a single photoluminescence (PL) peak with the smallest FWHM at 4.2 K was observed from a single QW on the (411)A substrate, indicating that extremely flat interfaces are realized in GaAs/AlGaAs QWs grown on (411)A GaAs substrates. The flat interfaces have been applied to GaAs/Al<sub>0.3</sub>Ga<sub>0.7</sub>As resonant tunneling diodes (RTDs) which exhibited a superior peak-to-valley (p/v) ratio (5.0 at 77K) to that (4.1) of a RTD simultaneously grown on (100) GaAs substrate, but their I-V characteristics were not so good because of thick barrier layers (10 nm) and low barrier height.<sup>3)</sup> In this paper, we report successful fabrication of GaAs/AlAs RTDs on a (411)A GaAs substrate by MBE for the first time, which exhibit much improved p/v ratio of 11.8 at 80K.

GaAs/AlAs double-barrier resonant tunneling (DBRT) structures with a 7.2 nm-thick GaAs well and 3 nm-thick AlAs barriers were grown simultaneously on (411)A and (100) GaAs substrates by MBE. Undoped GaAs/AlAs DBRT structure was grown at 640 °C and V/III ratio of 14 (in pressure) to form the atomically flat (411)A GaAs/AlAs interfaces. On the other hand, Si-doped GaAs layers in the RTD structure were grown at 580 °C and V/III ratio of 14 to realize n-GaAs with low compensation ratio similar to a Si-doped GaAs grown on (100) substrate.<sup>4)</sup> Growth rates of GaAs and AlAs were 1.0 μm/h. Figure 1 shows I-V characteristics (80K) of the (411)A RTD with a contact area of 120 μm in diameter. The p/v ratio for the (411)A RTD is 11.8 which is 57% higher than 7.5 for a (100) RTD. Figure 2 shows the peak and valley current densities of the (411)A and (100) RTDs as a function of the temperature. The valley current density is almost constant below 50 K due to the extinction of the current of thermally activated electrons over the AlAs barrier. The improved p/v ratio of the (411)A RTD is due to the drastic decrease of the valley current density. These results indicate that the (411)A GaAs/AlAs flat interfaces can be successfully applied to RTDs.

## References

- 1) S. Shimomura et al., Jpn. J. Appl. Phys. **32** (1993) L1728.
- 2) S. Hiyamizu et al., J. Vac. Sci & Technol. **B12** (1994) 1043.
- 3) S. Shimomura et al., to be published in Solid State Electron. (1996).
- 4) K. Shinohara et al., Semicond. Sci. Technol. **11** (1996) 125.

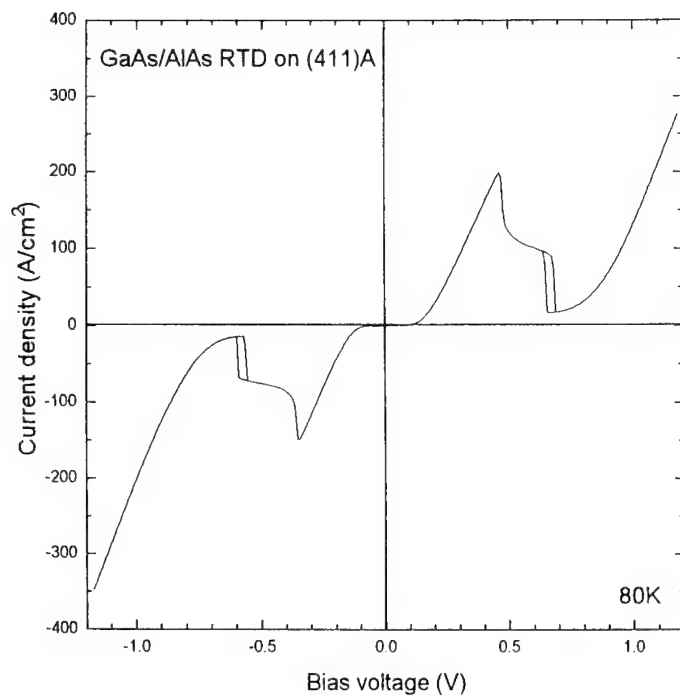


Fig. 1 I-V characteristics of a GaAs/AlAs RTD fabricated on a (411)A GaAs substrate with a contact area of  $120 \mu m$  in diameter.

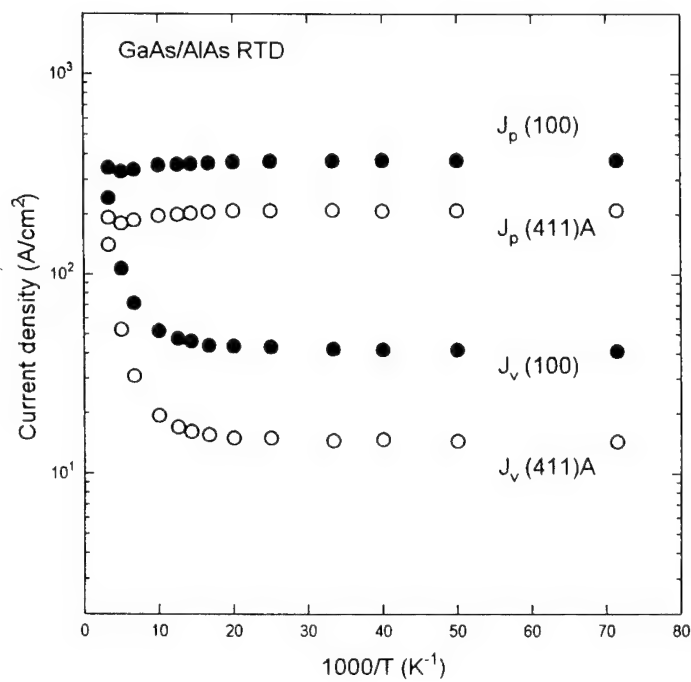


Fig. 2 Temperature dependence of the peak current density ( $J_p$ ) and the valley current density ( $J_v$ ) of GaAs/AlAs double barrier RTDs fabricated on (411)A and (100) GaAs substrates.

# Molecular beam epitaxy of $\text{Al}_{0.48}\text{In}_{0.52}\text{As}/\text{Ga}_{0.47}\text{In}_{0.53}\text{As}$ heterostructures on metamorphic $\text{Al}_x\text{Ga}_y\text{In}_{1-x-y}\text{As}$ buffer layers

M. Haupt, K. Köhler, P. Ganser, S. Emminger, S. Müller, and W. Rothemund

*Fraunhofer-Institut für Angewandte Festkörperphysik,*

*Tullastr. 72, D-79108 Freiburg, FRG*

*Phone: + 49-761-5159-648 Fax: + 49-761-5159-200, e-mail: haupt@iaf.fhg.de*

Ternary  $\text{Al}_x\text{In}_{1-x}\text{As}/\text{Ga}_y\text{In}_{1-y}\text{As}$  heterostructures are grown on GaAs with a lattice mismatch up to 4% by molecular beam epitaxy. Two buffer layer concepts to compensate the lattice misfit between the  $\text{Al}_x\text{In}_{1-x}\text{As}/\text{Ga}_y\text{In}_{1-y}\text{As}$  layers and the GaAs substrate using the quaternary  $\text{Al}_x\text{Ga}_y\text{In}_{1-x-y}\text{As}$  in a step and linear graded fashion, respectively, are presented. The Al and Ga-content of the ternary layers were chosen to be  $x = 0.48$  and  $y = 0.47$ , respectively, in order to have the same heterostructures grown lattice matched on InP as a reference.

On top of the buffer structure, which is kept at a practical thickness of 1  $\mu\text{m}$ , the appropriate structures were grown. The HEMT structure has a  $\delta$ -doping concentration of  $5 \times 10^{12} \text{ cm}^{-2}$  separated by a 5 nm spacer layer from the 40 nm  $\text{Ga}_{0.47}\text{In}_{0.53}\text{As}$  electron channel. The optimum growth temperature of the HEMT structure was 530°C measured by pyrometer, for both, lattice matched growth on InP as well as lattice relaxed growth on GaAs.

Before growing the actual buffer layer for the linear grading beginning with  $\text{Al}_{0.51}\text{Ga}_{0.49}\text{As}$ , a 100 nm GaAs layer is grown. The grading was performed using computer controlled temperature ramping for Ga and In finally conforming to the lattice constant of  $\text{Al}_{0.48}\text{In}_{0.52}\text{As}$ . The step graded buffer the layer sequence consists of two layers beginning with 500 nm of  $\text{Al}_{0.33}\text{Ga}_{0.31}\text{In}_{0.36}\text{As}$  and continuing with 500 nm of  $\text{Al}_{0.48}\text{In}_{0.52}\text{As}$ .

Focusing on the surface morphology for the linear graded HEMT structure we observed a 'cross-hatching' of the surface, which indicates the existence of misfit dislocations with a 2D growth mode or layer by layer growth still present [1]. For the step graded buffer the morphology of the surface is the result of a 3D growth mode. Growth temperatures  $T_B$  for the buffer above 400°C and below 300°C give a strong increase in roughness. In the range between 300°C and 400°C we observe nearly identical roughness values for both step and linear grading with a slightly better surface morphology of the heterostructure for the linear graded buffer. The lowest rms roughness value of 2.6 nm was found at a substrate temperature  $T_B$  of 350°C for the linear graded buffer. The same HEMT structure grown lattice matched on InP yielded a rms roughness of 0.2 nm.

Hall mobilities of the HEMT structures with both buffer types increase when the temperature is lowered from 300K to 77K. The Hall mobility  $\mu_{77\text{K}}$  shows higher values for the linear graded structures with a maximum of 38000  $\text{cm}^2/\text{Vs}$  at 450°C. For the step graded structures we measured a maximum of 26000  $\text{cm}^2/\text{Vs}$  at a  $T_B$  of 400°C. Electron concentrations of  $3.0 \times 10^{12} \text{ cm}^{-2}$  were measured for all samples. A decrease of the mobilities for  $T_B$  below 350°C and above 450°C is observed for both buffer types. An electron mobility of 50000  $\text{cm}^2/\text{Vs}$  at 77K was measured for the same HEMT structure grown lattice matched on InP.

The interface roughness, though similar in the absolute rms roughness values, but originating from different growth modes, has also a strong influence on the photoluminescence (PL) properties of structures, measured on the two different buffers on GaAs, and for reference purposes also on InP. The quantum well (QW) structure for the photoluminescence studies consisted of five quantum wells with well thicknesses of 20, 10, 4, 3 and 1 nm grown at the same optimum growth temperature of 530°C. The superior interface quality of the QW's grown on the linear graded buffer, compared to the growth on the step graded buffer, is obvious from the reduced PL line width. Hall mobilities and QW-PL linewidths show that relaxed structures on linearly graded buffers are of almost equal quality as lattice matched structures on InP.

[1] P. J. Goodhew, *J. Phys. Chem. Solids* 55, 1107 (1994)

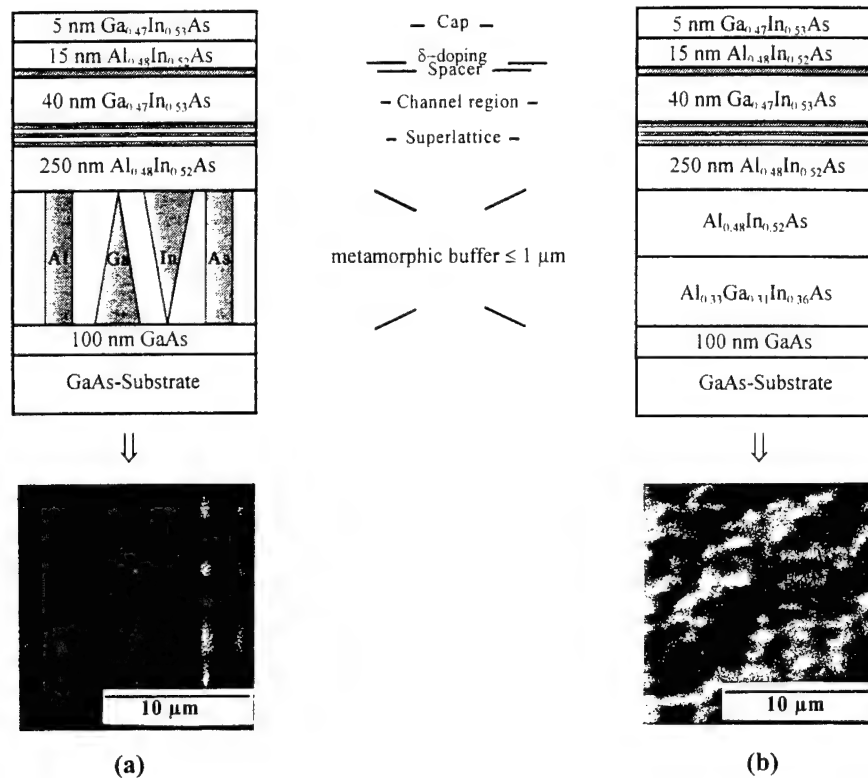


**Fig. 1.** MBE grown  $\text{Al}_{0.48}\text{In}_{0.52}\text{As}/\text{Ga}_{0.47}\text{In}_{0.53}\text{As}$  HEMT and buffer structure for linear (a) and stepwise (b) compensation of the lattice misfit. The Nomarski micrographs are shown underneath each layer structure.

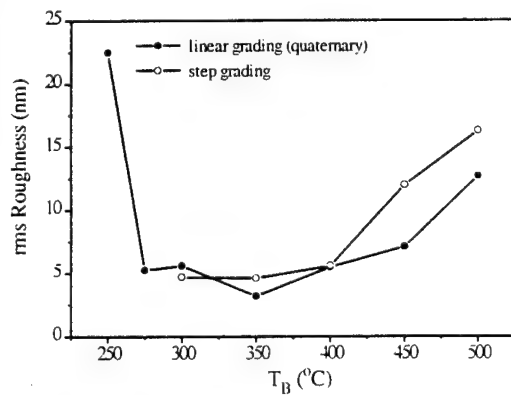


**Fig. 2.** Surface roughness as a function of the buffer growth temperature  $T_B$ .

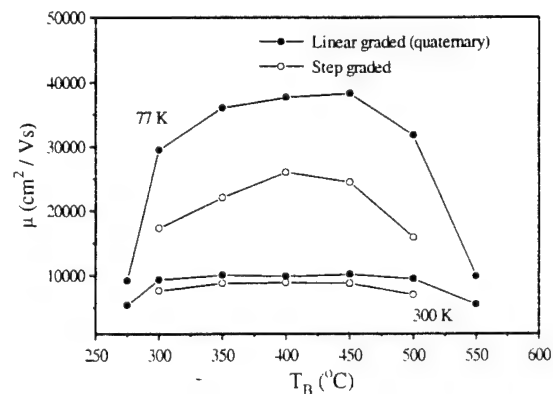


**Fig. 3.** Hall mobilities at 300K and 77K of  $\text{Al}_{0.48}\text{In}_{0.52}\text{As}/\text{Ga}_{0.47}\text{In}_{0.53}\text{As}$  HEMT structures grown on linear and step graded buffers as a function of the buffer growth temperatures.

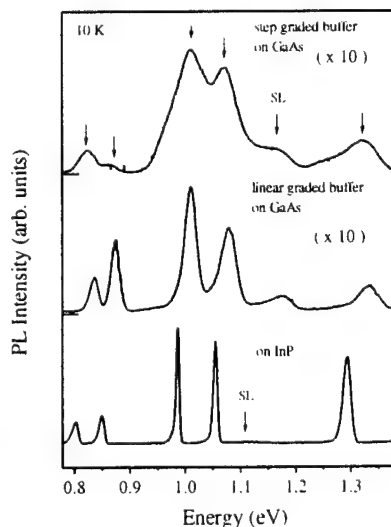


**Fig. 4.** PL spectra of the samples studied with five quantum wells lattice matched on InP and with lattice relaxed linear and step graded buffer on GaAs. From left to right the arrows indicate the well widths 20, 10, 4, 3, and 1 nm, respectively. The luminescence of the superlattice grown before the quantum well layer sequence is denoted by SL.



## DESIGNING DELTA-DOPED QUANTUM WELL STRUCTURES SUITABLE FOR POWER FET APPLICATIONS

J.M. ROBERTS<sup>†#</sup>, J.J Harris<sup>†</sup>, M. Hopkinson<sup>‡</sup>, C. Roberts<sup>\*</sup>

<sup>†</sup>Semiconductor IRC, Electrical & Electronic Engineering Dept., UCL, London WC1E7JE.

<sup>#</sup>Tel: (+44) 171 419 3843, Fax: (+44) 171 387 4350, email: j.roberts@eleceng.ucl.ac.uk.

<sup>‡</sup>EPSRC III-V Central Facility, University of Sheffield.

<sup>\*</sup>Semiconductor IRC, Imperial College, Prince Consort Rd, London SW72BZ.

A study of the effects of material composition and Si delta-( $\delta$ -) doping plane position on the transport properties of several  $\delta$ -doped GaAs/AlGaAs and InGaAs/InP quantum well (QW) structures is presented. The intention being to determine the design rules for high carrier concentration, high mobility structures suitable for high frequency power FET applications such as microwave generation.

Previous works on  $\delta$ -doped structures have generally shown low carrier mobilities <sup>1, 2</sup> due to the high levels of ionised impurity scattering present, a result of the spatial coincidence of the electrons and donors. Self-consistent Poisson-Schrödinger modelling suggests that by edge doping the QW an electron-donor separation is created which decreases the amount of ionised impurity scattering thereby improving carrier mobilities. Such separations can be further increased by compositionally grading the QW. The digital alloying technique has been used to produce these graded edge  $\delta$ -doped  $\text{In}_x\text{Ga}_{1-x}\text{As}$  QWs.

Measurements have shown a 13% mobility ( $\mu$ ) improvement in the edge  $\delta$ -doped QWs over the uniformly doped and centre  $\delta$ -doped structures (Fig. 1). Also observed is an 11% improvement in the electron saturation drift velocity ( $v_s$ ) in the same sample set (Fig. 2). Improvements in mobility of 100% (to  $2300 \text{ cm}^2/\text{Vs}$ ) (Fig. 1) and 67% in saturation drift velocity (to  $1.77 \times 10^7 \text{ cm/s}$ ) (Fig. 2) have been observed in the digitally graded, strain balanced,  $\text{In}_x\text{Ga}_{1-x}\text{As}$  structures when compared to the lattice matched edge  $\delta$ -doped  $\text{In}_{0.53}\text{Ga}_{0.47}\text{As}/\text{InP}$  QWs. Increasing the linearity of the grade is expected to increase electron-donor separations resulting in further enhanced carrier mobilities and saturation drift velocities. The saturation drift velocity results are the best we have seen for such highly doped structures (the carrier concentration was determined as  $4 \times 10^{12} \text{ cm}^{-2}$ ).

Investigation of the high field data has revealed a relationship between  $v_s$  and  $\mu$  of the form  $v_s \propto \mu^{0.8 \pm 0.4}$ . This relationship underlines the impact a high carrier mobility has on the high frequency operation of a transistor device.

X-ray diffraction data performed on the digitally graded structures is also presented confirming that these structures are strain balanced.

<sup>1</sup> J.J. Harris, Review Paper, Journal of Materials Science: Materials in Electronics, **4**, (1993) 93 -105.

<sup>2</sup> G. Gillman, B. Vinter, E. Barbier and A. Tardella, Appl. Phys. Lett., **52**, (1988) 972.

Fig. 1 Transport data for the GaAs/AlGaAs (■ and ●) and  $\text{In}_x\text{Ga}_{1-x}\text{As}/\text{InP}$  (□ and ○) QWs. (C $\delta$ -dope = Centre  $\delta$ -doped and E $\delta$ -dope = Edge  $\delta$ -doped)

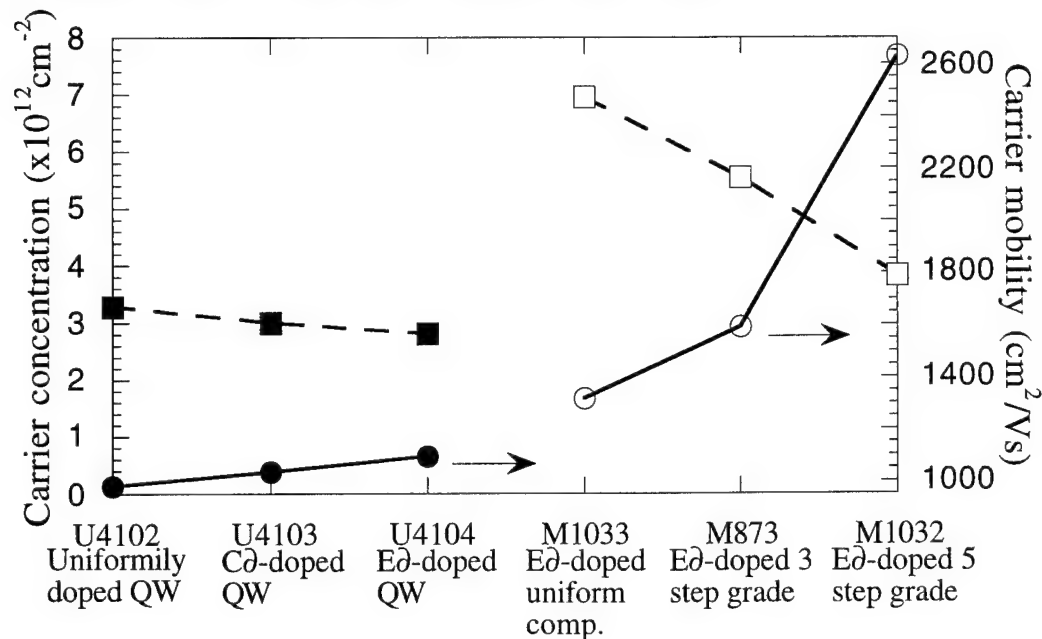
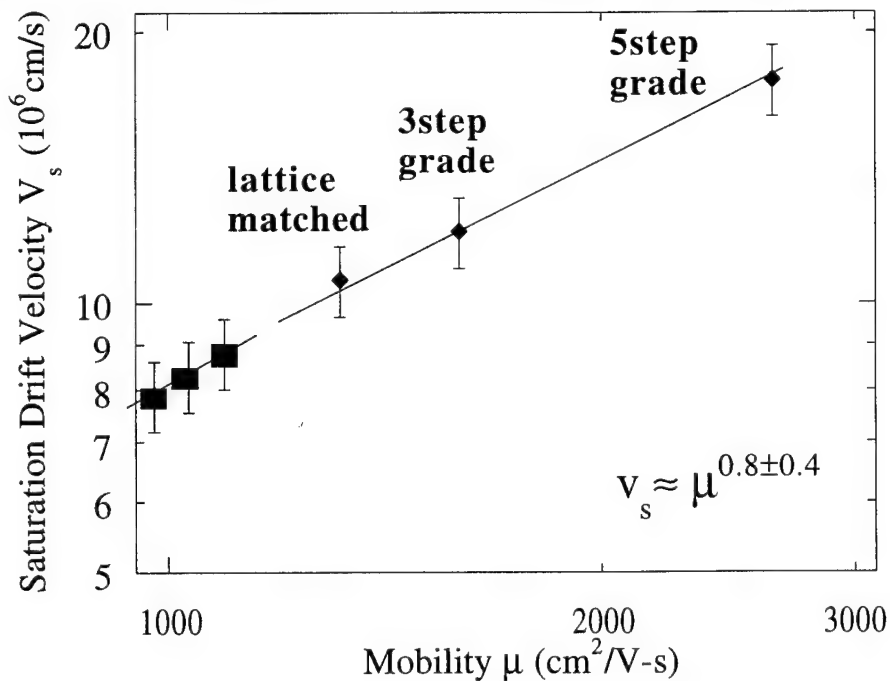


Fig. 2 Electron saturation drift velocity versus low field carrier mobility for the GaAs/AlGaAs (—■—) and  $\text{In}_x\text{Ga}_{1-x}\text{As}/\text{InP}$  (—◆—) samples.



# High Voltage Gain, High Breakdown Voltage, and Device Linearity Improvement by Pseudomorphic FET with Triple Delta-Doped Channel

Wen-Shiung Lour, Jiann-Ru Chen, and H.R. Chen<sup>1</sup>

Department of Electrical Engineering, National Taiwan-Ocean University,  
2 Peining Road, Keelung, TAIWAN, Republic of China.

<sup>1</sup>Department of Electrical Engineering, Private Kung-Shan Institute of Technology  
and Commerce, Tainan Hsien, TAIWAN, Republic of China

## Abstract

We report on an AlGaAs/InGaAs/GaAs pseudomorphic FET with a triple delta-doped channel (we call it TD-HFET), which emerges the concept of a conventional MISFET, a  $\delta$ -FET, and a graded-channel FET. The typical TD-HFET grown by MBE is shown in Fig. 1. The portion of the InGaAs layer was triple delta-doped to  $1.2 \times 10^{12}$ ,  $4 \times 10^{11}$ , and  $1 \times 10^{11} \text{ cm}^{-2}$ . The measured room temperature Hall mobility and sheet density are  $3800 \text{ cm}^2/\text{V}\cdot\text{s}$  and  $1.8 \times 10^{12} \text{ cm}^{-2}$ , respectively. The high mobility is a result of a  $\delta$ -FET similar design and suggests a reduction in impurity scattering in graded delta-doped channel. Figure 2 shows the device doping profiles by C-V measurements. Instead of three doping peaks, a single graded charge distribution is obtained. The peak concentration is derived to be  $2.8 \times 10^{18} \text{ cm}^{-3}$ . The calculated total sheet concentration is  $1.6 \times 10^{12} \text{ cm}^{-2}$ . Obviously, the measured data from Hall and C-V measurements are reasonable since the epitaxial density is designed to be  $1.7 \times 10^{12} \text{ cm}^{-2}$ . Fig. 3(a) shows the I-V curve of the drain-to-source characteristic. The drain-to-source breakdown voltage is as high as 27.2 V. The gate-to-drain breakdown voltage at gate leakage current of 1 mA/mm is also measured to be 30 V. The improvement of both gate-to-drain and drain-to-source breakdown voltages are attributed partly to the use of a large energy-gap insulator, partly to the design of a  $\delta$ -FET, and partly to the less impact ionization in the alleviated electrical field at the upper of the triple layer. Figure 3(b) shows the dc characteristics of a TD-HFET. The high forward gate-to-source voltage is attributed to the large turn-on voltage. No significant leakage current (1 mA/mm) was found at  $V_{gs}=+1.2 \text{ V}$ . The  $g_m$ ,  $I_{DS}$ , and  $g_{ds}$  as a function of gate-to-source voltage is depicted in Fig. 4. The peak extrinsic transconductance and the maximum associated drain-to-source current are 160 mS/mm at  $V_{gs}=+0.5 \text{ V}$  and 248 mA/mm at  $V_{gs}=+1.4 \text{ V}$ , respectively. Note that the transconductance play a broad plateau with an associated K value of 140 mS/mm $\cdot$ V. Clearly, the graded delta-doped that resulting in graded-doped profile provides the device linearity improvement. The current density with transconductance larger than 100 mS/mm is ranged from 25 to 240 mA/mm, which is 86 percent of the available current density. The dc output conductance at drain-to-source voltage  $> +1.5 \text{ V}$  is smaller than 0.3 mS/mm. This yields an open-drain voltage gain as high as 530.

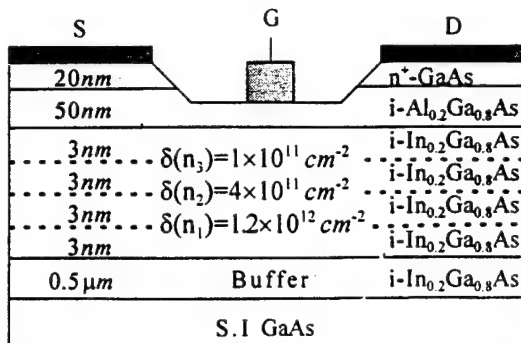


[Fig.1] The schematic cross section of the achieved TD-HFET.

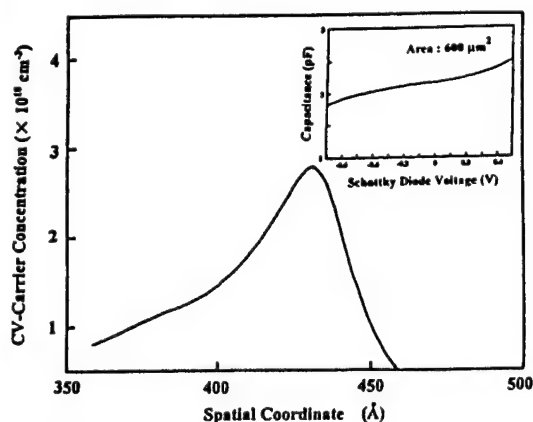


[Fig.2] Carrier concentration of our triple delta-doped epi-layer deduced from C-V measurements. The peak carrier concentration is  $2.8 \times 10^{18} \text{ cm}^{-3}$  and the measured capacitance is also depicted in the inset of figure.

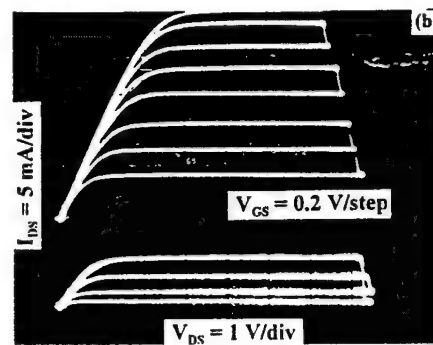
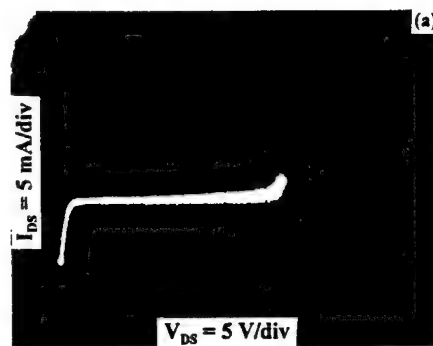


[Fig.3] (a) Forward drain-to-source I-V characteristics with  $V_{gs} = 0 \text{ V}$ . (b) Output I-V characteristics of a  $1 \times 100 \mu\text{m}^2$  TD-HFET. Note that the maximum  $V_{gs}$  is  $+1.4 \text{ V}$ .

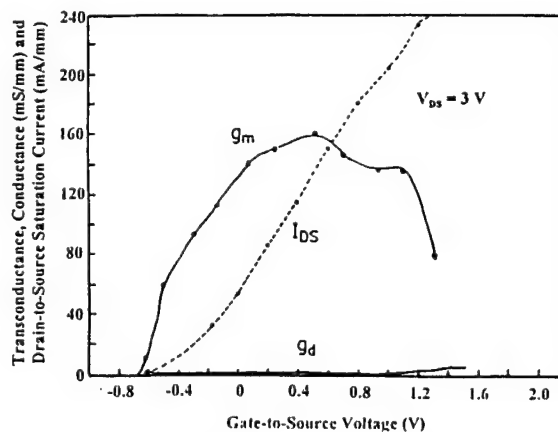


[Fig.4] The extrinsic transconductance, drain-to-source current density, and output conductance as a function of the gate-to-source voltage.

## Photoluminescence Characterization of MBE Grown AlGaAs/InGaAs/GaAs Pseudomorphic HEMTs

M. Wojtowicz, D. Pascua, A.-C. Han, T. R. Block, and D. C. Streit  
TRW Electronics and Technology Division  
Redondo Beach, CA 90278

The need for AlGaAs/InGaAs/GaAs HEMT devices for low noise and power microwave circuits continues to increase. In order to reduce costs and supply stable material, the device structure must be monitored and screened as close to the growth process as possible. Low temperature photoluminescence (PL) provides very useful technique to monitor the InGaAs channel material properties providing the relation between the spectral features and the InGaAs channel material characteristics is understood. We have correlated the PL spectral features of both low noise and power HEMT structures with the InGaAs channel material characteristics. This allows us to use PL for monitoring the channel characteristics of MBE grown HEMT material to provide consistent material for power and low noise applications.

The material profiles used in this study are shown in Fig. 1. Even though all InGaAs/AlGaAs/GaAs HEMTs have two heterointerfaces, we will call the structure with a single AlGaAs/InGaAs interface a single heterostructure profile and the structure with two AlGaAs/InGaAs interfaces a double heterostructure profile. The theoretical PL spectra was calculated from the wavefunction and energy states which were, in turn, calculated using a self-consistent solution of Poisson's and Schrödinger's equations. Energy state broadening and a excess e-h pair distribution was used to calculate the spectral broadening.

Fig. 2 shows representative measured and calculated PL spectra for both structures. Solid lines are the measured spectra while the dashed lines show the calculated spectra. Both measured and calculated spectra are normalized to the peak amplitude. Very good agreement is obtained between the measured and calculated spectra. Two peaks are observed in both structures where the lower energy peak corresponds to the e1-hh1 transition while the higher energy peak corresponds to the e2-hh1 transition. In the single heterostructure profile, the ionized donors above the channel attract the electrons and repel the holes which reduces the intensity of the e1-hh1 transition relative to the intensity of the e2-hh1 transition. In the double heterostructure profile, the ionized donors below the channel repel the holes from the bottom interface which increases the e1-hh1 transition intensity and decreases the e2-hh1 transition intensity relative to the single heterostructure profile. The additional donors in the double heterostructure also reduce the energy of the e2 state and increase the energy of the hh1 state. This has the net affect of increasing the e1-hh1 transition energy and decreasing the e2-hh1 transition energy.

In summary, we have developed an accurate model to describe the photoluminescence spectra of AlGaAs/InGaAs/GaAs HEMTs. The model applies to both low-noise and power profiles and allows us to use PL as an effective MBE material characterization tool.

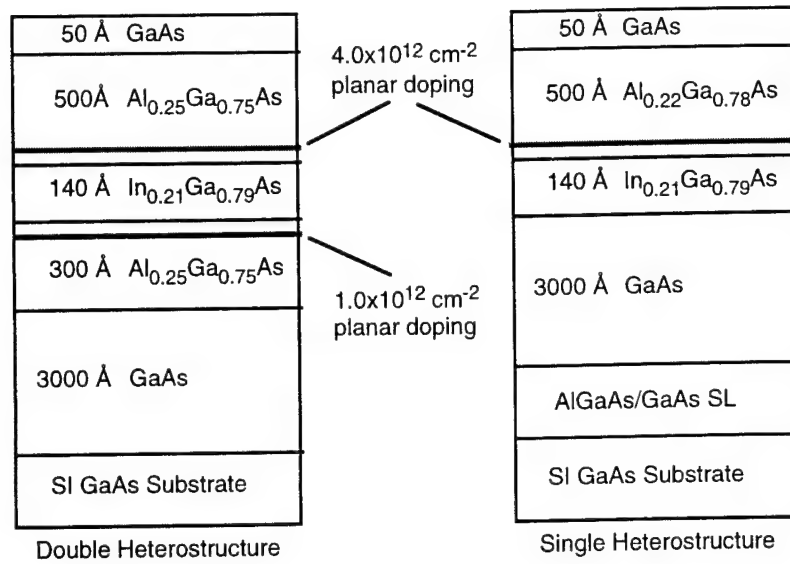


FIG. 1. Single and double heterostructure HEMT material profiles. The primary difference between the two structures is the additional 300 Å AlGaAs buffer region and buffer doping in the double heterostructure profile.

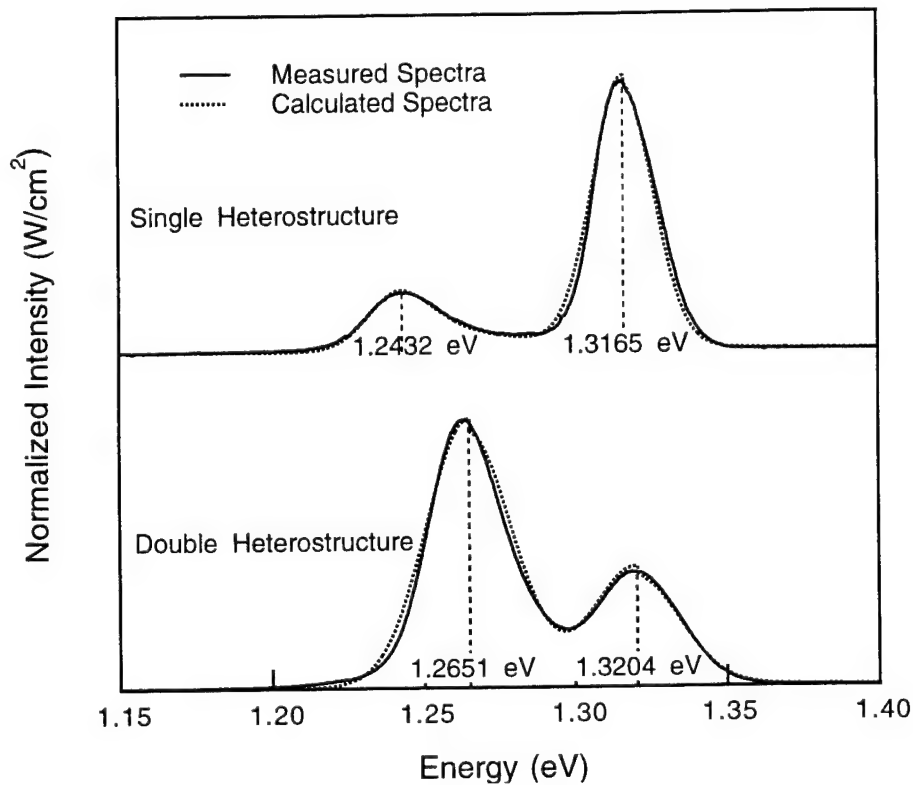


FIG. 2. Comparison of measured and calculated PL spectra for a single and double heterostructure HEMT. Solid lines are measured data and the dotted lines are the calculated spectra. Good agreement is obtained for both structures.

## Sub-40 $\mu$ A Continuous-Wave Lasing in an Oxidized Vertical-Cavity Surface-Emitting Laser with Dielectric Mirrors

D.L. Huffaker, L.A. Graham, H. Deng, D.G. Deppe, C. Lenox, and B.G. Streetman

Microelectronics Research Center  
Department of Electrical and Computer Engineering  
The University of Texas at Austin, Austin, Texas 78712-1084

Realizing ultralow lasing threshold in vertical-cavity surface-emitting lasers (VCSELs) is important for reduction of power consumption in highly parallel optical interconnects, and is a topic of interest in understanding the fundamental limits of operation in microcavity lasers. Recent results show that index-confinement within the otherwise planar Fabry-Perot microcavity is effective in controlling lateral diffraction loss and reducing the optical mode volume, and the increased coupling which accompanies the optical mode volume reduction allows significant reduction in lasing threshold [1,2]. In this talk we show that further improvement in lasing threshold can be achieved by reducing the intracavity loss, specifically through tight control of the p-type doping profile [3].

The VCSELs are grown by molecular beam epitaxy in a Varian Gen II system. Steam oxidation at 460°C for times of 5 and 7 min. are used to realize oxide openings (lateral cavity dimensions) of 7 $\mu$ m and 3 $\mu$ m. The p-type contact is designed so that a heavily p-doped GaAs contact layer can be removed selectively from the VCSEL cavity region. A newly designed low loss MgF/ZnSe distributed Bragg reflector (DBR) is also used to achieve threshold currents as low as 38 $\mu$ A in a 3 $\mu$ m diameter device, and as low as 98 $\mu$ A in a 7 $\mu$ m diameter device. Very low loss can be obtained from the MgF/ZnSe DBR by controlling the ZnSe electron beam deposition rate. Device characteristics with varying mirror pairs are studied to determine the trade-off between threshold current and efficiency.

We also report on similar low loss cavity designs for highly multimode operation, which may be of importance for multimode fiber applications. With the oxide confinement and a low loss vertical cavity, a 6 $\mu$ m VCSEL can support a 150Å-wide multimode lasing spectra at a low bias current of 600 $\mu$ A ( $1.2I_{th}$ ).

- [1] D.L. Huffaker, D.G. Deppe, K. Kumar, and T.J. Rogers, Appl. Phys. Lett. 65, 97 (1994).
- [2] D.G. Deppe, D.L. Huffaker, J. Shin, and Q. Deng, IEEE Photon. Tech. Lett. 7, 965 (1995).
- [3] G.M. Yang, M.H. MacDougall, and P.D. Dapkus, Electron. Lett. 31, 886 (1995).

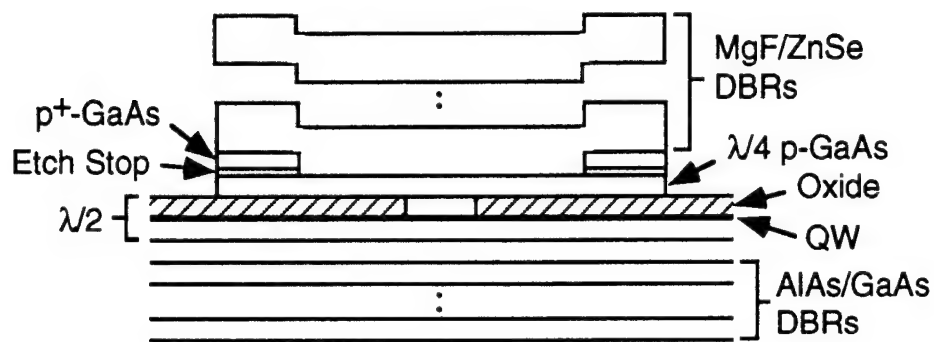


Figure 1: Schematic illustration of oxide VCSEL. The intracavity contact has been improved to remove the p<sup>+</sup>-GaAs contact layer from the cavity region and a low loss MgF/ZnSe DBR is used for the upper mirror.

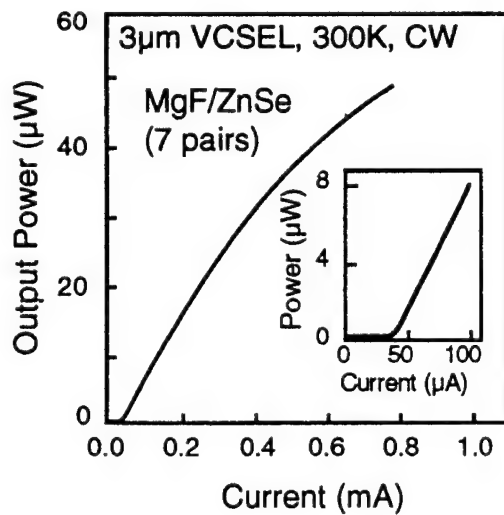


Figure 2: Light versus current curves measured CW at room temperature for a 3μm diameter VCSEL using seven DBR pairs.

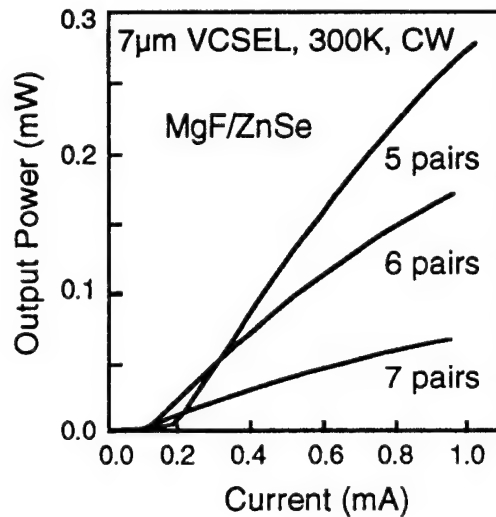


Figure 3: Light versus current curves measured CW at room temperature for 7μm diameter VCSELs with either five, six or seven DBR pairs.



## Full gaseous source growth of separate confinement MQW 1.55 $\mu\text{m}$ laser structures in a production MOMBE

M. Popp, H. Heinecke\*

University of Ulm, Dept. of Semiconductor Physics, D-89069 Ulm, Germany

H. Baumeister, E. Veuhoff

Siemens AG, ZFE T KM 3, D-81730 Munich, Germany

For the production of device structures high uniformity and multi-wafer processing is mandatory. We have shown earlier that these criteria can be fulfilled for the InP-based material system in our production MOMBE machines [1]. However, the doping in MOMBE is still an area of concern with respect to reproducible process development and transfer into production.

We have used the in MOVPE qualified doping gases  $\text{DEZn}$  [2] and  $\text{Si}_2\text{H}_6$ . The disilane was injected via a high-temperature gas cell allowing for thermal precracking of this doping gas. The design of this injector excludes any possible clogging due to Si-deposition. Fig. 1 gives the dependence of the net electron concentration in InP in dependence of the precracking temperature. The growth rate was set to 1.3  $\mu\text{m}/\text{h}$  at a growth temperature of 510  $^\circ\text{C}$ . This plot reveals that the dissociation of  $\text{Si}_2\text{H}_6$  starts at 600  $^\circ\text{C}$  and yields an optimum operation at 900  $^\circ\text{C}$ . As expected a linear dependence of the electron concentration on the  $\text{Si}_2\text{H}_6$ -flux is measured. The Hall-mobility of these Si-doped InP layers agree well with MOVPE standards and Si doped InP by MOMBE using Si effusion cells.

Using the disilane and  $\text{DEZn}$  doping double separate confinement MQW laser structures for an emission at 1.55  $\mu\text{m}$  were produced. The basic layer sequence was: Si-doped InP-cladding layer /  $\text{Ga}_{0.18}\text{In}_{0.82}\text{As}_{0.39}\text{P}_{0.61}(\text{Q1.15})$  confinement /  $\text{Ga}_{0.25}\text{In}_{0.75}\text{As}_{0.54}\text{P}_{0.46}(\text{Q1.25})$  / MQW / Q1.25 / Q1.15 / Zn-doped InP-cladding / Zn-doped GaInAs. It is important to note that we observe for GaInAs grown at 510  $^\circ\text{C}$  a change in lattice mismatch of + 100 ppm/ $^\circ\text{C}$  as reported earlier, for Q1.55 ( $\text{Ga}_{0.42}\text{In}_{0.58}\text{As}_{0.90}\text{P}_{0.10}$ ) this coefficient is reduced to + 85 ppm/ $^\circ\text{C}$  and for Q1.25 material there is a negative value of - 110 ppm/ $^\circ\text{C}$ . This negative temperature coefficient is the result of a decreasing As-incorporation when the growth temperature is increased. For the Q1.05 material ( $\text{Ga}_{0.11}\text{In}_{0.89}\text{As}_{0.24}\text{P}_{0.76}$ ) this coefficient is again positive (+ 100 ppm/ $^\circ\text{C}$ ). These results are confirmed by the mapping data over full 2" wafers and by the data on the variation of the growth temperature. The mechanism of this particular change in the As/P-incorporation mechanism around the Q1.25 material is still unclear and under investigation now.

The MQW-region in the above mentioned laser structure was grown with unstrained GaInAs wells or 0.6 % / 0.8 % / 1.0 % compressive strained quaternary wells, all yielding 1.55  $\mu\text{m}$  emission. Table 1 demonstrates that the broad area lasers with five QW and 1 % compressive strain yield the best threshold current densities of about 1.1 kA/ $\text{cm}^2$ . The structure is Si-doped up to the second confinement layers. The Zn-doping starts after a recess zone in the InP cladding layer. The doping recess on both sides of the MQW-structure has a distinct effect on the laser characteristics. The temperature dependence of the quaternary growth and the mapping data over 2" wafers will be discussed in the presentation.

- [1] B. Marheineke, M. Popp, and H. Heinecke  
J. Crystal Growth, in press (presented at ICCBE-5, San Diego, 1995)
- [2] E. Veuhoff, H. Baumeister, R. Treichler, M. Popp, and H. Heinecke  
J. Crystal Growth, in press (presented at ICCBE-5, San Diego, 1995)

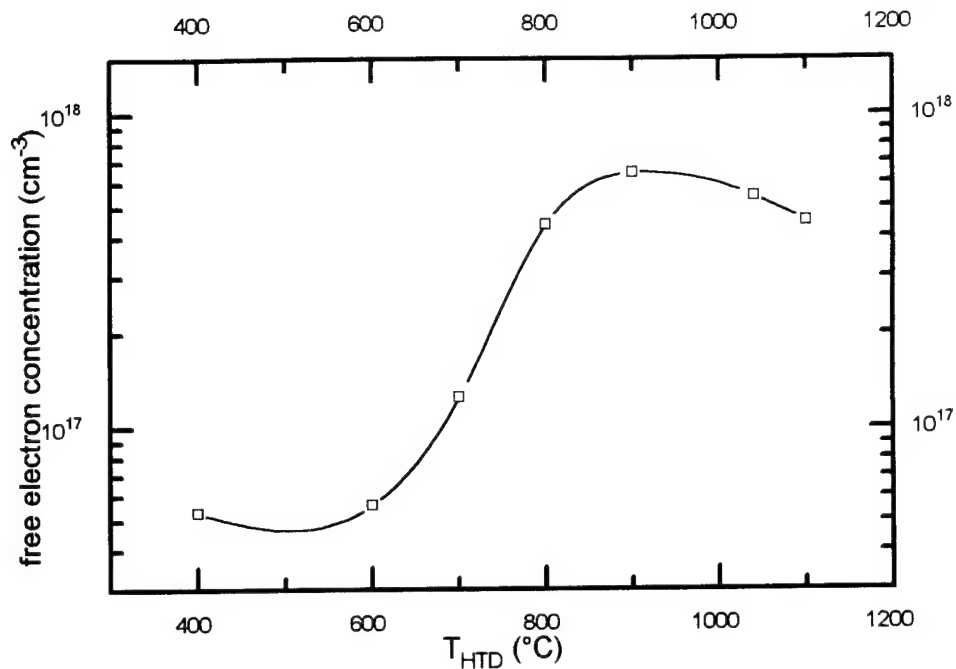


Fig. 1: Free electron concentration in InP layers as function of the disilane precracking temperature.

quantum wells	$j_{\text{th}}$ (kA/cm <sup>2</sup> )
unstrained-GaInAs	2.0
0.6 % strained-GaInAsP	1.3
0.8 % strained-GaInAsP	1.3
1.0 % strained-GaInAsP	1.1

Table 1: Threshold current densities of the 1.55  $\mu\text{m}$  broad area (50/100  $\mu\text{m} \times 400 \mu\text{m}$ ) lasers.

\* corresponding author:

Tel: +49-731-502-6101 Fax: -6108 e-mail: heinecke@sunrise.e-technik.uni-ulm.de

## Improved electro-absorption properties in 1.3 $\mu$ m MQW waveguide modulators by modified doping profile

X. B. Mei, K. K. Loi, W. S. C. Chang, and C. W. Tu

Department of electrical and computer engineering, University of California, San Diego, 9500 Gilman Drive, La Jolla, CA 92093-0407,

E-mail: xmei@sdcc3.ucsd.edu, Phone: (619) 534-3014, Fax: (619) 534-2486

In electroabsorption (EA) waveguide modulators for small-signal analog applications, a large slope in the absorption coefficient-voltage curves is desirable. A conventional p-i-n structure is employed. For 1.3 $\mu$ m applications, we have used strain-compensated InAsP/GaInP multiple quantum wells (MQWs) as the i-region, which is sandwiched between an n-type and a p-type In<sub>0.87</sub>Ga<sub>0.13</sub>As<sub>0.29</sub>P<sub>0.71</sub> cladding layer. The two cladding layers are doped to  $5 \times 10^{17} \text{ cm}^{-3}$ , low enough to reduce the free carrier absorption. The problem with the conventional structure is that the depletion region extends from the i-region into the cladding layers under reverse bias and causes a decrease in the electric field, and thus the quantum confined Stark effect (QCSE), at a given bias voltage. Therefore, it is desirable to alleviate this problem for high slope efficiency.

By inserting a highly doped ( $2 \times 10^{18} \text{ cm}^{-3}$ ) and thin ( $\sim 200 \text{ \AA}$ ) In<sub>0.87</sub>Ga<sub>0.13</sub>As<sub>0.29</sub>P<sub>0.71</sub> layer (pulse-doped layer) in the p and n InGaAsP cladding layers at each side of the i-region, we have obtained a larger QCSE at a given bias voltage in a modified MQW structure than in the conventional structure. Since the two pulse-doped layers are very thin compared to the waveguide thickness ( $\sim 1.7 \mu\text{m}$ ), they confine the depletion region to only the i-region without causing serious free carrier absorption. We find that the QCSE in the sample with pulsed-doped layers is 29% larger at 2V than that in the conventional structure. This increase in QCSE results in an increased slope in the absorption coefficient-voltage curves. By comparing the experimental data with the theoretical calculation on QCSE, the amount of improvement in the confinement of the depletion region is estimated.

In summary, we demonstrated an improved QCSE by confining the depletion region with pulse-doped layers on each side of the MQWs.

## **CBE growth of 850nm GaAs/AlGaAs quantum-well lasers.**

TJ Whitaker, PDJ Calcott, T MARTIN, MJ Kane, GW Smith, RJ Balmer, and M Houlton

DRA(Malvern), St Andrews Road, Gt Malvern, Worcestershire,  
WR14 3PS, United Kingdom

Tele: +44-(0)1684-895288      Fax: +44-(0)1684-894311      E-mail: tmartin@dra.hmg.gb

In respect of source capacity, epilayer uniformity, defect density, flexibility and selective area growth CBE offers potential production advantages over the conventional epitaxial techniques of MBE and MOVPE. However, although a large number of high-performance CBE-grown device structures based on phosphorus-containing alloys have been demonstrated, very few GaAs/AlGaAs optical devices have been reported. In this paper we present data from a systematic study of the growth and performance of GaAs/AlGaAs quantum-well lasers, and report what is to our knowledge the first 850nm quantum-well laser to be grown using all gaseous source CBE.

GaAs/AlGaAs quantum-wells have been grown using pre-cracked arsine, triethylgallium and triisopropylgallium and ethyldimethylaminealane, and characterised using spectrally and temporally resolved photoluminescence. The room temperature photoluminescence lifetime has been studied as a function of well thickness, growth temperature and growth rate and the data obtained will be presented and compared with that obtained using MBE growth. Building on these lifetime studies doped laser structures have been grown using hydrogen sulphide and carbon tetrabromide as dopant sources.

Although it is generally accepted that lasers with low threshold current require the use of high growth temperatures (650-700°C), primarily to reduce oxygen incorporation, we have successfully demonstrated threshold currents of 500 A cm<sup>-2</sup> using growth temperatures as low as 540°C (50µm wide x 500µm long stripe with two 10nm quantum-wells). Results from SIMS analysis of the oxygen incorporated into the laser structures will be presented which demonstrate differences between CBE and MBE growth, consistent with the low threshold currents observed using CBE.

Finally we will appraise the correlation between quantum well lifetimes and laser performance and review future developments with respect to the selective area growth of GaAs/AlGaAs lasers.

## **GSMBE Growth and Characterization of InGaAs/InP Strained-layer MQWs in a P-i-N Configuration**

WANG XIAOLIANG, Sun Dianzhao, Kong Meiyong, Hou Xun\* and Zen Yiping  
Institute of Semiconductors, Chinese Academy of Sciences, P.O. Box 912, Beijing 100083,  
P.R.China Phone: 86-010-2558131ext.279 Fax: 86-010-2562389 E-mail: NMIRD@mimic.cnc.ac.cn  
\*Xi'an Institute of Optics and Precision Mechanics, Chinese Academy of Sciences, P.O.Box 80,Xi'an  
710068,P.R.China

Strained layer semiconductor structures offer an additional degree of freedom over electronic properties which present considerable potential for development of new and improved electronic and optoelectronic devices. In this work, we report the growth of the strained layer InGaAs/InP multiple quantum wells (SLMQWs) using a home made GSMBE system and the use of optical techniques to study on the energies of the exciton transitions in the InGaAs/InP SLMQWs as a function of strain.

The InGaAs/InP SLMQWs samples were designed to grow coherently on (100)-oriented InP substrates in a P-i-N configuration. The undoped SLMQWs in the i-region consists of twenty InGaAs quantum wells with thicknesses of 50Å separated by 200Å thick InP barriers. Five samples were grown, one lattice-matched with  $x=0.53$  (sample C), two under compression with  $x=0.60$  (sample D) and  $x=0.68$  (sample E), and the remainder under tension with  $x=0.39$  (sample A) and  $x=0.46$  (sample B). The indium concentration  $x$  varied from  $x=0.39$  to  $x=0.68$ .

Double crystal x-ray diffraction patterns and their computer simulation are used to determine the structural parameters and indium composition in the well of the samples. The indium concentration and SLMQWs dimensions determined from computer fitting are in good agreement with those estimated from the growth parameters, indicating that the growth process can be well controlled. Also, the low temperature PL and absorption spectrum are used to determine the exciton transition energies. We find that when indium concentration  $x$  in the 50Å InGaAs quantum wells vary from 0.39 to 0.68, the exciton transition energies decrease from about 0.985eV to 0.806eV. Good agreement is achieved between exciton transition energies obtained experimentally at low temperature with those calculated using the deformation potential theory. Finally, the photovoltaic (PV) measurements at room temperature show that the exciton absorption peaks can be clearly seen, indicating that the samples having good quality.

InP:Be 5000 Å
i - InP 2000 Å
20 Periods SLMQWs well=50 Å Barrier=200 Å
i - InP 2000 Å
InP:Si 2000 Å
N - InP Substrate

FIG. 1 The PIN multiquantum wells structure.

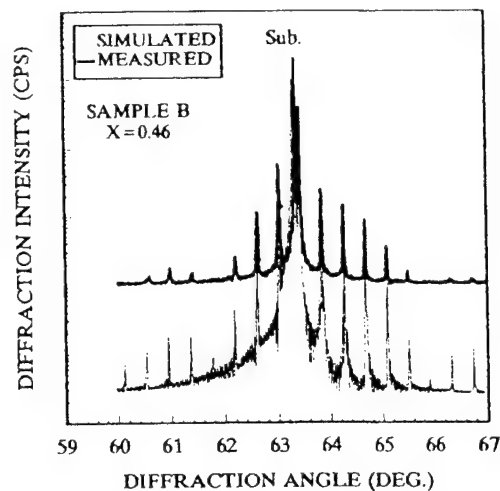


FIG.2 Double crystal rocking curve for sample B.

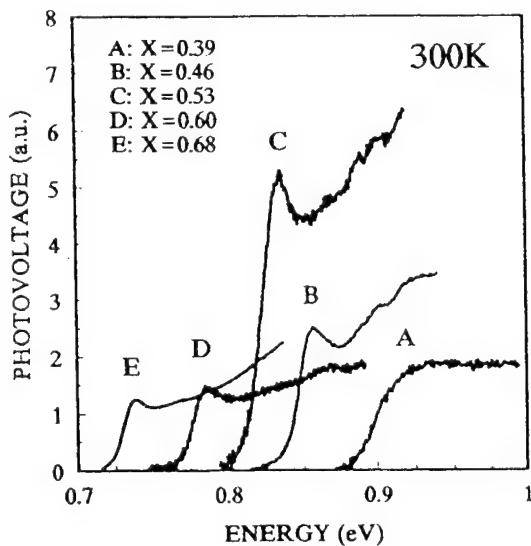


FIG.3 Photovoltaic spectra of four strained-layer and one lattice-matched  $\text{In}_x\text{Ga}_{1-x}\text{As}/\text{InP}$  MQWs PIN structures measured at room temperature.

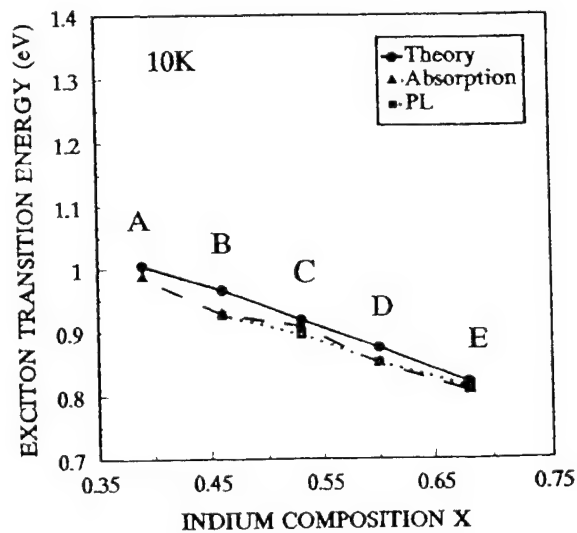


FIG.4 Exciton transition energies in  $\text{InGaAs}/\text{InP}$  MQWs as a function of indium composition  $X$  for sample A, B, C, D and E.

# Characterisation of bulk-GaInP and (GaAs/GaInP) p-i-n diode structures grown by solid-source MBE

M.Hopkinson, J.P.R.David and R.Ghin.

*Department of Electronic and Electrical Engineering, University of Sheffield,  
Mappin Street. Sheffield S1 3JD. UK.*

*Phone: +44 114 2825211 Fax: +44 114 2726391  
e-mail: m.hopkinson@sheffield.ac.uk*

GaInP may be used as a direct replacement for  $\text{Al}_x\text{Ga}_{1-x}\text{As}$  in bulk and quantum well (QW) device structures and offers potential improvements due to factors such as improved surface recombination velocity, higher breakdown voltage, the absence of DX-centre effects and high etch selectivity. However the abruptness of GaAs-QW interfaces and doping profiles in GaInP-based structures must be contrasted with the excellent properties of (Al)GaAs-based structures. We have investigated the properties of bulk-GaInP and (GaAs/GaInP) multi-quantum well (MQW) p-i-n diode structures grown by solid source MBE and compared these with equivalent (GaAs/AlGaAs) structures.

GaAs/GaInP MQW structures were grown at  $\sim 500^\circ\text{C}$  using  $\text{As}_2$  and  $\text{P}_2$  alternately switched using valved cracker sources. We find that to achieve abrupt interfaces precise control over the  $\text{As}_2$  flux during GaAs growth is required. Using an incorporated (As/Ga) flux ratio ( $R_i$ )  $\leq 1.5$  we find excess  $\text{P}_2$  incorporates into GaAs resulting in unintentional  $\text{GaAs}_x\text{P}_{1-x}$  QW's. Conversely, at high  $R_i$  ( $\geq 2.2$ ), we observe evidence for excess As incorporation into the GaInP barrier. Fig.1. shows 10K PL data from several 50 period (80Å GaAs/120Å GaInP) MQW samples, together with an equivalent GaAs/ $\text{Al}_{0.3}\text{Ga}_{0.7}\text{As}$  structure for reference. The latter has a high PL intensity and narrow linewidth ( $\sim 3.3\text{meV}$ ). Optimised ( $R_i \sim 1.8$ ) GaAs/GaInP MQW structures exhibit similar PL wavelength and intensities to the GaAs/AlGaAs structure, whilst PL linewidths are somewhat broader at typically 5-7meV. An example of non-intentional  $\text{GaAs}_x\text{P}_{1-x}$  QW's, grown using lower than optimum  $R_i$ , is also included in the figure. X-ray analysis indicates  $x \sim 0.12$  for this structure. The PL linewidth is considerably degraded, yet despite the strain, the PL intensity is quite comparable to the optimised structures. Fig.2 shows x-ray diffraction data from an optimised MQW structure, together with dynamical simulation results. The agreement with the simulated data is good, which provides additional confirmation of abrupt GaAs/GaInP QW interfaces.

To assess the electrical properties of GaInP, with particular regard to dopant behaviour, a series of GaInP bulk p-i-n diode structures have been grown. Fig.3 shows I-V data from a device with an i-region thicknesses ( $d_0$ ) =  $1\mu\text{m}$ . The excellent low reverse leakage current ( $< 1\text{nA}$ ) and abrupt high breakdown voltage ( $\sim 65\text{V}$ ) is typical of these structures. Fig.4. shows C-V, depletion-depth, data for  $d_0 = 0.4$  and  $1.0\mu\text{m}$  p-i-n structures. The observed carrier concentration slopes down from  $\sim 10^{18}$  to  $\sim 10^{15}\text{cm}^{-3}$  over a depth range  $\sim 0.2\mu\text{m}$ . The behaviour is significantly worse than for AlGaAs, the data from which would appear abrupt on such a scale. Samples with  $d_0 = 2\mu\text{m}$  indicate that a low background carrier concentration  $\sim 5 \times 10^{14}\text{cm}^{-3}$  is ultimately reached. From SIMS analysis we attribute the broadening of the carrier concentration profile almost solely to Be diffusion. Attempts to grow devices with thin i-region thicknesses ( $d_0 < 0.4$ ) resulted in compensated or even pseudo-abrupt junctions. There is some evidence for enhanced Be diffusion in the proximity of Si doped layers, an effect previously observed for Zn-doping in phosphides. Aspects of the diffusion of Be are undergoing additional study.

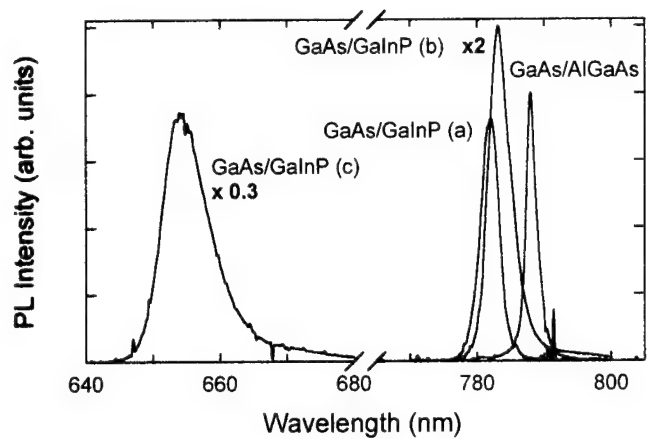


**Fig.1:** 10K photoluminescence data from GaAs/GaInP and GaAs/AlGaAs MQW structures. For the GaInP-based structures; (a)= optimised interface, (b)= as (a), but with AlInP cap, (c)= (non-intentional) GaAsP/GaInP graded MQW.

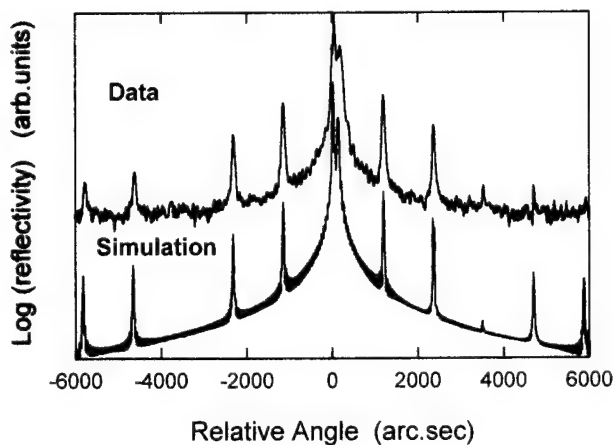


**Fig.2:** Double crystal x-ray diffraction data and simulation for a 50-period GaAs/GaInP MQW with abrupt interfaces. The curves are displaced for clarity.

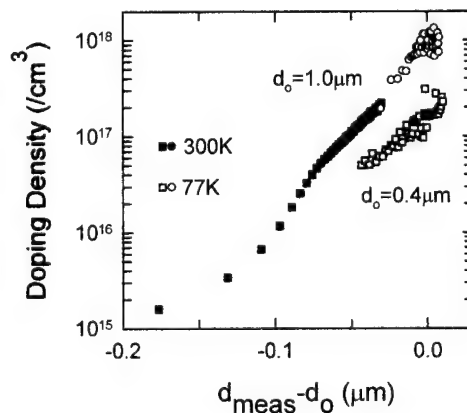
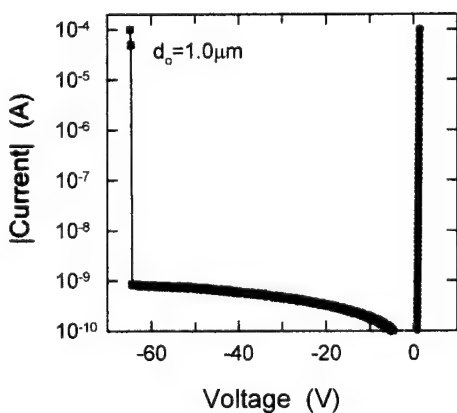


**Fig.3:** Current-voltage and **Fig.4:** capacitance-voltage (depletion depth) data for GaInP p-i-n (n-i-p) structures.



# Symmetric Triangular-barrier Optoelectronic Switch (S-TOPS) by Gas Source MBE

H. Sakata, Y. Nagao and Y. Matsushima

KDD R&D Laboratories  
2-1-15 Ohara, Kamifukuoka-shi, Saitama 356, Japan  
Phone:+81-492-78-7831 FAX:+81-492-78-7516  
e-mail : sakata@pico.elb.lab.kdd.co.jp

In order to apply to an optical signal processing, several kinds of optoelectronic switching devices which used a negative differential resistance (NDR) have been studied so far. We have already proposed a novel device, Triangular-barrier Optoelectronic Switch (TOPS)[1]. It consisted of an  $n^+-i-\delta p^+-i-n^+$  doping profile in InAlAs/InGaAs heterostructure and showed clear S-shaped NDR. In order to fabricate the well-controlled  $\delta$ -doped layer in the InP-based semiconductors, a gas source MBE (GS-MBE) should be a promising technique. Experimental I-V characteristics of TOPS at different input-light powers are shown in Fig.1. By utilizing this S-shaped NDR, we successfully obtained differential gain, bistable and latch characteristics by just changing the bias voltages [2]. However, unipolar S-shaped NDR was only observed due to its unsymmetric structure. If we can realize bipolar S-shaped NDRs, we can expect new applications of this device as an optoelectronic switch. In this paper, we propose a symmetric structure TOPS (S-TOPS) and demonstrate the optically controllable bipolar S-shaped NDRs in this device. To our knowledge, this is the first demonstration of optically controllable bipolar S-shaped NDRs using  $n^+-i-\delta p^+-i-n^+$  structure.

Figure 2 shows a device structure of the S-TOPS. It consisted of an  $n^+-i-\delta p^+-i-n^+$  symmetric structure of  $\text{In}_{0.53}\text{Ga}_{0.47}\text{As}$  and InP buffer layer. The device was grown by GS-MBE, in which 100%  $\text{AsH}_3$  and  $\text{PH}_3$  were used for group V sources, and Be and Si were used as p- and n-type dopants, respectively. The growth temperature was  $420^\circ\text{C}$  for InGaAs. The parameters of the  $\delta p^+$  layer such as a thickness and a sheet carrier concentration were critical to attain the NDR operation, which was caused by an avalanche multiplication near the  $\delta p^+$  layer. Experimental I-V characteristics of S-TOPS at different input-light powers are shown in Fig.3(a)-(c), in which the sheet carrier concentration  $n_{sp^+}$  of  $\delta p^+$  layer were varied as follows : (a)  $n_{sp^+}=1.8\times 10^{13}\text{cm}^{-2}$ , (b)  $n_{sp^+}=5.7\times 10^{13}\text{cm}^{-2}$ , (c)  $n_{sp^+}=4.5\times 10^{14}\text{cm}^{-2}$ . In Fig.3(a), we only obtained gain characteristic because electrons in i-layer can flow over the potential barrier when the photo-generated hole accumulate the gate layer and lower the potential barrier. The avalanche multiplication, however, does not occur in this case due to low potential height made by the  $\delta p^+$  doping. On the other hand, we obtained clear bipolar S-shaped NDRs and gain characteristic simultaneously in Fig.3(b). It is because of the positive feedback due to the avalanche multiplication and gain characteristic. In the case of further high doping such as Fig.3(c), we could not obtain the gain characteristic any more but just only photocurrent, because electrons could not flow over the potential barrier. From these results, we confirmed that it is important to optimize the sheet carrier concentration of  $\delta$ -doped layer for positive feedback. Fig.4 shows input-light vs. current characteristics in the device of Fig.3(b). We obtained latch characteristic with plus bias condition. We also obtained the same characteristics with minus biased, so that we can use this device as an bipolar optoelectronic switch. These characteristics also show the high potential of GS-MBE for fabricating well-controlled  $\delta$ -doped structure.

## References

- [1] H. Sakata, K. Utaka and Y. Matsushima, Proceeding of MBE8: J. Crystal Growth, 1995, 150, pp.1384-1388
- [2] H. Sakata, K. Utaka and Y. Matsushima, Electron. Lett. 1994, 30, pp.1792-1793

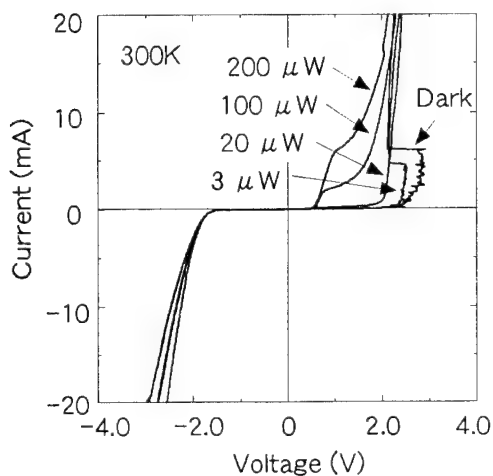


Fig.1. I-V characteristics of TOPS at different input-light powers

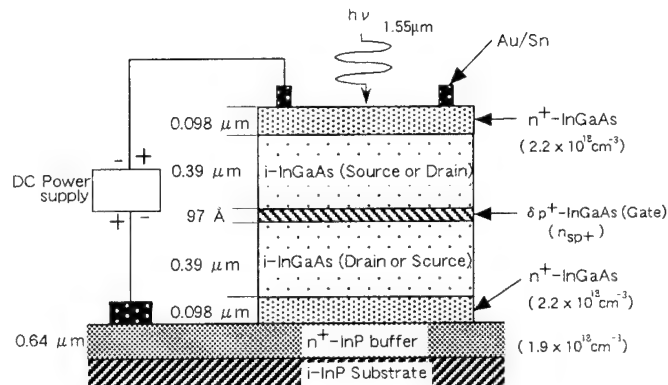
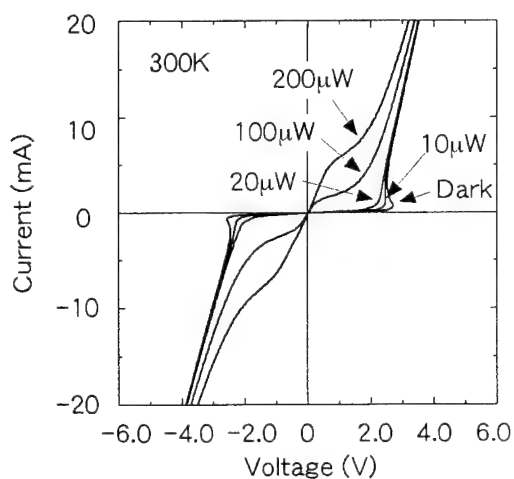
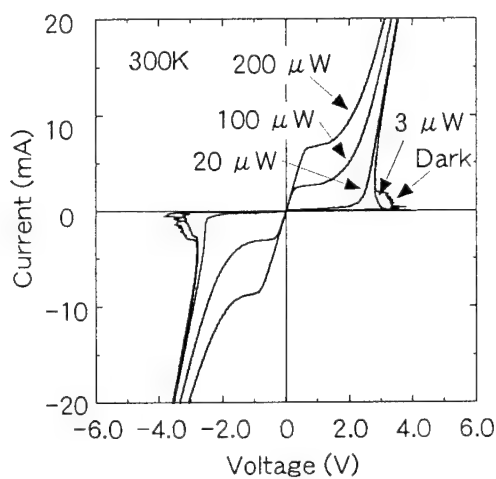


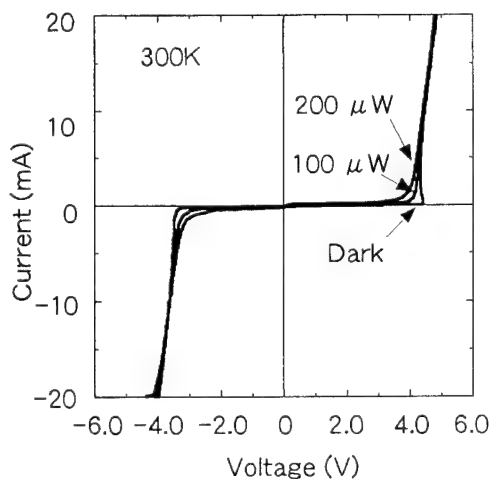
Fig.2. Device structure of S-TOPS



(a)  $n_{sp+} = 1.8 \times 10^{13} \text{ cm}^{-2}$



(b)  $n_{sp+} = 5.7 \times 10^{13} \text{ cm}^{-2}$



(c)  $n_{sp+} = 4.5 \times 10^{14} \text{ cm}^{-2}$

Fig.3. I-V characteristics of S-TOPS at different input-light powers as changing the sheet carrier concentration  $n_{sp+}$

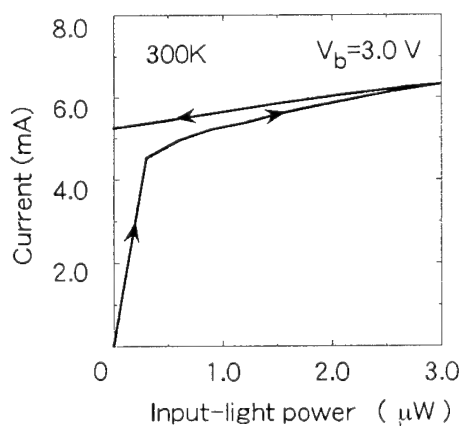


Fig.4. Input-light power vs. current characteristics ( $n_{sp+} = 5.7 \times 10^{13} \text{ cm}^{-2}$ )

**AlGaAs/GaAs, AlGaAs/InGaAs multiple quantum wells and Si-doped p-type quantum well infrared photodetectors grown on (311)A GaAs**

Albert Chin,<sup>(a)</sup> K. Lee,<sup>(b)</sup> J. Chu,<sup>(b)</sup> and S. S. Li<sup>(b)</sup>

<sup>a</sup>Dept. of Electronics Engineering, National Chiao Tung University, Hsinchu, Taiwan

<sup>b</sup>Dept. of Electrical and Computer Engineering, Univ. of Florida, Gainesville, FL 32611

Tel: 886-35-731841, Fax: 886-35-724361, e-mail: achin@william.ee.nctu.edu.tw

**ABSTRACT**

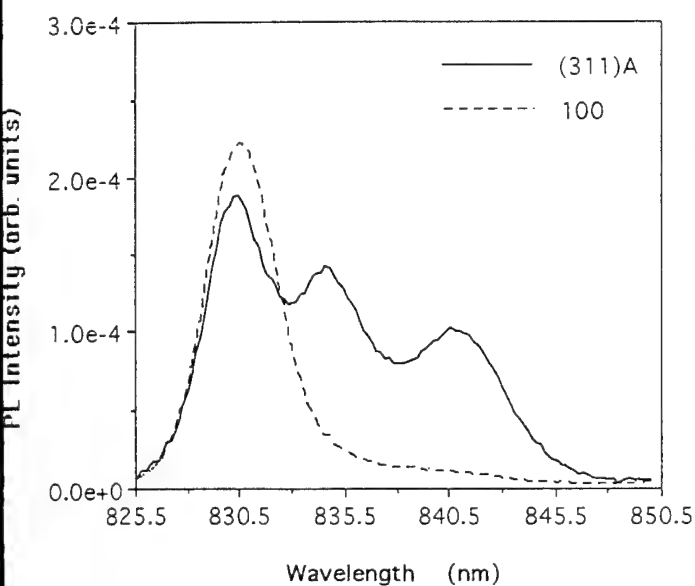
P-type quantum well infrared photodetectors (QWIP) has attracted much attention recently, because of the inherent capability of normal incidence radiation and even enhanced interband transition. To date, most of the p-type QWIP reported so far have used either beryllium (Be) or carbon (C) for the dopant species. However, both dopants have serious shortcomings. Be suffers from the problem of fast out-diffusion and asymmetrical I-V characteristics, while C is not compatible to the normal solid source MBE. Because high p-type concentration has been reported by Si-doped GaAs grown on (311)A orientation, we have studied the Si-doped p-type QWIP on this orientation. Owing to the very low diffusion coefficient of Si, a high growth temperature of 600 °C is used to grow the AlGaAs/GaAs p-type QWIP, which is ~50 °C higher than that grown by Be-doped (100) samples. The high growth temperature also improves the optical property of AlGaAs/GaAs multiple quantum wells (MQWs) as measured by photoluminescence (PL). A PL linewidth of 12 meV is measured from an undoped AlGaAs/GaAs MQWs grown on (311)A GaAs that indicates the good material quality on this orientation. Furthermore, more than an order of magnitude of PL intensity is measured from the 600 °C grown (311)A MQWs than that grown on (100) at 550 °C. Although strong PL intensity is also observed for AlGaAs/InGaAs MQWs grown on (311)A GaAs at 550 °C, multiple PL transitions are measured with peak energy red-shifts of 7 and 22 meV to that of side-by-side grown (100). We have used cross-sectional TEM to study this effect and the PL energy red-shift is due to the growth induced thickness modulation of quantum wells grown on (311)A orientation. The new Si-doped p-type AlGaAs/GaAs QWIP exhibits a symmetrical dark I-V characteristic at all the measured temperatures from 40 to 120 K. The strained p-type AlGaAs/InGaAs QWIP exhibits a slightly asymmetrical dark current characteristic, but is markedly less asymmetrical than that doped by Be. The slight asymmetry in dark I-V characteristic may be due to the thickness modulation observed by cross-sectional TEM, while the spontaneously formed thickness modulation can be used for novel multi-color QWIP by a simple structure design and material growth.

Fig. 1. 15K PL spectra of InGaAs/AlGaAs multiple quantum wells (MQWs) grown on (311)A and (100) GaAs. Multiple PL emissions is observed from (311)A strained MQWs.

Fig. 2. Cross-sectional TEM image of InGaAs/AlGaAs multiple quantum wells grown on (311)A GaAs. A thickness modulation is observed.

Fig. 3. Dark I-V characteristic for the Si-doped AlGaAs/GaAs p-type QWIP.

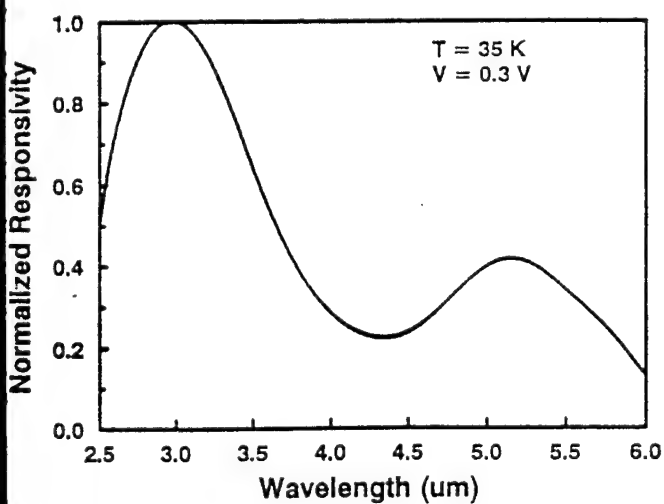
Fig. 4. Normalized responsivity for the Si-doped p-type QWIP.



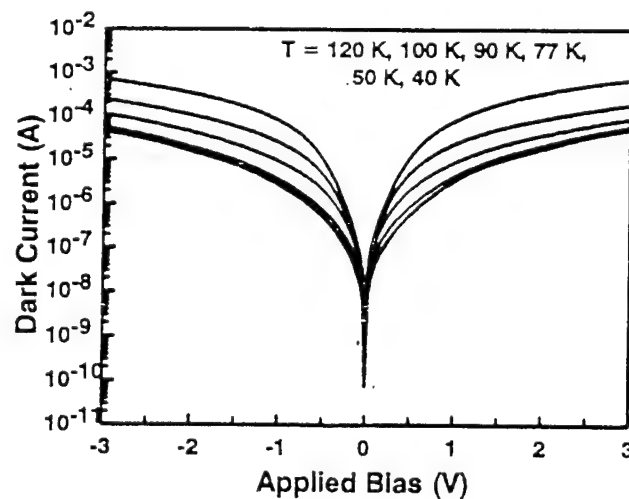
(1)



(2)



(4)



(3)

## CBE growth of tensile-strained GaAsP/GaAlAs quantum well heterostructures for laser application

J.Ch.Garcia, A.Lebkiri, A.Fily, Ph.Collot, J.Massies (\*), M.Leroux (\*)

Laboratoire Central de Recherches Thomson CSF 91404 Orsay cedex France

(\*) CRHEA/CNRS Rue Bernard Grégory 06560 Valbonne France

Tel: 33 1 69 33 90 99

Fax: 33 1 69 33 07 40

e-mail: [garcia@lcr.thomson.fr](mailto:garcia@lcr.thomson.fr)

Progress in the development and synthesis of aluminium containing organometallic precursors such as trimethyl amine alane (TMAAl) or dimethyl ethyl amine alane (DMEAAl) has led to the possibility of growing high purity GaAlAs materials by chemical beam epitaxy (CBE) [1]. Up to now, these advances have been mainly used to realise bipolar or two dimensional electron gas transistors. There is only a few reported results on the optical properties of CBE grown GaAlAs [2]. In this communication, we report on the CBE growth conditions of high quality GaAlAs ( $x_{Al}$  : 20-60%) and tensile-strained GaAsP quantum wells ( $y_P$ : 5-29%) on GaAs (001) using TMAAl and alternative precursors of group V elements (TBAs, TBP). Cracking conditions of TBAs and TBP have been improved in order to reduce the carbon incorporation. Low levels of carbon and oxygen were detected by SIMS analysis of AlGaAs layers, independent of the aluminium concentration used ( $[O] \approx 5-8 \cdot 10^{17} \text{cm}^{-3}$ ,  $[C] \approx 2-5 \cdot 10^{17} \text{cm}^{-3}$ ).

Figure 1 represents the room temperature photoluminescence (PL) energy of heavy-hole (HH) and light-hole (LH) related transitions as a function of phosphorus composition in 100Å thick GaAsP/Al<sub>0.25</sub>Ga<sub>0.75</sub>As quantum wells. The observation of HH-LH splitting by room temperature PL, even for large P concentration, is indicative of the high purity and interface quality of these QWs. The QW photoluminescence energy as a function of P mole fraction is well accounted for by envelope function calculations including strain effect. At least for  $y_P \leq 25\%$ , a good agreement is obtained between experimental and calculated E1-HH1, E1-LH1 energy transitions as shown in figure 1. At low P compositions, the smallest transition energy corresponds to HH. The relative position switching of the HH and LH bands has been observed for a composition of 5% in agreement with recently reported results on MOCVD grown similar structures [3]. These calculations have been used to optimize GaAlAs/GaAsP laser structures. Characteristics of separate-confinement heterostructure laser diodes emitting in the 0.74-0.85  $\mu\text{m}$  wavelength range will be discussed in the light of material properties and design of laser structures.

[1] R.W.Freer et al *J. Crystal Growth*, **150**, 539 (1995)

[2] B.Courboules et al. *Appl. Phys. Lett.* **65** 836 (1994)

[3] F.Agahi et al. *IEEE Phot. Tech. Lett.* **7**, 140 (1995)

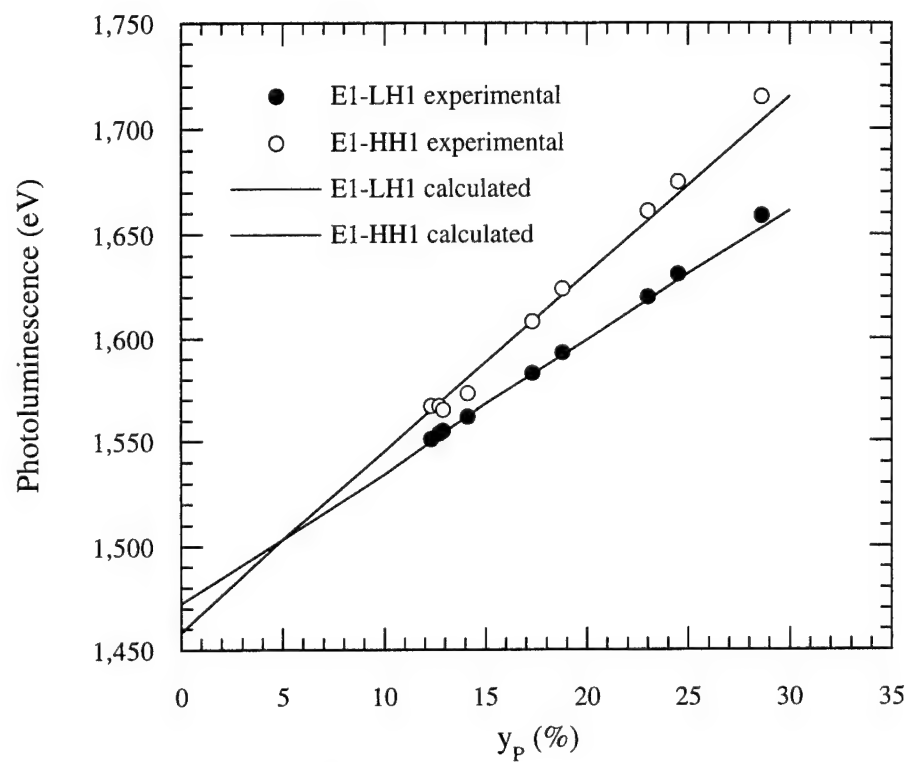


Fig. 1 Experimental photoluminescence energies versus phosphorus composition in the QW. The plot shows also the calculated energies (solid lines) for aluminium composition in the barriers of 25%.

# Strain compensation in highly carbon doped GaAs/AlAs distributed Bragg reflectors

A. Mazuelas, R. Hey, M. Wasserman, and H. T. Grahn\*

Paul-Drude-Institut für Festkörperelektronik,

Hausvogteiplatz 5-7, D-10117 Berlin, Germany

Tel. 49-30-20377351, Fax. 49-30-20377201, e-mail: mazuelas@pdi.wias-berlin.de

Solid source molecular beam epitaxy is used to synthesize highly carbon doped, strain compensated distributed Bragg reflectors (DBRs), which constitute part of complex optoelectronic devices such as vertical cavity surface emitting lasers (VCSEL), microresonators, and saturable absorbers. In order to obtain a high optical reflectivity, the DBR must have a large number of quarter-wavelength pairs and hence be of a considerable thickness. This fact together with the difference in the lattice parameters between the constituent materials results in a structural degradation by the generation of misfit dislocations. A carbon filament is used to produce highly p-doped GaAs/AlAs DBRs, which are at the same time strain compensated. We apply X-ray scattering methods to determine the best growth conditions, the effectiveness of the strain compensation (Fig.1), the onset of relaxation (Fig.2), and the overall structural quality of the DBRs. Atomic force microscopy is used to investigate the effect of the high C doping on the surface morphology (Fig.3). The residual strain with respect to the GaAs substrate can be reduced to less than  $1 \times 10^{-4}$ , which results in a large increase of the critical thickness of the carbon doped DBRs in comparison with the undoped or Be doped DBRs. By simulating X-ray diffraction patterns, the chemical profile as well as the structural parameters of the GaAs:C and AlAs:C layers are determined with high accuracy. The effective incorporation of carbon on lattice sites in AlAs:C is found to be twice as large as in GaAs:C using the same incident carbon flux. Optical and electrical characterization of the DBR:C are performed to establish high reflectivity and low series resistance. Carbon-doped, strain-compensated DBRs are promising candidates to be used as p-type mirrors in vertical cavity surface emitting lasers.

\* On leave at : Research Center for Quantum Effect Electronics, Tokyo Institute of Technology, 2-12-1 O-okayama, Meguro-ku, Tokyo 152, Japan

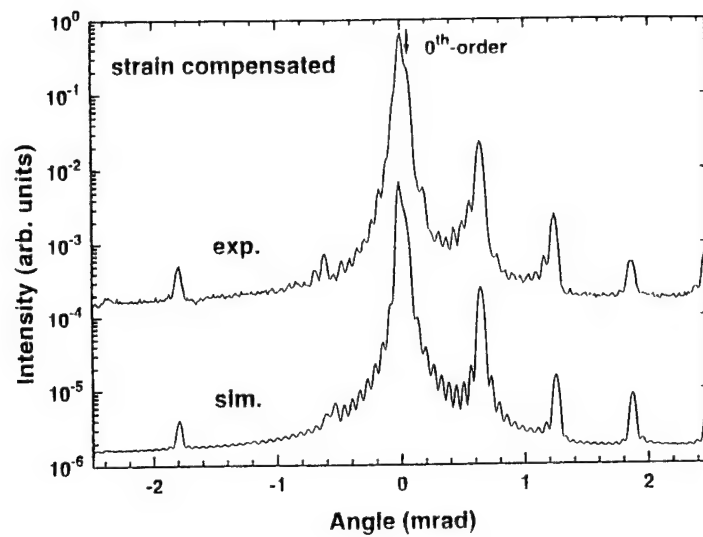


Fig. 1. Experimental and simulated rocking curves of a doped, 10-pair GaAs:C/AlAs:C DBR, which is strain-compensated with respect to the substrate.

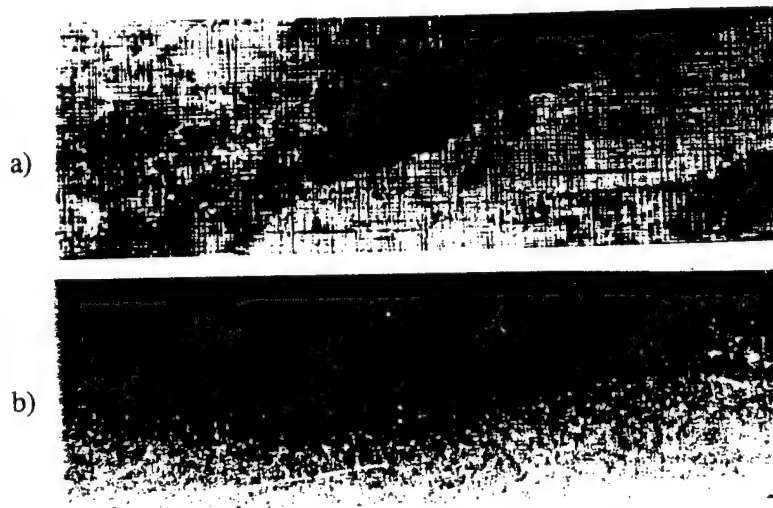


Fig. 2. X-ray topographs of two different 20 pair DBRs. While the undoped DBR in (a) contains a high density of misfit dislocations (relaxed), the doped DBR:C in (b) is free of misfit dislocations (strained).

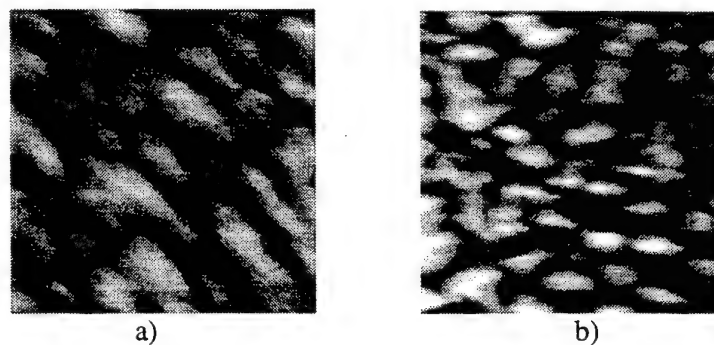


Fig 3. Atomic force microscopy images of an undoped, 20-pair DBR (a) and a strain compensated, 20-pair DBR:C (b).



**808nm HIGH POWER LASER GROWN BY MBE  
THROUGH THE CONTROL OF  
Be DIFFUSION AND USE OF SHORT-PERIOD SUPERLATTICE**

Donghai Zhu, Zhanguo Wang, Jiben Liang, Bo Xu,  
Zhanping Zhu, Jun Zhang, Qian Gong, Shengying Li

Laboratory of Semiconductor Materials Science,  
Institute of Semiconductors, Chinese Academy of Sciences

Beryllium (Be) diffusion plays an important role in the performance of GaAs/AlGaAs semiconductor lasers grown by MBE. Both increased oxygen incorporation and p-n junction displacement are related to Be diffusion. In this letter, we report the method of limiting the Be diffusion and incorporation of short-period superlattice in GRIN-SCH SQW high power lasers during molecular beam epitaxy.

The semiconductor crystals were grown by Riber 32p MBE system. The combination of Si doped graded index (GRIN) AlGaAs layer adjacent to n-AlGaAs cladding layer and undoped GRIN AlGaAs layer adjacent to p-AlGaAs cladding layer together with the reduced Be dopant concentration in p-AlGaAs cladding layer near the GRIN region at a range of 0.1  $\mu\text{m}$  prevent the Be diffusion during molecular beam epitaxy growth. Oxygen which forms nonradiative recombination centers is also minimized by this method. In the laser structure, superlattice among GaAs buffer and n-AlGaAs cladding layers are incorporated, which offer additional defense against O incorporation and make the epitaxial layer flat. A low Al composition AlGaAs layer is introduced as an getter buffer layer to remove the transient oxygen. High power broad-area lasers were fabricated, the threshold current density is near 200A/cm<sup>2</sup>, the external differential quantum efficiency is 85% per facet for uncoated lasers. Recorded CW output power at room temperature has reached 2.3W.

Address: Donghai Zhu  
Lab of semiconductor materials science  
Institute of semiconductors  
Chinese Academy of Sciences  
P.O.Box 912, Beijing 100083  
P.R. China

Fax: +86-10-2562389

# GaAs quantum well islands formed by sub-monolayer AlAs masking and thermal desorption

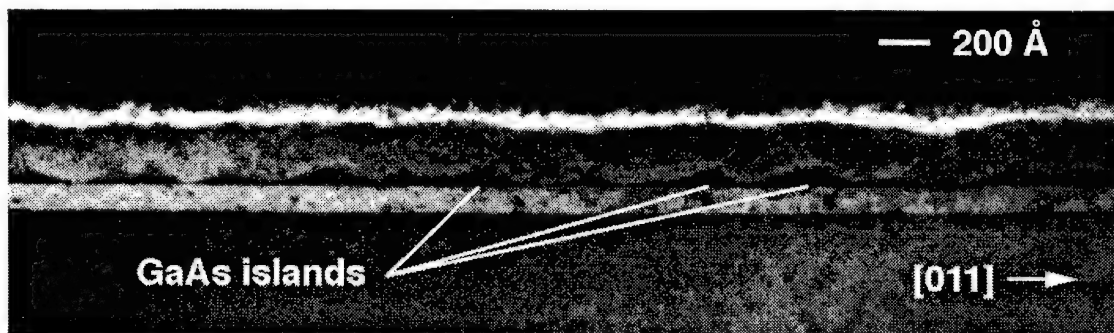
Timothy A. Strand\*, R. L. Naone, L. A. Coldren, P. M. Petroff, and E. L. Hu

*National Science Foundation Center for Quantized Electronic Structures (QUEST)*  
*University of California, Santa Barbara, CA 93106*  
\*email: 6500stra@ucsbuxa.ucsb.edu  
tel: 805-893-8154 fax: 805-893-4500

The high surface-to-volume ratios in small optoelectronic and electronic devices result in high levels of current lost to surface recombination. This recombination process is supplied by lateral carrier diffusion in the device's active region. We present here a means for reducing this lateral diffusion in a GaAs quantum well by patterning the quantum well into discrete islands.

We deposit a fractional monolayer of AlAs onto a GaAs quantum well at 530°C. The surface mobility of the AlAs, although small, leads to the formation of discrete islands with an approximate size of 100 x 150 Å. These monolayer, AlAs islands are stable under arsenic flux at temperatures well over 700°C, making them suitable as a mask for the desorption of the underlying GaAs quantum well. Thermal desorption at 700°C patterns the quantum well into discrete, quantum well islands. Due to the somewhat crystallographic nature of the desorption process, these GaAs islands are larger than the masking, AlAs islands, and have trapezoidal cross-sections.

We present data showing the size, shape, and distribution of these quantum well islands, as well as measurements of luminescence and lateral carrier diffusion. We demonstrate lateral diffusion lengths in quantum well island layers as small as 0.27 μm, and luminescence efficiency comparable to that of a non-patterned quantum well. We also discuss the applicability of this technique to forming quantum boxes.



Transmission electron micrograph of GaAs quantum well island layer (dark) in  $\text{Al}_{0.5}\text{Ga}_{0.5}\text{As}$ . The islands are trapezoidal in cross-section and have a width of 200-400 Å at the base.

# Molecular-beam Epitaxy of Self-assembled InAs

## Quantum Dots on non-(100) oriented GaAs

P.P.González-Borrero, E.Marega Jr., D.I.Lubyshev, E.Petitprez and P.Basmaji

Instituto de Física de São Carlos-Universidade de São Paulo

CP 369, 13960-970 São Carlos, SP, Brazil

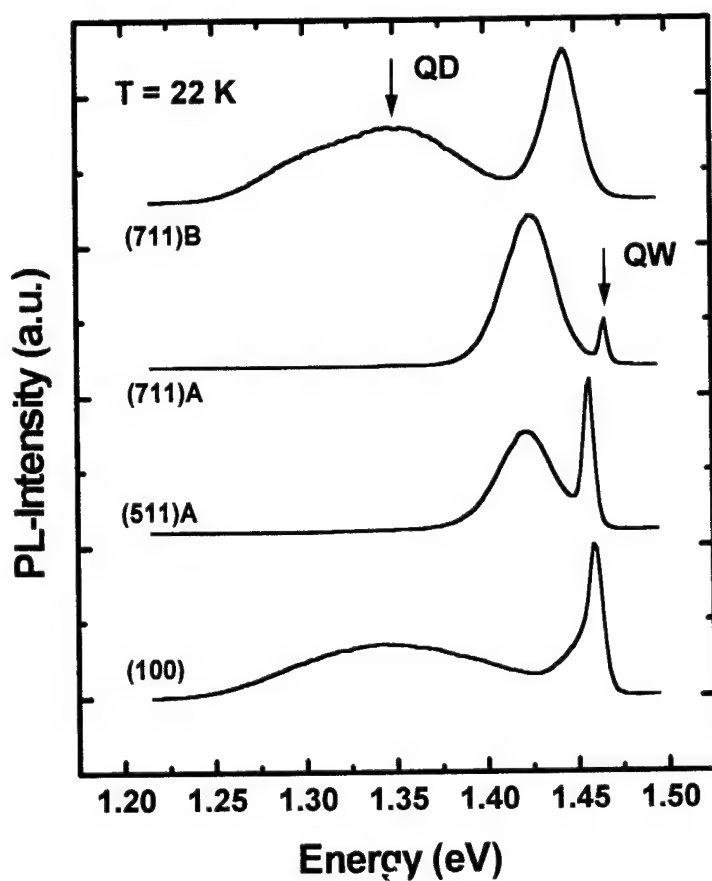
Heteroepitaxy of strained lattice-mismatch system -like InGaAs on GaAs and InAlAs on AlAs- opens new possibility to obtain nearly defect free quantum dots (QD) with characteristic sizes of 10-30 nm. These QD are usually produced by Stranski-Krastanow growth mode. The main QD parameters -as size redistribution, lateral size and shape form- are dependent from the mechanism of stress relaxation of a bi-dimensional (2D) layer to a three-dimensional (3D) island.

In this work, we report optical properties of InAs QD grown by molecular-beam epitaxy on GaAs (n11)A/B, where n is 1, 2, 5 and 7, and reference (100) substrates. The structure contains 20 periods of GaAs/AlAs (2nm/2nm) superlattice, a 0.5  $\mu\text{m}$  GaAs buffer layer, and a 3nm  $\text{In}_{0.2}\text{Ga}_{0.8}\text{As}$  quantum well (QW). The QD were separated from the QW by a 100 nm GaAs layer. For QD formation, 6 monolayer were deposited for (100) plane. To complete the structure, a 50 nm GaAs cap layer was grown. We have studied orientation and polarity effects by means of photoluminescence (PL) and polarization measurements. The PL spectra reveal difference on amplitude, integral luminescence, peak position and peak shape. The PL temperature dependence indicates an additional lateral confinement on (100), (211)B, (511)B, (711)B, (111)B, (211)A and (111)A surfaces. This dependence confirms QD formation on these planes. Our results also show an enhancement of the QD onset thermal quenching energy by a factor of 2.5 for these orientations. Based on our QD PL polarization measurements we suppose that QD have well developed microfacet configuration.

Contrary, the structure grown on (711)A and (511)A surface do not exhibit QD formation although present a broader PL peak related with recombination of a bidimensional InAs QW. These broad  $F_L$  signals are associated with presence of dislocation in relaxed InAs layer. We believe that the observed polarity (A/B) effects on stress relaxation is caused by different growth mode: Stranski-Krastanow (2D) for (100), (211)B, (511)B and (711)B surfaces, and Volmer-Weber (3D) for (711)A and (511)A one. The observed orientation and polarity effects on PL properties reveal that In adatom kinetic is an important mechanism of stress relaxation.

(contact person: P. Basmaji, IFSC-USP, CP 369, São Carlos, SP, Brazil;  
Fax: (55) (16) -(2713616) or -(2749206); e-mail: Pierre@ifsc.sc.usp.br)

Additional page to support our entitled work “*Molecular-beam epitaxy of Self-assembled InAs Quantum Dots on non-(100) oriented GaAs*” of authors: P.P. González-Borrero, E. Marega Jr., D. I. Lubyshev, E. Petitprez and P. Basmaji.



# InAs/GaAs self-organized quantum dots grown by ALMBE and MBE

A Bosacchi, P Frigeri, S Franchi\*, P Allegri and V Avanzini  
CNR - MASPEC Institute, Via Chiavari 18a, I-43100 Parma, Italy

Self-organized dots originating from deposits of highly strained materials on lattice-mismatched substrates are very simple systems which show low-dimensionality effects that can be exploited both for fundamental studies and for applications. One of the most important parameters of the dot populations is the island size and its distribution. While MBE is widely used for the preparation of quantum dot (QD) structures, new growth techniques are investigated since they may give useful benefits. ALMBE is considered interesting since the alternate supply of anions and cations gives rise to a significant increase of cation surface migration. It is expected that this feature would result in sharper size distributions since it may cause the selective enlargement of existing dots, instead of the continuous nucleation of new small islands.

The aim of this communication is to study how the features and the size distribution of self-organized InAs/GaAs QDs depend on MBE and ALMBE growth techniques and how the growth parameters and procedures of the upper and lower confining layers influence the PL properties of the structures.

We observe by AFM that in the 3D regime the mean diameters of ALMBE and of MBE dots increase with the InAs ML coverage  $\theta$ ; independently of  $\theta$ , ALMBE dots have mean diameters larger than those of the MBE ones (19 nm vs 14 nm and 21 nm vs 16 nm, for  $\theta = 2.4$  and 3.0 ML, respectively). Other interesting features are: i) the diameter distributions are always sharper in the case of ALMBE dots, ii) for relatively high InAs coverages (3.0 ML) MBE dots tend to coalesce, thus giving diameter distributions with a tail and a possible small peak at large diameters, and iii) for the same coverages the ALMBE dots have much sharper size distributions, that, for  $\theta = 3.0$  ML, have the main peak at 21 nm (FWHM of 4.5 nm) and a second smaller peak at  $\sim 4$  nm; this feature represents a second population of tiny dots that were almost absent at smaller coverages. The photoluminescence (PL) features of the ALMBE QDs as compared to those of the corresponding MBE ones are: i) smaller PL energies and ii) considerably lower FWHMs ( $\sim 40$  meV); these features are consistent with the larger diameters (at the same ML coverages) of ALMBE dots and their sharper size distributions.

As for the effect of growth parameters of caps, we observe that increasing the ALMBE growth temperature  $T_g$  from 360 °C to 460 °C, the PL transitions due to QDs shift to higher energies; this suggests that, also in the case of ALMBE, significant modifications of the QD morphology take place when caps are grown at relatively high  $T_g$ . When growing caps at 460 °C by ALMBE, we have results similar to those of other procedures used to reduce the interaction between QDs and caps and to improve the quality of the upper carrier-confining layers, such as the preparation of caps by MBE at 360 °C for 5 MLs and then at 560 °C. The quality of the bottom GaAs confining layers (on which the QDs are deposited) is definitely better when they are grown by MBE at relatively high temperatures (560 °C) than when they consist of MBE layers deposited at high  $T_g$  followed by thin ALMBE layers grown at the temperatures used for the ALMBE preparation of QDs. It is worth noting that structures with ALMBE dots and with optimized confining layers show significantly bright PL at 300 K.

The benefits of the above mentioned schemes and the resulting properties of the structures will be discussed in the framework of the current understanding of ALMBE and MBE growth mechanisms.

\* tel: +39-521-269209, fax: +39-521-269206, e-mail: franchi@prmasp.bo.cnr.it

# InAs/GaAs self-organized quantum dots grown by ALMBE and MBE

A Bosacchi, P Frigeri, S Franchi, P Allegri and V Avanzini

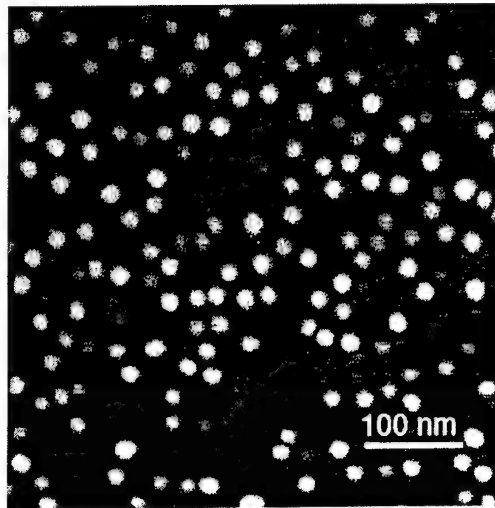


Fig. 1. AFM micrograph of InAs/GaAs QDs grown by ALMBE at 460 °C. The InAs coverage is 3.0 ML. The dots have been deposited on a MBE GaAs layer grown at 560 °C, after a 210 s interruption. The InAs dots have been deposited in 15 ALMBE cycles. The image has been obtained with a tip with a 20 nm radius.

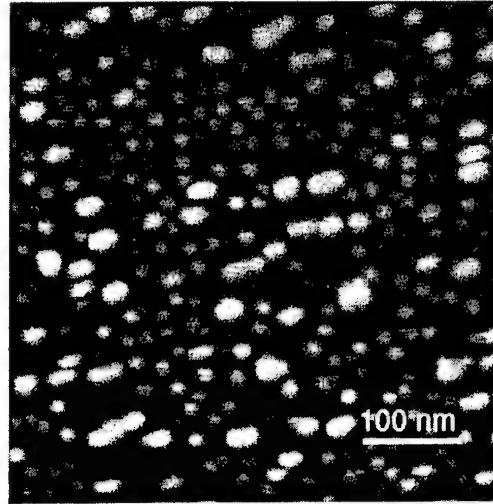


Fig. 2. AFM micrograph of InAs/GaAs QDs grown by MBE at 460 °C. The InAs coverage is 3.0 ML. The dots have been deposited on a MBE GaAs layer grown at 560 °C, after a 210 s interruption. The image has been obtained with a tip with a 20 nm radius.

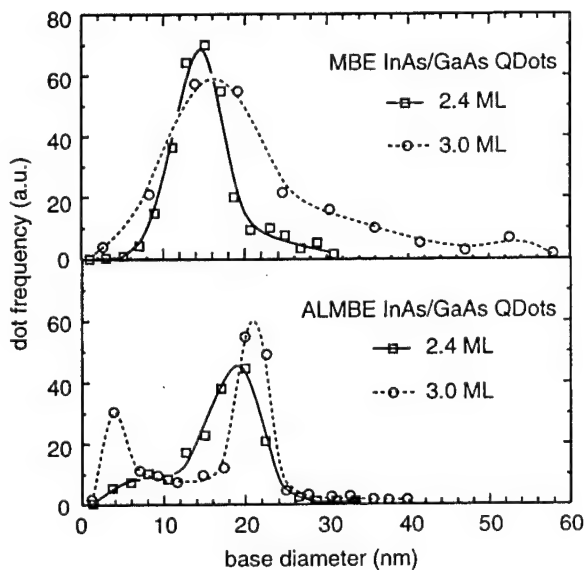


Fig. 3. Distributions of diameters of QDs grown by MBE and ALMBE with InAs coverages of 2.4 ML and 3.0 ML. The QDs have been prepared under the conditions described in the captions of Figs. 1 and 2. In the analysis of AFM images the convolution effects due to the 20 nm radius of the AFM tip are not taken into account.

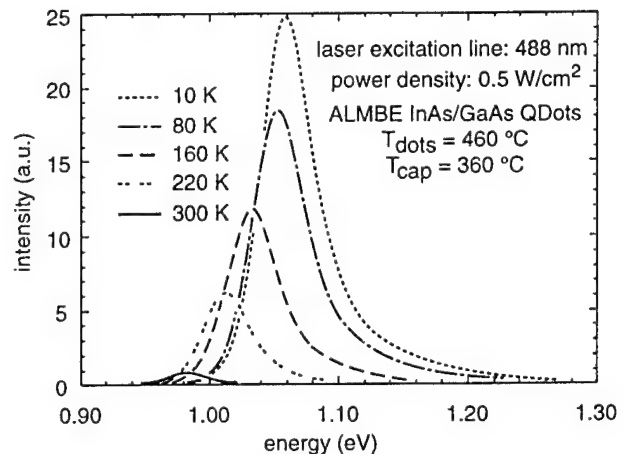


Fig. 4. Photoluminescence spectra at different temperatures of InAs/GaAs QDs grown by ALMBE at 460 °C; the upper confining layer has been grown at 360 °C by ALMBE. The dots have been deposited on a MBE GaAs layer grown at 560 °C, after a 210 s interruption. The spectral resolution is 1 meV.

## Temperature-insensitive photoluminescence at high temperatures in GaInAs strained multiple quantum wire heterostructures

D.E. Wohlert, S.T. Chou,<sup>a)</sup> and K.Y. Cheng<sup>b)</sup>

Department of Electrical and Computer Engineering, and Microelectronics Laboratory,  
University of Illinois at Urbana-Champaign, Urbana, Illinois 61801

Optoelectronic communications require lasers to emit at a stable wavelength. However, the bandgap of semiconductors changes with temperature which results in a temperature sensitive emission wavelength. This problem is currently remedied by employing a distributed feedback (DFB) structure in the design of laser diodes. Temperature dependent wavelength shifts are found to be about  $1 \text{ \AA}/^\circ\text{C}$  for  $1.55 \text{ }\mu\text{m}$  DFB lasers [1]. A further improvement on DFB lasers would be to have a semiconductor structure whose bandgap does not change with temperature to begin with.

Stable peak wavelength photoluminescence (PL) has been observed in  $\text{Ga}_x\text{In}_{1-x}\text{As}$  strained multiple quantum wire (MQWR) heterostructures for sample temperatures from room temperature up to around  $100^\circ\text{C}$  (see Fig. 1). The MQWR samples were grown by solid source molecular beam epitaxy using the strain induced lateral layer ordering (SILO) process. By growing quantum wells with  $(\text{GaAs})_2/(\text{InAs})_{2,2}$  short-period-superlattices,  $\text{Ga}_x\text{In}_{1-x}\text{As}$  lateral superlattices were formed *in situ*. The  $[\bar{1}10]$  oriented lateral quantum wells, along with the traditional quantum wells in the  $[100]$  growth direction, form quantum wires. The formation of the lateral  $\text{Ga}_x\text{In}_{1-x}\text{As}$  superlattices depends on the amount of strain, which depends on the growth conditions, present in the MQWR regions [2].

The PL behavior from 77 to 300 K of samples with a strongly strained MQWR active region differ greatly from those with moderate strain. Strongly strained samples have a net blue shift, with increasing temperature, of peak PL wavelength of about  $3 \text{ \AA}/^\circ\text{C}$ , whereas the net peak PL wavelength shift of moderately strained samples is negligible between 77 and 300 K. However, the peak PL wavelengths of both types of samples stabilize at  $1.61$  to  $1.62 \text{ }\mu\text{m}$  for temperatures above 300 K as seen in Fig. 2. The temperature dependent shift of peak PL wavelength between 300 and 380 K for these MQWR heterostructures is, on average, less than  $0.25 \text{ \AA}/^\circ\text{C}$ . Experimental and theoretical analysis indicates that multi-axial strain fields induced by the SILO process in the MQWR active regions are responsible for this phenomena. Lasing wavelength shifts of about  $1 \text{ \AA}/^\circ\text{C}$  between 77 and 300 K have been observed in  $\text{Ga}_x\text{In}_{1-x}\text{As}$  MQWR lasers. High temperature stimulated emission of MQWR lasers is presently being studied.

[1] Y. Abe, K. Kishino, Y. Suematsu, S. Arai, *Electron. Lett.* **17**, 945 (1981)

[2] S.T. Chou, K.Y. Cheng, L.J. Chou, and K.C. Hsieh, *J. Appl. Phys.* **78**, 6270 (1995)

<sup>a)</sup> Present Address: EE Department, Chung-Cheng Institute of Technology, Ta-Hsi, Tao-Yuan, Taiwan (335), Republic of China

<sup>b)</sup> Contact: Professor K. Y. Cheng, Microelectronics Laboratory, University of Illinois, 208 N. Wright St., Urbana, IL 61801, Phone: 217-333-6642, FAX: 217-244-6375, email: k-cheng@uiuc.edu

Figure 1

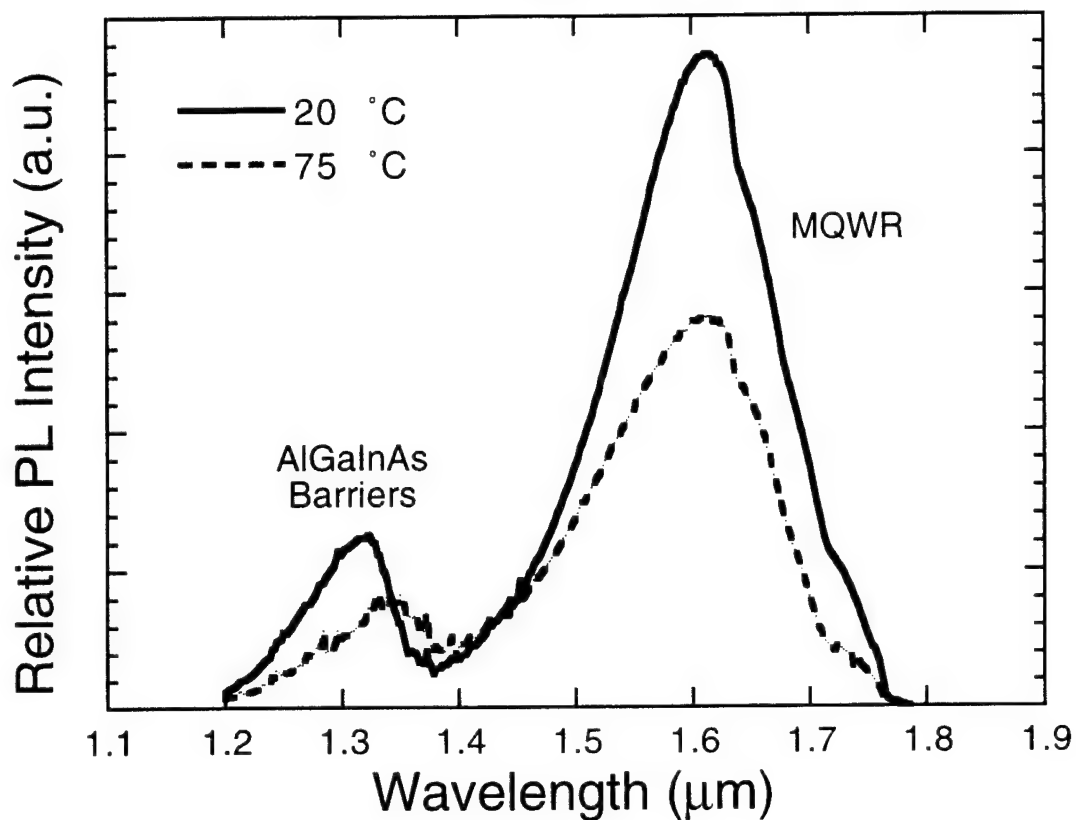
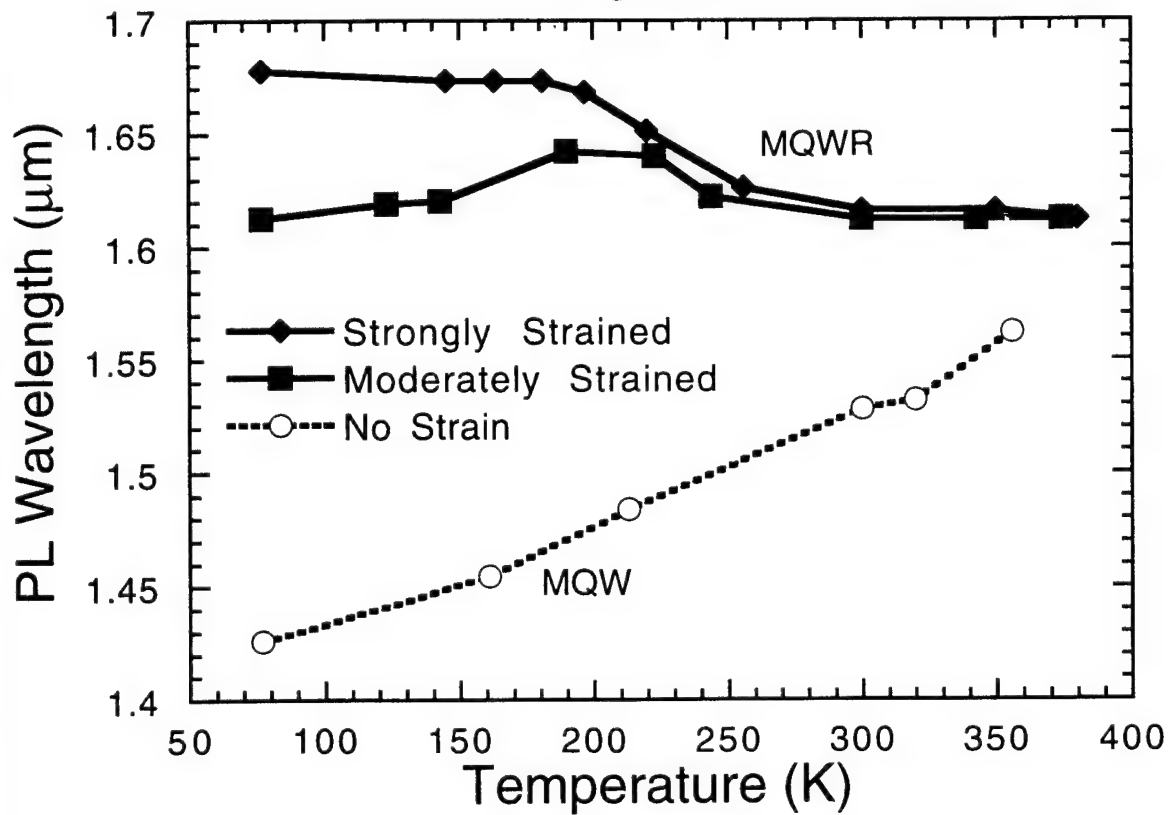


Figure 2





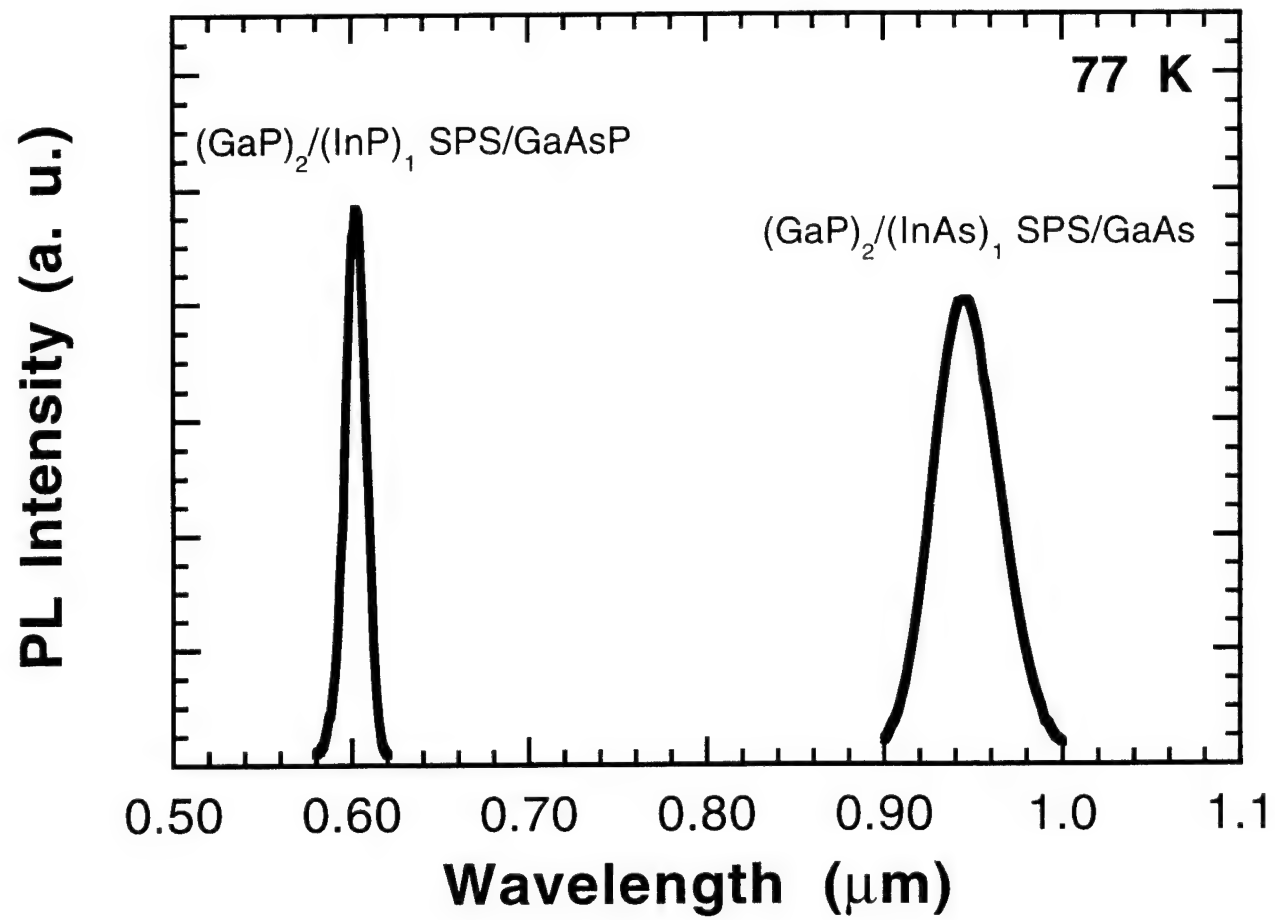
## Growth of GaInAsP Quantum Wire Heterostructures Using the Strain-Induced Lateral-Layer Ordering Process

A. C. Chen, A. M. Moy, K. Y. Cheng,<sup>a)</sup> L. J. Chou, and K. C. Hsieh  
 Department of Electrical and Computer Engineering and Microelectronics Laboratory,  
 University of Illinois at Urbana-Champaign, Urbana, Illinois 61801

Interest in quantum wire (QWR) lasers has been spurred by theoretically predicted advantages over their quantum well counterparts. Advantages include lower threshold current densities, higher modulation bandwidths, and higher characteristic temperatures. Utilizing the strain-induced lateral layer ordering process (SILO), it has been previously established that the growth of short-period superlattices (SPS) of  $(\text{GaP})_m/(\text{InP})_n$  on GaAs or  $(\text{GaAs})_m/(\text{InAs})_n$  on InP leads to a composition modulation along the  $[110]$  direction. This modulation provides a lateral dimension of confinement which can be coupled with standard quantum wells to produce multiple quantum wires (MQWRs). In the GaInP/GaAs and GaInAs/InP material systems, the number of monolayers was chosen to be  $m \cong n \cong 2$ , in order to fulfill the near strain-balance requirement. As a consequence, photonic devices fabricated with the SILO process exist in very limited wavelength ranges.

In this study, we have extended this concept to achieve GaInAsP QWRs using the SILO process, which cover a wide range of wavelengths, using non-equal number of monolayers in SPS but still satisfying the near strain-balance condition.  $\text{Ga}_x\text{In}_{1-x}\text{P}$  MQWRs were grown on ternary  $\text{GaAs}_{0.66}\text{P}_{0.34}$  substrates using the modified near strain-balance mechanism. Utilizing  $(\text{GaP})_2/(\text{InP})_1$  SPS, we are able to provide the necessary conditions for the SILO process to occur on the smaller lattice  $\text{GaAs}_{0.66}\text{P}_{0.34}$  substrates. QWRs with 77 K photoluminescent (PL) emission near  $6000 \text{ \AA}$  were obtained. Additionally, we have grown  $(\text{GaP})_2/(\text{InAs})_1$  SPS on GaAs substrates to further explore the near strain-balance mechanism in the SILO process. Using the technique, QWRs with 77 K PL emission near  $1 \mu\text{m}$  were obtained. The samples grown using the non-equal number of monolayers in SPS exhibit the same MQWR properties as those in the equal monolayer case. A strong composition modulation can be seen along the  $[110]$  direction as well as a strong PL anisotropy. Shown in Figure 1 is the 77 K PL emission of the  $(\text{GaP})_2/(\text{InP})_1$  MQWRs on GaAsP substrates and the  $(\text{GaP})_2/(\text{InAs})_1$  MQWRs on GaAs. This technique further utilizes the SILO process as a powerful tool in obtaining quantum confined heterostructures at extended wavelength ranges.

<sup>a)</sup> Contact: Professor K. Y. Cheng, Microelectronics Laboratory, University of Illinois, 208 N. Wright St., Urbana, IL 61801, Phone: 217-333-6642, FAX: 217-244-6375, email: k-cheng@uiuc.edu



## Formation of Self-Aligned $\text{In}_{0.5}\text{Ga}_{0.5}\text{As}$ Quantum Dots on GaAs by Molecular Beam Epitaxy

Jen-Inn Chyi, Tzer-En Nee,\* Ching-Ting Lee,\* Jia-Lin Shieh, and Jen-Wei Pan

Department of Electrical Engineering, National Central University

Chung-Li, Taiwan 32054, R.O.C.

\*Institute of Optical Sciences, National Central University

Chung-Li, Taiwan 32054, R.O.C.

Tel: +886-3-425-8241, Fax: +886-3-425-5830, chyi@mbox.ee.ncu.edu.tw

Semiconductor quantum dots is an area of great interest for low dimensional quantum devices. The formation of self-aligned quantum dots during epitaxial growth is one of the key issues in the fabrication of these devices. In this work, we have successfully developed the technique to form  $\text{In}_{0.5}\text{Ga}_{0.5}\text{As}$  self-aligned quantum dots on GaAs by molecular beam epitaxy.

The preparation of step-bunching, which facilitates the formation of self-aligned quantum dots was carried out on (100) GaAs substrates misoriented towards (111)A by  $4^\circ$ . It was realized by growing the GaAs buffer layer in the step-flow regime and performing a post-growth annealing at  $580^\circ\text{C}$ . The resultant step edges, running parallel to the  $[1\bar{1}0]$  direction, were uniformly distributed over a large area. The bunched steps also extended over a fairly long distance without interruption as compared to the reported results using MBE technique.

Images taken by atomic force microscopy (AFM) showed that the self-aligned  $\text{In}_{0.5}\text{Ga}_{0.5}\text{As}$  quantum dots, which varied from 20 nm to 30 nm in diameter depending on growth conditions, were formed spontaneously at the edge of the terraces. The density of the quantum dots could be changed by controlling the nucleation conditions, such as the substrate temperature and As flux.

We have also studied the effects of strain on the formation of quantum dot since the nucleation of quantum dot is closely related to the surface energy which may be modified by lattice strain. Both strained and relaxed  $\text{In}_{0.1}\text{Ga}_{0.9}\text{As}$  buffer layers were prepared for this study. The shape and the nucleation site of the quantum dots formed on these two buffer layers were significantly different as shown by the AFM images. Detailed experimental results on  $15^\circ$  misoriented substrates will be presented.

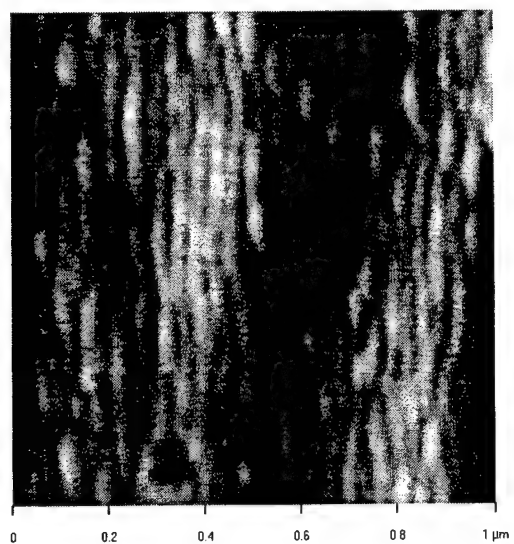
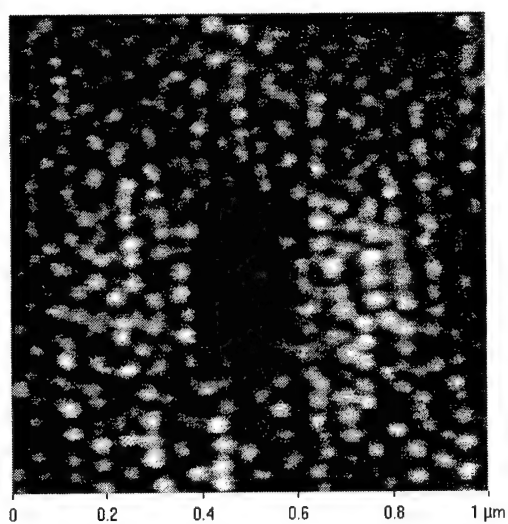
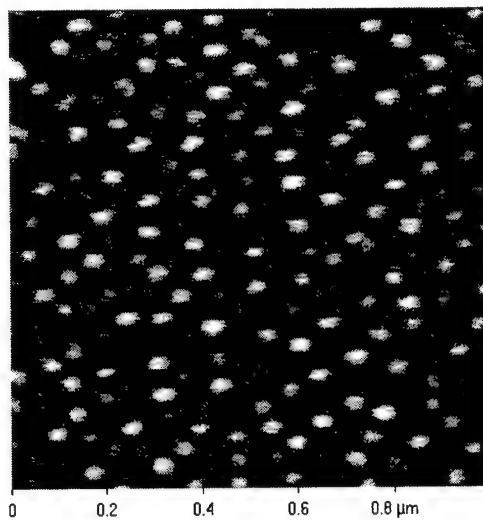


Fig. 1 AFM image of step-bunch formed on misoriented (100) GaAs substrate by molecular beam epitaxy.



(a)



(b)

Fig. 2 AFM images of self-aligned quantum dots grown on misoriented (100) GaAs under different nucleation conditions.

## **MBE Growth and Magnetotunnelling Transport Properties of a Single GaAs/AlAs/GaAs Barrier Incorporating InAs Quantum Dots**

M.Henini, I.E.Itskevitch, T.Ihn, P.Moriarty, A.Nogaret, P.H.Beton, L.Eaves,  
P.C.Main, J.R.Middleton and J.Chauhan

Department of Physics, University of Nottingham, Nottingham NG7 2RD, UK.

**Abstract:** The optical properties of self-organised InAs quantum dots on GaAs, formed by Stranski-Krastanov growth mode, have been intensively studied in recent years. In this paper we describe the growth of a novel type of structure in which the dots are incorporated in the AlAs tunnelling barrier of an n-i-n single barrier GaAs/AlAs/GaAs heterostructure. This type of structure provides us with a novel means of studying the quantum dots by means of magnetotunnelling spectroscopy. The samples were grown in a Varian MBE GEN-II system and the growth temperature was 550°C as monitored by a pyrometer, except during the growth of InAs when the growth temperature was lowered to 520°C. The growth rates are one monolayer/s (ML/s) for GaAs, 0.5 ML/s for AlAs and 0.066 ML/s for InAs. The formation of InAs dots was monitored by RHEED, and the average thickness of InAs deposited is 1.8 ML.

The low temperature current-voltage curves exhibit a series of pronounced peaks which are absent in a control sample grown without InAs in the AlAs barrier. The high quality of the AlAs on GaAs interface is demonstrated by the sharpness of the peaks and their behaviour in a magnetic field  $B$ . For  $B$  applied parallel to the current, each peak splits into a set of sharp components at fields as low as 0.4 T. They correspond to the Landau level quantisation of the occupied electron states in the emitter accumulation layer. This proves that each peak arises from tunnelling out of these Landau states into a single discrete zero-dimensional state in the tunnel barrier. From the decrease of the peak amplitude for increasing  $B$  perpendicular to the current, we estimate the spatial extent of these states to be 7-10 nm, consistent with the size of InAs islands measured by scanning tunnelling microscopy.

Author to contact: Dr M.Henini

Tel/Fax: +44 (115) 951 5195/951 5180

e-mail: ppzmmh@ppn1.physics.nottingham.ac.uk

# Luminescence anomaly in band gap tailored InGaAlAs quaternary alloy grown by MBE

*A.Ramam and S J Chua*

*Centre for Optoelectronics  
Department of Electrical Engineering  
National University of Singapore  
10 Kent Ridge Crescent  
Singapore 119260  
Tel : (65) 7722502  
Fax : (65) 7771103  
E-mail : elera@leonis.nus.sg*

**Abstract :** The band gap of the InGaAlAs alloy can be engineered between the emission wavelengths of the two bounding ternary alloys (InGaAs and InAlAs) and poses a serious challenge to the InGaAsP material. InGaAlAs epilayers with Al composition varying from 0.04 to 0.45 have been grown lattice matched to InP substrate by solid source MBE technique. The lattice mismatch obtained for the independently grown InGaAlAs epilayers is within 0.03%, with half widths in the range of 20-35 arcsec. The bandgap of the material estimated from RT photoluminescence (PL) peaks, as shown in Fig.1, varied from 0.8eV to 1.42 eV with FWHMs in the range 60-80 meV. Raman spectra on all the samples showed distinct phonon vibrational mode peaks of the three binary (InAs, GaAs and AlAs) compounds with the intensity ratios being equivalent to the mole fraction of the elements. These well characterized epilayers are studied under a temperature variation of 4-300K in PL experiments and are reported in this paper. An interesting phenomenon of 'dip behavior', in the variation of emission energy with temperature is observed in the range 30-80K, as shown in Fig.2. As the temperature is raised from 4K to 30K, a red shift is initially observed in the peaks. Between 30K and 80K a blue shift occurs and beyond that the normal red shift takes over following the Varshni equation. This behavior (known as 'inverted S') was observed [1] in InAlAs material and was associated with exciton localization. However, in our present work we observe that this characteristic behaviour which is seen to originate from the onset of multiple transitions, vanishes for Ga rich InGaAlAs epilayers. In fact, for Al mole fraction greater than 0.22, the phenomena is predominant. It is interesting to note that for Al mole fraction about 0.22 [2], the bandline-up crosses over from type I (InGaAs/InP) to type II (InAlAs/InP). Fig.3 compares the energy variation with temperature as a function of Al mole fraction. Free and bound exciton energies cannot account for the shift in energy values observed. A strong exciton localization is associated with the high Ga content layers.

## References:

- [1] S.M Olsthoorn, F.A.J.M Driessen, A.P.A.M Eijkelenboom and L.J Giling, J. Appl. Phys. 73, 7798, (1993).
- [2] J. Bohrer, A.Krost and D. B Bimberg, Appl. Phys. Lett, 63, 1918, (1993).

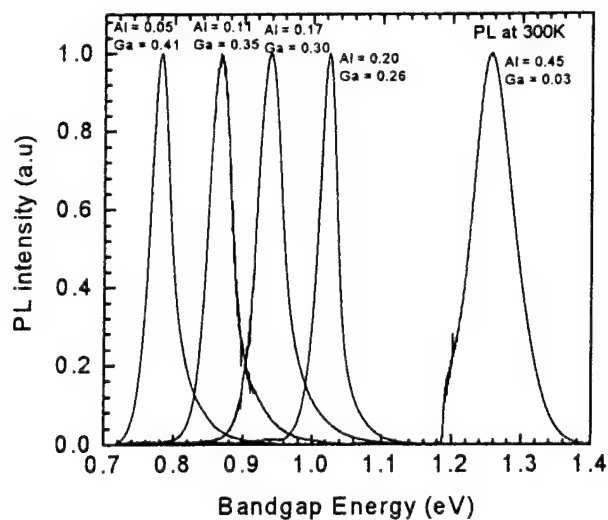


Fig.1 PL spectra of bandgap engineered InGaAlAs epilayers

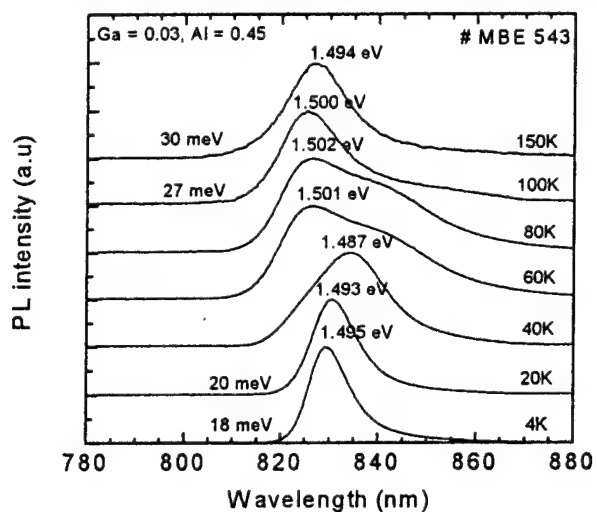


Fig.2 PL spectrum of a sample at variable temperature

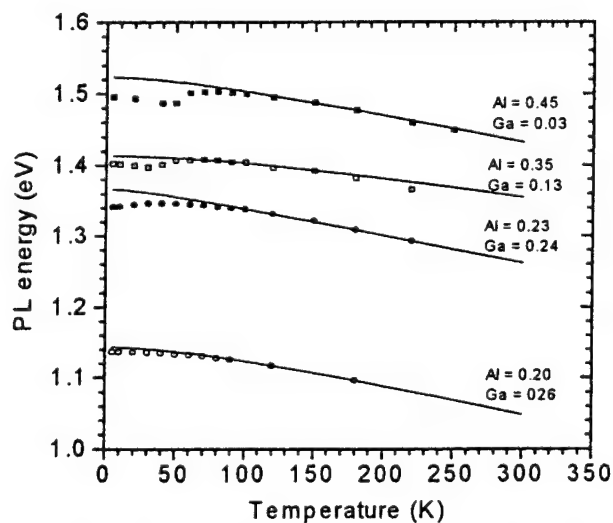


Fig.3 Variation of PL energy with temperature, with varying Al mole fraction.

## Determination of the Aluminum Content in $\text{Al}_x\text{Ga}_{1-x}\text{As}$ Layers: the Final Chapter

Z.R. Wasilewski, M.M. Dion, D.J. Lockwood, and P. Poole

*Institute for Microstructural Sciences, National Research Council of Canada,  
Montreal Road, Ottawa, ON K1A 0R6, Canada*

*tel. (613) 990 4557, fax.(613) 941 4667, e-mail:Zbig.Wasilewski@nrc.ca*

R.W. Streater and A.J. SpringThorpe

*Nortel Development,\* P.O.Box 3511, Station C, Ottawa, Ontario K1Y 4H7, Canada*

Of all the semiconductor materials used in the electronics science and industry AlGaAs is arguably second only to silicon in terms of its technological importance. As AlGaAs properties strongly depend on the aluminum composition, it is not surprising that much effort has been put into establishing reliable ways of measuring the latter. Of all the characterization tools available, double crystal x-ray diffraction (DCXRD), photoluminescence (PL), and Raman spectroscopy have proven to be the most popular due to their non-destructive character and high compositional resolution. However, in the multitude of equations proposed over the last twenty years to relate observed peak positions with the aluminum content of the layer, many are mutually exclusive. The increasing technological importance of AlGaAs has spurred renewed activity in the area. In spite of this effort the divergence has actually widened in some cases. The scatter of proposed AlAs material parameters needed for DCXRD interpretation is presently such<sup>1-3</sup> that the same layer can be assessed as having either 30% or 34% of aluminum content depending on the individual belief system. In the context of MBE growth, such scatter is unacceptable since, if used as a feedback in growth calibration, it can in some cases lead to an error in the AlAs growth rate approaching 20%. In a more general context, this uncertainty causes serious problems in establishing an effective device development loop: design → growth → fabrication → testing → design, particularly when some or all of the stages are contracted out.

The composition calibration and measurement scheme described in the present paper aims at providing a badly needed common platform for the growers and the users of epitaxial AlGaAs layers. To achieve this, we have cross-calibrated in this work the three characterization tools mentioned above:

DCXRD, PL and Raman spectroscopy. Central to this cross-calibration is the actual layer composition, which has to be measured independently. In previous work a wide variety of methods was used starting from sophisticated nuclear reaction techniques,<sup>4</sup> through ex-situ microprobe,<sup>1</sup> in-situ RHEED oscillation techniques,<sup>2,5,6</sup> and finishing with a model-based, "boot-strap"-like approach.<sup>3</sup> For the present work, in order to have a reliable measure of the possible error involved, we have devised a method that is based on a premise similar to the RHEED oscillation technique but, unlike the latter, it is not sensitive to possible flux transients, arsenic overpressure<sup>6</sup> or molecular beam geometries. The method relies on an independent measurement of the growth rates  $\mathcal{R}$  for GaAs, AlAs and AlGaAs, and the layer composition is calculated as  $x = \mathcal{R}_{\text{AlAs}} / (\mathcal{R}_{\text{AlAs}} + \mathcal{R}_{\text{GaAs}})$ .<sup>7</sup> Since the information on the local growth rates was embedded in the layer structure by design, we were able to take advantage of the lateral compositional gradient which can be obtained for AlGaAs by growing the layer without substrate rotation. We have grown two layers which provide quasi-continuous compositional change in the technologically important ranges of  $0.28 < x < 0.40$  and  $0.60 < x < 0.72$ . We also grew a number of single composition layers with low, high and medium Al composition values as well as a pure AlAs layer.

For each of the characterization techniques used we discuss the precautions to be taken and the factors which should be addressed in order to avoid misinterpretation and fully utilize the accuracy of the formulas provided. Among them are effects such as variations in the GaAs lattice constant between different substrate types which, albeit small, can lead to considerable errors in the layer compositions derived from the rocking curve simulations for thin or low aluminum content AlGaAs layers.

- <sup>1</sup> M. S. Goorsky, T. F. Kuech, M. A. Tischler, and R. M. Potemski, *Appl.Phys.Lett.* **59**, 2269-2271 (1991).
- <sup>2</sup> K. Tanner, A. G. Turnbull, C. R. Stanley, A. H. Kean, and M. McElhinney, *Appl.Phys.Lett.* **59**, 2272-2274 (1991).
- <sup>3</sup> M. Krieger, H. Sigg, N. Herres, K. Bachem, and K. Köhler, *Appl.Phys.Lett.* **66**, 682-684 (1995).
- <sup>4</sup> T. F. Kuech, D. J. Wolford, R. Potemski, J. A. Bradley, K. H. Kelleher, D. Yan, J. P. Farrell, P. M. S. Lesser, and F. H. Pollak, *Appl.Phys.Lett.* **51**, 505-507 (1987).
- <sup>5</sup> G. S. Solomon, D. Kirillov, H. C. Chui, and J. S. Harris, Jr., *J. Vac. Sci. Technol. B* **12**, 1078-1081 (1994).
- <sup>6</sup> K. H. Chang, C. P. Lee, J. S. Wu, D. G. Liu, D. C. Liou, M. H. Wang, L. J. Chen, and M. A. Marais, *J.Appl.Phys.* **70**, 4877-4882 (1991).
- <sup>7</sup> Although this formula is widely believed to hold true for the growth temperatures below about 640°C, the design of the layer was such as to allow for independent verification of the underlying assumptions, using high-precision SIMS profiling.

\* Formerly Bell-Northern Research



# Non-destructive Whole Wafer Well Thickness Measurements on Ultra-High Speed Tunnelling Structures by Excitation Photoluminescence.

P.D. Buckle, P. Dawson\*, M. Missous and W.S. Truscott

Department of Electrical Engineering and Electronics  
and

\*Department of Pure and Applied Physics  
University of Manchester Institute of Science and Technology  
P.O. Box 88, Manchester M60 1QD, United Kingdom.

The advent of ultra-high speed devices ( $<1$  ps) places increasing demands on the precision and control of the material growth, both vertically and across the wafer. Recent device proposals require thickness control on a sub-monolayer level, and if this is to be achieved commercially then it is essential to have fast whole wafer measurements to give feedback for the growth process.

We report the use of photoluminescence excitation (PLE) as a rapid non-destructive method for characterising whole 'as-grown' wafers. These wafers incorporate high frequency ( $>1$  THz) tunnelling structures with heavily doped top and bottom contact layers. This characterisation technique has enabled a series of different structures to be grown by MBE in which the wafer to wafer standard deviation of a nominally fixed well width was less than 1.5% (0.3 monolayers) and the mean well width was within 3% of the target value. Conventional photoluminescence cannot be observed in such tunnelling structures because of the fast escape of the confined carriers from the quantum well active regions. However PLE is measured by detecting luminescence originating from the heavily doped regions of the material.

The PLE was measured on a series of GaAs/AlGaAs triple-barrier tunnelling structures grown by MBE on semi-insulating GaAs substrates at 580 C. The upper contact layer was  $0.5\text{ }\mu\text{m}$  thick and doped at  $7 \times 10^{18}\text{ cm}^{-3}$ , the corresponding values for the lower contact were  $1\text{ }\mu\text{m}$  and  $3 \times 10^{18}\text{ cm}^{-3}$ . At 6 K the observed line width was 1.4 meV for a  $67\text{ }\text{\AA}$  well and shifts in the PLE across the wafer as small as 0.2 meV could be measured. Using PLE the effects of well width variation and strain can be clearly distinguished by observing both light and heavy hole transitions.

Dr. P.D. Buckle, Dept. Of Electrical Engineering and Electronics, UMIST, P.O. Box 88, Manchester M60 1QD, U.K., phone (44) 161 200 3187, fax (44) 161 200 4770; email [buckle@fs4.ee.umist.ac.uk](mailto:buckle@fs4.ee.umist.ac.uk)

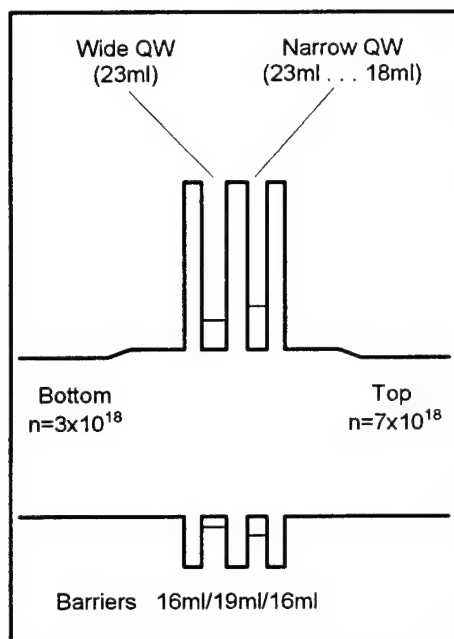


Figure 1.

Schematic band diagram of a triple barrier resonant tunneling structure (TBRTS) proposed for THz device applications.

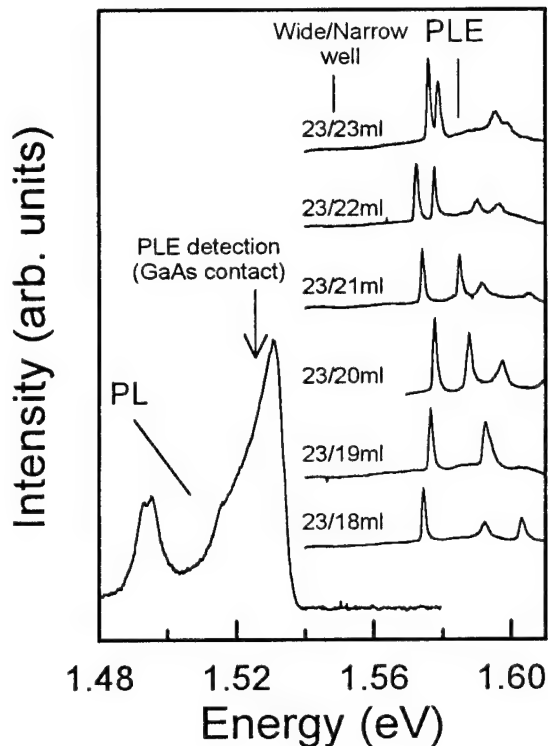


Figure 2.

PL and PLE for a range of TBRTS wafers. Note the absence of PL at the energy of the QW transitions. PLE spectra however show strong enhancements attributed to E1-HH1 and E1-LH1 absorption in the wide and narrow QWs of the active region.

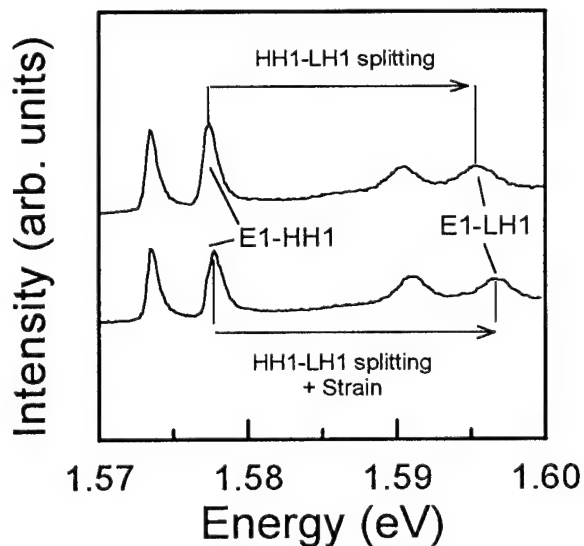


Figure 3.

Variations in the HH1-LH1 splitting are observed which cannot be accounted for by well width fluctuations across the wafer alone, and indicates detrimental strain induced by the wafer mounting technique.

# The Roles of Substrate Perfection and Strain in Channel Layers of InP-based Pseudomorphic High Electron Mobility Transistors

K.M. Matney and M.S. Goorsky

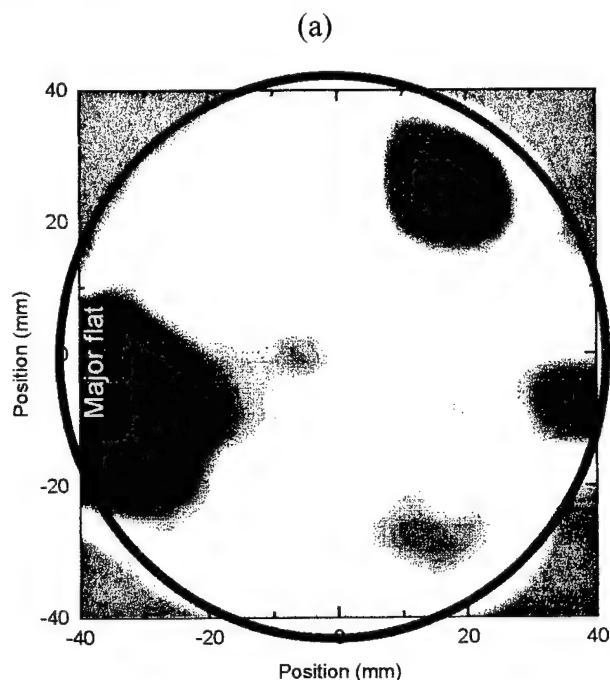
University of California, Los Angeles, Department of Materials Science and Engineering, Los Angeles, CA 90095-1595

D.C. Streit and T.R. Block

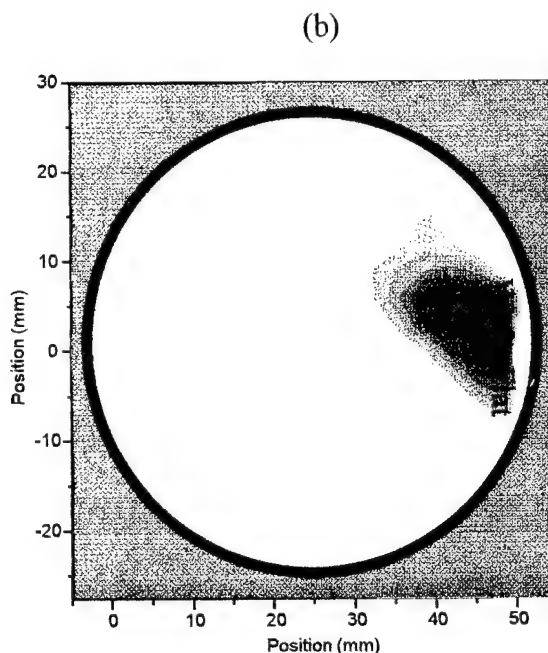
TRW, Electronic Systems Group, Redondo Beach, CA 90278

## Abstract

The crystalline quality of InP-based pHEMT structures grown by molecular beam epitaxy is strongly influenced by substrate perfection and by the sign of strain in the channel layers. Triple axis x-ray wafer mapping of two and three inch InP substrates is performed to determine variations in crystallographic quality across the substrates. In general, the larger substrates show a ~ 20% increase in the FWHM of triple axis omega scans - which directly relate to structural defects. In some cases, the area of high quality material is greater in the smaller wafers. A decrease in crystal quality is also observed near the wafer flats, indicating the presence of residual damage from grinding the flats. This is not typically observed in GaAs, and is attributed to the lower intrinsic strength of InP. Pseudomorphic HEMT structures grown on these different substrates are studied using double and triple axis diffraction techniques as well as Hall measurements. The crystalline quality of a 150 Å InGaAs channel layer across the wafer is shown to relate to defects in the underlying substrate. Triple axis techniques also show that mosaic structure in the epitaxial layers is greater for an epilayer strained in compression rather than tension - given an equal magnitude of mismatch. These advanced X-ray techniques provide a powerful, non-destructive means of determining substrate crystalline quality, and the structural quality and related performance of subsequently grown epitaxial layers.

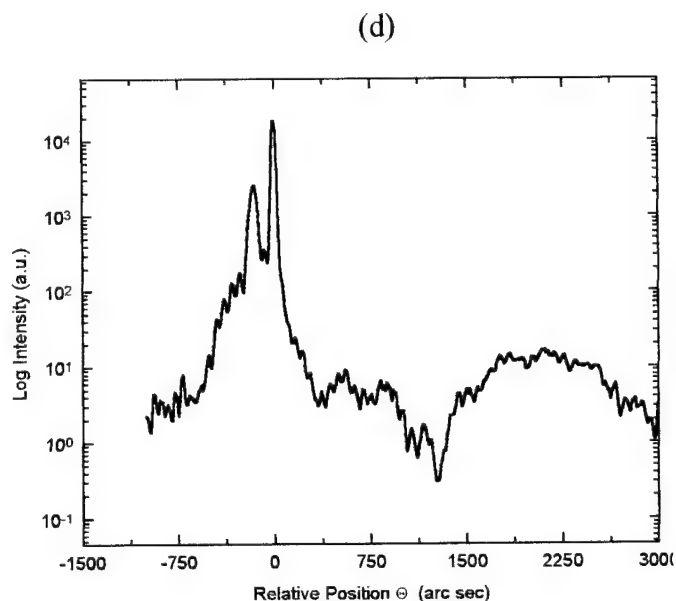
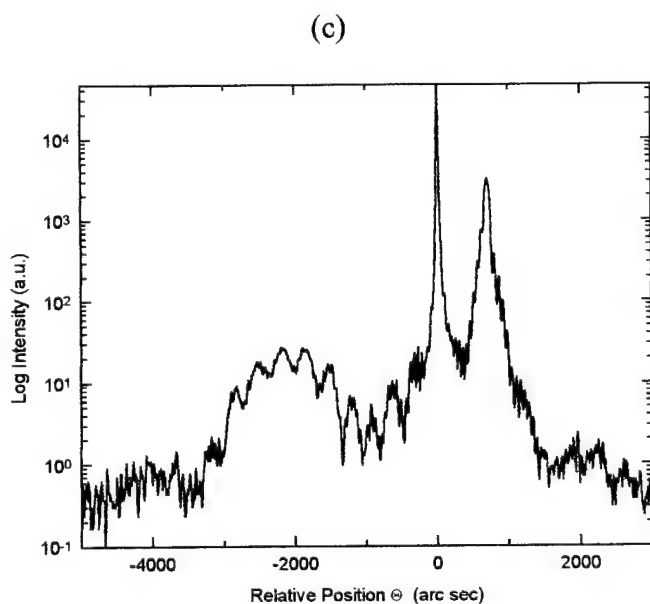


3" InP Wafer Map



2" InP Wafermap

Triple axis X-ray diffraction wafermaps of three inch (a) and two inch (b) InP substrates. The z-scale color map corresponds to areas of excellent (blue) to mediocre (green) to highly defective (red) crystalline quality.



Double axis X-ray scans of InGaAs epilayers in tensile (c) and compressive strain (d). The epilayers have similar mismatch, however, the compressively strained layer exhibits greater decay in the pendollosung X-ray fringes, due to misfit dislocations and mosaic tilts in the epilayer.

# Scanning Tunneling Spectroscopy and First-Principles Investigation on GaAs(001)(2x6)-S Surface formed by Molecular Beam Epitaxy

Shiro Tsukamoto, Takahisa Ohno, and Nobuyuki Koguchi

National Research Institute for Metals

1-2-1 Sengen, Tsukuba, Ibaraki 305, JAPAN

Tel.: +81-298-53-1054, Fax: +81-298-53-1093, E-mail: tsuka@nrim.go.jp

Sulfur-terminated(S-terminated) GaAs(001) surface is an important factor of droplet epitaxy which is a useful technique for fabricating quantum dot structures[1]. In order to establish this technique and to understand the droplet growth mechanism, the details of the S-terminated surface need to be investigated.

Recently, a novel S-termination method has been developed by exposure to S vapor in molecular beam epitaxy(MBE) system[2]. Using this method, the S-terminated GaAs(001) surface can be formed without etching surface. This etching effect usually occurs with ordinary S-treatments(e.g.,  $(\text{NH}_4)_2\text{S}_x$ -treatments)[3]. Then, not diffused (2x1), commonly reported, but clear (2x6) reconstruction was observed by reflection high-energy electron diffraction[2], scanning tunneling microscopy(STM)[2,3], and high-temperature STM[4]. In this paper, we study this (2x6) structure with scanning tunneling spectroscopy (STS) technique and compare with theoretical result in order to understand first growth sites of the Ga atoms during the droplet epitaxy.

At first, in order to evaluate a calculation model, we compared a S-S bond length from STM results with that from the theoretical calculation. By the STM observation, it was found that the separation between S atoms of S dimer was about 0.23 nm as shown in Fig.1. According to electron counting model, in order to form this (2x6)-S on GaAs(001) surface, one electron needs to be transferred from each S dimer to Ga dangling bonds on the missing dimer region[1]. Thus, we investigate the S-S bond length with and without one electron using the first-principles pseudopotential method. Figure 2 shows the model which was used for our calculation. As a result, the separations are calculated as 0.3897nm and 0.2370nm, with and without one electron, respectively. Experimental result well agreed with the latter condition. This indicates that this calculation model is only a part of the (2x6) structure but able to describe the whole structure with fulfillment of the electron counting (local-charge neutrality) heuristics.

By the STS measurement on this (2x6) structure, a conductivity spectrum as shown in Fig.3 was obtained. The voltage width of  $dI/dV=0$  indicates the energy band gap of GaAs (1.45 V) which is reasonable at room temperature. There is a peak in conduction band side. Usually GaAs(001) surface dose not show such a peak in STS. Figure 4 is an electronic structure of this S dimer without one electron calculated by the same model shown in Fig.2. It exhibits an unoccupied flat band which is mainly caused by antibonding band of S-S bond. This result also well agreed with the sharpness and energetic position of the peak in Fig.3. Therefore, this peak should relate with S dimers.

In conclusion, we compared the experimental results with the theoretical calculation. Then, it was found that there were unique agreements between them, indicating that there may be long-range electron transfers on this (2x6) structure and these transfers may change the surface charge density in atomic scale. Therefore, when Ga atoms are deposited on this (2x6) structure, this changed surface charge density may rule the first growth sites of the Ga atoms.

[1] N. Koguchi and K. Ishige, Jpn. J. Appl. Phys. 32 (1993) 2052.

[2] S. Tsukamoto and N. Koguchi, Jpn. J. Appl. Phys., 33 (1994) L1185.

[3] S. Tsukamoto and N. Koguchi, Appl. Phys. Lett., 65 (1994) 2199.

[4] S. Tsukamoto and N. Koguchi, J. Cryst. Growth., 150 (1995) 33.

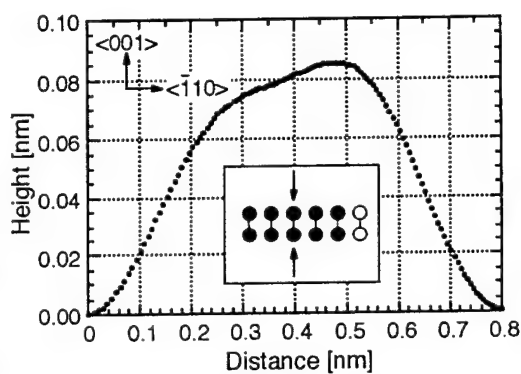


Fig.1 Cross-section of S dimer in (2x6)-S.  
( $V_{\text{sample}} = -3.0\text{V}$ ,  $I = 0.2\text{nA}$ )

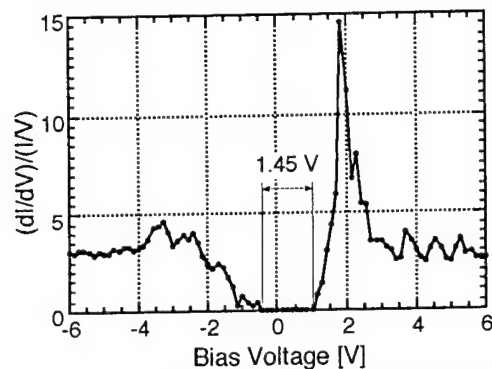


Fig.3 Conductivity spectrum of (2x6)-S surface.

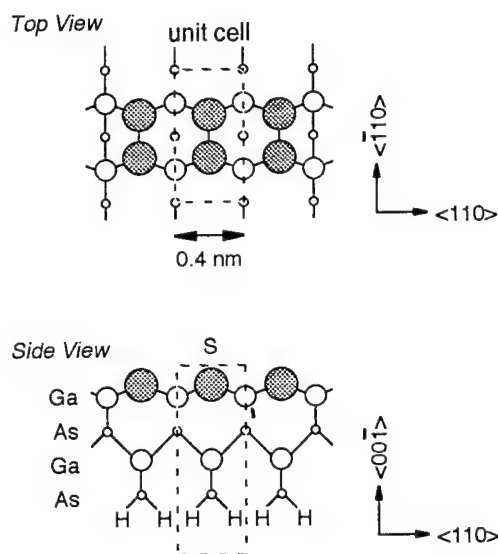


Fig.2 A model for first-principles pseudopotential calculation. S-S bond length with and without one electron in one S dimer was investigated.

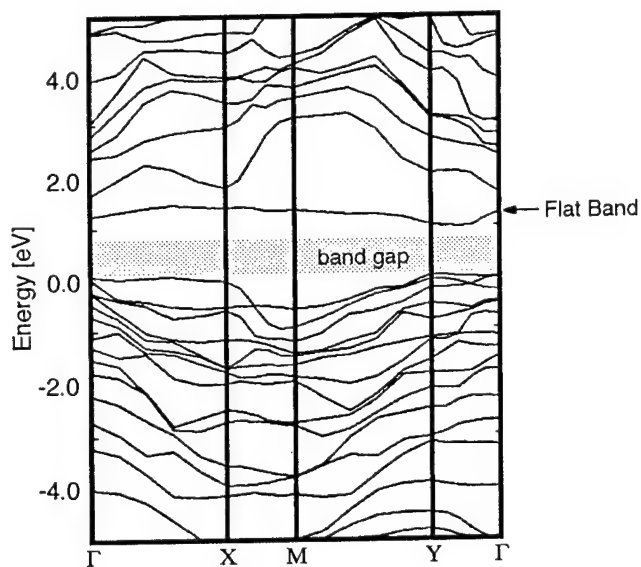


Fig.4 Calculated electronic structure. Shown band gap is an effective value by this calculation method. Discrepancy with experiment is about 47%.

## Growth mode induced surface morphology and its relation to optical and electrical properties of GaAs single quantum wells

R. Hey, I. Gorbunova, M. Ramsteiner, U. Jahn, K. Friedland, L. Däweritz and K. H. Ploog  
Paul-Drude-Institut für Festkörperelektronik, Hausvogteiplatz 5-7, D-10117 Berlin, Germany  
☎ ++49-30-20377354, Fax ++49-30-20377201, e-mail hey@pdi.wias-berlin.de

A series of GaAs single quantum wells was prepared on almost exactly and on misoriented GaAs(001) substrates by solid-source MBE with the aim to examine possibilities of surface and interface engineering and its impact on the properties of the layer system. The GaAs quantum wells (QW) grown with an interruption of 40 s at the upper interface were 4.8 nm thick and the barriers consisted of 1 nm AlAs / 2 nm GaAs short-period superlattice (SPSL). The upper barrier was capped by 4.8 nm GaAs. By appropriate quenching the surface morphology was not changed. Hence, this surface is regarded as being representative for the upper well interface neglecting modification by overgrowth.

Growth temperatures ( $T_s$ ), beam equivalent pressure (BEP) ratios of As<sub>4</sub>-to-Ga and the growth rate were chosen to ensure growth predominantly by the two-dimensional nucleation mode (Fig. 1a,d) or by the step-flow mode (Fig. 1b,c) as evidenced by a  $(2 \times 4)\alpha$  (Fig. 1c,d) or a weak  $(3 \times 1)$  (Fig. 1a,b) surface reconstruction. Due to the distinct growth conditions the step systems caused by an unintentional miscut of the substrates exhibit very different terrace and step edge profiles. High arsenic pressures and high  $T_s$  lead to a pronounced step edge roughening by forming larger Ga-terminated and As-terminated step segments (Fig. 1c). Thus, the total length of the step edge per unit length is maximum compared to a reduced arsenic flux which results in less roughened step edges (Fig. 1b). At  $T_s = 640^\circ\text{C}$  the layer surface contains a high number of holes and islands on the terraces (Fig. 1a) indicating a collapse of the pure step-flow mode due to an incomplete GaAs condensation. At lower  $T_s$ , layers grow in the 2D-nucleation mode (Fig. 1d).

The optical characterization of the layer system was done by micro-photoluminescence (PL) and PL-excitation spectroscopy. The emission spectra of all QWs and all SPSLs show a rich fine structure and their envelopes correspond to the conventional PL signals with FWHM values of 6-8 meV (Fig. 2) and 8-14 meV, respectively. The spikes in the micro-PL spectra are very narrow ( $\text{FWHM} \leq 0.1 \text{ meV}$ ). With increasing arsenic pressure the fine structure in the spectra becomes more pronounced and the Stokes-shift (14 meV) is largest for these growth conditions. The micro-PL spectra are reproducible but exhibit a strong spatial variation across the wafer. It is assumed that this property together with the Stokes-shift is attributed to the localization of excitons at potential fluctuations introduced at topological defects at step edges or compositional gradients across the interfaces. Local gradients of the composition or intermixing are mainly caused by Ga segregation probably at step edges or boundaries of the surface reconstruction domains on the terraces.

Step-flow conditions at low BEP-ratio were applied to the growth of remotely doped 10 nm single QW including the same kind of SPSL barriers. Occupying the lowest quantized level, carrier densities up to  $1.3 \times 10^{12} \text{ cm}^{-2}$  and electron mobilities as high as  $1.3 \times 10^6 \text{ cm}^2/\text{Vs}$  at 0.3 K were obtained.

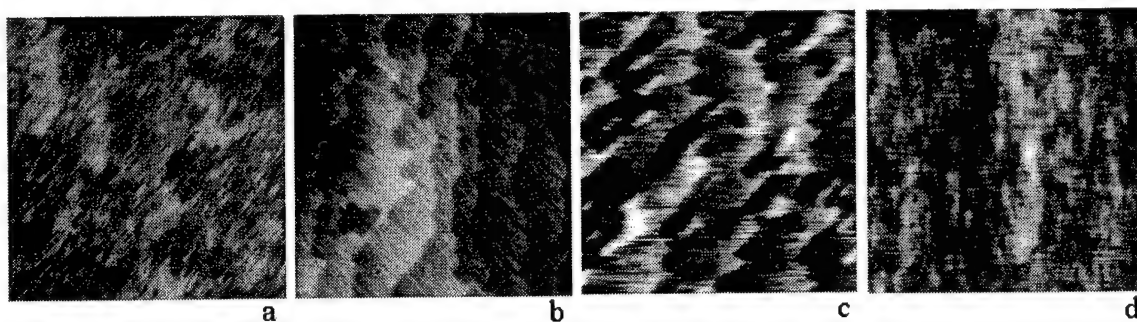


Fig.1. Atomic force microscopy images ( $2\ \mu\text{m} \times 2\ \mu\text{m}$ ) of the cap layer surfaces of the quantum well layer system prepared at different growth conditions.  $T_s$  and BEP ratios of arsenic-to-gallium were  $640^\circ\text{C}/10$  (a),  $610^\circ\text{C}/10$  (b),  $610^\circ\text{C}/30$  (c) and  $550^\circ\text{C}/10$  (d). Substrates were unintentionally misoriented by about  $0.03^\circ$ - $0.05^\circ$  towards (011).

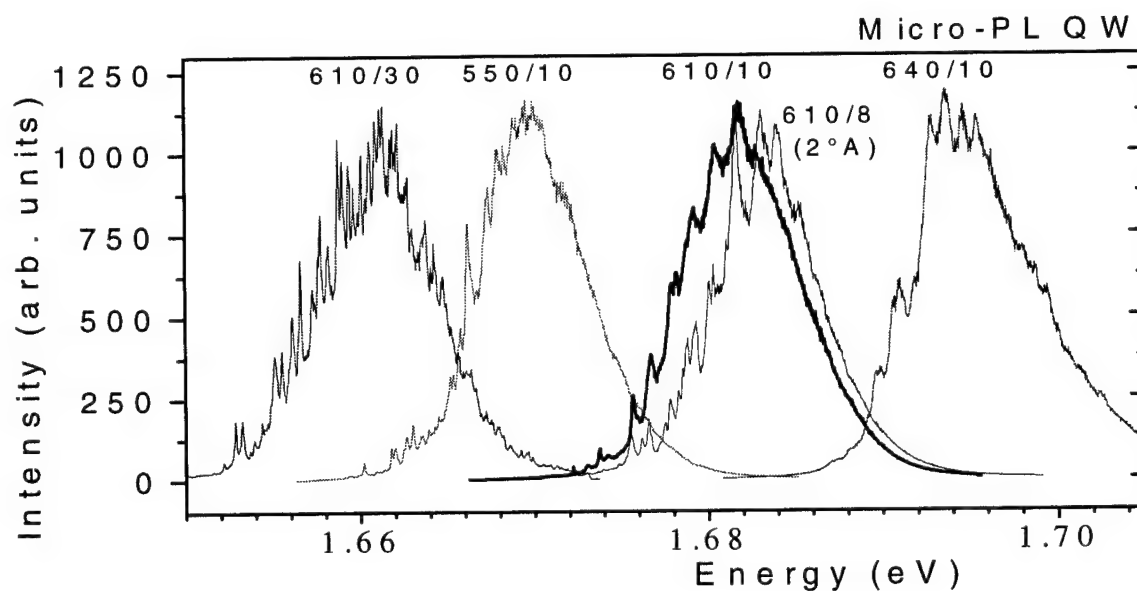


Fig.2. Micro-PL spectra of the quantum well emissions (normalized intensities).  $2^\circ\text{A}$  denotes the miscut of the (001) surface towards (111)Ga. All other substrates were unintentionally misoriented by  $0.03^\circ$ - $0.05^\circ$  towards (011).  $T_s$  and BEP-ratio of arsenic-to-gallium are indicated above each spectrum.



## Does scanning tunneling microscopy provide a realistic picture of the step array of vicinal GaAs(001) surfaces grown at high temperature ?

L. Däweritz, H. Nörenberg\*, P. Schützendübe, and K. Ploog

Paul-Drude-Institut für Festkörperelektronik, Hausvogteiplatz 5-7, D-10117 Berlin, Germany

\*University of Oxford, Department of Materials, Parks Road, Oxford OX1 3PH, U.K.

Tel.: (49-30) 203 77 359, Fax: (49-30) 203 77 201, daeweritz@pdi.wias-berlin.de

The morphology of the real surface and the kinetic processes on it have 2D character. The RHEED intensity recording as a widely used technique to control the growth mechanism provides, however, in principle 1D information. STM studies, on the other hand, give detailed 2D information on the local surface structure. For high substrate temperatures which are of interest for the growth of laterally ordered structures it becomes, however, problematic to quench in the structure of the growth surface. In a comprehensive 2D RHEED study we show for the first time that at growth temperatures  $>580^\circ\text{C}$  (and low As coverage) ordered steps on a  $2^\circ$  misoriented GaAs(001) surface bunch after growth interruption *within less than 1s* and are, therefore, not accessible to STM studies after quenching.

We have used a  $90^\circ$  double RHEED set-up for a real-time study of the morphology of vicinal GaAs(001) surfaces ( $2^\circ$  misorientation toward (111)A or  $(\bar{1}\bar{1}1)$ B) in the transition range between the 2D and the step-flow growth mode. The intensity behaviour of the specular and fractional-order beams was recorded *simultaneously* in the orthogonal  $[110]$  and  $[\bar{1}\bar{1}0]$  azimuths (Fig. 1).

At high temperatures where growth proceeds entirely in the step flow mode, vicinal A and B surfaces show a similar intensity behaviour of the specular beam for the direction parallel to the steps. The same is true for the direction perpendicular to the steps. This is clear evidence that the intensity behaviour is caused by the evolution of the step structure. In the parallel and perpendicular directions it reflects the step edge roughness and the step ordering, respectively.

On the vicinal A surface the temperature at which the RHEED intensity oscillations disappear is about  $20^\circ\text{C}$  higher in the  $[\bar{1}\bar{1}0]$  azimuth than in the  $[110]$  azimuth. This is due to the formation of islands elongated in  $[\bar{1}\bar{1}0]$  direction which change their axis ratio as a function of temperature. Due to strong step meandering the vicinal B surface is more isotropic and no measurable difference between the disappearance temperatures of the oscillations in the two orthogonal  $\langle 110 \rangle$  azimuths is found.

During growth in the transition range between 2D and step flow mode the vicinal A surface becomes uniformly stepped, whereas on the vicinal B surface the terrace width fluctuation increases. This is explained by an asymmetry in the step edge attachment with a *downward diffusion of adatoms over B-type steps*. At near-equilibrium conditions above  $\sim 580^\circ\text{C}$  a *kinetic smoothing* occurs also on the vicinal B surface. In this case the terrace width equalization is linked to a disordering of the reconstruction and therefore not the result of the step attachment asymmetry but rather a consequence of the energetics. The unbunched B and A surfaces are metastable at this temperature and recover after growth interruption within less than 1 s to the equilibrium bunched surface. For the A surface this can be directly observed in the RHEED spot profile.

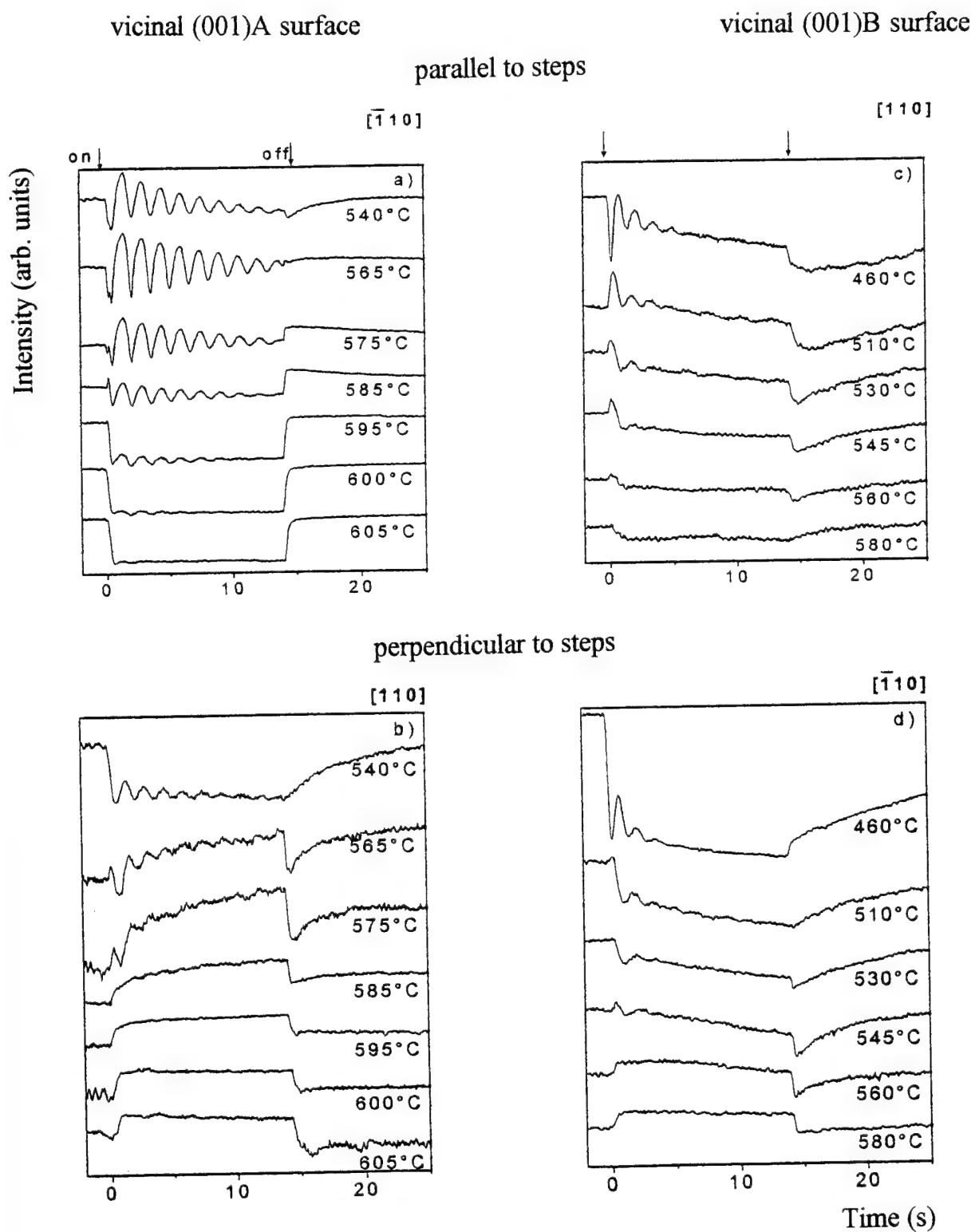


Fig. 1. Specular-beam RHEED intensity recorded simultaneously in the azimuth parallel (a, c) and perpendicular to the misorientation steps (b, d) during GaAs growth on vicinal GaAs(001) misoriented toward (111)A (a, b) and  $(\bar{1}\bar{1}1)$ B (c, d).

## Photoluminescence of low temperature AlGaAs / GaAs multiple quantum wells

W. Feng, F. Chen, Q. Huang, and J. M. Zhou

*Institute of Physics, Chinese Academy of Sciences, P. O. Box 603-(36), Beijing  
100080, People's Republic of China .*

Fax: (86-010)-2562605, Tel: (86-010)-2551205, e-mail: wfeng@aphy02.iphy.ac.cn

We have performed photoluminescence (PL) study of low temperature (LT)  $\text{Al}_{0.3}\text{Ga}_{0.7}\text{As}/\text{GaAs}$  multiple quantum wells (MQW). The MQW structure was grown by MBE on GaAs (001) substrate at 310 °C, and consists of 75 periods of 100Å  $\text{Al}_{0.3}\text{Ga}_{0.7}\text{As}$  barriers and 70Å GaAs wells. For comparison, a sample with the same MQW structure was grown at 600°C and implanted with proton to a dose of  $10^{14} \text{ cm}^{-2}$  at 180keV. All the MQW samples were subjected to rapid thermal anneal from 500 to 900 °C for 30 seconds. The PL spectra of the LT MQWs and the proton-implanted MQWs exhibit different dependencies on annealing temperature. For proton-implanted MQWs, the PL intensity is monotonously enhanced upon anneal, due to the decrease of the point defects. In contrast, the PL from LT MQWs annealed below 600 °C shows three orders of magnitude decrease in intensity, compared with the as-grown LT MQWs. With higher anneal temperature, PL intensity of LT MQWs begins to recover. At 900 °C anneal, the PL intensity becomes comparable with that of normally-grown MQWs. When annealed, the point defects are decreased both in the LT MQWs and the implanted MQWs. This decrease of point defects will result in an enhancement in PL, as is observed for the implanted MQWs. But, the excess arsenic in as-grown LT MQWs will collect in arsenic precipitates once annealed. The anomalous behavior of PL in annealed LT MQWs clearly reveals the effect of arsenic precipitates on the PL characterizations. The variation in PL of LT MQWs with anneal temperature can be explained in term of formation of arsenic precipitates which form Schottky barriers with respect to the matrix. The photoexcited carriers are trapped by and recombine at these precipitates, causing the drastic decrease of PL. Further annealing decreases the number of precipitates and increases the spacing between precipitates, leading to the recovery of PL. For LT MQWs annealed above 600 °C, we observed that the PL spectra become broadened and shift toward high energy. The shift and broadening of PL spectra can be attributed to the interface intermixing and roughening in the LT MQWs.

# EFFECTS OF MORPHOLOGY AND STRAIN ON PHOTOEMISSION OSCILLATIONS MEASURED DURING THE GROWTH OF RESONANT TUNNELING DEVICES

J. J. Zinck and D. H. Chow  
Hughes Research Laboratories, Malibu, CA

Photoemission oscillations (PEO) have been shown to be a viable technique for measuring monolayer thicknesses from rotating substrates during MBE growth<sup>1</sup>. Using the PEO technique, we have demonstrated that a higher degree of correlation between peak current density and barrier thickness is achievable with respect to dead reckoning for InAs/AlSb RTDs<sup>2</sup>. However, variability in oscillation contrast has made application of PEO as an *in situ* control sensor problematic for particular material systems. For example, the ability to resolve GaSb oscillations measured during growth of a near lattice matched and coherently strained InAs/AlSb/GaSb RTD is dependent on whether or not the initial substrate is lattice-matched to the active layer material. Figure 1 compares the photoemission signature measured during growth of the GaSb well region of an RTD deposited on a) GaAs and b) InAs substrates. Oscillations are clearly resolved for GaSb in the lattice-matched case. Atomic force microscopy images of the two devices reveal that the morphologies are quite different, as shown in Figure 2. Despite the existence of a superlattice smoothing layer for the RTD grown on GaAs, the surface is quite rough with respect to the device grown on InAs. It is known from cross-sectional TEM data<sup>3</sup> that the device grown on GaAs has a threading dislocation density on the order of  $10^8/\text{cm}^2$  and it is tempting to infer that the strain field and/or additional step structure associated with the dislocations influences the growth mode of GaSb in this system. Interestingly, the ability to resolve AlSb barrier oscillations is unaffected by the choice of substrate, suggesting that, in contrast to the case of Ga, the diffusion length of Al is small enough that the gross morphology of the surface is not sampled. These data, in addition to PEO measured from InGaAs/AlAs RTD's grown on InP will be discussed and the implication of these observations for *in situ* process control of high speed devices for circuit applications will be discussed.

1. J. J. Zinck and D. H. Chow, Appl. Phys. Lett. **66**, 3524 (1995).
2. J. J. Zinck and D. H. Chow, Appl. Phys. Lett. **68**, 1406 (1996).
3. D. H. Chow, unpublished.

Please address correspondence to:

J. J. Zinck  
Hughes Research Laboratories  
MS RL92  
3011 Malibu Canyon Road  
Malibu, CA 90265  
310-317-5913 voice  
310-317-5483 fax  
jzinck@msmail4.hac.com

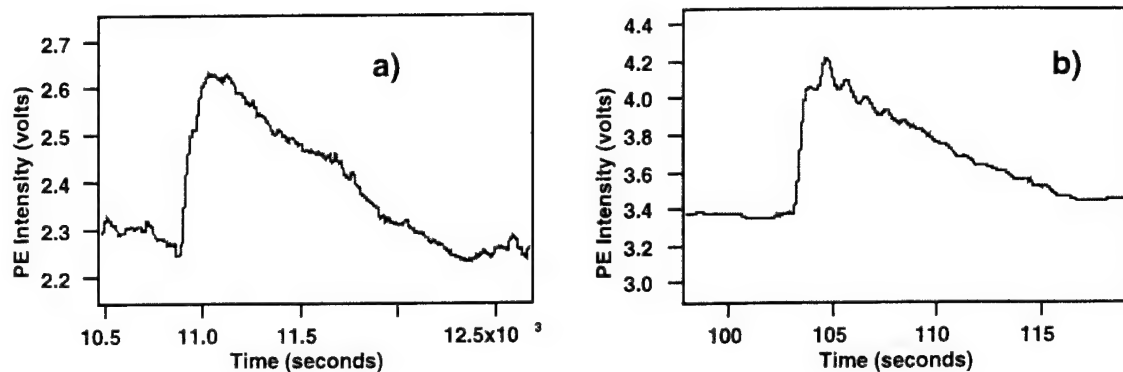


Figure 1. Photoemission oscillations measured during the growth of the GaSb well of an RTD grown on a) GaAs substrate; b) InAs substrate.

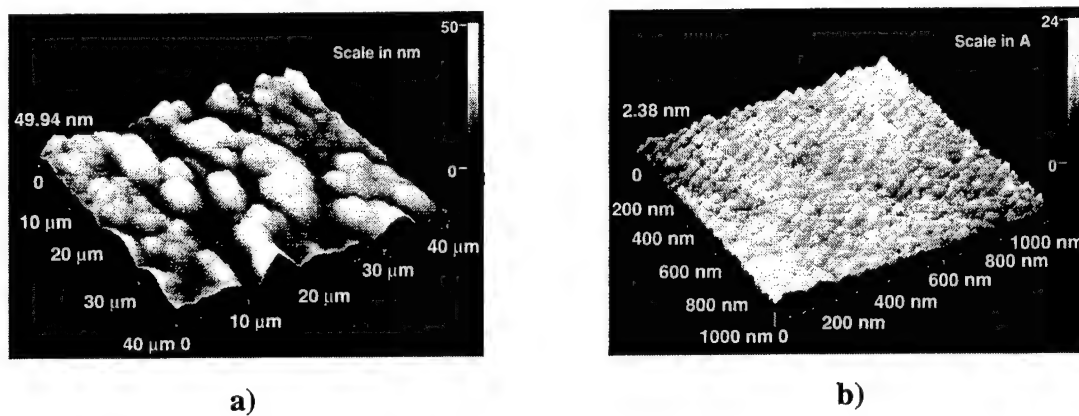


Figure 2. Atomic force microscopy images ( $10\mu\text{m} \times 10\mu\text{m}$  area) of an InAs/AlSb/GaSb RTD grown on a) GaAs substrate; b) InAs substrate.

## X ray Fluorescence: A Complementary In-Situ MBE Probe

Joseph Pellegrino

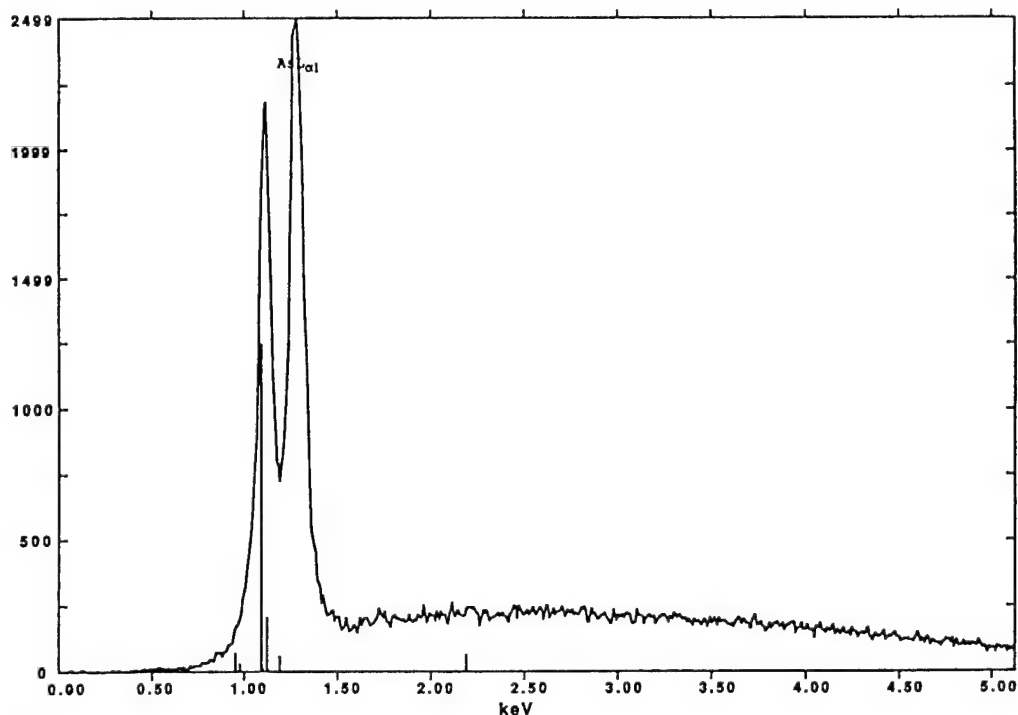
Semiconductor Electronics Division, National Institute of Standards and Technology,

Gaithersburg MD, 20899-0001

phone (301) 975 2123, fax (301) 948 4081, joe@apollo.eeel.nist.gov

A specially designed energy dispersive x-ray detector has been mounted on an MBE chamber to monitor composition and lattice matching criteria during growth. A commercial growth chamber was equipped with an additional vertical port placed at glancing incidence to the substrate in the growth position. Electrons of modest energy and current (6 keV, 100 microamps) produced by the additional electron gun are incident upon the sample and produce fluorescence that results in x-ray photons with characteristic excitation energies. These x-rays are analyzed by using a silicon lithium detector. The detector resolution is 133 eV. An attractive feature of the grazing electron beam is that it minimizes damage to the substrate by virtue of an areal footprint which easily exceeds a 75 mm wafer. The detector is presently mounted on an oven port and sits upon a telescoping track which can extend to within 2 cm of the substrate. A unique heated window design prevents contamination of the detector during the deposition. The plot shows data from the detector for the growth of GaAs. Quantitative analysis of the spectra using ZAF theory in the thin-film approximation is used to obtain composition values (not shown).

This work addresses the use of x ray fluorescence as an in-situ characterization tool and compares it with other in-situ and ex-situ probes. Multi-wavelength ellipsometry data, also obtained in real time, will be presented and correlated with the fluorescence and other probe results (RHEED, x-ray diffraction). The development of in-situ fluorescence monitoring provides an important and complementary probe of the composition during growth. The x-ray photons should not be sensitive to polarization and rotation effects and will provide a unique correlation with the optical and electron beam probes.



GaAs

Generated.

Analyst: Joe Pellegrino keV: 6.00 Cu

Detector Resolution: 158.00 eV Take-off

Markers for Ga, 31

0.00

# Substrate Temperature Change in III-V Molecular Beam Epitaxy

Keith R. Evans and J. E. Ehret  
Wright Laboratory (WL/ELDM)  
Wright-Patterson Air Force Base, Ohio 45433-7323

C. R. Jones and R. Kaspi  
University Research Center, Wright State University  
Dayton, Ohio 45435

The ability to control substrate temperature during molecular beam epitaxy (MBE) is critical for realizing high quality semiconductor heterostructures. The most common substrate temperature sensor is the non-contact thermocouple, which is inexpensive and simple to implement. However, it is prone to large systematic errors, both under constant temperature conditions and during intentional temperature change. The latter often occurs at a heterointerface (e.g., AlGaAs at 700 °C grown on GaAs at 600 °C). In this work we study the relationship between the thermocouple-indicated temperature and the actual surface temperature during such intentional temperature changes for various growth conditions, substrate conductivity, and substrate temperature controller settings.

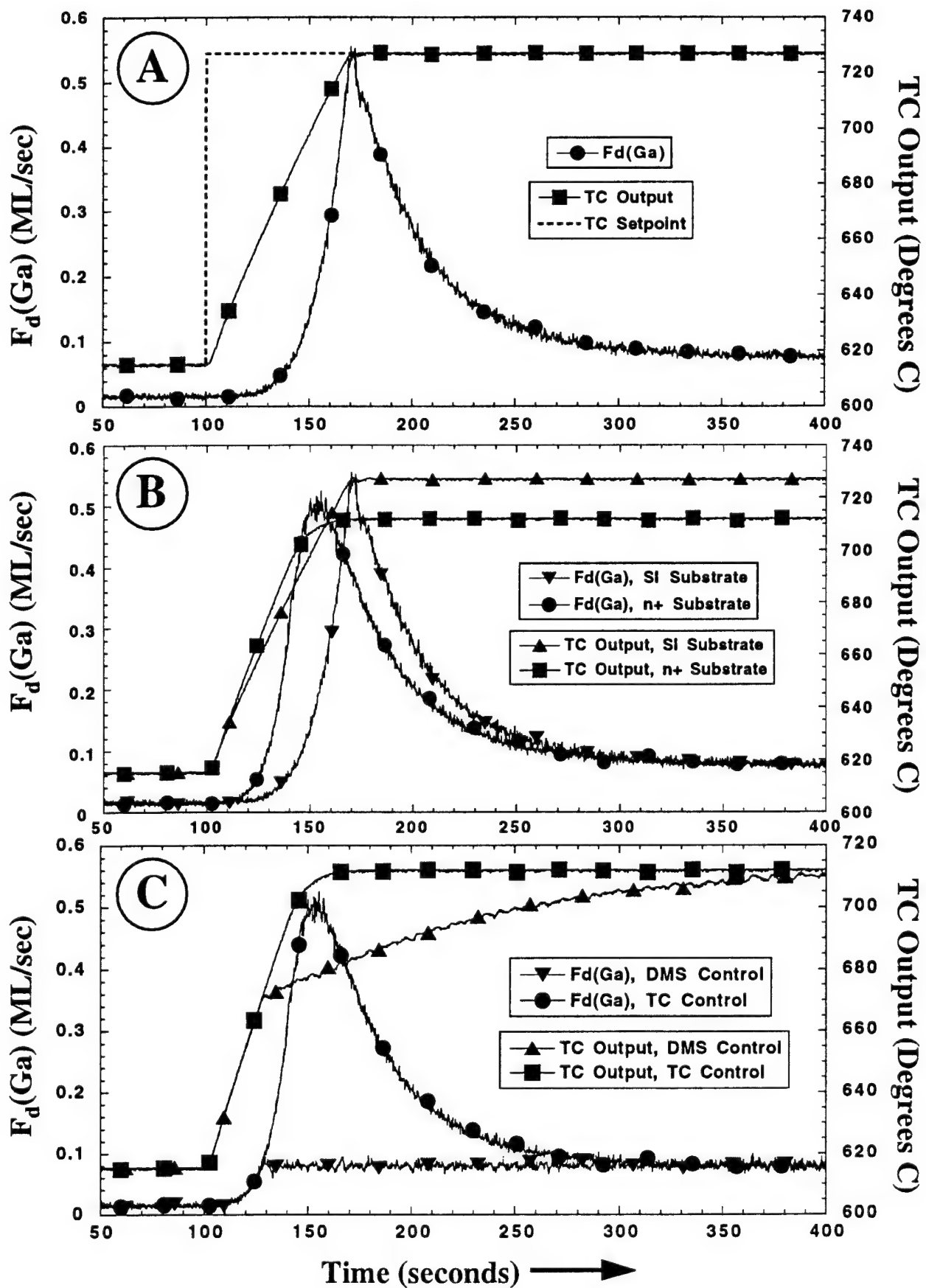
The dynamic relationship between the thermocouple -indicated temperature ( $T_{TC}$ ) and the actual GaAs surface temperature ( $T_s$ ) was followed in time after instantaneous changes were made in the setpoint temperature ( $T_{stpt}$ ). The actual GaAs surface temperature was inferred from the Ga desorption rate [ $F_d(Ga)$ ], which was measured by desorption mass spectrometry (DMS). The basic experiment is shown in Figure A. The thermocouple setpoint temperature  $T_{stpt}$  (dashed line) is changed from 615 to 727 °C at  $t=100$  sec. The behavior of  $T_{TC}$  (right) relative to  $T_{stpt}$  is characterized by an initial ~ 70 second lag, with little if any overshoot, while  $F_d(Ga)$  (left), which provides a direct measure of the surface temperature, undergoes significant overshoot which corresponds to an overshoot in  $T_s$  of 36 °C! The peak magnitude of  $F_d(Ga)$  is greater than 0.5 monolayer/sec, which is ~ 50% of typically employed incident Ga fluxes. Such a  $T_s$  overshoot would clearly produce a significantly graded interface during, for example, AlGaAs/GaAs interface formation.

Similar data was taken for a variety of temperature setpoints, substrate conductivity, and temperature controller (PID and maximum current) settings. For example, Figure B compares the response of a conductive n+ substrate and a semi-insulating (SI) substrate. The initial setpoint was 615 °C for both; the final setpoint was 712 and 727 °C for the n+ and SI substrates, respectively. The Ga desorption rate and thus surface temperature for the n+ substrate respond more quickly than for the SI substrate, due to the smaller effective bandgap of the n+ substrate, which results in the absorption of a larger fraction of heater radiation. Similar arguments explain why a (727-712=15 °C) lower final  $T_{stpt}$  results in the identical surface temperature for the n+ vs SI substrate. Thus, TC-sensing leads to significant errors in both steady-state and dynamic  $T_s$  control.

Figure C compares thermocouple feedback (TC-control) and  $F_d(Ga)$  feedback (DMS-control), for which  $T_{TC}$  or  $F_d(Ga)$  are compared with their respective setpoints and the resulting error signal is supplied as input to the substrate heater power supply. In contrast to TC-control, the DMS-control approach provides a smooth and rapid  $T_s$  evolution with essentially no overshoot.

We will discuss the general impact of these results on MBE-grown III-V device structures. Additionally, we will present practical solutions to the problem of  $T_s$  control and overshoot, some of which do not require DMS sensing.

**Acknowledgments:** The authors thank C. Huang, L. Kyle, and C. Litton for technical support. Authors RK and CRJ were supported by US Air Force Contract # F33615-95-C-1765. This work was partially supported by the US Air Force Office of Scientific Research (AFOSR).





## Reflectivity Difference Spectroscopy Study on Thin Film ZnSe grown on GaAs by Molecular Beam Epitaxy

C. C. Kim, Y. P. Chen, M. Daraselia and S. Sivananthan  
Microphysics Lab, Dept. of Physics, University of Illinois at Chicago, Chicago, IL

D. J. Smith and S.-C.Y. Tsen  
Center for Solid State Science, Department of Physics and Astronomy,  
Arizona State University, Tempe, AZ

Reflectivity difference spectroscopy (RDS) has been recognized for some time as a useful diagnostic tool because of its sensitivity to the surface atomic and electronic structure. Much work has been carried out for the elemental and III-V systems, but little work, so far, has been done for II-VI systems. ZnSe-based alloys have received attention for their potential as laser diodes in the blue-green region of the spectrum. The short lifetime in the laser diode has been ascribed to poor interface quality arising from stacking faults and high dislocation density.

Our objective in this work was to establish whether the RDS could be used, both during and after growth, to assess the quality of a typical II-VI material and thus to control it. ZnSe films were grown on GaAs substrates with various growth conditions by molecular beam epitaxy. Their optical anisotropy was determined by *ex-situ* and *in-situ* RDS. The RDS spectra consistently revealed the interference patterns below the bandgap as shown in Fig 1. The comparison with spectroscopic ellipsometry (SE) data revealed that the RDS data could be utilized to determine the thickness, alloy composition and temperature during growth. The *in-situ* RDS data which determined the thickness and temperature during growth will be presented. (See Fig. 2 as an example.) The *ex-situ* RDS spectra were also compared with the results from transmission electron microscopy (TEM) and Hall measurement. The comparison with the Hall effect shows that the magnitude of the optical anisotropy is slightly correlated with the carrier concentration. The comparison with the TEM results shows that both the structure and magnitude in the  $E_1$  region carries the information on the surface morphology. As reported for III-V systems [1], the origin of the optical anisotropy around the  $E_1$  region is strongly correlated with the surface roughness. Furthermore, both the structure and magnitude around the bandgap shows strong correlation with the ZnSe/GaAs interface quality.

[1] B. R. Bennett, J. A. Del Alamo, M. T. Sinn, F. Peiro, A. Cornet, D. E. Aspnes, J. Elec. Mat. **23**, 423 (1994)

Contact Author: Dr. C. C. Kim

Address: Department of Physics, University of Illinois at Chicago, 845 W. Taylor St.,  
Chicago, IL 60607-7059

Tel: 312-413-2786, Fax: 312-996-9016, Email: kim@uicws.phy.uic.edu

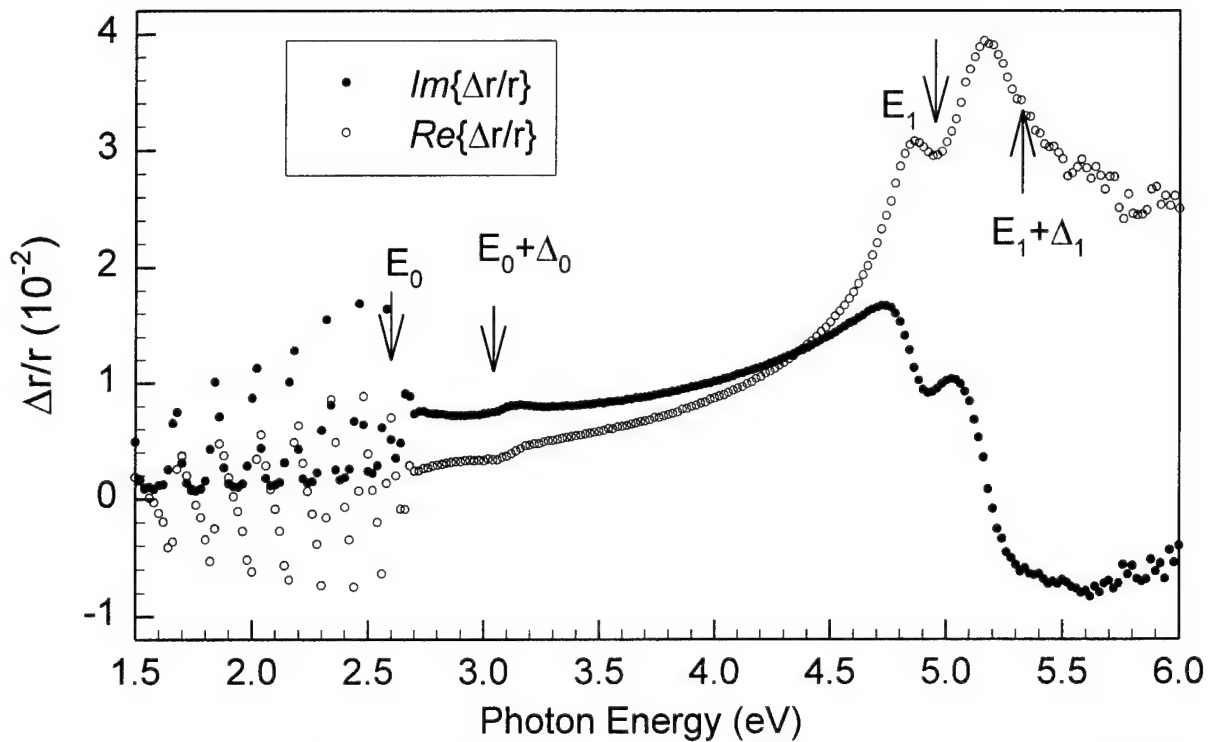


Figure 1. Ex-situ reflectivity difference spectra of ZnSe/GaAs between 1.5 eV and 6 eV. The interference patterns are shown below the band gap of ZnSe. The critical point structures are also shown.

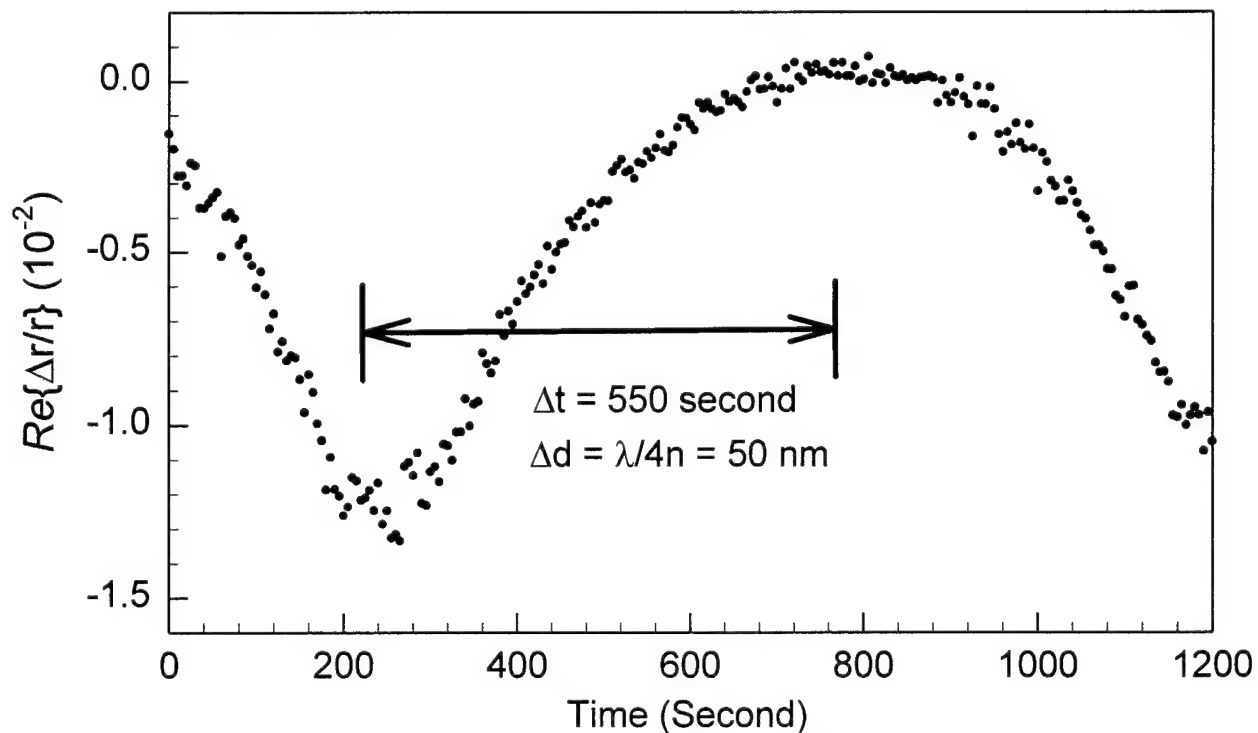


Figure 2. In-situ reflectivity difference spectra of ZnSe/GaAs during growth. The data are taken at 500 nm as a function of time. The thickness is deduced from the variation of the data.

# **Real-Time Monitoring of RHEED using Digital Signal Processing Techniques**

R. F. Kromann, R. N. Bicknell-Tassius\*, A. S. Brown and J.S. Dorsey  
School of Electrical Engineering  
Georgia Tech Research Institute\*  
Georgia Institute of Technology  
Atlanta, GA 30332-0250  
Office Phone and fax numbers: (404) 894-9885, (404) 894-4832  
e-mail: rb91@prism.gatech.edu

The reflection high energy electron diffraction (RHEED) technique has been widely applied to the study of molecular beam epitaxy growth kinetics. RHEED oscillations have been used to not only to measure growth rates, but also to accurately determine alloy compositions and surface diffusion lengths. One limitation of the RHEED technique is that to date it has been almost exclusively applied to non-rotating substrates. Thus it has had limited application in real-time monitoring/control and the study of surface kinetics during growth of realistic device structures. It is important to study realistic structures due to coupling between the layers in a multilayer structure.

A RHEED system has been developed that allows real-time monitoring of RHEED information throughout a multilayer growth run with rotation. This system consists of a standard RHEED system coupled with high speed video capture hardware and advanced digital signal processing software. In Figure 1 is plotted the specular spot intensity vs time for a complete MBE growth run consisting of a AlGaAs buffer layer and a single InGaAs quantum well. As can be seen, little useful information is readily available due to the large amount of noise introduced into the signal by substrate rotation. This same data is plotted in Figure 2 after it has been passed in real-time through a DSP filter to remove this noise. In Figure 3 is plotted the specular spot intensity during the growth of the InGaAs quantum well, showing the recovery of the specular spot intensity during the growth interrupts and its variation during the quantum well growth.

As an application of the RHEED monitoring during rotation, a desorption monitoring system has been developed that allows tight control of the oxide desorption process. This system has been used to investigate desorption effects on InGaAs/AlGaAs single quantum well structures for systematically varied process parameters. The method and extent of desorption have been shown to be very significant and SIMS measurements have shown that the amount of oxygen incorporation varies by two orders of magnitude depending on the oxide desorption process.

Signal processing software has been developed to extract not only the specular spot intensity, but also the position, intensity and width of multiple diffraction spots. This allows us to quantitatively monitor in real-time the condition of the growth surface. Results of a series of InGaAs quantum well structures for various growth parameters will be discussed.

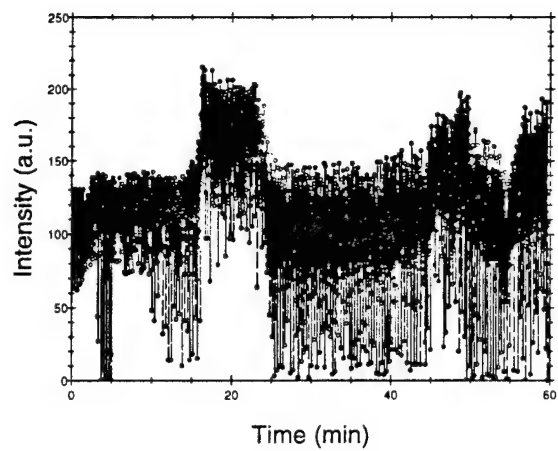


Figure 1.

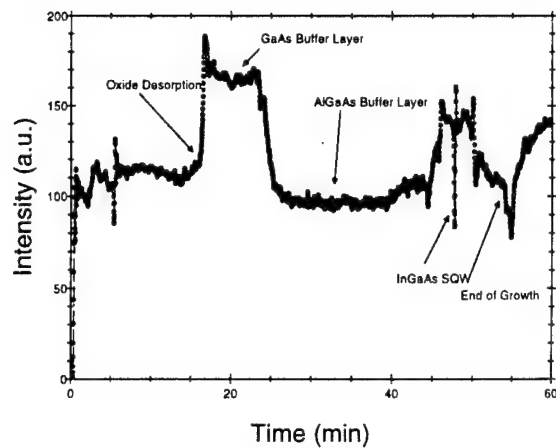


Figure 2.

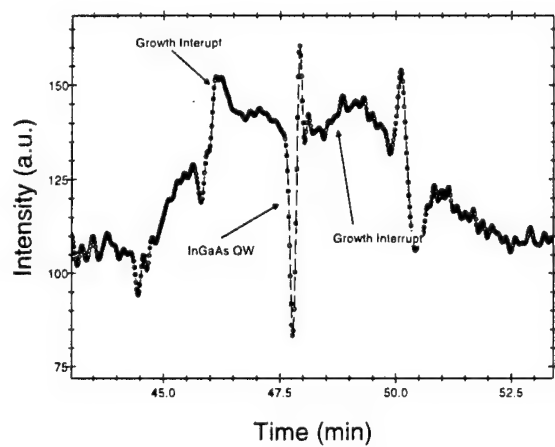


Figure 3.

## Concept of Sensor Simulator for Real-time Monitoring and Control of Molecular Beam Epitaxy Growth

J. J. Zhou\*, Y. Li, P. Thompson, D. L. Sato and H. P. Lee  
Department of Electrical and Computer Engineering  
University of California, Irvine, CA 92715  
Tel: (714)824-8309 Fax:(714)824-3732  
\*email: jzhou@ece.uci.edu

X. Liu  
Department of Electronic Engineering  
Tsinghua University, Beijing, P.R. China

*In situ* non-invasive sensors form the basis for real-time monitoring and control of epitaxial growth and device processing. Recent progress in sensor and integrated sensor technology together with ever declining computational overhead have pushed closed-loop MBE growth system closer to reality. If sensor-based MBE systems is to evolve into full-fledge closed-loop systems, widespread use of sensor simulator as a generic design and analysis tool will become indispensable. Such a simulator can be used not only for the validation of the control codes, but also provides valuable insight on the design and optimization of control algorithms (virtual interface, end-points detection methods etc, among others) prior to actual experimentation. Simulation test allows the designer to examine the behavior of a proposed control system so that necessary modification can be implemented early in the development cycle before time and resources are committed. In this talk, we will discuss the general methodology of employing sensor simulator for closed-loop control under MBE growth environment from a user's perspective. We described in detail how a prototype sensor simulator based on pyrometric interferometry (PI) monitoring is used for the closed-loop growth of AlAs/GaAs DBR structures. Although the simulator is used in the framework of a model-referenced control system, the general concept of sensor simulator can be implied from the studies. Our virtual control system consists of virtual sensor, sensor signal processing (based on Least Square Phase Estimation (LSPE) algorithm) and control units. The sensor simulator emulated the time-evolution of the PI signal based on model-calculation [1]. In some cases, the effect of growth rate transients, temperature variations (a sensitive parameter for pyrometric interferometry monitoring), systemic measurement drift (such as change in the intensity of the probing source) and measurement white noise are also incorporated into the sensor simulator. The virtual control-loop is executed by matching the sensor output with the endpoints of the reference signal (calculated versus incremental thickness) obtained either through (1) model-calculation, or (2) empirical data of a well calibrated structures (master copy). The expected reflectance spectrum is then calculated from the layer thickness obtained from the virtual controller. A major concern in the design of the control system arises from the fact that the outputs of the reference and simulated sensors are obtained in thickness and time domains respectively. We have used the sensor simulator to find the optimal parameters of the LPSE that minimize control errors due to the time-to-thickness transformation. In a separate example, the simulator is used to match experimentally measured sensor signal, and has confirmed a coding error in the time-to-thickness data interpolation algorithm which would be rather difficult to detect otherwise.

<sup>1</sup> H.P.Lee, E.Ranalli, and X.Liu, Appl. Phys. Lett., **67**, 1824 (1995).

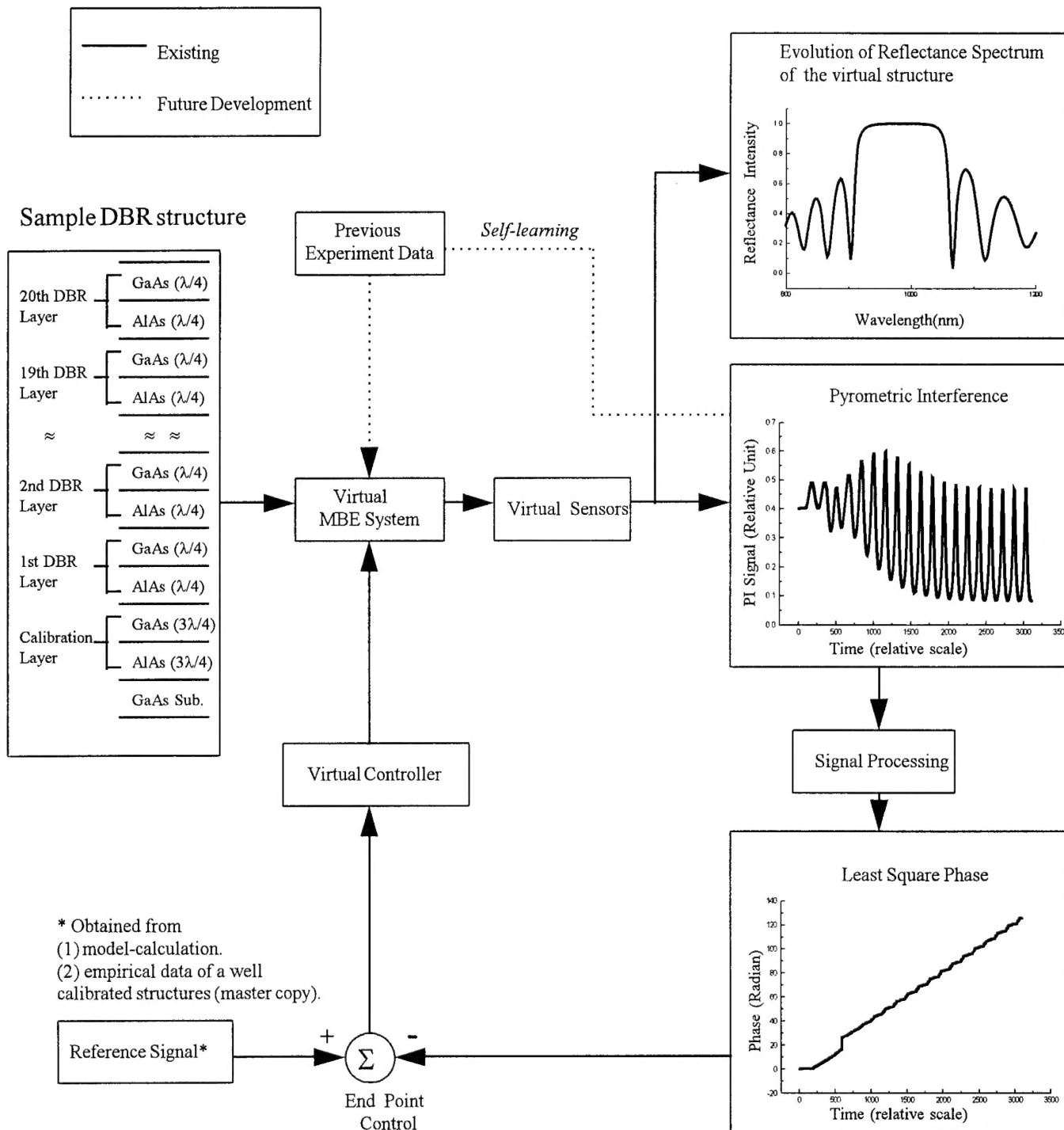


Figure1: The role of sensor simulator in generating PI signal vs. time during the MBE growth of DBR structure for close-loop control.

# In situ BEEM study of interfacial dislocations and point defects

H. von Känel, T. Meyer, H. Sirringhaus, and E.Y. Lee

Laboratorium für Festkörperphysik, ETH Zürich, CH-8093 Zürich

Recently, it has become possible for the first time to image misfit dislocations at epitaxial  $\text{CoSi}_2/\text{Si}(111)$  interfaces by ballistic-electron-emission microscopy (BEEM) [1]. In BEEM hot charge carriers are injected into a heterostructure grown on top of a semiconducting collector by the tip of an STM [2]. Those carriers which are able to pass all interfaces on their way to the collector give rise to the BEEM or collector current. This current is sensitive to the height of the potential barriers lying between the point of injection and the collector, as well as to any scattering processes a hot carrier may be subject to. Both can be studied by BEEM with a spatial resolution in the nanometer range. As an example we consider epitaxial metal/semiconductor heterostructures. Thin films of  $\text{CoSi}_2$  have been grown by MBE on both  $\text{Si}(111)$  and  $\text{Si}(100)$  and studied in situ by BEEM at 77 K. At  $\text{CoSi}_2/\text{Si}(100)$  interfaces interfacial dislocations lead to pronounced variations of the Schottky barrier height. By contrast no barrier height fluctuations are found at  $\text{CoSi}_2/\text{Si}(111)$  interfaces, except in regions where the crystal structure of the silicide deviates from the usual fluorite one. The highest sensitivity to scattering by interfacial defects is found on unreconstructed surfaces, since reconstructions can give rise to large variations of the BEEM current on an atomic scale. Thus we find that at unreconstructed  $\text{CoSi}_2/\text{Si}(111)$  interfaces scattering centers of atomic dimensions can easily be imaged by BEEM, in addition to the common misfit dislocations. The density of these point defects is found to be of the order of  $10^{13} - 10^{14} \text{ cm}^{-2}$  depending on the details of the growth procedure. This density is too low for the point defects to be detectable by transmission electron microscopy. It is on the other hand of the order of magnitude expected from the surface roughness previously determined by measuring the thickness dependence of the residual resistivity [3].

[1] H. Sirringhaus, E.Y. Lee, and H. von Känel, *Phys. Rev. Lett.* **73**, 577 (1994)

[2] W.J. Kaiser and L.D. Bell, *Phys. Rev. Lett.* **60**, 1406 (1988)

[3] H. von Känel and G. Fishman, *Phys. Rev. B* **45**, 3929 (1992)

contact person:

H. von Känel, tel. (0041)1 633 22 61, FAX (0041)1 633 10 72

e-mail: vkaenel@solid.phys.ethz.ch

## ***in situ* STM characterisation of Ga<sup>+</sup> focused ion beam interactions with MBE grown GaAs(100)**

S J Brown, P D Rose, E H Linfield, D A Ritchie, G A C Jones

University of Cambridge, Cavendish Laboratory, Madingley Road,  
Cambridge, CB3 0HE, UK

Using a combined system (Fig. 1) which incorporates molecular beam epitaxy (MBE), a Ga<sup>+</sup> focused ion beam (FIB), and an ultra high vacuum scanning tunnelling microscope (UHVSTM), we have studied the interaction of high energy Ga<sup>+</sup> ions with the GaAs(100) surface *in situ*. This unique apparatus allows contamination free analysis of the MBE grown and ion beam exposed surfaces, since all wafer transfers are in UHV (<10<sup>-10</sup> mbar). The use of a high energy Ga<sup>+</sup> focused ion beam (FIB) in the fabrication of GaAs/AlGaAs back-gated high electron mobility transistors is a well established technique[1], where implanted regions of the backgate become highly resistive for areal doses >10<sup>13</sup> ions cm<sup>-2</sup>. There is, however, speculation regarding the mechanism of this process in the crystal lattice. We will show topographic and spectroscopic data of the exposed and cross sectional surfaces using the UHVSTM to characterise the structure of the implanted regions.

In our experiments, a 30 keV Ga<sup>+</sup> FIB exposed 0.5 μm lines on a MBE grown GaAs(100) surface, with a line dose that varied from 1-8x10<sup>8</sup> ions cm<sup>-1</sup>. In the UHVSTM, we then observed the preservation of surface topography in the exposed areas, with only small scale disorder of the surface atomic structure. Spectroscopic studies showed an extended depletion region of the surface states beyond the FIB spot size. Spatially resolved and single point spectroscopy were used to characterise this altered electronic surface structure (Fig. 2). Cross sectional studies on the cleaved (110) surface were also performed to investigate the crystal lattice disorder.

We have thus demonstrated STM imaging of FIB defined regions in a MBE grown layer. This is an important step in the development of a fabrication procedure for nanometre scale devices, in which the UHVSTM is used to fabricate nanoscale features in a FIB defined structure.

[1] E.H. Linfield, G.A.C. Jones, D.A. Ritchie, and J.H. Thompson, *Semicond. Sci. Technol.* **8**, 415 (1993).

Stuart J Brown

Tel +44 1223 337471

Fax +44 1223 337271

e-mail [sjb1013@cus.cam.ac.uk](mailto:sjb1013@cus.cam.ac.uk)



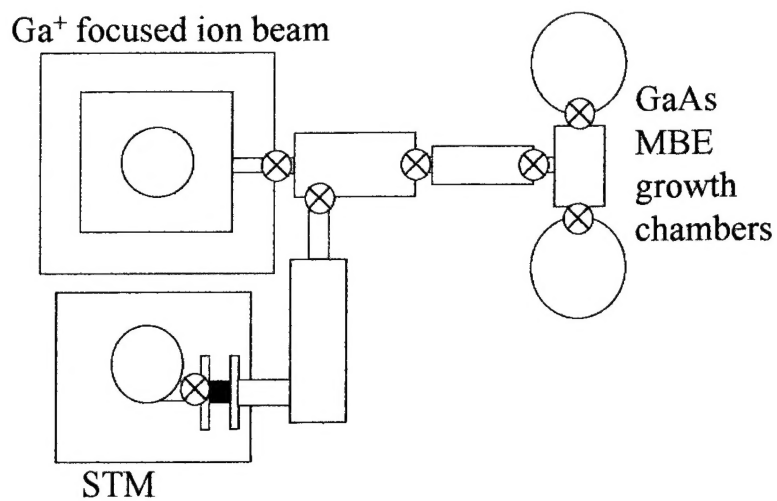


Figure 1: Schematic of combined system layout.

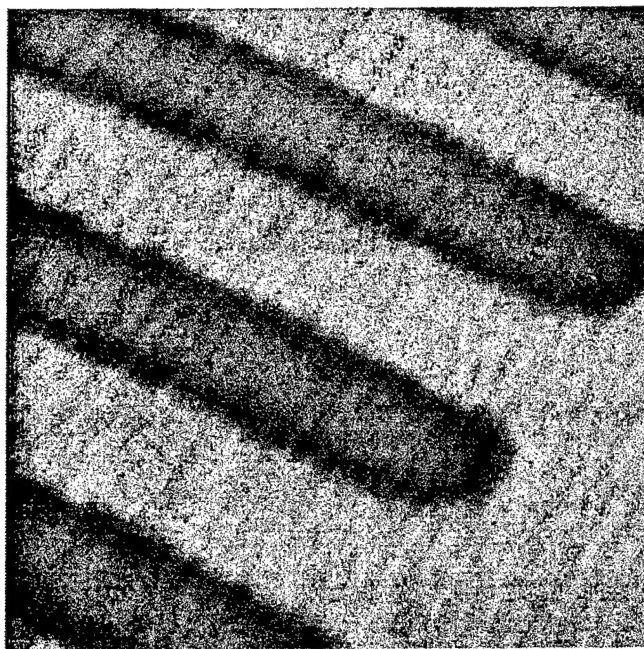


Figure 2: 4.5  $\mu\text{m}$  x 4.5  $\mu\text{m}$  STM spatial current image showing change in surface states due to ion beam exposure.